EVOLUTION OF THE IN-SITU STRESS STATE IN AN UPSTREAM CONSTRUCTED TAILINGS DAM

YASHAY NARAINSAMY

A project report submitted in partial fulfilment of the requirements for the degree of
DOCTOR OF PHILOSOPHY (CIVIL ENGINEERING)
In the
FACULTY OF ENGINEERING
UNIVERSITY OF PRETORIA

January 2025

© University of Pretoria

PROJECT REPORT SUMMARY

EVOLUTION OF THE IN-SITU STRESS STATE IN AN UPSTREAM CONSTRUCTED TAILINGS DAM

YASHAY NARAINSAMY

Supervisor: Professor S. W. Jacobsz
Department: Civil Engineering
University: University of Pretoria
Degree: Doctor of Philosophy (Civil Engineering)

In recent years, there have been several large tailings dam failures around the world that have resulted in significant negative environmental and social consequences. These failures are clearly a cause for concern and have led to a major review of the current design and operational practices of tailings dams. The outcomes of the independent panel investigations into the causes of these failures have highlighted several areas of uncertainty, mostly involving undrained shearing and the mobilisation of undrained shear strengths.

Within the context of undrained shearing, a specific area of uncertainty is the in-situ stress state. Although it is known that the in-situ stress state theoretically influences the undrained shear response for sandy soils, there are very few reported attempts to measure the in-situ stress state in literature. The objective of this study was therefore to design, construct, verify and implement a remote monitoring system capable of measuring the in-situ stress state in an upstream constructed tailings dam.

Such a system was developed, and it comprised several commercially available sensors, as well as some sensors constructed at the University of Pretoria. To measure the total earth pressures, two Earth Pressure Cells (EPCs) were used. These were installed in tailings dams such that the vertical and horizontal stresses could be measured. Tensiometers were used to measure the pore pressure, and a moisture probe was used to record the soil moisture content. Several other components such as dataloggers, batteries, and solar panels were included to ensure the completeness of the system.

© University of Pretoria

A rigorous verification process followed the development of the system which comprised testing of the individual sensors, as well as long-term testing of the entire system. Once the system was verified, it was installed on three active tailings dams.

Data from 27 months of monitoring of the in-situ stresses in an upstream constructed gold tailings dam are presented. Although there was some variability during the early monitoring periods, the in-situ stresses stabilised and remained within a fairly narrow band after a few months. It was found that the in-situ stress state is not isotropic. Rather, the stress state, described using the geostatic stress ratio, was found to vary between 0.4 and 0.6 for the gold tailings dam monitored. Shorter-term data obtained from an iron ore and platinum tailings site showed similar stress states.

To place these findings within a behavioural framework, a series of oedometer and triaxial compression tests were conducted on the gold tailings. It was found that gold tailings exhibited a unique Normal Consolidation Line (NCL) and unique Critical State Line (CSL) for remoulded samples prepared using the Moist Tamping technique. In terms of the undrained shearing response, it was found that the gold tailings is influenced by both the density and stress anisotropy. It was specifically found that these parameters influence the yield undrained shear strength and Brittleness Index. This is important as both of these parameters are used directly in design and safety evaluations in some international guidelines. Relatively small changes in both void ratio and stress anisotropy resulted in meaningful changes in yield undrained shear strength and brittleness index.

In terms of the performance of the EPCs, it was found that these sensors appear susceptible to temperature influences that cannot be corrected using the thermal correction factors provided by the manufacturer. In this study, a number of laboratory and field experiments were conducted where EPCs under constant load were subjected to large variations in temperature. This thermal influence was found to vary between 0.3 and 6.5 kPa/°C.

In summary, this study presented experimental data showing the large influence the in-situ stress state can have on the undrained shearing behaviour of loose gold tailings. In particular, the influence on the yield undrained shear strength and Brittleness Index were highlighted. A remote monitoring system, capable of monitoring the in-situ stress state in upstream constructed tailings dams was presented. The system is cost-effective and simple to install. The system installed on the gold site remains fully functional 27 months after installation and will likely continue providing reliable data for many years to come.

© University of Pretoria

“*If I have seen further, it is by standing on the shoulders of giants.”*

Sir Isaac Newton, 1675

© University of Pretoria

ACKNOWLEDGEMENTS

I wish to express my appreciation to the following people and organisations who made this thesis possible:

- My supervisor, Professor SW Jacobsz, for all your guidance and support through both my Masters and Doctoral studies.
- Professor Gerhard Heymann, for being an inspiration to me and all the other students in the department.
- Dr Nico Vermeulen, Professor Florian Hörtkorn, and Dr Luis Alberto Torres-Cruz for your mentorship throughout my career, you have truly been remarkable role models.
- The “G-Wizards”: Faith Abimaje, Jack Basson, Arno Crous, Opeyemi Fajire, Gregory McDonald, Ruan Murison, and Magai Thon. Thank you for all the help in the laboratory and for making my time on campus special. I could not have asked for better colleagues and friends.
- My family, for their continued love and support.
- Our laboratory technician, Mr Jan Vermaak, may your soul rest in peace.
- Fraser Alexander Tailings and The South African National Research Foundation (NRF) for financial support during my studies.

© University of Pretoria

TABLE OF CONTENTS

		PAGE
1	INTRODUCTION	1-1
1.1	BACKGROUND	1-1
1.2	OBJECTIVES OF THE STUDY	1-2
1.3	SCOPE OF THE STUDY	1-3
1.4	METHODOLOGY	1-3
1.5	ORGANISATION OF THE REPORT	1-4
2	LITERATURE REVIEW	2-1
2.1	INTRODUCTION	2-1
2.2	TAILINGS AND TAILINGS DAMS	2-1
2.2.1	Gold tailings	2-1
2.2.2	Tailings dams	2-6
2.2.3	Typical features of a modern tailings dam	2-8
2.2.4	Historical Water and Tailings Dam Failures	2-10
2.2.5	Current Tailings Dam Management Framework	2-31
2.3	EXISTING BEHAVIOURAL FRAMEWORK FOR SOILS	2-37
2.3.1	Soil behaviour in compression	2-38
2.3.2	Soil behaviour in shear	2-42
2.3.3	Unsaturated soil behaviour	2-53
2.3.4	Previous testing on gold tailings	2-55
2.4	LABORATORY TESTING OF SOILS	2-60
2.4.1	Sample preparation methods	2-60
2.4.2	Oedometer testing	2-61
2.4.3	Triaxial testing	2-61
2.4.4	Drying Boxes	2-65
2.5	GEOSTATIC STRESS RATIO	2-68
2.5.1	Importance of K_0	2-69
2.5.2	Factors influencing K_0	2-70
2.5.3	Empirical methods to estimate K_0	2-72
2.5.4	Laboratory measurement of K_0	2-73
2.5.5	Field measurement of K_0	2-74
2.5.6	Measurements on site	2-77
2.6	SENSORS FOR GEOTECHNICAL APPLICATIONS	2-88
2.6.1	Earth Pressure Cells	2-88

© University of Pretoria

2.6.2 High Capacity Tensiometers 2-103
2.6.3 Suction probes 2-104
2.6.4 Comparison of suction sensors 2-105
2.6.5 Moisture content probes 2-106
2.7 SUMMARY 2-109

3 LABORATORY ELEMENT TESTING 3-1

3.1 INTRODUCTION 3-1
3.2 ANALYSIS OF DATA FROM LITERATURE 3-1
3.3 GOLD TAILINGS CHARACTERISTICS 3-4
3.3.1 Physical characteristics 3-4
3.3.2 Mineralogical characteristics 3-5
3.3.3 Site conditions 3-10
3.4 OEDOMETER TESTING 3-13
3.4.1 General procedure 3-14
3.4.2 Uniqueness of the 1D-NCL 3-17
3.4.3 Influence of particle crushing 3-20
3.4.4 Summary 3-21
3.5 TRIAXIAL TESTING 3-22
3.5.1 General procedure 3-22
3.5.2 Key behavioural aspects 3-25
3.5.3 Indicator characteristics of the triaxial samples 3-30
3.5.4 Critical State Line (CSL) Testing 3-32
3.5.5 Influence of stress level 3-37
3.5.6 Influence of density 3-41
3.5.7 Influence of stress anisotropy 3-44
3.5.8 Influence of sample preparation method 3-49
3.5.9 Uniqueness of the NCL 3-53
3.5.10 Summary 3-56
3.6 COMBINED OEDOMETER AND TRIAXIAL TEST RESULTS 3-57
3.7 SUMMARY 3-59

4 REMOTE MONITORING SYSTEM 4-1

4.1 INTRODUCTION 4-1
4.2 REQUIREMENTS OF THE REMOTE MONITORING SYSTEM 4-1
4.3 COMPONENTS OF THE REMOTE MONITORING SYSTEM 4-4
4.3.1 Overview 4-4

© University of Pretoria

4.3.2 Sensors 4-4
4.3.3 Logging equipment 4-9
4.3.4 Power unit 4-9
4.3.5 Cabling 4-10
4.3.6 Enclosure (logger box) 4-12
4.3.7 Software 4-12
4.3.8 Summary 4-13
4.4 DESIGN OF THE REMOTE MONITORING SYSTEM 4-14
4.5 VERIFICATION OF THE REMOTE MONITORING SYSTEM 4-15
4.6 SUMMARY 4-15

5 LABORATORY VERIFICATION TESTS 5-1

5.1 INTRODUCTION 5-1
5.2 TENSIOMETER CALIBRATION TESTS 5-1
5.2.1 General procedure 5-1
5.2.2 Results 5-3
5.3 MOISTURE PROBE CALIBRATION TESTS 5-6
5.3.1 General procedure 5-6
5.3.2 Results 5-9
5.4 EARTH PRESSURE CELL VERIFICATION TESTS 5-14
5.4.1 General procedure 5-15
5.4.2 Results 5-20
5.5 INTERPRETATION OF DATA FROM THE REMOTE MONITORING SYSTEM 5-24
5.5.1 Determination of total stresses 5-24
5.5.2 Determination of pore pressures 5-25
5.5.3 Determination of water content 5-25
5.5.4 Determination of geostatic stress ratio ($\boldsymbol{K0}$) 5-25
5.5.5 Determination of vertical and horizontal effective stresses 5-26
5.6 DRYING BOX TESTS 5-29
5.6.1 Test 1: Long-term performance 5-29
5.6.2 Test 2: Performance during first filling 5-44
5.6.3 Test 3: Performance during temperature changes 5-48
5.6.4 Temperature effects on the EPCs 5-58
5.7 SUMMARY 5-59

6 FIELD MONITORING 6-1

6.1 INTRODUCTION 6-1

© University of Pretoria

6.2 GOLD TAILINGS SITE 6-1
6.2.1 Site description 6-1
6.2.2 Installation details 6-6
6.2.3 Results 6-11
6.3 IRON ORE TAILINGS SITE 6-24
6.3.1 Site description 6-24
6.3.2 Installation details 6-25
6.3.3 Results – shallow installation 6-29
6.3.4 Results – deep installation 6-40
6.4 PLATINUM TAILINGS SITE 6-47
6.4.1 Site Description 6-47
6.4.2 Installation details 6-48
6.4.3 Results 6-51
6.5 TEMPERATURE EFFECTS OF THE EPCS 6-57
6.6 COMBINED RESULTS 6-58
6.6.1 In-situ stress states 6-58
6.6.2 Stress ratios 6-60
6.6.3 Stress paths 6-62
7 INTERPRETATION OF LABORATORY AND FIELD DATA 7-1
7.1 INTRODUCTION 7-1
7.2 INTERPRETED STRESS RATIOS 7-1
7.3 BEHAVIOURAL FRAMEWORK 7-3
7.4 TEMPERATURE INFLUENCES ON THE EPCS UNDER CONSTANT LOAD 7-4
7.5 SUMMARY 7-1
8 CONCLUSIONS AND RECOMMENDATIONS 8-1
8.1 INTRODUCTION 8-1
8.2 CONCLUSIONS 8-1
8.2.1 The influence of K_c on the undrained shear response of the gold tailings 8-1
8.2.2 The uniqueness of the NCL for the gold tailings 8-2
8.2.3 The performance of several geotechnical sensors for long-term monitoring of gold tailings 8-4
8.2.4 Development and implementation a remote monitoring system capable of measuring the in-situ stress state in an upstream constructed tailings dam 8-5
8.2.5 Evaluation of the in-situ stress state in an upstream constructed tailings dam 8-6
8.3 RECOMMENDATIONS 8-7

© University of Pretoria

8.3.1 Additional field testing to estimate the in-situ stress ratio, K 8-7
8.3.2 Additional sites for field monitoring 8-7
8.3.3 Additional calibrations for the Earth Pressure Cells 8-8
8.3.4 Additional sensors for field installations 8-8
8.3.5 Additional Laboratory Element Testing 8-10

9 REFERENCES 9-1

© University of Pretoria

LIST OF FIGURES

Figure 2.1: Change in particle size with distance from discharge point (after Blight, 2009) .2-2
Figure 2.2: Preconsolidation pressures for the East Geduld gold slimes (after Donaldson, 1965).....2-4
Figure 2.3: Effect of sun drying on void ratio of gold slimes (after Blight, 1988) 2-5
Figure 2.4: Typical wall-raising methods for tailings dams: (a) upstream, (b) downstream, (c) centreline (after Vick, 1983).....2-7
Figure 2.5: Locations of the tailings and water dam case histories investigated.....2-10
Figure 2.6: Sketch showing the postulated series of events that led to failure at Merriespruit (after Wagener, 1997) 2-12
Figure 2.7: Results from the field sampling campaign at Merriespruit (after Fourie et al., 2001) 2-13
Figure 2.8: Results from a piezocone probe conducted near the decant facility on Merriespruit (Fourie et al., 2001) 2-14
Figure 2.9: Cross section through the failure section at Mount Polley (after Morgenstern et al., 2015).....2-16
Figure 2.10: Aerial photograph showing the setback at the Left Abutment (after Morgenstern et al., 2016) 2-19
Figure 2.11: Cross section of the Fundão Left Abutment showing: (a) the design intent, (b) the site conditions in November 2015, and (c) the proposed failure mechanism (after Morgenstern et al., 2016) 2-20
Figure 2.12: Cross section through the Feijão tailings dam: (a) after Robertson et al. (2019), and (b) after CIMNE (2021) 2-22
Figure 2.13: Supporting evidence for the Feijão tailings showing: (a) bonding, after Robertson et al. (2019); and (b) no bonding, after CIMNE (2021).....2-24
Figure 2.14: Photograph of the Edenville Dam failure 36s after initiation of failure (after France et al., 2022) 2-27
Figure 2.15: Stability analysis for the Edenville left embankment (after France et al., 2022) .2-29
Figure 2.16: Soil brittleness classification (after ICOLD, 2022) 2-36
Figure 2.17: Idealised soil behaviour in compression for: (a) fine-grained soils (clays), and (b) coarse-grained soils (sands) (after Jefferies & Been, 2015).....2-39
Figure 2.18: Triaxial test results on Erksak 330/0.7 sand (after Jefferies & Been, 2000)...2-40
Figure 2.19: Unload-reload loops for the LDUL-3/PV sample (after Jefferies & Been, 2000) 2-41
Figure 2.20: Influence of density on the undrained shear response of Ottawa sand (after

© University of Pretoria

Castro, 1969) in: (a) $q - \gamma$ space, and (b) $q - p'$ space 2-46
Figure 2.21: Influence of stress level on the undrained shear response of Toyoura sand (after Ishihara, 1993) in: (a) $q - \varepsilon a$ space, and (b) $q - p'$ space.....2-47
Figure 2.22: Influence of sample preparation method on the undrained shear response for loose Lagunillas sandy silt (after Zlatovic & Ishihara, 1997) in: (a) $q/p0' - \varepsilon a$ space, (b) $q/p'0 - p'/p'0$ space 2-49
Figure 2.23: Influence of fabric of the undrained behaviour of gold tailings (after Chang et al., 2011).....2-50
Figure 2.24: Influence of mode of shear on the undrained behaviour of Toyoura sand (after Yoshimine et al., 1998).....2-51
Figure 2.25: Key components of a Soil Water Retention Curve (after Fredlund, 2017) 2-54
Figure 2.26: Grading curves of previous testing regimes on gold tailings 2-56
Figure 2.27: Diagrammatic layout of a triaxial test (after Bishop & Henkel, 1962) 2-62
Figure 2.28: Examples of local Drying Boxes after (a) Westraad (2004), and (b) Wortmann (2007).....2-65
Figure 2.29: Examples of International Drying Boxes after: (a) Daliri (2013), and (b) Rozina et al. (2015).....2-66
Figure 2.30: Numerical simulations of silty tailings at various initial stress states (after Jefferies et al., 2019) 2-69
Figure 2.31: Influence of density on K_0 (after Obrician, 1969).....2-71
Figure 2.32: Influence of stress history on K_0 (after Obrician, 1969) 2-72
Figure 2.33: Numerical simulations of the evolution of the in-situ stress state at the Cadia NTSF (after Jefferies et al., 2019).....2-79
Figure 2.34: Photographs of the Lusatian overburden dumps showing: (a) the location of the monitoring stations, and (b) sensor installation at location 4a (after Rosenzweig et al., 2020) 2-82
Figure 2.35: Lateral stress measurements at Muskeg River Mine: (a) considering geological history, and (b) an alternate view (after Shuttle et al., 2021).....2-84
Figure 2.36: Stress state along the critical slip surface (after France et al., 2022) 2-85
Figure 2.37: Cross-section of the bridge abutment at Guildford (after Symons & Murray, 1988) 2-94
Figure 2.38: Influence of temperature on the interpreted: (a) lateral stresses and, (b) vertical stresses at Guildford (after Symons & Murray, 1988) 2-95
Figure 2.39: Cross-section through the box culvert at Site 1 (after Yang, 2000) 2-96
Figure 2.40: Results from the EPCs at Site 1 showing: (a) interpreted vertical stresses and, (b) seasonal temperature variations (after Yang, 2000).....2-97
Figure 2.41: Results from the thermal calibration of pressure cell 1 (after Daigle & Zhao, 2004)

© University of Pretoria

.....2-99
Figure 2.42: Typical components of the Tuks HCT (after le Roux, 2019).....2-104
Figure 2.43: Key components of the TEROS 21 WPS (after Tripathy et al., 2016) 2-105
Figure 2.44: Sketch of the TEROS 12 moisture probe (after METER Group, 2018).....2-108
Figure 3.1: Typical undrained shear response observed for the Quebec gold tailings in: (a) $q - \varepsilon a$ space, and (b) $q - p'$ space (after Fotovvat & Sadrekarimi, 2022) 3-2
Figure 3.2: Comparison of yield undrained shear strengths for the Quebec gold tailings (after Fotovvat & Sadrekarimi, 2022) 3-4
Figure 3.3: Sample collection at the gold site showing: (a) sample being extracted, and (b) extracted sample on surface.....3-11
Figure 3.4: Summary of void ratio measurements taken on site during the monitoring period 3-12
Figure 3.5: Photographs taken on site showing the layering at the gold tailings site 3-13
Figure 3.6: Oedometer test results on the gold tailings 3-19
Figure 3.7: Quantification of the degree of convergence of the 1D-NCL of the gold tailings..3-20
Figure 3.8: Influence of imposed stress on particle crushing of the gold tailings 3-21
Figure 3.9: Summary of the specific gravity test results on the gold tailings.....3-31
Figure 3.10: Results from the grading analyses conducted on the gold tailings moisture content samples 3-32
Figure 3.11: Results from the CSL testing for the gold tailings in: (a) $e - p'$ space, and (b) $q - p'$ space.....3-33
Figure 3.12: Failure points of all 21 MT samples in: (a) $e - p'$ space, and (b) $q - p'$ space ..3-34
Figure 3.13: Influence of density on the shear behaviour of the gold tailings showing: (a) deviator stress, (b) excess pore pressure, and (c) volumetric strain 3-38
Figure 3.14: Influence of stress level on the stress paths of the gold tailings 3-39
Figure 3.15: Results from the triaxial tests showing the influence of density in: (a) $q - \varepsilon a$ space, and (b) $q - p'$ space.....3-43
Figure 3.16: Consolidation stress paths for the anisotropically consolidated gold tailings samples.....3-45
Figure 3.17: Influence of stress anisotropy on the undrained shear response of the gold tailings at low strain levels 3-46
Figure 3.18: Results from the triaxial tests showing the influence of stress anisotropy in: (a) $q - \varepsilon a$ space, and (b) $q - p'$ space 3-48
Figure 3.19: Results from the triaxial tests conducted as part of Batch 5 in: (a) $q - p'$ space,

© University of Pretoria

and (b) $e - p'$space 3-51
Figure 3.20: Results from the triaxial testing to identify the NCL 3-54
Figure 3.21: Influence of density and stress anisotropy on brittleness and undrained shear strength of gold tailings in: (a) $q - \varepsilon a$ space, and (b) $q - p'$ space 3-57
Figure 3.22: Combined triaxial and oedometer test results 3-58
Figure 3.23: Summary of key CSSM features of the gold tailings 3-59
Figure 4.1: Details of the Geosense VWTPC-4000 EPC (after Geosense Ltd, 2016) 4-5
Figure 4.2: Sketch of the erse Kablo LIYCY cable used for this study (after erse Kablo, 2021) 4-11
Figure 4.3: Photographs showing the cable splicing at the platinum site: (a) before epoxy filling, (b) after epoxy filling, and (c) completed splices 4-12
Figure 4.4: Components of the remote monitoring system inside the enclosure 4-15
Figure 5.1: Sketch showing the setup for the tensiometer calibration 5-2
Figure 5.2: Raw calibration data for tensiometer 1B, used for the gold tailings site.....5-4
Figure 5.3: Interpreted calibration data for tensiometers 1A and 1B, used for the gold tailings site 5-5
Figure 5.4: Results from selected dry-out tests on the Tuks tensiometers 5-6
Figure 5.5: Sketch showing the key components of the setup used for the moisture probe calibration tests 5-8
Figure 5.6: Photograph showing the setup used for the moisture probe calibration tests....5-8
Figure 5.7: Selected results from the moisture probe calibration Test 3.....5-10
Figure 5.8: Performance of the TDR sensor using the Mineral Soils relationship.....5-11
Figure 5.9: Performance of the TDR sensor using the Topp et al. (1980) relationship 5-12
Figure 5.10: Comparison of the various SWRCs developed for the gold tailings.....5-13
Figure 5.11: Fredlund & Xing (1994) curve fits for the gold tailings showing: (a) VWC, and (b) Sr plots.....5-14
Figure 5.12: Sketch showing the configuration of the EPC compliance testing setup 5-15
Figure 5.13: Displacement transducer verification using a precision stand 5-16
Figure 5.14: Results from the displacement verification testing 5-17
Figure 5.15: Sketch showing the three displacement transducer locations for the EPC compliance testing.....5-18
Figure 5.16: Results from the transducer verification process showing: (a) the transducer response, and (b) the measurement error 5-19
Figure 5.17: Results from the compliance testing of the EPCs 5-20
Figure 5.18: Example of variation in deflection along the face of the EPC 5-21
Figure 5.19: Variation in compliance of the EPCs installed at the gold site 5-22
Figure 5.20: Variation in compliance for the EPCs installed at the iron ore site 5-22

© University of Pretoria

Figure 5.21: Variation in compliance of the EPCs installed at the platinum site 5-23
Figure 5.22: Results of all the compliance tests conducted on the EPCs.....5-24
Figure 5.23: Visual representation of the three assumptions considered for the S_r calculation 5-28
Figure 5.24: Summary of the three S_r assumptions on the calculated K_0 values for the gold tailings site 5-29
Figure 5.25: Key features of the Drying Box 1 experiment.....5-32
Figure 5.26: Selected photographs showing key stages of the Drying Box 1 experiment..5-34
Figure 5.27: Drying Box 1 pore pressure data for: (a) the entire test, and (b) the first seven months 5-36
Figure 5.28: Results from Drying Box 1 showing: (a) pore pressures over the entire test duration, (b) correlation between the HCTs, and (c) the slow response of the WPS.....5-38
Figure 5.29: Photographs of the sensors used for Drying Box 1 showing: (a) all three sensors, (b) the cracked epoxy-cased HCT, and (c) the intact steel-cased HCT.....5-39
Figure 5.30: Results from Drying Box 1 showing: (a) total stresses, (b) pore pressures, (c) VWC, and (d) stress ratios 5-41
Figure 5.31: Temperature effects on the EPCs for the Drying Box 1 experiment showing: (a) temperatures, (b) Setup 1 EPC frequencies, (c) Setup 2 EPC frequencies, and (d) interpreted total stresses 5-43
Figure 5.32: Sensor layout for Drying Box 2 5-45
Figure 5.33: Results from the Drying Box 2 showing: (a) total stresses, (b) pore pressures, (c) VWC, and (d) stress ratios 5-47
Figure 5.34: EPC response during filling for Drying Box 2 5-48
Figure 5.35: Overview of the short-term tests conducted for Drying Box 3.....5-50
Figure 5.36: Layout of the Drying Box 3 test for Stage 2.....5-51
Figure 5.37: Results from Stage 2 of the Drying Box 3 experiment showing: (a) recorded temperatures, and (b) interpreted total stresses 5-52
Figure 5.38: Setup for Stage 4 of the Drying Box 3 experiment 5-53
Figure 5.39: Results from Stage 4 of the Drying Box 3 experiment showing: (a) recorded temperatures, (b) total vertical stresses, and (c) total horizontal stresses.....5-54
Figure 5.40: Results from the Drying Box 3 experiment showing: (a) Stages 3, and (b) Stage 4.....5-55
Figure 5.41: Detailed long-term results from the Drying Box 3 experiment showing: (a) temperature, (b) Setup 1 EPC frequencies, (c) Setup 2 EPC frequencies, and (d) interpreted total stresses.....5-57
Figure 5.42: Summary of results of the long-term testing as part of the Drying Box 3 experiment 5-58

© University of Pretoria

Figure 6.1: Monthly rainfall records at the gold tailings dam over the monitoring period 6-3
Figure 6.2: Key monitoring data at the gold tailings dam over the review period showing: (a) monthly deposition, (b) elevation, and (c) RoR 6-5
Figure 6.3: Monthly piezometer water column heights at the gold tailings dam over the monitoring period.....6-6
Figure 6.4: Photographs showing the gold site: (a) planning, (b) installation, and (c) the logger boxes installed on the slope 6-7
Figure 6.5: Sensor installation at the gold tailings site, Station 3 6-8
Figure 6.6: Station 3 at the gold tailings site: (a) on the day of installation, and (b) on day 13 of monitoring 6-9
Figure 6.7: Cross section showing the installation details at the gold tailings dam.....6-10
Figure 6.8: VWC and suction responses at the gold site after: (a) first rewetting, and (b) wetting and drying in month six.....6-12
Figure 6.9: Results from the gold site, prior to the step-in showing: (a) total stresses, (b) pore pressures, (c) VWC, and (d) stress ratios 6-15
Figure 6.10: Results for the gold tailings site over the entire monitoring period showing: (a) total stresses, (b) pore pressures, (c) VWC, and (d) stress ratios 6-17
Figure 6.11: VWC and suction values measured at the gold tailings site 6-18
Figure 6.12: Selected stress paths for Station 2 6-19
Figure 6.13: Interpreted stress paths for all three stations at the gold site during November 2022 6-19
Figure 6.14: Combined stress path results for the gold site 6-20
Figure 6.15: Month-end Sr and suction values at the gold tailings site.....6-20
Figure 6.16: Month-end vertical and horizontal effective stresses at the gold site.....6-21
Figure 6.17: Seasonal ground temperature variations at the gold site 6-22
Figure 6.18: Influence of temperature on the EPCs installed at Station 1, after the step-in showing: (a) temperatures, (b) EPC frequencies, and (c) interpreted total stress 6-23
Figure 6.19: Grading curves for the iron ore tailings, compared to the gold tailings 6-25
Figure 6.20: Photographs taken for the iron ore shallow installation showing: (a) planning, (b) installation, and (c) the erected logger boxes 6-27
Figure 6.21: Photograph for the deep installation showing: (a) planning, (b) installation, and (c) the erected logger box.....6-29
Figure 6.22: VWC and suction measurements during the first wetting and drying cycles at the shallow iron ore installation 6-30
Figure 6.23: Temperature influences prior to recommissioning showing: (a) temperatures, (b) EPC frequencies, and (c) interpreted total stresses 6-32
Figure 6.24: Results from the shallow installation at the iron ore site showing: (a) total stress,

© University of Pretoria

(b) pore pressure, (c) VWC, and (d) stress ratios 6-34
Figure 6.25: VWC and suction responses at the shallow iron ore site for: (a) both stations, and (b) Station 2 only 6-35
Figure 6.26: VWC responses at the iron ore site (shallow installation).....6-36
Figure 6.27: EPC response post deposition ceasing showing: (a) temperatures, (b) EPC frequencies, and (c) interpreted total stresses 6-38
Figure 6.28: Stress paths for the shallow installation at the iron ore site 6-39
Figure 6.29: Month-end stress ratios for the iron ore tailings site 6-40
Figure 6.30: Results from the deep installation at the iron ore site showing: (a) temperatures, (b) EPC frequencies, (c) interpreted total stresses, and (d) water content estimates 6-42
Figure 6.31: Results from the remote monitoring system at the deep installation at the iron ore site showing: (a) temperatures, (b) total stresses, and (c) VWC 6-44
Figure 6.32: Photograph showing the large desiccation cracks noted near the penstock at the iron ore site 6-45
Figure 6.33: Daily temperature variations before and after backfilling of the excavation ...6-46
Figure 6.34: Grading curve of the platinum tailings, compared to the gold tailings.....6-48
Figure 6.35: Photograph for the platinum installation showing: (a) planning, (b) installation, and (c) the erected logger boxes 6-49
Figure 6.36: VWC and suction data for the first rewetting phase at the platinum site 6-52
Figure 6.37: Results from the remote monitoring stations at the platinum site showing: (a) total stress, (b) pore pressures, (c) VWC, and (d) stress ratios 6-54
Figure 6.38: VWC and suctions responses at the platinum site 6-55
Figure 6.39: Stress paths for the platinum site.....6-56
Figure 6.40: Month-end stress ratios at the platinum tailings site.....6-57
Figure 6.41: Stress ratios for the: (a) gold, (b) iron ore, and (c) platinum sites 6-59
Figure 6.42: Summary of the interpreted stress ratios for the: (a) gold, (b) iron ore, and (c) platinum sites 6-61
Figure 6.43: Interpreted stress paths for the: (a) gold, (b) iron ore, and (c) platinum sites 6-63
Figure 7.1: Estimated month-end S_r values during the field monitoring.....7-1
Figure 7.2: Estimated month-end stresses over the course of the field monitoring 7-2
Figure 7.3: Summary of the thermal effects on the interpreted stress response from the EPCs under constant load.....7-6

© University of Pretoria

LIST OF TABLES

Table 2.1: Summary of XRD results on gold tailings mined from the Witwatersrand Supergroup (after Vermeulen, 2001) 2-6
Table 2.2: Summary of minimum FoS values for various scenarios (after ICOLD, 2022) 2-37
Table 2.3: Summary of key terminology used to describe the shearing behaviour of soils 2-44
Table 2.4: Summary of key characteristics of gold tailings from the literature 2-59
Table 2.5: Summary of previous Drying Box experiments 2-67
Table 2.6: Summary of K_0 estimates from literature 2-87
Table 2.7: Summary of factors influencing EPC performance (after Weiler & Kulhawy, 1982) 2-100
Table 2.8: Summary of EPC thermal correction factors from the literature 2-102
Table 2.9: Comparison of various suction measurement sensors 2-106
Table 3.1: Indicator parameters of the gold tailings assessed as part of this study 3-5
Table 3.2: Results from the XRD testing on the gold tailings 3-5
Table 3.3: Process water composition of the gold tailings, compared to national drinking water limits 3-7
Table 3.4: Summary of key aspects of the oedometer tests 3-16
Table 3.5: Examples of triaxial Test IDs, with a detailed description 3-24
Table 3.6: Four key aspects of soil behaviour relating to tailings dam design and safety evaluation procedures 3-26
Table 3.7: Summary of key critical state parameters for the gold tailings 3-35
Table 3.8: Summary of key aspects of the triaxial tests for Batch 1 (CSL Testing) 3-36
Table 3.9: Summary of key aspects of the triaxial tests for Batch 2 (influence of stress level) 3-40
Table 3.10: Key parameters for the triaxial tests conducted as part of Batch 3 (influence of density) 3-42
Table 3.11: Key parameters for the triaxial tests conducted as part of Batch 4 (influence of stress conditions during consolidation) 3-47
Table 3.12: Key parameters of the triaxial tests conducted as part of Batch 5 (influence of fabric) 3-52
Table 3.13: Summary of key triaxial data for Batch 6 (NCL investigation) 3-55
Table 4.1: Key aspects of the remote monitoring system 4-2
Table 4.2: Summary of actions applied for this study regarding key aspects affecting the performance of EPCs 4-6
Table 4.3: Summary of key components of the remote monitoring system 4-13
Table 5.1: Key aspects of the moisture probe calibration tests 5-9

© University of Pretoria

Table 5.2: Overview of the three Sr assumptions considered 5-27
Table 5.3: Summary of the six short stages of Drying Box 3.....5-49
Table 5.4: Summary of temperature influence noted for the EPCs under constant load ...5-59
Table 6.1: Key rainfall characteristics of the gold site (after Adamson, 1981) 6-2
Table 6.2: Key events at the gold site.....6-9
Table 6.3: Composition of the iron ore tailings (basin sample).....6-25
Table 6.4: Key events at the iron ore site.....6-26
Table 6.5: Composition of the platinum tailings (basin sample) 6-48
Table 6.6: Key events at the platinum site 6-50
Table 6.7: Summary of temperature influence on EPCs under constant load 6-58
Table 7.1: Summary of field measured K_0 values 7-3
Table 7.2: Summary of temperature influence noted for the EPCs under constant load 7-5
Table 7.3: Summary of EPCs tests conducted to investigate thermal effects under constant load 7-1

© University of Pretoria

LIST OF ABBREVIATIONS

AEV	Air Entry Value
AP	Air Pluviation
ASTM	American Society for Testing and Materials
CASM	Clay and Sand Model
CD	Consolidated Drained
CoP	Code of Practice
CPT	Cone Penetration Test
CSD	Constant Shear Drained
CSL	Critical State Line
CSSM	Critical State Soil Mechanics
CT	Computed Tomography
CU	Consolidated Undrained
DE	Deposition Event
DMRE	Department: Mineral Resources and Energy
DR	Dilative Response
DSS	Direct Simple Shear
DWAF	Department: Water Affairs and Forestry
DWS	Department: Water and Sanitation
DSO	Dam Safety Office
EC	Electrical Conductivity
EGLE	Michigan Department of Environment, Great Lakes, and Energy
EoR	Engineer of Record
EOTF	End of Test Freezing
EPC	Earth Pressure Cell
ERPM	East Rand Proprietary Mines
ETF	External Tailings Facility
FEA	Finite Element Analysis
FERC	Federal Energy Regulatory Commission
FLAC	Fast Lagrangian Analysis of Continua
FoS	Factor of Safety
FSO	Full Scale Output
GDS	Global Digital Systems
GISTM	Global Industry Standard on Tailings Management
HAE	High Air Entry

© University of Pretoria

HBM	Hottinger Baldwin Messtechnik
HCT	High Capacity Tensiometer
HDS	Hydraulic Dry Stacking
ICMM	International Council on Mining and Metals
ICOLD	International Commission on Large Dams
IFT	Independent Forensic Team
IL	Instability Locus
IP	Ingress Protection
ISO	International Organisation for Standardisation
LCC	Limiting Compression Curve
LDUL	Load Unload
LF	Liquefaction Failure
LL	Limited Liquefaction
LLDPE	Linear Low-Density Polyethylene
LVDT	Linear Variable Differential Transformer
MAMSL	Metres Above Mean Sea Level
MHSA	Mine Health and Safety Act
MRM	Muskeg River Mine
MT	Moist Tamped
NC	Normally Consolidated
NCL	Normal Consolidation Line
NGL	Natural Ground Level
NTSF	Northern Tailings Storage Facility
OHSA	Occupational Health and Safety Act
OC	Overconsolidated
OCR	Overconsolidation Ratio
PMF	Probable Maximum Flood
PNCL	Pseudo Normal Consolidation Line
PSD	Particle Size Distribution
PV	Wet Pluviated
PVC	Polyvinyl Chloride
PW	Process Water
QSS	Quasi Steady State
RE	Rainfall Event
RoR	Rate of Rise
SABS	South African Bureau of Standards
SANAS	South African National Accreditation System

© University of Pretoria

SANCOLD	South African National Committee on Large Dams
SANS	South African National Standard
SBP	Self-Boring Pressuremeter
SD	Slurry Deposited
SIM	Subscriber Identity Module
SMA	SubMiniature version A
SMD	Surface Mounted Device
SWRC	Soil Water Retention Curve
TDR	Time Domain Reflectometry
TSF	Tailings Storage Facility
TUK	Transvaalse Universiteitskollege
TW	Tap Water
TXC	Triaxial Compression
TXE	Triaxial Extension
UD	Undisturbed
USB	Universal Serial Bus
USCS	Unified Soil Classification System
UU	Unconsolidated Undrained
WES	Waterways Experiment Station
WP	Water Pluviation
WPS	Water Potential Sensor
WS	Water Sedimented
XRD	X Ray Diffraction
1D-NCL	One-Dimensional Normal Consolidation Line

© University of Pretoria

LIST OF SYMBOLS

α	Calibration coefficient for the Tuks tensiometer [kPa/mV/V)]
a	SWCC fitting parameter as per Fredlund & Xing (1994)
β	Response from the Tuks tensiometer at zero pressure (mV/V)
c_v	Coefficient of vertical consolidation (m^2/year)
Δ	Stress cell deflection (mm)
d	Stress cell active face diameter (mm)
D	Stress cell diameter (mm)
D_r	Relative density (%)
D_{50}	Median soil grain size (mm)
d/D_{50}	Stress cell active diameter to soil grain size ratio
e_i	Void ratio at the start of the test (initial void ratio)
e_c	Void ratio at the end of consolidation
e_{cs}	Void ratio at critical state
e_{min}	Minimum void ratio
e_{max}	Maximum void ratio
ε	Apparent dielectric permittivity
ε_a	Axial strain
f_0	Initial pressure cell frequency reading (Hz)
f_1	Current pressure cell frequency reading (Hz)
f_h	Pressure cell frequency reading for horizontal stress (Hz)
f_v	Pressure cell frequency reading for vertical stress (Hz)
G_s	Specific gravity
γ	Shear strain
I_B	Brittleness index
k	Coefficient of permeability (m/s)
k	Linear calibration factor, used for the EPC stress interpretation (kPa/Hz^2)
k_1	Thermal coefficient provided by the manufacturer (kPa/°C)
K	Stress ratio, for field conditions
K_0	Geostatic stress ratio, also referred to as the coefficient of lateral earth pressure at rest
K_a	Apparent dielectric constant
K_a	Active earth pressure coefficient
K_c	Stress ratio, for triaxial compression conditions

© University of Pretoria

K_p	Passive earth pressure coefficient
λ_e	Slope of the CSL in the $e - \ln p'$ projection
m	SWCC fitting parameter as per Fredlund & Xing (1994)
n	SWCC fitting parameter as per Fredlund & Xing (1994)
p	Uncorrected pressure reading (kPa)
P	Pressure (kPa)
p'	Mean effective stress (kPa)
p'_c	Mean effective stress at critical state (kPa)
p'_y	Mean effective stress at the onset of yielding (kPa)
p'_0	Mean effective stress at the start of the shear phase (kPa)
p_k	Temperature corrected pressure, using the thermal coefficient provided by the manufacturer (kPa)
φ'	Effective friction angle (°)
ψ	State parameter
ψ	Matric suction (kPa)
ΔP	Pressure variation (kPa)
q	Deviator stress (kPa)
q_{cs}	Deviator stress at critical state (kPa)
q_y	Deviator stress at the onset of yielding (kPa)
RAW	Raw data reading from the TEROS 12 moisture probe
R	Registration ratio
S	Soil-cell stiffness ratio
s	Critical state stress invariant (kPa)
$S_{u(critical\ state)}$	Critical state undrained shear strength (kPa)
$S_{u(yield)}$	Yield undrained shear strength (kPa)
$\frac{S_{u(yield)}}{p'_0}$	Yield undrained strength ratio
σ'_h	Horizontal effective stress (kPa)
σ_h	Horizontal total stress (kPa)
σ'_v	Vertical effective stress (kPa)
σ_v	Vertical total stress (kPa)
σ^*	Bishop effective stress (kPa)
T/D	Stress cell thickness/diameter ratio, also referred to as aspect ratio
T	Stress cell thickness (mm)
T	Thermal calibration factor, used for EPC stress interpretation (kPa/°C)
T_0	Initial temperature (°C)

© University of Pretoria

T_1	Current temperature (°C)
t	Time (s)
t	Critical state stress invariant (kPa)
t_{90}	Time for 90% consolidation (s)
τ	Shear stress (kPa)
u_a	Pore air pressure (kPa)
u, u_w	Pore water pressure (kPa)
Γ_1	Altitude of the CSL in the $e - \ln p'$ projection at p'=1 kPa
θ	Volumetric water content (m^3/m^3)
v	Specific volume, equal to $e + 1$
v_5	Specific volume at an applied vertical total stress of 5 kPa
v_{2400}	Specific volume at an applied vertical total stress of 2.4 MPa
V_{diff}	Voltage difference recorded by the Tuks tensiometer (mV/V)
w	Gravimetric water content (%)
χ	Empirical factor related to degree of saturation and soil type (dimensionless)

© University of Pretoria

1 INTRODUCTION

1.1 BACKGROUND

Tailings dams are some of the largest man-made structures in the world and can have significant negative social and environmental impacts if not designed, constructed, operated and closed appropriately. Recently, there have been several prolific global tailings dam failures that have resulted in significant negative social and environmental impacts. For example, the Fundão tailings dam failure in 2015 resulted in the contamination of over 670 km of a major river (Morgenstern et al., 2016). Similarly, the Feijão tailings dam failure in 2019 resulted in the death of over 250 people (Robertson et al., 2019).

Clearly, these are unacceptable consequences. The global tailings industry has recognised this, and in 2020 the Global Industry Standard on Tailings Management (GISTM) was released (Oberle, 2020). The intent of this document was to provide clear, objective, minimum requirements for the design, construction, operation and closure of tailings dams with the ultimate goal of improving tailings dam safety. The International Council of Mining and Metals (ICMM) is an international organisation dedicated to a safe, fair and sustainable mining and metals industry. With large members involved in many countries all over the world, the commitment by the ICMM to comply with the GISTM is significant.

Although the publication of the GISTM is a step in the right direction, there are still significant uncertainties involved with its implementation. This has been recognised and there has been an attempt to address this in terms of administrative clarity. For example, in 2021 two supporting guideline documents to the GISTM were published (ICMM, 2021a, 2021b). Even with these guideline documents, there still remains a need for tailings-specific research and that is where this study becomes relevant.

A key area of uncertainty within the GISTM is related to the in-situ stress state of soil. This stress state can be evaluated using the geostatic stress ratio, K_0, which is simply the ratio between the horizontal and vertical effective stress in the soil. Although the equation is simple, determination of these parameters is not. So much so that in their theme lecture at the International Conference on Geotechnical Engineering for Coastal Development, Jamiolkowski et al. (1991) stated that the assessment of the horizontal effective stress remains a sort of black hole in soil engineering. This was followed up at the opening address of CPT'95 where Jamiolkowski (1995) stated that it is evident that there is an urgent need for developing

© University of Pretoria

non-destructive methods for the evaluation of K_0 in situ. These are bold statements and in the author's view, they remain relevant to this day. Further, it appears that these statements about the uncertainty regarding the in-situ horizontal effective stress is especially true for mine tailings.

The purpose of this research is therefore to attempt to reduce some of the current uncertainty regarding the behaviour of mine tailings in undrained shear. A specific focus was the measurement of the in-situ stress state in an active tailings dam. To provide some context as to why knowledge of the in-situ stress state is important, a behavioural framework was also defined with a particular focus on the influence of the stress state on the undrained shear response of the gold tailings. The choice of the tailings material and tailings dam site was made based on the composition of the current tailings dams in South Africa.

1.2 OBJECTIVES OF THE STUDY

There were five objectives of the study, two key objectives and three lesser objectives. These are defined below.

1. The primary objective of the study was to design, construct, test and implement a remote monitoring system capable of measuring the in-situ stress state in an active upstream constructed tailings dam.
2. A secondary objective was the use the remote monitoring system on an active upstream constructed tailings dam to measure the changes in the in-situ stress state. The system should specifically measure the resulting change in in-situ stress state due to routine deposition events and subsequent drying cycles for as long a period as possible.

In addition to the two key objectives, three smaller objectives were identified:

3. Define a behavioural framework for the gold tailings, with a specific focus on the influence of the stress ratio (K_c) on the mechanical response during undrained shearing in triaxial compression.
4. Within the behavioural framework defined for the gold tailings, investigate the uniqueness of the Normal Consolidation Line (NCL).
5. Investigate the performance of the various sensors used in terms of their long-term performance for monitoring of gold tailings.

© University of Pretoria

1.3 SCOPE OF THE STUDY

Although the defined objectives of this study can be applied in a broad sense, the scope of this study was limited to the following aspects:

1. This study was limited to the investigation of gold tailings from a single, upstream constructed tailings dam located in the East Rand in Gauteng. Although additional tailings types were initially investigated, these eventually proved unsuccessful for long-term monitoring and therefore only short-term data are presented for the other tailings types.
2. The in-situ stress state was represented as a stress ratio of the horizontal and vertical effective stresses.
3. Laboratory element testing was limited to triaxial compression tests and oedometer tests.
4. Element testing was limited to remoulded samples. The majority of the samples were remoulded using the Moist Tamping method with a limited number of samples prepared using the Slurry Deposition method.
5. No direct field methods to verify the in-situ stress state were used.
6. No numerical modelling was conducted.
7. Although some aspects of unsaturated soil mechanics were considered, the behaviour of the gold tailings was predominantly assessed within a saturated soil mechanics framework.
8. Unless otherwise stated, the work presented in this thesis remains the work of the candidate. Assistance from other students and laboratory technicians during the field installations and laboratory testing is acknowledged where applicable and is greatly appreciated.

1.4 METHODOLOGY

A multi-phase approach was taken to achieve the desired objectives of this study. The main stages of the study can be summarised as follows:

1. Firstly, a literature review was conducted to identify the current state of knowledge in the field of tailings engineering, with a particular focus on gold tailings, upstream constructed tailings dams, laboratory testing and field monitoring.

© University of Pretoria

2. The next stage comprised the design of the remote monitoring system. Clear requirements were identified for the system, and individual component was specifically chosen.
3. Once the system was designed, it needed to be tested. The individual sensors were tested and then the entire system was tested in a long-term laboratory trial. The intent of the trial was to verify the performance of the system in controlled laboratory conditions.
4. Once the performance of the system was verified, the next step was to deploy the system to the test site. Three test sites were chosen, and the remote monitoring stations were successfully installed. After installation, data were routinely collected remotely to investigate the true in-situ stress state in active tailings dams. This monitoring phases was supplemented with site visit to collect samples, take photographs, and inspect the monitoring system.
5. During this monitoring period, while the remote monitoring system was actively recording data, additional laboratory tests were conducted. At this stage, concerns were noted at two of the sites and it seemed that recording of reliable long-term data would not be possible. It was therefore decided that testing would only be focused on the gold tailings. The intent of these tests was to define the behavioural framework of the gold tailings, with a specific focus on the influence of density and stress state.
6. A thorough review of the laboratory and field data was then conducted, the results of which are summarised and presented in this report.

1.5 ORGANISATION OF THE REPORT

The report consists of the following chapters and appendices:

- Chapter 1 provides the background, objectives and scope of the study.
- Chapter 2 provides a literature review of key concepts of the study.
- Chapter 3 provides an overview of the laboratory element testing that was conducted on the gold tailings. The intent of the testing was to provide a behavioural framework for the soil, within which the observed field data could be presented and interpreted.
- Chapter 4 provides an overview of the requirements and the design of the remote monitoring system.
- Chapter 5 provides the results from the laboratory verification tests on the individual sensors, as well as the entire system.

© University of Pretoria

- Chapter 6 provides the results from the field monitoring at the three test sites.
- Chapter 7 contains an interpretation and discussion of the laboratory and field data.
- Chapter 8 provides the conclusions and recommendation of the study.
- A list of References is provided

© University of Pretoria

2 LITERATURE REVIEW

2.1 INTRODUCTION

A literature review was conducted to investigate the current state of knowledge for key aspects related to this study. A specific focus was placed on gold tailings and upstream constructed tailings dams. The existing behavioural framework for sandy soils is discussed and areas of uncertainty, with specific regard to gold tailings are highlighted. Finally, sensors for geotechnical monitoring are reviewed and discussed. A summary of key findings from the literature review is also provided.

2.2 TAILINGS AND TAILINGS DAMS

2.2.1 Gold tailings

The term tailings (or slimes) is used to refer to the crushed rock particle produced as a by-product of the mining process (Vick, 1983). To ensure optimum resource extraction, the ore is typically ground to silt-size particles, pumped in a slurry form, and hydraulically deposited onto large stockpiles called Tailings Storage Facilities (TSFs) or tailings dams.

Different ore types create different tailings types, so while gold mining produces gold tailings, platinum mining produces platinum tailings, etc. The tailings differ from each other in terms of physical and chemical characteristics. These differences lead to the soils having different behavioural characteristics, even under the same external conditions. It is therefore important to classify the tailings that is being considered.

The focus of this research is gold tailings sourced from an active tailings dam in the East Rand in Gauteng, South Africa. Mining at the site is from the Witwatersrand Supergroup. Historically, investigative work on gold tailings from the same group has been conducted by Vermeulen (2001), Papageorgiou (2004) and Chang (2009). Additional details regarding the scope and findings of these studies are provided in Section 2.3.4

One of the simplest ways to classify a soil is by its grading, which describes the composition of the soil in terms of particle size. It is known that the grading of a soil can affect key properties of the soil. For example, Fourie & Papageorgiou (2001) showed how for the Merriespruit gold tailings the fines content influenced the intercept of the Critical State Line (CSL), as well as the critical state friction angle.

© University of Pretoria

In a conventional tailings dam, the tailings exists in various gradings in the dam. This is typically due the deposition method employed which results in the coarser material settling near the outer wall and the finer material settling near the centre of the dam. Figure 2.1 shows results from grading samples obtained from the beach of a kimberlite (diamond) tailings dam. The grading of each sample is represented by a relative particle size ratio. It can be seen that there is a general decrease in particle size as the distance from the point of deposition increases. Although this was shown for a kimberlite tailings dam, these characteristics are generally true for other tailings dams, including gold tailings. Whenever discussing soil properties and behaviour, it is therefore always important to link this behaviour with the grading of the soil under consideration. In terms of dam safety, it is usually the coarser fraction that is of importance as it is this material that lies within the structural zone of a tailing dam. Details of the structural zone are provided in Section 2.2.3.

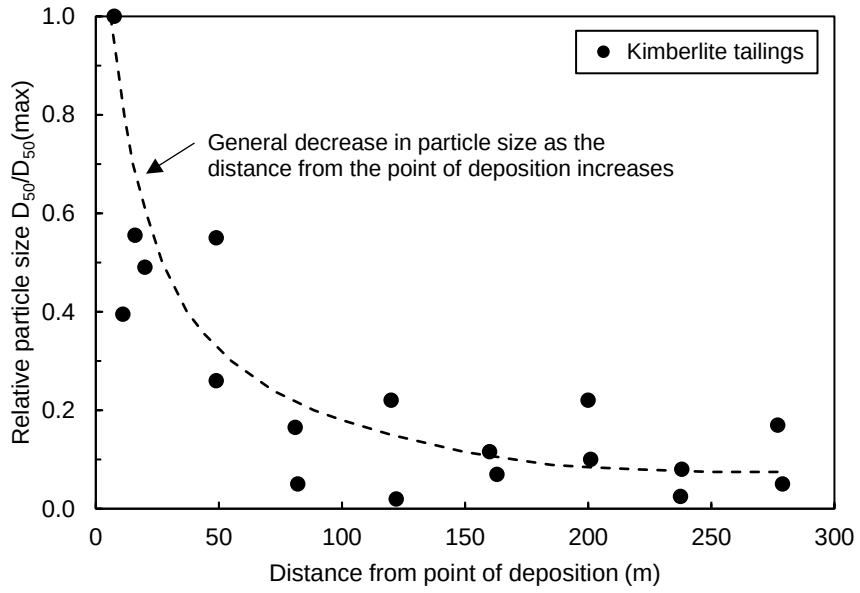


Figure 2.1: Change in particle size with distance from discharge point (after Blight, 2009)

Initially, it was suspected that aspects such as sun-drying greatly improved the geotechnical properties of the tailings, compared to samples which were not allowed to dry. However, there was limited published experimental data to support this view. Donaldson (1960) was perhaps the first researcher to investigate this aspect.

A number of oedometer tests were conducted on undisturbed gold tailings samples obtained from the East Geduld gold slimes dam in the East Rand of Gauteng. The samples, 76.2 mm in diameter, were obtained using a piston sampler, similar to that used by Collins (1954). The intent of the testing was to determine the preconsolidation pressure, i.e. the maximum pressure to which the soil had been subjected to. Knowledge of the preconsolidation pressure, together with the current

© University of Pretoria

pressure conditions (which could be estimated using the depth below the surface and the bulk density of the overlying tailings), allowed for the estimation of the degree of overconsolidation of the sample. Samples with a preconsolidation pressure greater than the current pressure were considered overconsolidated (OC), while samples with a preconsolidation pressure equal to the current stress state were considered normally consolidated (NC). It should be noted these comparisons do not consider the effect of matric suctions, which would have an influence on the equivalent effective stress state of the soil.

Figure 2.2 shows the results from these oedometer tests. For each test, the preconsolidation pressure is plotted at the depth from which the sample was taken. Also shown is the line representing the estimated stress conditions within the dam when the samples were obtained. Data points lying on this line represent samples in a NC state, while data points to the right of this line represent samples in an OC state. Data points to the left of the line are theoretically not possible and are likely a result of sampling disturbance. These samples are considered to be in a NC state.

Although there is significant scatter in the data, some key observations that can be made. Firstly, it is clear that the material above the phreatic surface appears to be in an OC state, and by some margin. However, below the phreatic surface this is less noticeable. In fact, it can be interpreted that all the samples below the phreatic surface are NC (despite the fact that these samples would have experienced a similar stress history to the samples above the phreatic surface, and are now just simply re-saturated). It was noted that similar findings, regarding the state of the tailings above and below the phreatic surface, were obtained when considering the results from the vane shear tests and the corresponding laboratory shear tests.

Based on the results by Donaldson (1960), it can be concluded that desiccation caused by sun-drying clearly results in tailings with greater stiffness and strength characteristics than can be explained for an equivalent NC sample. Since it is known that no previous load was applied to the tailings, this improvement in both stiffness and strength must be attributed to the sun drying induced desiccation. However, once the tailings re-saturates, this influence is reduced significantly and the difference between the desiccated sample, and an equivalent NC sample becomes almost negligible.

© University of Pretoria

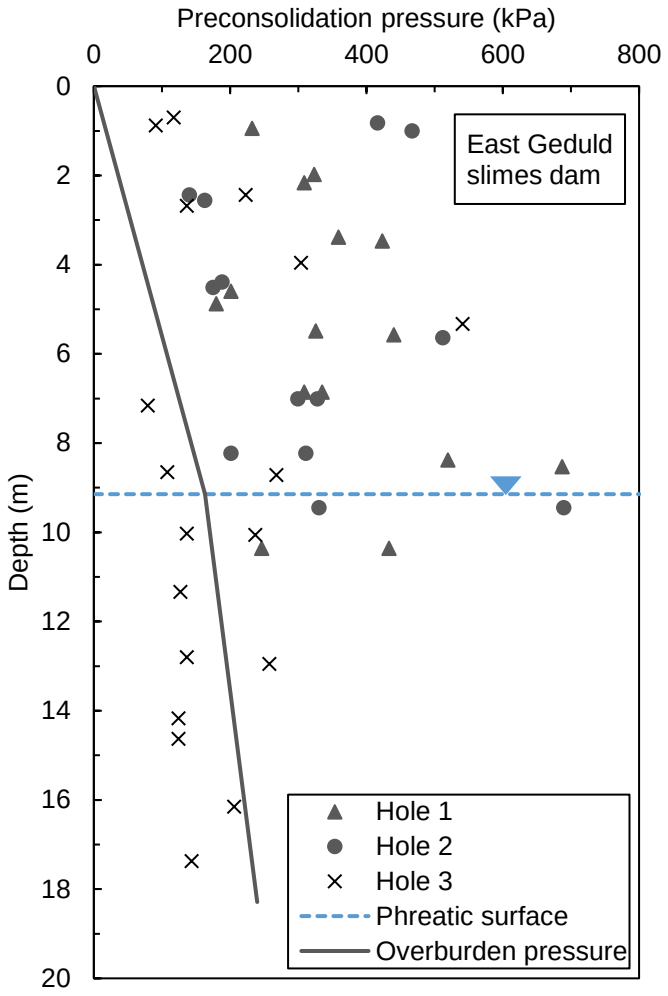


Figure 2.2: Preconsolidation pressures for the East Geduld gold slimes (after Donaldson, 1965)

A similar investigation was conducted by Blight (1988), where the compression behaviour of gold tailings was compared for a number of conditions. Figure 2.3 shows a series of compression curves of gold slimes. Unfortunately, unlike Figure 2.2, very little information is provided regarding the data used to generate this plot.

Despite this lack of information, this figure has been used by many researchers even in recent years (e.g. Reid et al., 2018) to support the statement that gold tailings exists in a heavily overconsolidated state in the field. It is believed that the purpose of this figure is to show the benefits of sun drying, specifically at future points in time once the material has been re-saturated. However, the author is of the opinion that these benefits are mostly lost once the tailings is re-wetted. This opinion is based on the experimental evidence presented in Figure 2.2, and is discussed further in Section 2.2.4 as part of the discussion on the Merriespruit failure. This opinion is also supported by Reid et al. (2018), where it was found that for gold tailings in Direct Simple Shear, the influence of desiccation on shear strength was negligible once the specimens had been

© University of Pretoria

re-saturated and consolidated to effective vertical stresses greater than 250 kPa.

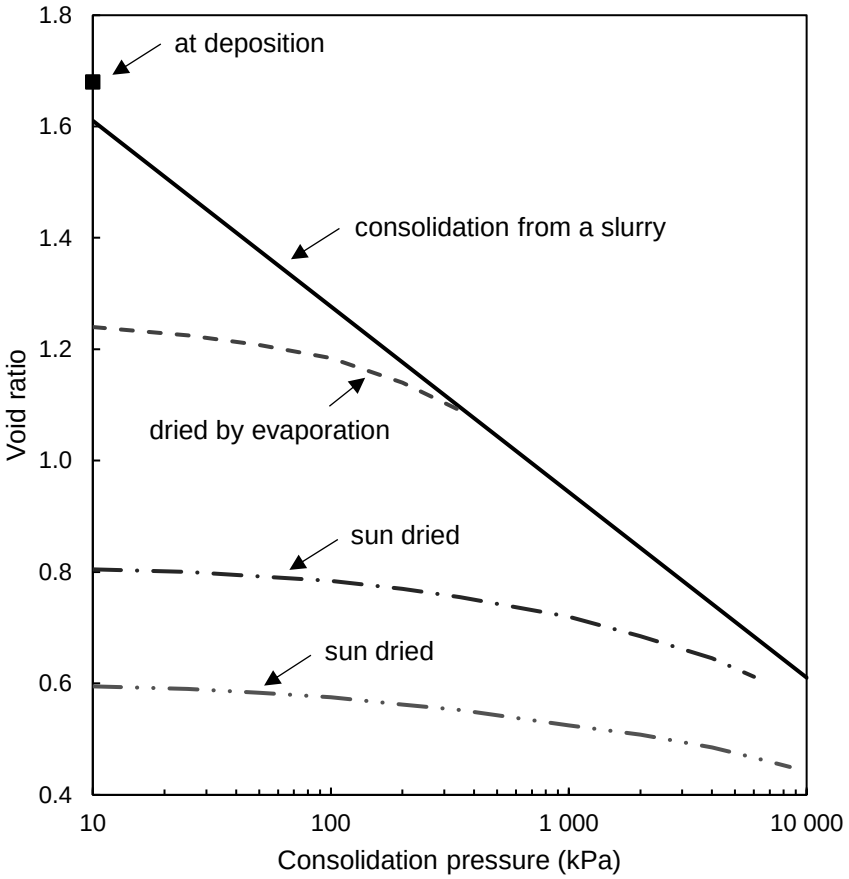


Figure 2.3: Effect of sun drying on void ratio of gold slimes (after Blight, 1988)

Although knowing the physical characteristics of the soil under consideration is important, knowledge of the mineralogical components of a soil can also be useful. One method that can be used to determine the mineralogical composition of a soil is X-Ray Diffraction (XRD). XRD is a versatile, non-destructive analytical method for the identification and quantitative determination of crystalline phases present in a sample (König et al., 2017). There are various implementation methods that can be used to analyse a material using the XRD technique.

One of these methods is the Rietveld method (Rietveld, 1969). The Rietveld method directly reports the relative weight fractions of all crystalline phases included in the model, which thus sum to 100%. However, not all solids are crystalline. Some are amorphous, like glass, and do not have any regular interior arrangement of atoms (Cullity, 1956). Solids of this nature cannot be determined directly by XRD due to their lack of crystalline structure. Therefore, while the relative values for phase concentrations would be correct, the absolute amounts would be overestimated in proportion to the amount on non-analysed phases present (e.g. Scarlett et al., 2004). To address this, alternative interpretation such as the traditional external standard approach (O'Connor &

© University of Pretoria

Raven, 1988) can be taken. In the method, the absolute weight fractions are calculated and thus also the amorphous/unidentified phase content.

Table 2.1 shows a summary of the XRD results on the gold tailings mined from the Witwatersrand Supergroup as reported by Vermeulen (2001). It can be seen that the bulk of the gold tailings comprises quartz, with some clay minerology in the form of illite and kaolinite.

Table 2.1: Summary of XRD results on gold tailings mined from the Witwatersrand Supergroup (after Vermeulen, 2001)

	Mispah (Fine)	**Mispah (Coarse)**	**Pay Dam (Fine)**	**Pay Dam (Coarse)**
Quartz	75	83	59	79
Muscovite	9	8	7	9
Pyrophyllite	4	1	17	5
Illite	6	5	11	3
Clinochlore	3	2	3	3
Kaolinite	2	1	3	1
Pyrite	-	-	1	-

2.2.2 Tailings dams

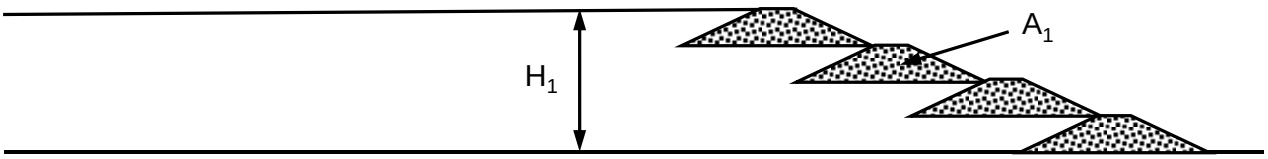
A key difference between tailings dams and conventional water dams is the method of construction, or wall raising. Unlike conventional water retaining dams where the entire embankment is constructed prior to filling, construction is an ongoing process in a tailings dam. These structures typically have long operating lives so the construction phase can last several decades. These extended construction periods have some drawbacks, including potential changes in mineral extraction technology which can result in different mechanical or chemical properties of the tailings. This is especially important for upstream constructed facilities where the tailings itself is used for the outer wall raising.

In general, there are three types of construction methods for tailings dams, and these are shown in Figure 2.4. Upstream construction, shown in Figure 2.4(a), is the oldest and most common method used in South Africa (e.g. Wates & Lyell, 2018). For this construction method, the previously-deposited tailings is used to as part of the wall raising material. Although it can be the most cost-effective option, it is the most susceptible to liquefaction and post-earthquake deformations (e.g. Vick, 1983).

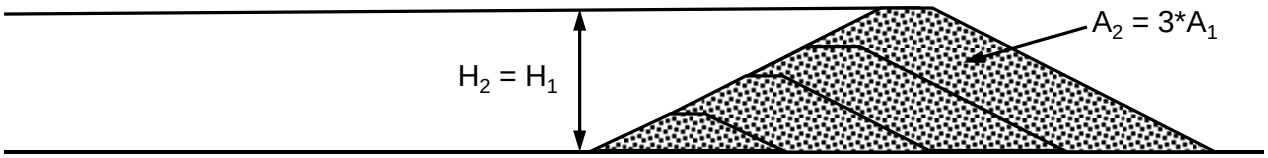
© University of Pretoria

Downstream construction, shown in Figure 2.4(b), is a more stable option compared to upstream construction as the structural zone contains competent material. However, significantly more fill material is required to construct the outer wall. This material can either be imported, or selected fractions of the tailings can be used (for example, the coarse fraction of cyclone tailings). For the same dam height, H_1, three times as much volume of embankment fill material can be required when compared to the upstream method as shown in Figure 2.4(b). Downstream methods also require careful planning as the footprint of the dam increases with each successive lift.

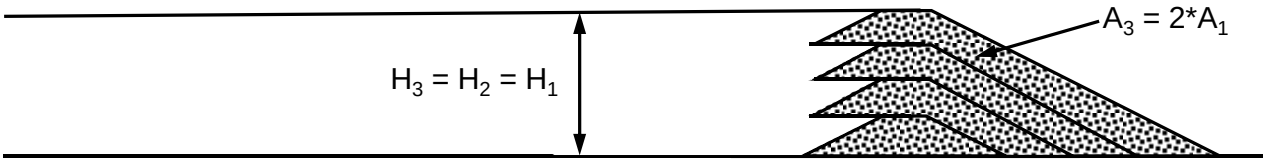
The centreline method, shown in Figure 2.4(c), shares advantages with both the upstream and downstream methods. For example, less embankment fill material is required than the downstream method and there is an improvement in the seismic resistance when compared to the upstream method. The type of construction method is usually based on a range of site-specific factors including tailings type, deposition rate, seismic activity in the region, local communities, local legislation, etc.



(a) Upstream



(b) Downstream



(c) Centreline

Figure 2.4: Typical wall-raising methods for tailings dams: (a) upstream, (b) downstream, (c) centreline (after Vick, 1983)

The focus of this research is on upstream tailings dams. This was chosen as these dams are the most common type in South Africa, and are also considered to be of a higher risk when compared

© University of Pretoria

to downstream or centreline constructed dams (e.g. Franks et al., 2021).

2.2.3 Typical features of a modern tailings dam

Modern tailings dams have several key features to ensure adequate slope stability and operational efficiency. These features are discussed in this section.

2.2.3.1 Structural zone

The structural zone refers to the outer portion of the tailings dam embankment that controls the structural stability of the tailings dam. For upstream constructed tailings dams, this zone is constructed using the tailings itself. For modified centreline and downstream constructed dams, this material is typically imported.

A key advantage of the centreline and downstream construction methodologies is that the type of imported material, as well as the placement method, can be specified. This makes it easier to control the density of the material which can greatly improve the dams resistance to liquefaction. Naturally, this typically comes with an increased cost when compared to upstream constructed dams.

Additionally, new technologies are leading to new deposition techniques such as Hydraulic Dry Stacking (HDS). HDS is a co-disposal technique that is designed to improve the conditions of material placed in the structural zone in upstream constructed facilities. It is currently being trialled, and the preliminary results seem promising (e.g. Newman et al., 2022; Newman et al., 2023). Alternatively, the use of mechanical cyclones, and the subsequent compaction of the tailings has been attempted in some cases (e.g. de Mello Martins et al., 2022). However, these technologies and approaches remain in trial phases, and it is unclear whether these methods will be able to scale to meet the production volumes required by modern mines.

2.2.3.2 Internal drainage system

A key aspect of any modern tailings dam is the internal drainage system. The intent of this system is to ensure that the pore pressures within the dam, specifically within the structural zone, are kept as low as possible. This helps for three main reasons. Firstly any reduction in pore pressure will increase the effective stress in the soil which generally improves the stability of the dam. Secondly, an effective internal drainage system assists with consolidation. As tailings dams are continuously being raised, the previously deposited tailings are constantly being loaded. Adequate consolidation

© University of Pretoria

of the underlying tailings typically improves both the stiffness and strength of the tailings, both of which contribute to stability.

Thirdly, a key requirement for static liquefaction is saturation of the soil. However, it has been shown that full saturation is not necessary for static liquefaction in some cases (e.g. Lü et al., 2018; Świdziński & Smyczyński, 2022). Regardless, a well-designed and operated internal drainage system can assist in ensuring that key sections of the structural zone remain free draining and essentially unsaturated, thereby significantly improving the resistance to liquefaction. A well-designed, and effective internal drainage system is therefore crucial for a modern tailings dam.

2.2.3.3 Surface water drainage system

Another key feature of modern tailings dams is a surface water drainage system. Traditionally, these have been gravity-based systems such as penstocks. However, in recent years, there has been a move towards pumped systems. This change is primarily driven by the North American view that traditional penstock gravity decant systems are fragile systems which have been shown to be problematic (e.g. FEMA, 2005).

However, in a country like South Africa where energy security is a challenge, it remains to be seen whether the benefits of a potentially more robust system outweigh the risks of interrupted power supply. There are also additional operational costs associated with pumping that are not required for gravity decant systems. Regardless, both pumped and traditional penstock decant systems have been, and continue to be used effectively in South Africa.

The purpose of the surface water decanting system is to limit the volume of water stored on the tailings dam. This is done for a number of reasons but foremost is related to dam safety, specifically to ensure that there is sufficient storage capacity to safely contain large storm events. There is strong evidence that unnecessarily storing excess water on a tailings dam increases the likelihood of failure as well as the effect of any potential failure (e.g. Smith & Connell, 1979; Rico et al., 2008). This is generally best managed with a robust freeboard plan and a dedicated return water dam. In water scarce countries such as South Africa, an optimum design of these features is critical.

2.2.3.4 Monitoring system

Even with the best design and construction, monitoring is key to ensure continued compliance to the design, as well as to ensure that key assumptions made during the design phase remain appropriate. Traditional monitoring systems include those that measure pore pressures, drainage system flowrates (both from the penstock and basal drainage systems), pond water levels and

© University of Pretoria

daily rainfall. More manual measurements include freeboard measurements, deposition tonnages and deposition densities. All of these measurements provide valuable information to the design engineers and operators. Optimum monitoring systems are essential in providing a continuous view on the health of a tailings dam. A more detailed discussion on several of the sensors used for these measurements is provided in Section 2.6.

Currently, the biggest area of concern regarding tailings dam safety is related to undrained shearing. This is partly due to the fact that these failures occur rapidly, typically with no warning and with no time for slope stabilization or even evacuation measures. Unfortunately, as far as the author is aware, there are currently no monitoring systems capable of detecting precursors to undrained shearing failures.

2.2.4 Historical Water and Tailings Dam Failures

Tailings dams are some of the largest man-made structures in the world and have the potential to cause significant social and environmental damage if not appropriately designed, constructed, and operated. In this section, several key tailings dam failures (and a water dam failure) are discussed. Figure 2.5 shows the locations of the case histories that were investigated.

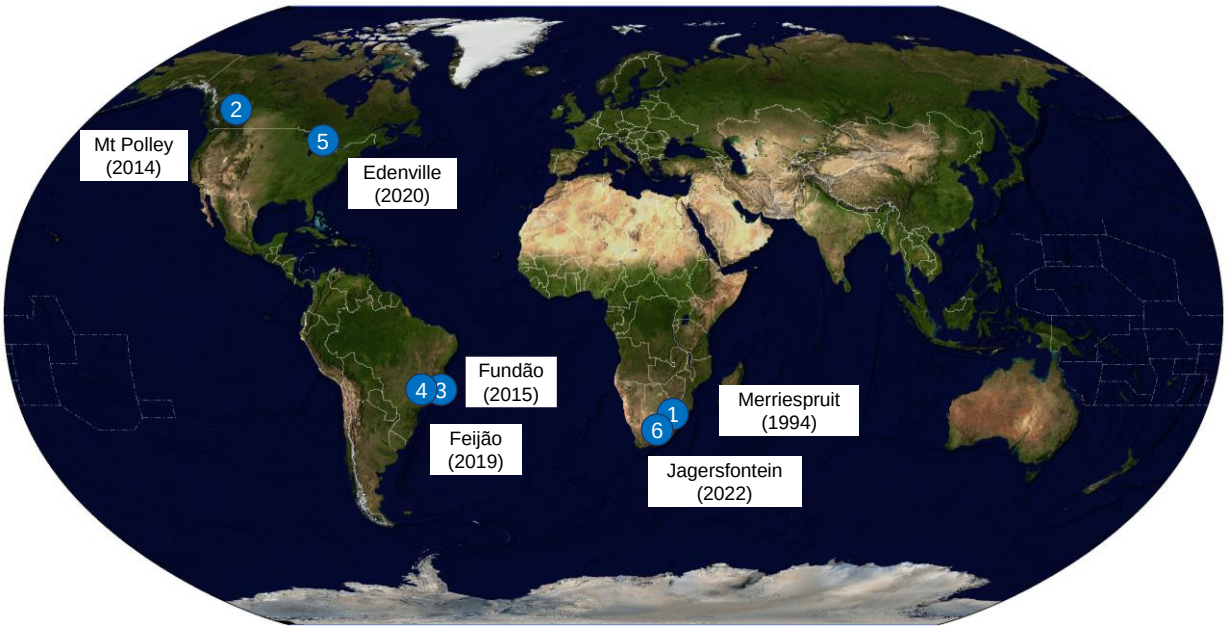


Figure 2.5: Locations of the tailings and water dam case histories investigated

2.2.4.1 Merriespruit tailings dam, South Africa

The Harmony Gold Mine Complex was located in the vicinity of the Town of Virginia in the Free

© University of Pretoria

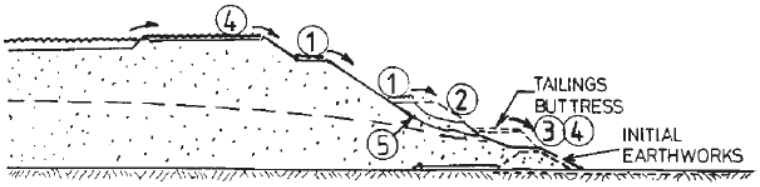
State Province of South Africa. On the evening of 22 February 1994, after a moderate rainfall event, the Merriespruit Tailings Dam 4 failed resulting in the uncontrolled release of 600 000 m^3 of tailings and the unfortunate death of 17 people.

Construction of the Merriespruit Tailings Dam 4 started in 1987. The dam was designed as an upstream constructed facility and was meant to be operated with two compartments. At the time of failure, the dam was 31 m high which meant the dam had been constructed at an average Rate of Rise (RoR) of 1.94 m/year. The dam was meant to be dormant. However, investigations conducted after the failure revealed that deposition was occurring on the dam at the time of the failure.

Figure 2.6 shows a sketch of the series of events that led to the failure at Merriespruit as postulated by Wagener (1997). After the rainfall event on the afternoon of 22 February 1994, there was an overtopping event at the Northern wall of Dam 4A. This was caused as a direct result of the operating pool being located against the outer wall; the loss of the division berm between compartments 4A and 4B which resulted in all the rain falling on both compartments ending up on the Northern wall, as well as the poor freeboard (approximately 300 mm) that was in place prior to the rainfall event.

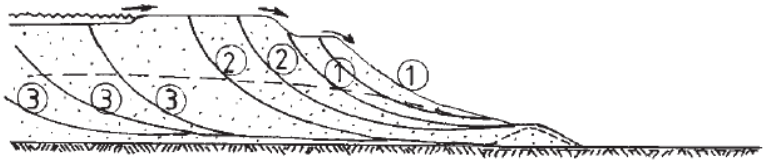
This overtopping event eroded the loose tailings that was placed on the lower berms to fill in the gulleys created by earlier slips. The removal of this tailings led to more small slip failures occurring. This led to a series of slip failures retrogressively moving up the slope, resulting in the final slip failure which enabled the release of approximately 600 000 m^3 of tailings from the dam. The town of Merriespruit was less than 400 m from the toe of Dam 4 and since the failure occurred in the evening, there was little time for warning and evacuations.

© University of Pretoria



1. Berms overtop after thunderstorm
2. Loose tailings infill to earlier failures on lower slope erodes
3. Tailings buttress starts to fail
4. Pool commences overtopping and erodes slopes and buttress
5. Unstable lower slope fails and failed material is washed away

a) CRITICAL SECTION OF NORTH WALL DURING EARLY STAGES OF FAILURE



1. Lower slopes fail and are washed away
2. Domino effect of local slope failures which are washed or flow away
3. Major slope failures with massive flow of liquid tailings

b) CRITICAL SECTION OF NORTH WALL DURING FAILURE

Figure 2.6: Sketch showing the postulated series of events that led to failure at Merriespruit (after Wagener, 1997)

Although there was the terrible consequence of the loss of 17 lives, this incident did prompt a thorough review of the safety of tailings dams in South Africa. In fact, the failure at Merriespruit led directly to the development of the South African National Standard on Mine Residue (SANS 10286) which is still in place in 2024. This document specifies minimum requirements for the design, construction, operation, and closure of tailings dams in South Africa.

A key learning from this incident, specifically with regard to the numerous post-failure analyses that were conducted, was that it forced tailings practitioners in South Africa to critically evaluate the long-held view that due to the desiccation process, mine tailings are generally in a heavily overconsolidated state and will have a dilative tendency upon undrained shear. Therefore failure mechanisms such as static liquefaction are not applicable. This view was supported by earlier research in South Africa (e.g. Donaldson, 1965; Blight, 1988).

However, as discussed in Section 2.2.1, closer inspection of these results reveals that there is

© University of Pretoria

much uncertainty regarding the sampling and testing procedure conducted. This is specifically true to the data presented by Blight (1988). In addition, although this improvement in stiffness and strength may be true for the material at the surface, it is likely not true for the material at greater depths, particularly below the phreatic surface. Perhaps the best evidence that the tailings at Merriespruit was in a loose state is from the field testing that was conducted after the failure. The next two paragraphs deal with results from a sampling study, as well as a Cone Penetration Test (CPT) probing campaign. In the author's opinion, these results are clearly not indicative of soils in a heavily overconsolidated state.

Figure 2.7 shows the results from the field sampling campaign conducted by Fourie et al. (2001). Notice the number of occurrences for samples with void ratios far in excess of 1.0. These are very loose samples and, as will be shown in Section 3.5.6, gold tailings specimens at these loose densities generally exhibit collapse behaviour in undrained shear.

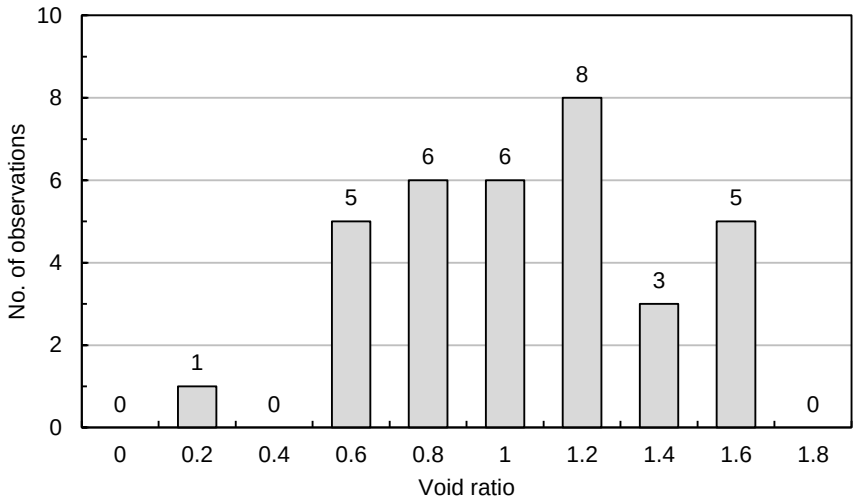


Figure 2.7: Results from the field sampling campaign at Merriespruit (after Fourie et al., 2001)

Figure 2.8 shows a result from a CPT probe conducted near the decant facility at the Merriespruit Dam 4. Note the consistently low tip resistances (approximately 0.5 MPa) and high dynamic pore pressures. This is indicative of a loose material and not of a soil in a heavily overconsolidated state.

© University of Pretoria

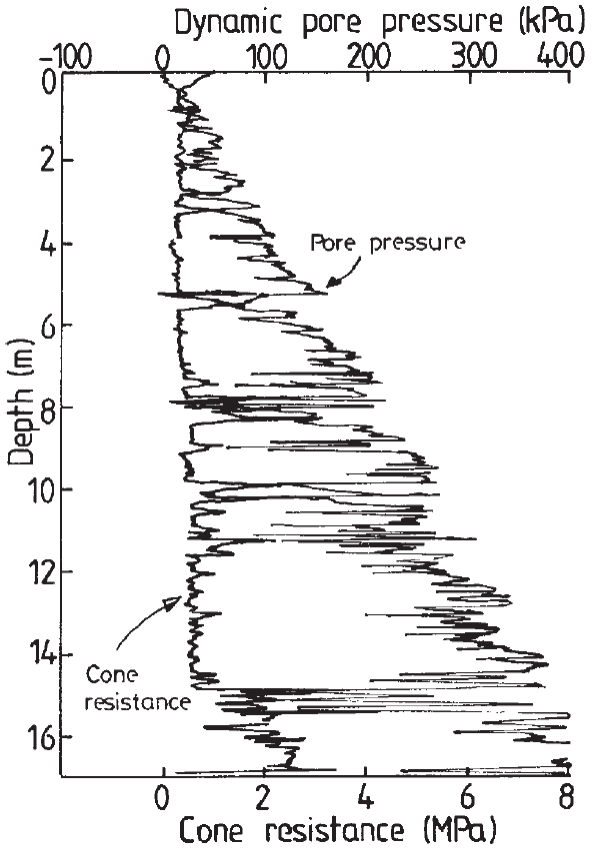


Figure 2.8: Results from a piezocone probe conducted near the decant facility on Merriespruit (Fourie et al., 2001)

2.2.4.2 Mount Polley tailings dam, Canada

The Mount Polley Mine is a gold and copper mine located 56 km North-East of the Town of Williams Lake in British Columbia, Canada. On 4 August 2014, the Mount Polley Tailings dam failed and resulted in the uncontrolled discharge of millions of cubic meters of tailings into an environmentally sensitive area. Thankfully there were no reported injuries nor deaths, however, there was significant environmental damage that was caused. As with the previous case studies, much of the information presented here was obtained from the independent investigation report (Morgenstern et al. 2015).

Construction of the dam started in 1996 and, at the time of failure, the dam was 40 m high. The dam was raised using the modified-centreline construction method with a rockwall downstream slope. Traditionally, these types of facilities have been considered robust and highly unlikely to fail. Although this is true for failure surfaces through the waste rock, this opinion neglects to consider slip surfaces through the foundation soils. Incredibly, at the time of failure, it was reported that there were 10 Mm^3 of water stored on the dam. This certainly negatively influenced the extent of the impact of the failure.

© University of Pretoria

It was concluded that the key issue regarding the failure at Mount Polley was a localised geological unit, referred to at the Upper Glaciolacustrine Unit (Upper GLU). Based on the results from the post-failure site investigation, this unit appeared to be less than 150 m wide and only 2.5 m thick at its thickest. Further, this unit was approximately 8 m below Natural Ground Level (NGL). Figure 2.9 shows a cross section through the embankment at the failure sections. The Upper GLU Unit is shown in turquoise.

The geological history of site meant that the Upper GLU unit was in a heavily overconsolidated state prior to the construction of the tailings dam. However, once the applied load to the Upper GLU (as a result of the rock wall and tailings) reached the historical maximum, the Upper GLU became normally consolidated and exhibited a significant reduction in stiffness. The discontinuous nature of the Upper GLU (i.e. the fact that the GLU only existed below the rock outer wall and not the retained tailings) allowed an unfavourable slip surface geometry to develop through the outer wall. The low shear strength of the Upper GLU, combined with its reduced stiffness (due to becoming normally consolidated), and the unfavourable geometry were ultimately attributed to have led to the failure.

During the failure investigation it was found that the design did not consider the effect of this Upper GLU layer. In particular, the following was stated regarding the geotechnical site investigations that were conducted prior to the failure (i.e. the investigations upon with the design and subsequent safety evaluations of the tailings dam were conducted):

*"The **type and extent** of the **pre-failure site investigations** were **not sufficient to detect** this stratum [n]or **identify its critical nature**"* (Morgenstern et al., 2015)

It should be noted that the initial design called for an outer slope of 1(V):2(H), however, due to operational constraints, the slope was built to a temporary, interim slope of 1(V):1.4(H). The intent was that once the quantities of waste rock became available again, the design slopes would be created. An analysis conducted by Morgenstern et al. (2015) showed that, had the outer wall been completed to the design slopes, a FoS of 1.27 would have been calculated, even considering the presences of the Upper GLU layer. Unfortunately, the failure occurred before this could occur.

© University of Pretoria

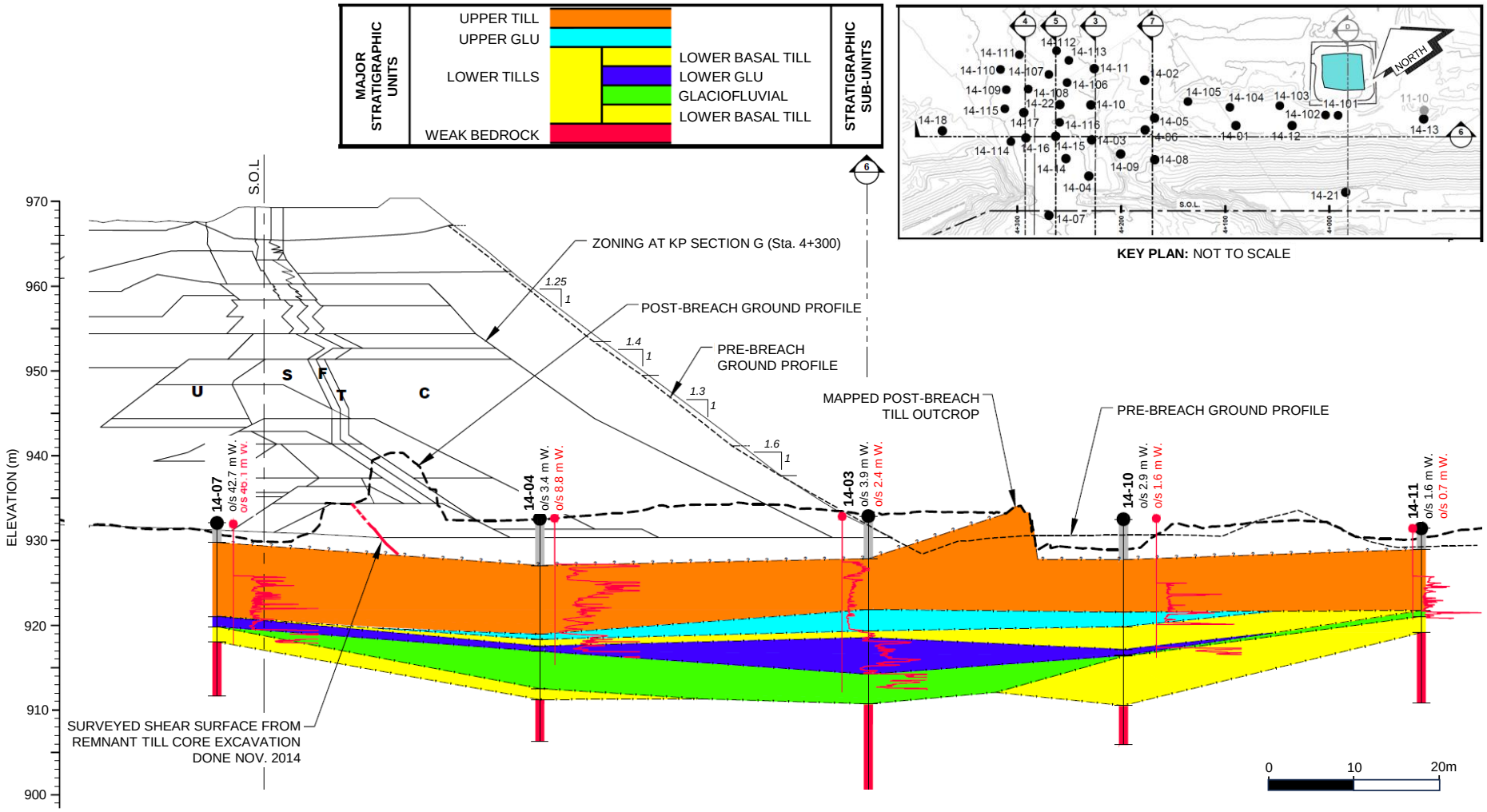


Figure 2.9: Cross section through the failure section at Mount Polley (after Morgenstern et al., 2015)

© University of Pretoria

2.2.4.3 Fundão tailings dam, Brazil

The Germano Iron Ore Mining and Processing Complex is located 5 km North-West of the Town of Bento-Rodrigues in Minas Gerais, Brazil. Failure of the Fundão tailings dam occurred on 5 November 2015, resulting in nine deaths and significant environmental damage (Morgenstern et al., 2016). The tailings dam was commissioned in 2008, and at the time of the failure, was 110 m high.

Two distinct waste streams are produced by the processing plant: sands and slimes. The sands are coarse-grained and nonplastic, while the slimes are fine-grained and clayey in nature. These materials are produced in specific quantities and a key feature of the design was to ensure physical separation of the sand and slimes. As part of the design, the slimes would be stored behind Dike 2 and the sands behind Dike 1 (the main embankment).

There were three key pillars to the design and operation of the Fundão tailings dam and these are shown in Figure 2.11(a). The first key design aspect was a 200 m wide beach zone at the outer wall with the finer slimes impounded behind the sands. The maintenance of the 200 m wide beach required a certain volume of sands to be produced which was linked to a 70/30 split by volume between the sands and the slimes produced by the processing plants.

The dam was located in a seismically active region, and it was known that sandy soils placed in a loose state are susceptible to cyclic liquefaction and associated sudden strength loss. However, it has been shown on numerous occasions that the resistance to cyclic liquefaction greatly increases as the degree of saturation of the sands decreases (e.g. Yoshimi et al., 1989; Mele et al., 2019). The second key pillar of the design was therefore the inclusion of a robust internal drainage system which would ensure the sands remained dry (and therefore resistant to cyclic liquefaction). To monitor the effectiveness of the blanket drainage system, a comprehensive piezometer network was designed and installed.

The third and final key design aspect was a surface water decant system. The purpose of this system was to remove supernatant water from the surface of the tailings dam. This would provide the processing plant with supplementary water for ore processing but more importantly reduce the volume of standing water on the tailings dam, thereby limiting recharge of the flow regime in the sands. The system consisted of two high-capacity drainage galleries: the main drainage gallery and the secondary drainage gallery which were intended to serve the material retained behind Dikes 1 and 2, respectively.

© University of Pretoria

Unfortunately, during construction and operation, there were significant deviations from the design. For example, a significant internal erosion event was noted at the base of Dike 1 in 2009. A formal investigation revealed serious construction flaws in the base drains and filters, including a portion of a drain outlet that was never completed. It was deemed not feasible to repair the basal drainage system and all the drains were sealed to prevent future erosion issues. To replace the internal drainage system, a blanket drain was planned to be installed on top of the existing sands.

In 2010, there was a change in the plant which resulted in a change in the 70/30 split between the sand and the slimes. This meant that an intermediate Dike (Dike 1A) needed to be constructed to temporarily store the additional slimes while the sand structural zone “caught up” in terms of elevation. In 2010, a sinkhole appeared above the main drainage gallery. Subsequent investigations found serious construction defects in the drainage gallery. It was decided that water from Dike 2 would be re-routed to Dike 1 via an overflow channel so that surface water could be abstracted using the secondary drainage gallery. During this period, slimes encroached into the sands zone and in some cases, came within 60 m of the outer wall.

Similar structural defects were found in the secondary drainage gallery. Subsequent investigations led to the recommendation that the secondary drainage gallery also be sealed. However, since the sealing operation would take time, and the dam would continue to be raised in this time, concerns were raised regarding the structural integrity of the gallery if the dam were to be raised as per the original design. It was therefore decided that a temporary setback would be created. This setback (shown in Figure 2.10) would maintain plant production, limit additional load being placed on the compromised drainage gallery, and maintain access to the drainage gallery for the sealing works.

© University of Pretoria



Figure 2.10: Aerial photograph showing the setback at the Left Abutment (after Morgenstern et al., 2016)

Unfortunately, the issues at the site continued. In 2013, serious seepage and structural cracks were noted at the toe of the setback. A stabilising buttress was designed, and construction started shortly thereafter. Incredibly, while battling to mitigate the seepage and stability concerns, a third processing plant was commissioned 2014. At the same time, the blanket drain that was installed as a replacement to the basal drainage system reached its drainage capacity. This severely limited the ability to dewater the sands in the structural zone.

In the months preceding the failure, the dam was raised at a rapid pace, with an average annual RoR of 18 m in 2013, 13 m in 2014, and 13 m in the first 10 months of 2015. In October 2015, the month before the failure, the dam was raised 2.9 m. This equates to an annualised RoR of 35 m/year.

As shown in Figure 2.11(b), at the time of failure, not one of the three key pillars of the design were in place at the Left Abutment. The failure of the main drainage gallery and the creation of the overflow channel led to slimes intruding into the sands zone on several occasions. Similarly, the sealing of the basal drainage system, combined with the excess surface water, led to the sands zone becoming saturated. Although the setback at the Left Abutment (which was done to facilitate the safe closure of the compromised secondary drainage gallery) resulted in a flatter overall slope, it resulted in an unfavourable geometry for the localised setback slope itself, which was constructed over the intrusive slimes layers.

The independent panel concluded that failure of the Fundão tailings dam was due to a “lateral

© University of Pretoria

extrusion" of the slimes layer and subsequent static liquefaction of the overlying, loose, saturated sands. Figure 2.11(c) shows key aspects of the proposed failure mechanism. The high RoR of the setback resulted in the rapid loading of the slimes. The geometry of the setback resulted in the sands downstream of the intrusive slimes having less vertical confining stress and this allowed for the lateral extrusion of the rapidly loaded slimes.

The loose, non-cohesive sands above the slimes (and below the setback) moved in conjunction with the slimes. This movement of the sands resulted in a reduction in lateral confining stress to the sands (downstream of the setback). Since the sands were in a loose and saturated state, this reduction in lateral confining stress resulted in collapse of the material just downstream of the setback. This collapse initiated the flow liquefaction failure.

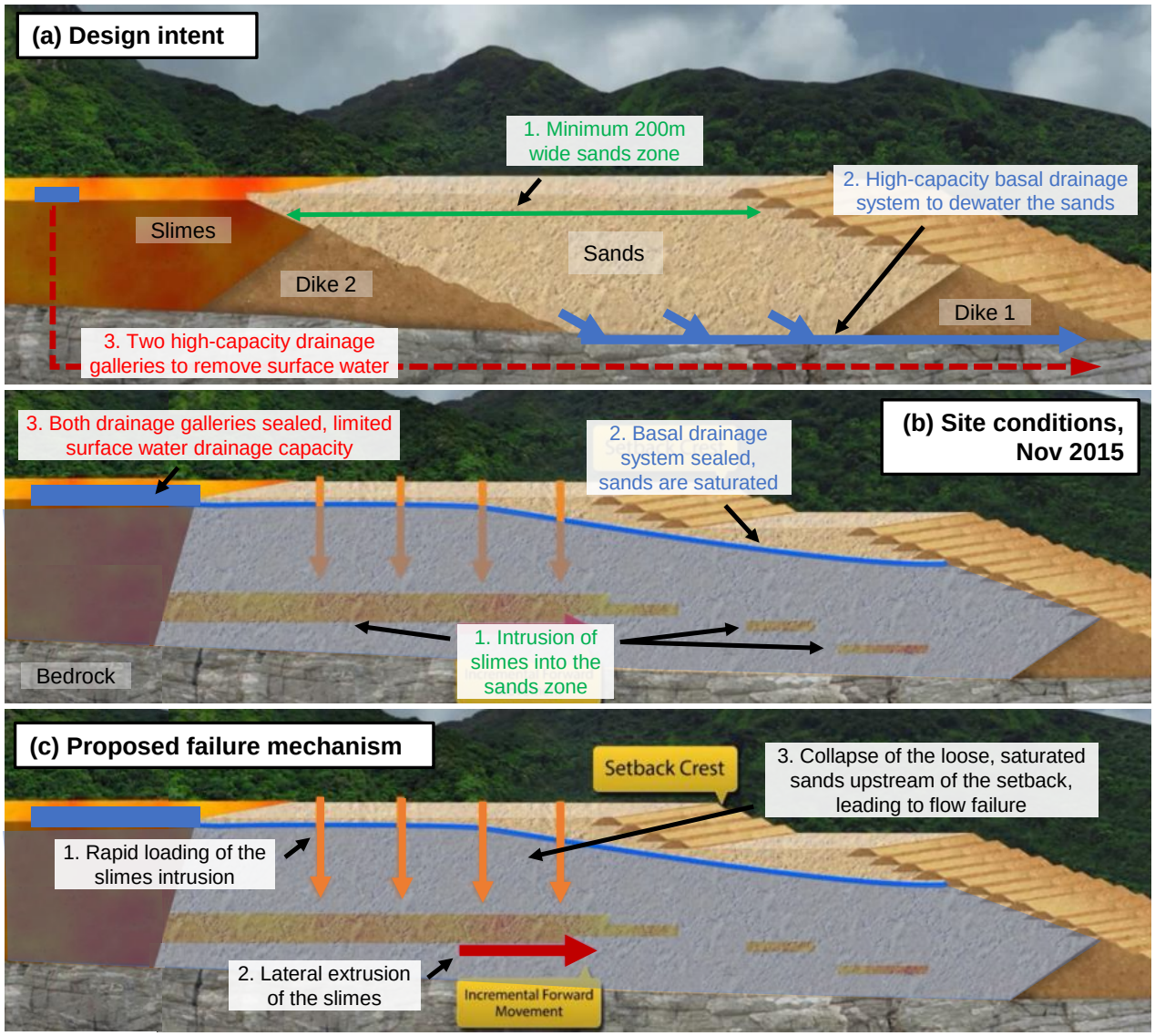


Figure 2.11: Cross section of the Fundão Left Abutment showing: (a) the design intent, (b) the site conditions in November 2015, and (c) the proposed failure mechanism (after Morgenstern et al., 2016)

© University of Pretoria

A total of 32 Mm^3 of tailings material was released as a result of the failure and the downstream town of Bento Rodrigues was severely impacted. Within a few days, the impact of the failure was noted at the mouth of the Doce River, more than 670 km from the Fundão tailings dam. This failure had significant environmental consequences and recovery and rehabilitation is still ongoing to this day.

This case history highlights how initial construction defects can have significant long-term consequences, as well as the negative influence that intense production pressure that is a constant feature in many large mines can have on a tailings dam.

2.2.4.4 Feijão tailings dam, Brazil

The Córrego de Feijão Iron Ore Mining and Processing Complex is located 9 km North-East of the Town of Brumadinho in Minas Gerais, Brazil. Failure of the Feijão Tailings Dam B1 occurred on 25 January 2019 when 9.7 Mm^3 of tailings was released. The ensuing mudflow resulted in catastrophic environmental damage and at least 250 deaths. An independent expert panel was established to investigate the cause of the failure (Robertson et al., 2019).

A unique aspect of this case study is that the moment of failure was captured on video (Chadwick, 2019). This case is also interesting as it was a failure of a dormant dam, with the last deposition occurring in 2016, almost three years prior to the failure. The dam was operated with no decant facility and satellite images taken over the years show several instances of the pond being located against the outer wall. This configuration is known to result in the tailings settling in a very loose state (e.g. Reid, 2021). Interestingly, a few months after the release of the independent report, a second investigation was commissioned (CIMNE, 2021). Although the same field data were analysed as part of the second investigation, additional samples were obtained from site and new laboratory testing was conducted.

As part of their respective investigations, the panels worked through an immense amount of laboratory and field data. For example, in the case of the Robertson et al. (2019) investigation, the panel reviewed data from over 110 piezometers and 210 laboratory tests. This is in addition to the 37 000 data points from the CPT probing that was conducted. For the CIMNE (2021) investigation, the 37 000 CPT data points were re-analysed and an additional 70 advanced laboratory tests were conducted. A key aspect of both investigations was the influence of the drilling activities associate with borehole B1-SM-13, which occurred on the day of the failure.

© University of Pretoria

Figure 2.12 shows the key cross sections used by both investigations to determine the cause of the failure of the Feijão tailings dam, with the cross section employed by the Robertson et al. (2019) investigation shown in Figure 2.12(a) and the cross section used by the CIMNE (2021) investigation in Figure 2.12(b). It is clear that an incredible level of detail was deemed necessary in both investigations.

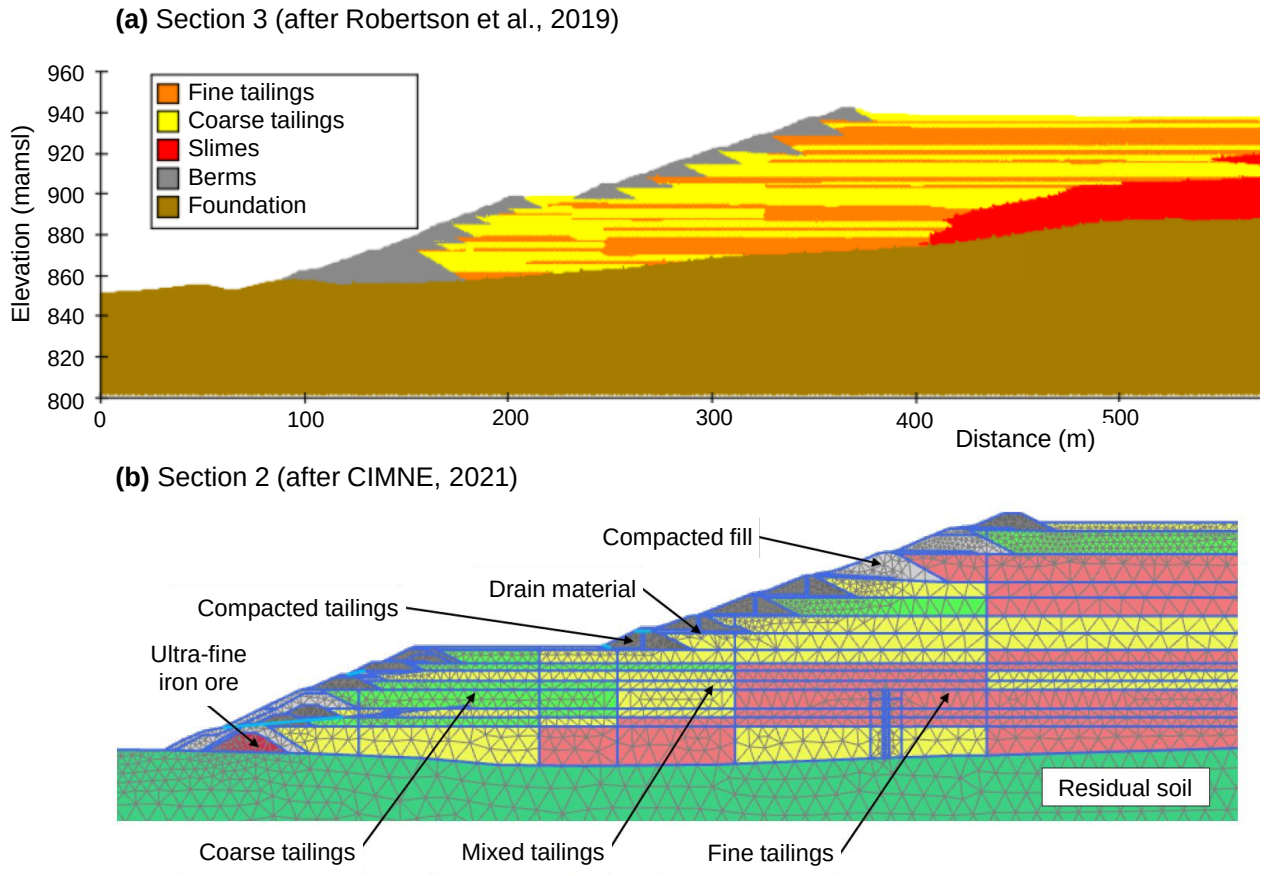


Figure 2.12: Cross section through the Feijão tailings dam: (a) after Robertson et al. (2019), and (b) after CIMNE (2021)

Conflicting and contradicting findings were published for the two investigations. For the Robertson et al. (2019) investigation, it was proposed that a combination of loss of suction due to increased rainfall, combined with internal creep which was sufficient in magnitude to break the bonded tailings, led to failure. The triggering of failure due to liquefaction induced by the drilling of borehole B1-SM-13 was investigated and summarily dismissed as not being a plausible trigger mechanism.

Conversely, for the CIMNE (2021) investigation, it was proposed the drilling activities associated with borehole B1-SM-13 were in fact the trigger of the failure. It was found that the localised increase in pore pressure was sufficient to induce a strain-softening response in the surrounding soil which ultimately resulted in the collapse of the slope. No evidence of bonding of the tailings

© University of Pretoria

was found and rather than a reduction in suction (or increase in saturation), it was found that there was a general decrease in saturation of the slope in the months preceding the failure. In addition, even with extensive numerical modelling, it was found that failure could not have been initiated as a result of internal creep.

In summary, both investigations proposed different, and conflicting reports on the cause of the failure of the Feijão tailings dam. Both investigations rigorously considered the causes propose by the other investigation and proposed with reasonable explanations why they couldn't be the case. It is incredible that even with video footage of the failure, and with the leading minds in the field with access to resources such as advanced testing and numerical modelling, there is no consensus regarding the true cause of the failure.

What is even more intriguing is that the proposed failure mechanisms are conflicting. For example, Robertson et al. (2019) showed SEM images and CPT interpretations indicating bonding (see Figure 2.13(a) for the SEM images). However, independent SEM imaging and re-analysis of the CPT data by (CIMNE, 2021) showed no evidence of bonding (see Figure 2.13(b) for the results from the re-analysis of the CPT data). Similarly, the CIMNE (2021) investigation showed a general decrease in saturation, while the Robertson et al. (2019) investigation showed an increase in saturation in the months preceding failure.

© University of Pretoria

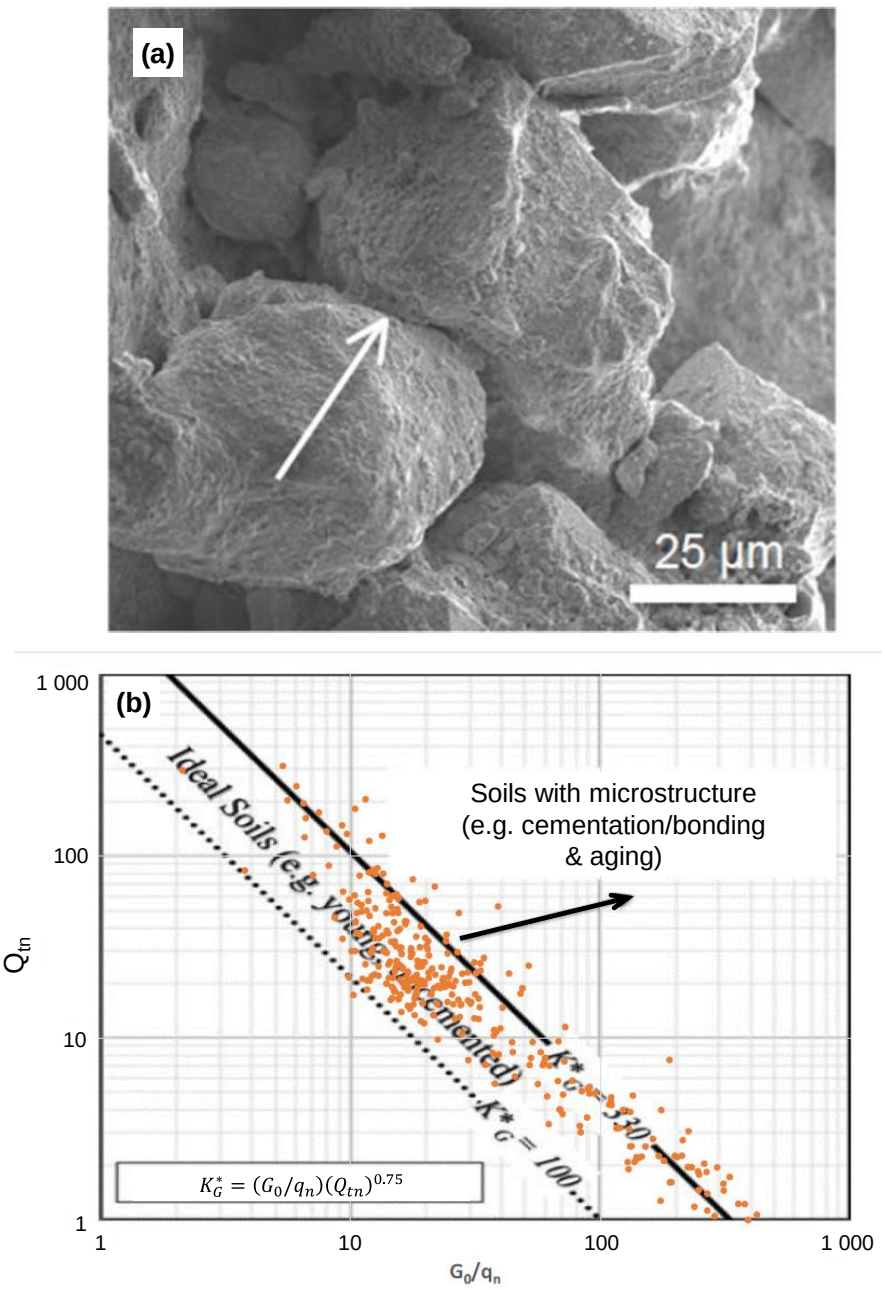


Figure 2.13: Supporting evidence for the Feijão tailings showing: (a) bonding, after Robertson et al. (2019); and (b) no bonding, after CIMNE (2021)

2.2.4.5 Edenville water dam

The Edenville Dam is the only water retaining dam that is discussed in this section. This is an important case history as it was perhaps the first modern failure of a water dam where failure was attributed to static liquefaction. It is very likely that this failure will influence both water dam and tailings dam legislation in the near future. The details contained in this section were predominantly obtained from the independent investigation report (France et al., 2022).

© University of Pretoria

Edenville Dam is one of four dams located in series along the Tittabawasse River in Central Michigan. The purpose of these dams was to generate electrical power and each dam had an associated hydroelectric facility. At the time of the failure, the Edenville Dam was approximately 10.5 m high and was regulated by the Michigan Department of Environment, Great Lakes, and Energy (EGLE) as the Federal Energy Regulatory Commission (FERC) had revoked the Edenville dam licence in 2018. One of the key reasons for the revoking of the FERC licence was due to the inability of the spillway to safely pass the Probable Maximum Flood (PMF). The revocation of the FERC licence meant that the only facilities available to control the reservoir level at the Edenville Dam were the spillway gates. Without an operating licence, water could not be released through the powerhouse, and the lower-level sluiceways had been inoperable for decades.

After a moderate rainfall event, the Edenville Dam failed on 19 May 2020, and resulted in the uncontrolled release of a significant volume of water. The 24-hour rainfall event itself was estimated to be between a 25- and 50-year recurrence interval event. However, as a result of an unusual combination of rainfall characteristics and watershed conditions, the resulting flood event was representative of a 100-to-200-year event. The failure of the Edenville Dam led directly to the overtopping failure of the downstream Sanford Dam some three hours later.

Like the Feijão tailings dam failure, the Edenville Dam failure was caught on video (MLive, 2020). With the limited documentation available on the history of the dam, as well as limited monitoring information for the specific section that failed in the days leading up to the failure, the video footage played a key role in the investigation that followed the failure. It was noted that without the video footage, the evidence for static liquefaction would have been less conclusive and there is a chance that an alternative failure mode could have been inferred.

Thankfully, no injuries nor deaths were reported as approximately 11 000 residents in the downstream vicinity were evacuated as part of the emergency response prior to the failure. This was a particularly sensitive issue in the United States as a similar incident had occurred a few years before when more than 180 000 residents were ordered to evacuate after stability concerns were noted at the Oroville Dam (France et al., 2018). Despite the evacuations, the failure of the Edenville and Sanford dams was reported to have affected 3 000 homes and caused damages in the order of $190 million for residents, in addition to $55 million in damage to public infrastructure (France et al., 2022).

Construction of the Edenville Dam started in 1923. The dam comprised a left and right embankment with a spillway and powerhouse in between. The left embankment, where failure occurred was approximately 240 m in length. Upon review of the design documentation, the Independent

© University of Pretoria

Forensic Team (IFT) found that the design of the Edenville Dam was not substantially inadequate if the dam had been built according to the design plans and construction specifications. However, during the course of the investigation, it became clear that the actual construction of the dam deviated substantially from the design plans and construction specifications, apparently with the knowledge of the designer. This resulted in the safety margins of the dam being below average when compared to dams of similar type and size that were built between 1910 and 1930 in the United States.

In particular, the following deficiencies in the construction were noted:

- Lack of compaction of the fill material. This resulted in sections of the dam being created with very loose to loose sands which created the fundamental physical conditions required for static liquefaction.
- Poor control over the downstream slope angle. This resulted in the slope being 1(V):1.6(H) in the upper part of the failure section, compared to the design downstream slope 1(V): 2(H).
- Poor under-drainage construction. An investigation conducted in 2012 revealed that no underdrains had been constructed in the vicinity of the failure section. This meant that the saturation of the slope in this area would be increased, compared to the rest of the embankment.

The reservoir impounded by the Edenville Dam is known as Wixom Lake, which had a storage volume of 44.4 Mm^3. Figure 2.15 show an output from the stability assessment of the Edenville left embankment considering the reservoir level under normal operating conditions. In this assessment, the strength parameters as identified in the 1987 inspection report were used. A FoS of 1.04 was calculated using drained strength parameters, which is significantly lower than the value of 1.5 as required by FERC. This lower FoS value was attributed to a steeper downstream slope than the adjacent sections where the wall height was greater. In these sections, the calculated FoS was greater than 1.5 and the phreatic surface was monitored using piezometers. This low FoS value is clearly indicative of a dam with marginal stability.

As part of their investigation, the IFT closely examined three potential primary failure mechanisms for the Edenville Dam: overtopping, internal erosion, and instability. An overtopping failure was ultimately ruled out as there was no evidence (neither from the video recording, photographs, nor eyewitness accounts) of water flowing across the crest nor evidence of water on the downstream face until less than four minutes before the failure. An internal erosion failure was ruled out due to a combination of factors including the fact that no turbid discharge water was detected; and that the kinetics of the failure, specifically the global acceleration and velocity of the failure mass, were

© University of Pretoria

not consistent with historical observations of internal erosion failure.

As will be shown in Section 2.5.6, a numerical analysis was conducted which showed that the stress state in the embankment was such that only a small trigger event was required to initiate collapse. Based on the knowledge of the collapse behaviour of loose, saturated, sandy soils it was noted that even a gradual rise in pore pressure in an embankment containing such soils could trigger collapse behaviour. This collapse could be initiated without any significant changes in shear stress and at a stress state below the drained failure envelope. It is not disputed that on the day of the failure, the reservoir level was at its highest elevation.

Further, laboratory tests showed that the loose embankment material was susceptible to collapse. All this lead the IFT to conclude that the failure at Edenville was a result of wetting-induced collapse of the loose sandy soils in the downstream face of the dam, and subsequent static liquefaction failure of the embankment. It was ultimately found that static liquefaction was the most likely cause of failure. This was based predominantly on the video footage which showed a rapid instability failure of a localised portion of the downstream section of the dam. This localised failure was followed by the collapse of the upstream remnant of the embankment.

Figure 2.14 shows a photograph of the failed section 36 s after the initiation of failure. In this image it is clear to see that the extent of the failed embankment section is limited to a length of 12 m to 24 m along the axis of the dam.



Figure 2.14: Photograph of the Edenville Dam failure 36s after initiation of failure (after France et al., 2022)

Another interesting aspect of the report was the discussion on the existing guideline documents

© University of Pretoria

for water storage dams in the United States. A specific attempt was made to determine how loose, saturated, sandy soils should be evaluated, and if there was any guidance of designing against static liquefaction. The following extract from the report details their findings: "…in fact, references and guidance documents for dam design and analysis indicate that drained strengths should be used for sands and silty sands for all load conditions except for rapidly applied loads, such as earthquakes". Therefore, at the time of the failure, static liquefaction was not treated as a plausible failure mechanism for water storage dams in the United States.

As with the Merriespruit tailings dam failure, the independent investigation report was quite clear in their opinion that the failure was foreseeable and preventable.

"With respect to the human judgements, decisions, actions, and inactions during the project history leading up to the May 2020 event, ***the dam failures were foreseeable and preventable****"* (France et al., 2022).

In addition, as was found with the Mount Polley tailings dam failure, there were deficiencies in the design and safety evaluations of the dam to such an extent that the key issue that resulted in the failure was not identified.

"During the nine decades after the construction, particularly once the dam came under FERC regulation about three decades before the failures, embankment stability analyses were performed for two locations where there were specific stability or seepage concerns, but these analyses were not sufficient in scope to evaluate the stability of the entire 6 000 ft length of the Edenville embankments. Therefore, ***the stability deficiency of the embankment section that failed was never recognised****"* (France et al., 2022).

The Edenville Dam failure is therefore an important case history offering valuable lessons. A key outcome of this failure is the question of whether static liquefaction should be considered as a possible failure mode for water dams? This is currently being addressed by regulators in the United States and it is likely that a decision will be made in the near future.

© University of Pretoria

Color	Name	Material Model	Unit Weight (pcf)	Cohesion (psf)	Effective Cohesion (psf)	Effective Friction Angle (°)	Piezometric Line
	1987 – Fine to Medium Sand Fill	Mohr-Coulomb	120		0	35	1
	1987 – Natural Sand	Mohr-Coulomb	120		0	34	1
	1987 – Sandy Clay Hardpan	Undrained (Phi=0)	130	4,500			1
	1987 – Silt and Sand Fill	Mohr-Coulomb	105		0	32	1

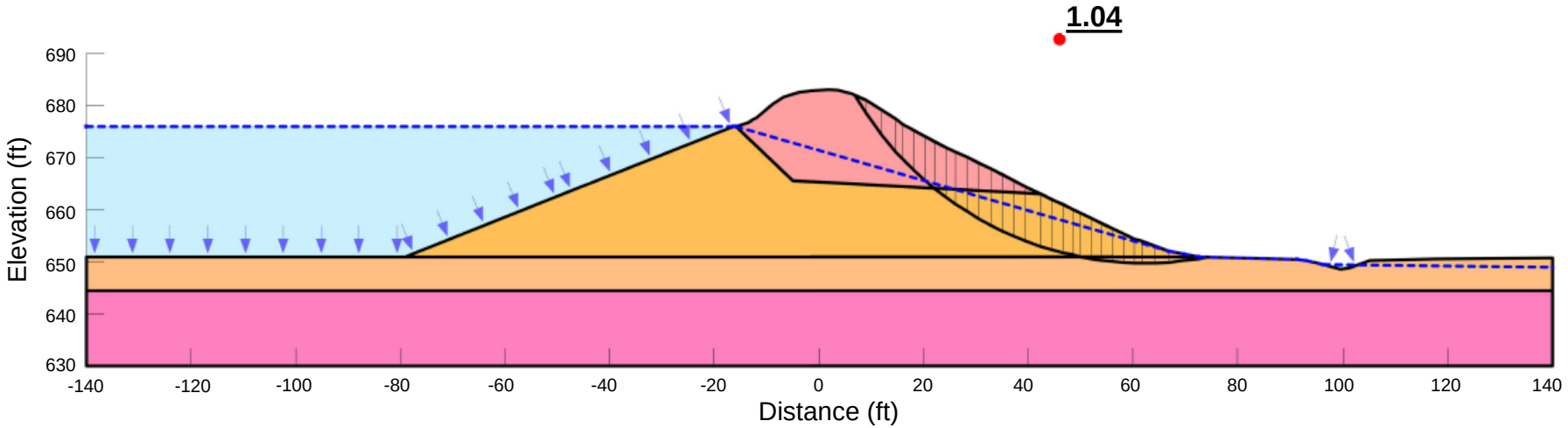


Figure 2.15: Stability analysis for the Edenville left embankment (after France et al., 2022)

© University of Pretoria

2.2.4.6 Jagersfontein tailings dam, South Africa

The Jagersfontein Diamond Mine is located in the town of Jagersfontein in the Free State Province of South Africa. The mine is world-renown and has produced two of the ten largest rough diamonds ever discovered: the 995 carat Excelsior in 1893 and the 650 carat Reitz in 1895 (Philip, 2016). Mining at the site started almost 150 years ago but operations have been continuously interrupted during the years for various reasons, including regional wars, depressed commodity prices, and changes in ownership.

In 2022, the only activities occurring on the site were reprocessing of old surface stockpiles. After processing, the waste material was stored on the Jagersfontein tailings dam. Unfortunately on 11 September 2022, the Jagersfontein tailings dam failed, resulting in significant environmental damage and the death of at least one person (Dludla, 2022). As at the time of writing, the independent investigation report is still being developed and is only expected to be published in 2024 (DWS, 2023). Therefore, there is limited scientific information available regarding exactly why failure occurred. However, there is other publicly available information available which is useful in understanding some of the conditions of the dam, as well as the consequences.

For example, a commercial satellite operator used satellite imagery to estimate that at the time of the failure, the dam was 55 m high, and that a total of 5 Mm^3 of tailings material was released as part of the failure (Rivet, 2023). In a separate study, it was shown that the failure impacted the Kalkfontein Dam, some 56 km downstream from the tailings dam (Torres-Cruz & O'Donovan, 2023). The Kalkfontein Dam is a large water dam with a full storage capacity of 325 Mm^3. It is used for agricultural purposes by many of the regional farmers and its pollution is a significant concern.

There is still much uncertainty surrounding this failure and it is imperative that an appropriate scientific investigation is completed and published timeously.

2.2.4.7 Summary

In this section, six case histories of failures involving a large water and five tailings dams were presented. It is clear that the failure of these dams was not a chance occurrence. In each case, even those where the exact cause of failure is unclear, there is a clear pattern of poor decisions or actions (or inactions) which led to the deteriorating state of the dam and ultimately failure. In most cases, these potential adverse consequences of these actions or decisions were known and were done anyway, often in the pursuit of production targets. The impact of the temporary measures implemented at Mount Polley and Fundão are classic examples of this.

© University of Pretoria

What is also of importance is that even with the best regulations in place, these failures still occur. This sentiment that improving governance will not end tailings dam failure is one that seems to be shared by other researchers (e.g. Jefferies, 2022). A key example is the Edenville Dam where there are decades of inspections, internal audits and external audits that certified the dam as stable. The Feijão failure is another example. In this case there were hundreds of sensors in the dam and a video camera monitoring the slope. Both these dams still failed, despite being certified stable a few months prior. It should be noted that there are some uncertainties relating to the credibility of those stability audits for the Feijão dam (e.g. SEC, 2022; SEC, 2023) but that is outside the scope of this review.

Despite their tragic consequences, previous incidents provide valuable learning opportunities, and these should be taken advantage of to ensure these mistakes are not repeated in the future.

2.2.5 Current Tailings Dam Management Framework

It is important to highlight some of the current regulatory requirements as this will assist in providing context for the relevance of this research to the local and global tailings industry. In this section three documents relating to the design and operation of tailings dams are discussed. There are many more excellent documents available, such as those published by other governments, regulators, and even mining companies. However, for the scope of this study, it was decided that these three documents are of particular importance and need to be highlighted.

2.2.5.1 South African National Standard 10286 (SANS 10286)

The South African Bureau of Standards (SABS) is the statutory body in South Africa in charge of developing, publishing and maintaining South African National Standards (SANS). Following the Merriespruit tailings dam failure in 1994, which resulted in 17 deaths, SABS 0826 (later renamed to SANS 10286) was published.

SANS 10286 details the minimum requirements for the planning, design, construction, operation, decommissioning and closure of mineral residue deposits in South Africa (SABS, 1998). Although SANS by nature are non-statutory documents, SANS10286 is considered to be slightly different to other standards. This is due to the fact that the Mine Health and Safety Act (MHSA) of 1996 requires all mines to compile and adhere to a Code of Practice (CoP) document which, amongst other aspects deals with the design and operation of the mines tailings dams (RSA, 1996). The MHSA further states that all CoP documents must comply with the requirements as directed by the Chief Inspector of Mines. In 2000, the Chief Inspector of Mines published a document prescribing

© University of Pretoria

that all CoP documents should comply to the SANS 10286 (DME, 2000). In this way, SANS 10286 can be considered different to general SANS documents are there is a trail of official government documents specifically mentioning the document as a requirement to meet clearly defined requirements in an Act of Parliament which is law.

At the time of writing, SANS 10286 was in the process of being updated. Although the draft document exists, it is perhaps premature to comment on the contents of this document as it has not yet been through the public comment process. Since the proposed changes from the 1998 version are substantial, the public comment process is likely to result in some changes. Therefore, comments will be based on the existing version of the document.

In addition to conventional tailings dams, the document includes jurisdiction over waste rock dumps. The document is broad in nature and does not prescribe minimum FoS values. Rather, minimum inspection and reporting requirements are set-out. The frequency of these inspections and the contents of the associated reports depends on the classification of the dam. Tailings dams are classified based on potential risks to people and the environment. For dams with a high risk, a registered professional engineer must be appointed as the responsible person for the dam.

Although the SANS document is old, there is limited scientific evidence that the guidance provided in the document is deficient. In fact, a comparison in 2018 showed that at the time, the South African standard compared well with its peers (Wates, 2018). Regarding the Jagersfontein tailings dam failure in 2022, as far as the author is aware, there is no scientific evidence that the dam failed as a result of deficiencies in the current standard.

However, it should be noted that the current version of SANS 10286 contains no specific requirements regarding dealing with undrained shearing which has been shown to be an area of concern for tailings dams. Instead, the standard falls back on providing the responsible engineer with freedom to decide on whatever criteria he or she feels necessary. Regardless, there is a clear push to incorporate aspects of new standards such as the GISTM and ICOLD Bulletin 194 into the South African standard. It remains to be seen to what extent this will be achieved.

2.2.5.2 Global Industry Standard on Tailings Management (GISTM)

The International Council for Mining and Metals (ICMM) is an international organisation dedicated to a safe, fair and sustainable mining and metals industry. Following the failure of the Feijão tailings dam in January 2019, which resulted in over 250 deaths, there was significant concern raised regarding the perceived lack of governance within the tailings industry. The ICMM, the United

© University of Pretoria

Nations Environment Programme, and the Principles for Responsible Investment co-convened the Global Tailings Review to establish an international standard on tailings management. This initiative was led by Dr Bruno Oberle and in 2020, the Global Industry Standard on Tailings Management (GISTM) which was published (Oberle, 2020).

The GISTM contains 77 requirements in six categories: affected communities; integrated knowledge base; design, construction, operation and monitoring of tailings storage facilities; management and governance; emergency response and long-term recovery; and public disclosure and access to information.

Following the publication of the GISTM, the ICMM members committed in August 2020 to implement the GISTM within three years for all facilities with an “Extreme” or ”Very High” hazard classification (as per Annexure 2 of GISTM), and all other facilities within five years. To support this commitment, ICMM published two additional documents in 2021. The first document, the Tailings Management Good Practice Guide was developed to support the interpretation of the 77 requirements within the GISTM and promote good engineering practices for tailings management (ICMM, 2021a). The second document, the Conformance Protocols for the GISTM, was developed to help operators and independent third parties to assess implementation of the GISTM and to demonstrate conformance (ICMM, 2021b).

Requirement 4.6 of the GISTM states that brittle failures modes should be identified and addressed using conservative design criteria, independent of trigger mechanisms, to minimise their impact on the performance of the tailings facility. For design engineers this is a critical aspect of the new standard, and it is this requirement that is likely to determine whether tailings dams should be declared safe or not according to the GISTM. However, despite the publication of the supporting documents, there is still significant uncertainty from both practicing engineers and academics regarding how this requirement should be implemented in practice (e.g. Fourie & Reid, 2021; France et al., 2022; Jefferies, 2022). The particular concern is the specification that brittle failure mechanisms should be addressed independent of the trigger mechanisms. Although this is a conservative approach, there is a cost associated with retrofitting existing designs. These costs can become quite substantial as almost all existing tailings facilities were not designed to this standard.

In light of the above, Requirement 4.7 does make an allowance for deviations from Requirement 4.6 but only under strict conditions, and with the support of senior management. As the GISTM is still in the early stages of implementation and auditing, these details are still being worked out and there are likely to be changes based on learnings from this initial implementation period.

© University of Pretoria

Aside from the technical requirements, the GISTM is also administratively demanding and there is a real concern that there simply aren't sufficient personnel worldwide to meet the demands of the GISTM (e.g. Hatton et al., 2020). To illustrate this point, Spencer (2021) showed that complex tailings facilities where the consequence of failure is high, can require as many as 24 hours per week from the Engineer of Record (EoR). For these types of facilities, the EoR needs to be a senior engineer, typically with more than 10 years of experience. This means that a senior engineer could spend more than half a typical work week on just one facility, which may not be practical.

Like the current SANS document, no explicit FoS values are specified in the GISTM, nor in the associated guideline documents.

2.2.5.3 International Commission on Large Dams Bulletin 194 (ICOLD Bulletin 194))

The International Commission on Large Dams (ICOLD) is an international, non-governmental organisation that provides a forum for the exchange of knowledge and experience in dam engineering. A particular focus of ICOLD is to ensure that dams are built and operated safely, efficiently, economically, and without detrimental effects on the environment. To achieve this, ICOLD regularly publishes technical documents. A particular type of publication is a bulletin which is a state-of-the-art report on a single precise subject, written by experts and incorporating recommendations from engineers all over the world.

South Africa has a number of large water dams and hosts the South African National Committee on Large Dams (SANCOLD). SANCOLD is a member of ICOLD and in that way ICOLD publications are relevant in a South African context. In 2022, ICOLD published Bulletin 194 which is focused on Tailings Dam Safety.

Globally, it is common for tailings engineers to use guideline documents published for water dams. South Africa is no exception as the SANCOLD guidelines on freeboard are routinely applied to tailings dams, specifically those who meet the criteria for classification and registration as dams with a safety risk. In this way, it is believed the ICOLD Bulletin will be relevant to tailings engineers in South Africa. A key difference between ICOLD Bulletin 194 and the SANS and GISTM documents is that the ICOLD Bulletin provides minimum FoS values that should be achieved for various scenarios.

Although the document itself is useful, it is the Appendices that are of particular interest for this study. Appendix A focuses on material behaviour and Appendix B deals with stability assessments.

© University of Pretoria

Although a useful framework is provided, the author is of the opinion that there is perhaps a mismatch between the method provided and its usefulness for upstream constructed tailings dams. A key discrepancy is the classification of the soil state. Within the Bulletin 194 framework, soil behaviour, specifically the undrained shear response, is treated as a soil characteristic. This is in direct contradiction to the essence of critical state theory, where this behaviour is closely linked to the state of the soil. In the case of tailings dams, the material in the structural zone is known to vary. This is especially true for upstream constructed facilities. For example, a recent study at the Candelaria Mine by Robertson et al. (2023), based on previous observations by Robertson (2017), showed how by increasing the stress level imposed on the tailings, the brittleness of the tailings was reduced. In this case, the increase in stress was as a result of the construction of a rock pad on the tailings.

Other examples for tailings include the numerical results from the Cadia Northern TSF (NTSF) analysis which show how K_0 changes with time (Figure 2.33). Figure 2.30 shows how the K_0 value can influence the stress-strain response of a soil. In other words, brittleness is not a soil characteristic and can change depending on the state. This concept has been shown experimentally for many soils.

Therefore, methods that consider this type of approach should be used with caution. The key concern is that the heterogeneity of the tailings is not considered in a practical manner. Using this approach, a cross section may need to be divided into many sections, as was done for the Feijão investigation, which can become quite cumbersome. However, it may be that this is the only way in which slopes that may be unstable in undrained shearing can be identified. This is a different issue and is not dealt with further in this study.

Regardless, the document has been published and will likely be used. Therefore, a review of the existing requirements is provided. Figure 2.16 shows the summary chart from Appendix B that is used to classify the brittleness of soils. Depending on the material's stress-strain response, soils are either classified as generally non-brittle, moderately brittle (transitional), or highly brittle. Minimum FoS values under various scenarios are provided for each classification.

Each classification is then discussed in detail, with a specific focus on both static and seismic stability. As the seismicity of South Africa can be considered moderate by world standards (e.g. Brandt, 2011), and generally characterised by low to minor earthquakes (e.g. Alabi et al., 2013), the focus of the review will be on the static stability analyses. Full details regarding the seismic analyses can be found in the document itself.

© University of Pretoria

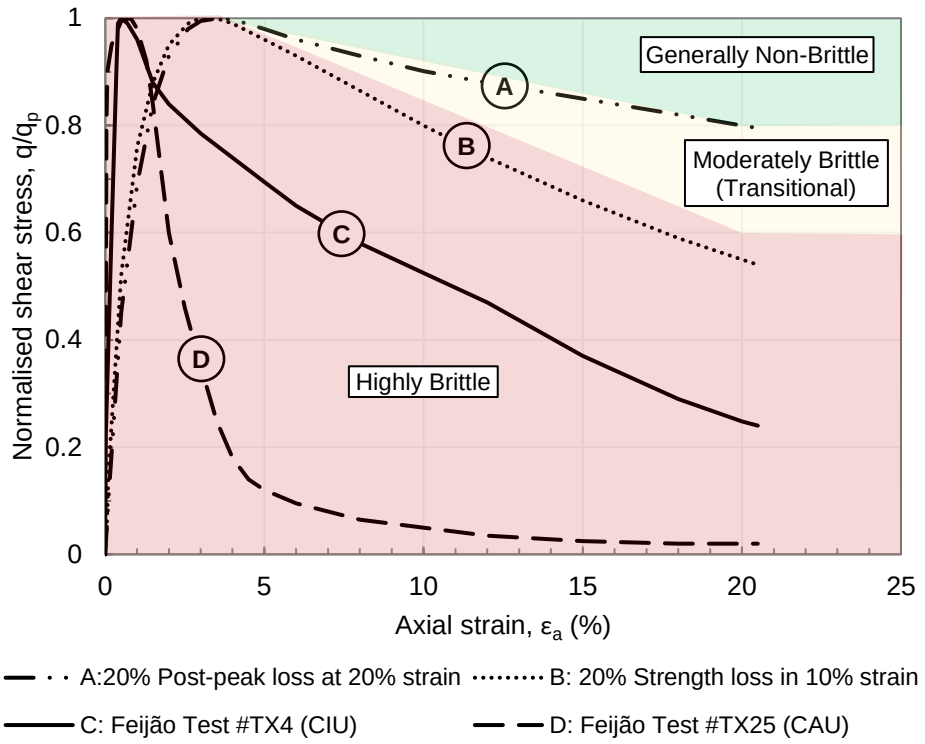


Figure 2.16: Soil brittleness classification (after ICOLD, 2022)

Table 2.2 provides a summary of the minimum FoS values for various cases. The cases are based on the brittleness of the soils within the structural zone. Two key undrained shear strengths are mentioned: peak and residual. Although the terminology is not strictly the same, these strengths relate to the same strength mobilised at the points marked yield and critical state in Figure 2.20.

For all cases, a minimum FoS for static conditions of 1.3, and a minimum FoS for post-earthquake conditions of 1.1 are required. When reading into the document, it becomes obvious that static conditions cover both drained and undrained peak shear strengths while post-earthquake conditions consider residual strengths. Therefore a minimum FoS of 1.5 considering peak undrained shear strengths has also been added. Depending on the case, these values can be reduced as shown in Table 2.2.

© University of Pretoria

Table 2.2: Summary of minimum FoS values for various scenarios (after ICOLD, 2022)

Case	Region in Figure 2.16	Brittleness Index (I_B)	Drained FoS	Undrained FoS (peak strengths)	Undrained FoS (residual strengths)
General	N/A	N/A	1.5	1.5	1.1
Case 1: No strain-softening	N/A	0	1.5	1.3	1.3
Case 2: Limited strain-softening	Non-Brittle (Green)	< 0.2	1.5	1.3	1.1
Case 3: Moderate strain-softening	Moderately Brittle (Yellow)	0.2 < I_B > 0.4	1.5	1.5	1.1
Case 4: High strain-softening	Highly Brittle (Red)	> 0.4	1.5	N/A	1.1

2.2.5.4 Summary

As a results of the recent tailings dam failures, there has been an increase in the development and publication of both new and updated standards and guideline documents for the management of tailings dams. Three such documents were discussed: SANS 10286, the GISTM and ICOLD Bulletin 194. All three documents provide stringent requirements regarding the governance of tailings dams.

The purpose of the next few sections is to describe how certain aspects of soil behaviour, specifically those described in the above-mentioned documents are influenced by various conditions experienced on active tailings dams. A particular effort will be made to show the relevance and importance of this study into this aspect, and how the results from this study could be implemented to ultimately improve tailings dam safety.

2.3 EXISTING BEHAVIOURAL FRAMEWORK FOR SOILS

Based on the information presented earlier, it should be clear that aside from the operational risks, the current geotechnical risks for tailings dams lies in the undrained behaviour of the tailings. This section provides an overview of the current understanding of the behaviour of sandy soils (such as mine tailings). A particular emphasis is placed on the factors that influence the undrained behaviour.

© University of Pretoria

2.3.1 Soil behaviour in compression

Before delving into the specifics of soil behaviour in compression, it is necessary to define some common terminology. Compression is the process of gradual reduction in volume of a soil due to an increase in effective stress. It is common to present the results of compression behaviour in a semi-log plot with the density (or void ratio) on the vertical axis, and the applied stress level on the horizontal axis, in a logarithmic scale. Depending on the stress conditions imposed, and the assumptions made, the stress is either presented in terms of vertical effective stress (σ'_v) or mean effective stress (p').

There are several test methods available to investigate the compression behaviour of soil and each test has specific stress and strain boundary conditions. These conditions directly influence the results of the tests and need to be carefully considered. Two popular tests to investigate the compression behaviour of soils are the oedometer test and the triaxial test. In a standard oedometer test, conditions of zero lateral strain are enforced. These conditions are referred to as one-dimensional compression conditions. In a standard triaxial test, conditions of equal lateral and axial stress are imposed. These conditions are referred to as isotropic compression conditions.

The virgin compression curve obtained under one-dimensional conditions is referred to as the One-Dimensional Normal Consolidation Line (1D-NCL), while the virgin compression curve obtained under isotropic compression conditions is referred to as the Normal Consolidation Line (NCL). The NCL is also referred to as the isotropic compression line. It has been shown experimentally that the 1D-NCL is parallel to the NCL for fine-grained soils such as clays of high plasticity (e.g. Atkinson & Bransby, 1978), as well as for coarse-grained soils such as clean sands (e.g. Coop, 1990). However, there remains some uncertainty regarding whether this is true for intermediate soils such as mine tailings.

When considering the compression behaviour of soils, it is important to know the type of soil being considered as it is known that fine-grained soils and coarse-grained soils have distinctly different compressibility characteristics. In particular, fine-grained soils such as clays of high plasticity appear to have a unique NCL that is parallel to the CSL as shown in Figure 2.17(a). This is in contrast to the behaviour of coarse-grained soils such as clean sands which appear to exhibit an infinite number of NCLs, which are not parallel to the CSL, as shown in Figure 2.17(b). Note that these behaviours are limited to low to moderate stress levels where particle crushing (and thereby changing of the grading characteristics of the soil) are not a feature.

© University of Pretoria

One of the objectives in Section 3.4 is to investigate whether from a practical perspective, the gold tailings behave more like fine-grained soils with a unique NCL, or more like coarse-grained soils with an infinite number of NCLs. This is important to know as it will influence laboratory testing plans and can also influence decisions for expected future site conditions.

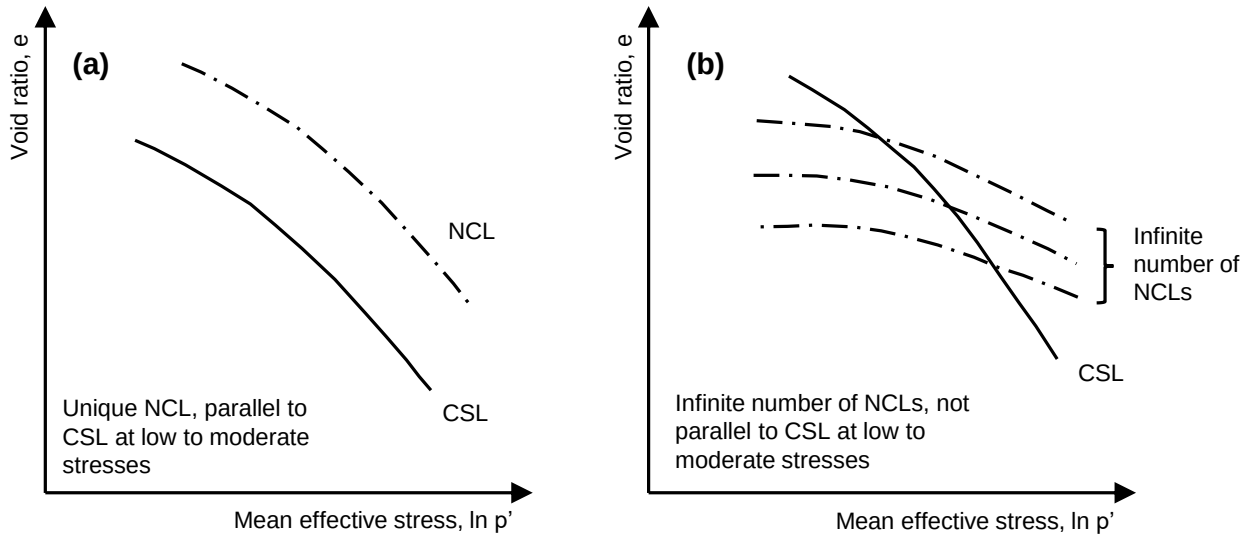


Figure 2.17: Idealised soil behaviour in compression for: (a) fine-grained soils (clays), and (b) coarse-grained soils (sands) (after Jefferies & Been, 2015)

There have been several studies showing that this idealised compression behaviour of fine-grained soils is true for clays of high plasticity (e.g. Rendulic, 1936; 1937; Skempton, 1944). However, the compression behaviour of coarse-grained soils is perhaps less well-known. One such study, by Jefferies & Been (2000), was conducted on Erksak 330/0.7 sand.

Figure 2.18 shows the results from these tests. The sand had a D_{50} value of 0.330 mm and a fines content (material by mass passing the 0.075 mm sieve) of 0.7%. In addition to the compression curves of the sand with various initial states, the CSL and the pseudo NCL (PNCL) are indicated. The CSL was defined based on the results from the shear phase of the triaxial tests. However, the PNCL is based on the Cam Clay proposition that the NCL is parallel to the CSL when presented in an $e - \ln p'$ or $e - \log p'$ projection (e.g. Schofield & Wroth, 1968). The spacing ratio is used to define the offset of the PNCL from the CSL and the original Cam Clay spacing ratio of 2.73 was used.

© University of Pretoria

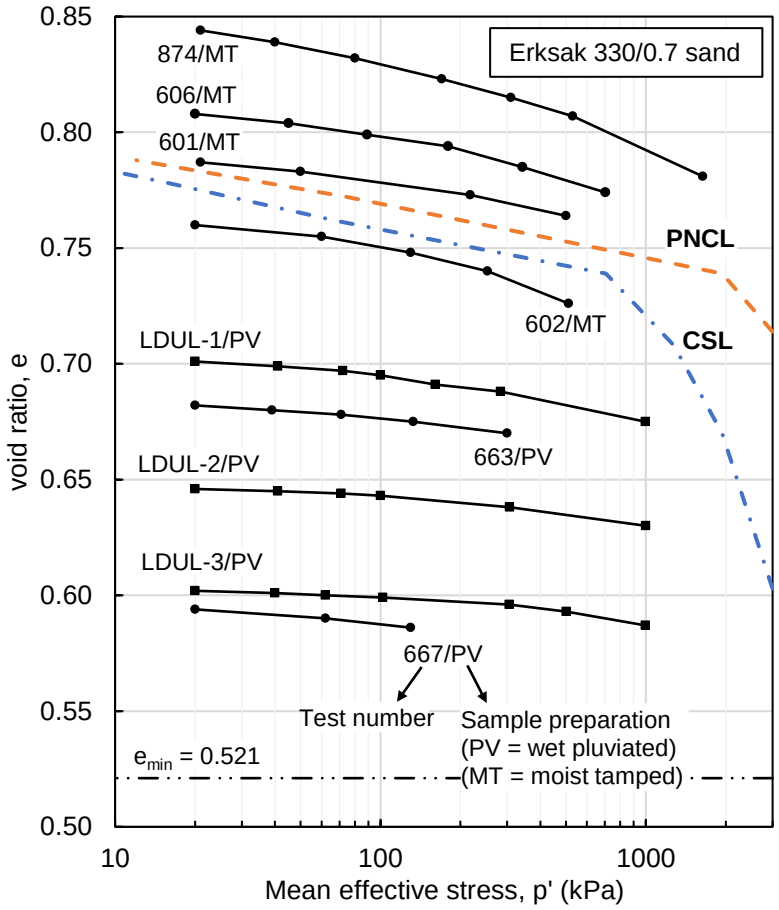


Figure 2.18: Triaxial test results on Erksak 330/0.7 sand (after Jefferies & Been, 2000)

The purpose of the testing was to investigate the concept of an infinite number of NCLs for sandy soils. For each compression curve shown in Figure 2.18, it was argued that these are true NCLs for the following reasons:

1. The samples were prepared under low stresses, either by gentle Moist Tamping (MT) or Wet Pluviation (PV). This is true even for the initially dense samples such as samples LDUL-3/PV and 667/PV. It appears to be a characteristic of clean sands that a range of initial densities can be achieved without imposing a stress history on the sample. Therefore the samples were never overconsolidated in their initial state.
2. The virgin compression and unload-reload loops form a classic elastic-plastic form as shown in Figure 2.19.
3. Although no unique NCL was identified (Figure 2.18), a PNCL was defined using the Cam Clay theory. If this PNCL were a true NCL, and the compression curves were in fact simply swelling lines, then material consolidated at states looser than the PNCL should exhibit a rapid reduction in volume to reach the PNCL. However samples 874/MT, 606/MT and 601/MT lie above the PNCL, and no collapse was observed for these samples. Rather, a

© University of Pretoria

smooth, stable response during compression was observed.

For this study, the uniqueness of the NCL for the gold tailings will be investigated according to the above-mentioned aspects.

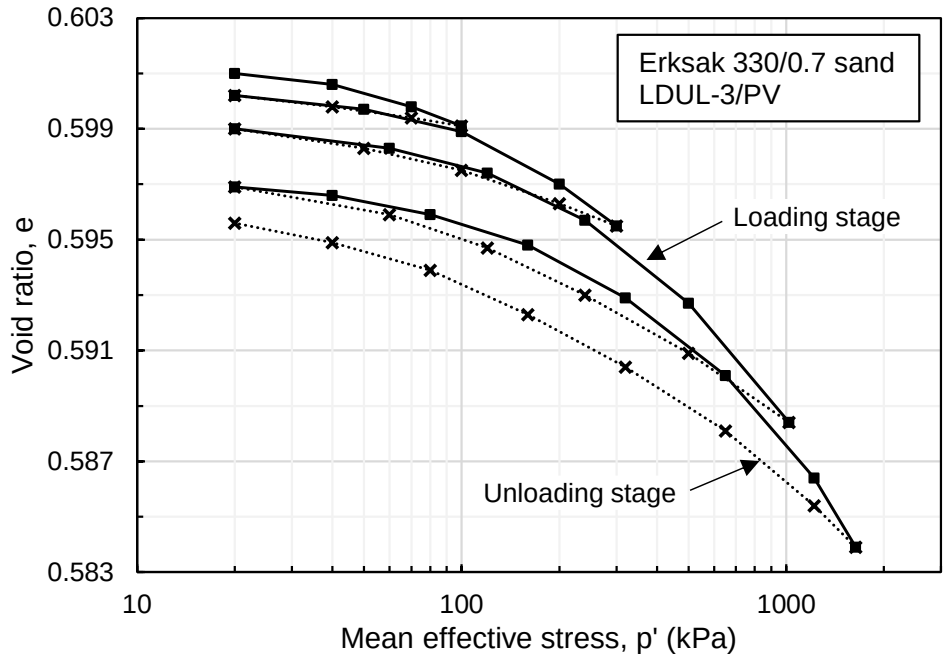


Figure 2.19: Unload-reload loops for the LDUL-3/PV sample (after Jefferies & Been, 2000)

2.3.1.1 Quantifying convergence

As part of the investigation into the uniqueness of the NCL, it will become necessary to comment on the converge (or lack of convergence) of various compression curves. Although this can be done visually, it would be more useful to use a method that is repeatable and provides a magnitude of convergence. Ponzoni et al. (2014) proposed such a method where a parameter, m, is used to quantify the degree of convergence of a number of compression curves.

To implement the method, the specific volume (v) of the sample is compared two stress levels: the initial stress level, and the stress level at which convergence is being assessed, typically the last loading increment. v describes the density of a sample and is numerically equal to $1 + e$. The specific volumes at these two stress levels are plotted on a graph where the vertical axis shows the specific volume at the stress level at which convergence is being assessed, and the horizontal axis shows the initial specific volume.

© University of Pretoria

Each test is represented by a single point. This process is repeated for each test conducted, typically with the aim of having tests starting at different specific volume values but being subjected to the same level of applied stress. The slope of the linear trendline drawn between the points obtained for all of the samples is described as the parameter m. m varies between 0 and 1, with an m value of 0 indicating a unique compression curve and an m value of 1 indicating that the compression curves are parallel.

This method has been used by several researchers to classify transitional soils (these soils are described in Section 2.3.2. For example, Li (2017) conducted a series of oedometer tests on Brazilian gold tailings and found an m value of 0.13 for an applied stress of 7 MPa. At stress levels of 20 MPa, the m value reduced to 0 indicating a unique compression curve.

In terms of other soils, Ponzoni et al. (2014) conducted an extensive series of oedometer and triaxial tests on silts and silty clays from the Venice Lagoon. Based on the results from over 200 oedometer tests, an m value of 0.40 was determined and the material was classified as possibly transitional (i.e. not exhibiting a unique NCL).

In terms of other tailings materials, Li (2017) conducted a series of oedometer tests on Chinese copper tailings at applied stress levels of up to 7 MPa. An m value of 0.64 was determined and the material was classified at transitional. Similarly, Cartwright et al. (2022) conducted a series of compression tests on Australian mineral sands tailings up to an applied stress of 5.6 MPa. An m value of 0.71 was determined and the soil was also classified as transitional.

2.3.2 Soil behaviour in shear

Initially, the compression and shear behaviour of soils was always considered independently. This changed with the development of Critical State Soil Mechanics (CSSM). Popularised by Schofield & Wroth (1968), CSSM was perhaps the first accepted attempt to unify both the compressive and shear behaviour of soil. As more soils were investigated, it became apparent that not all soils conform to the principles of CSSM. These soils have been termed transitional soils. Transitional soils are those for which the initial density continues to affect its compression and shearing behaviour to large strains to the extent that unique NCLs and CSLs cannot be found by means of traditional testing (Coop, 2015). Therefore, any investigative laboratory testing regime must be designed to clearly identify soils which are transitional or not.

Within the CSSM framework, the state of the soil influences it behaviour. This state is described

© University of Pretoria

by five key factors: the density, the current stress conditions, previous stress conditions (stress history), the fabric (particle orientation), and the type of loading applied to the soil. In the subsequent sections, an attempt is made to show the influence of each of these factors on the shear behaviour of mine tailings. However, high-quality published data on mine tailings is limited. Therefore certain principles are shown for sandy soils. A particular focus is placed on the undrained shear response.

2.3.2.1 Terminology

Since it is known that the behaviour of a soil is dependent on its state, it is important to be able to classify the state of a soil. Initially, relative density was used to describe the state of sandy soils. Although this proved to be a useful parameter, it soon became clear that a key aspect was missing. For example, Been & Jefferies (1985) showed that for Kogyuk sand with the same relative density, vastly different behaviour during undrained shear was noticed, depending on the stress level.

A new parameter that considered both density and stress level was proposed to describe the state of sandy soils. This parameter was defined as the state parameter and, as shown in Equation (1), is the difference in void ratio between the current void ratio and the void ratio at critical state, at the same stress (Been & Jefferies, 1985).

$$\psi = e - e_{cs} \tag{1}$$

Where:

ψ = State paramater

e = Current void ratio

e_{cs} = Void ratio at critical state

At this point, it will be quite useful to explain some terminology used to describe the shearing response of a soil under various conditions. Table 2.3 provides a summary of these terms, as well as references to examples of each type of behaviour. An important point highlighted in Table 2.3 is that a soil can be contractive but not strain softening. It is the strain-softening behaviour that is a concern for stability analyses.

© University of Pretoria

Table 2.3: Summary of key terminology used to describe the shearing behaviour of soils

Term	**Description**	**Example (Figure 2.20)**	**Example (Figure 2.21)**
Contractive	This classification is based on the observed volume change or pore pressure response. In drained shear, contractive samples with exhibit a decrease in total volume, while in undrained shear contractive samples will exhibit an increase in pore pressure.	1,2,3	2,3,4
Dilative	This classification is based on the observed volume change or pore pressure response. In drained shear, dilative samples with exhibit an increase in total volume, while in undrained shear dilative samples will exhibit a decrease in pore pressure.	N/A	1
Strain-softening	This classification is based on the observed magnitude of strength mobilised during shearing. Strain-softening soils will typically (but not always) show an initial increase in strength during shearing until a peak value is reached. After this point, there is a reduction in strength as the strain increases until critical state is reached.	3	4
Strain-hardening	This classification is based on the observed magnitude of strength mobilised during shearing. Strain-hardening soils will an increase in strength during shearing until a peak value is reached. After this point, the strength either remains constant or increases as the strain increases until critical state is reached.	1	1,2
Phase Transfer	Some soils do not exhibit purely strain-softening or strain-hardening behaviour during shearing. Depending on the state, some soils initially exhibit strain-softening but then undergo a phase transfer and then exhibit strain-hardening.	1,2	3,4

Although it is useful to categorise the undrained shear response of a soil into strain-hardening and

© University of Pretoria

strain-softening, it is clear that even for strain-softening soils, various extents of strain-softening can exist. Therefore, it would be more useful if the magnitude of strain-softening could be quantified. To address this, Bishop (1971) defined the Brittleness Index (I_B) as shown in Equation (2). I_B ranges from 0 to 1, where 0 indicates a soil that does not strain soften (i.e. the yield and critical state undrained shear strengths are numerically equivalent) and 1 indicates a soil that completely collapses (i.e. the shear strength drops to 0 kPa at large strains).

$$I_B = \frac{S_{u(yield)} - S_{u(critical\ state)}}{S_{u(yield)}} \quad (2)$$

Where:

I_B = Brittleness Index

$S_{u(yield)}$ = Yield undrained shear strength (kPa)

$S_{u(critical\ state)}$ = Critical state undrained shear strength (kPa)

2.3.2.2 Influence of density

The first test results that are shown are those performed by Castro (1969) who investigated the influence of density at the start of the shear phase to the undrained shear response for Ottawa sand in triaxial compression. The samples were prepared in the same manner (using the Moist Tamping sample preparation method, see Section 2.4.1 for more details regarding this method) and were consolidated to the same mean effective stress of approximately 400 kPa. However, the samples were prepared such that at the start of the shear phase, each sample had a different void ratio. The results are shown in Figure 2.20. Figure 2.20(a) shows the stress-strain response in $q - \gamma$ space, while Figure 2.20(b) shows the stress paths in $q - p'$ space.

It can be seen that for a relatively small change in void ratio, there is a distinctly different undrained shearing response. The loosest sample (with a void ratio of 0.748 at the start of the shear phase) exhibited an initial increase in shear strength up to a peak value at approximately 1.5% axial strain. This was followed by a rapid drop in strength to the critical state undrained shear strength. This behaviour was termed a Liquefaction Failure (LF).

The sample with a slightly denser packing (with a void ratio of 0.689) exhibited a rapid increase to a peak value followed by a small drop in shear strength. With increasing strain, a slight increase in shear strength was observed. This behaviour was termed Limitation Liquefaction (LL). The densest sample (with a void ratio of 0.675) exhibited a continuous increase in shear strength with strain. This behaviour was termed a Dilative Response (DR). Therefore, even at the same confining stress, a change in void ratio can result in significantly different undrained shear responses and

© University of Pretoria

therefore, different undrained shear strengths.

The distinction between these three behaviours is important as these yield and critical state undrained shear strength values are used directly in design and safety evaluation stability assessments in some jurisdictions (e.g. ICOLD, 2022).

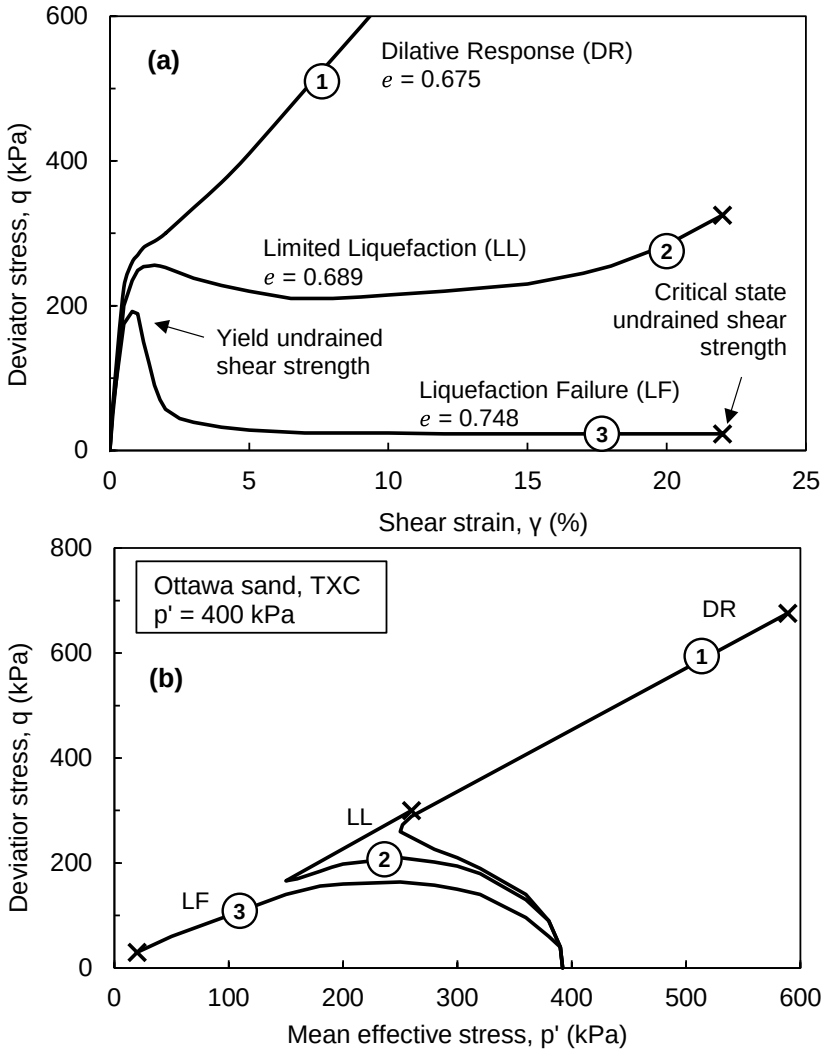


Figure 2.20: Influence of density on the undrained shear response of Ottawa sand (after Castro, 1969) in: (a) $q - \gamma$ space, and (b) $q - p'$ space

2.3.2.3 Influence of effective stress

In another study, the influence of stress level on the mechanical response during undrained shearing of Toyoura sand was investigated (Ishihara, 1993). Toyoura sand is a narrowly-graded, clean sand with no fines and is coarser than the gold tailings considered as part of this study. As part of the testing, samples were prepared using the MT sample preparation method and were consolidated to different mean effective stress values but to the same void ratio.

© University of Pretoria

Figure 2.21 shows the results from these tests. Figure 2.21(a) shows the stress-strain curves in $q - \varepsilon_a$ space, while Figure 2.21(b) shows the response in $q - p'$ space. It can be seen that the sample sheared at a confining stress of 0.1 MPa exhibited a strain-hardening response, while the sample sheared at a confining stress of 3.0 MPa exhibited a strain-softening response. Therefore, even at the same void ratio, a change in confining stress can result in significantly different yield undrained shear strengths. However, for a given void ratio, regardless of stress conditions, there is a unique critical state undrained shear strength. These results are all entirely consistent with the CSSM framework.

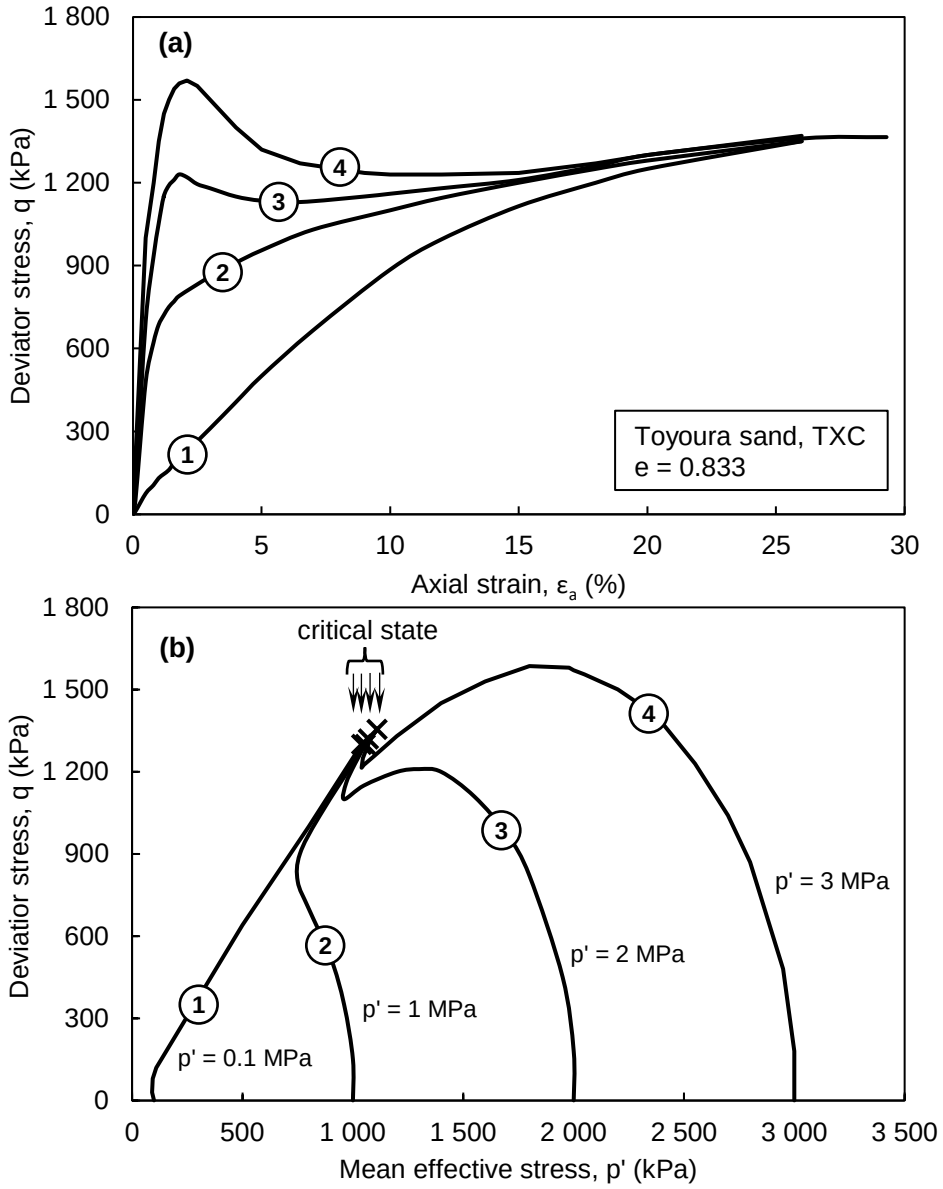


Figure 2.21: Influence of stress level on the undrained shear response of Toyoura sand (after Ishihara, 1993) in: (a) $q - \varepsilon_a$ space, and (b) $q - p'$ space

© University of Pretoria

2.3.2.4 Influence of fabric

As part of their investigation into the mechanical behaviour of loose, sandy soils, Zlatovic & Ishihara (1997) conducted a series of triaxial compression tests on the Lagunillas sandy silt. The grading of this material is similar to the grading of the gold tailings assessed as part of this study. The results from these triaxial tests are shown in Figure 2.22. Normalised curves were presented where the deviator stress and mean effective stress values were normalised by the mean effective stress value at the start of the shear phase. Figure 2.22(a) shows the response in $q/p'_0 - p'/p'_0$ space, while Figure 2.22(b) shows the response in $q/p'_0 - \varepsilon_a$ space. Three samples were prepared using three different sample preparation techniques, were consolidated isotropically, and were sheared undrained. The three sample preparation methods were: MT, Air Pluviated (AP), and Water Sedimented (WS). Additional details regarding these sample preparation methods are provided in Section 2.4.1

As shown in Figure 2.22(b), three distinct responses were noted for the three sample preparation methods. Each sample was prepared such that they had similar void ratios at the end of consolidation, with these void ratio values ranging between 0.83 and 0.86. Although a similar normalised yield undrained shear strength was noted for all three samples, the observed behaviour deviated for each sample after yielding. The MT and AP samples exhibited strain-softening behaviour while the WS sample exhibited strain-hardening behaviour. Using the terminology defined by Castro (1969), the MT sample exhibited a LF response, the AP sample exhibited a LL response and the WS sample exhibited a DR.

As discussed in Section 2.3.2.2, even small changes in the void ratio (density) of a loose sandy soil can have a large influence on the stress-strain response in undrained shear. Since the void ratio at the start of shearing was not identical for all three specimens, the curves shown in Figure 2.22 capture both the influence of density and fabric. Therefore, the figure also highlights how the selection of the sample preparation method can influence the loosest density achievable in the laboratory, which influences the stress-strain response.

© University of Pretoria

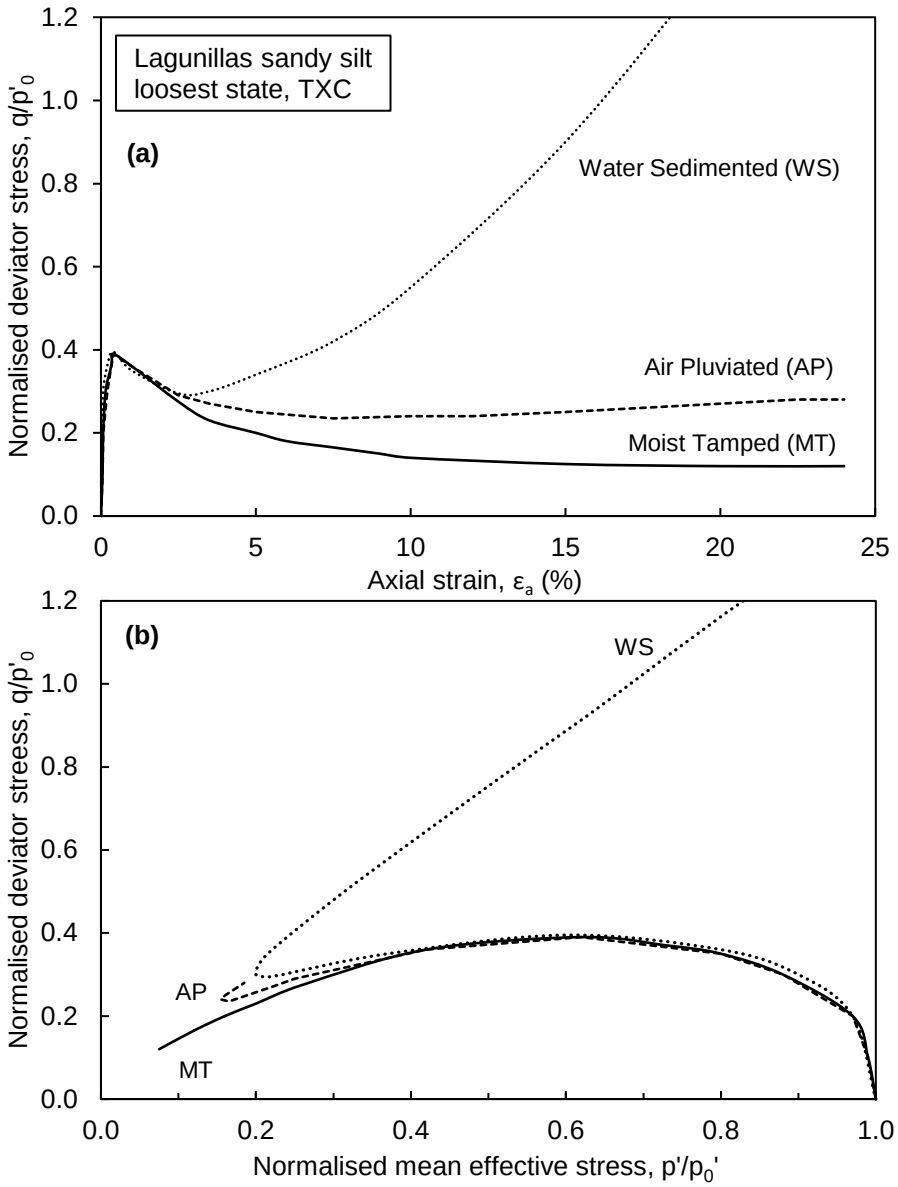


Figure 2.22: Influence of sample preparation method on the undrained shear response for loose Lagunillas sandy silt (after Zlatovic & Ishihara, 1997) in: (a) $q/p'_0 - \varepsilon_a$ space, (b) $q/p'_0 - p'/p'_0$ space

Similar results were found by Vaid & Sivathayalan (2000) for clean sands. In their study, loose Syncrude sand was tested in Direct Simple Shear (DSS) and loose Fraser River sand was tested in both triaxial compression (TXC) and triaxial extension (TXE). Fraser River sand is a coarse, clean sand. For both materials, and for all three modes of shear, it was found that there was a difference in the undrained shear response. The MT samples exhibited a strain-softening response and the SD samples exhibited a strain-hardening response.

Now that it has been established that the method of sample preparation influences the undrained shear response, the next logical question is how do these methods compare to the in-situ fabric? In other words, which sample preparation method is most appropriate if the intent is to create a

© University of Pretoria

sample that can reproduce the same undrained shear response as a sample with the in-situ fabric?

Chang et al. (2011) spent some time investigating this aspect. As part of their research, the undrained shearing response of samples prepares using the MT and SD methods were compared to the undrained shearing response of an Undisturbed (UD) sample. The undisturbed sample was sourced from the East Rand Proprietary Mines (ERPM) Dam 4 in Gauteng, South Africa. Figure 2.23 shows the results from these tests. It can be seen that the SD sample exhibited a response that matched the response from the undisturbed sample better than the MT sample. Although there were a few exceptions, specifically for specimens representing the coarser fraction of the tailings, this observation was generally consistent throughout the results presented. Corrêa & Oliveira Filho (2019) came to similar findings regarding the performance of the MT sample preparation method, when compared to the SD method for iron ore tailings.

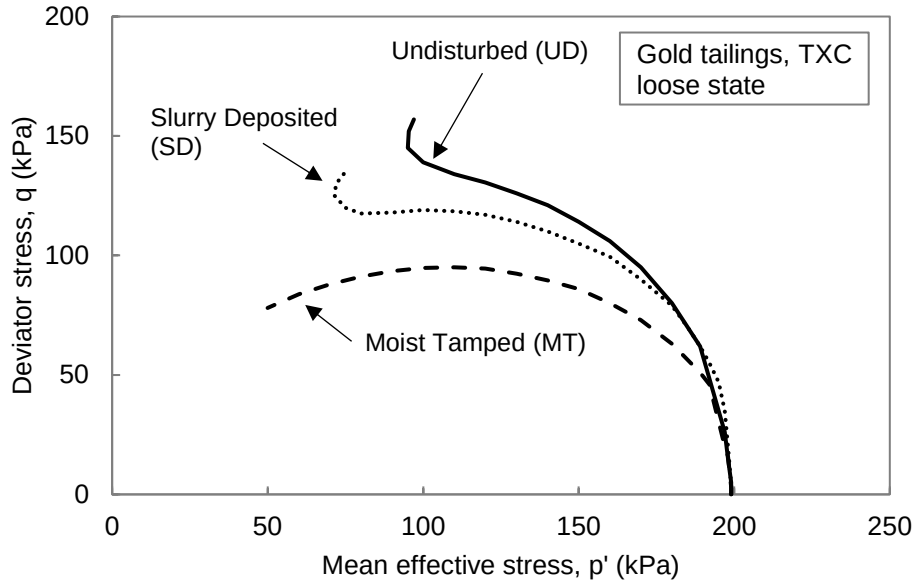


Figure 2.23: Influence of fabric of the undrained behaviour of gold tailings (after Chang et al., 2011)

2.3.2.5 Influence of mode of shear

Figure 2.24 shows the results from a series of laboratory tests conducted by Yoshimine et al. (1998) and summarised by Sadrekarimi (2014). In these tests, loose samples of Toyoura sand were prepared using the AP method. The samples were consolidated to the same effective stress and were sheared undrained. However, three distinct modes of shear were employed: TXC, DSS, and TXE. It is clear that the yield undrained shear strengths are different, with the yield undrained shear strength determined by TXC testing being greater than the DSS strength, which in turn is greater than the TXE strength. This trend appears to be consistent for loose, sandy soils as shown

© University of Pretoria

by Sadrekarimi (2014) who investigated a large database of undrained shear tests.

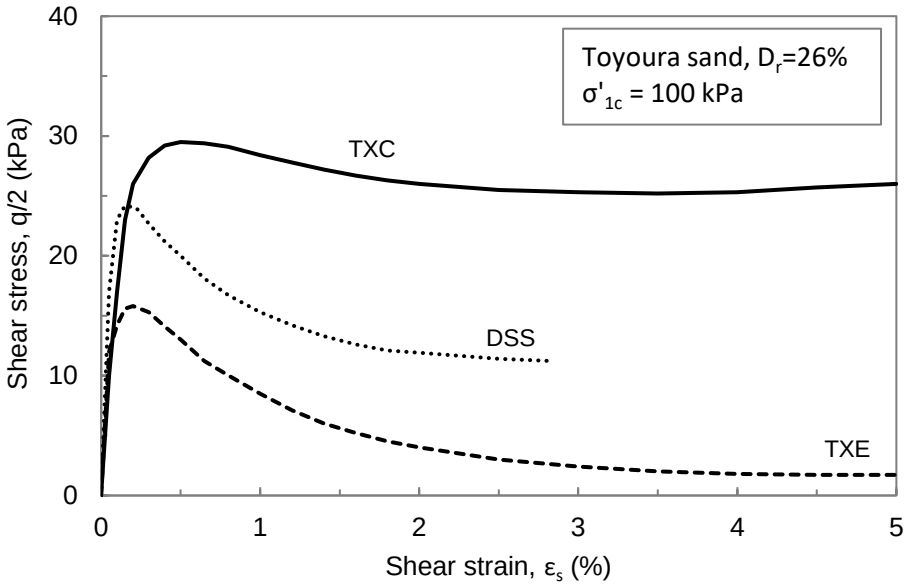


Figure 2.24: Influence of mode of shear on the undrained behaviour of Toyoura sand (after Yoshimine et al., 1998)

In another investigation, Vaid & Sivathayalan (2000) showed results from TXC and TXE tests on Fraser River sand. The samples were created in the same manner (moist-tamped) and consolidated to the same mean effective stress (values ranges from 100 kPa to 800 kPa) to similar, loose void ratios at the start of the shear phase. The samples sheared in triaxial compression exhibited a strain-hardening response while the samples sheared in triaxial extension exhibited a strain-softening response.

In an earlier investigation, Riemer & Seed (1997) showed that in addition to having different mechanical responses during undrained shear, tests on Monterey #9 sand showed distinctly different CSLs depending on the mode of shear. The Monterey #9 sand is a narrowly-graded medium sand. This is an intriguing finding as under classical critical state theory, the mode of shear should not influence the CSL. However, upon closer inspection of the results, it becomes apparent that the proposed CSLs for the three modes of shear presented have remarkably similar slopes when plotted on an *e-p'* diagram and in fact the major difference between the three CSLs is the intercept, which is a maximum of 0.03 in terms of void ratio.

Although there is remarkable consistency in the results obtained from the three methods, we have since become aware of the inherent variability involved in triaxial testing of sandy soils, particularly loose samples. As discussed in Section 2.3.4, Reid et al. (2021) showed that perhaps the most

© University of Pretoria

accurately that the CSL can be determined using modern triaxial testing equipment is within a void ratio of 0.04. Since the void ratio difference presented by Riemer & Seed (1997) is 0.03, it could be interpreted that from a practical perspective, the CSL is independent of the mode of shear for the Monterey #9 sand.

2.3.2.6 Influence of stress anisotropy

Kato et al. (2001) performed a series of undrained triaxial compression tests on isotropically and anisotropically consolidated samples of clean Toyoura sand. As part of their investigation, it was found that the CSL remained unique regardless of the stress state imposed during consolidation. Further, it was found that even for anisotropically consolidated samples, a unique critical state point was obtained. In other words, despite the different initial stress states, when the samples were sheared under undrained conditions, it was the void ratio at the start of the shear phase that dictated the behaviour at large strains. This is entirely consistent with critical state theory where the intersection of the CSL and an undrained plane is a single point.

In another series of tests, Doanh et al. (1997) conducted undrained triaxial compression tests on loose Hostun RF sand. Amongst other research objectives, the intent was to investigate the influence of the imposed stress conditions during consolidation (K_c) on the undrained shear response. It was found that the peak strength reached during undrained shearing increased with decreasing K_c, and that this peak value occurred at lower strains when compared to samples consolidated to higher K_0 values. Although this has been established for clean sands such as Hostun RF sand, there is some uncertainty whether this behaviour is expected for mine tailings. This is one of the objectives of this research.

2.3.2.7 Particle crushing

When subjecting soils to high stresses, it is important to consider particle crushing as this can result in a change in particle size distribution of the soil. This is especially important for investigations into the compression behaviour of soil where is it known that soils with different grain sizes exhibit different compression characteristics. As described by Zhang et al. (2020), the debris caused by particle crushing continuously fill the pores between the particles, thereby reducing the compressibility of the new soil.

In the literature, there are various reports of the magnitude of particle crushing for mine tailings. For example, Carrera et al. (2011) conducted a series of triaxial compression tests on fluoride tailings with mean effective stress values ranging from 60 kPa to 1 978 kPa. No appreciable evidence of particle crushing was noted. Similarly, Li (2017) conducted a series of oedometer and

© University of Pretoria

triaxial compression tests on Brazilian gold tailings and found no evidence of particle crushing, even on samples subjected to mean effective stress levels of 7 MPa.

Conversely, Bedin et al. (2012) performed a series of triaxial compression tests on the same Brazilian gold tailings as assessed by Li (2017), albeit with a coarser grading. In that study, particle crushing was evident at stress levels as low as 600 kPa. This difference in grading could perhaps explain the difference in particle crushing.

Similarly, in a series of triaxial compression tests on copper tailings, Zhang et al. (2020) found that particle breakage occurred from an applied mean effective stress as low as 200 kPa and continued all the way through to 5 MPa. However, the magnitude of particle breakage was limited. It was found that the D_{50} reduced from 0.165 mm as per the initial grading to 0.131 mm due to the applied load of 5 MPa.

Clearly, there is some uncertainty regarding the magnitude of particle crushing (if any) for mine tailings. Therefore, in this study, particular emphasis was placed determining the grading curves of the samples which were subjected to large stresses.

2.3.3 Unsaturated soil behaviour

With respect to tailings dams, where much of the soil mass is in an unsaturated state, it is important to not just consider saturated soil mechanics. In this section, two particular aspects of unsaturated soil mechanics are explored: the relationship between suction, degree of saturation and volume change; and an equivalent definition of effective stress for unsaturated soils.

2.3.3.1 Soil Water Retention Curve (SWRC)

A Soil Water Retention Curve (SWRC) describes how a soil changes as it wets up or dries out. Key aspects that are considered in a SWRC include the volume of the soil, the matric suction, and the degree of saturation. There are many ways to present a SWRC, but the most common is on a chart with the degree of saturation on the vertical axis (in a natural scale), and the matric suction on the horizontal axis (in a logarithmic scale). An example of such a curve is shown in Figure 2.25. Key components of a SWRC include the air entry value, and the residual suction value.

© University of Pretoria

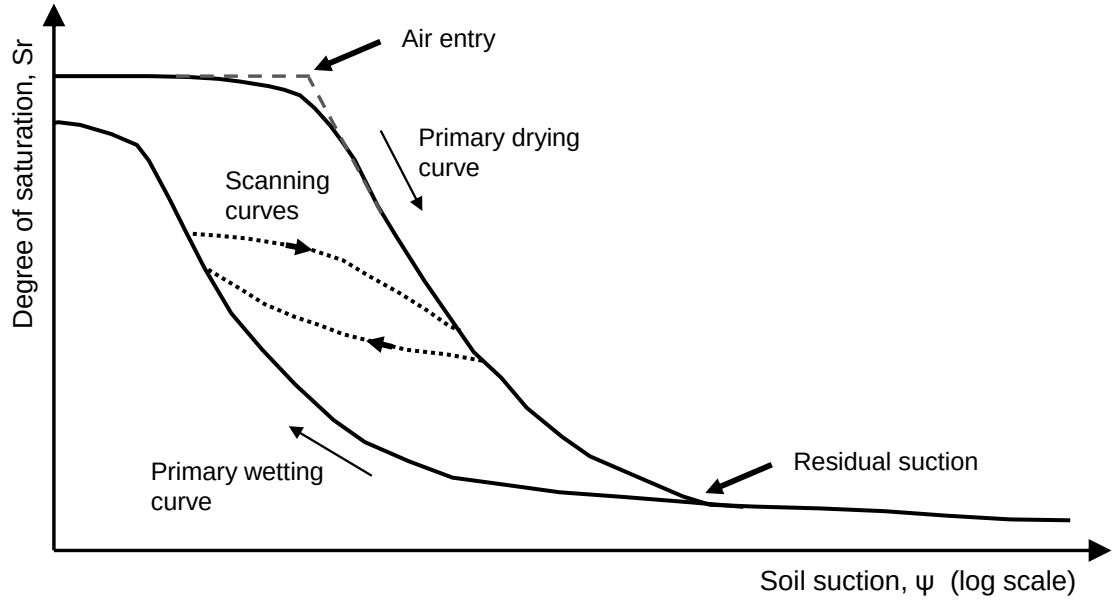


Figure 2.25: Key components of a Soil Water Retention Curve (after Fredlund, 2017)

It is important to note that a SWRC is not a characteristic curve for a soil. There is substantial experimental evidence to suggest that these curves are dependent on density and stress level. It is also known that the initial soil conditions, as well as the wetting/drying procedures influence the SWRC (e.g. Romero et al. 1999; Gallage & Uchimura, 2010).

For a given soil state, there are two limiting curves within which can exist an infinite number of curves. These limiting curves are referred to as the primary wetting curve, which is obtained when a soil sample is saturated from an initially dry condition; and the primary drying curve, which is obtained when a soil sample is dried from an initially saturated condition. For any other starting conditions, the soil will follow a scanning curve which will eventually join either the primary wetting or drying curve at extreme conditions.

There are several methods available to obtain these curves using laboratory experiments, with perhaps the most popular method being the pressure plate method described by Fredlund (2019). Recently, the tensiometer method for determining SWRCs (e.g. le Roux, 2019) has gained popularity in South Africa.

Each SWRC can also be represented by a mathematical equation and several methods are available. A popular method is the one proposed by Fredlund & Xing (1994). With their method, using the saturated and residual water contents, a SWRC can be represented using three curve fitting parameters (a, n and m). These parameters are related to the geometric shape of the SWRC and guidance on how to determine these parameters is provided by Fredlund & Xing (1994).

© University of Pretoria

2.3.3.2 Bishop effective stress

Although effective stresses play a much smaller role in unsaturated soil mechanics when compared to saturated soil mechanics, it is sometimes useful to obtain an equivalent stress value for comparison purposes. Despite the fact that such comparisons inherently have significant limitations, they can be useful in some instances.

A popular method to calculate an equivalent effective stress for an unsaturated soil is the approximation suggested by Bishop (1959). This approximation includes a dimensionless parameter χ to account for the degree of saturation of the soil, as well as the soil type. Upon further inspection of the approximation, some uncertainties, specifically related to the aspects of volume change and shear strength of unsaturated soils were noted (e.g. Bishop & Blight, 1963). To address these concerns, several researchers have since proposed slight modifications to the initial approximation. One such approach is that proposed by Bolzon et al. (1996) where the χ parameter is replaced with degree of saturation. The modified equation showed good correlation to experimental test data on kaolin clay.

Several alternative methods have since been proposed to estimate an equivalent effective stress for an unsaturated soil, with some researchers even suggesting a closed form solution (e.g. Lu et al. , 2010). However, on a fundamental level, all these estimations suffer from the same limitation that effective stress is not a particularly good parameter to use to characterise the state of an unsaturated soil (e.g. Zhang & Houston, 2024). Therefore, the approach suggested by Bolzon et al. (1996), shown in Equation (3), was used for this study based on its relative simplicity and correlation with experimental data.

$$\sigma^* = \sigma + S_r(u_a - u_w) - u_a \quad (3)$$

Where:

σ^* = Bishop effective stress (kPa)

σ = Total normal stress (kPa)

u_a = Pore air pressure (kPa)

u_w = Pore water pressure (kPa)

2.3.4 Previous testing on gold tailings

As can be expected, there has been substantial research into the behaviour of gold tailings over the years. Figure 2.26 shows the grading curves of the gold tailings tested by other researchers. It

© University of Pretoria

can be seen that there is a fair spread of the data, with the average grading of the gold tailings tested as part of this study falling in the middle.

Perhaps the most well-known investigation into the shearing behaviour of gold tailings is the laboratory round-robin conducted by Reid et al. (2021). In the study, 16 International laboratories were provided with bulk samples of gold tailings obtained from an active tailings dam in Australia. No constraints were provided regarding the testing or interpretation methodologies, the laboratories were simply asked to determine the CSL for the material. A few outliers were noted, mostly due to inadequate procedures followed to determine the end of test moisture contents. However, once these results were excluded, a unique CSL was identified across all the test results to within a void ratio of 0.04.

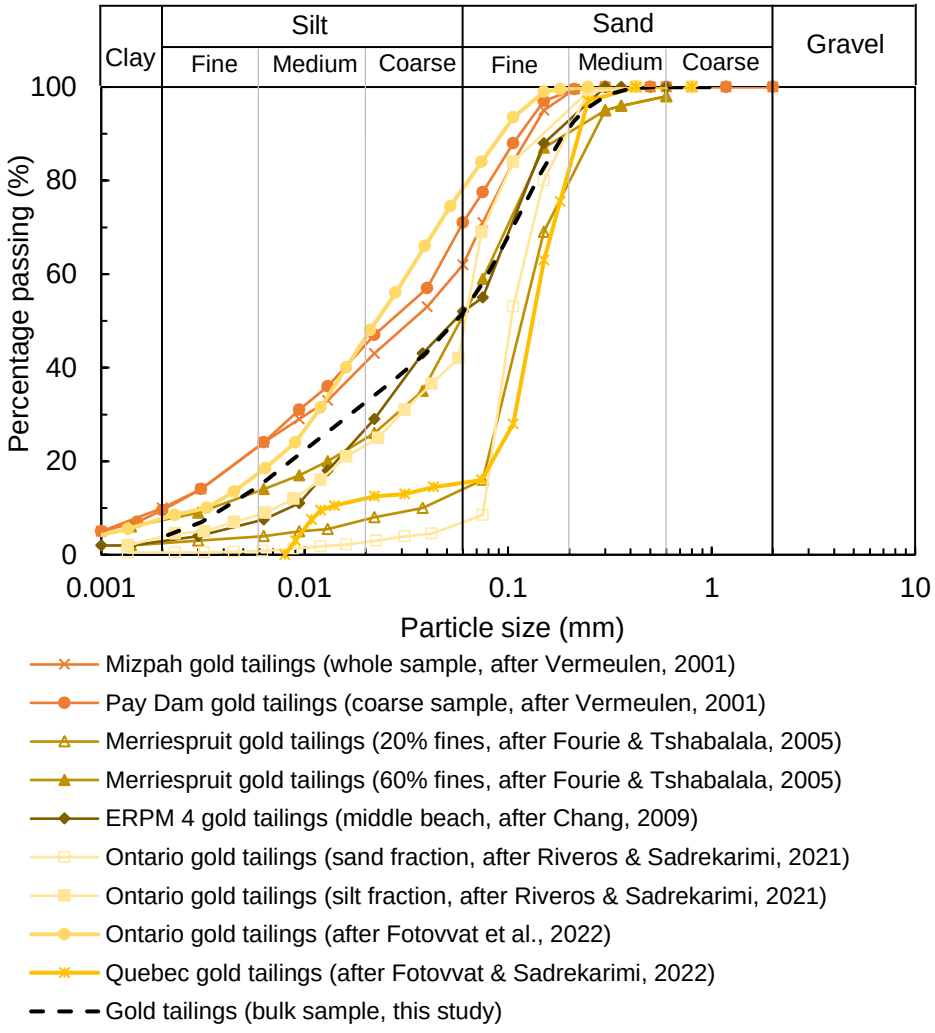


Figure 2.26: Grading curves of previous testing regimes on gold tailings

In terms of gold tailings mined from the Witwatersrand Supergroup, three particular studies are of interest: Vermeulen (2001), Papageorgiou (2004) and Chang (2009). Vermeulen (2001)

© University of Pretoria

investigated the composition and state of tailings from the Mizpah and Pay dams. Both dams were located in the Free State in South Africa. The Mizpah tailings dam still exists today (HGM, 2023) but Pay dam was remined several years ago.

Papageorgiou (2004) conducted a comprehensive laboratory investigation into the liquefaction behaviour of the Merriespruit gold tailings. These tests were supplemented by Tshabalala (2003) and Fourie & Tshabalala (2005). It was found that the fines content has an influence on the critical state friction angle as well as the location of the CSL in $e - \ln p'$ space.

Riveros & Sadrekarimi (2021) conducted a number of DSS tests on gold tailings obtained from a mine in Ontario, Canada. As was noted for the gold tailings from the Witwatersrand supergroup, these Canadian gold tailings were mostly quarzitic in terms of mineralogical compositions. These tailings did however contain components of phlogopite, chalcopyrite, beryl and chlorite. These minerals are not typically found in gold tailings mined from the Witwatersrand supergroup. The samples were prepared using the MT and SD preparation techniques to loose initial states.

The purpose of the study was to determine the undrained response of the silt and sand fractions of the tailings under different hydraulic boundary conditions and different fabrics. It was concluded that the effects of fabric for the undrained shearing behaviour of gold sand tailings is small for practical purposes. However, for the gold silt tailings, it was found that fabric does influence the undrained shear response. The SD samples exhibited initial contraction followed by dilation while the MT samples exhibited contractive behaviour only. This is similar to the behaviour observed for the silty South African gold tailings tested by Chang (2009), discussed in Section 2.3.2.

In another study, Fotovvat & Sadrekarimi (2022) performed a number of TXC and TXE tests on both isotropically and K_0-consolidated samples of gold tailings sourced from a mine in Quebec, Canada. The intent was to investigate the influence of mode of shear and stress conditions during consolidation on the liquefaction behaviour of gold tailings. The material has a similar grading and specific gravity of the tailings considered as part of this study. It was found that the samples sheared in TXE exhibited a more brittle response when compared to the samples sheared in TXC. Two different CSLs were determined for the TXC and TXE tests. Details regarding the influence of the stress conditions imposed during consolidation on the undrained shear response are discussed in Section 2.3.2.

Fotovvat et al. (2022) conducted a series of triaxial tests to investigate the drained instability of gold tailings sourced from Ontario and Quebec in Canada. The Quebec material was the same tailings tested by Fotovvat & Sadrekarimi (2022). However, the Ontario material was different to

© University of Pretoria

the Ontario gold tailings tested by Riveros & Sadrekarimi (2021). Similar to the work done by Sasitharan et al. (1993), it was highlighted that failure can occur under specific drained conditions at stress states significantly lower than the drained failure envelope. Failure was shown to coincide with intersection of the stress path and the collapse surface as described by Sladen et al. (1985).

Recently, extensive testing on mine tailings has been undertaken at the University of Western Australia. These tests have resulted in numerous publications on the behaviour of mine tailings under various conditions. Specifically related to gold tailings, Fanni et al. (2019) discuss the influence of pore water chemistry on the determination of the CSL and provide some guidance on how to address this. In another publication, Fanni et al. (2022) discuss the behaviour of loose gold tailings at large strains and provide some guidance on how to reliably measure liquefied shear strengths in the laboratory.

Although the tests described above contributed to the understanding of the general behaviour of gold tailings, there is still much uncertainty regarding the compression and shear behaviour of gold tailings. This is specifically true in the context of South African gold tailings mined from the Witwatersrand Supergroup. Table 2.4 shows key characteristics of gold tailings tested by other researchers.

© University of Pretoria

Table 2.4: Summary of key characteristics of gold tailings from the literature

Material	**Minimum void ratio, e_{min}**	**Maximum void ratio, e_{max}**	**Specific gravity, G_s**	**Median grain size, D_{50} (mm)**	**K_0**	**Friction angle, φ'(°)**	**Slope of the CSL, λ_e**	**Reference**
Mispah dam, whole tailings	0.480	1.800	2.74	0.030		34.6	0.066	Vermeulen (2001)
Pay dam, penstock coarse			2.74	0.025		31.5	0.068	
Merriespruit, 20% fines	1.326	1.827	2.69	0.120	0.44	26.7	0.075	Papageorgiou (2004)
Merriespruit, 20% fines	1.326	1.827	2.72	0.120	0.44		0.068	Fourie & Tshabalala (2005)
Merriespruit, 60% fines	0.655	0.696	2.69	0.060	0.59	30.0	0.031	Papageorgiou (2004)
Merriespruit, 60% fines	0.655	0.696	2.72	0.060	0.59		0.014	Fourie & Tshabalala (2005)`
ERPM 4			2.69	0.053		33.6		Chang (2009)
Ontario silt tailings	0.590	1.280	3.28	0.062			0.064	Riveros & Sadrekarimi (2021)
Ontario sand tailings	0.790	1.350	3.10	0.104		27.0	0.058	
Quebec tailings	0.680	1.080	2.75	0.134	0.57	38.6	0.060	Fotovvat & Sadrekarimi (2022)
Ontario tailings	0.620	2.080	2.75	0.023	0.55	39.8	0.080	Fotovvat et al. (2022)

© University of Pretoria

2.4 LABORATORY TESTING OF SOILS

2.4.1 Sample preparation methods

As discussed in Section 2.3.2, the state of the soil is known to influence the response of the soil. This is especially important for loose, saturated mine tailings. However, obtaining undisturbed samples of these soils is challenging. Therefore the majority of laboratory testing on tailings involved remoulded samples. This section describes key aspects of some popular sample preparation methods.

The most common sample preparation method for mine tailings is the Moist Tamping (MT) method as it has been shown to allow for the repeatable creation of both loose and dense samples. This an important point as it is known that the density plays an important role in the undrained shear behaviour of sandy soils. In the MT method, a predetermined mass of moist material is compacted into a split mould to a target density, usually in several layers. The under-compaction technique, as described by (Ladd 1978), attempts to improve the final sample homogeneity by reducing the target density of the lower layers to account for the additional compactive effort that will be applied to subsequent layers.

Air Pluviation (AP) is another sample preparation method that is popular for coarse-grained soils. In this method, a predetermined mass of dry soil is dropped from a hopper with a specific drop height and at a target placement rate. The density of resulting sample can be controlled by varying both the placement speed and the drop height (e.g. Vaid & Negussey, 1988).

An alternative technique is the Water Pluviation (WP) method as described by Vaid & Negussey (1988). In this method, the sample is created in layers by pouring a predetermined mass of dry material into a split-mould that is filled with de-aired water. This pouring is performed at a slow rate and the soil essentially displaces the water under its self-weight, resulting in a saturated sample. This method has since been modified by many researchers (e.g. Carraro & Prezzi, 2008; Wang et al., 2011) and is also referred to as the Water Sedimentation (WS) or Slurry Deposition (SD) method.

Modern approaches to this method include mixing the dry tailings with water at a moisture content above the liquid limit and allowing the slurry to air dry. Specimens for testing are then recovered from this mixture. This approach allows for the development of loose samples and is referred to as the air dried technique (e.g. Reid et al., 2022c).

© University of Pretoria

Loose samples prepared by the MT or AP methods, have been shown to exhibit significant collapse during flushing and saturation (e.g. Sladen & Handford, 1987). SD samples have shown to be more resistant to this collapse due their stress history (e.g. Vaid & Negussey, 1988; Reid et al., 2022c).

2.4.2 Oedometer testing

The oedometer test is a simple test that is commonly used to investigate the compressive behaviour of soil. A key aspect of the standard oedometer test is the fact that the soil sample is placed in a stiff ring which restricts lateral movement of the sample during the test. This conditions of zero radial strain during consolidation is referred to as K_0 consolidation and is believed to be representative of the conditions that soils in the field experience as a result of consolidation under their own weight (e.g. Bishop & Henkel, 1962).

Some limitations of the standard test include the inability to confirm saturation, the inability to measure pore pressures, and the fact that no shear phase is possible. However, in most cases these limitations are far outweighed by the simplicity of the test and the ability to reach high stress levels.

Although there is no direct confirmation of the pore pressures, it is common to plot the observed compression behaviour in terms of vertical effective stress. This is due to the fact that at moderate to high stress levels, at the end of the consolidation phase the magnitude of the pore pressure in relation to the total applied stress is negligible and can be ignored. In other words, it is assumed that at the end of each loading or unloading stage when any excess pore pressures have dissipated, the applied load in terms of vertical total stress is numerically equivalent to the vertical effective stress in the sample.

2.4.3 Triaxial testing

2.4.3.1 Introduction

The triaxial test is a popular soil test that can be used to investigate both the compressive and shear behaviour of soil. Developed in the early 1910's, these tests have improved significantly over the years (Deák et al., 2012). Figure 2.27 shows a diagrammatic layout of an early triaxial test. Despite the many advances, the key components remain the same.

A key principle of the triaxial test is the ability to apply forces to the soil sample externally, while at the same time measuring the pore pressure internally. This is achieved by the use of a latex

© University of Pretoria

membrane to seal the sample. This is important as it allows for the calculation of the effective stress within the sample.

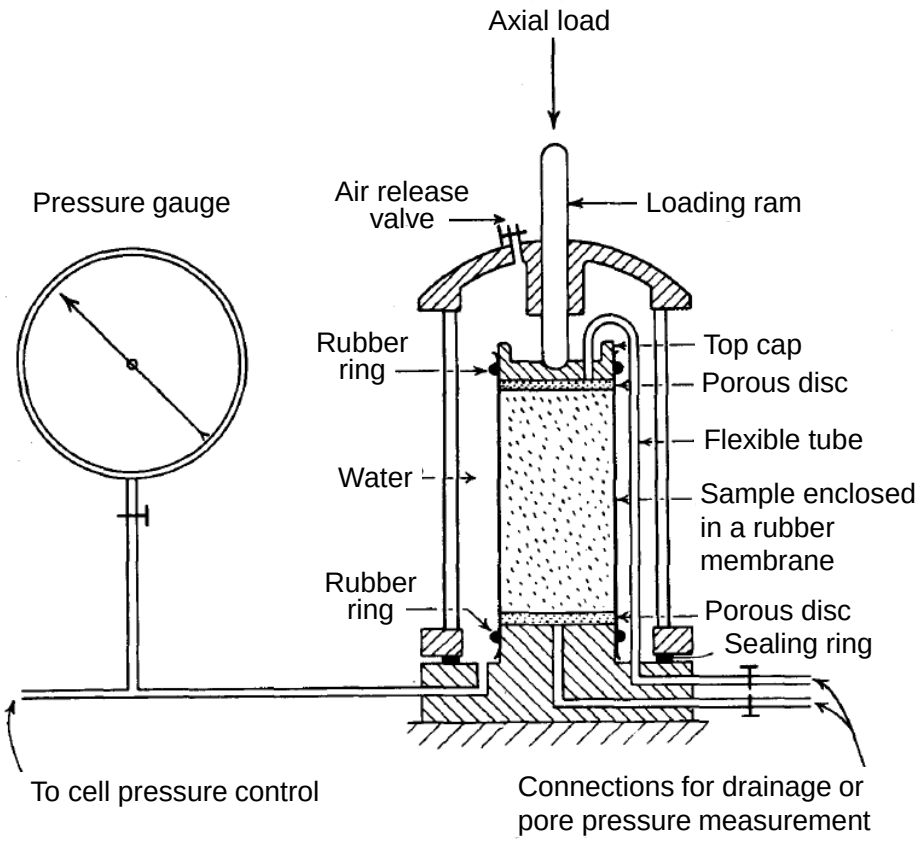


Figure 2.27: Diagrammatic layout of a triaxial test (after Bishop & Henkel, 1962)

2.4.3.2 Stages of a conventional triaxial test

In a conventional triaxial test, there are six main phases: sample preparation and installation, flushing, saturation, consolidation, shearing and decommissioning. Only three phases are briefly discussed here but there are many excellent references that provide a detailed description of all six phases (e.g. Bishop & Henkel, 1962; Lade, 2016; da Fonseca et al., 2021).

During the consolidation phase, a desired stress state is imposed on the sample so that shearing can commence. Consolidation can either be performed isotropically or anisotropically depending on the desired stress state. Since the pore pressure is typically only measured at the base of the sample and only one-way drainage is permitted, there is usually a pore pressure gradient within the sample during consolidation. This means that the true effective stress of the sample can only confidently be known at the start and end of consolidation. Consolidation is therefore usually conducted in stages.

© University of Pretoria

During the shearing phase, the sample can either be sheared under strain-controlled conditions, or load-controlled conditions. Depending on the desired hydraulic conditions, the drainage valve can either be closed or left open. The rate of shearing is important and is usually determined based on the observed behaviour during the consolidation stage (e.g. Bishop & Henkel, 1962). The results from the shear stage can be used to determine the CSL. When presented on an $e - \ln p'$ graph, the slope the CSL is represented by the symbol λ_e.

During the decommissioning phase, it is crucial to determine the end of test void ratio. Details of this process are discussed further in the next section.

2.4.3.3 General comments regarding triaxial testing

In previous sections, it was shown how even a small change in void ratio can significantly change the undrained behaviour of a soil. It is therefore important to accurately track the void ratio of a sample through the various stages of a triaxial test. Sladen & Handford (1987) showed how loose, sandy soils were susceptible to significant collapse during the flushing and saturation stages. This is important as it is not a trivial matter to accurately capture the change in volume of samples that collapse during flushing and saturation. This is due to the air in the sample which, unlike water, is compressible. It is therefore difficult to separate volume changes due to replacement of the air voids with de-aired water, and volume changes due to compression of the air phase within the sample.

“Backwards” based calculations are therefore generally preferred. In a “backwards” based calculation, the end of test void ratio is determined, and the void ratio during shearing and consolidation is determined based on this value. Since the samples have been verified as saturated during these phases, there is less uncertainty the components of measured volume change. Modern techniques to determine the end of test void ratio include the End of Test Freezing (EOTF) method as described by Jefferies & Been (2015), or the squeezing method as proposed by Verdugo & Ishihara (1996). Although the EOTF method is the preferred method (e.g. Jefferies & Been, 2015; da Fonseca et al., 2021; Reid et al., 2021), implementation of the method required modification of standard triaxial equipment. Conversely, the squeezing method requires no modifications and has been shown to provide comparable results to the EOTF method (e.g. Torres-Cruz, 2016). It should be noted that no comparisons were made in this study between the performance of the EOTF and squeezing methods for the gold tailings tested.

There is some debate on the use of enlarged and lubricated end platens, with researchers having varying opinions on their use. The intent of these modified platens is to reduce the development of

© University of Pretoria

stress concentrations at the ends of triaxial samples (Rowe & Barden, 1964). The enlarged end platen is specifically to cater for a potential increase in the diameter of dilative soil samples while the lubrication attempts to reduce the influence of platen restraint. For example, Jefferies & Been (2015) and da Fonseca et al. (2021) strongly recommend that enlarged and lubricated end platens be used for all triaxial testing. However, Zhang & Garga (1997) showed how the use of enlarged and lubricated end platens had a minimal effect on the stress-strain response of loose Unimin sand. Klotz & Coop (2002) noted how, even with the inclusion of enlarged and lubricated end platens, sample barrelling (and therefore stress concentrations) was still noted for medium dense Leighton Buzzard sand.

More recently, Sottile et al. (2023) showed in a series of numerical simulations on a clean sand how the inclusion of lubricated end platens resulted in more uniform stress distribution within the triaxial sample, compared to tests where non-lubricated end platens were considered. In fact, when the ends weren't lubricated, shear bands were noted to form within the specimens. These findings supported the experimental work by Omar & Sadrekarimi (2014) where triaxial tests on loose Ottawa sand showed that the use of enlarged and lubricated end platens reduced specimen bulging and resulted in more homogenous specimen defomation. However, as pointed out by Sachan (2011), the use of lubricated end platens influences the drainage boundary conditions and this needs to be carefully considered when performing drained triaxial tests.

There is still much uncertainty regarding the effectiveness of enlarged and lubricated end platens for routine triaxial testing. For this study, since it was primarily loose, contractive samples that were of interest, it was decided that enlarged and lubricated end platens would not be used. This is in line with triaxial testing by other researchers on mine tailings (e.g. Vermeulen, 2001; Papageorgiou, 2004; Chang, 2009; Torres-Cruz, 2016).

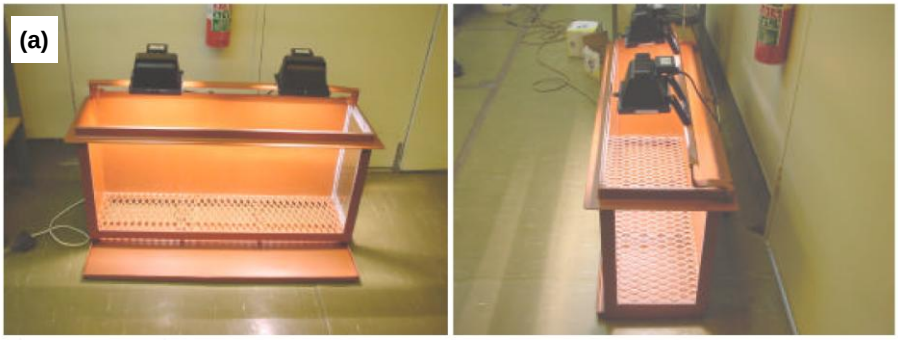
Another key issue related to the interpretation of triaxial test data is the occurrence of shear bands (strain localisation). This is a feature that is mostly linked to large strain response of dense samples in drained shear but can also occur in any triaxial compression test. When shear banding occurs, the local void ratio is no longer the same as the global void ratio due to the stress concentrations along the failure plane. To determine the true, local void ratio, techniques such as X-ray Computed Tomography (CT) are required. When this is done correctly, the stress paths can be plotted through to critical state (e.g. Desrues et al., 1996). However, in most cases when shear bands are formed, the use of advanced analysis using techniques such as X-ray CT are not possible. Therefore, it is common to no longer plot the global void ratio after the formation of a shear band.

© University of Pretoria

2.4.4 Drying Boxes

A Drying Box is an experiment that is conducted to simulate expected field conditions in a controlled environment. Drying Boxes have been shown to be particularly useful in simulating the deposition and subsequent drying phases that occur in tailings dams as part of routine operations. These tests are particularly well suited as a precursor to actual field deployments. One aspect that needs to be considered when performing Drying Box experiments is the boundary effects. In particular, it is common for shrinkage cracks to initiate at the boundaries. Therefore, the Drying Box should be sufficiently large such that these cracks do not meaningfully influence the drying process.

Drying Box tests have been performed locally (e.g. Westraad, 2004; Wortmann, 2007), as well as Internationally (e.g. Daliri, 2013; Rozina et al., 2015) with great success. Figure 2.28 shows photographs of the local Drying Boxes, while Figure 2.29 shows photographs of the International Drying Boxes. Table 2.5 provides a summary of key aspects from these previous experiments.



Drying Box after Westraad (2004)

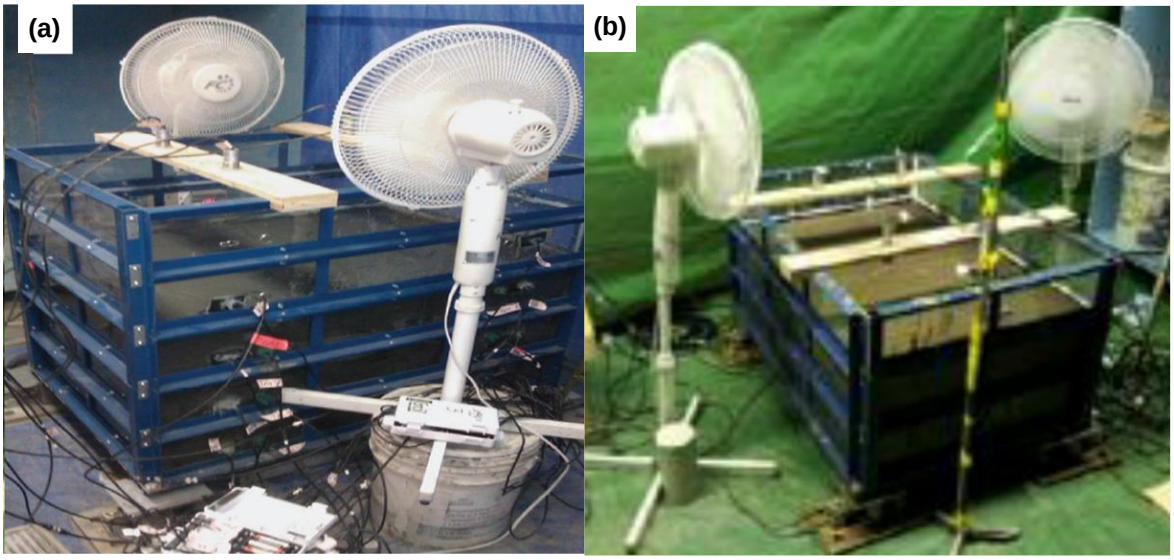
(b)



Drying Box after Wortmann (2007)

Figure 2.28: Examples of local Drying Boxes after (a) Westraad (2004), and (b) Wortmann (2007)

© University of Pretoria



Drying Box after Daliri (2013) Drying Box after Rozina et al. (2015)

Figure 2.29: Examples of International Drying Boxes after: (a) Daliri (2013), and (b) Rozina et al. (2015)

© University of Pretoria

Table 2.5: Summary of previous Drying Box experiments

No	Test Description	Duration (days)	Material	Measurements	Reference
1	A streel-reinforced glass Drying Box with dimensions of 0.30 m width, 1.0 m length, and 0.45 m height was used. Two layers were hydraulically deposited and the test was repeated four times. Two 250 W halogen lights were used to simulate sun drying.	9	Mispah gold tailings	Mass of the Drying Box, mass of water draining from the box, suctions at several locations in the box.	Westraad (2004)
2	A streel-reinforced glass Drying Box with dimensions of 0.43 m width, 0.6 m length, and 0.45 m height was used. Only one layer was hydraulically deposited but the Drying Box test was repeated five times. Four 250 W halogen lights were used to simulate sun drying.	24	Mispah gold tailings	Mass of the Drying Box, suctions at several locations in the box.	Wortmann (2007)
3	A steel-reinforced Plexiglas Drying Box with dimensions of 0.7 m width, 1.0 m length and 1.2 m height was used. Five layers were hydraulically deposited and two rainfall events were simulated. No lights were used to simulate sunlight, rather fans were used to simulate wind.	72	Thickened Tanzanian gold tailings	Mass of the Drying Box, mass of water draining from the box, suctions and volumetric moisture contents at several locations in the box.	Daliri (2013)
4	A steel-reinforced Plexiglas Drying Box with dimensions of 0.7 m width, 1.0 m length and 0.6 m height was used. Three layers were hydraulically deposited and two rainfall events were simulated. No lights were used to simulate sunlight, rather fans were used to simulate wind.	150	Canadian oils sands tailings	Mass of the Drying Box, mass of water draining from the box, suctions and volumetric moisture contents at several locations in the box.	Rozina et al. (2015)

© University of Pretoria

2.5 GEOSTATIC STRESS RATIO

A key objective of this research is to measure the in-situ stress state in a tailings dam. The true in-situ stress state has six components: three normal stresses and three shear stresses (e.g. Parry, 2004). For engineering purposes, it is often useful to consider two-dimensional simplifications of three-dimensional problems. One such approach is a plane-strain model, where it is assumed that the structure being modelled is infinitely long in the axial direction, such that strain in the axial direction is zero. Plane-strain conditions are commonly assumed for long embankments with a consistent cross section. Under these conditions, the in-situ stress state can be represented by a much simpler stress ratio.

One such method to describe the stress state of a soil is the geostatic stress ratio (K_0). K_0 is defined as the ratio between the horizontal and vertical effective stress as shown in Equation (4) (Shuttle et al., 2021). The use of K_0 allows the magnitude of anisotropy to be quantified which will be shown to be quite useful in characterising the stress state of a soil.

$$K_0 = \frac{\sigma'_h}{\sigma'_v} \tag{4}$$

Where:
K_0 = Geostatic stress ratio
σ'_h = Horizontal effective stress (kPa)
σ'_v = Vertical effective stress (kPa)

At this stage it is important to distinguish between the types of earth pressures. In addition to the at-rest earth pressure coefficient (K_0), there exists the active earth pressure coefficient (K_a) and the passive earth pressure coefficient (K_p). The difference between these earth pressures lies in the movement of the soil body required to mobilise these pressures. Active pressures involve expansion of the soil while passive pressures involve compression of the soil. At-rest pressures involve no change in lateral geometry of the soil. Significant work has been done in the areas of active and passive earth pressures (e.g. Rankine, 1856). This study is focused on the at-rest pressures.

In a large structure such as a tailings dam, the conditions of zero lateral strain seem appropriate. Therefore, it is assumed that factors that influence the at-rest pressure ratio (K_0), will also influence the stress ratios in the field.

© University of Pretoria

2.5.1 Importance of K_0

As the geostatic stress ratio describes the current stress state (which includes the stress history required to get to the stress state), it follows that the magnitude of the geostatic stress ratio must influence soil behaviour. Figure 2.30 shows the undrained shearing behaviour of three silty tailings samples. The results were obtained from numerical simulations using the NorSand constitutive model (Jefferies, 1993), and general silty tailings parameters after Been (2016).

Although the purpose of the figure is to illustrate the potential drained stress paths that could eventually lead to undrained collapse, the figure is also useful to describe the undrained shearing behaviour of soils at different anisotropic stress conditions. For example, Samples A, B and C could be distinguished based on different K_0 values. It can be seen that there is a gradual reduction in reserve strength after the initiation of undrained shearing from Sample A to Sample C. This occurs to such as extent that for Sample C, there is no reserve strength and collapse initiates immediately upon undrained shearing. As shown in Section 2.5.6, these anisotropic conditions can also exist due to sloping ground conditions, for example near the outer wall of a tailings dam.

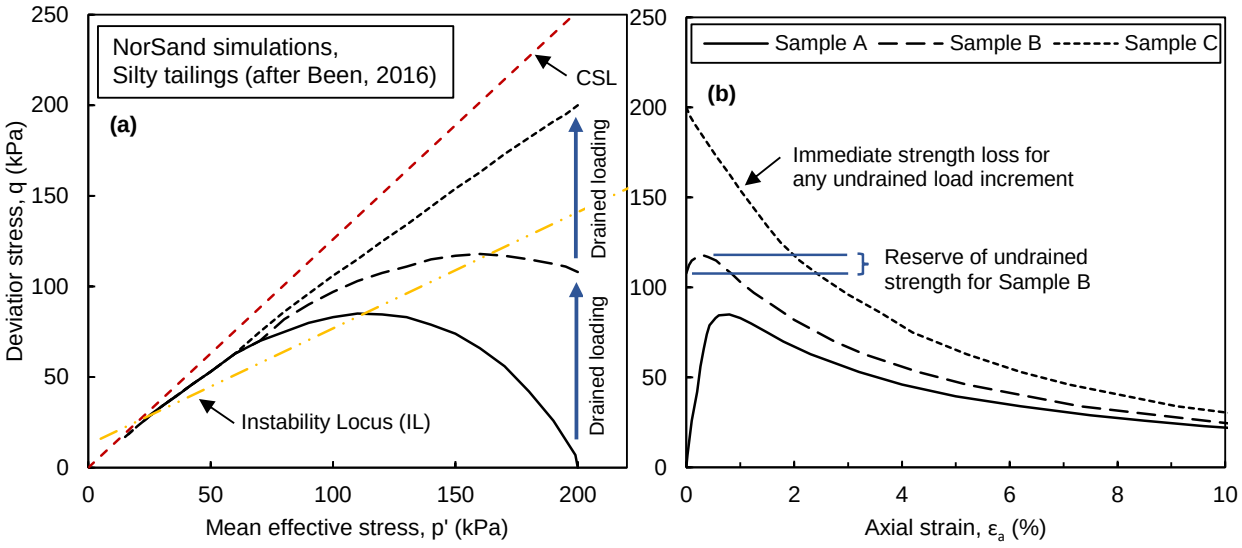


Figure 2.30: Numerical simulations of silty tailings at various initial stress states (after Jefferies et al., 2019)

In terms of numerical analyses, Reid et al. 2022a) conducted a study to investigate the influence of K_0 on the stability of a hypothetical, upstream constructed tailings dam. To initiate failure, the phreatic surface was slowly raised within the dam. Failure occurred when the embankment was saturated to such a state that the stress path crossed the instability line, a stress path referred to as Constant Shear Drained (CSD) (e.g. Sasitharan et al., 1993). It was found that, when failure occurred, the horizontal distance of the phreatic surface from the toe varied from 8 m to 23 m as K_0 was changed from 0.8 to 0.5. This is a meaningful difference in pore pressure conditions for a

© University of Pretoria

reasonably small change in K_0.

In separate studies, Zheng (2022) and France et al. (2022) also describe how the choice of K_0 played a significant role in the outcome of the stability assessment of the tailings dam and water retaining embankment under considerations, respectively. Knowledge of the in-situ K_0 value is therefore of great interest to geotechnical practitioners involved in designs and safety evaluations of tailings dams and water-retaining embankments.

2.5.2 Factors influencing K_0

Although it is known that the fabric and stress history influence the undrained shearing response of sandy soils, the influence of these aspects on the K_0 value is perhaps less clear. One particular study of interest is that conducted by Obrician (1969) on the influence of density, stress level and load history on K_0 for sandy soils. As part of the testing, Obrician (1969) designed an apparatus capable of measuring both axial and radial stresses, while at the same time maintain zero radial strain (a key requirement to measure true at-rest lateral earth pressures).

In the first set of tests, samples were prepared at a desired initial relative density (D_r) and then loaded under K_0-conditions in stages to 1 MPa. At each stage, the horizontal and vertical stresses were recorded, and the K_0 value was calculated. In this way, the influence of stress level on the calculated K_0 value could be determined. The initial density was then varied and the loading stages were repeated. The results from these tests are shown in Figure 2.31. It is clear that for the coarse sand, K_0 is influenced by the initial density as well as the current stress level. At the same stress level, K_0 was noted to decrease with increasing initial relative density while at the same initial density, K_0 was noted to decrease with increasing stress level. Chu & Gan (2004) came to similar findings regarding the influence of initial density on the calculated K_0 value noted for medium-loose silica sand during K_0-consolidation.

© University of Pretoria

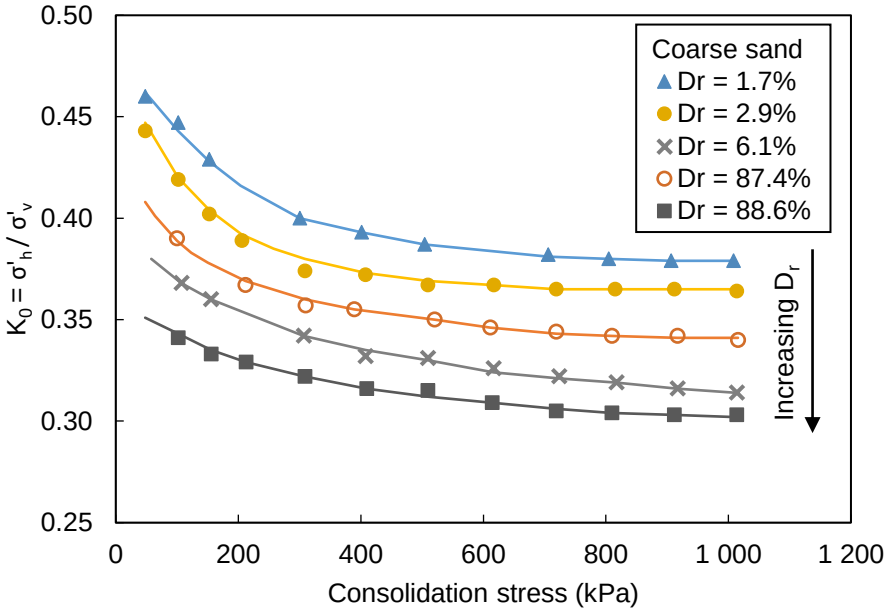


Figure 2.31: Influence of density on K_0 (after Obrician, 1969)

In a second series of tests, the influence of stress history was investigated. For these tests, a coarse to fine sand was used and unloading stages were also included. Figure 2.32 shows the results from the testing on the coarse to fine sand at an initial relative density of 51%. It is clear that there is a meaningful influence of stress history on the at-rest earth pressure. It was specifically found that the K_0 value increased along the unloading cycles and then decreased along the subsequent reloading cycles. At the same vertical stress, the K_0 value obtained for the loading cycle was significantly smaller than the K_0 value obtained for the unloading cycle. The influence of stress history on the calculated K_0 value was also noted by Fukagawa & Ohta (1988), during a series of K_0-consolidtion tests on medium-dense Toyoura sand.

© University of Pretoria

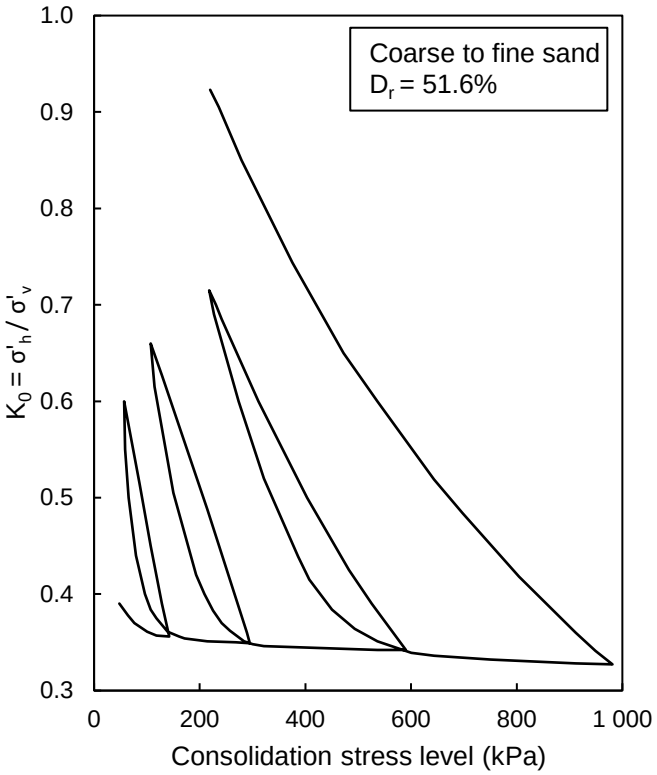


Figure 2.32: Influence of stress history on K_0 (after Obrician, 1969)

As discussed by Jefferies & Been (2015), two studies on the influence of cyclic loading on K_0 are also of interest. The tests were conducted on clean sands with initial void ratios between 0.5 and 0.6 (i.e. soils not in an initially loose state). In the first study, a calibrated membrane was used to measure the horizontal stress in a cyclic simple shear test (Youd & Craven, 1975). In the second study, an oedometer instrumented to measure lateral stress was mounted on a shaking table (Zhu & Clark, 1994). Both studies showed a clear increase in K_0 with increasing number of loading cycles.

Therefore, based on the experimental results discussed in this section, it can be concluded that for sandy soils, K_0 is influenced by the density, stress level and stress history.

2.5.3 Empirical methods to estimate K_0

There are several methods available to estimate K_0, with perhaps the equation proposed by Jaky (1944), as shown in Equation (5), being the most well-known. For a NC soil it was proposed that K_0 is simply a function of the critical state friction angle of the soil.

$$K_0 = 1 - \sin\varphi' \tag{5}$$

© University of Pretoria

Where:

φ' = Effective friction angle (°)

Although Equation (5) is frequently referenced in literature, the original publication was written in Hungarian and several researchers have translated the original text and found discrepancies with common interpretations. For instance, Handy (1983) noted that Equation (5) was actually only published by Jaky (1948) and that the equation proposed in the Hungarian text in Jaky (1944) contained additional terms which were subsequently removed. Additionally, the equation was not developed to define the lateral stress ratio under a broad, level, loaded area as is commonly assumed. Rather, the equation defined a stress ratio at the centre of a pile of sand whose surfaces are inclined at the angle of repose, φ' (e.g. Mesri & Hayat, 1993; Michalowski, 2005).

Despite the above, Equation (5) continues to be used and seems to provide reasonable results for many soil types as noted by Kulhawy & Mayne (1982). There have been several modifications to the original relationship to include aspects such overconsolidation ratio, but these are outside the scope of this study and are not discussed further.

2.5.4 Laboratory measurement of K_0

Laboratory test methods are generally preferred over field test methods as they can be conducted in a controlled environment, typically require less effort and cost less. However, the major limitation of laboratory tests is that the in-situ state of the soil needs to be re-created. For tailings, matching the field density may be the most difficult aspect. Additionally, the stress history imposed in the field is generally not known. These two aspects mean that laboratory-based K_0 tests are fairly limited.

In South Africa, Professors Blight and Ofer also developed a simple laboratory apparatus capable of measuring lateral earth pressures (e.g. Ofer, 1981; Blight & Ofer, 1984). The device was essentially a modified oedometer ring which was instrumented in such a way that the lateral stresses imposed by the soil sample on the ring could be measured. Unfortunately, the device remained a research tool and testing was mainly conducted on expansive clays.

An alternative approach is to perform a special consolidation phase in a triaxial cell. In this test, the loading ram is used in conjunction with the cell pressure controller such that the sample is consolidated in small steps while at all times maintaining no change in lateral geometry of the sample. This requires the use of a radial calliper and is referred to as K_0-consolidation. Provided

© University of Pretoria

the results from the calliper indicate that there has been minimal change in the diameter of the sample, this ratio of lateral and axial stress can be taken as the K_0 value for the sample. This process has been successfully performed on many soils by many researchers and is the approach used to generate the triaxial test results reviewed in Section 3.2.

At this stage, a key question to consider is whether the measured stress ratio should be scaled depending on the stress conditions. For example, should a stress ratio measured in a triaxial test (axis-symmetrical stress conditions) be used directly in a numerical analysis where plane-strain stress conditions are assumed? As described by Reid et al. (2022a) there are conflicting approaches taken in the literature. For example, Wanatowski & Chu (2012) presented experimental test results which suggest that the stress ratios should be scaled between the various stress conditions. Conversely, it appears that in some cases Morgenstern et al. (2016) considered the stress ratios determined from triaxial tests directly in their numerical models. For this study the stress ratios determined in the field were compared directly to the response of the soil due to the stress ratios imposed in the laboratory.

2.5.5 Field measurement of K_0

Several methods are available for field measurements of K_0 and a brief overview of some of these methods is provided in the following section. A more comprehensive description of these methods can be found in Hayat (1992) and Lindgård & Ofstad (2016).

2.5.5.1 Use of Earth Pressure Cells (EPCs)

Despite concerns regarding their accuracy (as discussed in Section 2.6.1, several researchers have shown how EPCs can be successfully used for long-term field monitoring if designed and installed correctly. For example, Rankka (1990) installed push-in, spade-shaped Glötzl, diaphragm-type EPCs in a number of glacial clay slopes in Sweden. The lateral earth pressures measured with these EPCs showed good correlation with the lateral earth pressures measured using a dilatometer and those estimated using numerical techniques. In general, the differences between the lateral earth pressures measured using the EPCs and those measured using the dilatometer was found to be less than 20 percent, with many regions showing differences of less than 10 percent.

In another study, Brackley & Sanders (1992) installed vibrating wire, diaphragm-type EPCs in an unsaturated, highly-expansive lacustrine clay deposit. The EPCs were 280 mm in diameter and 38 mm thick. The study was conducted over a period of three years at the Leeuhof test site in South Africa. Over this time it was noted that the horizontal pressures were two to three times

© University of Pretoria

larger than the vertical pressures recorded.

During the study, it was found that several of the EPCs stopped working during the monitoring period. Upon recovery of the EPCs, it was found that the EPCs were subjected to various degrees of corrosion. Therefore, a key learning from this work is that the EPCs should be corrosion resistant to ensure effective long-term performance. In terms of drift, zero readings were obtained for the EPCs when they arrived from the manufacturer, and again one year later (prior to installation). The zero readings were found to be consistent which supports the opinion that vibrating wire sensors are resistant to long-term changes in zero readings (e.g. Bordes & Debreuille, 1984).

More recently, Bruggemann & Gosden (2004) instrumented the main earthen embankment of the Thika Dam in Nairobi, Kenya. Unfortunately no reliable data were obtained as the cables were damaged due to poor waterproofing of the splice kits. After five years, only one of the initial EPCs was still functioning. Therefore, an important lesson to incorporate into this study is that appropriately robust splice kits are used to ensure the longevity of the monitoring system.

In terms of the use of EPC on mining sites, Rosenzweig et al. (2020) presented results from vibrating wire, hydraulic-type EPCs installed in an active overburden dump at a lignite mine in Eastern Germany. This is discussed further in Section 2.5.6.

Although the details are limited, Kudla et al. (2022) discussed the monitoring of an old Sedlitz mining pit. Eight EPCs were installed at various depths in loosely bedded sands with a fines content ranging between 2 and 8%. The same EPCs that were used by Rosenzweig et al. (2020) were used for this study. The vertical and horizontal stresses were monitored over a four-year period as the water table was gradually raised. Comparable field results were obtained to those observed in technical trials conducted at the Technical University of Freiber by the same researchers a few years earlier, indicating satisfactory performance of the EPCs.

2.5.5.2 Hydraulic fracturing

Hydraulic fracturing is a popular field method for estimating the in-situ lateral stress. As proposed by Bjerrum & Anderson (1972), the method works on the assumption that when an increase in fluid pressure is applied at a point in a soil, fissures develop in the soil in a direction perpendicular to the minor principal stress. Once the fissures have developed, the fluid pressure begins to drop. This process continues and the fluid pressure at which the fissures close is equal to the in-situ pressure acting perpendicular to the fissures. This pressure is assumed to be numerically equivalent to the at-rest lateral earth pressure. This method has been successfully implemented in

© University of Pretoria

clays by many researchers (e.g. Lefebvre et al., 1991).

As hydraulic fracturing is generally one of the failure modes that is considered when performing risk assessments, this test is rarely conducted on tailings dams. This method is most appropriate for clays where K_0 is less than 1.0. It is also important to consider the geometry of the piezometer used to monitor the pore pressures, as well as to ensure that sufficient time is allowed between the installation of the piezometer and the start of the test such that installation disturbances are minimised.

2.5.5.3 Flat dilatometer testing

The flat dilatometer is a push-in device similar to a cone penetrometer. The dilatometer itself consists of a stainless steel blade with a thin, flat circular, expandable steel membrane on one side (Marchetti, 1980). The dilatometer is pushed into the ground and at selected depths, the membrane is inflated by means of a pressurised gas. The pressure and deflection of the membrane are recorded as the membrane is inflated. This is typically repeated a few times. Several correlations are available to relate these measured parameters to soil properties. However, it is important to account for membrane stiffness and seating pressures when interpreting dilatometer data. Fortunately, these corrections are included in most standards test methods.

A key advantage of modern dilatometers is that they are designed to fit with standard cone penetration rods, so no additional rods or rigs are required. However, despite the numerous advantages of the test, flat dilatometer testing in South Africa still remains limited.

2.5.5.4 Self-boring pressuremeter

The Self-Boring Pressuremeter (SBP) is considered to be the least intrusive method to estimate K_0 in the field. However, as with all field tests, this is highly dependent on the skill of the operator. It is common to over-bore which causes significant disturbance of the soil and should be avoided.

The most common method of testing using the self-boring pressuremeter is to drill a borehole to just above the target test depth. The pressuremeter is then lowered into the hole and pushed ahead of the target depth. Jetting fluid is typically pumped around the pressuremeter as it is pushed into the soil to minimise disturbance (e.g. Shuttle et al., 2021). Once the pressuremeter is at the target depth, the pressuremeter is inflated and the corresponding pressure readings are recorded. However, even when performing this test according to the standard test method, there are some uncertainties regarding the interpretation. These uncertainties are particularly related to the lift-off pressure as well as corrections required for the membrane stiffness. Further details regarding

© University of Pretoria

these uncertainties and methods to address them are discussed by Shuttle et al. (2021).

2.5.5.5 Comparison of field measurements

In the previous sections, four field methods to determine K_0 were described. However, in addition to knowing the available field methods, it is important to understand the advantages and limitations of each method. This can be done by comparing the results from the various methods at test sites were the in-situ soil conditions are known.

Hamouche et al. (1995) conducted such a review, where three in-situ test methods for determining the in-situ K_0 values were reviewed: the self-boring pressuremeter, hydraulic fracturing, and the flat dilatometer. Three sensitive clay sites in Eastern Canada were considered for the study. Excellent correlation was noted between the three methods and the known in-situ K_0 at Sites A and B where the Overconsolidation Ratio (OCR) was between 1.1 and 1.4 and 2.4 and 4.7, respectively. Poor correlation was noted at Site C where the OCR was between 4.9 and 5.5.

Ideally, a similar comparison on sandy soils would be useful for this study but to the author's knowledge, no such investigation has been published.

2.5.6 Measurements on site

Although it is known that the geostatic stress ratio has an influence on the strength and compressibility characteristics of a soil, there are surprisingly few published case histories were in-situ geostatic stress ratio values have been measured, or even proposed for water-retaining embankments and tailings dams.

Although not strictly for either of the structures mentioned above, the study by Graham & Jefferies (1986) is one of the most well-known studies of in-situ measurements of K_0. As part of their investigation, 16 SBP tests were conducted in loose, hydraulically deposited Erksak sand that formed part of the founding structure of the Molikpaq offshore oil platform. Seven of the 16 tests were determined to provide reliable results and it was found that the equation proposed by Jaky (1944) provided a lower bound of the measured data, with an upper bound of $K_0 = 1.3$, and an average of $K_0 = 0.7$.

More recently, this range of values for the same dataset was validated by Ghafghazi & Shuttle (2008). In their study the original SBP results were independently analysed using iterative forward modelling, a numerical technique described in more detail later in this section. These studies are

© University of Pretoria

commonly referenced in geotechnical engineering software packages where $K_0 = 0.7$ is suggested as a reasonable value for use for loose or normally consolidated soils if no further information is available (e.g. Bentley Systems, 2023b).

Based on the literature available, only five relevant sites were found where attempts were made to quantify the geostatic stress ratio. These sites are reviewed in this section. A similar review was conducted by Narainsamy & Jacobsz (2023a).

2.5.6.1 Cadia Northern Tailings Storage Facility

On 9 March 2018, a slump occurred at the NTSF at the Cadia Valley Operations in Australia. No loss of containment occurred, and no injuries nor deaths were report. However, this incident was considered serious enough that an independent investigation was commissioned (Jefferies et al., 2019).

The NTSF is a modified centreline gold tailings facility which was approximately 60 m high at the time of the failure. As part of the independent investigation, a numerical analysis of the NTSF was conducted. The NorSand soil constitutive model was used to model the soil behaviour. NorSand is a powerful constitutive soil model based on CSSM principles and has been shown to be highly effective in capturing a wide variety of soil behaviour (e.g. Jefferies, 1993; Jefferies & Shuttle, 2005).

Both two and three-dimensional numerical models were analysed using the finite difference software Fast Lagrangian Analysis of Continua (FLAC) (Itasca, 2015). To incorporate the stress history imposed on the tailings during the life of the facility, the NTSF was virtually constructed in layers in the numerical model. The size and timing of the lifts was determined based on a review of available satellite images and construction records. Consolidation was allowed to take place between the lifts and the process was validated by comparing the results from the numerical model to the site records including topographic surveys, drain flow readings, and piezometer readings.

Based on the interpretation of the CPT data, an initial K_0 value of 0.7 was specified for the tailings at deposition. During subsequent deposition and consolidation, this K_0 value changed. By tracking individual soil elements within the model, it was possible to observe how this value changed with time. This is shown in Figure 2.33. At the time of the failure, the numerical investigation showed that the K_0 value in the region where the slump occurred had reduced to a value of approximately 0.5. It should be noted that the NorSand soil model has been shown to overpredict the K_0 value in many cases (e.g. Castonguay & Konrad, 2016). This is likely due to the shape of the yield surface

© University of Pretoria

used in the model. These calculated values could therefore likely be greater than those in the field.

Unfortunately, there were no direct field measurements of K_0 at the site to verify this value. However, the good correlation of the numerical model with the available site data, suggests that the simulated K_0 value is a good estimate. Using a φ' of 34° as determined from TXC testing conducted by the EoR managing the Cadia NTSF at the time of the failure, a K_0 value of 0.44 was estimated using the Jaky (1944) equation.

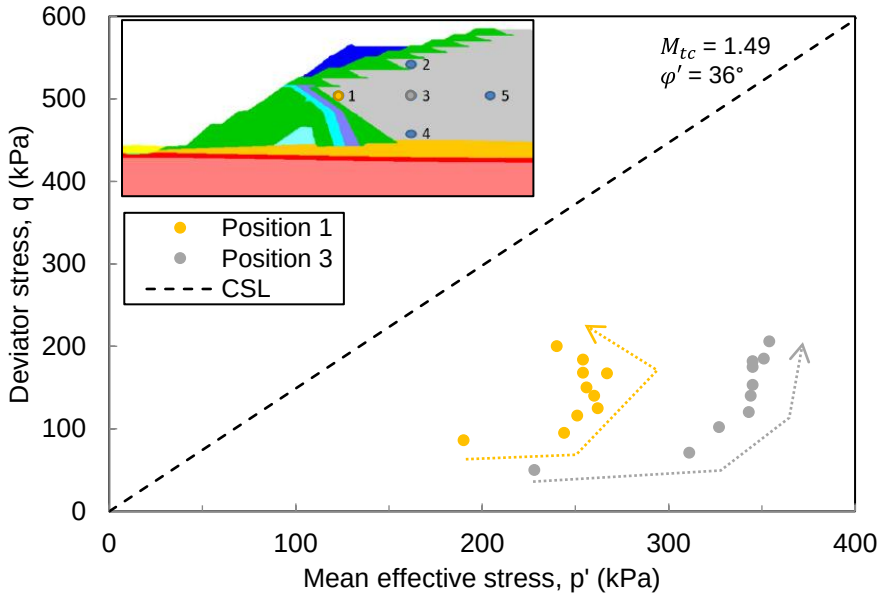


Figure 2.33: Numerical simulations of the evolution of the in-situ stress state at the Cadia NTSF (after Jefferies et al., 2019)

2.5.6.2 Feijão Dam B1

The Feijão tailings dam B1 was introduced in Section 2.2.4 and a detailed discussion was provided on the failure that occurred and the outcome of the two independent investigations that followed. As with the NTSF investigation, the NorSand soil constitutive model was used for the Feijão investigation by Robertson et al. (2019). The same procedure as the NTSF investigation was also followed. There was, however, a key difference. Since there was video footage available of the Feijão failure, it was possible to identify the shape and position of the true three-dimensional failure surface in the numerical models.

For the investigation, a similar approach to that followed by Olson (2001) was taken. Based on the speed of the failure, and the fact that the stability analyses conducted using drained shear strengths showed FoS values in excess of 1.5 (TÜV-SÜD, 2018), it was assumed that undrained shear strengths were mobilised during the failure. It was specifically assumed that yield undrained shear

© University of Pretoria

strengths were mobilised and that, at the moment of failure, a limit equilibrium analysis performed along the failure surface would result in a FoS of 1.0. Therefore, the yield undrained shear strength mobilised at the base of each slice was varied iteratively until a FoS of 1.0 was achieved.

This strength was normalised by the vertical effective stress acting at the base of each slice to obtain a yield undrained shear strength ratio $s_{u(yield)}/\sigma'_{v0}$. Since a three-dimensional stress state existed in the model, it was also possible to normalise the yield undrained shear strength by the mean effective stress to obtain a yield undrained shear strength ratio $s_{u(yield)}/p'_0$. By comparing these strength ratios, an average K_0 value was determined along the slip surface in the numerical model at the time of the failure. The value was determined to be 0.45. A limitation to this approach is the assumption that an equal yield undrained shear strength ratio was mobilised along the entire slip surface at the initiation of failure. This is perhaps an unlikely assumption but is inherent to the method used. However, the calculated strength ratio is still useful for comparative purposes.

The second investigation, by CIMNE (2021), used the same field test results as Robertson et al. (2019). However, a new sampling and laboratory testing plan was implemented. For the CIMNE (2021) investigation, the Clay and Sand Model (CASM) was used. Like NorSand, the CASM is also a critical sate model (Yu, 1998). The model was extended to include a visco-elastic component so that creep, which was identified as one of the causes of the failure by Robertson et al. (2019), could be appropriately modelled.

Unfortunately, not much information is provided in the report regarding how K_0 was determined as part of the investigation. However, it is made clear in the report that a K_0 value of 0.5 was used for the tailings material at the time of the failure. No direct field measurements of K_0 were made in either of the investigations. Using a φ' of 34° as determined by TXC testing for both investigations, a K_0 value of 0.44 was estimated using the Jaky (1944) equation.

2.5.6.3 Lusatian lignite overburden dumps

Prior to 1990, approximately 40 open-cast lignite mining operations were active in Eastern Germany. As part of the mining process, overburden material was removed and dumped using conveyor belts in previously mined areas. The dumps were created with loosely bedded sands with a fines content ranging between 2 and 8%. Over time, many of these mines were closed. After closure, dewatering was stopped, which resulted the local ground water rising by between 30 m and 50 m, thereby saturating the loosely dumped sands. This has resulted in over 100 liquefaction events being reported between 2006 and 2019 (Rosenzweig et al., 2020). By 2022, this number had risen to 125 (Kudla et al., 2022). This is a concern, and several research activities were

© University of Pretoria

commissioned to further investigate these incidents.

In one study, Rosenzweig et al. (2020) installed over 60 sensors at 16 installation locations on an active overburden dump in Lusatia. The intent of the instrumentation was to measure the in-situ stress state in the overburden material and monitor how this stress state changed during and after deposition. Figure 2.34(a) shows a photograph of the dump a few months after the installation when the sensors had been covered by routine conveyor deposition operations. The location of the 16 installations can be seen and the direction of the dump development is also highlighted for reference. To measure earth pressures, hydraulic-type vibrating wire EPCs were installed at various orientations. These EPCs, measuring 250 mm by 150 mm, were installed by hand at a depth of 0.5 m below surface. Figure 2.34(b) shows a photograph of the installation of the various EPCs at installation location 4a. Since the material was placed in a dry state, the pore pressures were assumed to be zero.

The sensors were monitoring over 15 months during which between 7 and 27 m of overburden was placed over the various installations. From 21 EPC pairs, K_0 values ranging between 0.28 and 0.71, with an average of 0.5, were determined. Excellent correlation was noted between the measured vertical stress and the estimated stress from the overburden height. At seven stations, this difference was found to be less than 10%. As an additional check, a numerical model of the dumping process was conducted, and comparable results were obtained between the measured stresses and the stress estimated from the numerical model. Using the Jaky (1944) equation, and a φ' of 30° as determined by TXC testing, a K_0 value of 0.50 was determined.

© University of Pretoria

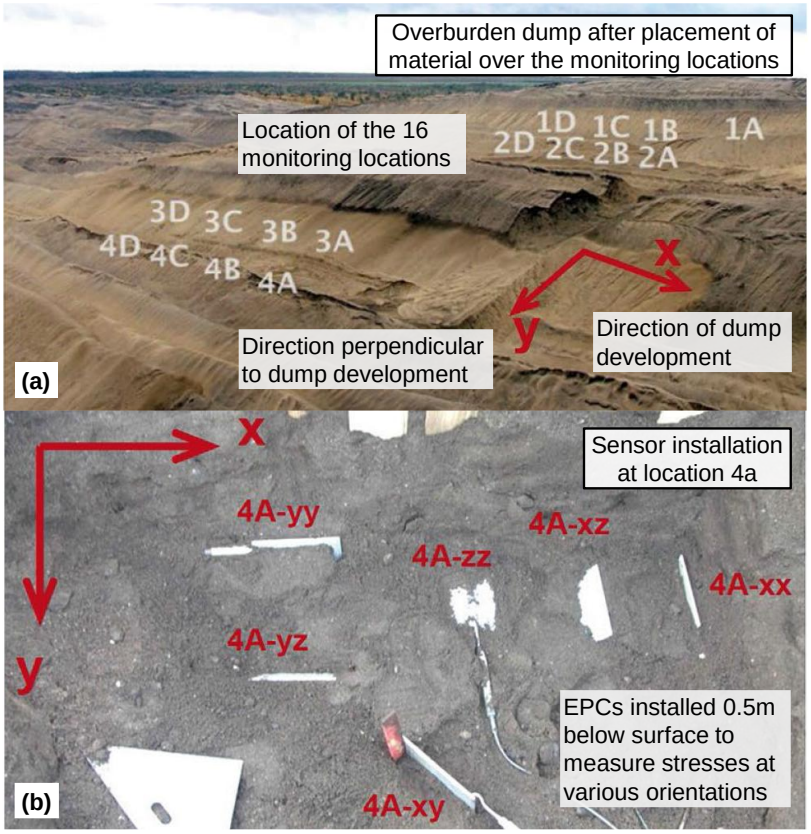


Figure 2.34: Photographs of the Lusatian overburden dumps showing: (a) the location of the monitoring stations, and (b) sensor installation at location 4a (after Rosenzweig et al., 2020)

2.5.6.4 Muskeg River Mine External Tailings Facility

The Muskeg River Mine (MRM) is an oil sands mine located in Alberta, Canada. The MRM has an External Tailings Facility (ETF) where the oil sands tailings are deposited. The ETF is an upstream constructed, ring-dyke facility and two distinct deposition methods are used. The tailings in the dyke's outer shell are deposited in wide layers and are compacted with either D7 or D8 bulldozers while the tailings inside these shells are hydraulically deposited (Shuttle et al., 2021). This is an interesting example as no failure event preceded the investigation. Rather, the investigation was conducted as part of routine operations. Additionally, this was the only case study where a field test was conducted to directly measure K_0.

Fourteen pressuremeter tests were conducted at two locations resulting in a total of 28 tests. Although the pressuremeter is considered the best tool for estimating lateral stress, there are some uncertainties in the interpretation of the results. These specifically relate to the "lift-off" pressure applied at the start of the test and the membrane stiffness. To deal with these uncertainties, a numerical analysis was conducted to improve the interpretation of the test results. A spreadsheet-based, iterative forward-modelling approach was used. In particular, cylindrical cavity expansion

© University of Pretoria

theory was implemented, with the Non-Associated Mohr-Coulomb failure model selected as the soil material model. Additional details regarding this process are provided in Shuttle et al. (2021).

Several deposition strategies are employed at the MRM ETF and this results in soils in different locations within the dam having different geological histories. These influences include compaction efforts immediately after deposition, as well as the loading induced by the seasonal freeze-thaw cycles. This geological history was considered during interpretation of the results.

Figure 2.35 shows the results from the pressuremeter tests at the MRM ETF. The horizontal effective stress determined from the pressuremeter tests and numerical modelling is shown on the horizontal axes, while the vertical effective stress estimated from the sample depth and overlying material density is shown on the vertical axis. Figure 2.35(a) shows a trendline corresponding to a geostatic stress ratio of 0.6 fitted through the measured data. A solid line is shown to correspond with the soil in a normally consolidated state while a dotted line is shown to correspond with the soil in an overconsolidated state. These soils are described as soils with a geological history. An initial offset of 60 kPa is applied to the dashed line and this value is associated with the bearing pressure of the plant used as part of the compaction process.

Interestingly, an alternate view was also presented. For the alternate view, the geologic history was ignored and a single K_0 value of 1.0 was assigned for the entire profile. This is shown in Figure 2.35(b). Using a φ' of 32° as determined by TXC testing, a K_0 value of 0.47 was determined using the Jaky (1944) equation.

© University of Pretoria

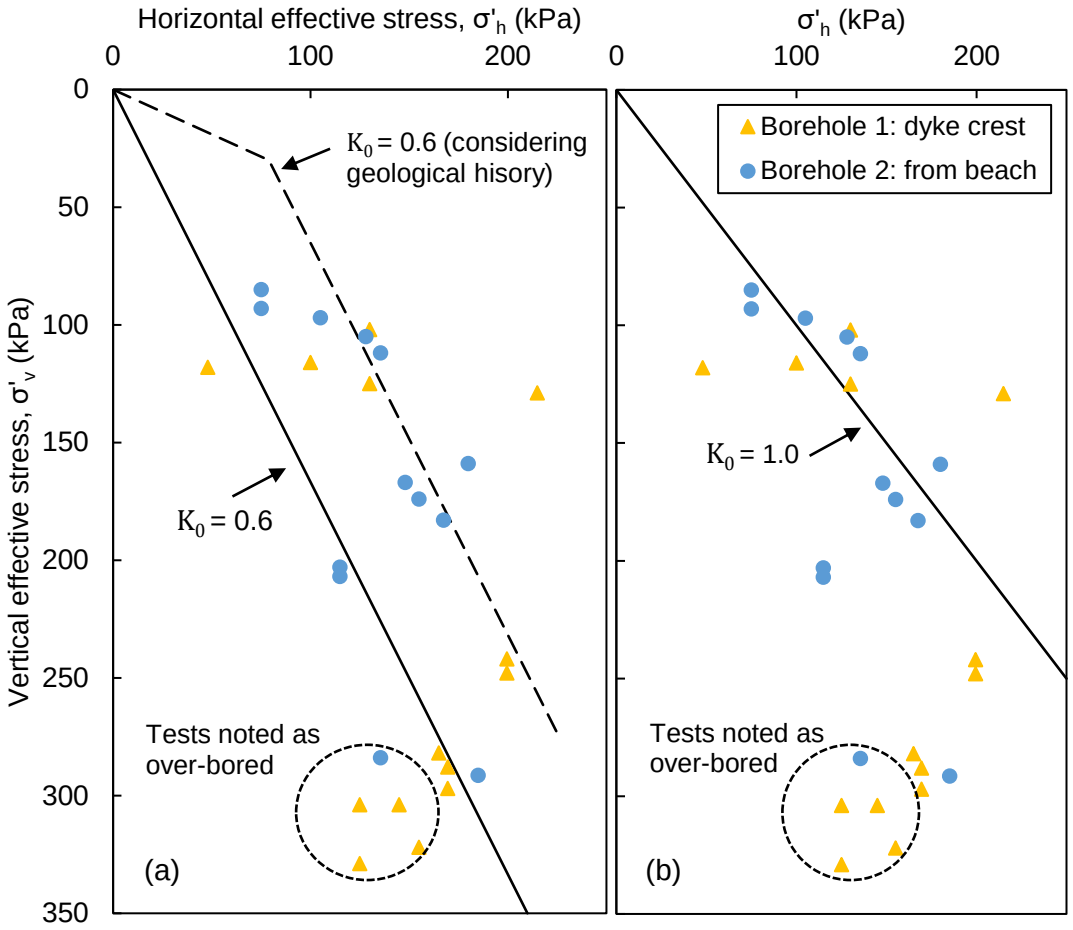


Figure 2.35: Lateral stress measurements at Muskeg River Mine: (a) considering geological history, and (b) an alternate view (after Shuttle et al., 2021)

2.5.6.5 Edenville Dam

As discussed in Section 2.2.4, the Edenville Dam failed in 2020. As part of the failure investigation, the IFT performed a numerical analysis of the embankment. As static liquefaction was deemed to have occurred, a trigger event to mobilise undrained shear strengths was required. Although no specific trigger was mentioned, a number of plausible triggers were listed, including a gradual rise in the water table, which did occur in the hours leading up to the failure.

Based on a review of the field data, a numerical model of the Edenville left embankment was created. A Finite Element Analysis (FEA) was conducted to simulate the loading conditions applicable to the embankment during its operational life. Based on the results from the FEA, a representative K_0 value of 0.6 was determined for the material. Unfortunately, little information was provided regarding the numerical modelling, so it is unclear what soil constitutive model was used.

© University of Pretoria

Figure 2.36 shows the stress state at the base of each slice along the critical slip surface identified as part of the stability analyses conducted. Also shown on the figure is the drained failure envelope and two Instability Locus (IL) lines, representing the estimated range of the ILs for the loose sands present at the left embankment at Edenville. These ILs represent effective friction angles of 18° and 22°, respectively.

The stress state was based on the results from the FEA conducted. It can be seen that the stress state for the slice at the toe lies above the drained failure envelope, while the stress state for the slice at the crest lies below the IL defined with an effective friction angle of 18°. As explained by France et al. (2022), the fact that some stress states at the toe exist in states above the drained failure envelope is not a violation of fundamental soil mechanics principles. It simply means that the excess stress would have been shed to adjacent elements once the slip surface started mobilised (i.e. stress redistribution). The majority of the stress states for the slices between the toe and crest lie between the ILs defined with equivalent friction angles of 18° and 22°, indicating that the embankment was on the verge of instability if undrained conditions were to be mobilised.

Using the Jaky (1944) equation, and a φ' of 31° as determined by direct shear box testing, a K_0 value of 0.48 was determined.

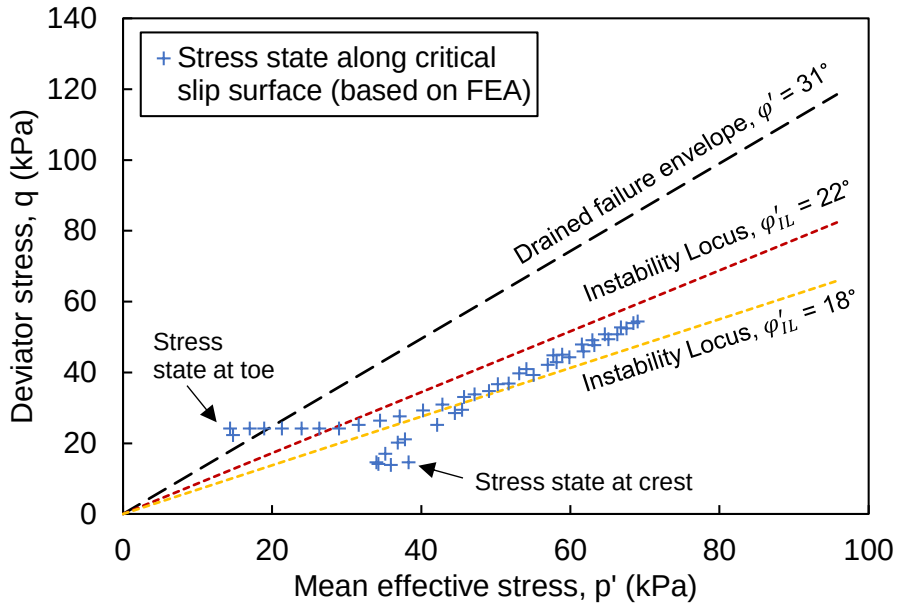


Figure 2.36: Stress state along the critical slip surface (after France et al., 2022)

2.5.6.6 Summary

A summary of K_0 estimates from literature is provided in Table 2.6. Three points are of interest.

© University of Pretoria

The first point is that, with the exception of the alternate view for the MRM oil sands tailings where a K_0 value of 1.0 was proposed, all the other sites showed that the materials in the structural zone were not in an isotropic stress state. Rather, the estimated K_0 values ranged from 0.45 to 0.60.

The second point is that good corelation was noted between the K_0 value estimated as part of the investigations and the K_0 value estimated using the Jaky (1944) equation for the gold and iron ore tailings. However, for these cases, no attempts were made to directly estimate K_0 so it is unclear how accurate the estimates are. In the case of the Lusatian overburden dumps where EPCs were installed, a wide range of K_0 values were obtained. However, the average K_0 value of 0.5 was identical to the value determined using the Jaky (1944) equation.

The third point of interest is that for the MRM site where direct measurements were attempted using the self-boring pressuremeter, a poor correlation was found between the estimated K_0 value and the K_0 values determined using the Jaky (1944) equation. Poor correlation was also noted for the Edenville water dam, however, there is more uncertainty regarding both the material present in the embankment at the time of the failure, as well as the method used to estimate the K_0 value.

Therefore, although there is some evidence that the use of the Jaky (1944) equation to estimate K_0 may be appropriate for tailings dams, care should be taken when using these methods. This is especially true in cases where no direct field measurements are attempted.

© University of Pretoria

Table 2.6: Summary of K_0 estimates from literature

Site	Material	Estimated in-situ K_0	K_0 after Jaky (1944)	Estimation method	Reference
Cadia NTSF	Gold tailings	0.50	0.44	Numerical back-analysis of the failure.	Jefferies et al. (2019)
Feijão Dam B1	Iron ore tailings	0.45	0.44	Numerical back-analysis of the failure.	Robertson et al. (2019)
Feijão Dam B1	Iron ore tailings	0.50	0.44	Numerical back-analysis of the failure.	CIMNE (2021)
Lusatian overburden dumps	Loosely bedded sands with a fines content between 2 and 8%.	0.50	0.50	Response from EPCs installed within the soil.	Rosenzweig et al. (2020)
Muskeg River Mine ETF	Oil sands tailings	0.60 considering geological history or 1.0	0.47	Self-boring pressuremeter tests.	Shuttle et al. (2021)
Edenville water dam	Zoned earth embankment with clean sand on the downstream slope and clay on the upstream slope.	0.60	0.48	Numerical back-analysis of the failure.	France et al. (2022)

.

© University of Pretoria

2.6 SENSORS FOR GEOTECHNICAL APPLICATIONS

It is well known that any design or safety evaluation is only as good as the input parameters used. Therefore, it is of great importance to select appropriate sensors to accurately and reliably measure the soil parameters of interest. In this section, several sensors are described that are used in the subsequent chapters to measure various soil parameters. For each sensor, a brief description of the working principle is provided, as well as key advantages and limitations.

2.6.1 Earth Pressure Cells

The first sensor that will be discussed is the Earth Pressure Cell (EPC). The purpose of an EPC is to measure the total normal stress at a certain point in a soil mass. There is significant scepticism within the geotechnical fraternity regarding the performance of EPC. For example, Hadala (1967) and Brown (1977) both noted that accuracies better than 20 percent cannot be expected from EPCs. Dunnicliff & Green (1988), some 10 years later had a similar opinion and noted that measurements with embedment earth pressure cells can rarely be made with high accuracy. This section attempts to address this concern by first describing the theoretical factors that influence the performance of earth pressure cells. A discussion is then provided in Section 4.3.2 on reasons why stress cells could be used effectively for this study.

2.6.1.1 Types of Earth Pressure Cells

There are two types of EPCs: diaphragm cells and hydraulic cells (Dunnicliff & Green, 1988). For diaphragm-type cells, the external earth pressure is sensed by a deformable, stiff, membrane which is typically supported by an integral stiff, edge ring. A deformation transducer is bounded on the interior face. For hydraulic-type cells, the cell typically consists of two circular steel plates, welded together along the outer edge. A liquid with high compressibility characteristics is placed within the void between the two plates and is hydraulically connected to a nearby transducer. The earth pressure is sensed by the fluid within the cell.

In addition to the two types of EPCs, there are two categories of EPCs: contact pressure cells and embedment pressure cells. Contact pressure cells are used when the pressures at the face of a structural element are of interest and embedment pressure cells are used when the stress within a soil mass is of interest. For this study, the hydraulic-type, embedment EPCs are of interest.

Modern pressure transducers use vibrating wire sensors. The operating principle of a vibrating wire sensor is that, like a piano string, the frequency of vibration of a length of tensioned wire will vary depending on the tension in the wire. Such a wire can therefore be used as a strain gauge. This is

© University of Pretoria

done by plucking the wire, measuring the frequency of the plucked wire, and relating the change in frequency to strain. Vibrating wire sensors therefore provide frequency readings every time the wire is plucked. In modern sensors, the wire is plucked magnetically by an electrical coil near the wire at its midpoint (Dunnicliff & Green, 1988).

In combination with the readings provided from a thermistor, the change in pressure being applied on the EPC can be determined. Calibration curves are typically either linear or polynomial. For most applications, the linear calibration curves are sufficient. An example of a linear calibration is shown in Equation (6).

$$\Delta P = k(f_1^2 - f_0^2) + T(T_1 - T_0) \quad (6)$$

Where:

ΔP = Pressure variation (kPa)

k = Linear calibration factor (kPa/Hz^2)

T = Thermal calibration factor (kPa/°C)

f_1 = Current pressure cell reading (Hz)

f_0 = Initial pressure cell reading (Hz)

T_1 = Current temperature (°C)

T_0 = Initial temperature (°C)

2.6.1.2 Factors affecting the performance of Earth Pressure Cells

Many factors influence the performance of EPCs and there has been significant research into this aspect. Perhaps the most rigorous investigation was that performed by Weiler & Kulhawy (1982). In their study, a literature review was combined with the results from the authors' recent experimental research. Fifteen factors that affect the performance of EPCs were identified. These factors were split into three categories and recommendations were provided for each factor, as discussed below and summarised in Table 2.7.

2.6.1.2.1 Stress cell properties and geometry

1. **Aspect ratio (T/D)** – This term describes the ratio of the thickness (T) to the diameter of the stress cell (D). It was proposed that EPCs with a small aspect ratio will produce the least disruptions of a uniaxial stress field. This was experimentally investigated by the Waterways Experiment Station (WES) in 1945 (Taylor, 1945), who recommended that a (T/D) ratio smaller than $1/5$ be used to minimise the error caused by cell thickness. Weiler & Kulhawy (1982) re-affirmed this design value. Dunnicliff & Green (1988), however,

© University of Pretoria

recommend an even stricter (T/D) ratio of less than 1/10. Unfortunately, limited evidence was provided showing whether this improvement is necessary for engineering purposes.

2. **Soil-cell stiffness ratio (S)** – This term describes the ratio of the stiffness of the surrounding soil to the stiffness of the pressure cell. It is known that a pressure cell stiffer than the soil will result in the cell measuring more stress than is present in the soil (i.e. over-registration), while a pressure cell that is less stiff than the surrounding soil will result in the cell measuring less stress than is present in the soil (i.e. under-registration) (e.g. Benkelman & Lancaster, 1940). This phenomenon has been investigated theoretically (e.g. Monfore, 1950; Tory & Sparrow, 1967) and experimentally (e.g. Peattie & Sparrow, 1954; Selig, 1964) and it was found that provided the cell is stiffer than the soil, the measurement errors remain negligible. Weiler & Kulhawy (1982) recommended that for diaphragm cells, a soil-cell stiffness ratio (S) less than 0.5 should be used to minimise this error.
3. **Diaphragm Deflection and Arching (d/Δ)** – This term describes the ratio of the active face diameter (d) to the deflection (Δ). As described by Weiler & Kulhawy (1982), the term arching in this context refers to the ability of a soil to support itself when an external support is removed. To measure the normal soil stress acting on the cell, there is some deformation of the pressure cell, and this deformation can cause some form of arching. Therefore, this factor needs to be considered for pressure cells. This aspect was investigated by the WES in 1944 (WES, 1944) and it was recommended that the cell diaphragm diameter to deflection ratio (d/Δ) be greater than 2000 to minimise this error.
4. **Stress Distribution on Stress Cell Face (Stress Concentrations)** – This term refers to the distribution of applied load to the face of the stress cell. Based on the numerical analyses conducted by Monfore (1950), it was noted that stress concentrations tended to develop near the edges of the pressure cell. To reduce this effect, it was recommended that the active area of the face be reduced by the introduction of a stiff annular ring around the cell. Monfore (1950) initially proposed that the area of the sensitive face be reduced to 45% of the total area ($d^2/D^2 < 0.45$). Subsequent experimental work by Peattie & Sparrow (1954) showed that this should be ratio should be reduced to 25% for more consistent results (i.e. $d^2/D^2 < 0.25$) however it was noted that these requirements may not be applicable for cells with a diameter greater than 75 mm, which was the largest cells that could be tested as part of their research.
5. **Stress Distribution on Stress Cell Face (Eccentric, Non-uniform and Point Loads)** – It is important that the soil provides a uniform load to the pressure cell and not a series of point loads, which could occur when the size of the soil grains is large, compared to the diameter of the pressure cell. This is particularly important when miniature pressure cells are used. To investigate this, Weiler & Kulhawy (1978) conducted a numerical analyses where the response from a pressure cell was compared for two loading scenarios: a series

© University of Pretoria

to point loads, and a uniform load. It was found that at a certain active cell diameter to grain size ratio, the two loading scenarios produced the same results meaning that there is no longer an influence of particle size on the response of the pressure cell. Therefore, for diaphragm cells, Weiler & Kulhawy (1978) proposed that an active cell diameter to soil grain size ratio (d/D_{50}) greater than 50 be used.

6. **Lateral Stress Rotation** – This term describes how the inclusion of a foreign object (such as a pressure cell) influences the free field stresses. The term specifically refers to how part of the free field lateral stress in the soil is disrupted and begins to act normal to the object. This component needs to be removed from the measured stress in order to quantify the true normal stress in the soil. For a rigid ellipsoidal inclusion, Askegaard (1963) noted that fraction of lateral stress acting normal to the cell is influenced by both the cell aspect ratio and the Poisson's ratio of the soil and proposed a method to remove this influence. However, a key input for this method is the true lateral stress in the soil which is not usually known.
7. **Lateral Stress Cross-Sensitivity** – This term in relation to the performance of EPC was defined by Brown & Pell (1967). Pressure cells are usually installed in a three-dimensional stress field and the influence of the stresses acting parallel to the diaphragm need to be considered. The term "lateral stress cross-sensitivity" therefore refers to the result of direct, non-uniform, in-plane (lateral) compression of strain-gauged diaphragm stress cells. As the strain gauges are used to measure radial and tangential bending strains rather than directly measuring vertical diaphragm deflection, the strain gauges are particularly sensitive to these in-plane stresses. As noted by Brown (1977), this factor is of particular importance when measuring radial strain in an axis-symmetrical stress field because the lateral stress on the cell is then non-uniform. For linear strain gauges, the problem is solved by rearranging the strain gauges so that the Wheatstone bridge does not measure in-plane stresses.

2.6.1.2.2 Properties of the soil in which the cell is placed

8. **Stress-Strain Behaviour of the Soil Under Calibration Conditions** – This refers to the stress boundary conditions applied to the soil during calibration. This aspect is of particular importance if either the calibration or field conditions correspond to K_0 conditions. This is due to the fact that it has been noted that there is a lateral stress build-up that occurs during cyclic K_0 loading (e.g. Dunn & Billam, 1966). This lateral stress build-up presents itself as hysteresis and needs to be considered.
9. **Placement Effects** – This refers to the strategy of installing the pressure cells into the soil. This phenomenon was initially described by Taylor (1945) where it was referred to as

© University of Pretoria

"pocket action". Essentially the principle is that if the soil surrounding the pressure cell is at a different density to the rest of the soil in which the free stress field is to the measured, then the measured pressure will not be the true soil pressure. Taylor (1945) described how a pocket of soil that is more compact than the surrounding soil will attract stress and cause the cell to over-register, regardless of the design and construction of the cell. Similarly, a pocket of soil that is less compact than the surrounding soil will under-register. It was noted that the error induced was between 10 and 20%. This was further investigated by Hadala (1967) who conducted a series of calibration chamber experiments. For sands, it was found that the simplest placement techniques were the most reproducible and resulted in the least scatter in the results. The method recommended for use was to place the cell gently on top of the last lift placed and then to continue backfilling as if the cell was not present. A different methodology was proposed for clays.

2.6.1.2.3 Environmental conditions

10. **Dynamic Stress Application** – This factor refers to the ability the pressure cell to capture rapid changes in applied stress, specifically in the case of dynamic loading. It is known that the cell and the soil will have different time-dependent responses to an applied stress. For fine-grained soils, there can be a long response time. In comparison, the response time of the cell is typically much quicker. However, this depends on the sensor being used. Resistance strain gauges and semiconductor strain gauged typically have response times of microseconds while vibrating wire strain gauges typically have longer response time and are generally not suitable for cases where dynamic loading is expected. Selig (1964) also found that if the mass of the cell is greater than the mass of the soil it replaces, additional inertia forces will be created by the cell during dynamic loading that need to be considered. In cases where high frequency loadings are expected, the resonant frequency of the cell should be three to five times the maximum frequency of the expected loading (e.g. Triandafilidis, 1974).
11. **Placement Conditions** – This factor specifically refers to the compaction of fills within which pressure cells are installed. Once the pressure cell has been installed, it is important to ensure that the stresses induced by the compaction process are not greater than the capacity of the cells. When selecting a pressure cell, the capacity of the cell must be sufficient to withstand the stresses induced during compaction (including the mass of any construction plant that may drive in the vicinity of the pressure cell), but must still be sensitive enough to measure the desired soil stresses.
12. **Corrosion and Moisture** – Pressure cells are usually installed in harsh working environments where there is access to water and oxygen which provide conditions

© University of Pretoria

conducive to corrosion and moisture ingress. Weiler & Kulhawy (1982) noted that a key aspect relating to corrosion resistance of a pressure cell lies in the choice of construction material. Due to its low density, aluminium is a popular choice, but it is known to be susceptible to corrosion. Stainless steel and titanium were proposed as viable alternatives. Some disadvantages of stainless steel include its increased density. However, although titanium is lighter, it is more expensive. Therefore, the final decision should be based on the site-specific conditions.

13. **Temperature** – Although it was known that changes in temperature influence the performance of EPCs, not much emphasis was placed on this factor in the early days of EPC development. At the time, Weiler & Kulhawy (1982) noted that errors as high as 23 kPa/°C as a result of temperature changes had been reported by some researchers (e.g. Selig & Tobin, 1967; Williams & Brown, 1971). Since then, there has been a more targeted approach to investigate this aspect.

    Dunnicliff (1997) noted that although thermal correction factors are provided by most manufacturers, these correction factors are for the transducer itself, and not for the entire cell assembly. Therefore, there could be temperature effects on the entire cell assembly which are not captured with the thermal correction factor provided in the datasheets. Dunnicliff (1997) noted that no correction methods had been widely proposed or accepted at the time and it was suggested that this could have been due to the fact that any correction would need to incorporate the extent of restraint provided to the pressure cell by its surroundings. This is difficult to do in the laboratory, as the extent of restraint would be different for different applications.

    Felio & Bauer (1986) may have been the first researchers to present experimental evidence on the influence of temperature on the performance of EPCs. As part of their research, several laboratory tests were conducted on the SOLINST pneumatic EPCs. These EPCs were 100 mm in diameter and were 5.4 mm in thickness. The EPCs were diaphragm type cells, with the cavity between the two flexible discs filled with pressurised oil. The pressure of the oil prior to any external loading was termed the prestress pressure.

    The EPCs were immersed in a water bath, where the temperature was varied from -4°C to 45°C. The EPCs were first calibrated under “no load” conditions and then under hydrostatic conditions to various applied stresses. The calibration factors obtained from the hydrostatic calibration were compared to the calibration factors provided by the manufacturer who performed the calibration at room temperature where the cell was placed between two air bags which were pressurised. It was found that the calibration coefficients remained the same, but the intercept (prestress pressure) changed at the various temperatures.

    A few years later, Symons & Murray (1988) presented results of long-term monitoring of EPCs installed behind a retaining wall in Surrey. In addition to the EPCs that were installed

© University of Pretoria

against the abutment (contact cells), a number of EPCs were installed in the soil behind the abutment at various depths and orientations (embedment cells). The locations of the EPCs are shown in Figure 2.37.

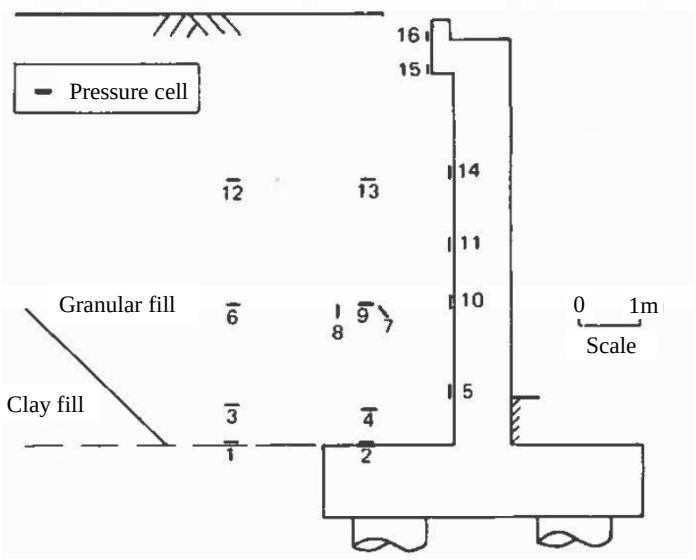


Figure 2.37: Cross-section of the bridge abutment at Guildford (after Symons & Murray, 1988)

Limited information was provided regarding the type of EPCs that were used. Data were collected for five years after completion of the structure and significant seasonal variations in measured pressures were noted. This was noted in both the EPCs measuring lateral and vertical earth pressures and is shown in Figure 2.38. Although only results from the contact EPCs were presented, similar trends were noted for the embedment EPCs.

© University of Pretoria

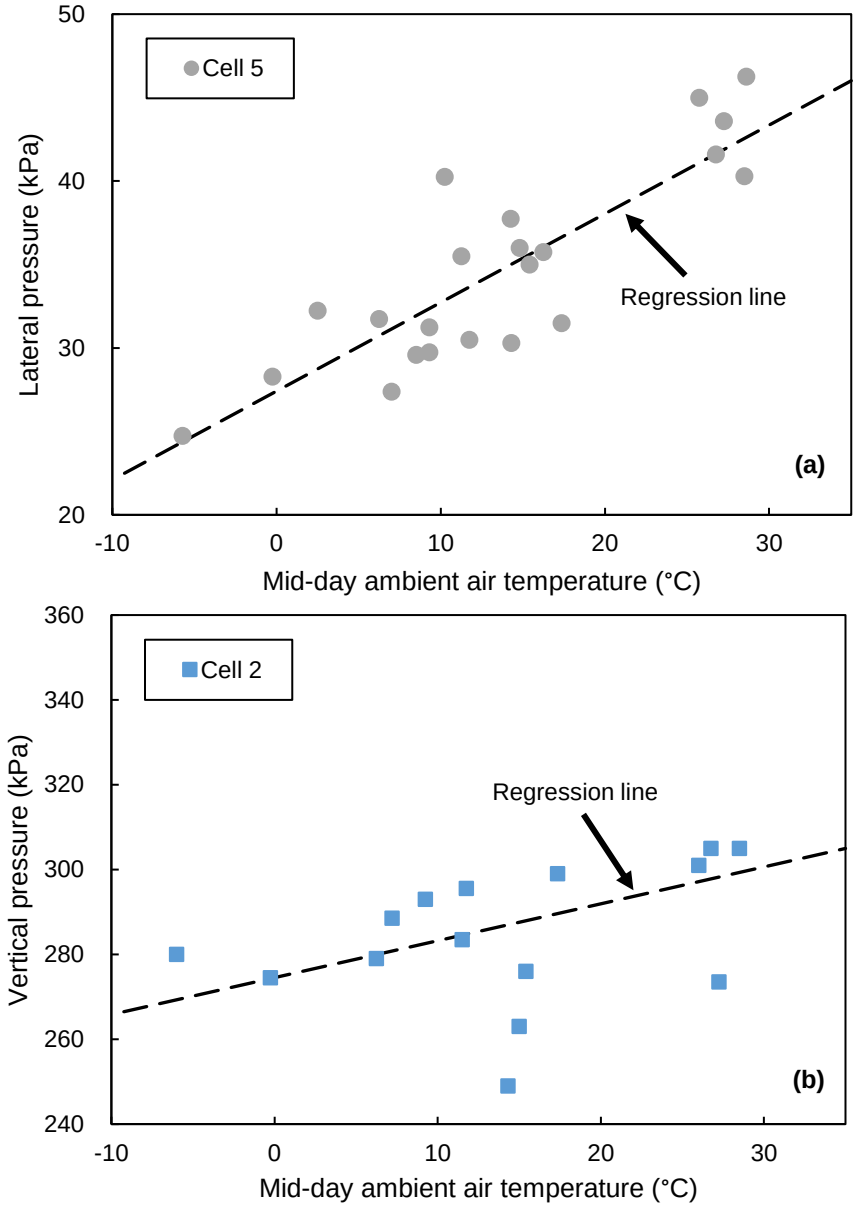


Figure 2.38: Influence of temperature on the interpreted: (a) lateral stresses and, (b) vertical stresses at Guildford (after Symons & Murray, 1988)

In 2000, Sellers (2000) conducted a numerical analysis of an EPC to determine a theoretical correction that would need to be applied to the measured stress in the cell due to temperature effects. A hypothetical circular cell was considered and the effect of an increase in temperature of 1°C was postulated. The analysis considered both a contact EPC and an embedment EPC. The increase in temperature would cause an expansion of the liquid within the cell which would be resisted by the confinement provided by the surrounding medium (soil in the case of the embedment cell, and concrete in the case of the contact cell). This tendency for expansion due to an increase in temperature and resistance in volume change due to the confinement would cause a pressure rise in the

© University of Pretoria

liquid. Two equations to estimate this pressure rise were derived for the cell assembly: one for contact cell, and one for embedment cells. These equations only required the geometric and stiffness properties of the soil and the EPC. Although this was a useful step forward, subsequent investigation found that the proposed equations tended to under-estimate the influence of temperature when compared to long-term field data. It was suspected that this under-estimate was due to the simplistic assumptions made during the development of the equations.

At the same time, Yang (2000) presented results from long-term field monitoring of EPCs installed on a concrete box culvert. Hydraulic-type, vibrating wire pressure cells (Geokon 4810) with a capacity of 345 kPa were used. The contact pressure cells, 230 mm in diameter and 6 mm thick, were installed on the culvert which was then backfilled by a 11.7 m high embankment of clayey weathered shale. A cross-section of the box culvert is shown in Figure 2.39. As the inside of the culvert was exposed to the air temperature, these EPCs were subject to large changes in ambient temperature. After completion of the embankment, more than three years of data were recorded.

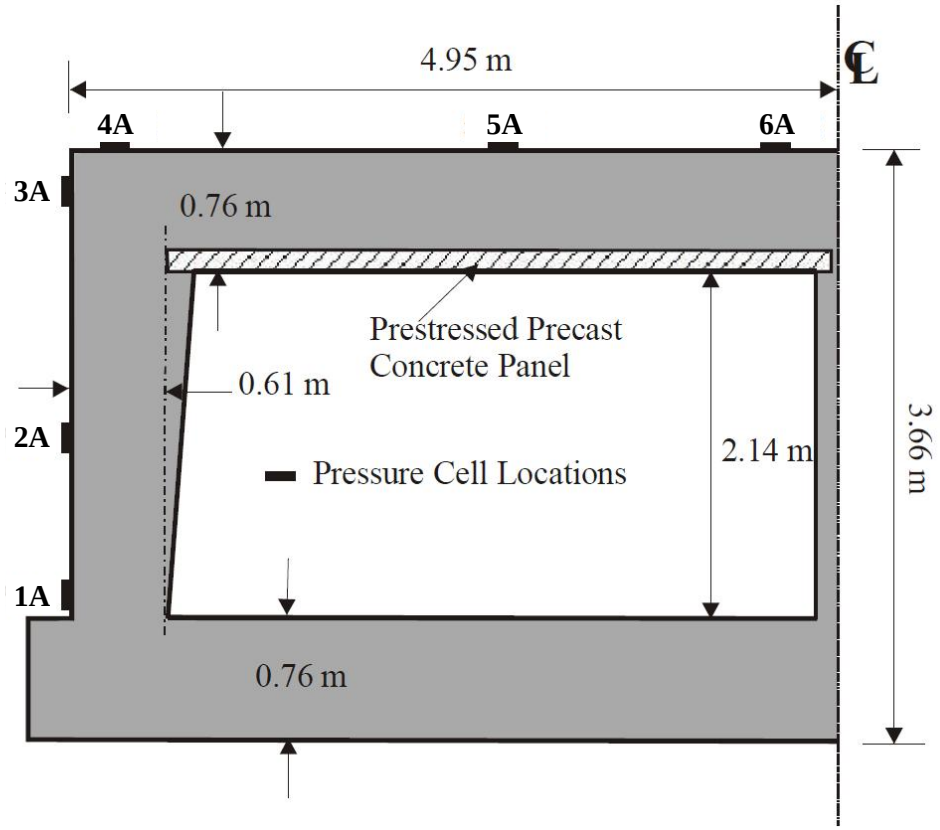


Figure 2.39: Cross-section through the box culvert at Site 1 (after Yang, 2000)

Upon review of the data, seasonal variations in measured earth pressure as shown in Figure 2.40 became apparent. Specific attention was given to the EPCs placed on top of

© University of Pretoria

the culvert. The recorded variations in earth pressure were in the order of 100 kPa (approximately 30% of the mean measured pressure over the period). A comparison between the interpreted pressures in Figure 2.40(a) and temperatures in Figure 2.40(b) show a clear correlation between the two readings. Note that this interpreted stress includes the thermal correction recommended by the manufacturer.

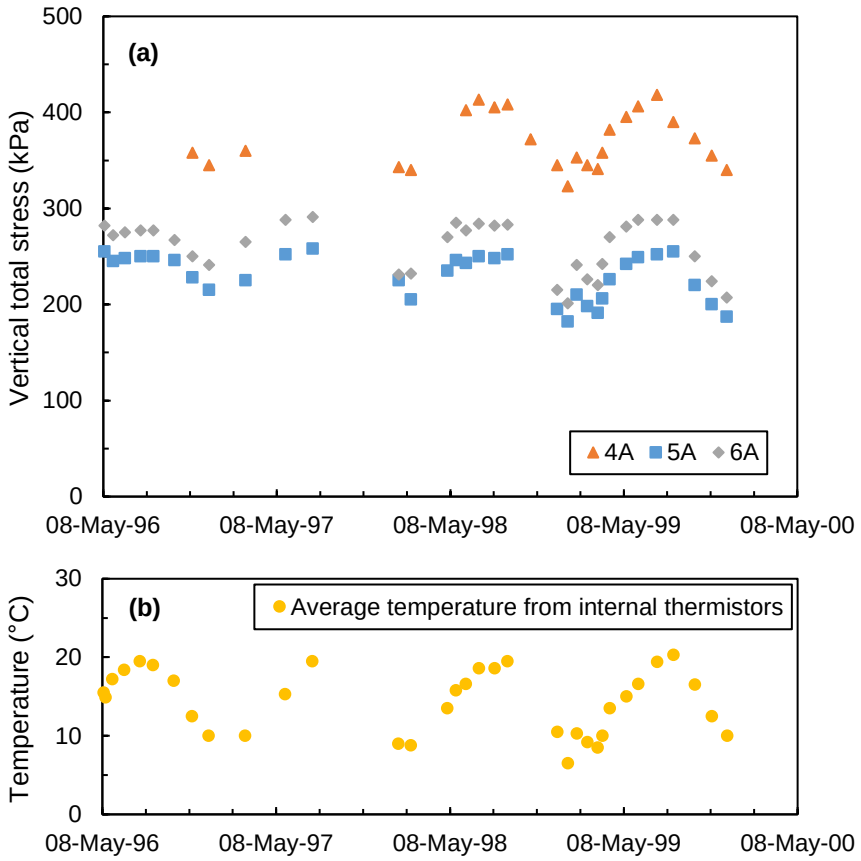


Figure 2.40: Results from the EPCs at Site 1 showing: (a) interpreted vertical stresses and, (b) seasonal temperature variations (after Yang, 2000)

To address this, Yang (2000) carefully worked through a list of factors that could influence these readings. These included: a reduction in compaction-induced stresses, structural movement, changes in moisture in the soil leading to true stress changes in potentially expansive soils, changes in moisture at the concrete interface leading to a slight expansion of concrete around the pressure cell, and thermal effects. Ultimately, it was concluded that it must be a thermal influence that was affecting the interpreted stresses.

In an attempt to correct the data, the equations proposed by Sellers (2000) were used. For a change in temperature of 13°C, a pressure correction of 7.6 kPa was determined. This is very different to the changes of 100 kPa that were recorded on site. Therefore, an

© University of Pretoria

alternative approach, based on the assumption that the true vertical total stress remained constant for the period after the embankment construction, was tried. The calculated empirical correction coefficient for this method varied between 5.62 kPa/°C and 6.99 kPa/°C for the EPCs. The corrected stresses showed much smaller seasonal variations and were deemed to be more representative of the true stresses in the soil.

By now, it was quite apparent that EPCs were susceptible to thermal influences. However, correction methods were limited to theoretical and empirical solutions, both of which were not satisfactory. This was identified by Daigle & Zhao (2004) who conducted a comprehensive laboratory investigation. In their study, hydraulic-type, vibrating wire EPCs were tested and cells with two specific diameters were used: 76 mm and 228 mm. The 76 mm diameter cells have an aspect ratio of 0.13 and fall into the category of "poor design" with a ratio greater than 0.1 as described by Dunnicliff & Green (1988). Optimal performance perhaps therefore cannot reasonably be expected from these sensors. The 228 mm diameter cells had an aspect ratio of 0.04 which meets the design criteria.

Unloaded and loaded tests were conducted at various steady state temperatures. The term "apparent pressure" was used to describe the variation in frequency readings caused only by temperature changes while loading conditions remained constant. A calibration chamber was used to test the cells under pressure. The chamber was filled with dry Ottawa sand and the cell was positioned in the centre of the chamber at mid-height. The pressure chamber was placed in an environmental chamber where the temperature was carefully controlled.

Typical results from the tests on the 76 mm diameter cell are shown in Figure 2.41. It can be seen that there is an influence of temperature for all the cases, and that the influence increases as the applied stress level increases. In each case, the reference pressure was taken at room temperature (22°C). The apparent pressures are also shown in terms of percentage of Full Scale Output (FSO). As summarised in Table 2.8, the observed thermal effects on the 228 mm diameter cell were lower than those observed for the 76 mm diameter cell.

© University of Pretoria

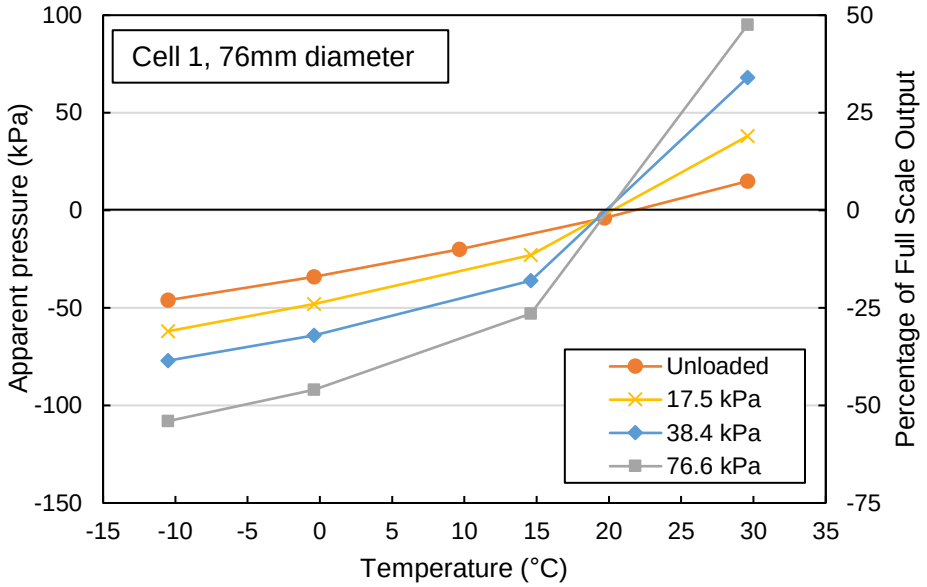


Figure 2.41: Results from the thermal calibration of pressure cell 1 (after Daigle & Zhao, 2004)

In summary, it was found that in cases where there are large variations in temperature, the temperature calibration factors provided on the manufacturer's calibration sheets can underestimate the thermal influence on the EPCs. It was also found that the magnitude of pressure applied to the cell influences these thermal effects

Corrections for thermal influences in the field are complex and there does not appear to be an accepted method for accounting for these influences. Perhaps the most reasonable approach is that suggested by Yang (2000). However, this method is only applicable in areas where soil stresses are assumed to be constant.

© University of Pretoria

Table 2.7: Summary of factors influencing EPC performance (after Weiler & Kulhawy, 1982)

	Factor	Description of error	Correction method	Reference
1	Aspect ratio (cell thickness to diameter ratio)	Cell thickness alters stress field around cell.	Use relatively thin cells ($\frac{T}{D} < \frac{1}{5}$), $\frac{T}{D} < \frac{1}{10}$ in some cases.	Askegaard (1963), Collins et al. (1972), WES (1944), Tory & Sparrow (1967), Dunnicliff & Green (1988)
2	Soil-cell stiffness ratio, S	Changing soil stiffness may cause a nonlinear calibration.	Design cells for high stiffness ($S < 0.5$) and use correction factors.	Monfore (1950), Peattie & Sparrow (1954), Selig (1964), (Tory & Sparrow, 1967)
3	Diaphragm deflection (arching)	Excessive deflection changes stress distribution over cell.	Design cell for low deflection ($\frac{d}{\Delta} > 2\,000 - 5\,000$).	WES (1944), Taylor (1947), Trollope & Lee (1957)
4	Cylinder or piston cell deflection	Much lower allowable deflection than for diaphragm cells.	Design cell for low deflection ($\frac{d}{\Delta} > 20\,000$).	Carder (1976), Kallstenius & Bergau (1956)
5	Stress concentrations at cell corners	Causes cell to over-register by increasing the stress over the active cell face.	Use inactive outer rims to reduce sensitive area ($\frac{d^2}{D^2} < 0.25 - 0.45$).	Hvorslev (1976), Monfore (1950), Peattie & Sparrow (1954)
6	Eccentric, nonuniform and point loads	Soil grain size too large for cell size used	Increase stress cell active diameter (diaphragm, $\frac{d}{D_{50}} \geq 10$; cylinder $\frac{d}{D_{50}} \geq 50$).	Brown & Pell (1967), Kallstenius & Bergau (1956), Weiler & Kulhawy (1978)
7	Lateral stress rotation	Presence of cell in soil causes lateral stresses to act normal to cell.	Use correction factors such as those proposed by Askegaard (1963).	Askegaard (1963), Bates (1969), Collins et al. (1972), Weiler & Kulhawy (1978)

© University of Pretoria

	Factor	Description of error	Correction method	Reference
8	Cross-sensitivity	Nonuniform direct lateral compression of cell causes error in measurement.	Change strain gauge arrangement or add outer rings.	Bates (1969), Brown & Pell (1967), Sparrow & Tory (1966), Weiler & Kulhawy (1978)
9	Stress-strain behaviour of soil	Cell measurement influenced by confining conditions.	Calibrate cell under near-usage conditions.	Dunn & Billam (1966), Weiler & Kulhawy (1978)
10	Placement effects	Physical placing of cells causes disturbance of soil.	Random error; use duplicate measurements.	Audibert & Tavenas (1975), Hadala (1967), Reiff & Linger (1967), Taylor (1945)
11	Proximity of structures and other stress cells	Interaction of stress fields of cell and structure causes errors.	Use adequate spacing: see text for criteria.	Reiff & Linger (1967)
12	Dynamic stress measurements	Response time, natural frequency and inertia of cell causes errors.	Use dynamic calibration.	Ingram (1965), Selig (1964), Shannon & Wilson Inc. (1972), Triandafilidis (1974)
13	Corrosion and moisture	May cause cell “failure” by attacking cell materials.	Use extra water-proofing precautions.	Bozozuk (1970), Kennard et al. (1967), Williams & Brown (1971)
14	Placement stresses	Overstressing during soil compaction may permanently damage cell.	Check cell design for yield strength.	Williams & Brown (1971)
15	Temperature	Changes “zero reference” of cells, does not change slop of calibration.	Calibrate or use balance resistors.	Reiff & Linger (1967), Williams & Brown (1971)

© University of Pretoria

Table 2.8: Summary of EPC thermal correction factors from the literature

ID	Description of installation	Type of EPC	Temperature variation (°C)	Proposed temperature correction (kPa/°C)	Manufacturer's thermal factor (kPa/°C)	Reference(s)
1	Pressure cells installed on a box culvert under an embankment of constant height, exposed to seasonal temperature changes over more than three years.	Hydraulic type, vibrating wire EPCs	6 - 20	5.62 – 6.99	0.05 – 0.12	Yang (2000), Yang et al. (2001)
2	Laboratory calibration of EPCs in an environmental chamber. 76 mm diameter cells ($\frac{T}{D} = 0.13$)	Hydraulic type, vibrating wire EPCs	-10 - 30	0.64 – 2.26	0.02 – 0.06	Daigle & Zhao (2004)
3	Laboratory calibration of EPCs in an environmental chamber. 228 mm diameter cells ($\frac{T}{D} = 0.04$)	Hydraulic type, vibrating wire EPCs	-10 - 30	0.22 – 0.42	0.08 – 0.36	Daigle & Zhao (2004)
4	Field data from both embedded and contact EPCs installed on and in the vicinity of a 1700 mm diameter concrete culvert under 1.5 m of granular material.	Hydraulic type, vibrating wire EPCs	0 - 22	0.6 – 3.0	N/A	Daigle & Zhao (2004)

© University of Pretoria

2.6.2 High Capacity Tensiometers

Pore pressures have been measured in embankments for several decades. Initially, the focus of these instruments was on measuring positive pore pressures. However, in recent years there has been a move towards the measurement of negative pore pressures (suctions). This is important for tailings dams as there are significant portions of the dam where the pore pressures are negative. Conventional piezometers are not designed to measure large negative pore pressures.

One instrument capable of measuring both positive and negative pore pressures in soil is a tensiometer. A tensiometer typically consists of a porous High Air Entry (HAE) ceramic disc connected to a pressure sensor through a fluid reservoir. The ceramic disc is placed in contact with the soil in which the pore pressure is of interest and, by an exchange of water between the pores of the soil and the fluid reservoir, pore pressures can be measured directly (Lu & Likos, 2004). A High Capacity Tensiometer (HCT) is a tensiometer with the ability to accurately and reliably measure suction values in excess of 100 kPa.

Low-cost HCTs have been successfully developed at the University of Pretoria for some years (e.g. Jacobsz, 2018). These sensors have been called the Tuks HCTs as a reference to the Afrikaans acronym that was used for the University at its establishment: Transvaalse Universiteitskollege (TUK). Figure 2.42 shows a cross section of a typical Tuks HCT. The Tuks HCTs make use of commercially available MS54XX miniature Surface Mounted Device (SMD) pressure sensor (TE Connectivity, 2018). Additional details of this sensors and the tensiometer assembly are provided in le Roux (2019). Note that the epoxy seal has been replaced with a steel casing in some of the tensiometers.

© University of Pretoria

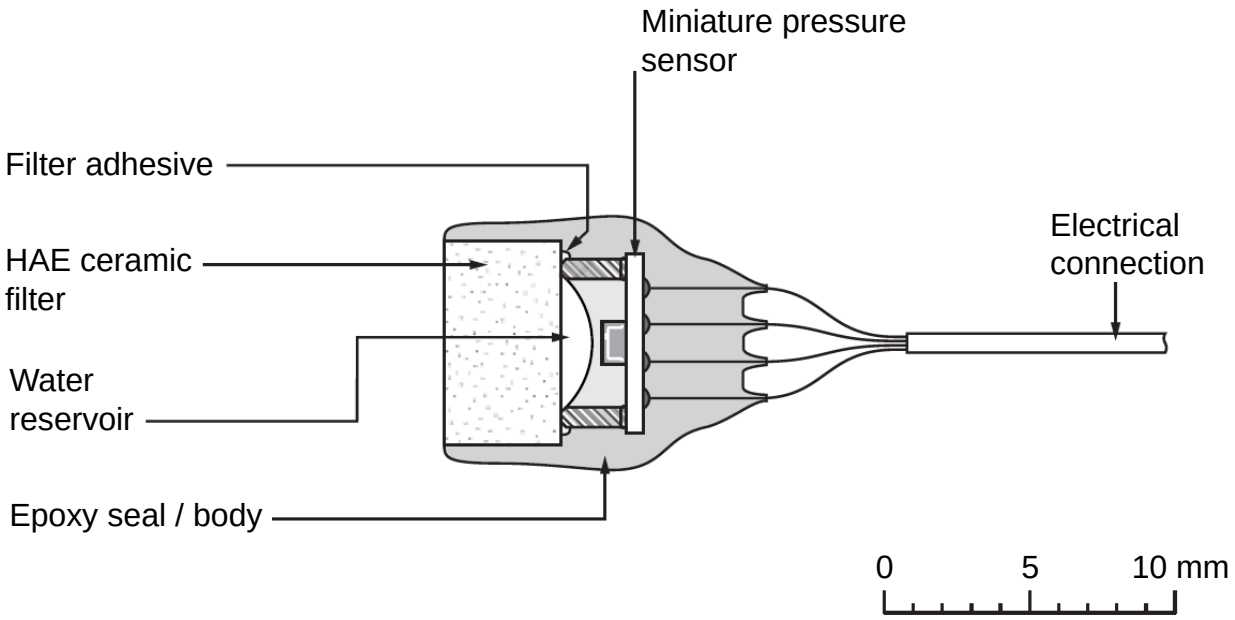


Figure 2.42: Typical components of the Tuks HCT (after le Roux, 2019)

Before use, each tensiometer is first saturated under a vacuum as recommended by Take & Bolton (2003). This significantly reduces the time and pressure required for saturation, as well as improves the resistance of the tensiometer to cavitation. Cavitation is the formation of gas or vapour bubbles in a liquid and is a major issue for HCTs. Once cavitation occurs, the response of the sensor to changes in external pressure become unreliable. Cavitation can be minimised by the design of the tensiometer to reduce potential locations for nucleation, as well as enhanced saturation procedures. Both aspects were considered in the development of the Tuks HCTs.

Each tensiometer is calibrated in the positive pore pressure range and then extrapolated to the negative pore pressure range. Such a technique has been shown to work well for the Tuks HCTs (e.g. le Roux, 2019). Additional details of the saturation and calibration processes are described in Section 5.2.1. For this study, the accuracy of the Tuks HCTs was only verified in the positive pressure range.

2.6.3 Suction probes

Although HCTs have been shown to perform well for many applications, they do have some limitations. These include the inability to reliably measure high suction values, as well as their susceptibility to cavitation. An alternative to the conventional HCT is a suction probe such as the Fixed-Matrix Water Potential Sensor (WPS). These sensors are not susceptible to cavitation and are capable of measuring suctions of up to 100 MPa.

© University of Pretoria

There are many commercially available sensors but for this study, the TEROS 21 sensor, produced by the METER group was used. The sensor comprises two fixed-matrix porous ceramic discs which are separated by a printed elective circuit board as shown in Figure 2.43 (METER Group, 2020).

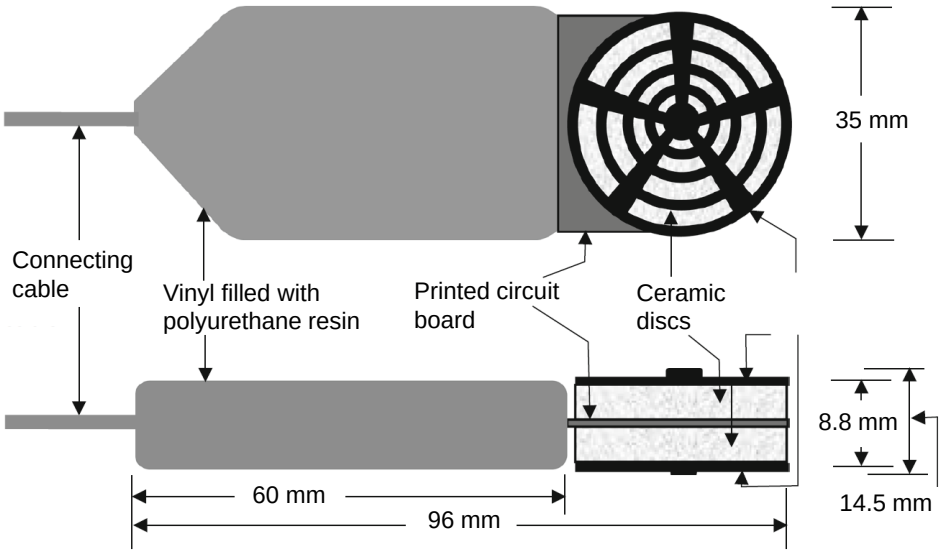


Figure 2.43: Key components of the TEROS 21 WPS (after Tripathy et al., 2016)

Since the pore distribution of the ceramic is known, the moisture content of the discs can be inferred by measuring the dielectric permittivity of the ceramic discs. As the SWRC of the discs is known, the matric suction in the discs can be estimated using the inferred moisture content. When the WPS is placed in contact with a soil, the matric suction in the ceramic discs equilibrates to the matric suction in the soil. This process occurs as a result of physical transfer of water between the ceramic discs and the surrounding soil.

The rate at which this equilibrium is reached is a function of the hydraulic conductivity of the soil as well as the matric suction gradient between the discs and the surrounding soil (Vandoorne et al., 2021). Each TEROS 21 sensor is factory calibrated and only the interpreted suction values are provided during use. Previous studies have shown that the TEROS 21 performs well for fine-grained soils and especially for suction values in excess of 1 500 kPa (e.g. Tripathy et al., 2016).

2.6.4 Comparison of suction sensors

Table 2.9 provides a summary of three sensors capable of measuring soil matric suction. It can be seen that there are advantages and disadvantages for each sensor type. The TEROS 21 WPS is

© University of Pretoria

resistant to cavitation and has a much larger suction operating range. However, these sensors do not perform well at low suction values, nor in the positive pressure range. Conversely the epoxy-cased Tuks HCTs are susceptible to cavitation and are fairly limited in their suction operating range when compared to the WPS. However, these sensors can be used for moderate positive pressures of up to 500 kPa. The steel-cased HCTs offer improved performance in the both the positive and negative pressure ranges over the epoxy-cased Tuks HCTs.

Table 2.9: Comparison of various suction measurement sensors

Sensor Type	Description	Operating Range	Accuracy	Reference
TEROS 21 WPS	A commercially available solid phase Water Potential Sensor (WPS)	-9 kPa to -100 MPa	10% of reading +2 kPa*	METER Group (2020)
Tuks HCT (epoxy-cased)	An in-house tensiometer constructed using a silicon micromachined pressure sensor with an epoxy casing	+500 kPa to -500 kPa	0.6% FSO	Jacobsz (2018)
Tuks HCT (steel-cased)	An in-house tensiometer constructed using a silicon micromachined pressure sensor with a steel casing	+700 kPa to -1 697 kPa	0.6% FSO	Jacobsz (2019)

*Accuracy rating only provided for suction values between 9 kPa and 100 kPa.

2.6.5 Moisture content probes

For an unsaturated soil, it is important to understand the moisture content of the soil. Traditional direct methods to determine soil moisture content require drying of a sample and comparing the wet and dry masses. These tests are time-consuming but perhaps more importantly, destroy the sample. Indirect methods, which are non-destructive and can be performed continuously have therefore been investigated.

One such technique is the use of Time Domain Reflectometry (TDR). Described by Fellner-Feldegg (1969) as an improvement over the Frequency Domain Reflectometry technique for wave characterisation, the TDR technique was perhaps first applied to the estimation of soil moisture by Davis & Chudobiak (1975). As part of their research, the TDR technique was demonstrated as a non-destructive test method to measure the dielectric constant of the soil, which is the first step to

© University of Pretoria

estimating the moisture content of the soil. In essence, the TDR technique enables the dielectric constant on a medium to be determined by using electrodes inserted into the medium.

Using this principle, Topp et al. (1980) investigated the relationship between Volumetric Water Content (VWC), θ, and the apparent dielectric constant, K_a. A rigorous laboratory testing regime was undertaken to investigate the influence of texture, density and soluble salt content on the relationship between K_a and θ_v for a given soil. It was found that the dielectric constant was almost independent of soil bulk density (1 140-1440 kg/m^3), soil texture (clay to sandy loam), salt content (salt-free water, 0.01 N $CaSO_4$, or 2 000 ppm NaCl solution), as well as temperature (10-36°C), and Equation (7) was proposed.

Based on the tests conducted, Topp et al. (1980) showed that Equation (7) could be used to estimate the VWC of a soil with an error of estimate of 0.013. The proposed relationship performed poorly when applied to the results on glass beads, vermiculite and organic soils. In this study, Equation (7) is referred to at Topp's equation.

$$\theta = -5.3 * 10^{-2} + 2.92 * 10^{-2} * K_a - 5.5 * 10^{-4} * K_a^2 + 4.3 * K_a^3 \quad (7)$$

Where:

θ = Volumetric water content (m^3/m^3)

K_a = Apparent dielectric constant

Recently, Susha Lekshmi et al. (2018) confirmed that Topp's equation performed well over a wide range of soils types and states. There are several commercially available TDR moisture sensors, each with their own advantages and limitations. For this study, the TEROS 12 probe, manufactured by the METER Group was selected. The TEROS 12 probe uses the TDR technique where an electrical pulse is generated from one needle. The pulse is received by the receiving needle and also reflected back. Based on the time for the pulse to arrive, and the degradation of the pulse, it is possible to estimate characteristics of the soil through which the pulse was transmitted.

Figure 2.44 shows a sketch of the TEROS 12 moisture content probe. This sensor comprises three sensing needles. Needles 1 and 2 are used to estimate the VWC of the soil, while Needles 2 and 3 are used to estimate the Electrical Conductivity (EC) of the soil. In addition, a thermistor installed in Needle 2 provides soil temperature measurements.

© University of Pretoria

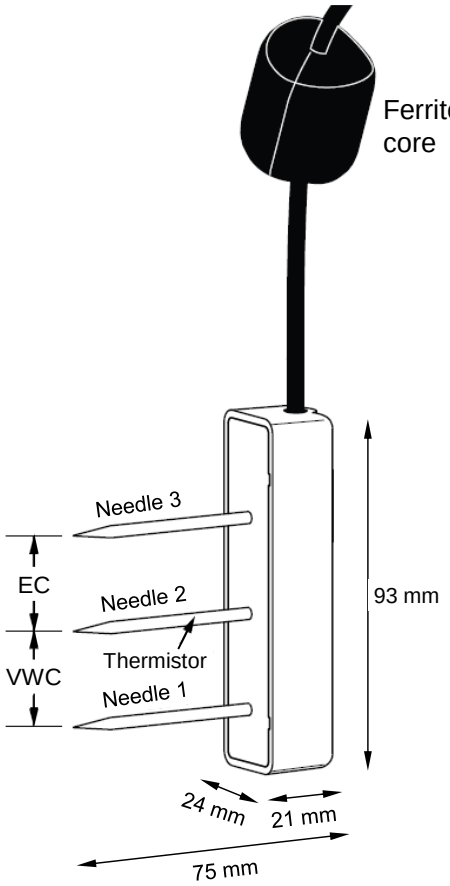


Figure 2.44: Sketch of the TEROS 12 moisture probe (after METER Group, 2018)

Equation (8) is proposed by the METER Group as a method of estimating the apparent dielectric permittivity of a soil (ε), based on the RAW reading obtained from the TEROS 12 probe. As discussed by Campbell Scientific Inc. (2019), the apparent dielectric permittivity (ε) is similar to, and can be used in place of, the apparent dielectric constant (K_a) as shown in Equation (7).

$$\varepsilon = 1.112 * 10^{-18} * RAW^{5.607} \quad (8)$$

Alternatively, METER Group propose a direct relationship between the measured RAW value from the TEROS 12 sensor and the volumetric water content of the soil. This relationship is based on in-house testing and is shown in Equation (9). This equation is only applicable for VWCs up to 0.70 m^3/m^3. In this study, Equation (9) is referred to as the Mineral Soils equation.

$$\theta = 3.879 * 10^{-4} * RAW - 0.6956 \quad (9)$$

© University of Pretoria

2.7 SUMMARY

The literature review conducted shows that there has been significant progress made in the understanding and prediction of soil behaviour since the early days of soil mechanics. Several key points were identified from the literature review that are applicable to this study and these are repeated here for reference.

Tailings and tailings dams

- Mine tailings generally classify as silty soils. This typically results in the tailings having distinctly different compression and shear behaviour when compared to traditional soils such as clays of high plasticity, or clean sands.
- The majority of tailings dams in South Africa are upstream constructed which, according to some sources, are considered riskier when compared to similar centreline and downstream constructed dams (e.g. Franks et al., 2021).
- Several key case histories of tailings and water dam failures were presented. In each case, failure occurred as a result of a series of incidents and in most cases, it was noted that the failures could have been prevented if the basic principles of dam engineering had been followed. Each case history provides valuable learnings which must not be ignored.
- The current tailings dam governance framework in South Africa was presented. Two International governance documents, which have been widely adopted globally, were discussed: The Global Industry Standard on Tailings Management (GISTM) (Oberle, 2020), and Bulletin 194 on Tailings Dam Safety published by ICOLD (2022).
- The South African standard is currently being updated to align with these two International documents. This is important as the GISTM specifically requires design against (undrained) brittle failure mechanisms while the ICOLD document provides specific FoS requirements for various degrees of soil brittleness. These are aspects that are not considered in the current South African standard.
- It was also noted how soil brittleness is treated as a material characteristic and not a state characteristic in the ICOLD document.

Compression behaviour of sandy soils

- The behaviour of plastic clays and clean sands is distinctly different. Fine-grained soils such as clays of high plasticity have been shown to exhibit a unique Normal Consolidation Line (NCL) that is parallel to the Critical State Line (CSL) when plotted in $e - p'$ space (e.g. Atkinson & Bransby, 1978).
- Conversely, coarse-grained soils such as clean sands have been shown to exhibit an infinite number of NCLs that are not parallel to the CSL (e.g. Jefferies & Been, 2000).

© University of Pretoria

- With gold tailings being an intermediate soil there is some uncertainty regarding its expected behaviour and this can lead to inconsistent interpretations for designs and safety evaluations.
- Transitional soils are those soils whose initial density continue to influence their behaviour at large strains. As noted by Coop (2015), when investigating soil behavioural frameworks, it is important to establish whether the soil under consideration is a transitional soil. This can be done using the m parameter proposed by Ponzoni et al. (2014).
- It was shown how the soil gradings changes within a tailings dam, and how the this grading can influence the compression and shear behaviour of mine tailings (e.g. Torres-Cruz, 2016). To ensure appropriate conclusions can be drawn from the testing, care must be taken to ensure that the grading of the soils remains constant.
- In terms of previous research conducted on gold tailings, it was found that the scope of these tests was not sufficient to investigate whether gold tailings should be viewed within the context of having a unique NCL or not. This remains an objective of this study.

Shearing behaviour of sandy soils

- In line with the fundamental principles of CSSM, it was also shown how the five key aspects of soil state (density, stress level, stress history, mode of shear and fabric) influence the undrained shearing behaviour of loose, sandy soils.
- For clean sands, Castro (1969) showed that for a small change in void ratio of 0.06, the behaviour of loose Ottawa sand changed from strain-hardening to strain-softening.
- For loose Hostun RF sand, Doanh et al. (1997) showed how the stress history of a soil (K_0) influenced the stress-strain response, and specifically the yield undrained shear strength.
- This is of importance as the in-situ density and stress history of tailings is known to vary, and that the undrained shear response greatly influences the results of designs and safety evaluations against undrained shearing.
- Details were provided regarding tests conducted on gold tailings by other researchers. Although these tests were not sufficiently rigorous to answer key questions posed as part of this study, they do provide some insight into the behaviour of gold tailings. Key CSSM parameters determined for these materials are provided in Table 2.4.

Laboratory testing of soils

- As shown by Reid et al. (2021), it appears that even with modern triaxial testing techniques, the CSL can only reasonably be expected to be estimated to within a void ratio of ±0.04.
- Several sample preparation techniques were described. It was shown that although the Moist Tamping (MT) preparation technique enables the creation of samples with precise

© University of Pretoria

and repeatable densities, there is strong experimental evidence that the fabric created by MT samples results in undrained shear behaviour that is different to that which can be expected based on the in-situ fabric (e.g. Chang et al., 2011).

Definition of the in-situ stress state

- The true in-situ stress state of a three-dimensional soil element comprises three normal stresses and three shear stresses. However, for most practical purposes this stress state can be simplified to a two-dimensional stress state. A common simplification involves the geostatic stress ratio, K_0, which is the ratio of the horizontal and vertical effective stress.
- The term K_0 refers to conditions of zero lateral strain. Since it is unclear whether this is strictly the case in the field, for this study the stress ratio will be used but the subscript "0" will be omitted.

Field measurements of K_0 for tailings dams

- In-situ measurements of the geostatic stress ratio in water retaining embankments and tailings dams appear to be rare. Where data have been published, many assumptions were made, and heavy reliance was placed on numerical modelling with little to no on-site verification.
- Two cases were presented where direct field measurements were attempted, and in both cased it was found that there was no clear, single K_0 value that could be assigned to the section of the embankment under consideration.
- Aside from the alternative view of the MRM ETF, where a K_0 value of 1.0 was proposed, the four other sites had estimated K_0 values distinctly different from 1.0, with K_0 values ranging from 0.45 to 0.60.
- For loose or normally consolidated soils, it was found that $K_0 = 0.7$ is a common assumption made for modelling purposes. This assumption is noted in the user manuals of some geotechnical engineering software packages (e.g. Bentley Systems, 2023b) and is based on the results from SBP tests in loose, hydraulically deposed sands the Beaufort Sea by Graham & Jefferies (1986). This work also found that the equation proposed by Jaky (1944) appeared to be a lower bound for the K_0 values measured on site.
- Since the geostatic stress ratio is defined in terms of effective stresses, and tailings commonly exists in an unsaturated state, some assumptions need to be made. Bishop effective stress, as modified by Bolzon et al. (1996) was shown as one such assumption.

Sensors for geotechnical applications

- Two soil suction sensors were discussed: the Tuks High Capacity Tensiometer (HCT), and

© University of Pretoria

the METER Group TEROS 21 Fixed Matrix Water Potential Sensor (WPS). These sensors work on different operating principles and also have different operating ranges

- To measure soil moisture content, the METER Group TEROS 12 moisture probe was discussed. This sensor uses the Time Domain Reflectometry (TDR) technique to estimate the dielectric permittivity of a soil which can be used to estimate its volumetric water content. Two estimation relationships were presented: The Topp equation (Topp et al., 1980), and the Mineral Soils equation (Campbell Scientific Inc., 2019).

Performance of EPCs

- There is significant uncertainty regarding the performance of embedment EPCs. These vary from the fact that the mere presence of the cell influences the free-field stress distribution to soil arching and thermal influences of the entire cell assembly.
- In terms of temperature effects, it was noted that the thermal correction factors provided most manufacturers are for the pressure transducer itself, and not for the entire cell assembly (e.g. Dunnicliff, 1997). Therefore, there could be temperature effects on the entire cell assembly which are not captured with the thermal correction factor provided in the datasheets. It was found that these effects can be large in some cases and that there appears that there is still no agreement on the preferred method to correct for these temperature effects (e.g. Daigle & Zhao, 2004).
- Fortunately, the many factors influencing the performance of EPCs have been well documents and methods to reduce and even eliminate these errors have been proposed. Perhaps the most extensive list developed was that presented by Weiler & Kulhawy (1982). This list has been updated over the years and is presented in Table 2.7.
- It was found that many factors relate to the design and installation of the EPCs. Since modern EPC manufacturers are aware of these factors, and make an effort to implement these recommendations, moderns EPCs are capable of providing accurate and reliable stress measurements.

© University of Pretoria

3 LABORATORY ELEMENT TESTING

3.1 INTRODUCTION

Mine tailings, typically being silty in nature are neither plastic clays nor clean sands and therefore some uncertainty regarding their compressibility characteristics exist. Similarly, there is some uncertainty regarding the undrained shear behaviour of gold tailings under certain conditions. The purpose of this chapter is to present results from an experimental investigation on gold tailings, with a specific goal to establish the behavioural framework for this soil. The intent is to then place any observed field behaviour within this framework.

3.2 ANALYSIS OF DATA FROM LITERATURE

Before embarking on new tests on the gold tailings of interest, a re-analysis of previous work by other researchers was conducted. This section therefore focuses on a review of triaxial compression tests on Quebec gold tailings available in the literature. A specific focus of the analysis was the influence of the stress anisotropy imposed during consolidation on the undrained shear response of the soils. The magnitude of stress anisotropy is described using the term K_c, which represents the ratio of the horizontal effective stress to the vertical effective stress. Aspects of this work have been summarised by the author in Narainsamy & Jacobsz (2022), and additional details of the review are provided in Appendix A

Figure 3.1 shows a typical undrained shear response observed for the Quebec gold tailings tested by Fotovvat & Sadrekarimi (2022). As was noted for the gold tailings from the Witwatersrand supergroup, these Canadian gold tailings were mostly quarzitic in terms of mineralogical compositions. These tailings did however contain components of albite and feroan. These minerals are not typically found in gold tailings mined from the Witwatersrand supergroup. The two samples were prepared in the same manner (Moist Tamping), were consolidated to approximately a mean effective stress of 150 kPa, and to similar void ratios. The only meaningful difference between the two samples was the stress state imposed during consolidation. For sample ICU1, isotropic stress conditions were maintained while for sample CKCU2, anisotropic stress conditions were maintained. Specifically, a K_c value of 0.57 was targeted at the end of the consolidation phase.

© University of Pretoria

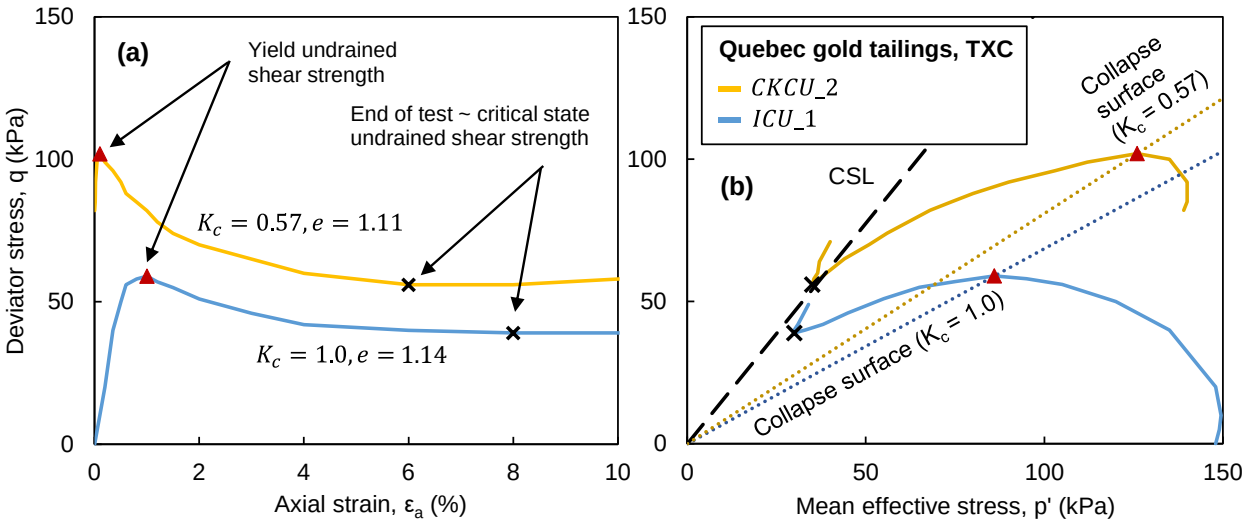


Figure 3.1: Typical undrained shear response observed for the Quebec gold tailings in: (a) $q - \varepsilon_a$ space, and (b) $q - p'$ space (after Fotovvat & Sadrekarimi, 2022)

There are three key differences between the two samples. These differences were consistently noted for all the tests reviewed, and are described below:

1. Difference in yield undrained shear strength.
2. Difference in axial strain require to reach the yield strength.
3. Difference in post-peak behaviour.

Difference in yield undrained shear strength

In Figure 3.1 the yield undrained shear strength is represented by a red triangular marker. It can be seen that the magnitude of the yield undrained shear strength is significantly different between the isotropically consolidated sample and the anisotropically consolidated sample. The isotropically consolidated sample yielded at a deviator stress of 59 kPa, while the anisotropically consolidated sample yielded at a deviator stress of 102 kPa. This is an important point to note as in some cases, the yield undrained shear strength is used as a direct input for stability assessments.

Difference in axial strain to reach the yield strength

The isotropically consolidated sample reached the yield strength at a strain level of 1.0% while the anisotropically consolidated sample reached a yield strength at a strain level of 0.1%. When considering undrained shearing, it has been postulated that loose, sandy soils will collapse upon intersecting the collapse surface (e.g. Sladen et al., 1985). Knowledge of the in-situ stress state is therefore of great importance to design engineers and regulators, especially when considering triggers that could lead to undrained events. It could be that some

© University of Pretoria

trigger events become plausible when it is known that only a small amount of strain is required to reach yielding.

Difference in post-peak behaviour

From the results shown in Figure 3.1, it can be seen that both the isotropically consolidated and anisotropically consolidated sample exhibited a strain-softening response. However, there is clearly a difference between the post-peak behaviour of the two samples. One approach to quantify the difference in response is to use the Brittleness Index (I_B) as defined by Bishop (1971). Using this index, values of $I_B = 0.35$ and $I_B = 0.45$ can be defined for the isotropically and anisotropically consolidated samples, respectively. This is a useful example as it provides an example of how the same soil can be classified on either side of the $I_B = 0.40$ value which has significant implications related to the design process as described by ICOLD (2022) and again perhaps highlights some of the limitations of using brittleness as a material classification, rather than a state classification.

Figure 3.2 shows a comparison of the yield undrained shear strengths of the isotropically consolidated samples (indicated with blue markers) and the anisotropically consolidated samples (indicated with yellow markers) of the Quebec gold tailings. When summarised in this form, it becomes quite clear that there is a distinct difference between the yield undrained shear strengths of the isotropically and anisotropically consolidated samples.

The yield undrained strength ratio (defined in terms of mean effective stress, rather than vertical effective stress as is common when assessing field data) for the isotropically consolidated samples is 0.20 which is expected for a sandy soil based on the literature review by Olson & Stark (2003). However, what is of interest is the yield undrained strength ratio for the anisotropically consolidated samples of 0.38. This value is almost double the value of the isotropically consolidated sample and, as discussed earlier, is important as this yield undrained shear strength is used directly for design and safety evaluation purposes in some guidelines (e.g. ICOLD, 2022). Although these ratios can readily be achieved in the laboratory, the use of yield undrained strength ratios significantly greater than those found in the literature should be done with caution.

This review was also conducted for triaxial tests conducted on three other sandy soils and similar results were found. Details of this review are provided in Appendix A

© University of Pretoria

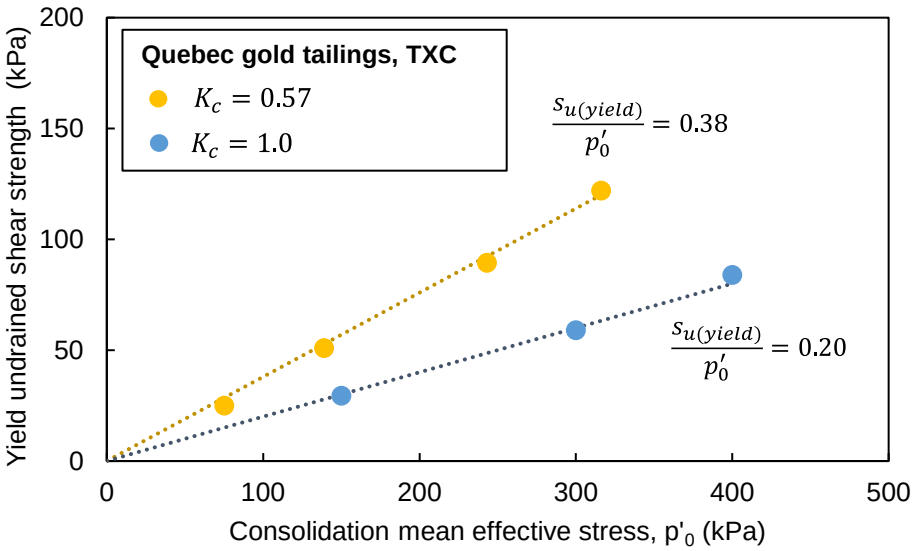


Figure 3.2: Comparison of yield undrained shear strengths for the Quebec gold tailings (after Fotovvat & Sadrekarimi, 2022)

3.3 GOLD TAILINGS CHARACTERISTICS

The focus of this study is on gold tailings obtained from an active tailings dam located in the East Rand of the Gauteng Province in South Africa. This section provides details regarding the physical and mineralogical characteristics of the gold tailings. Additional details of the site are presented in Section 6.2.1

3.3.1 Physical characteristics

Although it is known that the grading will vary within an active tailings dam, it was decided that instead of testing a range of gradings, a single representative grading would be used for all of the experimental work. The representative grading was chosen to match the grading in the structural zone of the tailings dam, which is key for design and safety evaluation activities.

Table 3.1 summarises the key indicator values for the gold tailings assessed as part of this study. Unless otherwise stated, average values are presented. The minimum void ratio was determined in accordance with ASTM D4253-16 (ASTM, 2016a) where Test Method 1A was used and an average void ratio was calculated for the two tests conducted. Similarly, the maximum void ratio was determined in accordance with ASTM D4254-16 (ASTM, 2016b). In this case, both Methods A and C were followed, and an average void ratio was determined.

© University of Pretoria

The specific gravity was determined using the gas pycnometer method as per ASTM D5550-14 (ASTM, 2014). The median grain size was determined using a grading curve generated by means of laser diffraction in accordance with ISO 13320:2020 (ISO, 2020). In terms of classification, the gold tailings can be classified as a nonplastic sandy silt according to the Unified Soil Classification System (USCS) as described in ASTM D2487-17 (ASTM, 2017).

Table 3.1: Indicator parameters of the gold tailings assessed as part of this study

Parameter	Symbol	Value	Test Method
Minimum void ratio	e_{min}	0.47	ASTM D4253-16
Maximum void ratio	e_{max}	1.57	ASTM D4254-16
Specific gravity	G_s	2.74	ASTM D5550-14
Median soil grain size	D_{50}	0.063 mm	ISO 13320:2020
Soil classification		s(ML) – nonplastic sandy silt	ASTM D2487-17

3.3.2 Mineralogical characteristics

XRD testing was performed on samples obtained from site at the laboratories at the University of Pretoria's Geology Department. Two samples were collected: a daywall sample, and a basin sample. The samples were coated with Carbon and interpretation was done in accordance with the Rietveld method (Rietveld, 1969). These results from the XRD testing have been summarised in Table 3.2. It can be seen that the gold tailings comprise predominantly of quartz with trace amounts of other minerals such as pyrophyllite and pyrite. The XRD spectrographs of the gold tailings are provided in Appendix B.

Table 3.2: Results from the XRD testing on the gold tailings

	Gold tailings (Basin)	Gold tailings (Daywall)
Quartz	94.6	95.7
Muscovite	0.9	0.5
Pyrophyllite	2.5	2.3
Illite	0	0
Clinochlore	0	0
Kaolinite	0	0
Pyrite	2.0	1.4

© University of Pretoria

It is known that the chemistry of the water can influence the electrical resistivity of a soil. This is particularly important as one of the sensors used in the remote monitoring system works on the principle that soil moisture content can be inferred from the electrical resistivity of a soil. Therefore, it is important to understand the chemistry of the water used both on site, as well as in the laboratory. To investigate this, a chemical analysis was conducted on water samples obtained from the geotechnical laboratory at the University of Pretoria, as well as from site.

Process water was collected from the discharge point at the crest of the dam. This water was sent to a South African National Accreditation System (SANAS)-accredited laboratory for testing.

The composition of the process water sample obtained from the gold tailings site is shown in Table 3.3. Also shown in the table are results from process water analysis of another gold tailings dam in Gauteng, specifically the Mispah tailings dam (Vermeulen, 2001). For each measured parameter, the acceptable limit for drinking water quality according to SANS 241:2015 has been provided.

To provide context for these values, commentary has been provided from the guideline document published by the Department of Water Affairs and Forestry (DWAF) (DWAF, 1996). The document provides a comprehensive overview of the rationale behind the development of the drinking water standard. Of particular interest for this study are the potential effects of ingestion of water containing elevated levels of particular minerals or elements.

It can be seen that for several of the elements, the concentrations found in the process water collected from site are above the recommended limits for drinking water. Therefore it will be important to conduct tests using both sources of water to determine if there is any influence of the water chemistry on the performance of the moisture content sensor.

© University of Pretoria

Table 3.3: Process water composition of the gold tailings, compared to national drinking water limits

	Gold tailings, this study	**Mizpah, after Vermeulen (2001)**	**Laboratory tap water**	**Drinking water limits (SABS, 2015)**	**Comments regarding the gold tailings process water (after DWAF, 1996)**
Date Tested	20/03/2023	03/03/1997	28/06/2023		
pH - Value @ 25 ºC	9.3	8.4	7.6	≥ 5.0 - ≤ 9.7	Within acceptable criteria.
Electrical Conductivity in mS/m @ 25°C	309	452	21.5	170	Above limit. See comments under Total Dissolved Solids (TDS), TDS is directly proportional to the Electrical Conductivity of water.
Total Dissolved Solids @ 180°C	2338	3560	126	1200	Above limit. There are several physiological effects which may be directly related to high concentrations of dissolved salts, including laxative effects, adverse effects for certain cardiac patients and hypertension sufferers, as well as some effects on kidney function.
Total Alkalinity as $CaCO_3$	112	40	64		No limit specified.
Chloride as Cl	254	310	15	300	Within acceptable criteria.
Nitrate as N	8.3	42	0.8	11	Within acceptable criteria.
Nitrite as N	14	N/A	N/A	0.9	Above limit. Upon absorption, nitrite combines with the oxygen-carrying red blood pigment, haemoglobin, to form methemoglobinemia, which is incapable of carrying oxygen.

© University of Pretoria

	Gold tailings, this study	Mizpah, after Vermeulen (2001)	Laboratory tap water	Drinking water limits (SABS, 2015)	Comments regarding the gold tailings process water (after DWAF, 1996)
Ortho Phosphate as P	<0.1	<0.5	0.1		No limit specified.
Sodium as Na	397	468	8	200	Above limit. Sodium intake can exacerbate certain disease conditions such as hypertension, as well as cardiovascular and renal diseases.
Potassium as K	34	78	3.5	50	Within acceptable criteria.
Calcium as Ca	266	640	15	150	Above limit. There is no conclusive evidence to support claims for the increased incidence of human kidney and urinary tract stones resulting from the long-term consumption of water with high concentrations of calcium. Rather, scaling is the principal undesirable effect of increased calcium levels. Scaling occurs in water heating appliances such as kettles and urns.
Magnesium as Mg	11	30	8	70	Within acceptable criteria.
Iron as Fe	36	<0.5	0.212	2	Above limit. The major effects of the presence of iron in domestic water are aesthetic. However, health effects such as tissue damage, may occur as a consequence

© University of Pretoria

	Gold tailings, this study	Mizpah, after Vermeulen (2001)	Laboratory tap water	Drinking water limits (SABS, 2015)	Comments regarding the gold tailings process water (after DWAF, 1996)
					of iron accumulation due to excessive ingestion at extremely high concentrations.
Manganese as Mn	0.834	0.8	<0.025	0.4	Above limit. The major effect of the presence of manganese in domestic water are aesthetic. However, health effects such as neurotoxic effects, may occur as a consequence of excessive ingestion at high concentrations.

© University of Pretoria

3.3.3 Site conditions

As was shown in Section 2.3.2, it is known that the response of a soil to changes in external loading is highly dependent on the state of the soil. One aspect of the soil state that can have a large influence of on the soil response is the void ratio. This has been shown to be especially true for the undrained shearing response of sandy soils. Since gold tailings is a sandy soil, and since the current uncertainty relates to undrained shearing, it therefore holds that it is important to know the density of the soil in the field, especially near the monitoring positions.

During the monitoring period, samples were taken at various depths adjacent the monitoring locations. A specially fabricated aluminium box was used for the sampling. The box was made using 1.5 mm thick steel plate and was 150 mm in length, 150 mm wide and 150 mm in height. The dimensions of the box were verified at the start and end of each day of sampling using a vernier calliper with a resolution of 0.01 mm. The wet and dry masses were determined using a calibrated mass balance with a resolution of 1 g and all the samples were oven-dried for at least 24 hours at a temperature of 105°C.

Figure 3.3(a) shows the sampler already pushed into the tailings and the tailings being removed from around the sampler. The box was gently tamped into the tailings until the top of the box was just below the surface. A steel plate was slid under the sampling box to assist with recovery of the sample. Figure 3.3(b) shows the extracted sample on surface. This particular sample was taken at a depth of 0.38 m below surface, adjacent to monitoring Station 3 at the gold tailings site. At this time, the sensors were approximately 1.1 m below the tailings surface.

Once the photograph was taken, the sample was carefully emptied into a sample bag, labelled and sealed. The sample was transported on the same day to the University of Pretoria where the wet mass was recorded. A total of 24 samples were obtained from site over the course of the monitoring period.

© University of Pretoria



Figure 3.3: Sample collection at the gold site showing: (a) sample being extracted, and (b) extracted sample on surface

Figure 3.4 shows a summary of the interpreted in-situ void ratios of the gold tailings. These void ratios were used to inform the parameters for the laboratory testing. It can be seen that the void ratios varied between 0.82 and 1.11, with an average void ratio of 0.97. For reference, the values have also been split between the three stations. Additional details regarding the three stress stations are provided in Section 6.2.2.

© University of Pretoria

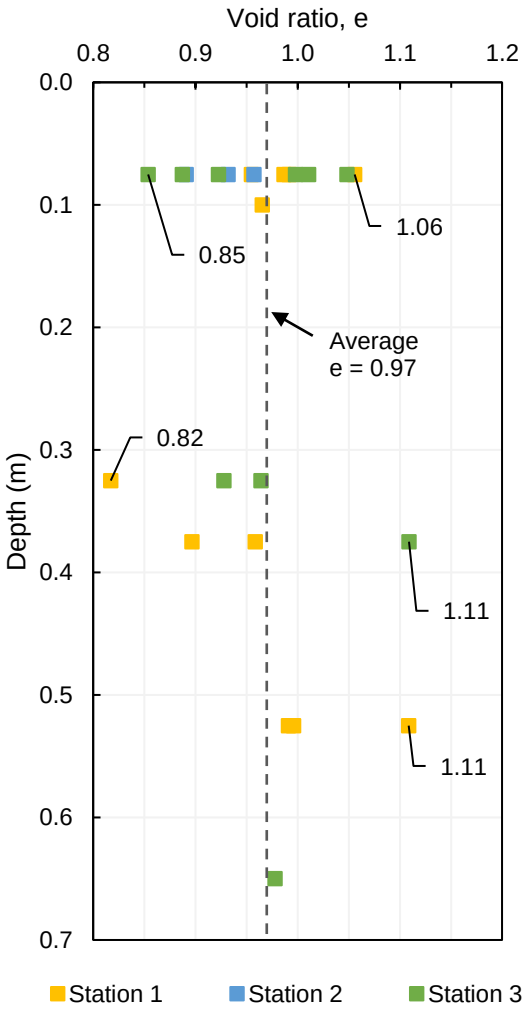


Figure 3.4: Summary of void ratio measurements taken on site during the monitoring period

Figure 3.5 shows a soil profile at the gold tailings site. This profile was exposed as part of an excavation that was created close to monitoring Station 1. At this point in time, the sensors were approximately 1.5 m below ground level. The measuring tape shows the depth below the tailings surface. It can be seen that the profile is not homogeneous. Rather, the profile is characterised by thin, alternating layers of coarse and fine tailings. This occurs due to the initial settling of the larger particles and is a well-known result of the deposition methodology employed at the site (e.g. Blight, 2009). Additional details of the site and the deposition methodology employed are provided in Section 6.2.1.

The finer material appears darker in colour, while the coarser material appears lighter in colour. This is due to the moisture content of the layers. The adjacent layers are assumed to be in suction equilibrium with each other. However, due to their particle sizes, the same suction value occurs at different moisture contents. The coarser material therefore exists at a lower moisture content than the finer material. This classification of the grading based on apparent colour (due to moisture

© University of Pretoria

content) was confirmed by the grading curves developed using samples of these layers, as shown in Figure 3.10.

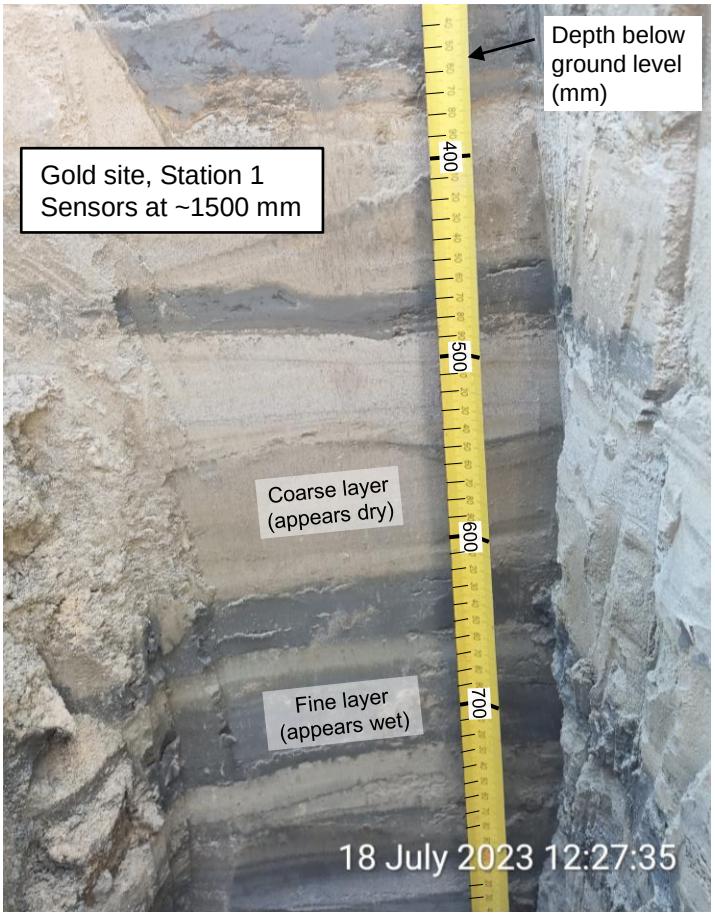


Figure 3.5: Photographs taken on site showing the layering at the gold tailings site

3.4 OEDOMETER TESTING

A key aspect of the oedometer testing was to investigate the uniqueness of the 1D-NCL for the gold tailings. The oedometer test is ideal for investigating this behaviour as it is capable of imposing high stresses on the sample and, due to the presence of the confining ring, there is little uncertainty regarding the void ratio of the sample during the test. Both of these aspects are crucial for any investigation regarding the uniqueness of the 1D-NCL, with the latter being especially true for loose samples, which is the target for this study.

As discussed earlier, when performing standard oedometer tests, the complete stress state is not known. The applied vertical total stress is known, based on the known applied mass, the lever arm ratio and the cross-sectional area of the sample. The pore pressure is assumed to be negligible and therefore the vertical effective stress is known. The oedometer ring provides lateral

© University of Pretoria

confinement to the sample and ensures zero radial strain. Although the radial strains are enforced as zero, there is no control of the lateral stresses which must exist. These stresses cannot be measured using a conventional oedometer apparatus and some assumptions need to be made if the complete stress state is of interest.

As discussed in Section 2.3.1, it has been shown experimentally that the 1D-NCL is parallel to the NCL for plastic clays and clean sands when plotted on a semi-log plot with void ratio on the vertical axis and mean effective stress on the horizontal axis (Atkinson & Bransby, 1978; Coop, 1990). However, there is some uncertainty regarding whether this is true for gold tailings. This assumption of whether the 1D-NCL is parallel to the NCL for gold tailings is one of the objectives of this laboratory testing campaign.

3.4.1 General procedure

The oedometer testing was conducted in accordance with ASTM D 2435 (ASTM, 2011). In particular, Test Method B was followed where time-based deformation readings were obtained for all the loading and unloading increments. Increments were considered complete when 100% of primary compression or swell had occurred, with a minimum waiting time of two hours.

Two different mass balances were used to confirm the masses of the mass pieces used for the loading increments. For mass pieces less than 6 kg, a mass balance with a capacity of 6 kg and a resolution of 0.01 g was used. For mass pieces with a mass greater than 6 kg, a mass balance with a capacity of 32 kg and a resolution of 1 g was used. Standard steel oedometer rings with a height of 18.9 mm and a diameter of 76.2 mm were used. The height and diameter of each oedometer ring was verified using a calibrated vernier calliper with a resolution of 0.01 mm, before and after each test. Care was taken to ensure that the samples were level with the top and bottom of the oedometer ring to minimise bedding errors.

Samples were prepared to the desired densities using the MT sample preparation technique. The samples were prepared at a moisture content of 15% and were created in a single layer. In addition to performing moisture content tests on the bulk mixture used the create the sample, initial moisture contents were verified by taking end-of-test moisture contents, assuming full saturation, and performing a backwards analysis.

The University of Pretoria has several ELE International 3 200 kPa consolidation frames with lever arm ratios of 1:10 and built-in ELE International mechanical dial gauges. These frames were used for the testing. Settlement readings were recorded using the dial gauges which had a range of

© University of Pretoria

25 mm and a resolution of 0.02 mm. A digital stopwatch, operated by an independent technician not involved in the reading of the dial gauges, was used to record the time between dial gauge readings to the nearest second.

As is it known that loose, sandy soils are prone to collapse upon saturation the first load increment of 5 kPa was performed in two steps. In the first step, the load was applied to the unsaturated soil and settlement was allowed to occur. Once primary settlement had been completed the second step commenced. In the second step, the cell was flooded with water while the applied load was kept constant at 5 kPa and compression was allowed to occur. The start and end of these two steps have been labelled as “wetting-induced collapse” in the appropriate figures.

A summary of the key aspects of the oedometer tests is shown in Table 3.4.

© University of Pretoria

Table 3.4: Summary of key aspects of the oedometer tests

Test	Test ID	Initial void ratio (e_i)	Initial relative density (%)	Specific volume at 5 kPa (v_5)	Specific volume at 2 400 kPa (v_{2400})	Comments
1	e_i=1.19	1.19	34.5	1.98	1.63	Loosest specimen. Minimal compaction effort required during sample preparation. Large settlement upon wetting ($\Delta e = 0.23$).
2	e_i=1.03	1.03	49.1	1.98	1.60	Loose specimen. Low compaction effort required during sample preparation. Moderate settlement upon wetting ($\Delta e = 0.09$).
3	e_i=0.80	0.80	70.0	N/A	N/A	Test was abandoned at the 400 kPa stress increment due to a dial gauge malfunction.
4	e_i=0.78	0.78	71.8	1.78	1.57	Sample was prepared by hand tamping. Moderated compaction effort was required during sample preparation.
5	e_i=0.62	0.62	86.4	1.62	1.54	Sample was statically compacted in a hydraulic press. A peak force of 25.5 kN (~5.7 MPa) was applied during compaction.
6	e_i=1.00	1.00	51.8	N/A	N/A	Test performed to obtain a sample for grading analysis. Minor settlement upon wetting ($\Delta e = 0.01$).
7	e_i=0.99	0.99	52.7	N/A	N/A	Test performed to obtain a sample for grading analysis. Minor settlement upon wetting ($\Delta e = 0.03$).

© University of Pretoria

3.4.2 Uniqueness of the 1D-NCL

As discussed in Chapter 1, one of the objectives of this study was to investigate the uniqueness of the NCL for the gold tailings. Knowledge of this aspect can greatly influence decisions made regarding laboratory test planning, as well as decisions made for future changes to an active tailings dam. This is particularly important when designing a laboratory test plan for CSL testing and numerical model calibrations as inadvertently imposing a stress history on a specimen during sample preparation can influence its usefulness for calibration purposes. Specifically, the objective was to investigate the uniqueness of the 1d-NCL for the average grading of the gold tailings for remoulded samples prepared using the MT sample preparation method.

The oedometer is an attractive apparatus for compression testing due to the simplicity of the test method and the ability to apply high stresses. However, as discussed earlier, the stress conditions imposed during oedometer testing are not the same as those required to define the NCL. Therefore, the compression curve obtained from oedometer testing is called the 1D-NCL. However, it has been shown experimentally by many researchers that the 1D-NCL is parallel to the NCL for both fine-grained and coarse-grained soils. Therefore knowledge of the 1D-NCL is still useful.

A total of seven oedometer tests were conducted as part of this testing. Unfortunately, the dial gauge malfunctioned on one of the dense samples (e_i= 0.80) so that test was abandoned during the 400 kPa loading increment. In addition, two of the tests (e_i = 0.99 and e_i = 1.00) were only performed to investigate the influence of particle crushing. These tests were stopped at the 100 kPa and 400 kPa loading increments, respectively.

Therefore, only four tests were conducted with complete loading and unloading stages. For each test, three distinct phases have been highlighted: wetting-induced collapse, loading (compression), and unloading (swelling). The two loosest samples, with initial void ratios (e_i) of 1.19 and 1.03, required minimal compaction effort and were deemed to be in a NC state at the start of the test. The two densest samples (e_i = 0.62 and e_i = 0.78) required some compaction effort during sample preparation and were deemed to be in an OC state at the start of the test.

The second densest sample (e_i = 0.78) was compacted by hand and required the use of a tamper and a hammer. The densest sample (e_i = 0.62) required the use of a hydraulic press to achieve the desired density. A load cell was attached to the hydraulic press to monitor the forces imposed on the sample during compaction. A peak force of 25.5 kN was recorded. This force is equivalent to an imposed total stress of 5.7 MPa which clearly indicates that this sample was in an OC state

© University of Pretoria

at the start of the test.

The time required for 90% consolidation (t_{90}) was determined using Taylor's construction method (Taylor, 1948). The estimated coefficient of vertical consolidation (c_v) values ranged from 239 m^2/year to 472 m^2/year, while the estimated coefficient of permeability (k) values ranged between 1x10^{-9} and 1x10^{-7} m/s. These values compare well with those found in the literature for gold tailings mined from the Witwatersrand Supergroup (e.g. Vermeulen, 2001; Papageorgiou, 2004; Chang, 2009).

Figure 3.6 shows the oedometer test results on the gold tailings. Visually, it appears clear that there exists a unique curve onto which each curve collapses onto at large stresses. However, simply converging to a single slope is not sufficient to establish whether a unique 1D-NCL exists. What is needed is to consider the stress history for each test as was discussed in Section 2.3.1.

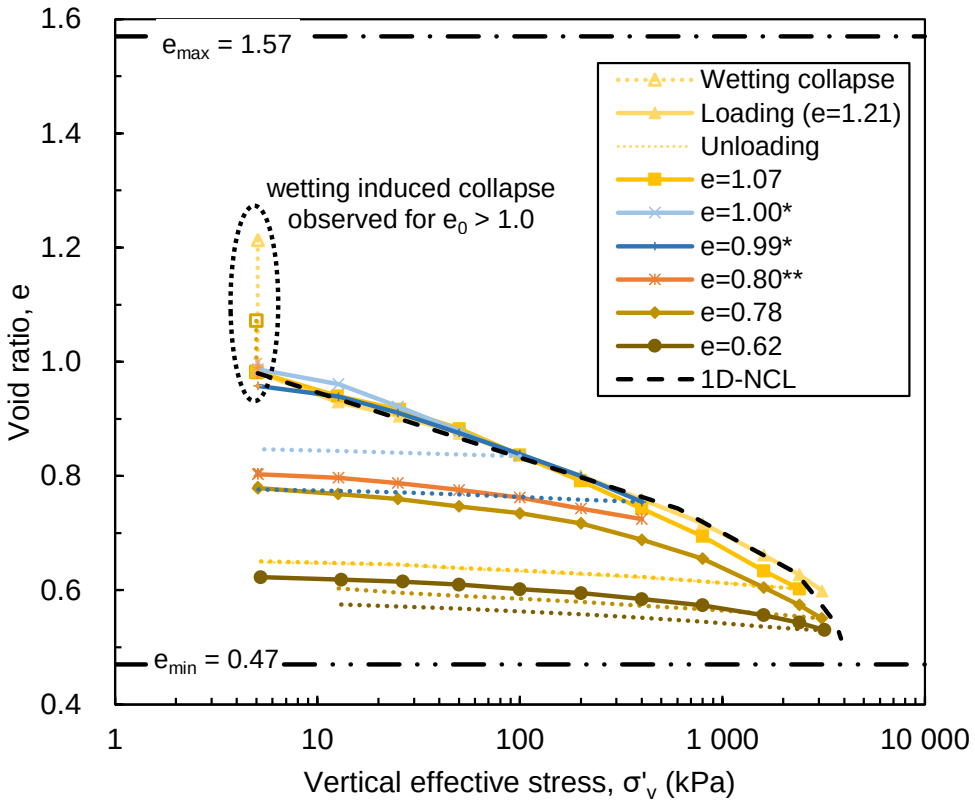
There are a few aspects of the compression curves shown in Figure 3.6 that are of interest. Firstly, the two loosest samples (e_i = 1.19 and e_i = 1.03) showed collapse during saturation. This behaviour is consistent with the CSSM framework for soils in a state looser than the 1D-NCL. Secondly, all four samples which were prepared to an initially NC state (e_i = 1.19, e_i = 1.03, e_i = 1.00, e_i = 0.99) showed consistent compression behaviour at low stresses. Further, all these samples tended sharply towards an apparently unique 1D-NCL at moderate stresses. The slope of these compression curves once they reach the proposed 1D-NCL are fairy similar and vary between 0.15 and 0.20. There is, however, a slight vertical offset between these curves.

Conversely, the three samples prepared at an initially OC state (e_i = 0.80, e_i = 0.78, e_i = 0.62), showed much flatter compression curves initially and then gradually tended towards the apparent unique 1D-NCL. The second densest sample (e_0 = 0.78) appeared to reach the 1D-NCL at the end of the 800 kPa loading increment. However, the densest sample (e_0 = 0.62) appears to still be approaching the 1D-NCL at the final stress increment of 3 200 kPa. This is consistent with the known applied stress of 5.7 MPa during sample preparation. Again, this behaviour is entirely consistent with the CSSM framework for soils with an initial state below the 1D-NCL.

The observed behaviour of the NC and OC samples is consistent with the idealised compression behaviour of fine-grained soils as shown in Figure 2.17(a). Although the compression curves of the gold tailings shown in Figure 3.6 look similar to the compression curves of the Erksak sand shown in Figure 2.18, there are two key differences. Firstly, the dense Erksak sand samples were prepared in a NC state, compared to the dense gold tailings samples (i.e. those with starting stress states below the 1D-NCL) which were prepared in an OC state. Secondly, the loose gold tailings

© University of Pretoria

samples (i.e. those with starting states above the 1D-NCL) showed significant collapse upon saturation at low applied stresses. This behaviour was not seen for the Erksak sand samples which were prepared with starting stress states above the PNCL.



* tests assigned for PSD analysis
**test abandoned, dial gauge malfunction

Figure 3.6: Oedometer test results on the gold tailings

To quantify the degree of convergence of the compression curves, the m value as proposed by Ponzoni et al. (2014) was calculated. Details regarding this method are provided in Section 2.3.2. Figure 3.7 shows a plot of the specific volume of the samples at an applied stress level of 2.4 MPa (v_{2400}) versus the initial specific volume (v_5), taken at 5 kPa for this study. Using this figure, an m value of 0.20 was calculated. This is comparable to value of 0.13 obtained for the Brazilian gold tailings at an applied loading of 7 MPa by Li (2017). In that research, it was found that the m value reduced to 0 at an applied loading of 20 MPa and the tailings was classified as having a unique 1D-NCL.

The m value of 0.20 obtained for the gold tailings is also lower than the value of 0.40, at which possible transitional behaviour was noted for the Venice Lagoon silts and silty clays (Ponzoni et al., 2014). This value is also significantly lower than the values of 0.64 and 0.71 that were obtained

© University of Pretoria

for Chinese copper tailings and Australian mineral sand tailings which were classified as transitional soils by Li (2017) and Cartwright et al. (2022), respectively. Therefore, for practical purposes, it can be concluded that there exists a unique 1D-NCL for the gold tailings tested.

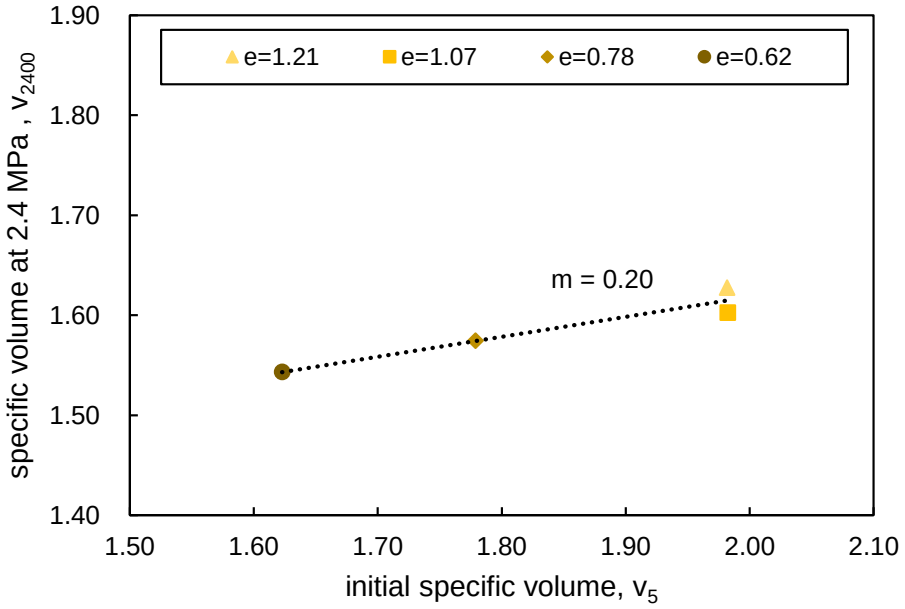


Figure 3.7: Quantification of the degree of convergence of the 1D-NCL of the gold tailings

3.4.3 Influence of particle crushing

To investigate the influence of particle crushing, a sample was taken after each test. The samples were labelled according to the maximum total stress applied to the sample during the test. The grading curves obtained from these samples were compared to the average grading curve of the bulk sample sourced from site, as well as the spread of gradings obtained from samples taken from the moisture content mixtures for the triaxial tests.

When returning material to the bulk sample storage area, care was taken to separate samples that had been subjected to stresses greater than 100 kPa. Therefore, a comparison of the gradings taken after the oedometer tests, and the gradings taken before the oedometer and triaxial tests, should only highlight any particle crushing that occurred during the oedometer testing.

The results of this investigation are shown in Figure 3.8. There is some evidence of an increase in fines content with an increase in applied loading. For instance, the D_{50} decreased from 0.063 mm to 0.055 mm for the initial grading and the grading for the sample that was subject to an applied loading of 3.2 MPa, respectively. However, this appears to be masked by the inherent variability in

© University of Pretoria

the gold tailings sample. Therefore, from a practical perspective, there appears to be limited particle crushing of the gold tailings, even at applied loads of up to 3.2 MPa.

The region shaded in blue in Figure 3.8 shows the extent of all the grading envelopes developed based on samples sourced from the bulk sample at the geotechnical engineering laboratory at the University of Pretoria. A total of 32 gradings tests were conducted to develop this region.

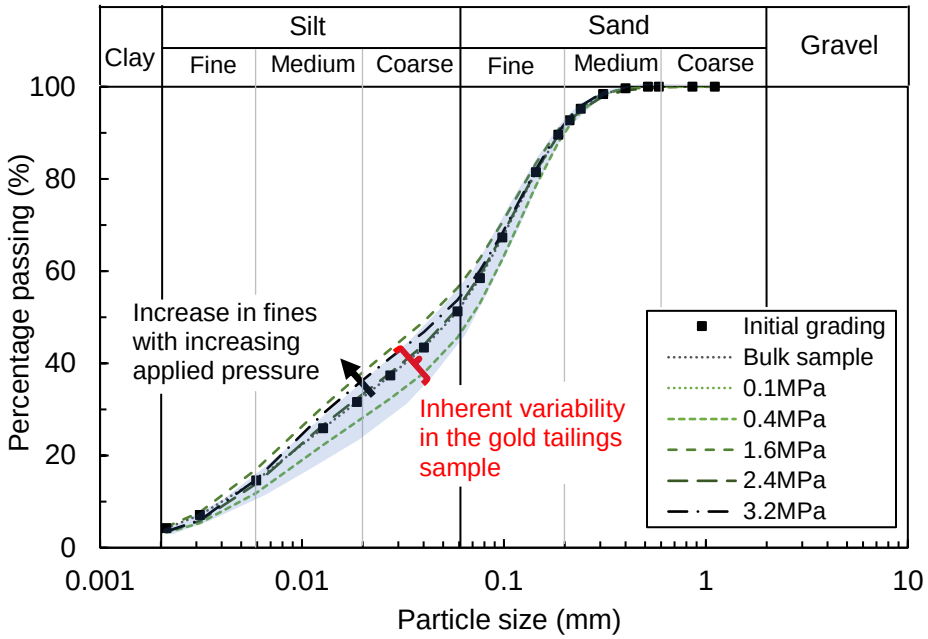


Figure 3.8: Influence of imposed stress on particle crushing of the gold tailings

3.4.4 Summary

A series of oedometer tests were conducted on the gold tailings to investigate two aspects: the uniqueness of the 1D-NCL, and the influence of stress level on particle crushing of the gold tailings. Regarding the uniqueness of the 1D-NCL, it was found that there does appear to be a unique 1D-NCL for the gold tailings tested.

Regarding the influence of imposed stress level on particle crushing, it was found that there is some evidence of an increase in fines with an increase in applied loading. However, the magnitude of this increase is small in comparison to the inherent variability in the grading of the gold tailings bulk sample from which the samples for the laboratory testing were sourced.

© University of Pretoria

3.5 TRIAXIAL TESTING

The NCL can be directly determined from the results of a standard triaxial test. This is due to the stress boundary conditions that are applied during consolidation. The NCL is also sometimes referred to as the Isotropic Compression Line. In addition to the investigation into the uniqueness of the NCL, the purpose of the triaxial testing was to define the CSL, as well as to investigate the undrained shear response of the gold tailings under various conditions. In particular, the influence of density and K_0 was investigated.

This section describes the triaxial testing conducted, as well as presents the results from these tests. Although the triaxial testing apparatus used for this testing has the capability of performing K_0-consolidation tests, the hardware required for these tests were not available at the time this study was being undertaken. These components included local strain instrumentation to record radial deformations, as well as an access ring required for the data communication cables for the local strain instrumentation. As a result, no K_0-consolidation tests were performed as part of the scope of this study.

3.5.1 General procedure

As part of a recent research collaboration, the University of Pretoria has procured state-of-the-art triaxial testing apparatus from Global Digital Systems (GDS) Instruments. Testing was performed in general accordance with the British Standard BS 1377 (BSI, 1990), with some minor changes as suggested in the guidelines provided by Jefferies & Been (2015). Testing was conducted in an access-controlled room where the temperature was regulated to ensure there was no undue influence of temperature changes on the pore pressure within the samples, as was observed by Torres-Cruz (2016).

With the exception of the slurry samples, which were mixed as a slurry and allowed to air dry in a large bucket as described by Reid et al. (2022c), the samples were prepared using the MT sample preparation method at a moisture content of 15%. Samples were created in eight layers of equal height but with different masses. The undercompaction technique as proposed by Ladd (1978) was used to create uniform samples to the desired initial void ratio. Samples were created with the use of a split-mould to a target diameter of 70 mm and height of 140 mm.

The mass of each layer was determined using a calibrated mass balance with a capacity of 800 g and a resolution of 0.001 g. Similarly, the height of each layer was controlled using an adjustable collar on the tamper, the height of which was set and verified using a calibrated vernier calliper

© University of Pretoria

with a resolution of 0.01 mm. Once all eight layers had been constructed, the split-mould was removed, and the final diameter and height of the sample were determined using the same vernier calliper.

During the test, the sample height was monitored using the Linear Variable Differential Transformer (LVDT) attached to the loading ram. A nominal contact load of 20 N (approximately 5 kPa, based on the sample surface area) was applied for the duration of the flushing and saturations stages. During consolidation, this load was maintained for the isotropic tests but was adjusted as required for the anisotropic tests.

All measurements were recorded digitally using the GDS triaxial data acquisition software, GDSLab v2.8.4 (GDS Instruments, 2017). The change in height of the sample was measured using a calibrated LVDT with a range of 50 mm and a resolution of 0.001 mm. The cell and back pressures and volumes were measured using second-generation GDS Instruments automated pressure controllers (V2), which have a resolution of 0.1 kPa and 1 mm^3 for the pressure and volume, respectively. These pressure controllers have a maximum operating capacity of 2 MPa and a storage volume of 200 cm^3. Pore pressures were measured at the base of the sample using a calibrated 2 MPa pressure transducer with a resolution of 1 kPa.

To improve the accuracy of the end of test void ratio determination, and to eliminate the uncertainties involved with the saturation-induced collapse of loose sandy samples, the gold tailings samples were squeezed using the method proposed by Verdugo & Ishihara (1996). At the end of the test, the wet and dry sample masses were determined using a calibrated mass balance with a capacity of 6 kg and a resolution of 0.1 g.

Each triaxial test performed can be uniquely identified in two ways. The first is the Test Reference Number, which has been shortened to “Test Ref” in the appropriate tables. This is simply an integer, and each successive test that was conducted was given the next integer. The purpose of the Test Reference Number was to assist with the correct association of grading samples, photographs and test data to the correct sample. Note that not all the tests conducted are presented.

The second manner in which each triaxial test can be identified is the Test Identifier, which has been shortened to “Test ID” in the appropriate tables. The purpose of the Test Identifier is to provide each test with a unique label that provides key information regarding the test. The following code was used for the Test ID:

© University of Pretoria

CXXXX_eX.X_KX.X_X

Where:

- **CXXXX - Consolidation stress and shear conditions, e.g.:**
  - CU100 – consolidated to p'=100kPa, sheared undrained
  - CD100 – consolidated to p'=100kPa, sheared drained
  - CU100(4) – consolidated to p'=400kPa, swelled to p'=100kPa, sheared undrained
  - Con100 – consolidated to p'=100kPa, no shear

- **eX.X - Target void ratio during sample preparation, e.g.:**
  - e1.0 – sample prepared to an initial void ratio of e=1.0
  - e0.8 – sample prepared to an initial void ratio of e=0.8

- **KX.XX - Target stress ratio during consolidation, e.g.:**
  - K1.0 – sample consolidated under a target stress ratio of K_c=1.0
  - K0.5 – sample consolidated under a target stress ratio of K_c=0.5

- **X - Additional test information, e.g.:**
  - SD – sample prepared using the SD method
  - LC – test performed under load-controlled conditions
  - 2 – duplicate test

To further clarify the Test ID, some examples have been provided in Table 3.5.

Table 3.5: Examples of triaxial Test IDs, with a detailed description

Test Ref	Test ID	Description
Test 12	CU100_e1.0_K0.5	The sample was consolidated to p'=100 kPa and sheared undrained. The sample was prepared to an initial void ratio of e=1.0 and consolidation was performed with K_c=0.5.
Test 28	CU100_e1.2_K1.0_2	The sample was consolidated to p'=100 kPa and sheared undrained. The sample was prepared to an initial void ratio of e=1.2 and consolidation was performed with K_c=1.0. This was a duplicate test at these conditions.
Test 29	CD100(8)_e0.8_K1.0_SD	The sample was consolidated to p'=800 kPa, unloaded

© University of Pretoria

		to p'=100 kPa, and then sheared drained. The sample was prepared to an initial void ratio of e=0.8 and consolidation was performed with K_c=1.0. The sample was prepared using the SD method.
Test 32	Con1500_e1.4_K1.0	The sample was consolidated to p'=1500 kPa. No shear phase was performed. The sample was prepared to an initial void ratio of e=1.4 and consolidation was performed with K_c=1.0.

3.5.2 Key behavioural aspects

Table 3.6 provides a summary of four key aspects of soil behaviour relating to tailings dam safety. These aspects include the influence of density on the undrained stress-strain response; factors influencing the yield undrained shear strength, factors influencing brittleness, and factors influencing the CSL. For each aspect, a description has been provided, as well as a short summary of the findings from this study.

© University of Pretoria

Table 3.6: Four key aspects of soil behaviour relating to tailings dam design and safety evaluation procedures

Aspect	Description	Findings from this study
The influence of density on the undrained stress-strain response	Not all soils behave poorly in undrained shearing. Rather, there is extensive theoretical and experimental evidence supporting the notion that the density of a soil plays a key role in the stress-strain response during undrained shearing. With all other aspects remaining equal, dense soils tend to exhibit strain-hardening behaviour, while loose soils tend to exhibit strain-softening behaviour. However, even for strain-softening soils, it is well established that not all contractive soils are strain-softening, and not all strain-softening soils have high brittleness (e.g. Robertson, 2017). Rather, this undrained shear behaviour is highly dependent on several factors, one of them being initial density. It has been shown for clean sands that a change in behaviour from limited strain-softening to significant strain-softening can occur over void ratio changes as small as 0.06 (e.g. Castro, 1969). However, there is limited published data on this aspect for gold tailings.	In this study, six gold tailings samples were consolidated to the same mean effective stress of 100 kPa, but at varying initial void ratios. The samples were then sheared under undrained conditions and the stress-strain response was observed and compared. As expected from the theory, and previous tests on sands, a range of stress-strain responses were noted. This varied from strain-hardening for the dense samples, and progressively changed to strain-softening for the loose samples. For the loose samples, it was specifically found that for a small change in void ratio of 0.04 (between e = 0.74 and e = 0.78), a marked change in behaviour from limited strain-softening to significant strain-softening was noted. This is important to know for a number of reasons, including the magnitude of sample disturbance for soft tailings samples, as well as the accuracy of method to infer the in-situ state. Errors in both cases have been shown to be larger than this value, even when modern techniques are used (e.g. Fourie et al., 2022).

© University of Pretoria

Aspect	Description	Findings from this study
Factors influencing the yield undrained shear strength	When assessing the undrained stability of an embankment, it is common to use the yield undrained shear strength, typically presented in the form of a stress ratio, $S_{u(yield)}/p'_0$. In some cases, this value is used directly in designs and safety evaluations (e.g. ICOLD 2022)). However, this parameter is not a material characteristic such as the critical state friction angle and varies with soil state. Although this is known, there is limited published experimental data regarding this. This is especially true for silty soils such as mine tailings.	In this study, the influence of both initial density and stress anisotropy (stress history) on the yield undrained shear strength was investigated. In terms of density, it was shown that for a change in void ratio from 0.74 to 0.78, a change in yield undrained strength ratio ($S_{u(yield)}/p'_0$) from 0.44 to 0.20 was noted. In terms of stress history, it was shown that for a change in K_c from 0.95 to 0.54, $S_{u(yield)}/p'_0$ changed from 0.20 to 0.36.
Factors influencing brittleness	Brittleness in the context of undrained shearing refers to the stress-strain behaviour of a soil after the peak strength value is reached. Brittle soils exhibit a large reduction in strength post-peak while non-brittle soils exhibit a small reduction in strength (if any). The Brittleness Index (I_B) as defined by Bishop (1971) is commonly used to classify the magnitude of brittleness of sandy soils. Like the yield undrained shear strength, brittleness is not a material characteristic. Rather, it is a state-dependent characteristic and has been shown theoretically to vary significantly depending on the state of the soil.	In this study, it was shown how two aspects of state can significantly influence the brittleness of a soil. Using the Brittleness Index (I_B), and the I_B = 0.4 boundary as suggested by ICOLD (2022) for separating soils with high brittleness and low brittleness, a few points can be made. For a small change in void ratio from 0.74 to 0.78, the samples changed from being classified as moderately brittle (I_B = 0.24) to being classified as highly brittle (I_B = 0.62). Similarly, for a change in K_c from 0.95 to 0.54, it was shown that I_B changed from 0.77 to 0.49. Although this change does not cross the 0.40 boundary, it is

© University of Pretoria

Aspect	Description	Findings from this study
	As was found with the yield undrained shear strength, although this is known, there is limited published experimental data regarding this aspect. This is especially true for silty soils such as mine tailings.	still a large difference and can have a meaningful impact of designs and safety evaluations. Since it is known that these conditions vary in the structural zone of a tailings dam, designs and safety evaluations that classify soils according to their brittleness need to be used with care.
Factors influencing the CSL	A key principle of CSSM is that understanding the state of a soil is key to predicting its future behaviour. However, the state only influences the soil behaviour at low and moderate strains. At large strains, when the sample approaches critical state, the soil behaviour is essentially independent of the initial state. This has been shown experimentally for many soils (e.g. Jefferies & Been, 2015). It is acknowledged that some soils, such as transitional soils as described by Coop (2015), do not conform to this principle. However, the gold tailings considered as part of this study is deemed to not be a transitional soil, as shown in Section 3.6. Knowledge of the CSL provides the framework in which	In this study, 21 MT samples were tested over a range of initial densities, stress levels, and hydraulic boundary conditions during shearing. A unique CSL was identified as a straight line in the $e - \ln p'$ space. Five SD samples were tested to supplement the MT tests. It was found that all five SD samples did not conform to the CSL defined using the MT samples. Rather, the SD samples were found to fit better with a CSL defined with the same slope (λ_e = 0.035), but with a different intercept (Γ_1 = 0.805), a difference of 0.07 compared to the CSL defined using the MT samples. This suggests that the sample preparation method does influence the critical state behaviour of the gold tailings which is in direct violation of one of the key principles of CSSM. This has been noted by other researchers for gold tailings (e.g.

© University of Pretoria

Aspect	Description	Findings from this study
	soils can be classified as contractive or dilative at large strains, which is the crucial first step in any design against undrained shearing. However, many laboratories use the MT sample preparation method as it facilitates the accurate creation of both loose and dense samples. This is important as it is known that the fabric created by MT is different to the fabric of the tailings in the field, which is perhaps better captured by using SD samples. A comparison between the large-strain behaviour of MT and SD samples is therefore of interest for the gold tailings.	Reid et al., 2022c) and iron ore tailings (e.g. Mmbando et al., 2023). However, all these studies were limited in nature. This aspect needs to be carefully considered as it can have a meaningful influence on methods which use the CSL for field investigations.

© University of Pretoria

3.5.3 Indicator characteristics of the triaxial samples

As discussed earlier, it is known that the grading of a soil influences both its compressibility and shearing characteristics. Similarly, since the density of each sample is defined in terms of void ratio, it is important to know the specific gravity of the sample and more importantly, if there are any changes with time or sampling procedures.

Since the material for the laboratory tests were sourced from a large, bulk sample (>1 m^3) that was obtained from site and stored in a container, there was some concern that there could be a sampling bias when obtaining samples from the storage container. This bias could be due to natural segregation and settlement of larger or denser particles. To combat this, a rigorous sampling procedure was undertaken for each test sample. A larger volume of material that required (typically three times the required volume) was collected the top, middle and bottom of the container where the bulk sample was stored. This material was then placed in an oven for 24 hours at 105°C. After drying, the sample was allowed to cool and then thoroughly mixed by hand.

To verify the performance of the sampling methodology, samples were taken from almost every test and tested to determine the grading and particle density. The samples were taken before any imposed loading to ensure that the influence of any particle crushing during the test was not inadvertently considered. Specific gravity testing was performed using the gas pycnometer method as described in ASTM D5550-14 (ASTM, 2014) while the particle size distribution curves were obtained using the laser diffraction method as described in ISO 13320:2020 (ISO, 2020). The laser diffraction method has been shown to provide comparable results to traditional sieve and pipette methods for silty and sandy soils (e.g. Wen et al., 2002).

Figure 3.9 shows a summary of all the specific gravity test results. The field samples are those taken on site and are shown in blue, while the laboratory samples are those taken from the bulk sample which was brought back to the laboratory and are shown in orange. It can be seen that there is an apparent bias with the laboratory sampling technique, resulting in the laboratory samples having a slightly lower G_s. In total, 10 field samples and 24 laboratory samples were sent for testing. For each test, three results were obtained resulting in a total of 30 data points for the field samples and 72 data points for the laboratory samples. An average G_s value of 2.72 was determined for the field samples and an average G_s value of 2.67 was determined for the laboratory samples.

© University of Pretoria

Although a difference was noted between the various samples, it was decided that the variation is small and that it would be more appropriate to use an average specific gravity of 2.74 for all the calculations regarding the gold tailings. This is in line with the specific gravity used for previous analyses of the same gold tailings at the University of Pretoria.

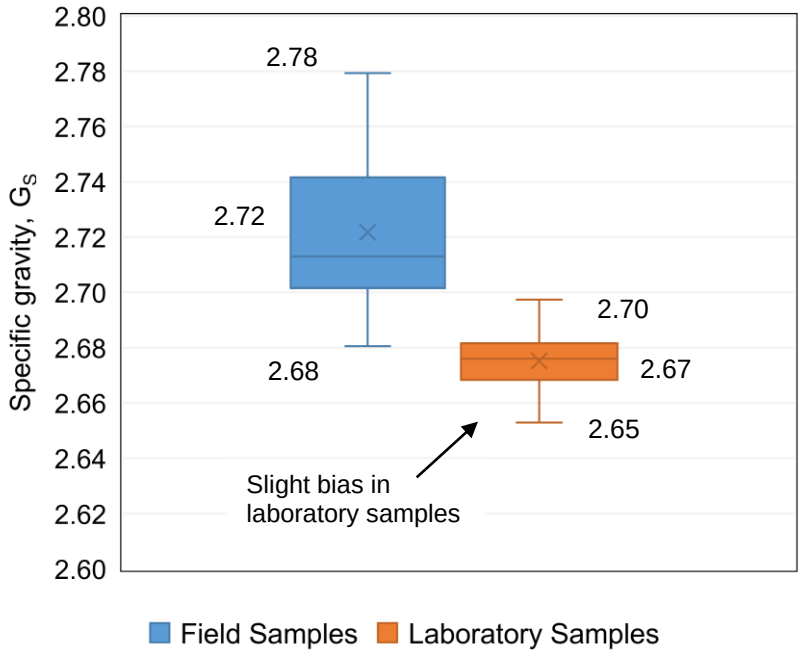


Figure 3.9: Summary of the specific gravity test results on the gold tailings

Figure 3.10 shows the grading curves obtained from the triaxial test moisture content samples. The region shown in blue indicates the range of the 32 grading curves that were obtained. Also plotted are the grading curves for the fine and coarse fractions of the tailings as obtained on site, as well as the grading curve of the bulk sample which was taken from the daywall and brought back to the laboratory. It can be seen that the grading curves did not vary significantly between the samples which shows that the sampling methodology worked effectively. It can therefore be concluded that any differences in the observed responses during the triaxial tests are due to other factors such as density, stress conditions during consolidation and hydraulic conditions during shearing, etc., and not grading nor particle density.

© University of Pretoria

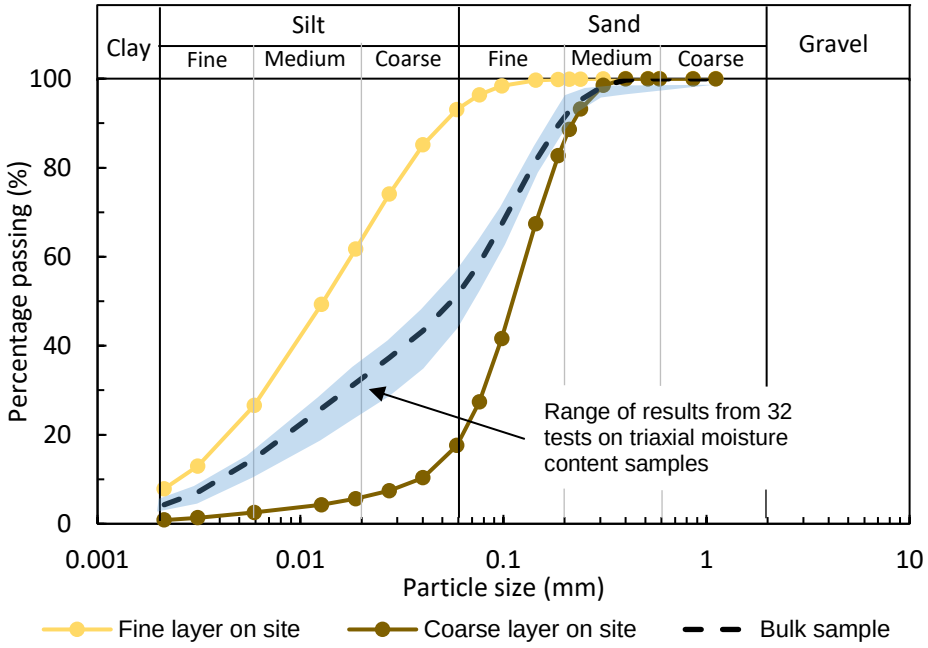


Figure 3.10: Results from the grading analyses conducted on the gold tailings moisture content samples

3.5.4 Critical State Line (CSL) Testing

The first goal of the triaxial testing was to establish the CSL. Table 3.8 shows the key details of the tests that were used to define the CSL for the gold tailings tested. The testing plan included dense and loose samples, as well as samples that were sheared drained and undrained. Figure 3.11 shows the results from the CSL testing on the gold tailings. Figure 3.11(a) shows the results of the consolidation and shear phases in an $e - p'$ plot. In this projection, the CSL has been defined as a straight line in a semi-ln plot. Figure 3.11(b) shows the results of the shear phases in a $q - p'$ plot. In this projection, the slope of the M-Line as well as the associated effective friction angle have been defined. These tests were selected as they represented a wide range of soil conditions.

To further emphasise the appropriateness of the proposed CSL, the results from all the samples prepared using the MT method are shown in Figure 3.12. The samples prepared using the SD method are not plotted as these tests are dealt with separately in Section 3.5.8. Details of these additional tests are described in the subsequent sections.

© University of Pretoria

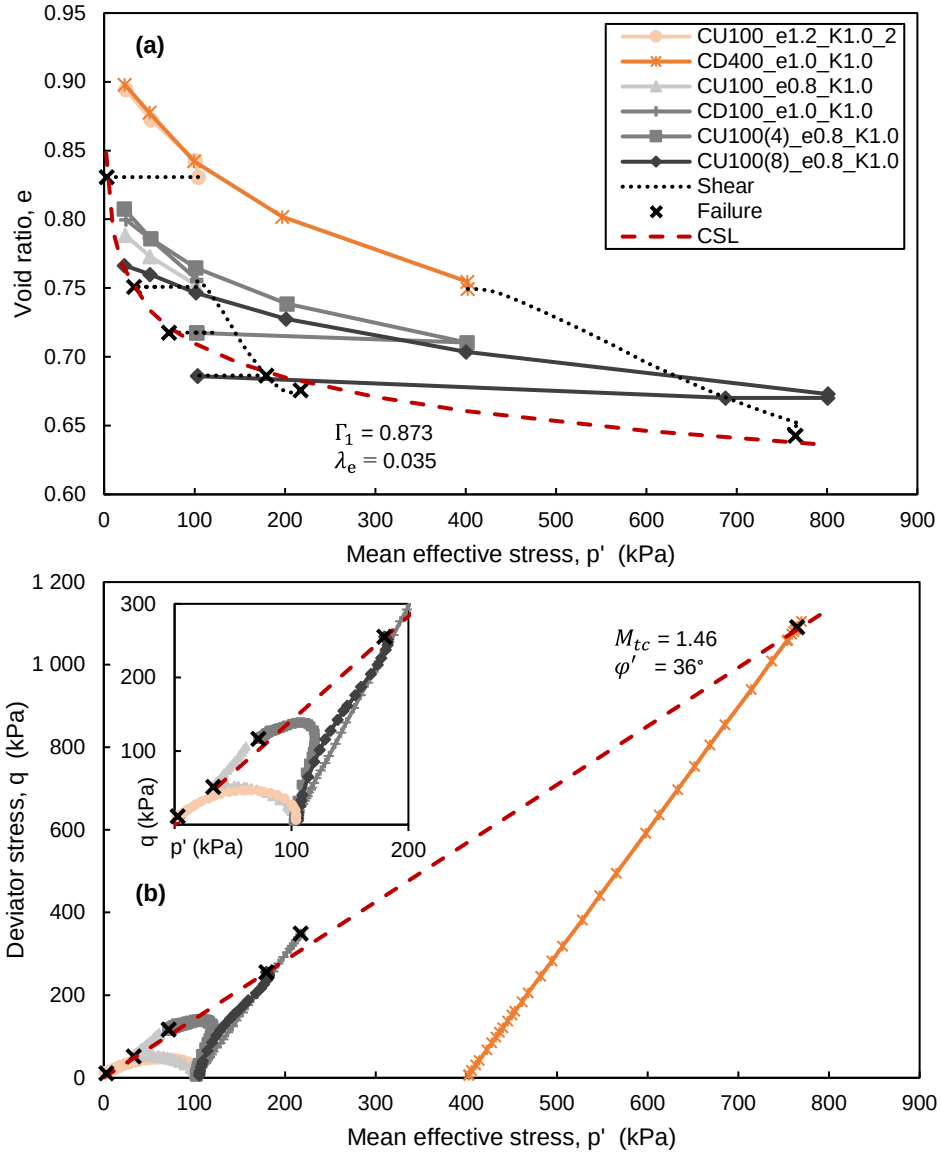


Figure 3.11: Results from the CSL testing for the gold tailings in: (a) $e - p'$ space, and (b) $q - p'$ space

© University of Pretoria

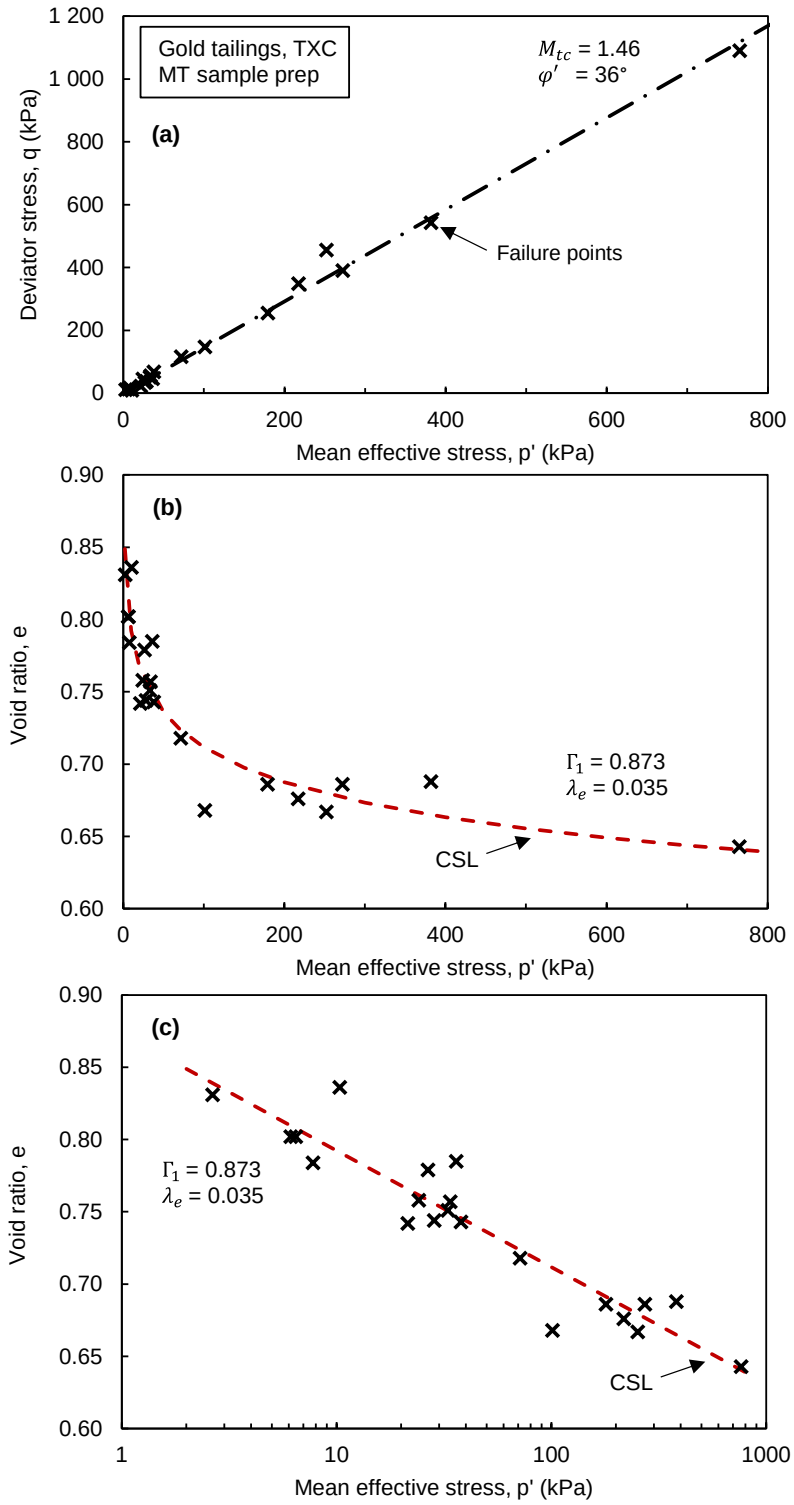


Figure 3.12: Failure points of all 21 MT samples in: (a) $e - p'$ space, and (b) $q - p'$ space

Based on the results from this batch of testing, key critical state parameters for the gold tailings were determined. These parameters are summarised in Table 3.7. These values are comparable to those obtained by others for testing on gold tailings mined from the Witwatersrand Supergroup (e.g. Vermeulen, 2001; Papageorgiou, 2004; Chang, 2009) as

© University of Pretoria

indicted in Table 2.4.

Table 3.7: Summary of key critical state parameters for the gold tailings

Parameter	**Symbol**	**Value**
Altitude of the CSL at p'=1 kPa	Γ_1	0.873
Slope of the CSL in $e - \ln p'$ space	λ_e	0.035
Slope of the CSL in $q - p'$ space, for triaxial compression	M_{tc}	1.461
Effective friction angle	φ'	36.0°

© University of Pretoria

Table 3.8: Summary of key aspects of the triaxial tests for Batch 1 (CSL Testing)

Test Ref	Test ID	Description	e_c	e_{cs}	p'_{cs} (kPa)	q_{cs} (kPa)
28	CU100_e1.2_K1.0_2	Loose sample, sheared undrained at p' = 100 kPa.	0.83	0.83	2.6	2.7
19	CD400_e1.0_K1.0	Loose sample, sheared drained at p' = 400 kPa.	0.75	0.64	764.9	1 090.0
6	CU100_e0.8_K1.0	Dense sample, sheared undrained at p' = 100 kPa.	0.75	0.75	33.0	51.2
5	CD100_e1.0_K1.0	Loose sample, sheared drained at p' = 100 kPa.	0.76	0.68	217.2	348.6
24	CU100(4)_e0.8_K1.0	Dense sample, overconsolidated to p' = 400 kPa, sheared undrained at p' = 100 kPa.	0.72	0.72	71.6	116.1
10	CU100(8)_e0.8_K1.0	Dense sample, overconsolidated to p' = 800 kPa, sheared undrained at p' = 100 kPa.	0.69	0.69	179.3	255.0

© University of Pretoria

3.5.5 Influence of stress level

Although not an explicit objective of this study, most testing plans to establish a CSL involve repeat tests at different stress levels. These samples are often created at the same initial density but consolidated to different effective stresses and then sheared under different hydraulic boundary conditions. This was the case for the gold tailings. Pairs of samples were tested in both drained and undrained shearing at mean effective stress values of 100 kPa, 200 kPa, and 400 kPa.

Figure 3.13 shows the results of the triaxial tests conducted to investigate the influence of stress levels on the shearing response of the gold tailings under drained and undrained conditions. Figure 3.13(a) shows the stress-strain response of the samples. As expected, the drained tests exhibited significantly larger shear strengths when compared to the undrained tests. Similarly, for samples with the same hydraulic conditions (i.e. drained or undrained), the shear strength of the soil increased with increasing confining stress. Further, all three drained tests exhibited strain-hardening behaviour while all three undrained tests exhibited strain-softening behaviour. This observed behaviour is entirely consistent with the CSSM framework.

Figure 3.13(b) shows the excess pore pressure response during shear for the undrained tests. As expected, no excess pore pressures were noted for the drained tests. For the undrained tests, it can be seen that after an initial increase, the excess pore pressures stabilised for all three samples. The magnitude of excess pore pressure increased with increased confining stress as expected.

Figure 3.13(c) shows the volumetric strain behaviour during shear for the drained tests. No volumetric strain was observed for the undrained tests. Unlike the excess pore pressures, the volumetric strain did not stabilise after an initial increase. However, these changes are small and there was little uncertainty that the samples had reached critical state.

© University of Pretoria

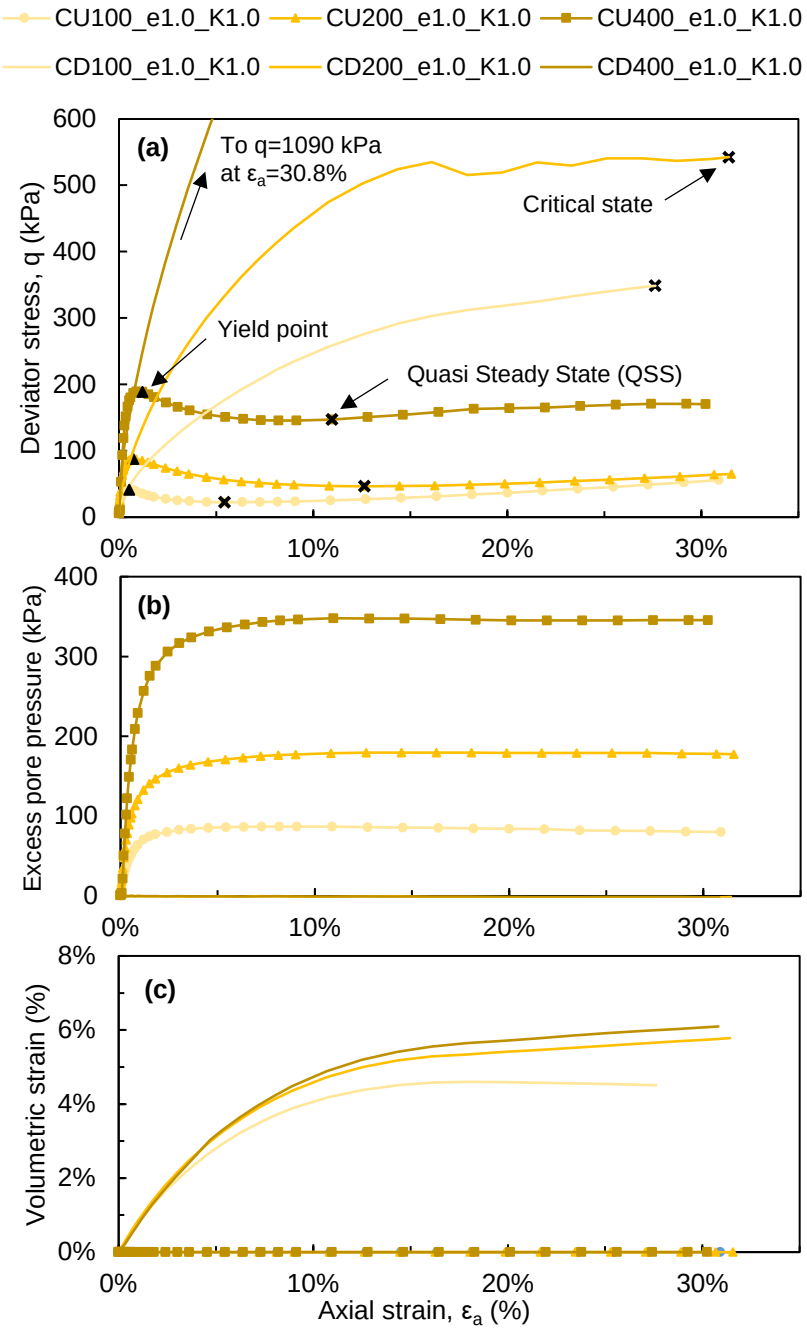


Figure 3.13: Influence of density on the shear behaviour of the gold tailings showing: (a) deviator stress, (b) excess pore pressure, and (c) volumetric strain

Figure 3.14 shows the stress paths of the for the six samples. In general, the samples show good agreement with the projection of the CSL. It can be seen that all three undrained samples exhibited a contractive tendency. In this projection, it is easier to see how the Quasi Steady State (QSS) marks a change in behaviour from a contractive tendency to a dilative tendency.

© University of Pretoria

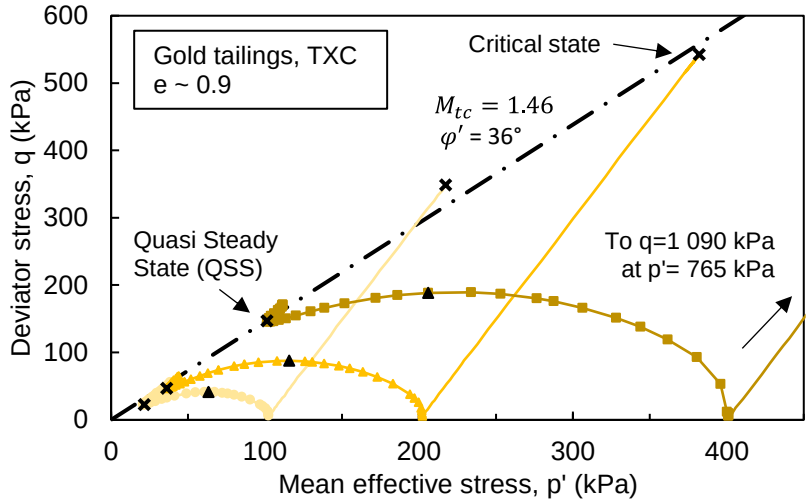


Figure 3.14: Influence of stress level on the stress paths of the gold tailings

A summary of the key parameters of each test is shown in Table 3.9. This series of tests is referred to as Batch 2.

© University of Pretoria

Table 3.9: Summary of key aspects of the triaxial tests for Batch 2 (influence of stress level)

Test Ref	Test ID	Description	e_c	e_{cs}	p'_{cs} (kPa)	q_{cs} (kPa)
4	CU100_e1.0_K1.0	Loose sample, sheared undrained at p' = 100 kPa.	0.90	0.74	21.4	22.3
5	CD100_e1.0_K1.0	Loose sample, sheared drained at p' = 100 kPa.	0.94	0.68	217.2	348.6
16	CU200_e1.0_K1.0	Loose sample, sheared undrained at p' = 200 kPa.	0.95	0.79	36.1	46.5
17	CD200_e1.0_K1.0	Loose sample, sheared drained at p' = 200 kPa.	0.94	0.69	382.0	542.3
18	CU400_e1.0_K1.0	Loose sample, sheared undrained at p' = 400 kPa.	0.93	0.67	101.2	147.0
19	CD400_e1.0_K1.0	Loose sample, sheared drained at p' = 400 kPa.	0.92	0.64	765.0	1090.3

© University of Pretoria

3.5.6 Influence of density

It is well-known that the density of the soil influences the undrained shear response. This has been shown experimentally many times for sandy soils. Perhaps the most referenced results are those produced by Castro (1969) where it was shown that for clean Ottawa sand, a void ratio change of only 0.06 resulted in a distinct change in stress-strain response.

However, there is some uncertainty whether gold tailings show similar changes in response to changes in void ratio, as well as the magnitude of the void ratio change that is required to change the behaviour from strain-hardening to strain-softening. This was investigated as part of this section.

Figure 3.15 shows the influence of density on the undrained shear response of the gold tailings. The void ratios provided are those at the end of the consolidation phase. Figure 3.15(a) shows the stress-strain curves in $q - \varepsilon_a$ space, while Figure 3.15(b) shows the stress paths in $q - p'$ space. It can be seen that a wide range of behaviours were observed for the six samples. The densest sample (e = 0.69) exhibited clear strain-hardening behaviour. This response progressively changed as the void ratio increased until at a void ratio of 0.84 (the loosest sample), strain-softening behaviour was noted.

Of particular interest is the change in behaviour between sample e = 0.74 and sample e = 0.78. For a relatively small volume change of 0.04, there is a distinct change in undrained shear response. Although this appears to be a small change in void ratio, it is believed to be well within the range of accuracy for the testing procedures implemented. For example, Reid et al. (2021) showed differences in the CSLs proposed for a gold tailings by different good quality geotechnical laboratories of at least e = 0.04, at the same effective stress. In this study, great care was taken to ensure accurate void ratio determinations, specifically considering the comments by several researchers on the subject (e.g. Papageorgiou, 2004; Omar & Sadrekarimi, 2014; da Fonseca et al., 2021). Additional details are provided in Section 3.5.10.

A summary of the key parameters of each test is shown in Table 3.10. This series of tests is referred to as Batch 3.

© University of Pretoria

Table 3.10: Key parameters for the triaxial tests conducted as part of Batch 3 (influence of density)

Test Ref	Test ID	Description	e_c	K_c	p'_0 (kPa)	ε_y (%)	q_y (kPa)	p'_{cs} (kPa)	q_{cs} (kPa)	$\frac{S_{u(yield)}}{p'_0}$	I_B
27	CU100_e1.4_K1.0	Loosest sample, sheared undrained at p' = 100 kPa.	0.84	0.95	100.4	0.58	39.5	10.4	9.2	0.20	0.77
9	CU100_e1.2_K1.0	Loose sample, sheared undrained at p'= 100 kPa.	0.78	0.95	102.2	0.55	44.5	7.8	17.0	0.22	0.62
6	CU100_e0.8_K1.0	Dense sample, sheared undrained at p' = 100 kPa.	0.75	0.95	101.5	0.87	53.1	33.0	51.2	0.26	0.04
23	CU100(2)_e0.8_K1.0	Dense sample, overconsolidated to p' = 200 kPa, sheared undrained at p' = 100 kPa.	0.74	0.95	102.5	1.42	90.1	37.9	68.1	0.44	0.24
24	CU100(4)_e0.8_K1.0	Dense sample, overconsolidated to p' = 400 kPa, sheared undrained at p' = 100 kPa.	0.72	0.95	102.4	2.31	138.5	71.6	116.1	0.68	0.16
10	CU100(8)_e0.8_K1.0	Dense sample, overconsolidated to p' = 800 kPa, sheared undrained at p' = 100 kPa.	0.69	0.95	105.4	8.38	255.0	179.3	255.0	1.21	0

© University of Pretoria

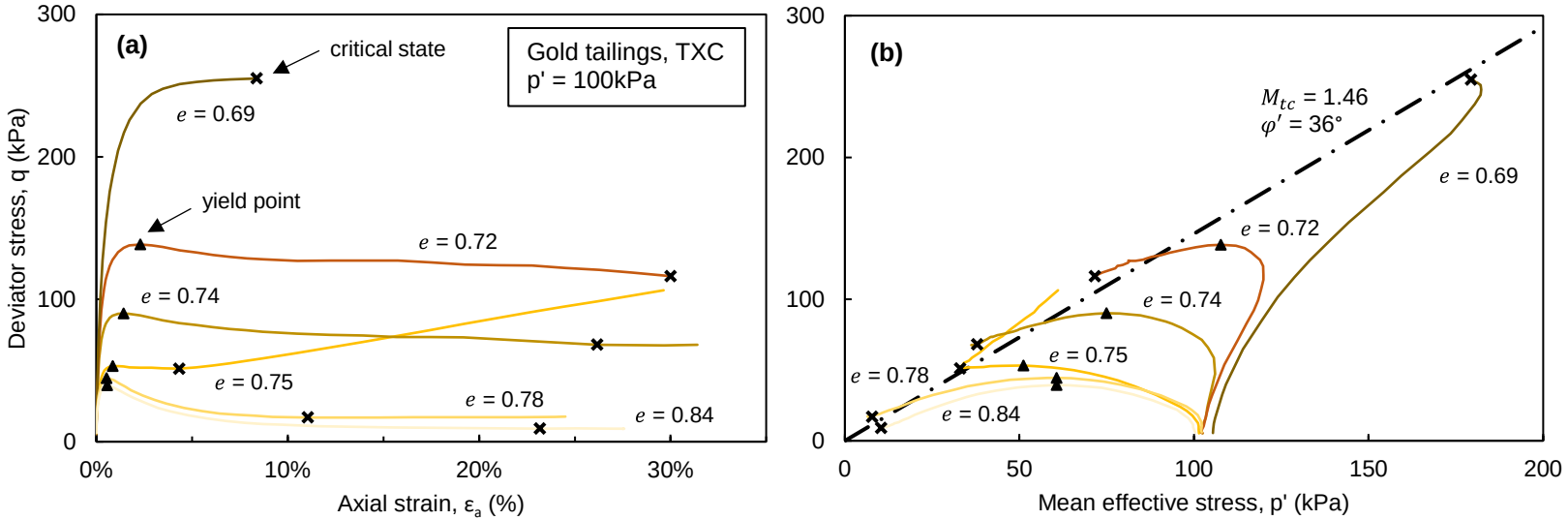


Figure 3.15: Results from the triaxial tests showing the influence of density in: (a) $q - \varepsilon_a$ space, and (b) $q - p'$ space

© University of Pretoria

3.5.7 Influence of stress anisotropy

A key aspect of this research was to investigate the in-situ stress state of gold tailings. As discussed in Section 2.5, the in-situ stress state can be described in terms of the geostatic stress ratio, K_0. However, knowledge of the geostatic stress ratio itself is not particularly useful to design engineers and regulators. What would be more useful is an understanding of the influence of the stress ratio on an aspect of the soil behaviour is directly related to design and safety evaluation aspects, such as the undrained shearing response.

To investigate this, a series of triaxial compression tests were performed on loose samples that were consolidated to the same mean effective stress but at different stress ratios. The undrained shearing response of the samples was then compared. The samples were prepared to the same initial void ratio of 1.0 and were anisotropically consolidated to a mean effective stress value of 100 kPa. Consolidation was performed in three incremental steps: 50 kPa, 70 kPa and 100 kPa.

Instead of the term K_0, which implies a condition of zero radial strain which was neither monitored nor enforced as part of this testing, the term K_c is used to describe the magnitude of stress anisotropy. This is in line with the terminology used by other researchers for anisotropic consolidation (e.g. Fotovvat et al., 2022).

At this stage it should be noted that there is a difference between the K_c value noted in the Test ID, and the K_c value presented in the figures and tables. This difference is due to the assumption regarding the sample cross sectional area. The K_c value presented in the Test ID is the K_c value that was input into the GDS software package. The software package assumes that the sample area is equivalent to the initial sample area (as measured after preparation but prior to installation). However, it is known that the samples reduced in volume during flushing and saturation. This change in volume was not considered in the GDS software.

To determine a more accurate cross-sectional area, the end of test conditions were used, and a backwards analysis was conducted using the area corrections as presented in BS 1377. The presented K_c value in the subsequent figures, as well as in the test description are based on these calculations.

Figure 3.16 shows the consolidation stress paths followed for the samples. The target stress ratio for each sample is also shown for reference. In general, a linear stress path was followed during the three consolidation phases. It can also be seen that Test 30 (CU100_e1.0_K0.4) failed during consolidation, so no shear phase is presented for this test.

© University of Pretoria

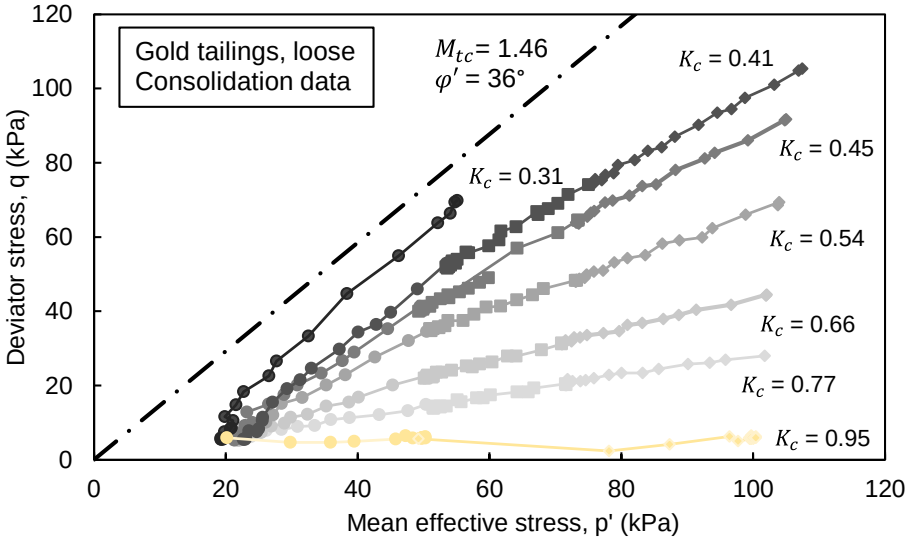


Figure 3.16: Consolidation stress paths for the anisotropically consolidated gold tailings samples

The complete results from the shear phases of the samples are shown in Figure 3.18. Figure 3.18(a) shows the stress-strain curves in $q - \varepsilon_a$ space, while Figure 3.18(b) shows the stress paths in $q - p'$ space. A few points are of interest in these figures. The first point is the yield undrained shear strength progressively increases as the K_c value decreases. For example, the yield undrained shear strength increased from 19 kPa to 53 kPa as the K_c value decreased from 0.95 to 0.41. In terms of the yield undrained shear strength ratio ($S_{u(yield)}/p'_0$), this value increased from 0.20 to 0.50, for the same change in K_c.

The second point is that this yield point occurs at progressively lower axial strains as K_c decreases. For example, yielding occurred at 0.58% axial strain for the K_c = 0.95 sample, while for the K_c = 0.45 sample, yielding occurred at 0.02% axial strain. The third point is that although there is some variability, there is a general decrease in brittleness as the stress anisotropy decreases. For example, I_B reduced from 0.77 to 0.48 as K_c reduced from 0.95 to 0.45.

It is clear that there is indeed an influence of stress anisotropy on the mechanical response during undrained shear for the loose gold tailings. This is specifically evident in the yield undrained strength, the strain level at which peak strength occurs, and the post-peak behaviour. This is in line with the findings of Doanh et al. (1997) for loose Hostun RF sand.

Figure 3.17 shows the observed behaviour of the gold tailings samples between an axial strain of 0 and 0.8%. In this view is it easier to see the trend of increasing yield strengths, at decreasing axial strain values, as the K_c value decreases. It is clear from the results that the yield undrained

© University of Pretoria

shear strength increases as the K_c value decreases. However, as described by Rosenzweig et al. (2020), this also indicates that as the stress ratio decreases, less addition shear stress is required to initiate collapse. Therefore, as the anisotropic stress ratio K_c decreases, less energy is required to induce collapse. This is an important point to note when considering undrained collapse trigger mechanisms.

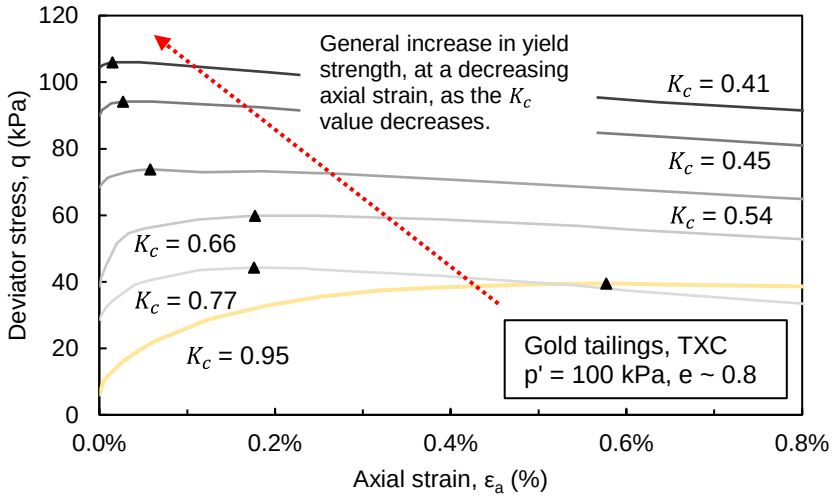


Figure 3.17: Influence of stress anisotropy on the undrained shear response of the gold tailings at low strain levels

A summary of the key parameters of each test is shown in Table 3.11. This series of tests is referred to as Batch 4.

© University of Pretoria

Table 3.11: Key parameters for the triaxial tests conducted as part of Batch 4 (influence of stress conditions during consolidation)

Test Ref	Test ID	Description	e_c	K_c	p'_0 (kPa)	ε_y (%)	q_y (kPa)	p'_{cs} (kPa)	q_{cs} (kPa)	$\frac{S_{u(yield)}}{p'_0}$	I_B
27	CU100_e1.4_K1.0	Loose sample, sheared undrained at p'=100kPa.	0.84	0.95	100.4	0.58	39.5	10.4	9.2	0.20	0.77
21	CU100_e1.0_K0.8	Loose sample, consolidated to K_c=0.77 and sheared undrained at p'=100kPa.	0.80	0.77	98.6	0.18	44.3	6.5	13.4	0.20	0.70
11	CU100_e1.0_K0.7	Loose sample, consolidated to K_c=0.66 and sheared undrained at p'=100kPa.′	0.80	0.66	100.6	0.18	59.9	6.1	14.7	0.30	0.75
20	CU100_e1.0_K0.6	Loose sample, consolidated to K_c=0.54 and sheared undrained at p'=100kPa.	0.74	0.54	103.6	0.06	73.8	28.5*	37.5*	0.36	0.49
12	CU100_e1.0_K0.5	Loose sample, consolidated to K_c=0.45 and sheared undrained at p'=100kPa.	0.76	0.45	104.3	0.03	96.9	26.7	33.5	0.46	0.65
31	CU100_e1.0_K0.45	Loose sample, consolidated to K_c=0.41 and sheared undrained at p'=100kPa.	0.76	0.41	106.7	0.02	106.0	33.8*	55.6*	0.50	0.48
30	CU100_e1.0_K0.4	Loose sample, attempted consolidation to K_c=0.31 but the sample failed during the consolidation phase.	0.76	0.31	N/A	N/A	N/A	N/A	N/A	N/A	N/A

*values at the phase transfer point provided.

© University of Pretoria

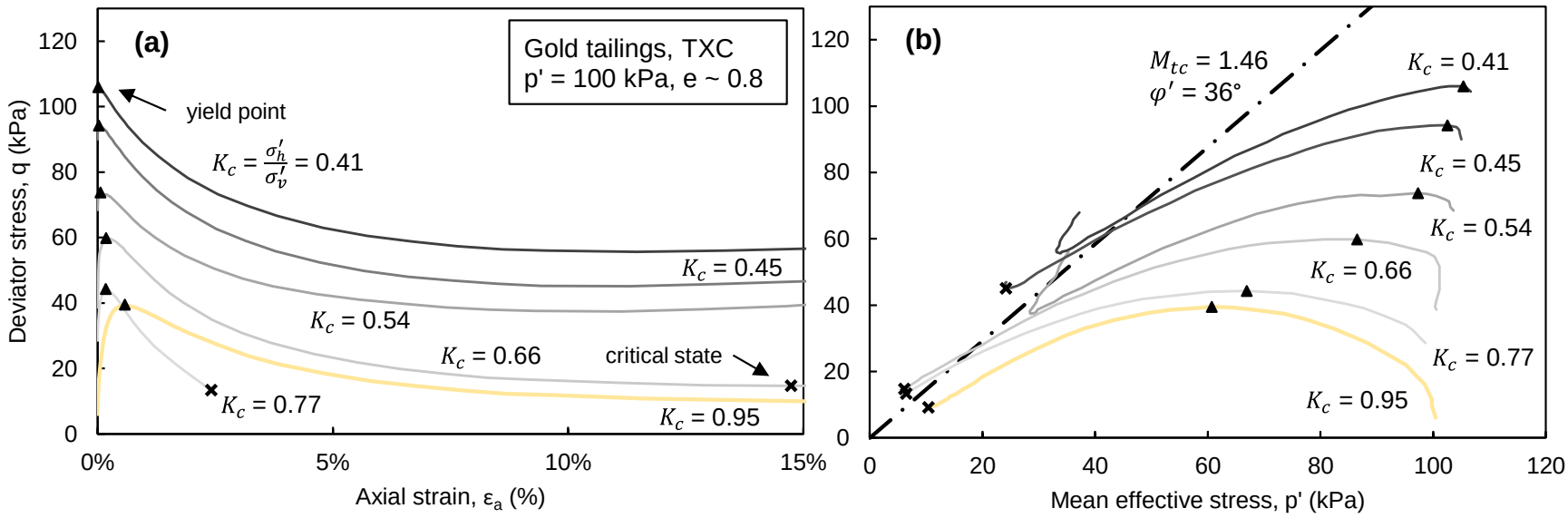


Figure 3.18: Results from the triaxial tests showing the influence of stress anisotropy in: (a) $q - \varepsilon_a$ space, and (b) $q - p'$ space

© University of Pretoria

3.5.8 Influence of sample preparation method

As discussed in Section 2.3.2, it is known that the sample preparation method influences the mechanical response during undrained shear for sandy soils. This has been specifically shown for gold tailings (e.g. Chang et al., 2011). However, it is also known that the density of a sample influences this response, and historically it has proven quite difficult to produce loose SD samples, specifically samples to match the loose densities expected in the field (e.g. Reid, 2021). However, recent innovations by Reid et al. (2022c) have provided alternatives for creating slurry deposited samples with looser densities. Unfortunately, even using these approaches, it was not possible to create loose SD samples in this manner for this study.

When the loose samples were recovered from the drying bucket, they had insufficient strength to maintain their structural integrity during the membrane installation. The samples started as right cylinder but slumped within seconds and formed a barrel shape near the base. Aside from the obvious inability to cover the sample with the membrane, the shape of the sample was deemed inappropriate for testing. By allowing the material to dry further, consolidation continued, and the samples gradually became more workable. Unfortunately, when the samples had consolidated sufficiently to maintain their shape during membrane installation, they were already fairly dense. It is likely that this approach could be refined further, however, this was not done for this study.

When plotting the results of these samples within the general framework established with the MT samples, it became apparent that these samples do not fit well within the framework. Although the samples were denser, there is little evidence to suggest that it was equipment limitations that prevented the samples from reaching critical state. Rather, it was believed that the SD samples were simply tending towards a different CSL, compared to the MT samples. To investigate this, three additional samples were tested but this time the shearing was conducted drained. This was done as it was believed it would be easier to identify whether the stress paths during shearing were tending towards the CSL or not when viewed in an $e - \ln p'$ projection, compared to the undrained tests.

Figure 3.19 shows the results of the triaxial tests on the SD samples. Figure 3.19(a) shows the results in $q - p'$ space, while Figure 3.19(b) shows the results in $e - p'$ space. Also shown on both figures is the CSL defined using the results from the MT samples. It is clear that there is a difference between the critical state locations of the SD samples, and the CSL (which was defined based on results from the MT samples). At low stress, there is good correlation between the friction angle determined using the MT and SD samples (see Figure 3.19(a)). However, there is some deviation

© University of Pretoria

at larger stress levels. Regarding the CSL in $e - p'$ space (Figure 3.19(b)), there is poor correlation between the MT and SD samples at critical states. As discussed in Section 2.4.3, the initially dense state of these SD samples could have resulted in the formation of shear bands at moderate strain levels. Therefore, there is some uncertainty regarding the reliability of these global void ratios and whether they truly represent the local void ratios that existed along the failure plane.

For reference, a line is shown with the same slope as the CSL defined for the MT samples, but with a different intercept. This line seems to fit the data well. Less reliance is placed on the test at high stresses as the test was approaching the equipment limitations.

It may be argued that although this is not desirable, it may be acceptable as many methods used to estimate the state of a soil only require the slope of the CSL, and not the intercept. For example, the suggested improvement of the Plewes et al. (1992) method as proposed by Torres-Cruz (2021) only requires knowledge of the slope of the CSL, and not the intercept.

However, arguments such as this miss a key component: the laboratory testing which needs to be conducted to establish the CSL to be used for the calibration testing of the methods. For these laboratory tests, knowledge of the complete CSL is crucial. This leads to another interesting aspect which is the layering of tailings and how this influences the CSL. However, this is outside the scope of this study and is not discussed further. For interest, this aspect has been explored by Reid et al. (2022b), with some intriguing findings.

Regarding this difference in CSL observed for MT and SD samples, this has been noted by other researchers for gold tailings (Reid et al., 2022c), and iron ore tailings (Mmbando et al., 2023). However, in all three cases only limited testing was conducted. Further testing is required to fully investigate the extent of this difference in behaviour between the MT and SD samples for the gold tailings considered as part of this study.

A test on a SD sample with a K_c value of 0.5 was also conducted (CU100_e0.8_K0.5_SD). However, this sample showed a clear dilative tendency during undrained shear which was attributed to the lower void ratio on the sample. Therefore, this result was not plotted against the results from the MT samples as the purpose of that comparison was to investigate the influence of stress anisotropy only. In this case there is a difference in sample preparation method, as well as void ratio, and both aspects are known to have a meaningful influence on the undrained shear response.

© University of Pretoria

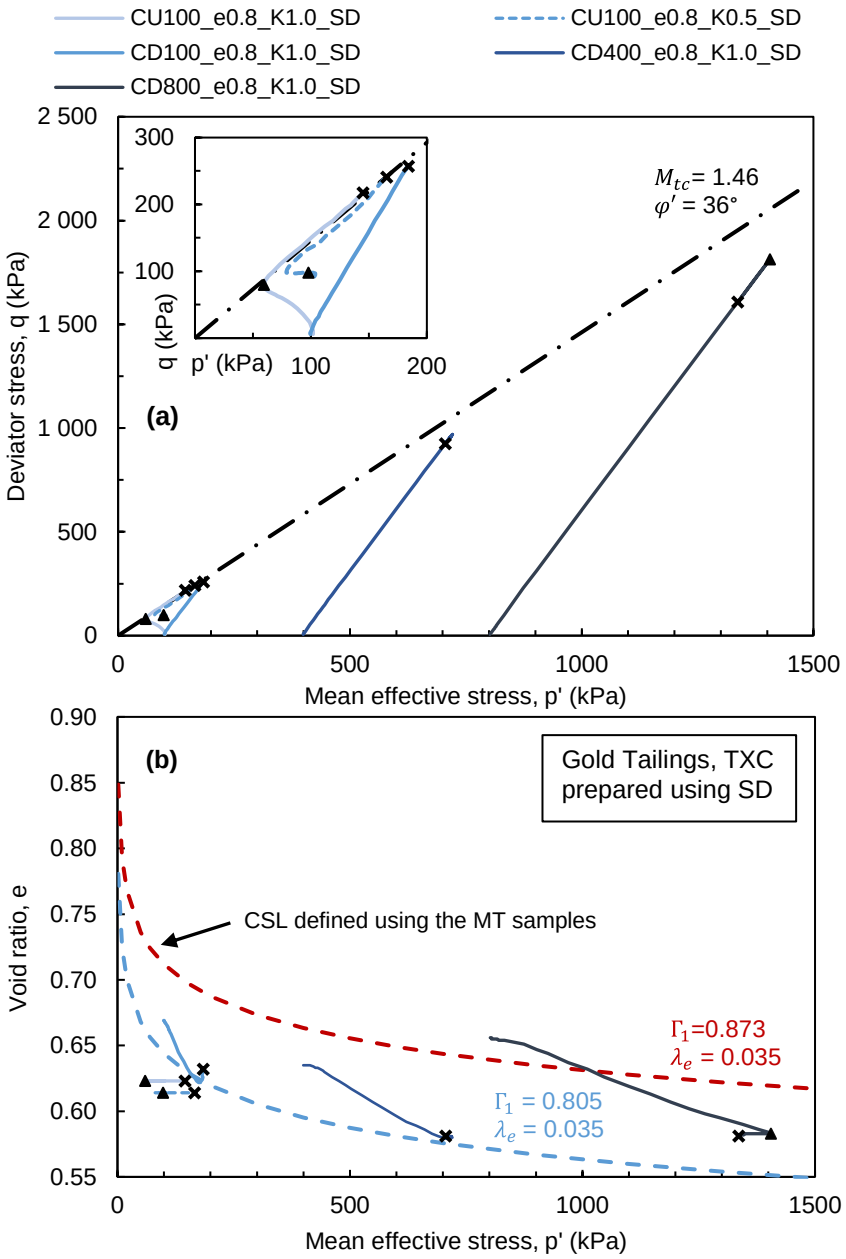


Figure 3.19: Results from the triaxial tests conducted as part of Batch 5 in: (a) $q - p'$ space, and (b) $e - p'$space

A summary of the key parameters of each test is shown in Table 3.12. This series of tests is referred to as Batch 5.

© University of Pretoria

Table 3.12: Key parameters of the triaxial tests conducted as part of Batch 5 (influence of fabric)

Test Ref	Test ID	Description	e_c	e_{cs}	K_c	p'_0 (kPa)	ε_y (%)	q_y (kPa)	p'_{cs} (kPa)	q_{cs} (kPa)	$\frac{S_{u(yield)}}{p'_0}$
25	CU100_e0.8_K1.0_SD	Sample prepared using the SD method, sheared undrained at p' = 100 kPa.	0.62	0.62	0.95	101.8	1.93	79.5	144.9	217.5	0.39
26	CU100_e0.8_K0.5_SD	Sample prepared using the SD method. Consolidated to K_c=0.5, and then sheared undrained at p' = 100 kPa.	0.61	0.61	0.45	103.0	0.13	98.0	165.5	240.6	0.48
34	CD100_e0.8_K1.0_SD	Sample prepared using the SD method, sheared drained at p' = 100 kPa.	0.67	0.63	0.95	99.5	N/A	257.3	184.2	257.3	N/A
36	CD400_e0.8_K1.0_SD	Sample prepared using the SD method, sheared drained at p' = 400 kPa.	0.64	0.58	0.95	339.3	N/A	924.1	705.8	924.1	N/A
35	CD800_e0.8_K1.0_SD	Sample prepared using the SD method, sheared drained at p' = 800k Pa.	0.66	0.58	0.95	802.1	15.82	1 607	1 336	1 607	N/A

© University of Pretoria

3.5.9 Uniqueness of the NCL

A final objective of the triaxial testing was to determine the uniqueness of the NCL. A total of four tests were conducted as part of this investigation: two samples prepared to a loose state, and two samples prepared to a dense state. Little to no compaction effort was required to prepare the loose samples. However, moderate to significant compaction effort was required to prepare the dense samples to initial void ratios of 0.84 and 0.74, respectively. At the start of the test, the two loose samples were therefore assumed to be in a NC state, while the two dense samples were considered to be in an OC state. To simplify the figure legends, and specifically to enable simple comparisons with the oedometer test data, the compression curves have been labelled according to their preparation void ratios.

Figure 3.20 shows the results from the triaxial testing. The NCL has been defined as two straight lines in this semi-log projection over two stress ranges. The intercepts and slopes of these two lines are shown in the figure and it can be seen that the slope of the NCL increases at higher stress levels.

Unlike the oedometer tests, in which the compression curves for the NC samples converged rapidly, there is a clear offset between the two NC samples for the triaxial tests (e = 1.18 and e = 1.10). This offset is approximately e = 0.04. This is the same value that was determined by Reid et al. (2021) to be the accuracy to which the CSL can reasonably be expected to be determined using modern triaxial testing techniques. Since the same approach that is used to determine the CSL is also used to determine the NCL in terms of the void ratio estimates, it seems reasonable to assume that this accuracy applies to the NCL as well.

The NCL has been drawn between these two curves with a slight bias toward the initially denser sample (e_i = 1.10), which experienced less collapse during flushing and saturation. The slopes of the compression curves for the 100 to 200 kPa for the two loose samples are similar and are significantly steeper when compared to the slopes of the dense samples at the same stress increment (as shown in Table 3.13). This is consistent with critical state theory regarding the compression behaviour of NC and OC samples.

For the 800 to 1 000 kPa increment, all the samples except for the densest sample (e_i = 0.74) have similar slopes. At this stage, it is postulated that the three loosest samples (e_i = 1.18, e_i = 1.10, e_i = 0.84) are on the NCL, while the densest sample (e_i = 0.74) is still approaching the NCL. It can be seen that the slopes of the unloading curves are similar for all four samples.

© University of Pretoria

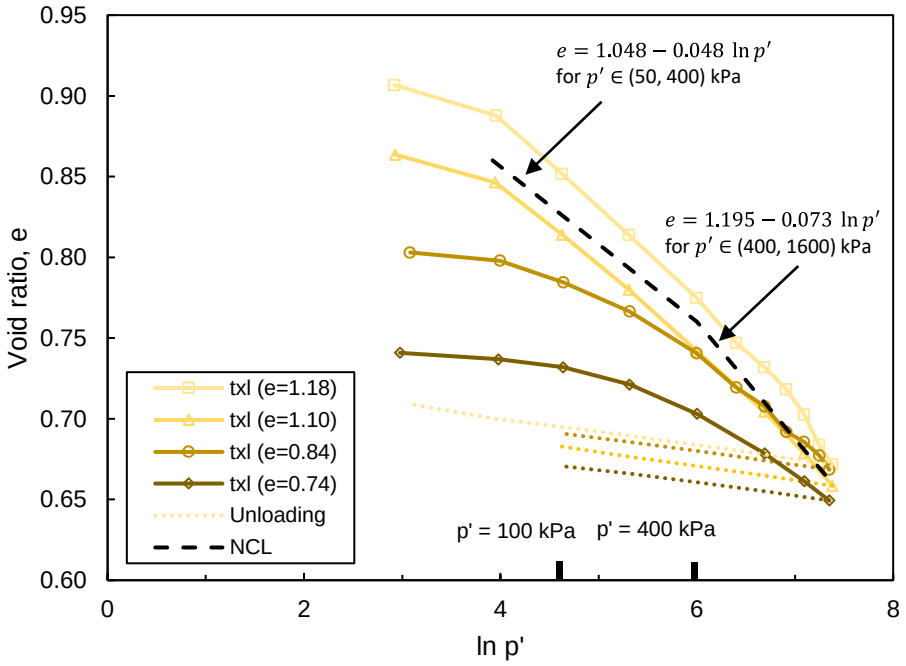


Figure 3.20: Results from the triaxial testing to identify the NCL

A summary of the key parameters of each test is shown in Table 3.13. This series of tests is referred to as Batch 6.

© University of Pretoria

Table 3.13: Summary of key triaxial data for Batch 6 (NCL investigation)

Test Ref	Test ID	Description	Preparation void ratio, e_i	Void ratio at 1 500 kPa	Slope of 100 to 200 kPa increment	Slope of 800 to 1 000 kPa increment	Average slope of unloading stages
32	Con1500_e1.4_K1.0 (e=1.18)	Loosest sample, consolidated in stages to p'=1 500 kPa. No shear phase.	1.18	0.67	0.056	0.062	0.009
37	Con1500_e1.2_K1.0 (e=1.10)	Loose sample, consolidated in stages to p'=1 500 kPa. No shear phase.	1.10	0.66	0.050	0.070	0.009
33	CU100(15)_e0.8_K1.0 (e=0.84)	Dense sample, consolidated in stages to p'=1 500 kPa and then sheared undrained.	0.84	0.67	0.027	0.071	0.009
38	Con1500_e0.7_K1.0 (e=0.74)	Dense sample, consolidated in stages to p'=1 500 kPa. No shear phase	0.74	0.65	0.016	0.043	0.008

© University of Pretoria

3.5.10 Summary

A comprehensive triaxial testing campaign was conducted on the gold tailings. Material was sourced from the daywall, and the MT sample preparation method was used for the majority of the samples. The influence of several aspects of soil state on the shearing response of loose gold tailings was investigated. These aspects included stress level, density, stress anisotropy during consolidation, and sample preparation method. Each aspect was found to influence the undrained behaviour of the gold tailings in a different manner. These influences are summarised in Section 2.3.2. In addition to the above, a unique NCL and a unique CSL were identified for the gold tailings.

Particular attention is drawn to two aspects of soil state and their influence on the undrained shearing response: density and stress anisotropy. Figure 3.21 shows selected results from the triaxial tests conducted as part of this study. In particular, two tests showing the influence of density and two tests showing the influence of stress anisotropy are shown. The samples with a change in void ratio are shown in yellow, while the samples with a change in stress anisotropy are shown in brown.

Of particular interest is the change in behaviour between sample e = 0.74 (labelled as 1) and sample e = 0.78 (labelled as 2). For a change in void ratio of only 0.04, there is a distinct change in undrained shear response. For a sample of this size, the change in void ratio represents a change in volume of 9.5 cm^3, or a volumetric strain of only 2%. In terms of brittleness, Sample 1 exhibited an I_B =0.24, while Sample 2 exhibited an I_B = 0.62. In terms of undrained shear strength, Sample 1 exhibited an $S_{u(yield)}/p_0'$ = 0.44, while Sample 2 exhibited an $S_{u(yield)}/p_0'$ = 0.22.

This is a useful example as it clearly illustrates how a small change in void ratio of 0.04 can result in a large change in both brittleness and undrained shear strength. Both aspects have major implications in the design and safety evaluation approaches suggested by some guidelines. For example, ICOLD (2022) specifies FoS values for peak conditions and these analyses use the yield undrained shear strength as a direct input. In addition, an I_B value of 0.4 is used to distinguish between soils which are moderately brittle and those which are highly brittle and distinctly different requirements are specified for these two conditions.

Similarly, the change in behaviour between sample K_c = 0.95 (labelled as B) and sample K_c = 0.54 (labelled as A) is also of interest. For a change in stress anisotropy of 0.41, there is a distinct change in undrained shear response. The K_c values represent the typical range of values expected

© University of Pretoria

in the structural zone of a tailings dam (e.g. Narainsamy & Jacobsz, 2023a). In terms of brittleness, Sample B exhibited an I_B = 0.77, while Sample A exhibited an I_B = 0.49. In terms of undrained shear strength, sample B exhibited an $S_{u(yield)}/p_0'$ = 0.20, while sample A exhibited an $S_{u(yield)}/p_0'$ = 0.36.

Although this example is not as extreme as the example showing the influence of density, these are still significant changes in both brittleness and yield undrained shear strengths for fairly small changes in stress ratio. This again highlights the care that needs to be taken when applying certain guidelines to tailings dams where it is know there is meaningful variability in soil state.

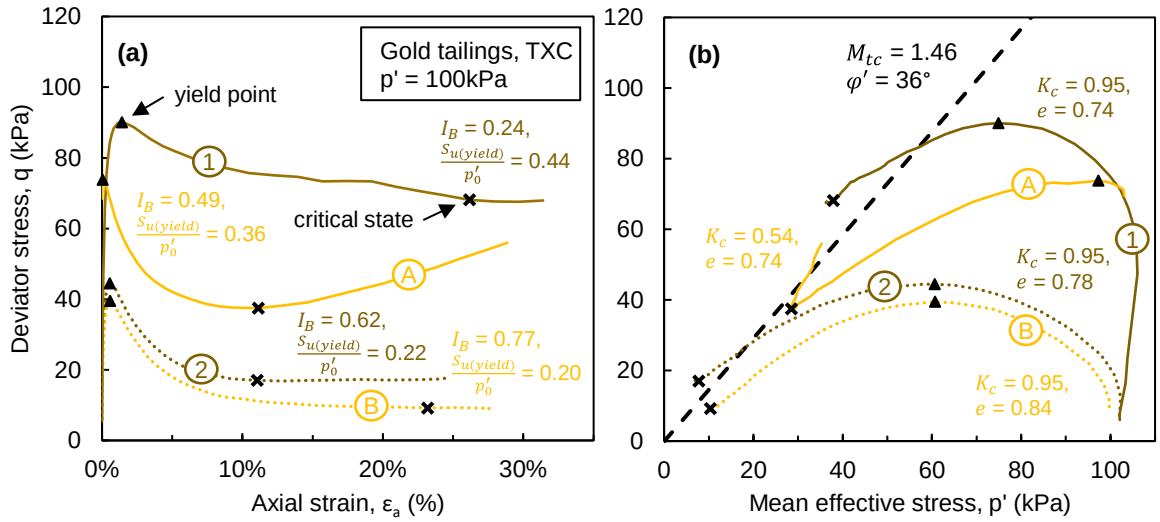


Figure 3.21: Influence of density and stress anisotropy on brittleness and undrained shear strength of gold tailings in: (a) $q - \varepsilon_a$ space, and (b) $q - p'$ space

3.6 COMBINED OEDOMETER AND TRIAXIAL TEST RESULTS

One of the objectives of combining the oedometer and triaxial test results is to evaluate whether the 1D-NCL and NCL are parallel to each other. To achieve this, it is necessary to plot the results from the oedometer and triaxial tests on the same set of axes. This requires knowledge of K_0. For this study, a K_0 value of 0.6 was assumed based on the work by Fourie & Tshabalala (2005) on the Merriespruit gold tailings. This material was mined from an ore body of similar geological origin (i.e. the Witwatersrand Supergroup) and has a similar grading as the gold tailings considered as part of this study. The mean effective stress (p') for the oedometer test data was calculated as shown in Equation (10).

© University of Pretoria

$$p' = \frac{1}{3}[\sigma'_v(1 + 2K_0)] \quad (10)$$

Figure 3.22 shows the combined results from the oedometer and triaxial tests, as well as the interpreted 1D-NCL and NCL. Due to system constraints, it was not possible to consolidate the triaxial samples to the same stresses that were achieved in the oedometer tests. To conclusively investigate the relationship between the 1D-NCL and the NCL, a higher capacity triaxial testing system is required. However, with the data available, it does not seem unreasonable to assume that, for practical purposes, the 1D-NCL and NCL are parallel at low to moderate stress levels. For example, between mean effective stress values of 50 kPa and 400 kPa, the slope of the 1D-NCL is 0.049, while the slope of the NCL is 0.048.

Therefore, based on the oedometer and triaxial test results presented in Sections 3.4 and 3.5, it was found that from a practical perspective, the gold tailings used as part of this study exhibits a unique NCL.

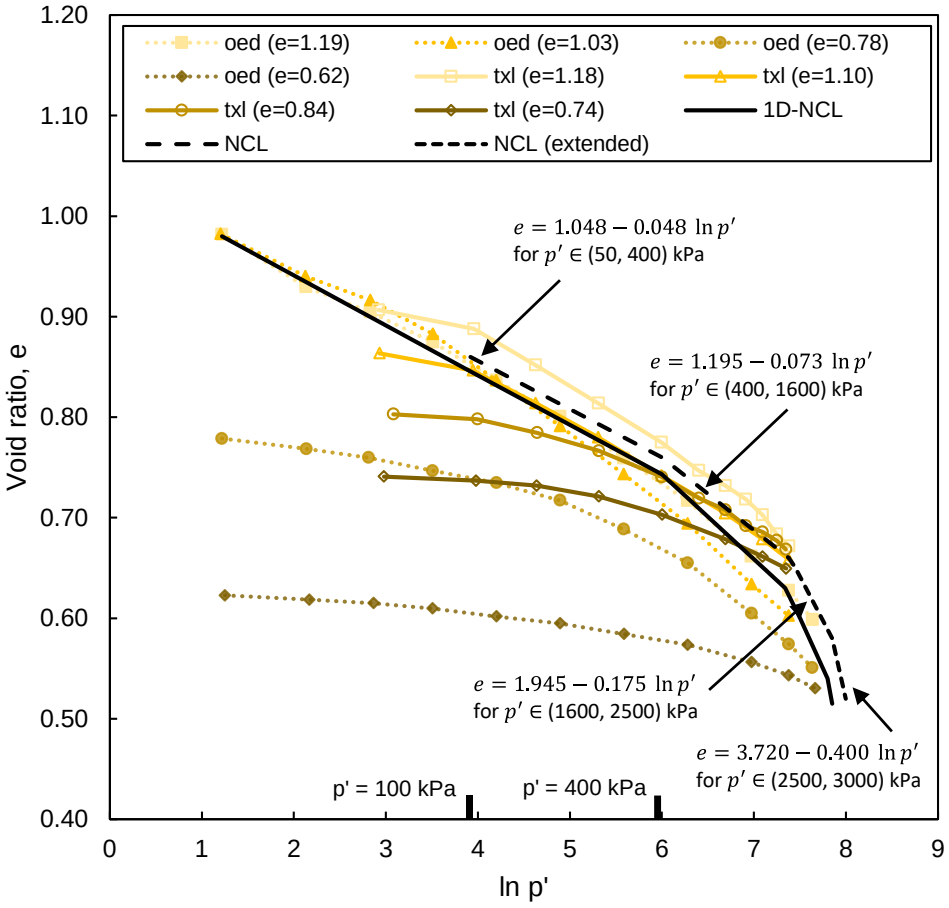


Figure 3.22: Combined triaxial and oedometer test results

© University of Pretoria

Figure 3.23 shows a summary of key CSSM features of the gold tailings determined as part of this study. For reference, the relevant equations for the various segments of the proposed NCL and CSL have been shown. The proposed lines have segments that are based on measured data, and segments that are extrapolated based on CSSM theory. For the NCL and CSL, the extended curves are based on the 1D-NCL. At high stresses, these curves have been shown to be parallel for sandy soils (e.g. Robertson, 2017).

Regarding the NCL and CSL, it was found that these lines are not parallel. However, for low to moderate mean effective stress levels of between 50 kPa and 400 kPa, the lines are meaningfully offset in the $e - \ln p'$ space. For example, for a NC sample, ψ changes from 0.126 to 0.100 as the mean effective stress increases from 50 kPa to 400 kPa. Therefore, for the purposes of defining whether the soil is contractive or dilative at large strains, the NCL and CSL can be considered parallel at low to moderate stresses.

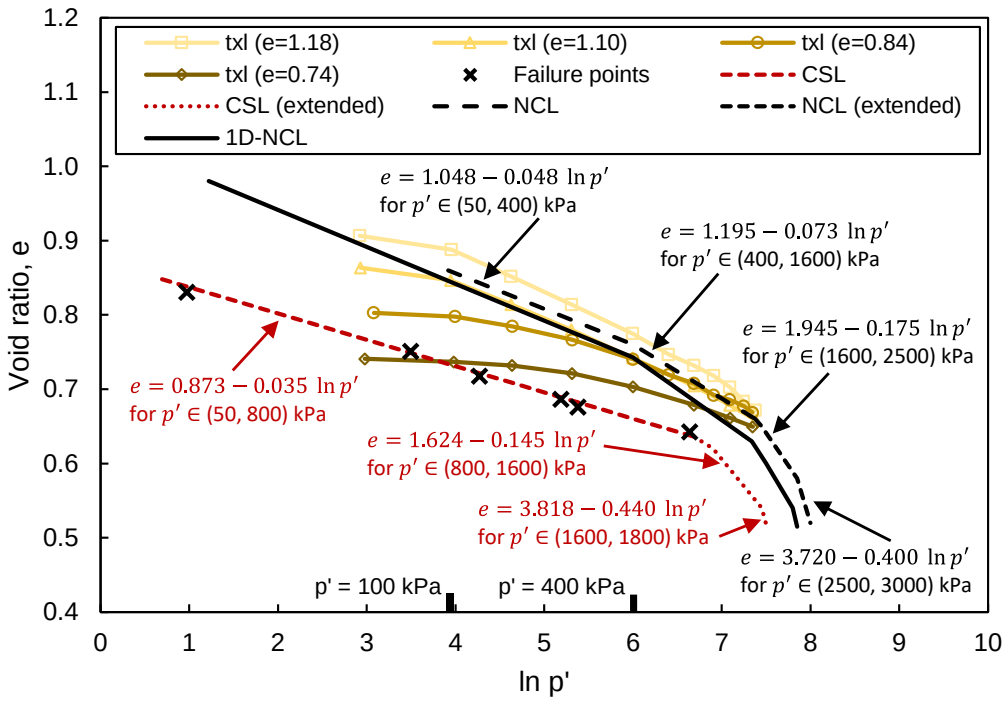


Figure 3.23: Summary of key CSSM features of the gold tailings

3.7 SUMMARY

A comprehensive series of oedometer and triaxial compression tests were conducted to investigate the behavioural characteristics of the gold tailings used as part of this study. As is it known that the grading of a sandy soil can greatly influence its compression and shearing behaviour, an effort was made to ensure that only a single grading was tested. This grading was chosen to represent the

© University of Pretoria

average grading observed on site.

Samples were prepared using different sample preparation techniques, to different initial densities, were consolidated under different stress conditions, and were sheared under different hydraulic boundary conditions. The compression and shear behaviour of the various samples were then observed and compared. Key findings are summarised here.

Based on the results from the oedometer testing, the following was found:

1. For the grading tested, there appears to exist a unique 1D-NCL for the gold tailings.
2. Even at stress levels of 3.2 MPa, no meaningful evidence of particle crushing was noted.

Based on the results from the triaxial testing a number of effects, specifically regarding the undrained shear response of the gold tailings, were observed:

1. Regarding the density at the start of the shear phase it was found that, as was seen for clean sands, the initial void ratio plays a key role in the undrained shear response of the gold tailings. For a change in void ratio from 0.69 to 0.84, the gold tailings exhibited a progressive change in behaviour from strain-hardening to strain-softening.
    a. For loose samples, a small change in void ratio of 0.04 changed the behaviour significantly (see Figure 3.15). In terms of brittleness, I_B changed from 0.24 to 0.62 as the void ratio increased from 0.74 to 0.78. Similarly, the yield undrained strength ratio, $S_{u(yield)}/p'_0$, changed from 0.44 to 0.22. These changes are significant.
2. Regarding the stress anisotropy imposed during consolidation, it was found that the undrained shear response is influenced by the magnitude of stress anisotropy. For a change in K_0 from 0.95 to 0.41, the gold tailings exhibited a progressive change in undrained shear response, with $S_{u(yield)}/p'_0$ changing from 0.20 to 0.50.
    a. In particular, it was found that for a change in K_c of 0.41 (from K_c = 0.95 to K_c = 0.54), both the brittleness and yield undrained shear strength changed. I_B changed from 0.77 to 0.49, while $S_{u(yield)}/p'_0$ changed from 0.20 to 0.36.
    b. In addition to the increase in yield undrained shear strength (Figure 3.18), it was found that for samples prepared at the same initial void ratio but consolidated under decreasing K_c values, there is a general increase in the axial strain required to reach the yield point (see Figure 3.17). As suggested by Rosenzweig et al. (2020), as K_c decreases, the soil has less capacity to handle an increase in shear stress before collapse is initiated. In other words a smaller trigger event is required to initiate collapse for soils with a smaller K_c, compared to soils with a higher K_c. This further motivates the importance of the knowledge of the in-situ stress state in tailings

© University of Pretoria

dams.

3. Regarding the influence of sample preparation method, two distinct CSLs were identified for the MT samples and the SD samples (as shown in Figure 3.19). The CSLs were defined using the same slope but with different intercepts. This is in direct contradiction to a key principle of CSSM that the sample preparation method should not influence the behaviour at critical state (i.e. that the CSL should be independent of initial fabric). However, similar observations have been made by other researchers on gold tailing (e.g. Reid et al., 2022b) and iron ore tailings (e.g. Mmbando et al., 2023). Additional testing is required to fully investigate these findings.

By assuming a K_0 value based on results by Fourie & Tshabalala (2005) on gold tailings mined from an ore body of similar geological origin, the results from the oedometer and triaxial tests could be directly compared. It was found that the 1D-NCL and NCL are not parallel. However, the slopes of these curves are similar, and for practical purposes, it can be assumed that the 1D-NCL and NCL are parallel for the gold tailings tested.

Aside from the finding regarding the influence of the sample preparation method on the CSL, these findings are all entirely consistent with CSSM principles and are useful for both practicing engineers and regulators. Results from these types of tests can greatly assist with planning of both routine and investigative laboratory testing, as well as future tailings dam design considerations.

© University of Pretoria

4 REMOTE MONITORING SYSTEM

4.1 INTRODUCTION

A key objective of the study was the design of a remote monitoring system. This chapter defines the requirements of the remote monitoring system, as well as describes the components that were selected for the system.

4.2 REQUIREMENTS OF THE REMOTE MONITORING SYSTEM

The first step in the design of the system was understanding the requirements of the system. Five key aspects were identified including accessibility, reliability, durability, longevity and capability. A summary of these requirements, and the solution implemented, is provided in Table 4.1.

© University of Pretoria

Table 4.1: Key aspects of the remote monitoring system

	Aspect	Definition	Requirement	Solution
1	Accessibility	Ability to communicate with the logger without having to visit site.	Since the tailings dams that were selected for monitoring are located some distance from the University, it is imperative that communication can occur remotely. This is important to ensure that the data can be collected regularly, and as well as to periodically confirm that the system is operating correctly.	Since South Africa has comprehensive cellular coverage and since mobile data is relatively affordable, it was decided that dataloggers with cellular capabilities would be used. The network service provided was chosen based on published coverage maps. No issues related to data coverage were noted for the duration of the monitoring period.
2	Reliability	Ability of the system to save the recorded data locally.	Since the study relied heavily on the monitoring data, it was deemed necessary to have the data saved in multiple, independent locations. Therefore the system chosen should be able to store the data locally, and once the periodic data were collected, these should be backed up.	A datalogger with sufficient on-board memory was selected. All measured responses from the loggers were saved locally once an hour. This data was remotely collected twice-weekly during the first month of monitoring, and then only once a week thereafter. Once obtained, the data were stored locally on the University's laboratory laptop and a cloud backup was made.
3	Durability	Ability of the system to survive the harsh conditions expected on site	Tailings dams provide some of the harshest environments for monitoring equipment. The remote monitoring system should therefore be able to withstand these effects. In particular, the sensors will be exposed to saturated mine tailings, while the cables and	Each sensor selected for use was manufactured using corrosion resistant materials and was waterproof. In addition, all the splices were performed with high-quality, waterproof splice kits and each splice was thoroughly tested before use. The logging equipment was housed in a waterproof and dustproof enclosure.

© University of Pretoria

	Aspect	Definition	Requirement	Solution
			logging equipment will be exposed to sunlight, rain and dust.	
4	Longevity	Ability of the logger to perform as required without intervention	The system should be capable of logging for an extended period of time without having to rely on an external power supply, or frequent battery replacements.	A high-capacity 12 V, 26 AH rechargeable gel battery was used to power the system. Based on the long-term Drying Box 1 experiment, this battery was shown to be capable of powering the system for at least six months. To further increase the longevity of the system, a solar panel was added to the system to continuously charge the battery.
5	Capability	Ability to measure the complete soil stress state	The complete stress state, as defined for this study, comprises the vertical effective stress and the horizontal effective stress. Therefore the combination of sensors selected should be capable of estimating these parameters reliably.	To measure the horizontal total stress, an EPC was suspended from a segment of reinforcing steel, while an EPC was placed within a slurry to measure the vertical total stress. To measure the pore pressure, two Tuks tensiometers were selected. In some laboratory tests, a TEROS 21 WPS was used to measure pore pressures, however, these were not installed in the field. A TEROS 12 moisture probe was used to estimate the VWC of the soil. The horizontal and vertical effectives stresses were calculated by considering both the total stresses and the measured pore pressure. As discussed in Section 5.5.5, the VWC was considered for the effective stress calculations.

© University of Pretoria

4.3 COMPONENTS OF THE REMOTE MONITORING SYSTEM

4.3.1 Overview

Based on the requirements set out in the previous section, several components were required to construct the remote monitoring system. This section describes the individual components that were selected to form part of the remote monitoring system.

4.3.2 Sensors

To measure the total stresses in the soil, Geosense Total Earth Pressure Cells (EPC) were selected. The EPCs chosen are 650 mm in length and comprise a circular sensing face and a 170 mm long, 25 mm diameter housing which contains the pressure transducer as shown in Figure 4.1. The sensing face is composed of two circular stainless-steel plates welded around their circumference and filled with a mixture of de-aired water and glycol.

The sensing face is hydraulically connected to the pressure transducer by means of a 6.2 mm diameter steel connecting tube. The sensing face has an active side and an inactive side with an outer diameter of 165 mm and a thickness of 7.5 mm. The active side has an inactive rim with an inner active diameter of 150 mm.

The EPCs used have a resolution of ±0.025% FSO, a reported accuracy of ±0.1% FSO, and a capacity of 345 kPa, over an operating temperature range of -20°C to +80°C (Geosense Ltd, 2016). The vibrating wire EPCs were chosen over the strain gauge cells as vibrating wire based sensors have been shown to be more reliable for long-term monitoring when compared to equivalent strain gauge based sensors (e.g. Bordes & Debreuille, 1984).

As was discussed earlier, it is known that there are several factors that influence the performance of EPCs and that if these factors are not considered appropriately, poor performance can be expected from the EPCs. Table 4.2 provides a summary of these 15 factors. For each factor, the steps taken as part of this study to improve the performance of the EPCs have been highlighted.

© University of Pretoria

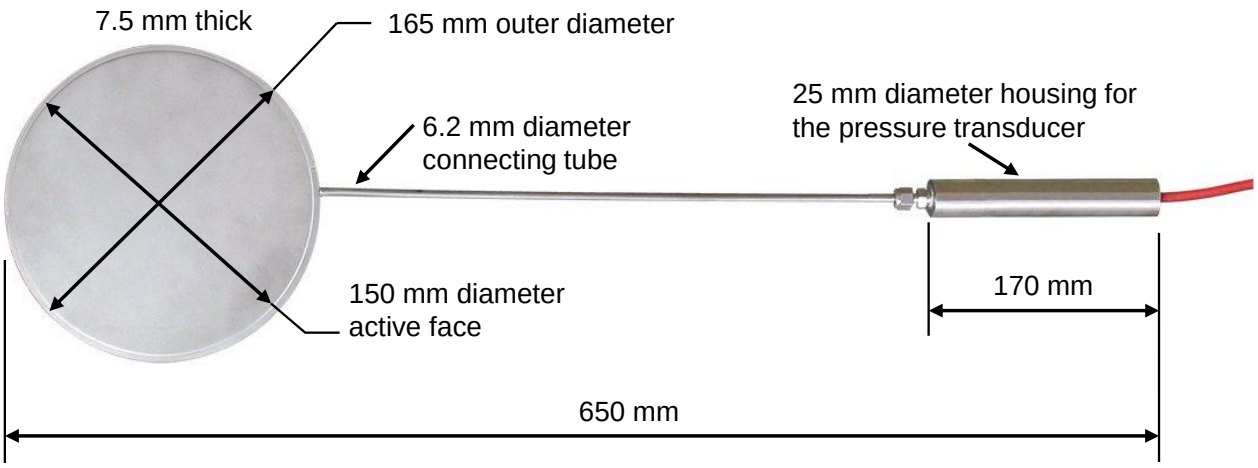


Figure 4.1: Details of the Geosense VWTPC-4000 EPC (after Geosense Ltd, 2016)

To measure the pore pressures in the soil, the Tuks HCTs were selected. In particular, the steel-cased tensiometers were selected over the epoxy-cased tensiometers. As an additional test, a commercial WPS was used for the initial laboratory experiments. However, it was later decided that this sensor would not be included for the site installations. This was based on the poor performance of the sensor at low stresses and in situations where rapid changes in suction are experienced (as discussed in Section 5.6.1).

To measure the moisture content of the soil, it was decided that the TEROS 12 moisture probes manufactured by the METER Group would be used. The TEROS 12 sensor is a compact, complete soil moisture system sensor (Campbell Scientific Inc., 2019). The sensor is often used in the agricultural sector due to its large one litre volume of influence as well as its high accuracy, durability and low cost.

© University of Pretoria

Table 4.2: Summary of actions applied for this study regarding key aspects affecting the performance of EPCs

	Factor	Recommended action	Action applied for this study
1	Aspect ratio (cell thickness to diameter ratio)	Use relatively thin cells ($\frac{T}{D} < \frac{1}{5}$), $\frac{T}{D} < \frac{1}{10}$ in some cases	With a thickness of 7.5 mm and a diameter of 165 mm, the EPCs used in this study have a $\frac{T}{D} = 0.05$, which meets the recommended requirements.
2	Soil-cell stiffness ratio, S	Design cells for high stiffness ($S < 0.5$) and use correction factors	With an average EPC stiffness of 612 MPa as measured during the compliance testing, and with an average gold tailings stiffness of 26 MPa, the EPCs have a calculated $S = 0.04$, which meets the recommended requirement.
3	Diaphragm deflection (arching)	Design cell for low deflection ($\frac{d}{\Delta} > 2\,000 - 5\,000$)	With an active face diameter of 150 mm and an average deflection of 0.047 mm, as measured during the compliance testing at applied pneumatic stresses of 200 kPa, the EPCs have a calculated $\frac{d}{\Delta} = 3191$, which meets the recommended requirement.
4	Cylinder or piston cell deflection	Design cell for low deflection ($\frac{d}{\Delta} > 20\,000$)	This factor is not applicable to the Geosense EPCs which are hydraulic-type EPCs and not diaphragm-type EPCs.
5	Stress concentrations at cell corners	Use inactive outer rims to reduce sensitive area ($\frac{d^2}{D^2} < 0.25 - 0.45$)	With an active diameter of 150 mm, the EPCs used in this study have a $\frac{d^2}{D^2} = 0.83$. This value lies outside the recommended range. However, it should be noted that these requirements were based on theoretical considerations (e.g. Monfore, 1950) and limited physical testing (e.g. Peattie & Sparrow, 1954). In their physical testing, Peattie & Sparrow, (1954) noted that it was not possible

© University of Pretoria

	Factor	Recommended action	Action applied for this study
			to test EPCs larger than 76.2 mm in diameter. It was also noted that if the regions of stress concentrations were restricted to a small distance in from the circumference of the cell, then the sensitive area ratio would not be of great importance for larger cells. The EPCs used in this study have an active diameter of 150 mm and it is therefore likely that this requirement may not be of great important for these EPCs.
6	Eccentric, nonuniform and point loads	Increase stress cell active diameter (diaphragm, $\frac{d}{D_{50}} \geq 10$; cylinder $\frac{d}{D_{50}} \geq 50$)	With a D_{50} of 0.063 mm, the EPCs installed in the gold tailings have a $\frac{d}{D_{50}} = 2300$, which meets the recommended requirements.
7	Lateral stress rotation	Use correction factors, such as those proposed by Askegaard, (1963).	The corrections proposed by Askegaard (1963) were based on analytical methods which included their own set of assumptions. It is unclear whether using these corrections would improve the results from the EPCs in this case, therefore no corrections were applied.
8	Cross-sensitivity	Change strain gauge arrangement or add outer rings	This factor is not applicable to the Geosense EPCs which are vibrating wire sensors and not strain gauge sensors.
9	Stress-strain behaviour of soil	Calibrate cell under near-usage conditions	Each EPC were delivered with a calibration datasheet developed by the manufacturer.
10	Placement effects	Random error; use duplicate measurements	The EPCs were installed in a shallow excavation. The excavation was loosely backfilled and then filled with slurry as part of routine operations. Three stress stations were installed in relatively close proximity (~20 m apart) for duplicate

© University of Pretoria

	Factor	Recommended action	Action applied for this study
			readings. Filling with slurry implies initial hydrostatic conditions and thorough embedment.
11	Proximity of structures and other stress cells	Use adequate spacing: see text for criteria	The EPCs were not placed near any other structures in the field.
12	Dynamic stress measurements	Use dynamic calibration	No dynamic measurements were made as part of this study.
13	Corrosion and moisture	Use extra water-proofing precautions	The EPCs used as part of this study are manufactured using stainless steel and are designed to be waterproof and corrosion resistant. A long-term laboratory trial was conducted to verify that the gold tailings had no corrosive effects on the EPC and that the EPCs were waterproof (see Section 5.6.1).
14	Placement stresses	Check cell design for yield strength	The EPCs were installed by hand, no construction-related stresses were imposed.
15	Temperature	Calibrate or use balance resistors	Temperature corrections were made using the EPC-specific temperature coefficient contained in the datasheet as per the manufacturer's recommendations.

© University of Pretoria

4.3.3 Logging equipment

Campbell Scientific develop and manufacture dataloggers, sensors and communication devices. The University of Pretoria has successfully used their range of dataloggers for several projects over the years. For this study, the CR300 datalogger was selected. This selection was based on a consideration of the operational requirements of the project, primarily the number of sensors that needed to be logged, the power consumption of the loggers, and the project budget.

Since the EPCs are vibrating wire sensors, a device capable of measuring the response from a vibrating wire sensor was required. The Campbell Scientific AVW200 module is one such device. A single AVW200 module is capable of interpreting the signal from two EPCs and so only one AVW200 module was required per system. The CR300 datalogger is capable of logging two Tuks tensiometers, the AVW200 module, and at least two sensors using the SDI-12 communication protocol. The CR300 datalogger and AVW200 modules can be powered by a standard 12 V battery, and the CR300 is able to transfer power from the 12 V battery to the AVW200 module, simplifying the power wiring requirements.

For the field tests, the response from the sensors was logged once an hour. However, this logging frequency was increased for the laboratory verification tests, as well as for the logging of the tensiometer installations on site. With some coding, the cellular module could be sent to a low-power sleep mode and only powered for a 15-minute window every three hours. This greatly reduced the power consumption of the system.

A dual band, SubMiniature version A (SMA) antennae with a 7 dB gain was used to boost the range of the internal modem so that the datalogger could connect to the local mobile telecommunications network.

4.3.4 Power unit

A Forbatt rechargeable gel battery (with product code FB26-12G) was used to power the remote monitoring system. The 12 V battery has a capacity of 26 AH. As discussed in the next chapter, smaller capacity batteries were initially trialled, however these ultimately proved inadequate to meet the power requirements for the remote monitoring system. The 26 AH battery, combined with the optimised logging code was shown to be capable of powering the entire remote monitoring system for up to six months with no external intervention being necessary. This is discussed in further detail in Section 5.6.1.

© University of Pretoria

A Growcol solar panel comprising 36 monocrystalline cells was used to charge the battery. The panel is 250 mm wide, 350 mm high, 17 mm thick and weighs approximately 1 kg. It has an anodised aluminium frame and has an Ingress Protection (IP) rating of IP65 which means that the enclosure is protected from total dust ingress and low pressure water jets from any direction (IEC, 2001). With a maximum power output of 10 W, the panel has an optimum operating current of 0.57 A, at a voltage of 17.8 V (Growcol International, 2021).

An SR-HP2410 smart solar control unit was used to regulate the power between the solar panel, battery and CR300 logger. The particular control unit chosen is lightweight and compact, with a width of 71 mm, height of 103 mm, thickness of 36 mm, and weight of just 100 g (SRNE Solar, 2018). The control using has a current capacity of 10 A. With an IP rating of IP30, the control unit is protected from tools and wires greater than 2.5 mm but not protected from liquids. The control unit therefore needed to be housed in the logger box.

As shown in Appendix C, the capacity of the solar panel, combined with the power usage of the remote monitoring system during the night, resulted in the batteries typically being restored to fully charged within a day if the weather was clear. On cloudy days, the time to replenish the batteries was increased to two days.

4.3.5 Cabling

Each commercial sensor is delivered with between 2 m and 5 m of cabling provided by the manufacturer. However, this length is insufficient for the field installations where the loggers were located many metres aways from the sensors. Therefore the cables needed to be spliced and extended. To achieve this, additional cabling and splice kits were required.

In terms of cabling, the four-core, flexible erse Kablo LIYCY cable was selected. A labelled sketch of this cable is shown in Figure 4.2. The cable has an outer diameter of 4.6 mm and is protected with a grey, oil-resistant Polyvinyl Chloride (PVC) outer sheath. Inside the sheath is a tinned copper braid screen and inside the screen is a pes tape wrapping. These layers protect the four bare copper cores in the cable. Each core has a PVC insulation cover and an area of 0.14 mm^2.

© University of Pretoria

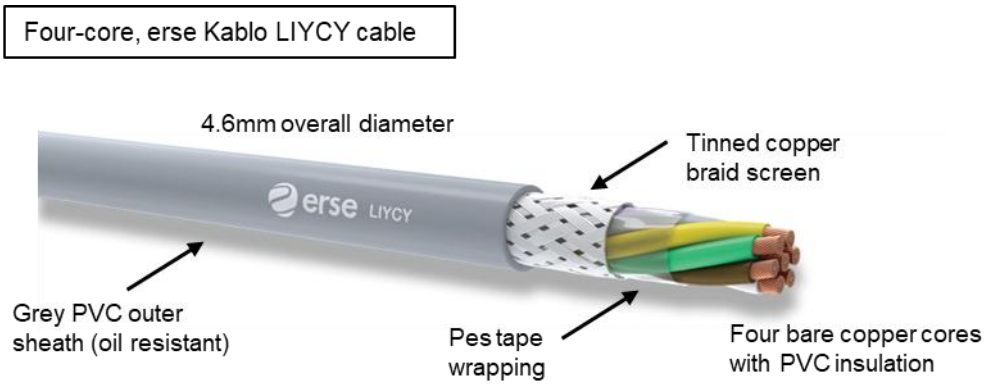


Figure 4.2: Sketch of the erse Kablo LIYCY cable used for this study (after erse Kablo, 2021)

In terms of splicing, it was decided that special attention would be given to this aspect considering how important this was shown to be by other researchers. For example, Bruggemann & Gosden (2004) showed how almost all the sensors installed in the embankment were lost after a few years due to the poor quality of the splice kits that were used. Although necessary, splices in a cable naturally create opportunities for broken connections. Therefore any splices would need to be well protected and thoroughly tested. Further, since these sensors were to be installed on an active tailings dam, the splices will need to be waterproof. For this study, the Metaplast MX1 low voltage joint kits were selected.

Figure 4.3 shows selected photographs taken during the cable splicing that was conducted at the platinum site. Figure 4.3(a) shows a photograph of the cables connected inside the splice kit, but before the epoxy was added. During this time, the connection was tested. Figure 4.3(b) shows the splice kits drying after being filled with the epoxy resin. Figure 4.3(c) shows the completed splices for all ten cables being placed in a protective sleeve.

© University of Pretoria

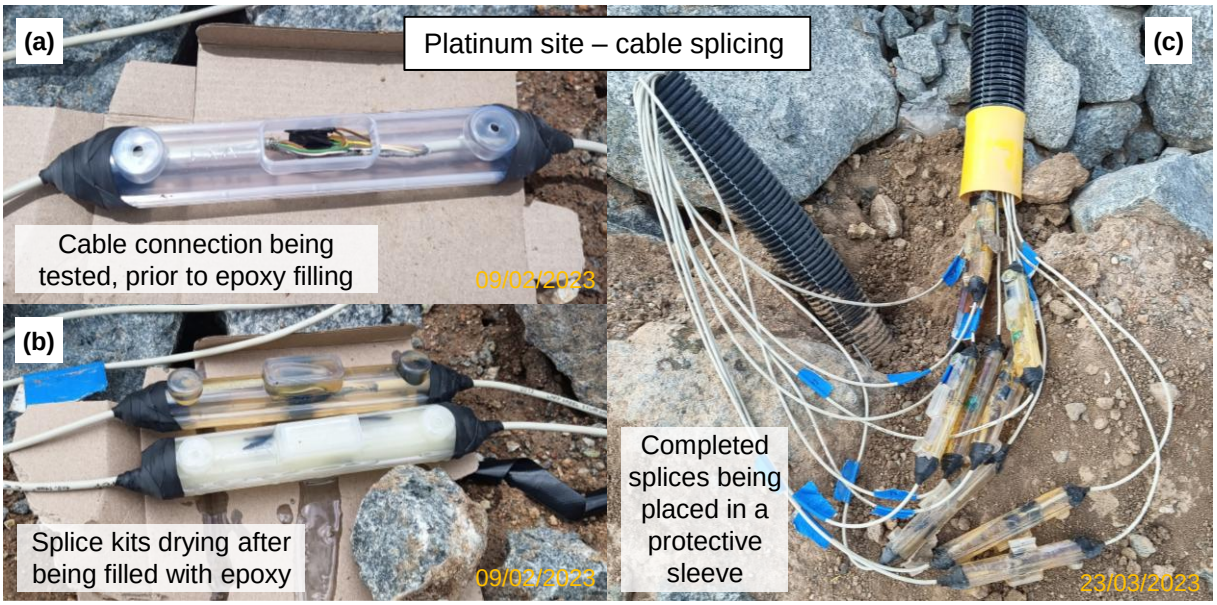


Figure 4.3: Photographs showing the cable splicing at the platinum site: (a) before epoxy filling, (b) after epoxy filling, and (c) completed splices

4.3.6 Enclosure (logger box)

Tailings dams provide some of the harshest environments that can be expected for field logging equipment. Typical hazards include direct sunlight, rainfall and dust exposure. To protect the logging equipment from these elements, an enclosure was selected to house the equipment. The particular enclosure selected was the Allbro Allbrox 3. Made from durable glass reinforced polyester, the logger box is 250 mm wide, 350 mm high, and 200 mm deep. With an IP rating of IP66, the logger box enclosure is protected from total dust ingress and high-pressure water jets from any direction.

Penetrations through the bottom of the box were made to provide access for the cables from the sensors, solar panel and antennae. Compression cable glands were used to ensure these holes remained waterproof.

4.3.7 Software

The Campbell Scientific equipment uses the LoggerNet datalogger support software for communication with the dataloggers. For this study, LoggerNet v4.7 was used. LoggerNet enables communication with the dataloggers through the use a Universal Serial Bus (USB) cable. For the remote monitoring system, loggers with cellular connectivity were chosen. With these loggers and Subscriber Identity Module (SIM) card.

© University of Pretoria

The logging code was created using CRBasic, which is a computer coding language used by all Campbell Scientific dataloggers.

4.3.8 Summary

A summary of the key components of the remote monitoring system is provided in Table 4.3. For each component, a brief description of the component is provided, as well as details regarding the specific model that was used in the study.

Table 4.3: Summary of key components of the remote monitoring system

	Component	Description	Model
1	Cabling	Flexible, four-core, screened cable with an oil-resistant PVC outer sheath.	esri Kablo LIYCY four-core screened cable.
2	Splice kits	Waterproof and dustproof splice kits to connect the extensions to the manufacturer's cable.	Metaplast MX1 low-voltage joint kit.
3	Solar panel	A small solar panel to charge the battery, thereby extending the working life of the remote monitoring system before battery replacements are required.	Growcol 350 mm x 250 mm, 10 W monocrystalline cell solar panel.
4	Solar panel control unit	A control unit capable of directing current from the solar panel to the battery, as well as directing current from the battery to power the datalogger. The control unit should stop supplying current to the battery when it is fully charged.	SNRE Solar, SR-HP2410 smart solar control unit.
5	Battery	12 V rechargeable battery to power the remote monitoring system.	Forbatt rechargeable 12 V, 26 AH gel battery (product code: FB26-12G).
6	Antenna	An antenna to boost the signal from the internal modem of the datalogger so that the datalogger can connect to a local cellular network for remote communication.	SMA 7bB gain antenna (product code: ANT 7DB).
7	Datalogger	Datalogger capable of logging the response from all the sensors, storing the data, and being accessible via a cellular network.	Campbell Scientific CR300 cellular datalogger.

© University of Pretoria

	Component	Description	Model
8	Vibrating Wire Analyser	Datalogger capable of logging the response from a vibrating wire sensor.	Campbell Scientific AVW200 spectrum analyser.
9	Vertical stress sensor	Vibrating wire, hydraulic-type Earth Pressure Cell (EPC).	Geosense 165 mm, 345 kPa EPC (Model: VWTP-4000).
10	Horizontal stress sensor	Vibrating wire, hydraulic-type EPC.	Geosense 165 mm, 345 kPa EPC (Model: VWTP-4000).
11	Pore pressure sensor	Sensor capable of measuring both positive and negative pore pressures.	Tuks High-Capacity Tensiometer (HCT), steel-cased.
12	Pore pressure sensor (alternate)	Sensor capable of measuring both positive and negative pore pressures.	METER Group TEROS 21, Gen 2 Water Potential Sensor (WPS).
13	Moisture content sensor	Sensor capable of measuring the moisture content of a soil, continuously and non-destructively.	METER Group TEROS 12 probe.
14	Enclosure (logger box)	A waterproof and dustproof enclosure to house the battery, dataloggers, and solar panel control unit.	Allbro Allbrox 3 with dimensions: 350 mm x 250 mm x 200 mm (Model: ALL-003).

4.4 DESIGN OF THE REMOTE MONITORING SYSTEM

A few iterations of the solar panel and logger boxes were evaluated and trialled in the laboratory. The final configuration of the logger box (enclosure) is shown in Figure 4.4. This photograph was taken at the platinum monitoring site and shows how all the components listed in Table 4.3 were configured on site.

© University of Pretoria

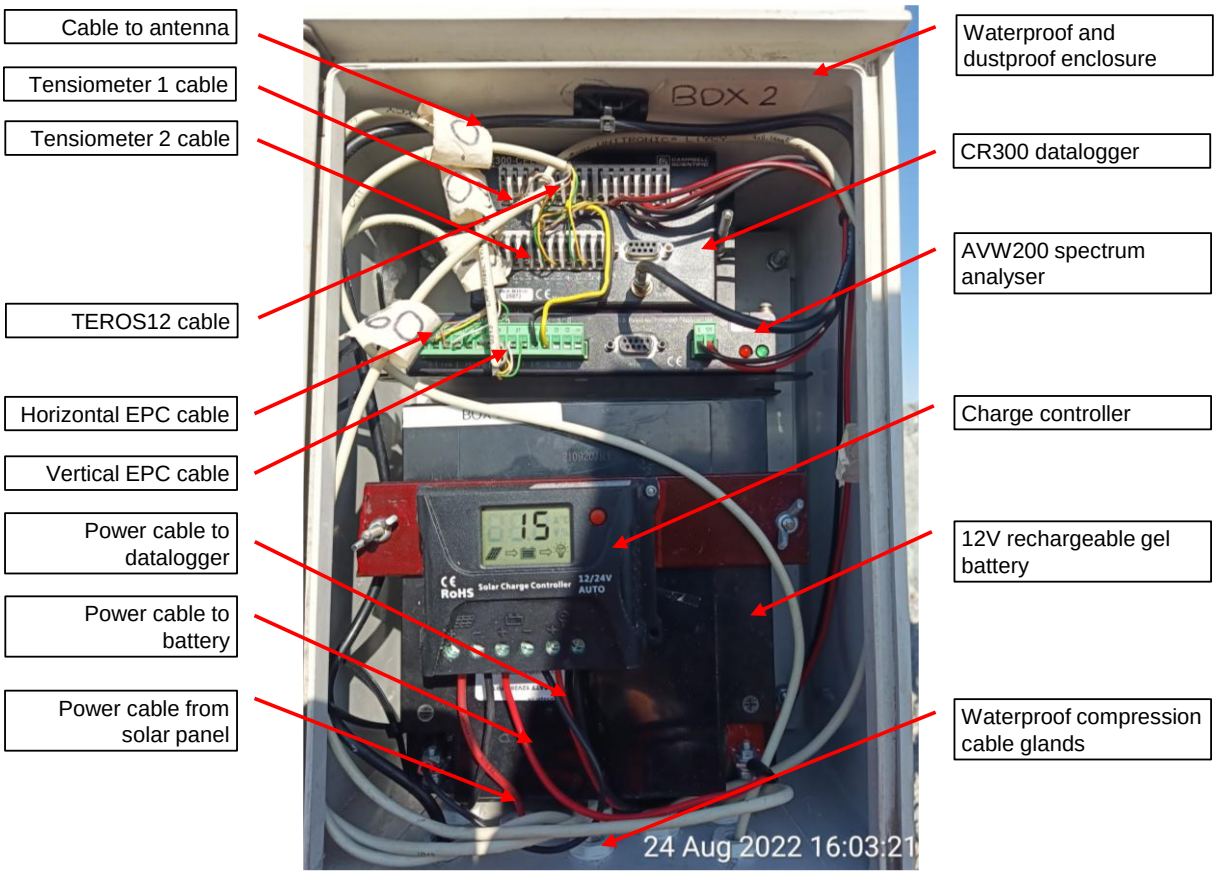


Figure 4.4: Components of the remote monitoring system inside the enclosure

4.5 VERIFICATION OF THE REMOTE MONITORING SYSTEM

To verify the performance of the system, it was decided that a series of tests would be conducted in a controlled environment. The objective of these tests was to verify the performance of the various individual components of the system, as well as the performance of the entire system under the conditions expected in the field. Details regarding these tests are provided in the next chapter.

4.6 SUMMARY

A key objective of the study was the design of a remote monitoring system capable of measuring the in-situ stress state on an active tailings dam. This chapter presented several aspects of this system, including the fundamental requirements of the system, as well as details of the various the components that were selected to meet these requirements. To complete the design and verification of the system, a series of short-term and long-term laboratory tests were conducted on individual components of the system, as well as on the entire system as a whole. The next chapter discusses these laboratory tests.

© University of Pretoria

5 LABORATORY VERIFICATION TESTS

5.1 INTRODUCTION

In this chapter, laboratory testing of the remote monitoring system is described. The intent of this testing was to verify the performance of the individual components of the system, as well as for the complete system.

5.2 TENSIOMETER CALIBRATION TESTS

As discussed in Section 2.6.2 the Tuks tensiometers have been shown to perform well at low to moderate suctions. However, this is only possible if the tensiometers are adequately saturated. This section describes the saturation and calibration process followed for each tensiometer.

5.2.1 General procedure

The tensiometer calibration tests were performed at the geotechnical engineering laboratories at the University of Pretoria. Figure 5.1 shows a sketch of the setup used for the tensiometer calibration. In general, the compressed air supply conduits have been indicated with green lines while the water supply conduits have been indicated with blue lines. The calibration was performed in a temperature-controlled room.

The water pressure readings were read off a calibrated Bourdon gauge. The gauge has a range of 1 MPa and a resolution of 20 kPa. A series of lever ball valves allows for the isolation of the air-water interface, de-aerator and Bourdon gauge as required.

© University of Pretoria

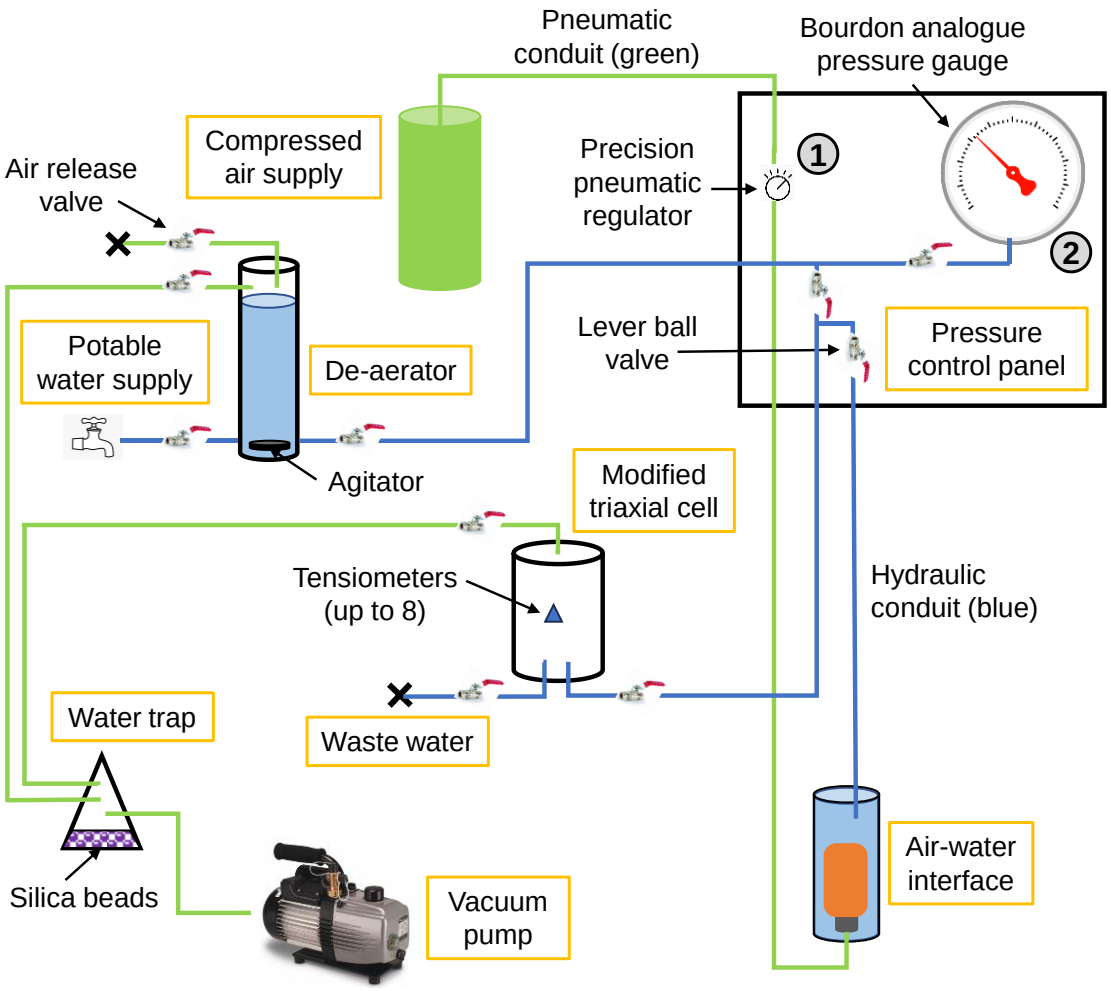


Figure 5.1: Sketch showing the setup for the tensiometer calibration

The calibration process comprised two distinct phases: saturation and calibration. Each process is briefly described in the following sections.

Saturation

The purpose of the saturation phase it to ensure that the reservoir and ceramic of the tensiometer is completely filled with de-aired water. This is a critical phase as poor saturation of the tensiometers is known to significantly affect its performance (e.g. le Roux, 2019). Prior to the start of the saturation phase, the tensiometers were placed in an oven at 65°C overnight to ensure the reservoir and ceramics were dry.

The first step in the saturation process is to ensure the water used is de-aired. This was achieved by using a de-aerator fitted with a mechanical agitator and connected to a vacuum pump. A minimum de-aerating time of 30 minutes was typically enforced.

The tensiometers were placed in the modified triaxial cell and the cell was filled with the de-aired

© University of Pretoria

water. Following the procedure described by Take & Bolton (2003), a vacuum was applied to the cell during filling. This significantly reduced the time required for saturation, as well as improved the cavitation resistance of the tensiometers. Once the cell was filled with de-aired water, air bubbles were bled from the cell and the tensiometers were allowed to equilibrate. Once an appropriate response was noted for all the tensiometers, the cell was pressurised to 500 kPa and the tensiometers were left overnight. The calibration process, described in the next section, was typically conducted the next morning.

Calibration

The intent of the calibration tests was to verify the performance of the tensiometers, as well as to determine the relevant calibration coefficients. A well-performing tensiometer would show a sharp change in voltage difference due to a change in applied pressure. During calibration, the tensiometers were connected to a Campbell Scientific CR300 datalogger and the voltage difference was recorded once a second.

Water pressure in the chamber was systematically raised in increments of 100 kPa from atmospheric pressure (0 kPa) to 600 kPa and then back to 0 kPa. The applied pressure was controlled using the precision regulator, indicated at position 1 in Figure 5.1, while the magnitude of applied pressure was read from the Bourdon gauge, indicated at position 2 in Figure 5.1. Load increments were typically held constant for at least 20s.

Pressures (P) were calculated from the raw tensiometer readings (V_{diff}) using two calibration coefficients α and β as shown in Equation (11).

$$P = \alpha\,(V_{diff} - \beta) \tag{11}$$

Where:

P = Pressure applied to the tensiometer (kPa)

α = Calibration coefficient [kPa/(mV/V)]

V_{diff} = Measured response from the tensiometer due to an applied pressure (mV/V)

β = Response from the sensor at zero pressure (mV/V)

5.2.2 Results

For each tensiometer used as part of this study, a calibration test was conducted. For simplicity, only key examples of these calibration curves are shown here. Figure 5.2 shows the raw calibration data for Tensiometer 1B, which was installed at the gold tailings site. A known pressure was applied

© University of Pretoria

to the modified triaxial cell, and the response of each sensor in mV/V was noted. Three calibration curves are shown. For each stress increment a minimum stabilisation time of 20 s was ensured. The results show a sharp response from the tensiometer to a change in applied pressure and the results are repeatable, indicating that the tensiometer is performing well.

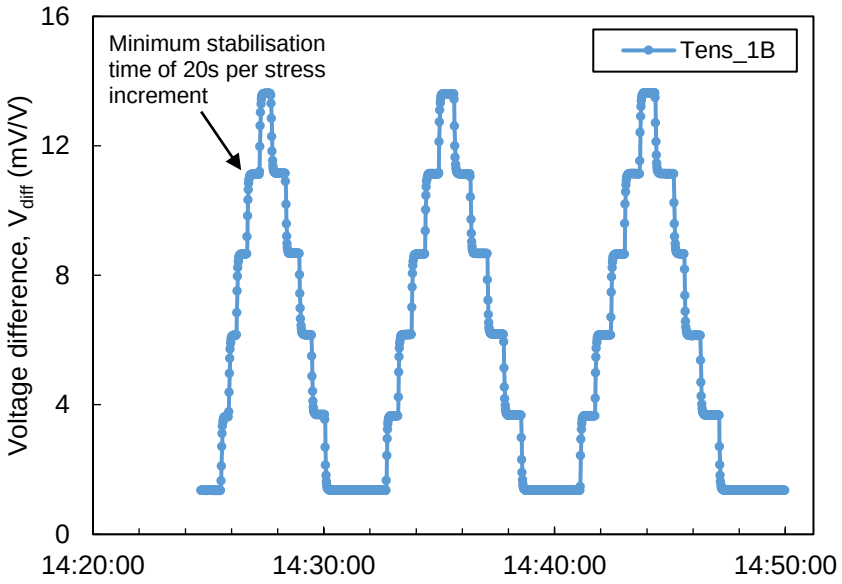


Figure 5.2: Raw calibration data for tensiometer 1B, used for the gold tailings site

The raw calibration data were interpreted, and a calibration coefficient was determined for each tensiometer. The calibration coefficient has units of kPa/(mV/V) and is used to relate the response from the tensiometer to the change in applied pressure as shown in Equation (11). Figure 5.3 shows the interpreted pressures using the chosen calibration coefficients (α) of 40.08 kPa/(mV/V) and 40.55 kPa/(mV/V) for Tensiometers 1A and 1B which were used for the gold site. The zero readings for these tensiometers in the laboratory were 0.479 mV/V and 1.355 mV/V, respectively.

© University of Pretoria

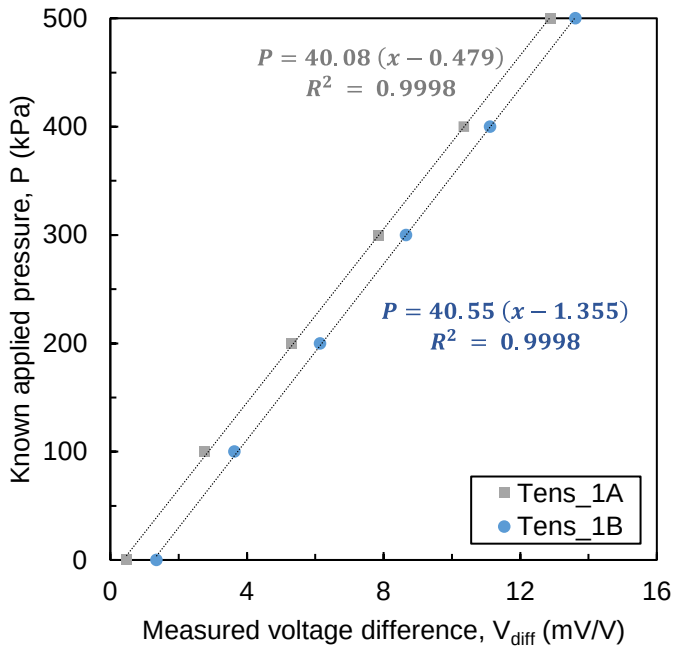


Figure 5.3: Interpreted calibration data for tensiometers 1A and 1B, used for the gold tailings site

Limited dry-out tests were conducted to test the capacity of the tensiometers. In a dry-out test, the tensiometers are left exposed to the air. The water at the face of the tensiometer dries out due to evaporation and this results in cavitation of or air-entry into the tensiometer. The intent of these tests is to verify the performance of the sensors to ensure that they are capable of providing reliable readings in the range of suctions that are expected.

Results from two such dry-out tests are shown in Figure 5.4. Tensiometer S1 achieved a suction reading of 270 kPa before cavitation, while tensiometer S2 achieved a suction reading of 837 kPa before cavitation. After cavitation, it can be seen that both tensiometers abruptly returned to a suction value of 95 kPa (close to absolute zero pressure at the University's elevation). Thereafter, the tensiometers gradually returned to their initial zero reading. After cavitation, the tensiometers no longer provided reliable pressure readings. Tensiometers in this state need to be dried out, re-saturated and re-calibrated before being used again.

A total of 56 tensiometers were used as part of the various aspects of this research and a saturation and calibration exercise was conducted for each tensiometer. Key calibration details for each tensiometer using the field and laboratory tests are shown in Appendix B.

© University of Pretoria

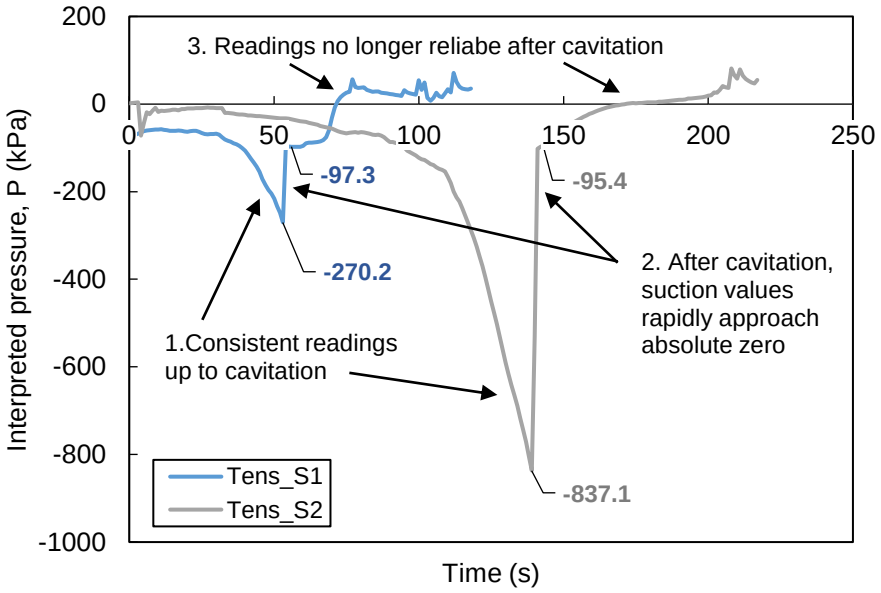


Figure 5.4: Results from selected dry-out tests on the Tuks tensiometers

5.3 MOISTURE PROBE CALIBRATION TESTS

As described in Section 2.6.5, the TEROS 12 moisture probe uses the TDR technique to estimate the dielectric permittivity of the soil. From this parameter, the VWC of the soil can be estimated using one of several empirical relationships (e.g. Topp et al., 1980; Campbell Scientific Inc., 2019). However, these relationships have traditionally been developed for natural soils and there is some uncertainty regarding the performance of these methods for gold tailings. This is specifically important as it is known that the dielectric permittivity of a soil is influenced by the chemistry of the pore water, which is different for gold tailings when compared to natural soils.

A series of drying experiments were conducted in the geotechnical engineering laboratories at the University of Pretoria to investigate the performance of the TEROS 12 probe for use in gold tailings. This section describes the experiments conducted, as well as the results obtained.

5.3.1 General procedure

The intent of the calibration tests was to dry a tailings sample from a saturated state and measure the changes in water content, total volume and suction as the sample dried. In this way, the primary drying curve could be defined for the soil, for the given starting void ratio. For each test, a pre-determined mass of dry tailings was thoroughly mixed with a similarly pre-determined mass of water. The masses were determined based on an assumed initial volume and a target density. To ensure the tailings was dry and did not have clumps, the material was oven-dried at 105°C for

© University of Pretoria

24 hrs. Once cooled, the material was sieved through a 2 mm sieve to remove any clumps.

For each test, the height required to reach the target volume was marked out on the drying container. This volume was determined by filling the container with potable water at room temperature and placing the container on a mass balance. The height of the water was marked once the desired mass was noted on the mass balance. The target volume included the volume of the sensors that would be added to the soil. During sample preparation, the desired mass of wet material was placed such that the height of the sample coincided with the marks on the container once all the material had been placed. To achieve the desired density, the wet material was carefully placed for the loose samples. Some vibration was necessary for the dense samples.

Figure 5.5 shows a sketch of the key components used as part of the calibration tests. Care was taken to ensure that no cables were hanging off the mass balance so any change in mass could only be attributed to loss of water due to evaporation. The total volume was tracked using photographs of the buckets taken at regular intervals.

A single TEROS 12 moisture probe was placed in the centre of the soil sample, with the sensing needles facing horizontally. In addition, two steel-cased Tuks tensiometers and a TEROS 21 WPS were also placed at mid-height within the soil mass. An external light source, with a 100 W light bulb, was used to accelerate the drying process. All masses were determined using a calibrated mass balance with a capacity of 10 kg and a resolution of 0.01 g.

Readings from the sensors were recorded once every five minutes for the tensiometers, moisture probe and suction probe. Readings from the mass balance were saved once every minute. Before each test, the internal clock on the CR300 datalogger was synced with the clock on the laptop computer used to log the readings from the mass balance.

The volume of the sample at the end of the test was determined by marking the height of the tailings on the bucket. The bucket was then cleaned and filled with potable water until the marked height was achieved. The mass of the water was determined using a mass balance mentioned above and the volume of water was calculated assuming a density of the water of 1 g/cm^3. The sample volume was determined by subtracting the volume of the sensors and their cables from the total volume determined by filling the bucket to the marked height.

© University of Pretoria

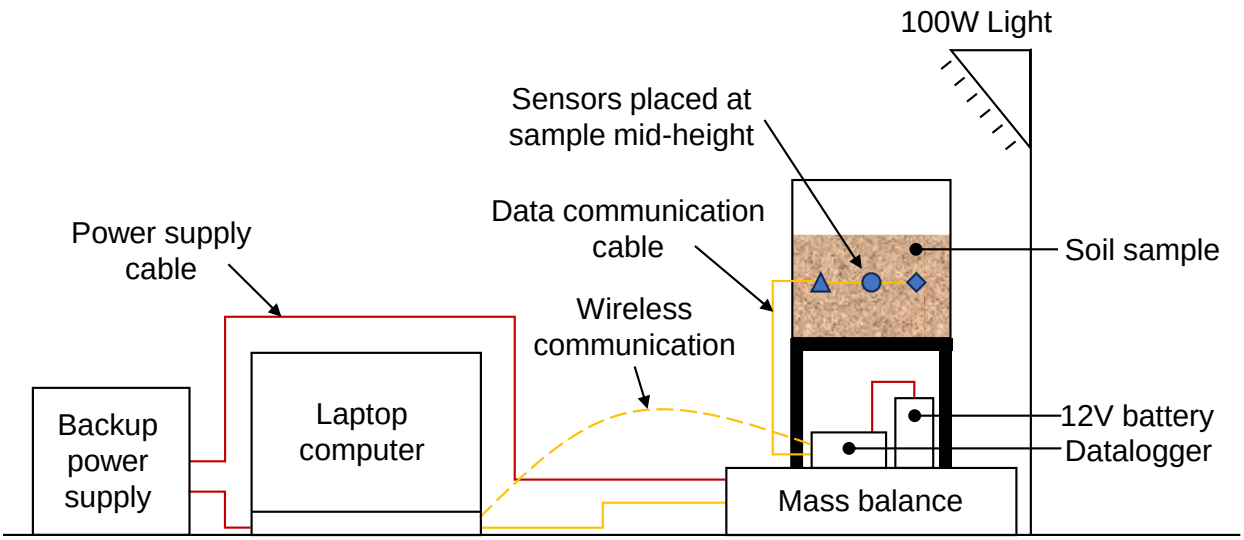


Figure 5.5: Sketch showing the key components of the setup used for the moisture probe calibration tests

Figure 5.6 shows a photograph of the moisture probe calibration test setup taken during Test 5. Each component shown in the sketch can be seen in the photograph.

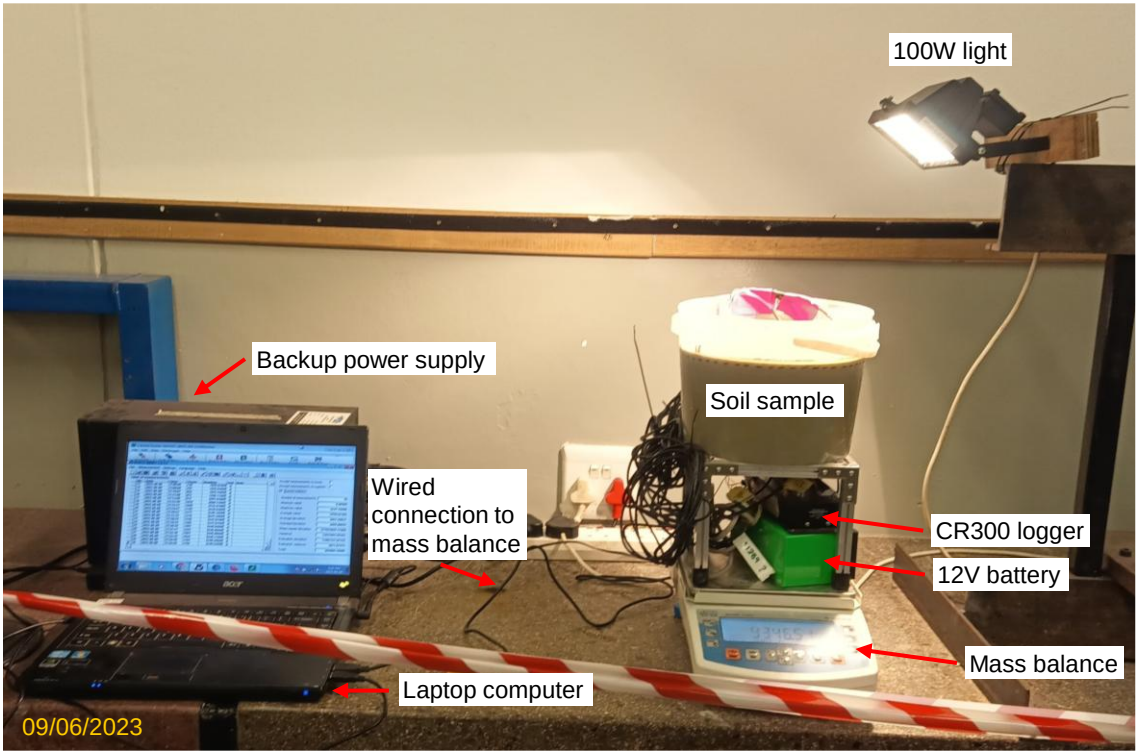


Figure 5.6: Photograph showing the setup used for the moisture probe calibration tests

© University of Pretoria

5.3.2 Results

Table 5.1 provides a summary of key aspects of the five moisture probe tests conducted. Test 1 was the densest sample tested. Although the sample was initially created at a looser state (e~0.9), the sample separated after placement into a soil phase at the bottom with a water phase at the top. After the excess water which had collected at the top of the sample was removed, it was found that the sample had consolidated to a denser state, with a void ratio of approximately 0.80. Throughout the testing, it was the point where no further standing water was present on the sample that was taken as the start of the test. Unfortunately Test 2 was interrupted by load shedding (i.e. a power outage) and the recovered data were deemed unreliable. Results from this test are therefore not plotted.

Test 3 was conducted on a loose sample, with an initial void ratio of 1.02. For this test, process water obtained from site was mixed with the dry tailings to obtain the slurry. The purpose of this test was to investigate the influence of the mine process water on the performance of the moisture probe. Test 4 was of an intermediate density (e~0.9) and Test 5 was a repeat of Test 3 (i.e. the loosest sample) but with tap water being used instead of the mine process water that was used for Test 3. Table 3.3 shows the composition of both the mine process water (used in Test 3) as well as the laboratory tap water (used in Tests 1,2,4 and 5).

Table 5.1: Key aspects of the moisture probe calibration tests

Test	Start void ratio	End void ratio	Start VWC	End VWC	Test duration (days)	Comment
1	0.80	0.80	0.45	0.08	11	First test, densest sample
2	0.95	0.76	0.41	0.06	15	Test interrupted by load shedding, data not reliable.
3	1.02	0.74	0.49	0.15	24	Loose sample, replace tap water with mine process water
4	0.88	0.72	0.38	0.03	32	Intermediate density
5	1.04	0.75	0.49	0.14	40	Repeat of Test 3, use tap water

Figure 5.7 shows selected results from Test 3. These results are typical of those obtained from the calibration tests. Figure 5.7 specifically shows the response of the two Tuks HCTs and the WPS, compared to the total mass of the sample over time. The mass of the sample follows an exponential

© University of Pretoria

decay function as the water evaporated. Excellent correlation was noted between the suction measurements reported for the two HCTs. However, a slower response was noted for the WPS.

The slower response of the WPS, compared to the HCTs can be described either in terms of measured suction at a specific time, or in terms of a time delay required to achieve the same suction. For example, at 15 days, the WPS showed a suction value approximately 20 kPa lower than the two HCTs. It took a further 4 days for the WPS to reach this suction value, when compared to the HCTs.

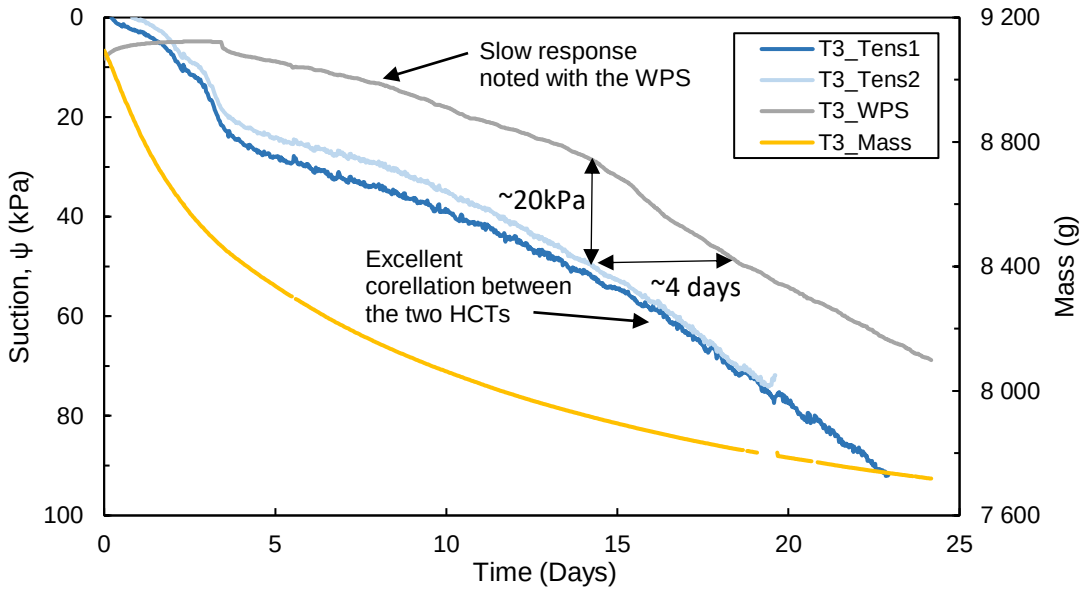


Figure 5.7: Selected results from the moisture probe calibration Test 3

Figure 5.8 shows a summary of the results from all four calibration tests on the TEROS 12 moisture probe. In the figure, the known VWC is compared to the VWC calculated using the Mineral Soils relationship as shown in Equation (9). The legend differentiates between samples prepared using Tap Water (TW) and Process Water (PW). It can be seen that the majority of the data points lie within ±0.05 of the line of equality. Further, there does not appear to be a clear influence of density nor water chemistry. It therefore appears that the interpretation of VWC for gold tailing using the TEROS 12 probe and the Mineral Soils relationship is independent of water chemistry and initial density.

© University of Pretoria

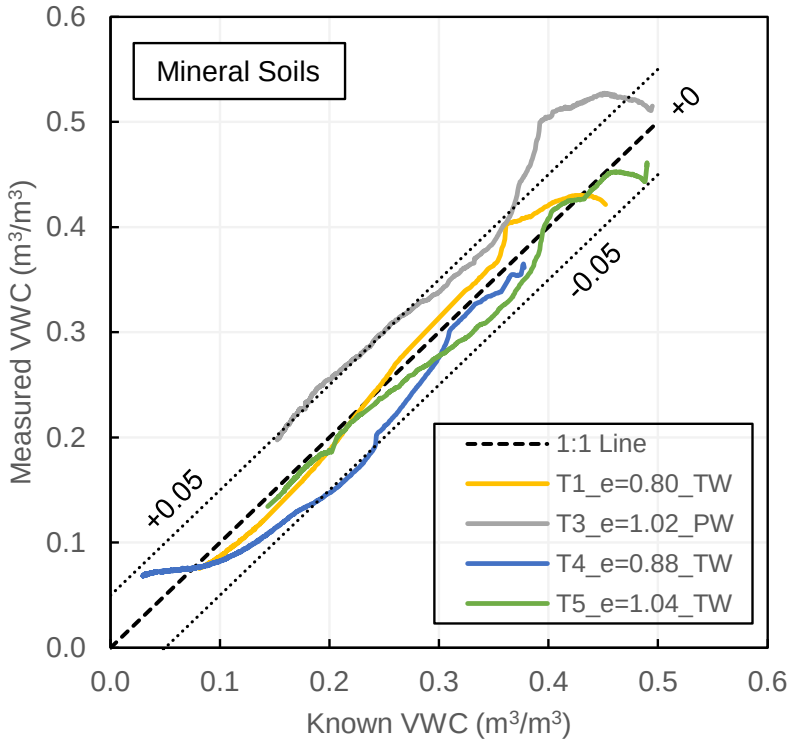


Figure 5.8: Performance of the TDR sensor using the Mineral Soils relationship

Figure 5.9 shows a summary of the results from all four calibration tests on the TEROS 12 moisture probe. In this figure, the known VWC is compared to the VWC calculated using the relationship proposed by Topp et al. (1980) as shown in Equation (7). It can be seen that although the majority of the data fit within ±0.05 of the line of equality, there are still some data points that lie outside this range. A poorer fit was noted when compared to the results shown in Figure 5.8 which were determined using the Mineral Soils equation. As was noted with the Mineral Soils interpretation, there does not appear to be a clear influence of density nor water chemistry. It therefore appears that the interpretation of VWC for gold tailings using the TEROS 12 probe and the Topp equation is independent of water chemistry and initial density.

© University of Pretoria

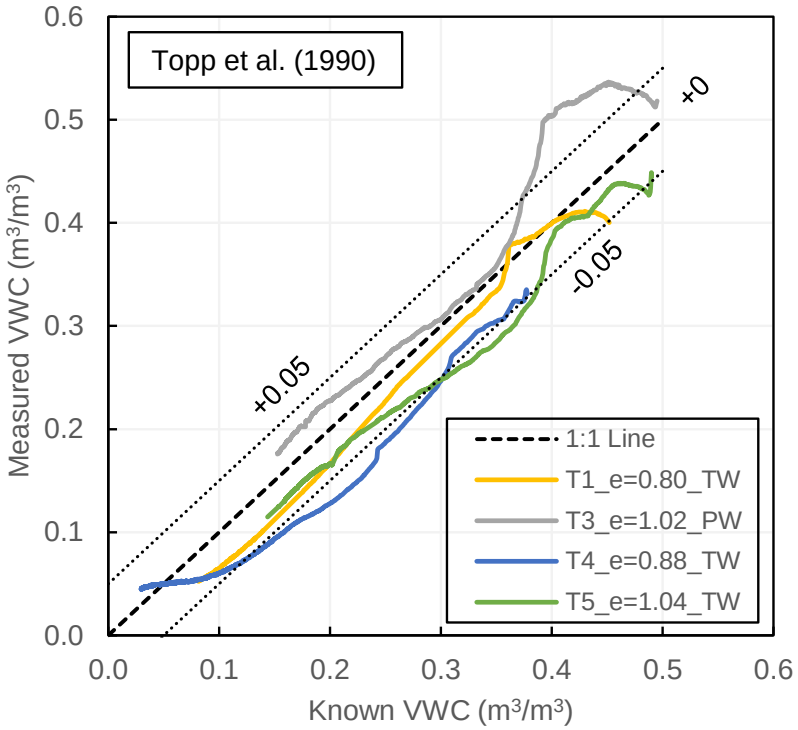


Figure 5.9: Performance of the TDR sensor using the Topp et al. (1980) relationship

Using the suction values measured by the Tuks HCTs, and by calculating the degree of saturation using the mass readings from the mass balance (assuming any loss of mass is only due to evaporation), it is possible to plot a SWRC for the gold tailings. Figure 5.10 shows the SWRCs developed using the results from the moisture probe verification tests. Data for an additional SWRC is also shown for reference. This SWRC was determined in accordance with the tensiometer method as described by le Roux (2019). The initial void ratios of the samples, as well as the interpreted Air Entry Values (AEVs) have been highlighted. It can be seen that it proved difficult to ensure initial saturation of the denser samples. In addition, the gold tailings can be characterised by a low AEV of between 4 kPa and 11 kPa.

© University of Pretoria

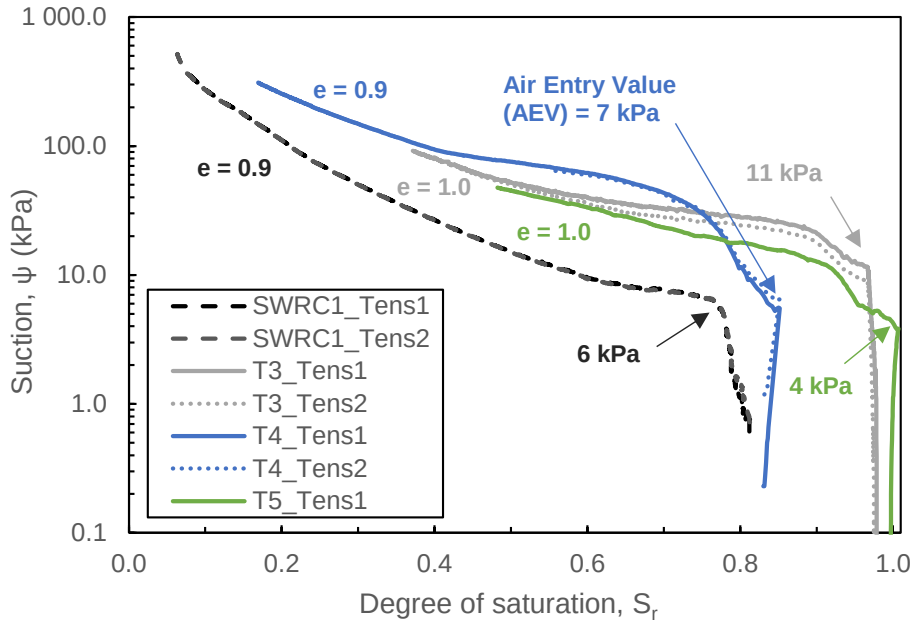


Figure 5.10: Comparison of the various SWRCs developed for the gold tailings

The measured drying curve for Test 5 was approximated using the equation proposed by Fredlund & Xing (1994) as shown in Figure 5.11. Figure 5.11(a) shows the VWC-ψ relationship while Figure 5.11(b) shows the Sr-ψ relationship. Excellent correlation can be seen for both relationships. The curve-fitting parameters a, n and m are shown in the figure. Curve fits for Tests 3 and 4 can be found in Appendix B.

© University of Pretoria

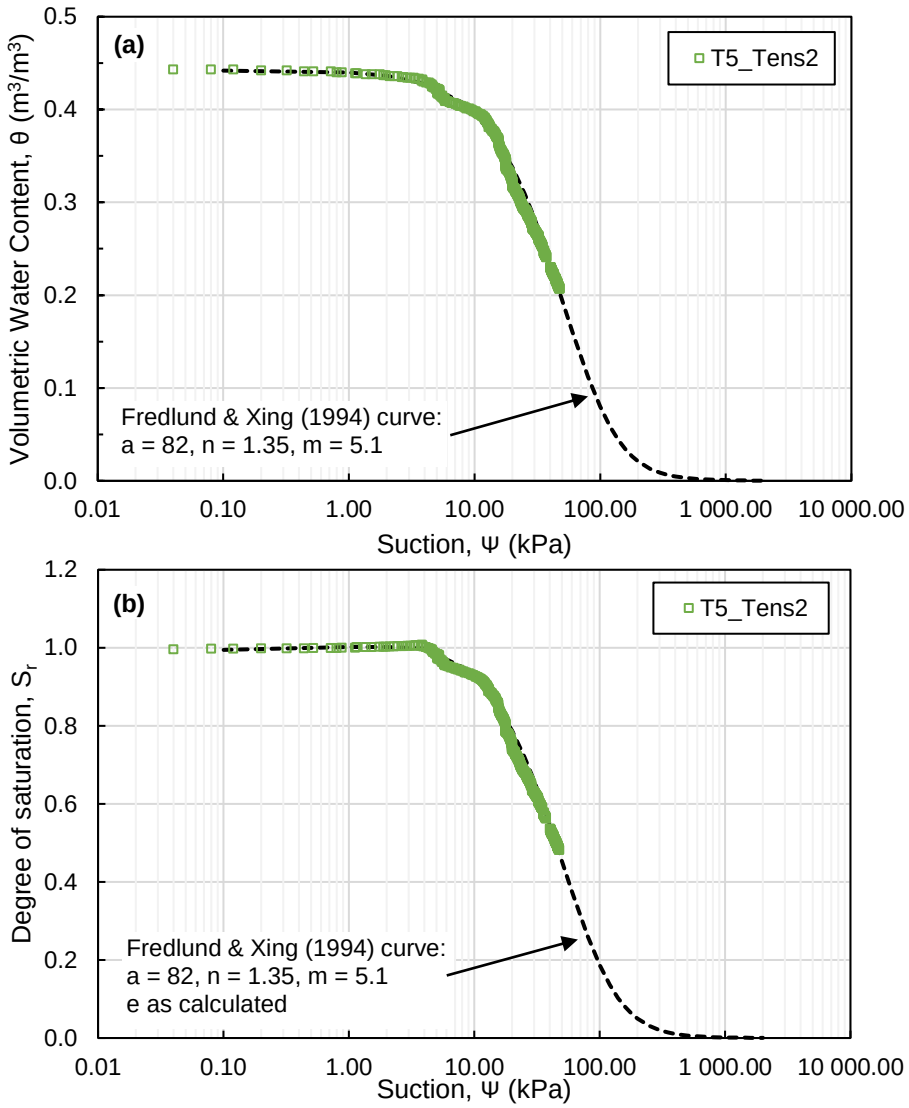


Figure 5.11: Fredlund & Xing (1994) curve fits for the gold tailings showing: (a) VWC, and (b) Sr plots

5.4 EARTH PRESSURE CELL VERIFICATION TESTS

A series of tests were conducted to investigate the compliance of the different EPCs. It is known that the stiffness of the EPCs influence their performance in soil. The intent of this testing was to investigate the magnitude of cell deflection for the expected applied total stresses, as well as to investigate the potential variability in deflection between the different cells when subjected to the same applied load.

One of the key areas of uncertainty regarding the performance of EPCs in soil is compliance issues. As discussed in Section 2.6.1, there are several types of EPCs available, each with its own set of advantages and disadvantages. The EPCs selected for use in this study are hydraulic-type cells. These cells by definition deform due to an external applied loading. This deformation can be a

© University of Pretoria

concern when measuring earth pressures if the soil is known to arch (i.e. span across the EPCs such that the true stress in the soil is not imposed on the EPC). This is especially important for EPCs installed to measure lateral earth pressures. To investigate the susceptibility of the EPCs to this phenomenon, it was decided that the deflection of the EPC would be measured as a function of an applied load.

5.4.1 General procedure

The compliance tests were conducted in a temperature-controlled room in the geotechnical engineering laboratories at the University of Pretoria. Figure 5.12 shows a sketch of the setup that was used for the EPC compliance testing. The testing apparatus involved the use of a modified pneumatic pressure vessel with a safe working capacity of 700 kPa. The pressure vessel was connected to a compressed air supply, and the pressure was regulated using a lever ball valve to increase pressure and an air release valve to reduce pressure.

The response from the EPCs was recorded using a Campbell Scientific AVW200 spectrum analyser, connected to a Campbell Scientific CR300 datalogger. The datalogger and spectrum analyser were powered by a 12 V, 4.6 AH lead acid battery and were connected to a laptop computer using a USB cable. Frequency and temperature measurements were recorded once every 10 s.

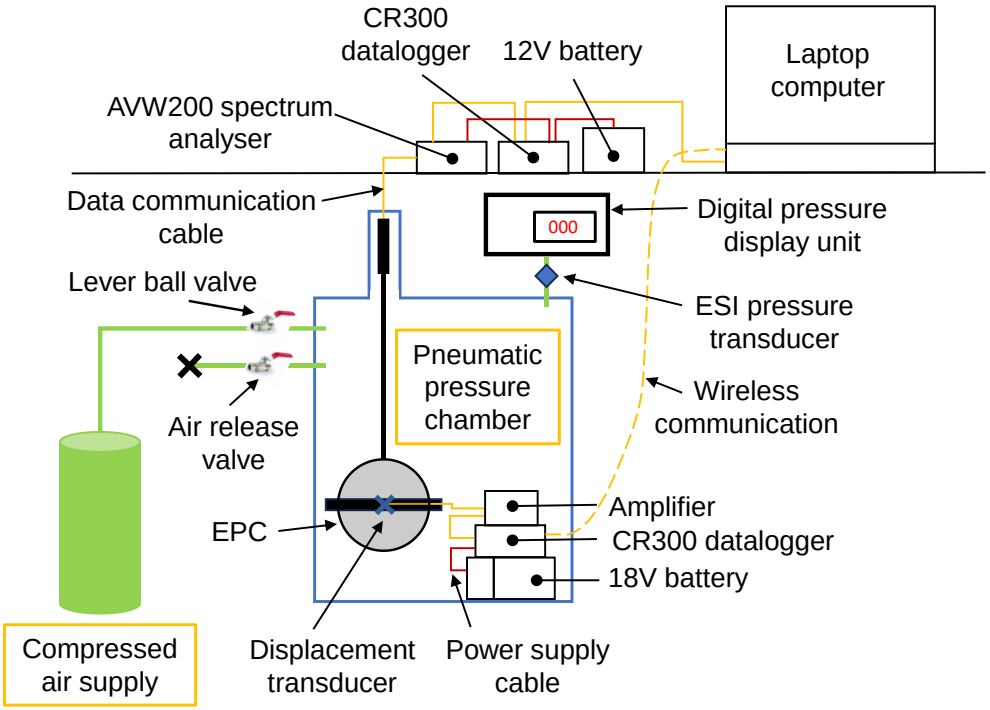


Figure 5.12: Sketch showing the configuration of the EPC compliance testing setup

© University of Pretoria

Cell deflections were measured using an Hottinger Baldwin Messtechnik (HBM) inductive miniature displacement transducer. The displacement transducer (Model WI/2mm-T) has a range of 2 mm. For this test, the displacement transducer was connected to an HBM Clip Electronic amplifier. The amplifier (Model AE501) was used to increase the response from the displacement transducer so that the response was within the measuring range of the datalogger.

A Campbell Scientific CR300 datalogger was used to record the response from the displacement transducer. The datalogger and amplifier were powered by an 18 V composite battery. The datalogger was connected to the same laptop computer noted earlier using a wireless connection. During the test, the response from the displacement transducer (in mV/V) was recorded once a second.

To verify the performance of the displacement transducer, a verification process was conducted. Figure 5.13 shows a photograph taken during this verification process.

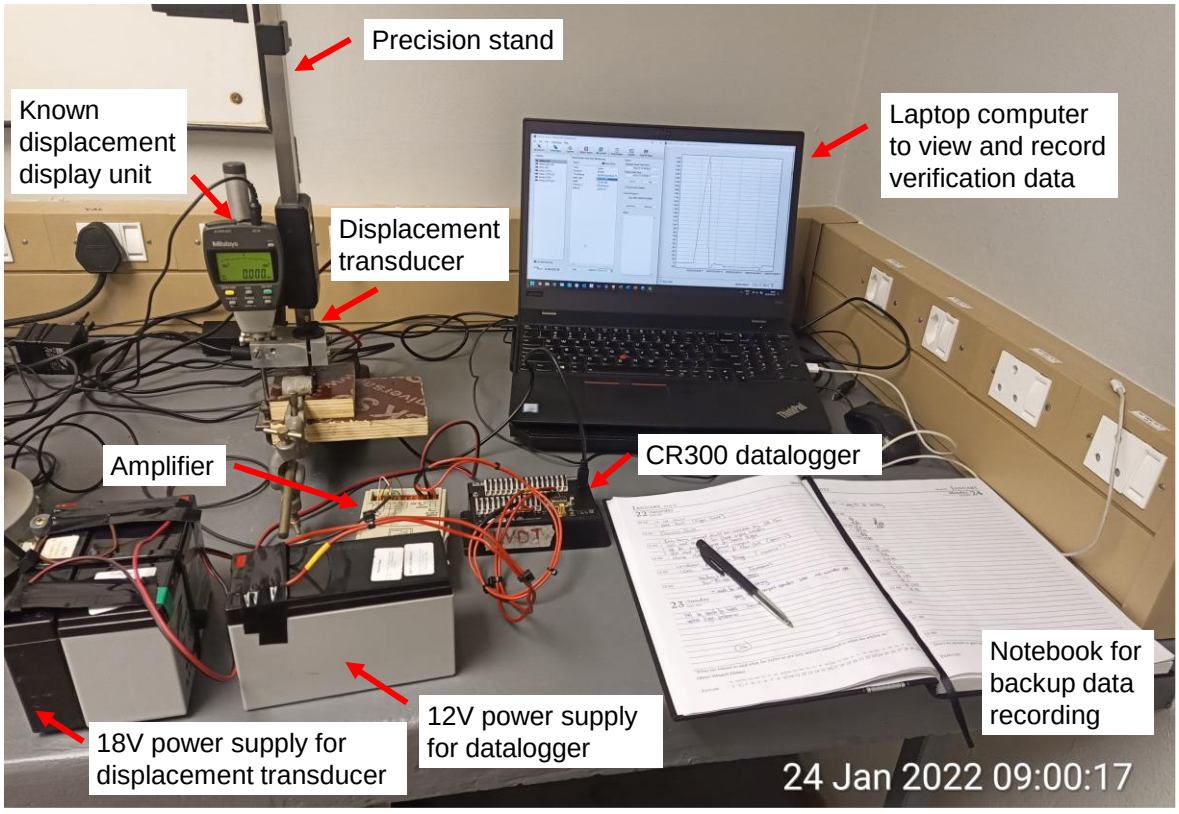


Figure 5.13: Displacement transducer verification using a precision stand

Figure 5.14 shows the results from this verification testing. A good fit was noted between the known applied displacement and the interpreted displacement using the linear calibration factor as

© University of Pretoria

recommended the manufacturer. The error was determined as the difference between the interpreted displacement and the known displacement. This error value varied from 0.001 mm to -0.008 mm as the known displacement was increased from 0 mm to 0.25 mm.

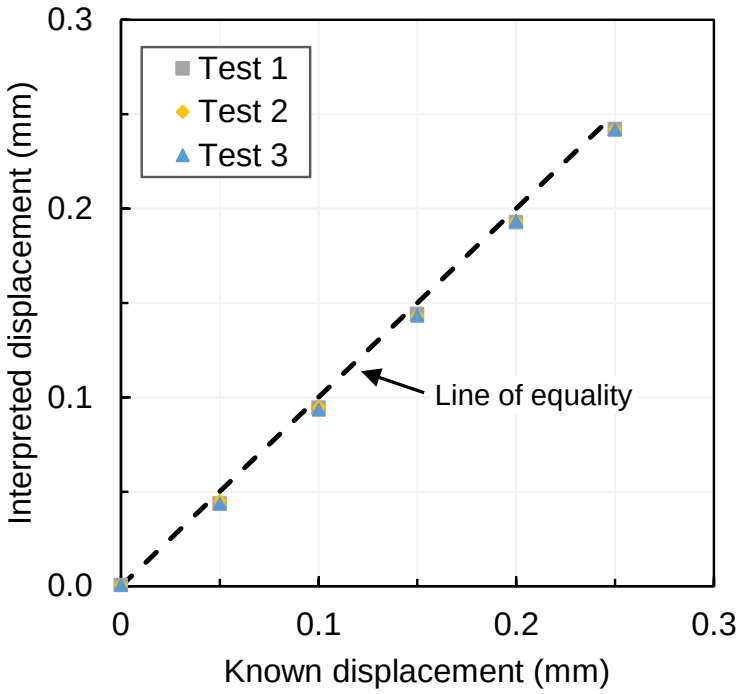


Figure 5.14: Results from the displacement verification testing

As part of the EPC compliance testing, one of the objectives was to investigate the deflection of the sensing face of the EPC at various locations due to an applied loading. Figure 5.15 shows a sketch indicating the three displacement transducer locations: Left (L), Middle (M) and Right (R). The majority of the testing was conducted at the middle (M) position. The tests that were conducted at the (L) and (R) positions are indicated as such.

© University of Pretoria

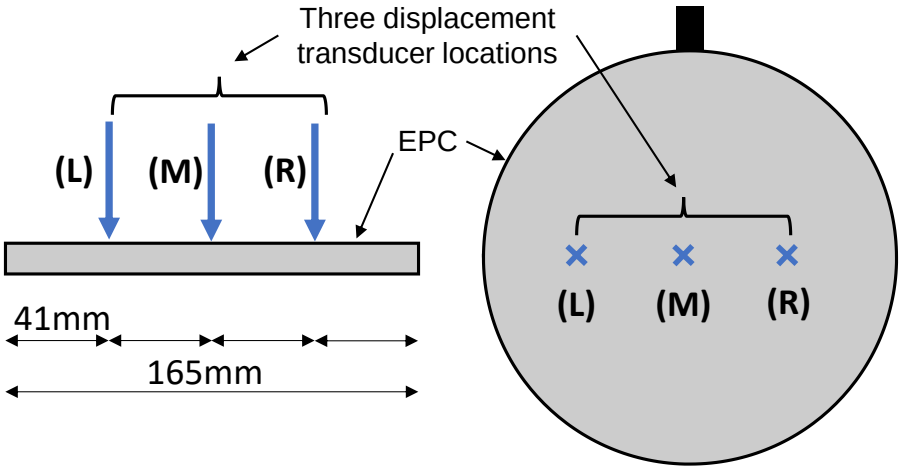


Figure 5.15: Sketch showing the three displacement transducer locations for the EPC compliance testing

An ESI Technology GENSPEC GS4200 pressure transducer , with a capacity of 1 MPa (ESI Technology, 2021) was used to verify the air pressure in the pressure vessel. The pressure transducer was configured to an amplifier and display unit such that the measured pressure was displayed with a resolution of 1 kPa. The accuracy of the pressure transducer was verified using the same calibrated Bourdon gauge as was used for the tensiometer calibration. The gauge has a capacity of 1.0 MPa and a resolution of 20 kPa.

As part of the verification testing of the pressure transducer, the system was filled with de-aired water and the air-water interfaces were used to impose a known applied hydraulic pressure to the pressure transducer. Each stress increment was typically held for at least 20 s. At the end of the stress increment, the pressure recorded on the display unit and the pressure noted on the Bourdon gauge were noted.

Figure 5.16(a) shows the response noted from the pressure transducer during the verification exercise. Figure 5.16(b) shows the difference between the measured transducer response and the known applied pressure, defined as the error. It can be seen that the error varies between 0 and 7 kPa, with the largest errors occurring at low stresses (<50 kPa). However, there is some uncertainty regarding the performance of this transducer to pneumatic loading. Therefore, the responses have only been used as an indication of the applied pressure.

© University of Pretoria

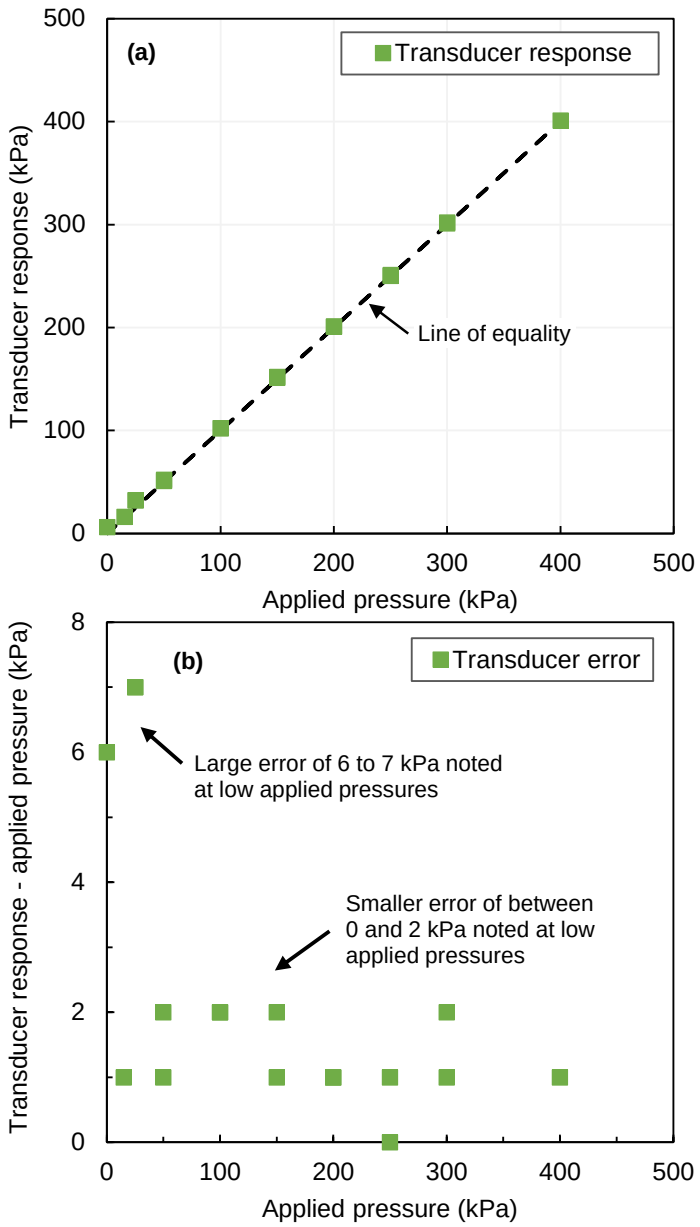


Figure 5.16: Results from the transducer verification process showing: (a) the transducer response, and (b) the measurement error

As a baseline test the displacement transducer was attached to an aluminium plate which, for practical purposes, would have undergone zero deflection due to the applied pneumatic load of 200 kPa. The purpose of this test to verify that the displacement transducer was not influenced by any other factors present during the compliance testing (such as temperature, pressure, etc). A maximum deflection of 0.001 mm was noted for this test, which is considered negligible.

Since it was known that the EPCs would be installed in tailings which would desiccate, there was a possibility that the tailings could impose some tensile forces on the EPCs during this process. Therefore, several tests were conducted where negative air pressures were imposed on the EPCs

© University of Pretoria

to investigate their performance under these conditions.

A summary of the key results from the EPC compliance testing is provided in Appendix B.

5.4.2 Results

Figure 5.17 shows the results from the verification tests conducted on all the EPCs. The applied pressure is plotted on the horizontal axis and the interpreted pressure is plotted on the vertical axis. The line of equality, as well as lines showing values 7.5% greater than, and 7.5% less than the line of equality are shown for reference. It can be seen the majority of the results fall within ±7.5% of the known applied pressure. This value is far greater than the quoted accuracy of the sensor of 0.25% of FSO and can be attributed to the fact that the system used for the verification tests was not sufficiently accurate to be used for independent calibration. Rather, the purpose of these tests was to investigate the compliance of the various EPCs under the same applied load. It is for this reason that the tests are referred to as verification tests and not calibration tests.

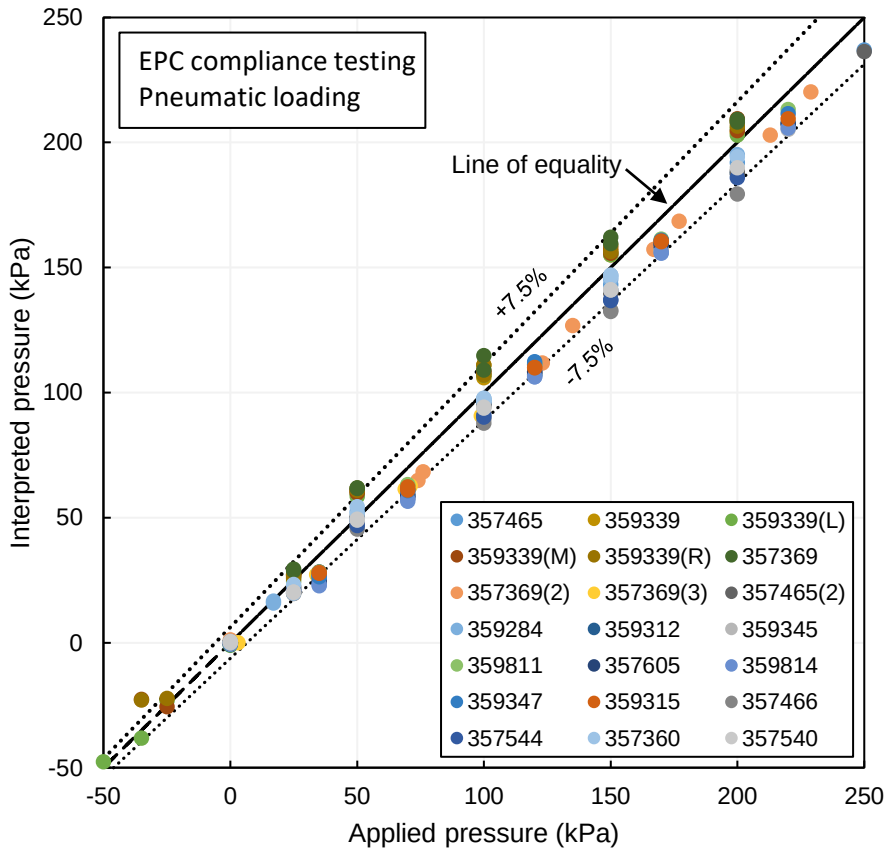


Figure 5.17: Results from the compliance testing of the EPCs

Figure 5.18 shows the results from one of the compliance tests on the EPCs where the deflection

© University of Pretoria

along the face of the EPC was investigated. In the figure, the deflection measured by the displacement transducer is shown for each applied stress increment. It can be seen that the response of the EPC is highly non-linear. In this test, suction was applied to the pressure chamber using a vacuum pump. Two points are evident from the graph. The first point is that the most deflection occurs at the centre, compared to the left and right positions. This is expected due to the design of the EPC. Similar deflection values were noted for the left and right displacement transducer locations.

The second point is that the magnitude of the deflection of the EPC is larger for suction (negative) applied pressures when compared to the deflection noted for positive applied pressures. For example, for the displacement transducer located in the middle at an applied air pressure of 50 kPa, deflection values of 0.03 mm and 0.02 mm were noted on the loading and unloading paths, respectively. However, at an applied air pressure of -50 kPa, significantly larger deflection values of -0.05 mm and -0.09 mm was noted. The negative value implied the thickness of the EPC increased (i.e. the face of the EPC expanded).

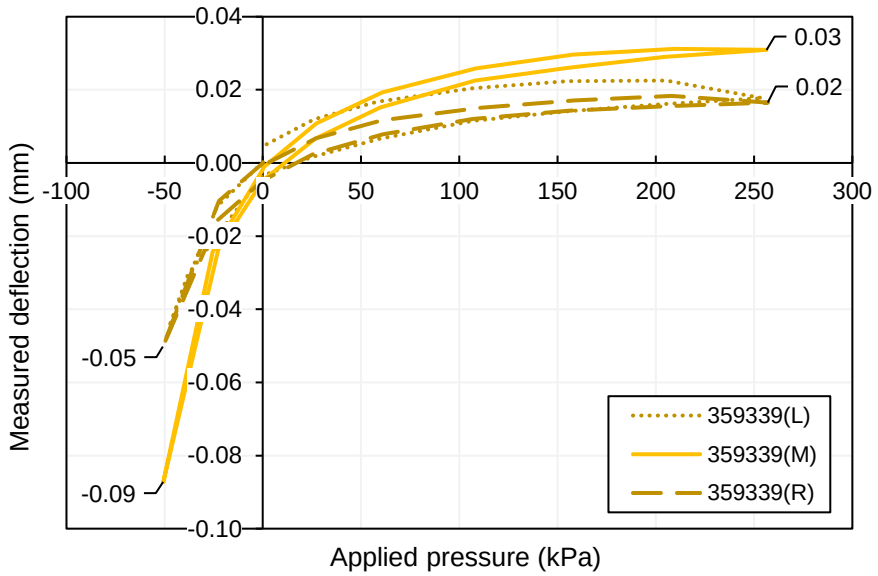


Figure 5.18: Example of variation in deflection along the face of the EPC

Figure 5.19 shows the results from the compliance tests conducted on the EPCs that were installed on the gold tailings site. Unfortunately, it was not possible to test all the EPCs before installation on site. Instead, duplicate tests were performed to investigate the repeatability of the observed deflection. In general, excellent repeatability was found for the three EPCs tested. Peak deflections of between 0.01 mm and 0.13 mm, under an applied pneumatic load of approximately 250 kPa, were noted for the EPCs.

© University of Pretoria

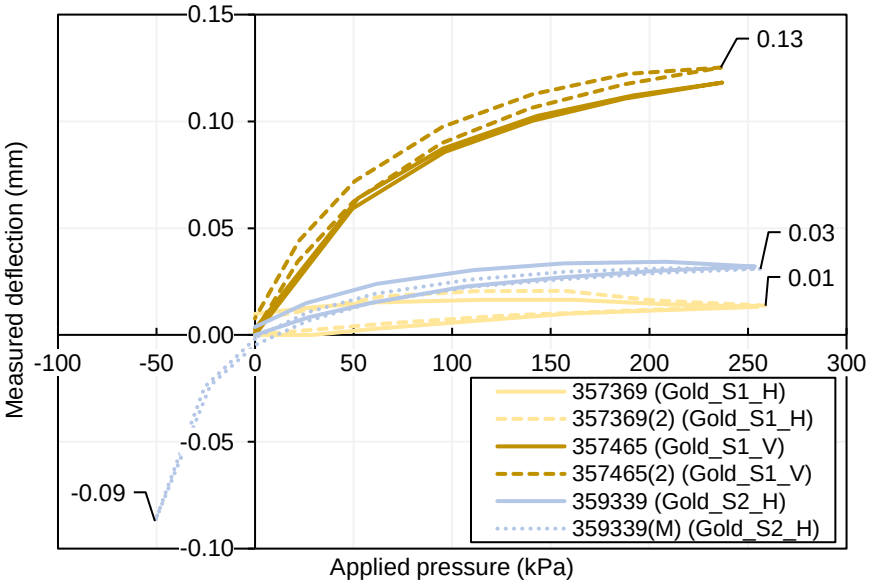


Figure 5.19: Variation in compliance of the EPCs installed at the gold site

Figure 5.20 shows the results from the compliance tests conducted on the EPCs that were installed on the iron ore site. It can be seen that for an applied loading of approximately 200 kPa, a much larger deflection of between 0.16 mm and 0.18 mm was noted for the EPCs installed at Station 3 (indicated in green), compared to the deflection noted for the EPCs installed at Stations 1 and 2 (indicated in yellow and blue). The EPCs installed at these stations exhibited deflections of between 0.01 mm and 0.04 mm.

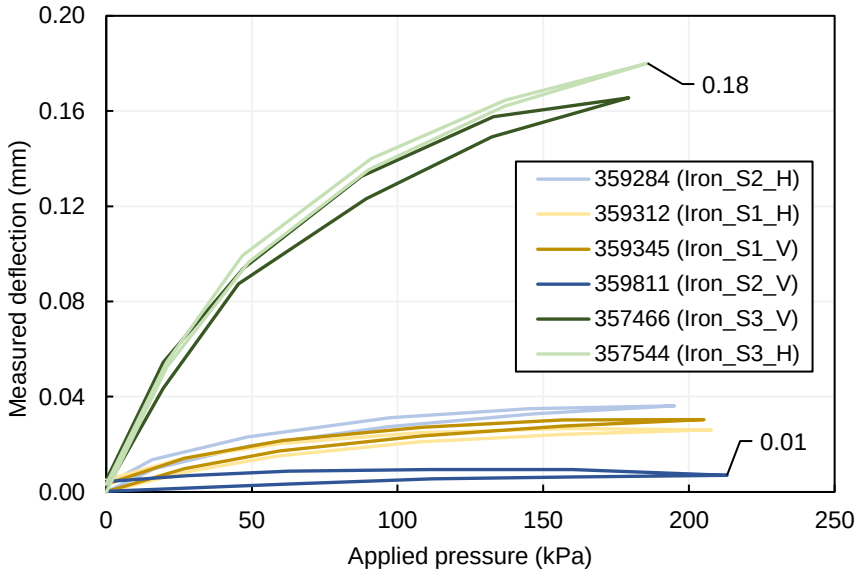


Figure 5.20: Variation in compliance for the EPCs installed at the iron ore site

© University of Pretoria

Figure 5.21 shows the results from the compliance tests conducted on the EPC that were installed on the platinum tailings site. It can be seen that the EPCs which were used to measure the horizontal stress showed significantly less deflection (0.012 mm to 0.02 mm), compared to the EPCs which were used to measure the vertical stress (0.0 1 mm to 0.0 3 mm). Interestingly, meaningful hysteresis was noted for the horizontal EPCs. However, these values are small (<0.005 mm) and therefore not too much emphasis is placed on these results. For reference, the deflection noted for the aluminium plate, which for practical purposes would have undergone zero deflection due to the applied pneumatic load of 200 kPa, was in the order of 0.001 mm.

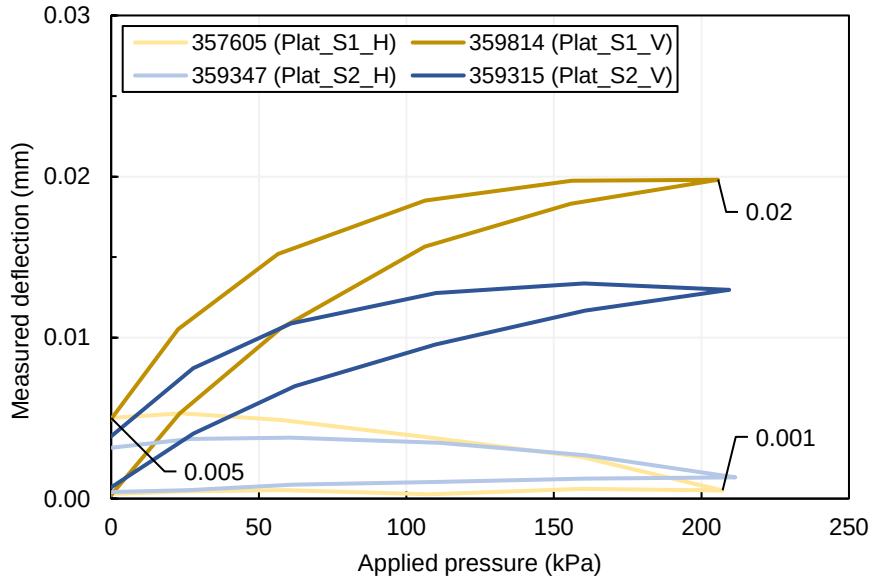


Figure 5.21: Variation in compliance of the EPCs installed at the platinum site

Figure 5.22 shows the results of the all the compliance tests conducted on the EPCs. Also indicated is the test on the aluminium plate (indicated with a black dotted line). The aluminium plate test was a baseline test to verify that the displacement transducer was not influenced by any other factors present during the compliance testing (such as temperature, pressure, etc). A maximum deflection of 0.001 mm was noted for this test, which is considered negligible.

Considering the responses from all the EPCs, it can be seen that there is a large variation in the measured deflection for the various EPCs for the same applied load. For example, a maximum deflection of 0.18 mm was noted for EPC 357 544, compared to a maximum deflection of 0.01 mm that was noted for EPC 359 811. The difference in measured deflection between the various EPCs is something that needs to be considered.

© University of Pretoria

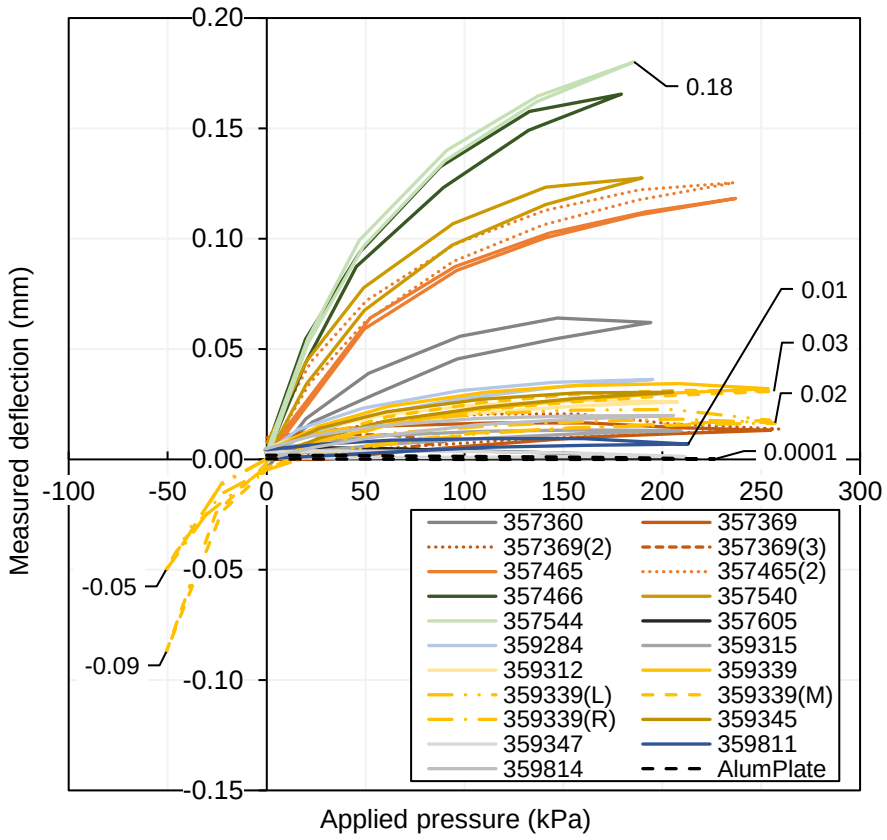


Figure 5.22: Results of all the compliance tests conducted on the EPCs

5.5 INTERPRETATION OF DATA FROM THE REMOTE MONITORING SYSTEM

The response recorded from the various sensors of the remote monitoring system were converted to engineering units using various relationships and calibrations. This section describes these processes.

5.5.1 Determination of total stresses

Total stresses measured by the EPCs were determined using the linear relationship shown in Equation (6) (Section 2.6.1). The zero readings were obtained prior to the start of the respective tests, and the calibration factors were taken from the datasheets provided by the manufacturer (see Appendix E). Additional details regarding the site zero readings are shown in Appendix C.

© University of Pretoria

5.5.2 Determination of pore pressures

Pore pressures were determined using the response measured by the HCTs and the linear relationship shown in Equation (11) (see Section 5.2). The zero readings were obtained prior to installation, and the calibration factors were taken based on the results from the calibration tests (see Appendix B). Additional details regarding the site zero readings are shown in Appendix C.

5.5.3 Determination of water content

Based on the laboratory calibration tests conducted in Section 5.3, it was found that the Mineral Soils equation tended to perform better than the Topp equation for the gold tailings. It was assumed that this improved relationship is also valid for the iron ore and platinum tailings. Therefore, all interpretation of the WPS was performed using the Mineral Soils relationship as shown in Equation (9) (Section 2.6.5).

5.5.4 Determination of geostatic stress ratio (K_0)

The geostatic stress ratio was determined using the horizontal and vertical effective stresses calculated as described in the following section of this chapter. In Section 4.3, the EPCs used in this study were shown to have been designed in accordance with the recommendations by Weiler & Kulhawy (1982). Additionally, as described in Chapter 6, the installation was conducted in accordance with the same guidelines and the vertical field measurements were indirectly validated using the known average bulk density of the overlying tailings and the tailings elevation as reported monthly by the operating contractor. Therefore, there is relatively little uncertainty regarding the accuracy of the vertical stress measurement. However there is some uncertainty regarding the accuracy of the horizontal stress measurement.

As the EPCs were installed in a slurry, there was initially uniform contact between the soil and EPCs due to the hydrostatic conditions. These conditions allow for the sensing membrane to deflect without affecting the measured values. However, as the material settled and dried out, this uniform contact may not have been maintained, and this could have led to incorrect readings from the EPC. Two mechanisms in particular are considered to have possibly influenced the stress response recorded by the EPC. Both mechanisms involve movement between the soil and the EPC which could result in poor contact and therefore poor transfer of the true in-situ stresses.

The first mechanism is due to inward deflection of the EPC as the load imposed by the soil is

© University of Pretoria

increased (i.e. as a result of additional deposition). As was shown in Section 5.4, these displacements vary across the face of the EPC with the most deflection occurring at the centre. For the stress levels experienced in the field during this study, the expected deflection at the centre of the EPC is in the order of 0.1 mm. The second mechanism is due to the outward deflection of the EPC as the load imposed by the soil is decreased (i.e. as a result of shrinkage during drying). As was also shown in Section 5.4, at the same stress level, cell deflections due to negative pressure (suction) are greater than the displacements due to positive pressure. For the suction magnitudes experienced in the field in this study, the expected deflection at the centre of the EPC is in the order of 0.03 mm.

It is difficult to quantify the true influence of these mechanisms. However, it is likely that these mechanisms would have resulted in an under-measurement of the true in-situ horizontal stress. Therefore, although the best efforts were made to measure and calculate accurate stress ratios, these calculated stress ratios should be considered a lower-bound value to the true in-situ stress ratios. Based on the work by other researchers using EPCs in the field (e.g. Rankka, 1990; Kudla et al., 2022), these under-measurements could be in the order of 10%-20%.

5.5.5 Determination of vertical and horizontal effective stresses

As discussed in Section 2.3.3, the determination of the effective stress in an unsaturated soil is not trivial. For this study, the Bishop effective stress (Bishop, 1959), as modified by (Bolzon et al., 1996) was used. This approach requires an estimate of the degree of saturation (S_r) of the soil.

For this study, three assumptions were considered regarding this estimation. For the first assumption, S_r was calculated using the VWC as determined from the moisture probe, as well as the average in-situ void ratio determined over the monitoring period (see Section 3.3.3). However, this was found to result in S_r values that did not match the known field conditions at certain times (for example immediately after installation and during initial deposition periods, when the soil was likely saturated).

For the second assumption, the VWC was again determined from the moisture probe but the void ratio was adjusted such that the S_r values matched the known values on site. This adjustment was in the order of $e = 0.2$. For the third assumption, the VWC was estimated using the suction measured by the HCTs and the approximation of the drying curve measured in the laboratory. The average in-situ void ratio (which was similar to the void ratio at which the SWRC test was conducted) was used. Although this assumption avoids any potential uncertainty regarding the

© University of Pretoria

estimation of the VWC by the moisture probe, the approach is limited by the fact that only a drying curve was measured in the laboratory. The conditions in the field include both wetting and drying phase and it is known that the drying and wetting response of a soil is distinctly different. A brief description of each assumption as well as key advantages and limitations of each assumption are provided in Table 5.2.

Table 5.2: Overview of the three Sr assumptions considered

	Description of assumption	**Advantages**	**Limitations**	**Average K_0* (±standard deviation)**
1	Use VWC determined from the moisture probe and average in-situ void ratio determined over the monitoring period.	Average measured in-situ void ratio used directly.	Calculated S_r does not match site observations at times.	0.451 (±0.048)
2^	Use VWC determined from the moisture probe, adjust void ratio to match S_r at known times.	Calculated S_r matches site observations.	Adjustment to average in-situ measured void ratio required.	0.482 (±0.044)
3	Use suction measured by the HCT to estimate VWC based on laboratory measured SWRC. Calculate S_r using average in-situ void ratio.	Avoids potential measurement errors with the moisture probe.	Only drying SWRCs were determined in the laboratory.	0.483 (±0.042)

*based on measurements at the gold site from 01/10/2022 to 06/30/2024.

^assumption 2 was selected for use for this study.

Figure 5.23 shows the interpreted S_r for the three assumptions when applied to the measurements at the gold tailings site. The results obtained using assumption 1 are shown in grey and the low calculated S_r values are evident. The results obtained using assumption 2 are shown in blue and the S_r values appear to plot in a more realistic range. The results obtained using assumption 3 are shown in orange and it can be seen how they track the laboratory measured SWRC.

© University of Pretoria

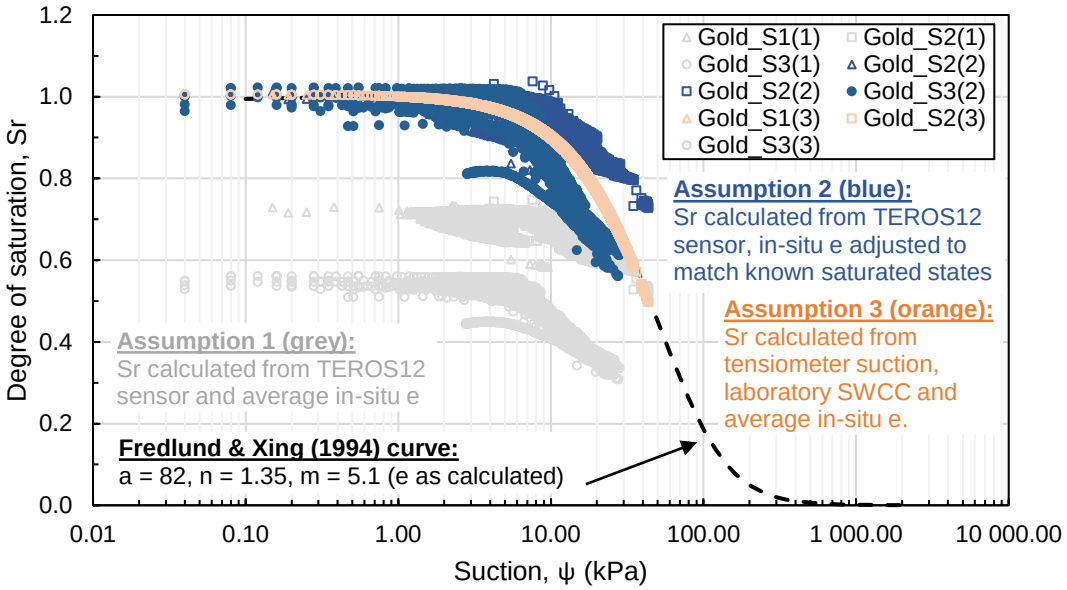


Figure 5.23: Visual representation of the three assumptions considered for the S_r calculation

To determine the influence of these assumptions on the calculated K_0 value, the horizontal and vertical effective stresses were determined using Equation (3) (Section 2.3.3), with the total stresses determined as described in Section 5.5.1. The resulting horizontal and effective stress pairs for the period from 01/10/2022 to 30/06/2024 for all three stations at the gold tailings site are plotted in Figure 5.24. For each assumption, the average K_0 value, as well as the standard deviation is shown. As can be seen, the resulting calculated K_0 values varied little between the three assumptions. This is likely due to the combination of relatively high total stresses and low suction values that were measured at the gold tailings site.

It was therefore decided that assumption 2 would be used for the interpretation for the field data for this study. This was deemed the approach that made the best use of the available field data, with as few assumptions as possible.

© University of Pretoria

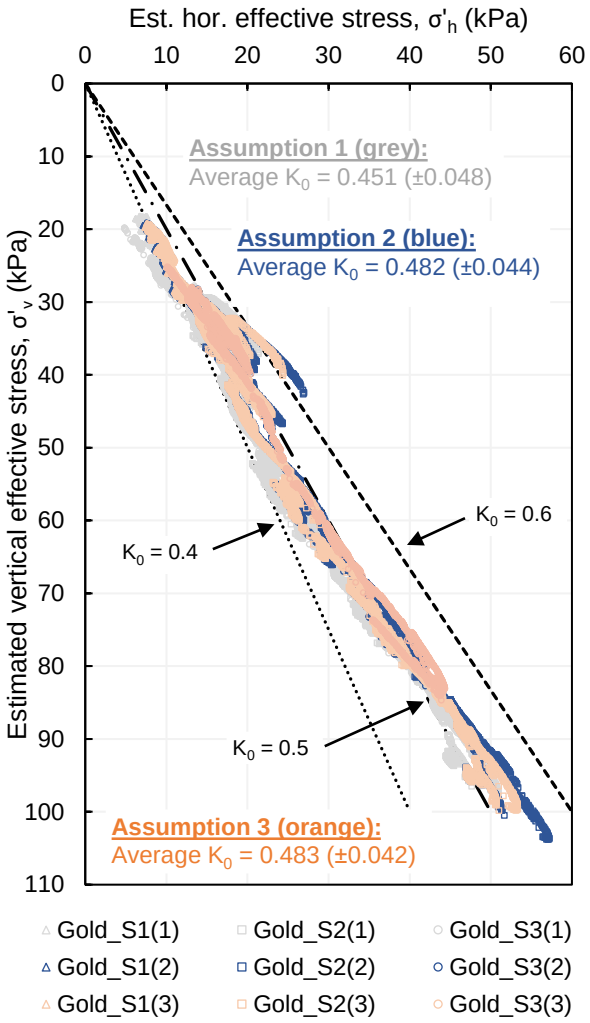


Figure 5.24: Summary of the three S_r assumptions on the calculated K_0 values for the gold tailings site

5.6 DRYING BOX TESTS

A key objective of this research was the development and verification of a remote monitoring system. To achieve this, laboratory experiments, referred to as Drying Box tests, were conducted to simulate the expected site conditions in a controlled laboratory environment. These tests are described in this section.

5.6.1 Test 1: Long-term performance

The intent of this test was to verify the performance of the complete remote monitoring system. Aspects of this test have also been summarised in a separate publication by the author (Narainsamy & Jacobsz, 2023b).

© University of Pretoria

5.6.1.1 General procedure

A Linear Low-Density Polyethylene (LLDPE) water tank with a wall thickness of 3 mm, an internal diameter of 1.1 m, and capacity of 1 kL was used for the Drying Box 1 experiment. A drainage system was installed at the base of the tank and comprised a 150 mm layer of 6 mm stone. A non-woven needle-punched geotextile, meeting the Class 1 (high survivability) requirements as specified by GRI-GT13a (GSI, 2017), was used a separation geotextile. A tap was used to control the flow of water out of this drainage system.

A large gold tailings sample (~1 m^3) was obtained from the gold tailings site in October 2021. The material was sourced from the daywall, near the existing and future monitoring locations, and is deemed to be representative of the material in the structural zone of the dam. A photograph of the material loaded onto the vehicle for transport is shown in Figure 5.26(a). The material was transported to the University, where it was labelled and stored in the geotechnical laboratory.

Before use, the gold tailings was oven-dried at 105°C for 24 hours. The use of dried tailings allowed for a repeatable preparation method, as well as the tracking of solids and water throughout the tests. After drying, the material was allowed to cool to room temperature and was sieved through a 2 mm sieve. This was to ensure that no clods of material were present to facilitate the mixing of the slurry. Ad-hoc samples were taken during this process and analysed in terms of PSD.

Prior to testing, a large container filled with potable water was used to verify the zero readings of the EPCs as recommended by the manufacturer (e.g. Geosense Ltd, 2016). The EPCs were left in the water overnight to allow for temperature equilibration. Zero readings were taken by raising each EPC individually until the active face was just below the surface of the water. Three readings were taken, and an average value was recorded. Due to inherent differences in the ambient pressure and temperature between Pretoria and Bury St Edmunds (where the manufacturer's zero readings were obtained), different values were obtained for the zero-reading frequency and temperature, compared to the values noted on the calibration datasheets. This difference was discussed with the manufacturer, and it was recommended that the local zero readings be used. In the same container the readings for the TEROS 12 moisture probe and TEROS 21 WPS in water were also verified. This process is shown in Figure 5.26(b).

Two duplicate setups were included for the test and each setup included the key components of the remote monitoring system. Figure 5.26(d) shows a layout of these two setups inside the Drying Box 1 experiment. The HCTs are not shown as they were only installed after the tailings had been deposited. Each setup included the following sensors:

© University of Pretoria

- two EPCs: one to measure vertical stress, and one to measure horizontal stress
- two Tuks HCTs
- one TEROS 12 moisture probe
- one TEROS 21 WPS

The stress imposed on the EPCs were interpreted using the linear calibration shown in Equation (6). The calibration coefficients were obtained from the manufacturer's datasheets and the zero readings were taken prior to commencement of the slurry placement. The pore pressures were determined using linear calibration as shown in Equation (11), and the calibration coefficients determined during the calibration exercise described in Section 5.2.1. Moisture contents were estimated using the raw data obtained from TEROS 12 moisture probe and the relationship proposed by Topp et al. (1980) and Campbell Scientific Inc. (2019), as shown in Equation (7) and Equation (8), respectively. Suction values were determined directly from the WPS.

Figure 5.25 shows key features of the Drying Box 1 experiment. In particular, the cumulative mass of dry tailings and water added to the Drying Box with time is shown. The cumulative mass of the water collected from the basal drainage layer is also shown, as well as the height of the tailings. A total of six Deposition Events (DEs) and four Rainfall Events (REs) were simulated over the 11-month test period. The four RE events comprised events of 1 mm, 5 mm, 20 mm and 50 mm. Each DE was done as quickly as possible and were usually completed within two hours. Each RE was specifically conducted over a one-hour period with equal volumes being added to the Drying Box every five minutes. This was done by means of spray bottles to ensure an even distribution of water on the surface of the tailings.

© University of Pretoria

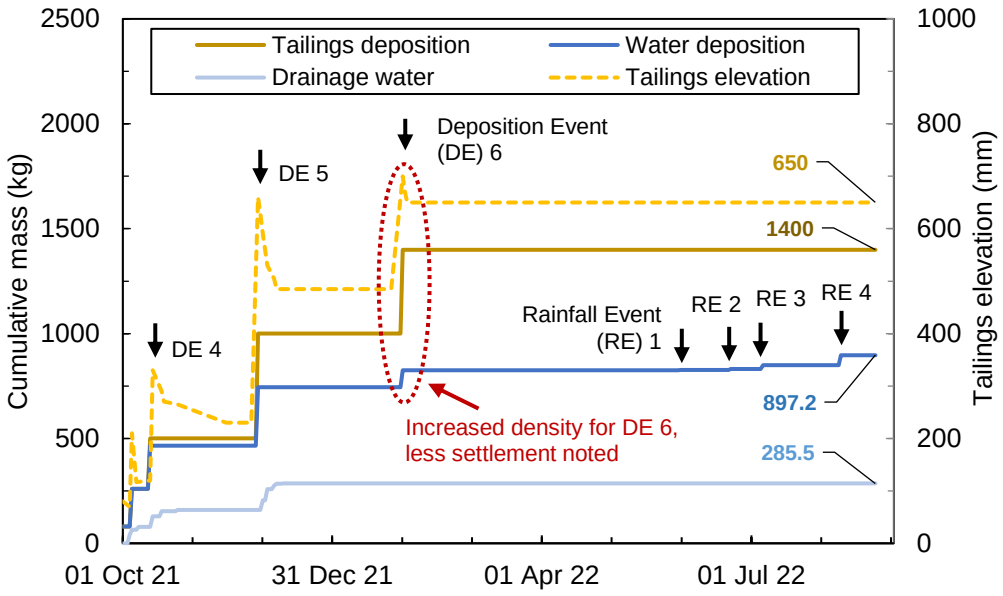


Figure 5.25: Key features of the Drying Box 1 experiment

The final height of the tailings at the end of the test was 650 mm. A total of 1 400 kg of dry gold tailings was added to the drying box, together with 897.2 kg of water. Of this, only 285.5 kg was collected from the drainage system. The remainder was either lost to evaporation or remained within the tailings pore spaces.

For each DE, the dry tailings mass and water mass was determined using a calibrated mass balance with a capacity of 70 kg and a resolution of 0.01 kg. For REs 3 and 4, representing the 20 mm and 50 mm events, the same mass balance was used. However, for REs 1 and 2 (representing the 1 mm and 5 mm events) a calibrated mass balance with a capacity of 6 kg and a resolution of 0.01g was used. The mass of water to be added for each RE was determined using the assumed density of water at room temperature (1 g/cm^3) and the product of the surface area of the tailings and the depth of the rainfall event being simulated.

The mass of water leaving the system was record daily by determining the mass of water collected in the drainage container as shown in Figure 5.26(f). The height of the tailings was determined every four hours during periods of rapid height changes (i.e. immediately after deposition) using the survey marker as shown in Figure 5.26(e). This recording frequency was reduced to once every 12 hours while consolidation was occurring, and then to once every 24 hours once the surface water had evaporated. Figure 5.26(e) shows the first filling of the Drying Box, while Figure 5.26(f) shows the Drying Box 4 days after the first filling. In this figure, the container used to collect the drainage water can be seen.

© University of Pretoria

Initially, the dry tailings was mixed in a mass ratio of 1:1 with tap water to a target bulk density of 1.45 t/m^3. This is in line with the density of the slurry as is deposited on site and was done for DEs 1, 2 and 3. However, it was noted that significant settlement occurred once the water had either evaporated of drained through the tailings and consolidation under self-weight had occurred. This became a concern as the capacity of the Drying Box was approached. To address this, the mixing ratio was change to 1 (tailings):0.8 (water) for DE 4, 1:0.5 for DE 5 and finally to 1:0.2 for DE 6.

Each lift was allowed to dry until a suction value of 50 kPa was recorded by the tensiometers.

© University of Pretoria

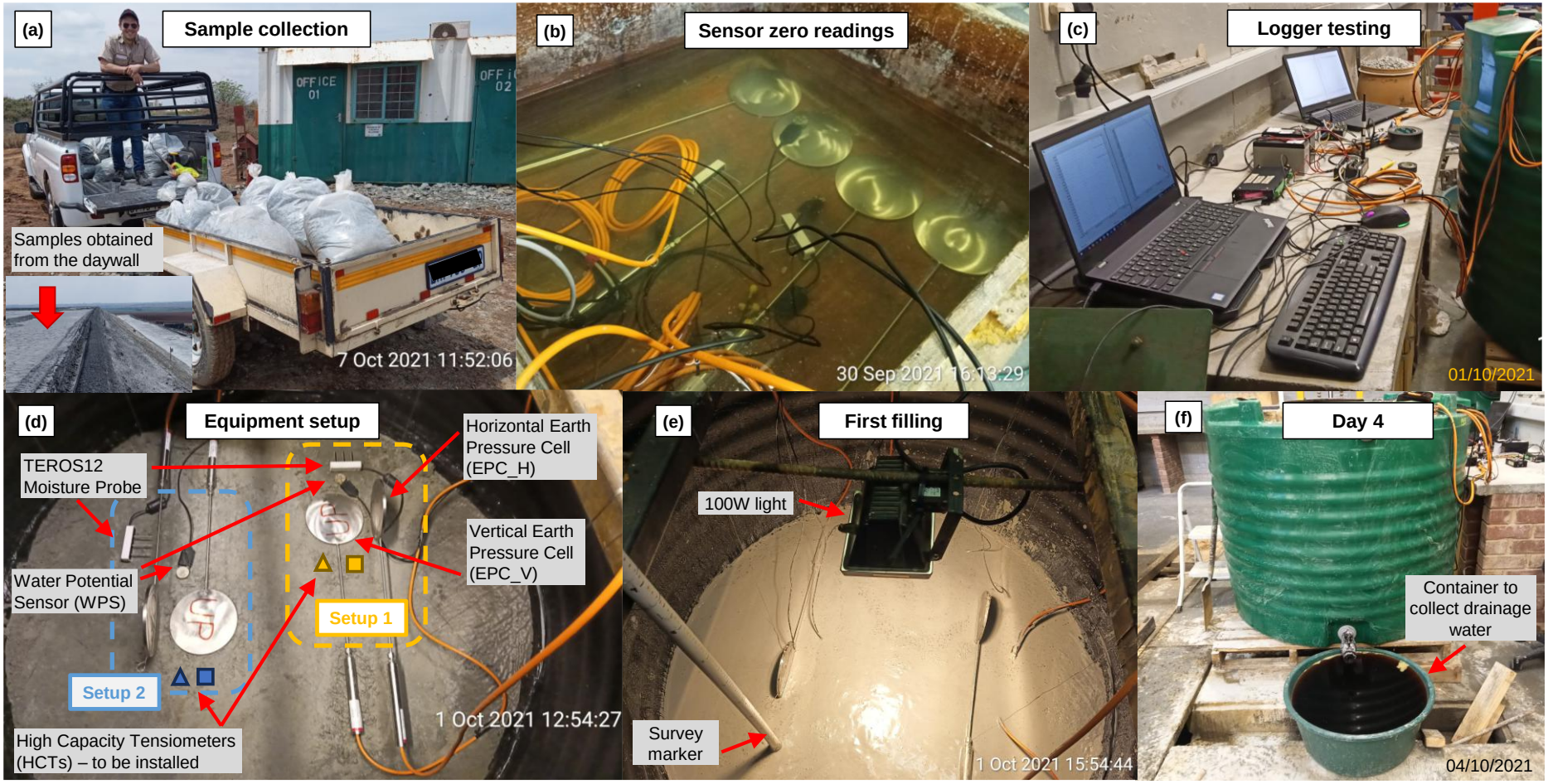


Figure 5.26: Selected photographs showing key stages of the Drying Box 1 experiment

© University of Pretoria

5.6.1.2 Results

The results from the test are presents in several sections. The pore pressures are assessed first, followed by the complete results from all the sensors. The section ends with a review of the temperature effects on the EPCs after the last DE.

Pore pressures

Figure 5.27(a) shows the pore pressure measurements for the entire test period. Results from the two tensiometers, as well as the TEROS 21 WPS are shown for each setup. The increase in pore pressure corresponds to the deposition events, while the decrease in pore pressure corresponds to the drying periods between deposition events. The representative pore pressure for Setup 2 was taken as the reading from tensiometer 1 for the first 15 weeks. After this tensiometer cavitated, the suction readings from the TEROS 21 WPS sensor were taken as the representative pore pressure for Setup 2. For Setup 1, the response from tensiometer 2 was used for the entire test duration.

Also shown in Figure 5.27(a) is the time lag between the Tuks tensiometer and the TEROS 21 WPS. As was done for the moisture probe verification tests, the time lag was defined as the difference in time required for the WPS to report the same suction as recorded by the Tuks tensiometer. In this case, it can be seen that this lag time varied. In January 2022, at suction values of approximately 25 kPa, this lag time was noted as 13 days. This increased to 16 days in March 2022 at suctions of 28 kPa, and then to 27 days in May 2022, at suction values of 40 kPa.

Figure 5.27(b) shows the pore pressure measurements over the first seven months of the experiment. Between January and March 2022, three of the initial four tensiometers cavitated. After the cavitation of first two tensiometers, it was decided that an additional tensiometer would be added. This tensiometer (Add_T1) was installed in January 2022. Unfortunately, the power supply to the logger for this additional tensiometer proved to be unreliable and data were not recorded for extended periods of time. However, when the pore pressures were recorded, excellent correlation was observed between the additional tensiometer and the remaining functioning tensiometer.

© University of Pretoria

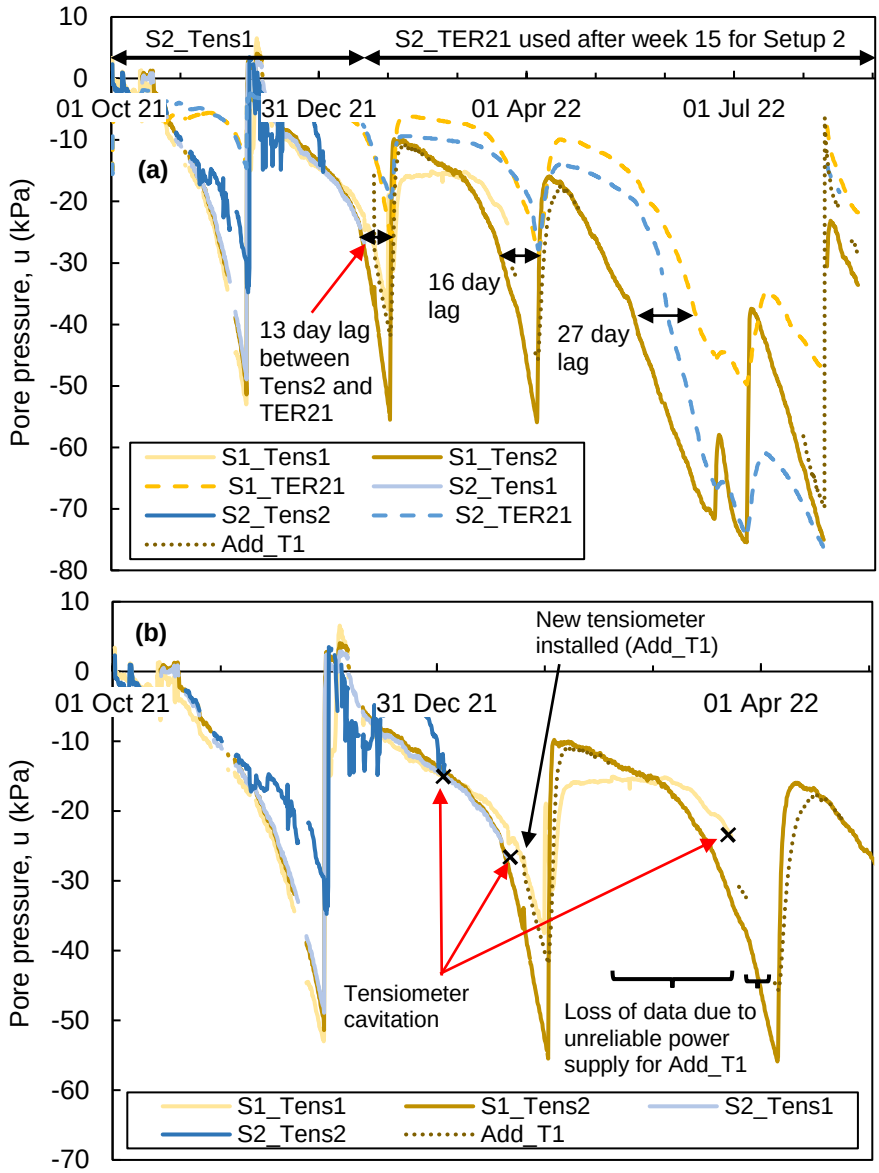


Figure 5.27: Drying Box 1 pore pressure data for: (a) the entire test, and (b) the first seven months

Figure 5.28 shows the response from the HCTs and the WPS for the entire duration of the Drying Box 1 experiment. Figure 5.28(a) shows the response from the three sensor types for the entire 11-month period, while Figure 5.28(b) and Figure 5.28(c) focus on the response during the first five months. The suctions (negative pore pressures) measured by the WPS are shown in blue, while the suctions measured by the epoxy-cased and steel-cased Tuks tensiometers are shown in orange and yellow, respectively. The DEs and REs are also shown for reference. Figure 5.29(a) shows a photograph of the three suction sensors that were used as part of the test.

Figure 5.28(b) shows the drying periods for the first four DEs. Excellent correlation can be seen between the two tensiometers from the start of the test to the middle of January 2022. However, there is a divergence between the two tensiometers after this point. Upon recovery of the

© University of Pretoria

tensiometers at the end of the test, it was noted that the ceramic of the epoxy-cased tensiometer was cracked (as shown in Figure 5.29(b)). No cracks were noted in the ceramic of the steel-cased tensiometer (as shown in Figure 5.29(c)). It is believed that this cracking of the ceramic led to the cavitation of the epoxy-cased tensiometers. The steel-cased tensiometers performed well for the entire 11-month testing period.

Also shown in Figure 5.28(b) is the performance of the WPS at low suction values. In particular, the periods directly after DEs 1 to 4 are indicated with dotted lines. During these periods, the suction values were close to zero (in fact during deposition, small positive pore pressures were measured). Both the epoxy-cased and steel-cased tensiometers were able to capture these low suction values. However, the WPS was not. This was expected as the TEROS 21 WPS is only rated to be able to reliably measure suctions in the range of 9 kPa to 100 MPa.

Figure 5.28(c) shows the same period as Figure 5.28(b) but this time highlights the slower response of the WPS due to a change in suction. Two particular examples are highlighted. The first period occurred during mid-November 2021 where both tensiometers recorded suction values of 28 kPa but the WPC only showed a suction of 7 kPa. This slow response is also seen in mid-January 2022 where both tensiometers recorded suction values of 20 kPa, compared to the suction value of 6 kPa recorded by the WPS.

© University of Pretoria

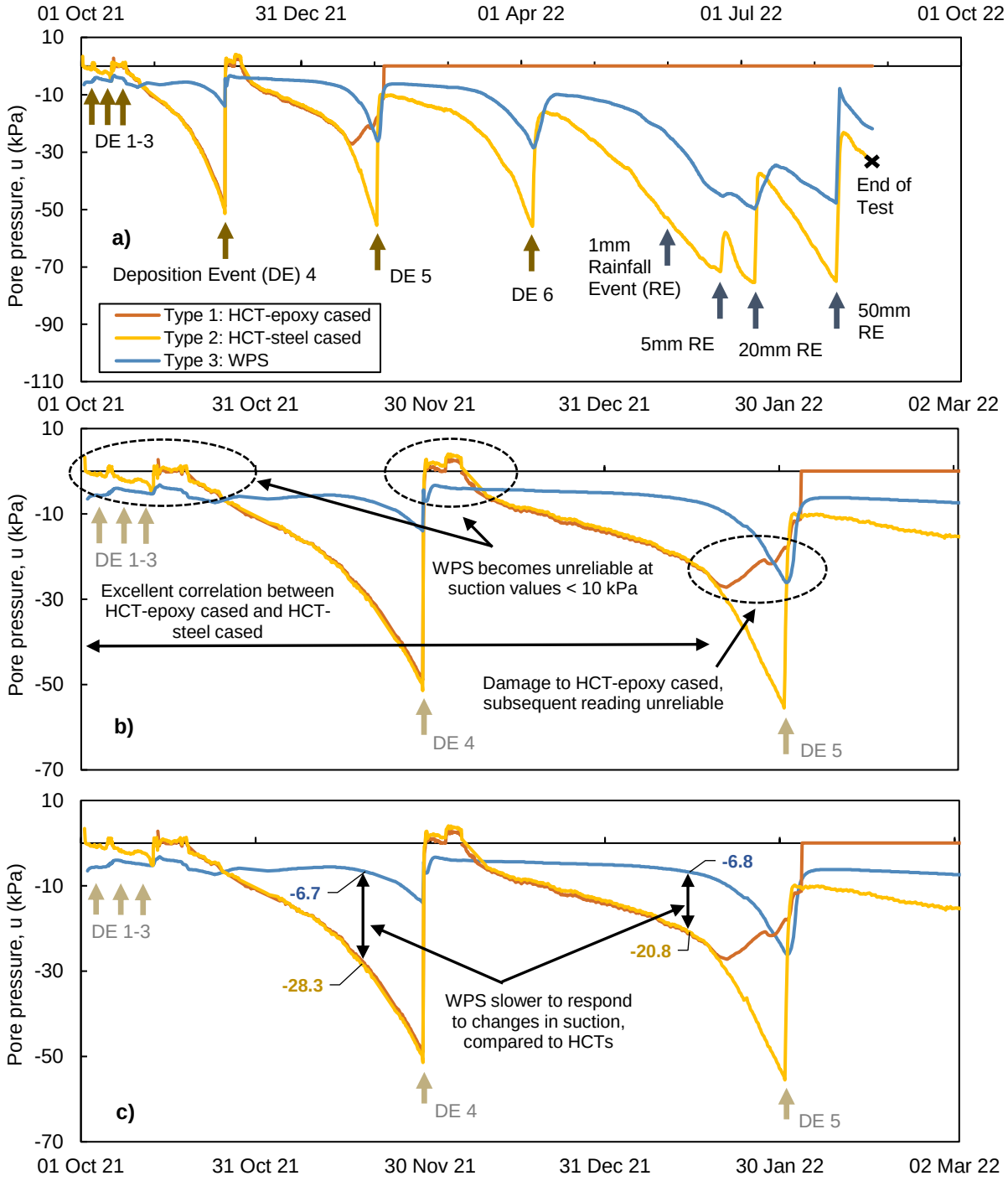


Figure 5.28: Results from Drying Box 1 showing: (a) pore pressures over the entire test duration, (b) correlation between the HCTs, and (c) the slow response of the WPS

© University of Pretoria

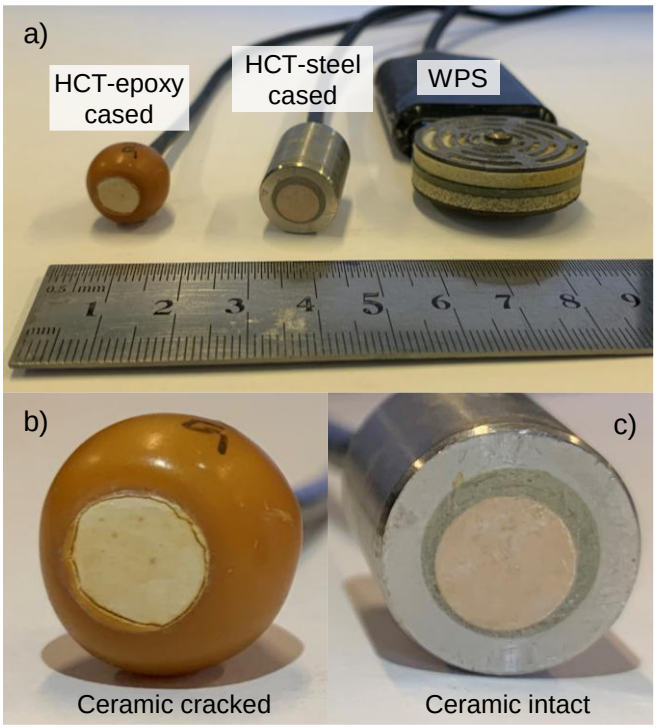


Figure 5.29: Photographs of the sensors used for Drying Box 1 showing: (a) all three sensors, (b) the cracked epoxy-cased HCT, and (c) the intact steel-cased HCT

Complete Results

Figure 5.30 shows the results from the two setups for the entire duration of the Drying Box 1 experiment. Figure 5.30(a) shows the response of the EPCs while the response from the tensiometers is shown in Figure 5.30(b). It can be seen that there was a noticeable drop in the interpreted total stress for a period in January 2022. This drop occurred when the external light was switched off due to a blown bulb. Interestingly, a corresponding increase in interpreted stress can be seen when the light was switched back on.

Due to the low total stresses imposed on the EPCs it is difficult to draw any meaningful conclusions from these results. At these low stresses the EPCs are greatly influenced by temperature variations which could obscure any trends in the data. Additionally, the full scale of the EPC should be considered. With a capacity of 345 kPa, the measured stresses of 2 to 8 kPa are small. These values are well within the reported accuracy of the EPC of ±0.1% (±0.35 kPa) but are still at only between 1 to 3% of the capacity of the EPCs, so some variation can be expected.

It can also be seen that the suctions determined from the tensiometers for Setup 1 and the suctions determined from the TEROS 21 WPS for Setup 2 appear to correlate to some extent at higher suction values. On these figures, the DEs and REs are also highlighted for reference. Although the

© University of Pretoria

influence of the DEs is clear on the response from the tensiometers and TEROS 21 WPS, the influence is less noticeable on the response from the EPCs.

Figure 5.30(c) shows the interpreted VWC using the Mineral Soils equation. It can be seen that there is good correlation between the VWC values estimated for the two setups. After DE 4, it is also clear that there is a progressively smaller influence of the DEs on the response noted from the TEROS 21 moisture probes. This is believed to be due to both the gradually increasing distance of the sensor from the surface of the tailings where the next layer was added, as well as the decreasing volume of water added for each DE. For the REs, it can also be seen that neither the 1 mm, 5 mm, nor 20 mm REs resulted in any meaningful response from the TEROS 12 moisture probes. A response was however noted for the 50 mm RE.

Figure 5.30(d) shows a plot of the stress ratios calculated for the two setups. After some initial variability during deposition, both setups indicated stress ratios approaching 1.0 at the end of drying. It should be stated that the geometry of the Drying Box was not designed in accordance with the general recommendations for calibration chamber to reduce edge-effects (e.g. Hadala, 1967). Therefore, there are likely some strain boundary conditions that influence the measurement of the lateral stress. In addition, due to the combination of low total stresses and high suction values it is believed that these stress ratios are not representative of the true stress ratios that would exist in the field. As a result of the temperature effects noted on the EPCs under constant load, the interpreted stress ratios after DE6 are not plotted.

Although not explicitly discussed here, the Drying Box 1 experiment also provided an opportunity to optimise the logging code and the specification of the battery used to power the system. It was found that the batteries used initially (12 V, 4 AH lead acid batteries) were inadequate to meet the power consumption requirements of the remote monitoring system. New, higher capacity batteries (12 V, 26 AH gel batteries) were ordered, and the logging code was optimised to power down the internal cellular modem, which was identified as a module with high power consumption, during periods of inactivity. The combined effect of the optimised logging code and the new battery reduced the battery power consumption of the remote monitoring system from 172 mV/day to 11 mV/day.

With this configuration, it was shown that the remote monitoring system could perform independently using the same power supply for over six months. Additional information can be found in Appendix B.

© University of Pretoria

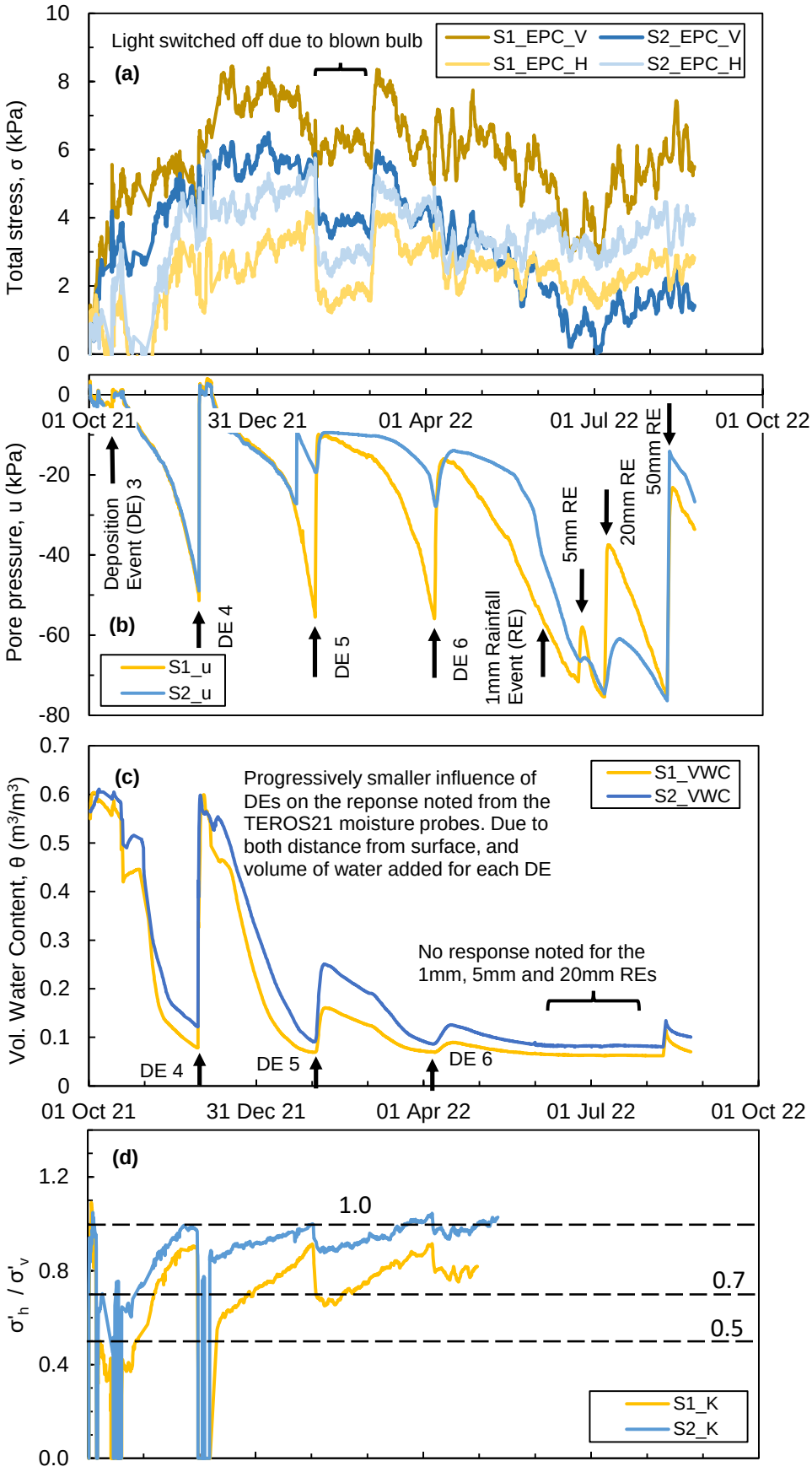


Figure 5.30: Results from Drying Box 1 showing: (a) total stresses, (b) pore pressures, (c) VWC, and (d) stress ratios

© University of Pretoria

Temperature effects

Figure 5.31 shows the results from the Drying Box 1 experiment, specifically for the five-month period after the last DE. The intent of this figure is to highlight the temperature influences on the response recorded by the EPCs under constant load. Figure 5.31(a) shows the temperature recorded by the four EPCs. In general, there is good correlation between the four EPCs, with a tight grouping of the EPCs per setup. It can be seen that over the five-month monitoring period, a change in temperature of approximately 7°C was noted for by the EPCs. This change in temperature is due to seasonal changes and is dampened due to the presence of approximately 0.65 m of tailings above the sensors. Temperature readings recorded by the logger outside the Drying Box indicated ambient temperature changes of 10°C, over the same period.

Figure 5.31(b) shows the response from the EPCs installed at Setup 1, while Figure 5.31(c) shows the response from the EPCs installed at Setup 2. It can be seen that there is a change in frequency for the four EPCs even though there is no change in stress being applied to the EPCs. This change in frequency varies for the four EPCs, with the values ranging from 2 Hz to 6 Hz. As the thermal factor only influences the interpreted stress when there is a change in temperature, these changes in frequency due to temperature cannot be corrected by adjusting the thermal calibration coefficient as shown in Equation (6). The unit change in frequency as a result of temperature changes for the four EPCs can be calculated as 0.6 Hz/°C, 0.9 Hz/°C, 0.6 Hz/°C, and 0.5 Hz/°C for the horizontal and vertical EPCs installed at Setup 1 and Setup 2, respectively.

Figure 5.31(d) shows the interpreted stress for the EPCs. It can be seen that there is a change in interpreted stress for all four EPCs, even though no further tailings was deposited. These changes in interpreted stress differ for the horizontal and vertical EPCs and vary between 1 kPa and 4 kPa. The unit change in interpreted stress as a result of temperature changes can be calculated as 0.3 kPa/°C, 0.6 kPa/°C, 0.1 kPa/°C and 0.6 kPa/°C for the horizontal and vertical EPCs for Setup 1 and Setup 2, respectively. Additional details for the test, specifically related to the temperature influences are discussed further in Section 6.5

© University of Pretoria

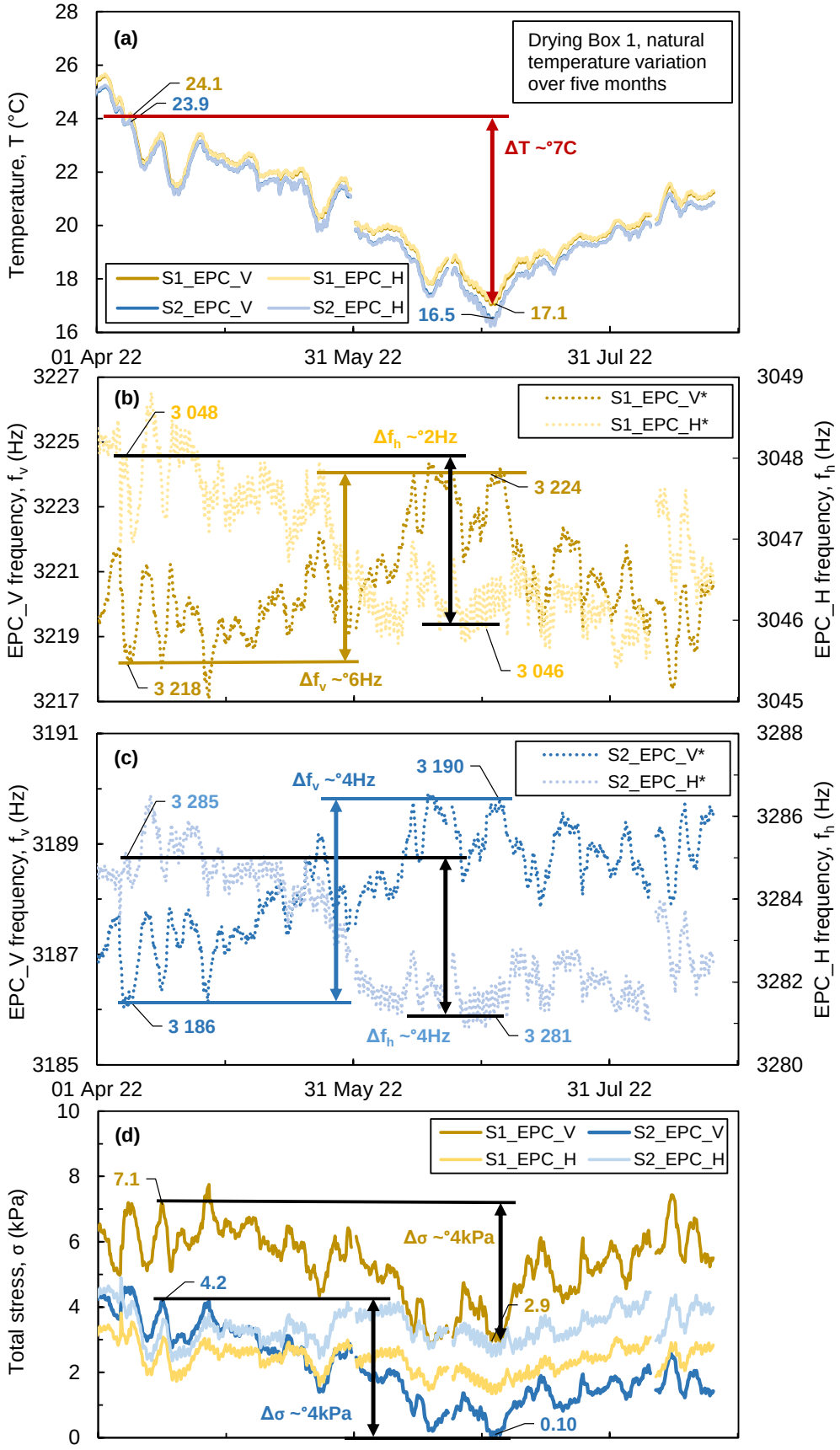


Figure 5.31: Temperature effects on the EPCs for the Drying Box 1 experiment showing: (a) temperatures, (b) Setup 1 EPC frequencies, (c) Setup 2 EPC frequencies, and (d) interpreted total stresses

© University of Pretoria

5.6.2 Test 2: Performance during first filling

Upon review of the data from site, it was found that the field tests showed initial negative interpreted stress for the horizontal EPCs. These values were small (in the order of 2-3 kPa). However, there was uncertainty regarding whether these were true tensile forces being imposed on the EPCs by the tailings, or whether these were artifacts of the EPCs interpretation, either due to an incorrect zero reading or due to thermal effects? The intent of the Drying Box 2 test was therefore to investigate the behaviour during these early periods of monitoring, specifically during the placement of the slurry and the subsequent drying and consolidation.

A key limitation that was overcome for this test was the interval between measurements. For the field tests, measurements were only taken once an hour. For this test, the interval between measurements was reduced to five minutes.

5.6.2.1 General procedure

Figure 5.32 shows a layout of the sensors for the Drying Box 2 experiment. This Drying Box is different to the Drying Box used for Test 1. The Drying Box was constructed using 20 mm thick laminated pine and has dimensions of 750 mm in length, 750 mm in width, and 450 mm in height. The box was made watertight by sealing the edges with silicone. A 50 mm thick gravel layer was placed at the base of the box and a separation geotextile of the same class as used for Drying Box 1 was placed above the gravel layer. A valve was connected to the side of the box to facilitate drainage. As was the case for Drying Box 1, two identical setups were used.

This test comprised two main DEs. The first DE occurred on 21 February 2023 when 130kg of dry tailings was mixed with 130 kg of water and the Drying Box was filled to a height of approximately 0.32 m. The second DE occurred the next day, once the majority of the free-standing surface water had drained through the tailings. For this DE, only 15 kg of tailings and water were added to reinstate the 0.32 m height of the tailings.

During the initial drying period, while there was still free-standing water on the surface of the tailings, only one 400 W light was switched on. This was done to prevent a recurrence of the damage that occurred due to moisture ingress for the first Drying Box experiment. The second 400 W light was switched on during the morning of 24 February 2023 when it was noted that all the free-standing surface water had evaporated.

© University of Pretoria

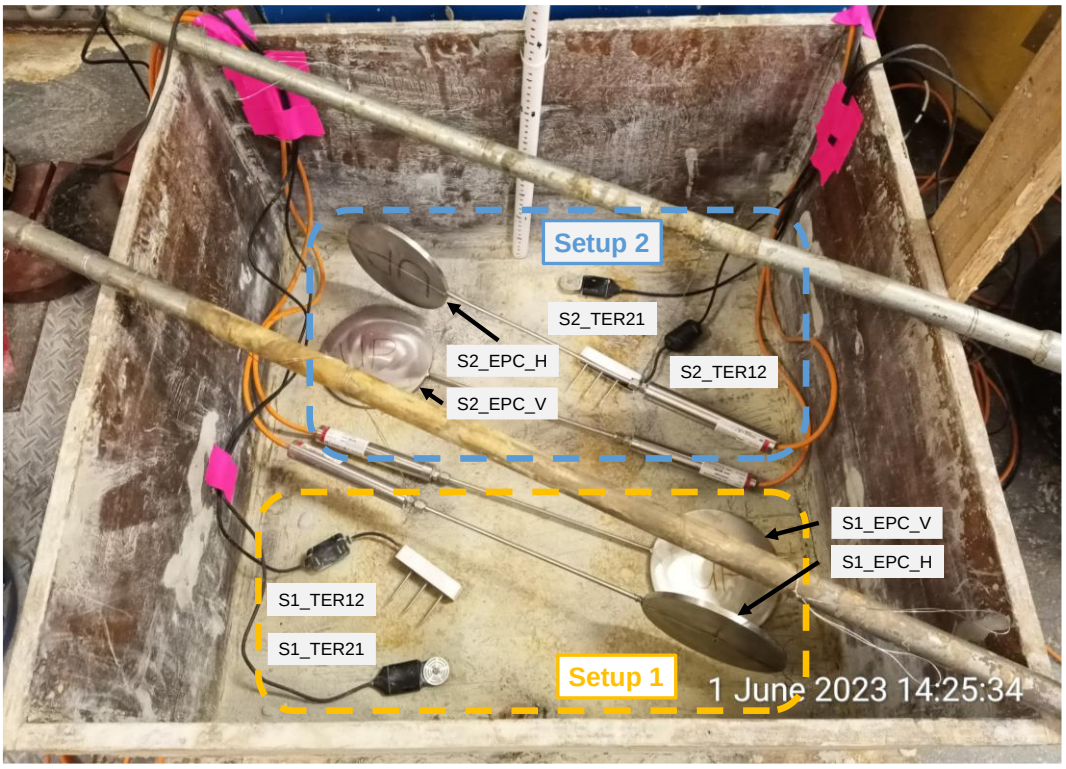


Figure 5.32: Sensor layout for Drying Box 2

5.6.2.2 Results

Figure 5.33 shows the results from the two setups over the entire 16-day duration of the experiment. Figure 5.33(a) shows the response from the EPCs, while Figure 5.33(b) shows the response from the tensiometers and TEROS 21 WPS. Although there is some scatter, it is clear that, besides an initial period during filling, all the interpreted stresses remained positive. By the end of the test, the suction values as recorded by the tensiometers approached 30 kPa. Again, the TEROS 21 WPS was shown to perform poorly at low suctions.

Figure 5.33(c) shows the interpreted VWC from the TEROS 12 moisture content probes and Figure 5.33(d) shows the interpreted stress ratio. Regarding the VWC interpreted from the TEROS 12 moisture probes, it was seen that in general there is good correlation between the two Setups. On 24 February 2023, when the second 400 W light was switched on after the free-standing water had either drained through the tailings or evaporated, a sharp increase in the VWC was noted for both setups. After this point, a rapid reduction in the interpreted VWC was noted.

Two features in this test are unexpected. The first is the increase in interpreted stress for the horizontal EPC at Setup 1 on 28 February 2023. The second is the decrease in estimated VWC noted for Setup 2 on 7 March 2023. Additional details of this test, including the raw data recorded from the sensors during these periods are provided in Appendix B.

© University of Pretoria

As was noted for the Drying Box 1 experiment, the interpreted stress ratio is dominated by the high suction values compared to the low total stress values. Therefore, aside from the fact that no sustained negative total stresses were recorded for the EPCs during initial drying, no meaningful conclusions are drawn regarding the stress ratio determined as part of this experiment.

© University of Pretoria

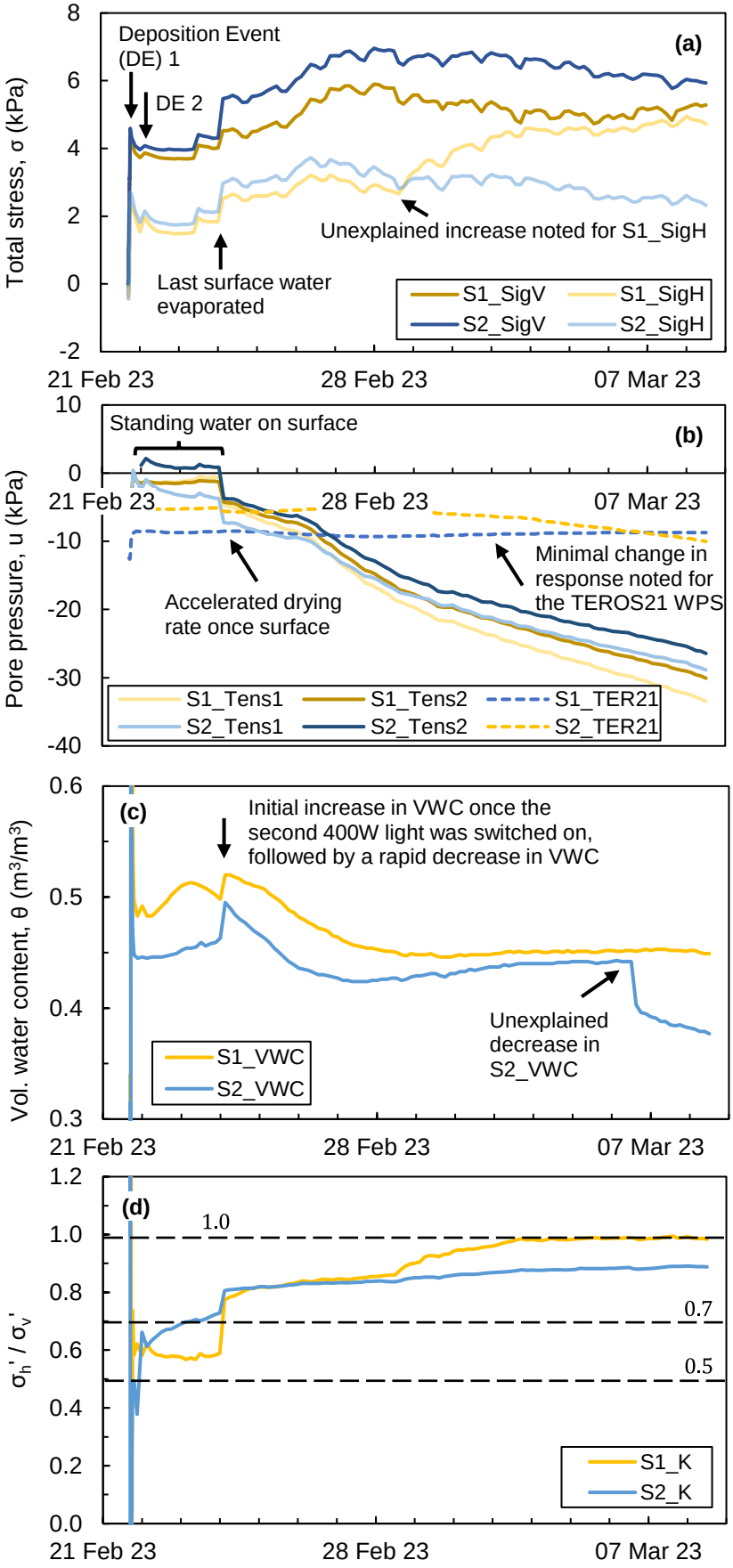


Figure 5.33: Results from the Drying Box 2 showing: (a) total stresses, (b) pore pressures, (c) VWC, and (d) stress ratios

© University of Pretoria

Figure 5.34 shows the interpreted stress from the EPCs for the first six hours of the experiment. The response from the EPCs was monitored every five minutes, and this was changed to once every 60 minutes at the end of deposition. There is a clear distinction between the vertical and horizontal stresses at both setups. Although limited negative interpreted stresses were noted during filling (<0.5 kPa), these were not seen again for the duration of the test. Therefore, based on the results from this test, no evidence of suction-induced tensile forces acting on the horizontal EPCs was observed. Rather, it is believed that any small interpreted negative stresses are a result of temperature influences on the entire cell assembly, or slightly inaccurate zero values.

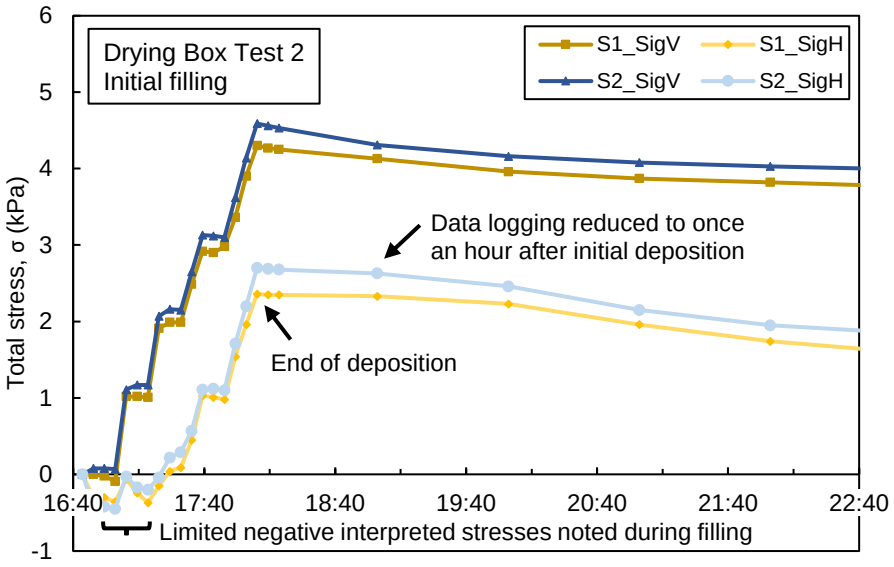


Figure 5.34: EPC response during filling for Drying Box 2

5.6.3 Test 3: Performance during temperature changes

As discussed in Section 2.6.1, it is known from the literature that there are thermal influences that affect the performance of EPCs that are over and above those accounted for with the temperature corrections provided in the Manufacturer's datasheet. The purpose of Drying Box 3 experiment was to investigate these thermal influences at zero load and at low applied stresses using hydraulic loading.

5.6.3.1 General procedure

With the exception of the tensiometers, the same experimental setup as described for Drying Box 2 was used for Drying Box 3. There were two main phases for Test 3. The first phase involved the behaviour of the remote monitoring system under short-term natural and artificial temperature

© University of Pretoria

changes at zero load, and at low hydrostatic pressures. The second phase considered the influence of longer, seasonal temperature variations at zero load. Six stages were conducted as part of the first phase and the details of each stage is described Table 5.3. The EPC zero readings were taken at the start of the test on 1 June 2023. All the interpreted stresses shown include the thermal correction as recommended by the manufacturer.

Table 5.3: Summary of the six short stages of Drying Box 3

Stage	Description	Duration (hrs)
1	Zero stress, natural temperature variations	24
2	Zero stress, artificial temperature variations	24
3	Low stress, natural temperature variations	24
4	Low stress, artificial temperature variations	24
5	Zero stress, natural temperature variations	48
6	Zero stress, artificial temperature variations	48

5.6.3.2 Results

The results are split into key stages of the test. Firstly, an overview of the six stages is provided. This is followed by the results from Stage 2, Stage 4 and then a combination of Stages 3 and 4. Finally, results from the long-term testing phase are presented. A more detailed presentation of the results from the Drying Box 3 experiment can be found in Appendix B.

Overview

Figure 5.35 shows an overview of the temperature recorded by each EPC for the short-term tests that were conducted as part of the Drying Box 3 experiment. Six stages were conducted and each stage had specific conditions imposed on the EPCs in terms of applied stress and temperature variations (as shown in Table 5.3). It can be seen that there are slight differences in the temperature recorded by the various EPCs. This is attributed to the location of the EPCs in relation to the light that was used to artificially vary the temperature. Since it is the change in the temperature that influences the interpreted stress, and since the corresponding temperature was used for each individual EPC, this was not deemed to be a concern.

© University of Pretoria

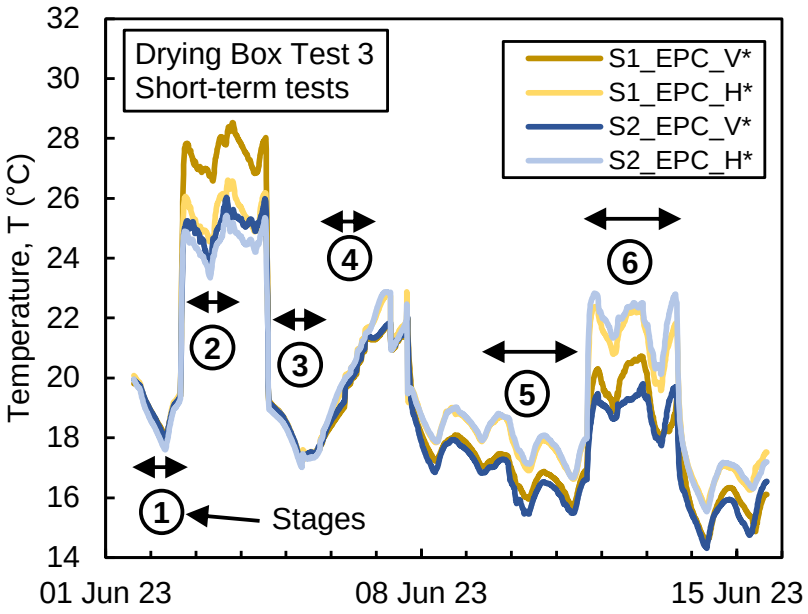


Figure 5.35: Overview of the short-term tests conducted for Drying Box 3

Stage 2: no stress, artificial temperature changes

Figure 5.36 shows a photograph of the Drying Box 3 experiment as it was configured for Stage 2 of the test. It can be seen that there is zero load on the EPCs and the two 400 W lights are switched on to provide an artificial increase in temperature for the entire EPC assemblies.

© University of Pretoria

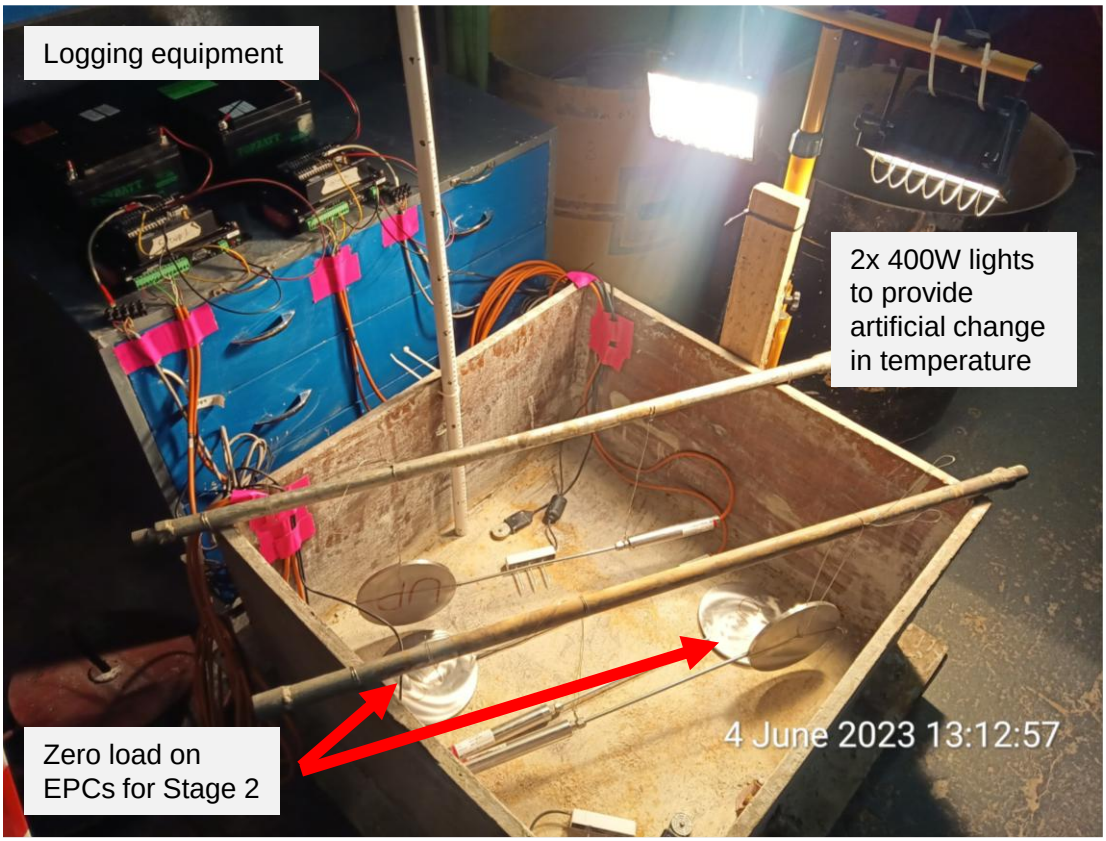


Figure 5.36: Layout of the Drying Box 3 test for Stage 2

Figure 5.37 shows the results from Stage 2 of the Drying Box 3 experiment. Figure 5.37(a) shows the recorded temperature, while Figure 5.37(b) shows the interpreted total stress for each EPC. It can be seen that for a change in temperature of approximately 6°C, there is an associated change in the interpreted stress of approximately 2 kPa for the vertical and horizontal stresses at Setup 2. The vertical and horizontal stress changes at Setup 1 were slightly lower. For the vertical EPCs at Setup 2, this change in interpreted stress due to temperature can be expresses as 0.4 kPa/°C. Additional details of this test are provided in Appendix B.

© University of Pretoria

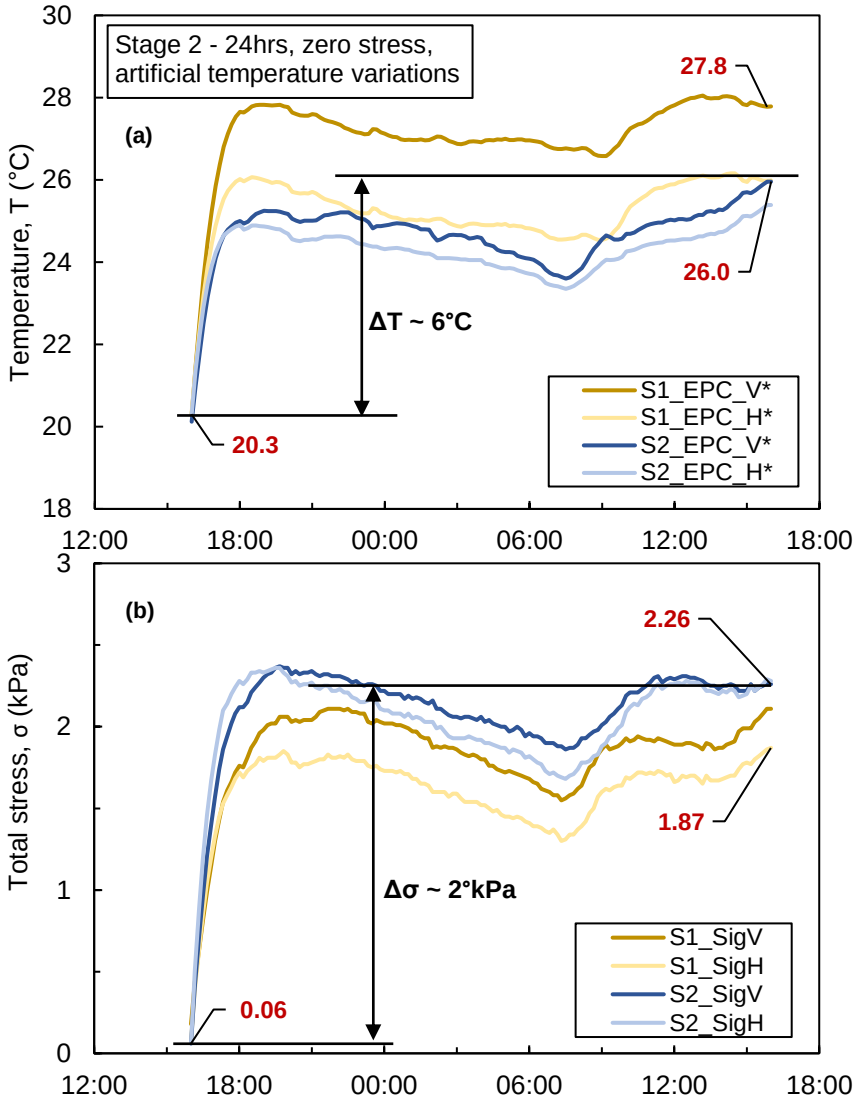


Figure 5.37: Results from Stage 2 of the Drying Box 3 experiment showing: (a) recorded temperatures, and (b) interpreted total stresses

Stage 4: low stress, artificial temperature changes

Figure 5.38 shows a photograph showing the setup for Stage 4 of the Drying Box 3 experiment. In the figure, the hydraulic loading of the EPCs can be seen. The water elevation was tracked using the survey marker which had increments of 1.0 cm. A hosepipe connected to a nearby tap was used to periodically add additional potable water to the Drying Box to maintain the required elevation. The true mid-height elevation was determined for each horizontal EPC prior to the commencement of the test. This elevation was verified at the end of the test to ensure no movement of the EPCs had occurred.

© University of Pretoria

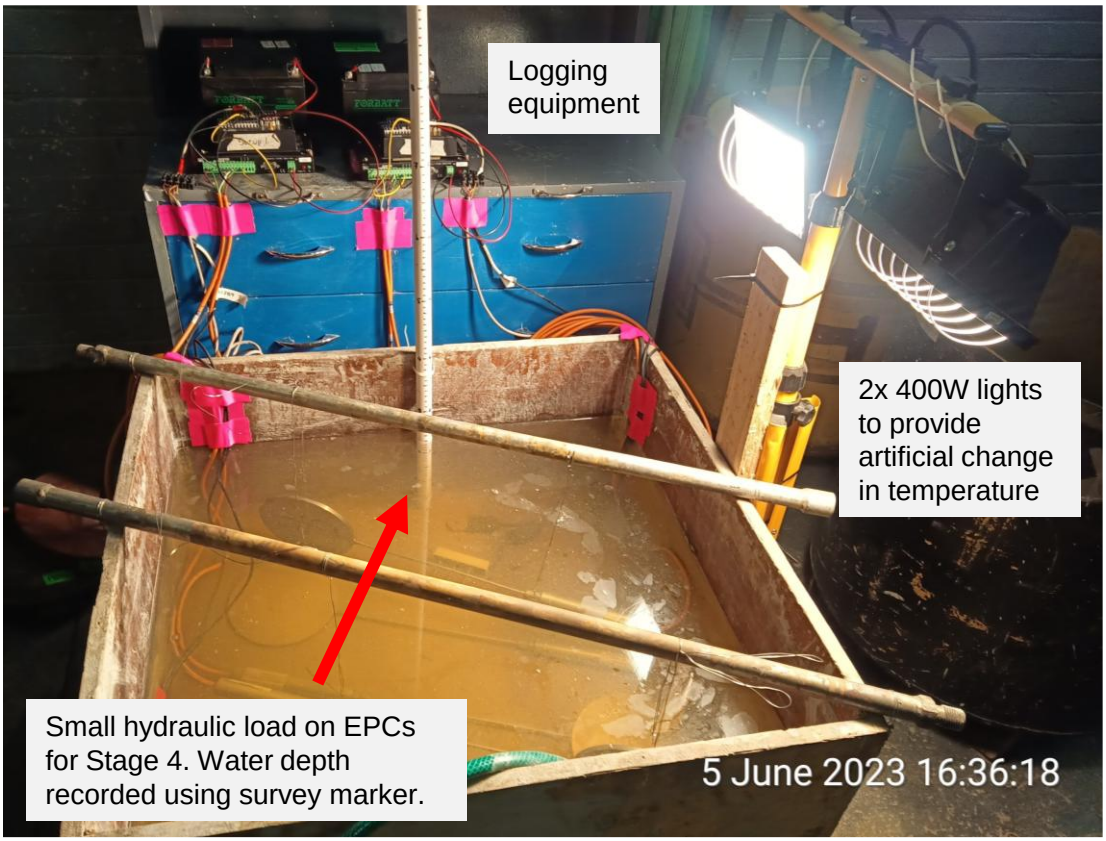


Figure 5.38: Setup for Stage 4 of the Drying Box 3 experiment

Figure 5.39 shows the results from Stage 4 of the Drying Box 3 experiment. Figure 5.39(a) shows the recorded temperatures, while Figure 5.39(b) and Figure 5.39(c) show the interpreted vertical and horizontal stresses for each EPC, respectively. For relevant figure, the known applied stress is also plotted for reference. This known stress is determined based on the measured height of water above the relevant EPC, and the assumed density of water. For the horizontal EPC, this height was taken to the mid-height of the EPC.

It can be seen that for a temperature change of 4°C, there is a corresponding change of approximately 1 kPa noted for both the vertical and horizontal stresses. For the vertical EPCs at Setup 1 and Setup 2, this change in interpreted stress due to temperature can be expressed as 0.3 kPa/°C and 0.4 kPa/°C, respectively. Similar changed were noted for the horizontal EPCs. Additional details of this test are provided in Appendix B.

© University of Pretoria

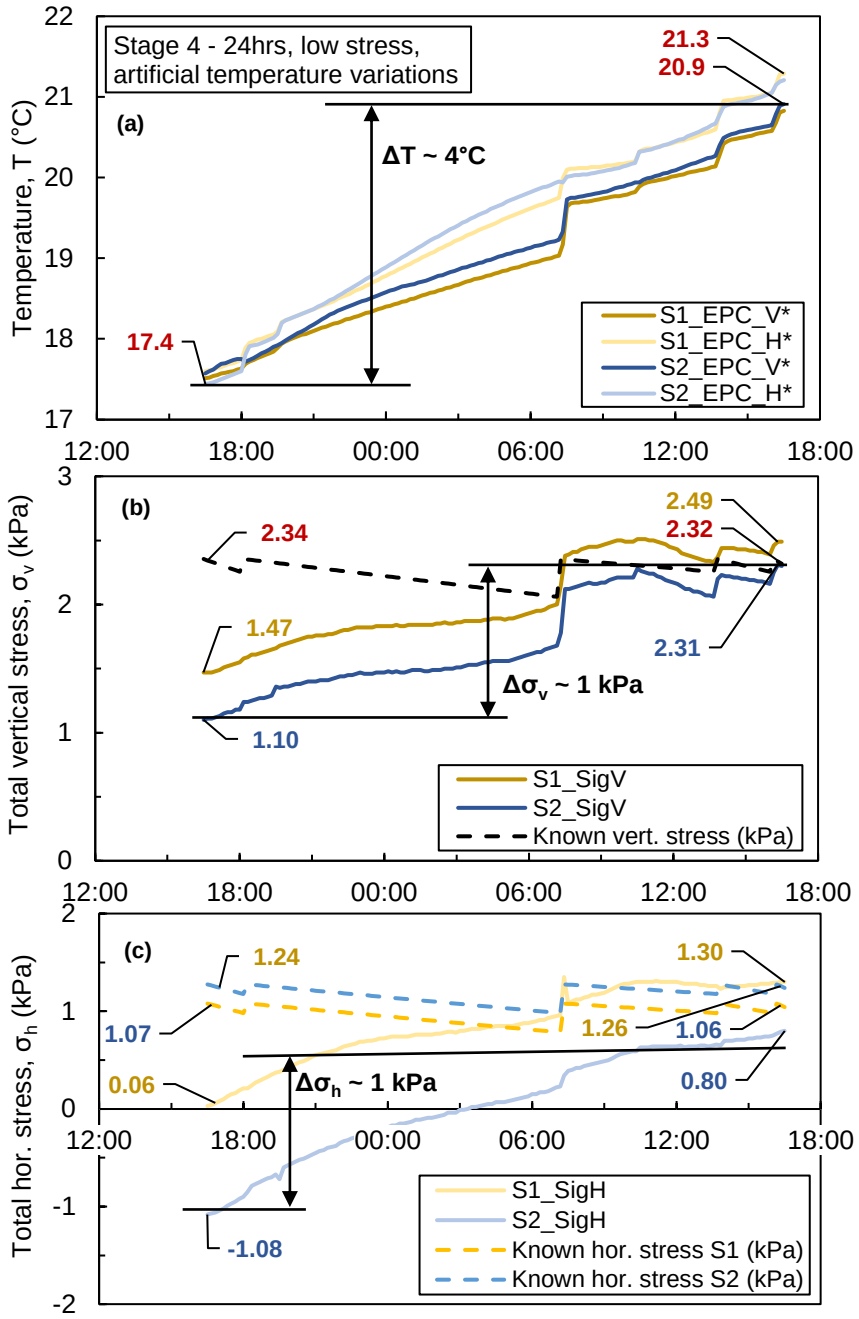


Figure 5.39: Results from Stage 4 of the Drying Box 3 experiment showing: (a) recorded temperatures, (b) total vertical stresses, and (c) total horizontal stresses

Stages 3 and 4: low stress conditions

Figure 5.40 shows a summary of the results from Stages 3 and 4 of the Drying Box 3 experiment. In these stages, the Drying Box was filled with water to apply a known pressure to the EPCs. The difference between the two stages lies in the nature of the temperature changes. Stage 3, shown in Figure 5.40(a), comprised natural temperature changes while Stage 4, shown in Figure 5.40(b),

© University of Pretoria

comprised artificial temperature changes.

For each stage, the interpreted pressure is plotted against the applied pressure. Also shown in the figure is the line of equality. It can be seen that there is a large difference between the applied and measures stress for both stages. This again highlights the perceived limitations of the EPCs at low stresses, specifically when there is a meaningful change in ambient temperature. It should be noted that the zero reading for each EPC was determined at the initial time of installation. This is the reason that no points lie on the line of equality for Stage 3.

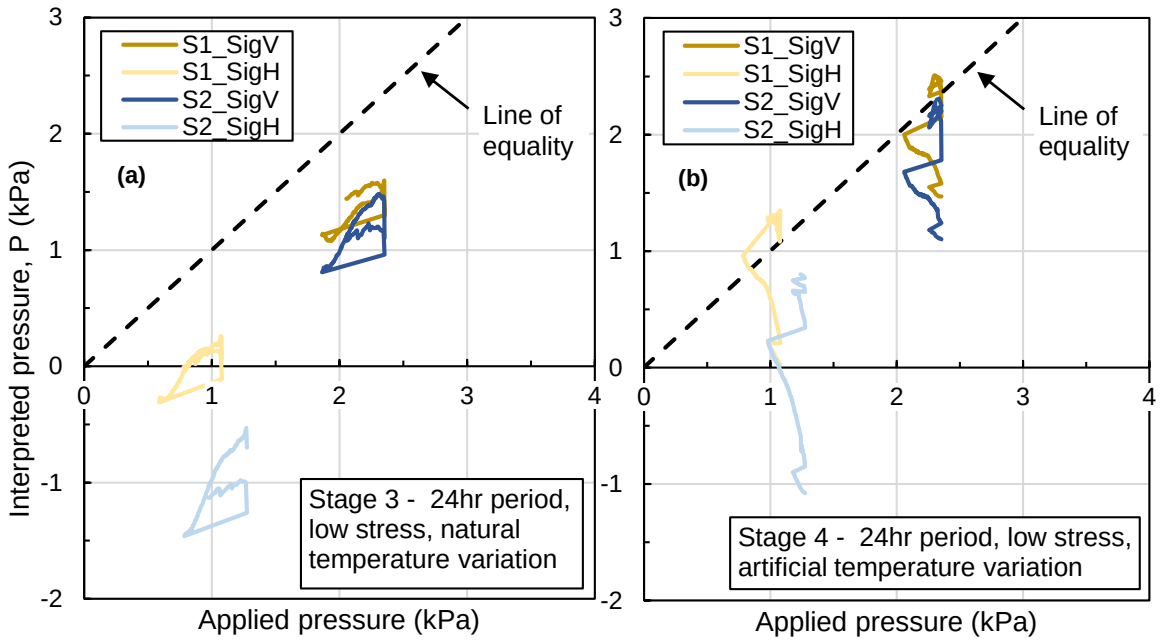


Figure 5.40: Results from the Drying Box 3 experiment showing: (a) Stages 3, and (b) Stage 4

Long-term testing

Figure 5.41 shows detailed results from the long-term testing that was conducted as part of the Drying Box 3 experiment. Figure 5.41(a) shows the temperature recorded by each EPC. In general, there is excellent correlation between the four EPCs. It can be seen that over the eight-month monitoring period, a change in temperature of approximately 15°C was noted. This change in temperature is due to seasonal changes and is larger than the change noted for the Drying Box 1 experiment. This is a result of the EPCs being exposed to the elements for this test, so there is no dampening effect due to the overlying tailings as was the case for the Drying Box 1 experiment.

Figure 5.41(b) shows the response from the EPCs installed at Setup 1, while Figure 5.41(c) shows the response from the EPCs installed at Setup 2. Again, it can be seen that there is a change in

© University of Pretoria

frequency recorded by the EPCs over the monitoring period. The change in the frequency for the four EPCs, with the values ranging from 2 Hz to 7 Hz. Unlike the results from Drying Box 1 experiment where there may be some uncertainty regarding the true stress, in this test these changes in frequency can only be a result of changes in temperature. As was noted for the Drying Box 1 test, these changes in frequency cannot be corrected by adjusting the thermal calibration coefficient as shown in Equation (6).

The unit change in frequency as a result of temperature changes for the four EPCs can be calculated as 0.3 Hz/°C, 0.1 Hz/°C, 0.1 Hz/°C, and 0.5 Hz/°C for the horizontal and vertical EPCs installed at Setup 1 and Setup 2, respectively.

Figure 5.41(d) shows the interpreted stress for the EPCs. It can be seen that there is a change in interpreted stress for all four EPCs, even though no change in stress was applied to the EPCs during this period (the EPCs were left under zero load as shown in Figure 5.36, with the exception that the lights were switched off for this stage of the test). These changes in interpreted stress are fairly similar for the horizontal and vertical EPCs and vary between 4 kPa and 7 kPa. The unit change in interpreted stress as a result of these temperature changes can be calculated as 0.3 kPa/°C, 0.2 kPa/°C, 0.4 kPa/°C, and 0.3 kPa/°C for the horizontal and vertical EPCs for Setup 1 and Setup 2, respectively.

Additional information regarding these temperature effects is provided in Appendix B.

© University of Pretoria

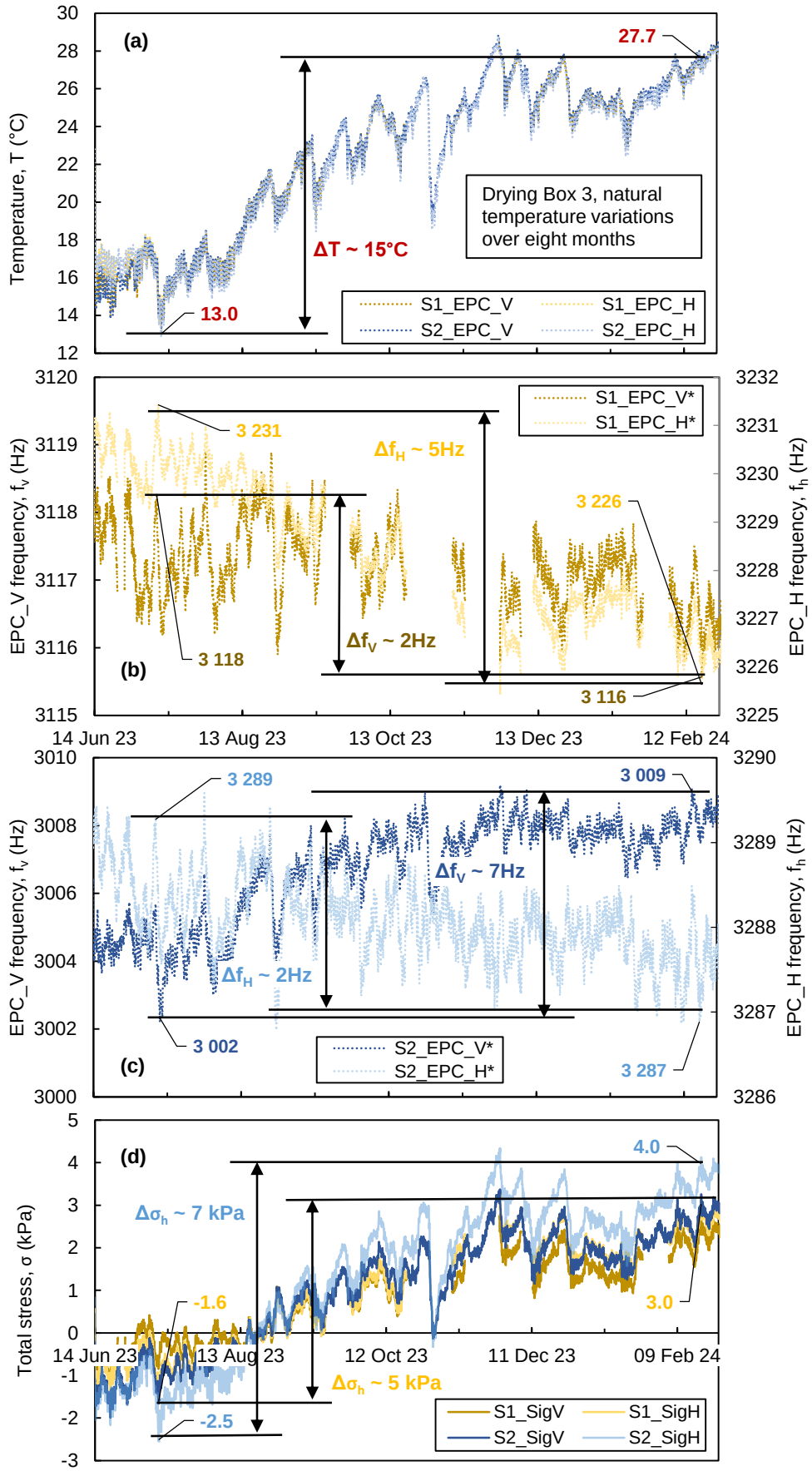


Figure 5.41: Detailed long-term results from the Drying Box 3 experiment showing: (a) temperature, (b) Setup 1 EPC frequencies, (c) Setup 2 EPC frequencies, and (d) interpreted total stresses

© University of Pretoria

Figure 5.42 shows a summary of the interpreted stress for the four EPCs, as well as the temperature recorded by the vertical EPC at Setup 2. It can be seen that there is a clear link between the interpreted stress and the recorded temperature. It is believed that this link is further exaggerated as a result of the fact that these EPCs are in an unloaded state. The reason for this link becomes clear when Equation (6) as shown on page 2-89, which is used to calculate the interpreted stress, is considered.

The equation comprises the sum of two components: a component dealing with the change in frequency, and a component dealing with a change in temperature. For this test, the component of the interpreted stress as a result of frequency changes due to pressure should be close to zero. Conversely, the temperature component should be large. Therefore, it follows that the temperature changes should be apparent in the interpreted stress.

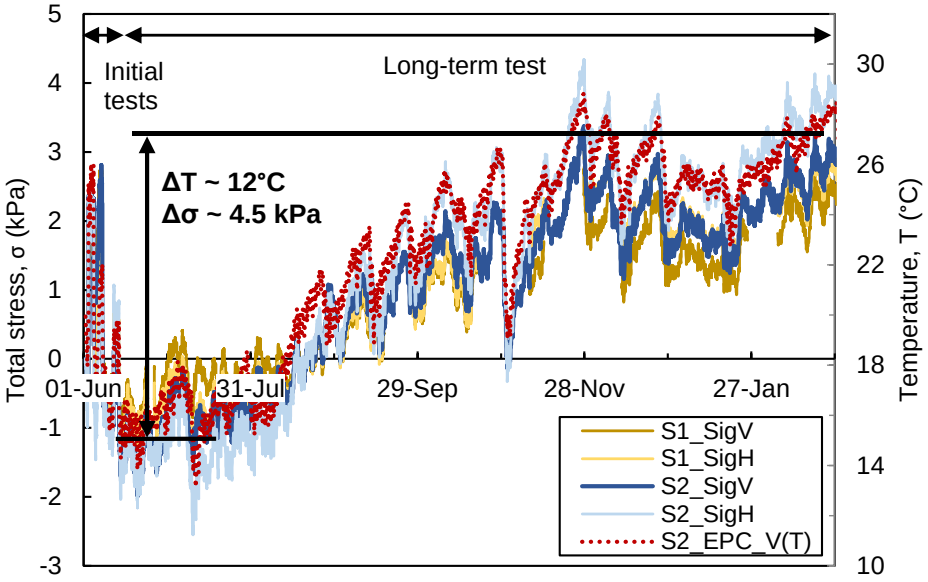


Figure 5.42: Summary of results of the long-term testing as part of the Drying Box 3 experiment

5.6.4 Temperature effects on the EPCs

Table 5.4 provides a summary of the temperature effects on the EPCs during the various Drying Box experiments. A total of 16 EPCs were tested over a range of time periods (between 24 hours and eight months). Imposed stress levels were limited to between 0 and 7.1 kPa and the temperatures investigated ranged from 13 to 28°C. It can be seen that for all the tests, the unit change in interpreted pressure due to temperature changes is similar in magnitude to the thermal correction factors provided by the manufacturer. However, it should be noted that this is a change observed despite the thermal correction being applied. In other words, all the values presented in

© University of Pretoria

this study are based on Equation (6), which already include the thermal corrections recommended by the manufacturer. Additional details regarding these tests can be found in Appendix B.

Table 5.4: Summary of temperature influence noted for the EPCs under constant load

	Starting stresses (kPa)	**Temperatures (°C)**	**Changes in interpreted stress (kPa/°C)**	**Manufacturer's thermal factors (kPa/°C)**
This study, laboratory tests	0 - 7.1	13 - 28	0.3 – 0.5	0.1 – 0.5

5.7 SUMMARY

This chapter presented laboratory verification tests on key components of the remote monitoring system. The intent was to verify the performance of the individual sensors, and then the entire system in a controlled environment before deployment to the field. In general, it was found that the calibration coefficients provided by the manufacturers were appropriate.

Tensiometers Calibration Tests

To verify its response to changes in applied positive pressure, each tensiometer was calibrated after saturation. A calibration coefficient was determined which was then used to extrapolate into the negative pressure range, as was done by le Roux (2019).

In addition, a limited number of dry-out tests were performed and suction values up to 837 kPa were achieved before the tensiometers cavitated. Key calibration parameters for each tensiometer used as part of this study are provided in Appendix B for reference.

Moisture Probe Calibration Tests

A series of drying experiments were conducted to investigate the performance of the TEROS 12 moisture probe for use in gold tailings. During the tests, the height of the tailings, as well as the mass of the tailings was tracked. In this way the true VWC could be calculated. A total of four tests were conducted where the initial density was varied between e = 0.88 and e = 1.04. The fourth test was a duplicate test at a void ratio of 1.0, but was conducted using process water obtained from site, instead of tap water from the laboratory. In this way, the influence of both initial density and water chemistry on the performance of the moisture probe were evaluated.

© University of Pretoria

Based on the results from the four tests, it was found that both the Mineral Soils and Topp et al. (1980) equations appeared to be independent of both density and water chemistry. Both methods resulted in the estimated VWC being within ±0.05 of the true VWC , with the Mineral Soils equation performing slightly better than the Topp et al. (1980) equation for the gold tailings.

In addition, soil suctions were monitored using the Tuks tensiometers. Since the volumetric properties of the soil were known, SWRCs could developed from these drying tests. These curves represented the drying curves for the soil, and compared well to drying curves developed for the same gold tailings using the tensiometer method as described by le Roux (2019). Based on these SWRCs, it was found that the gold tailings can be classified as having a low AEV of between 4 kPa and 11 kPa.

Earth Pressure Cell Verification Tests

EPC verification tests were conducted to measure of the deflection of the sensing face under various applied pneumatic loads. A total of 21 tests (on 15 different EPCs) were conducted to investigate the magnitude of deflection of the sensing face for various applied pneumatic loads.

A highly non-linear deflection response was noted for the EPCs. It was found that the deflection of the EPCs varied along the face of the cell, with the most deflection occurring at the centre. For the same magnitude of applied stress of 50 kPa, a greater deflection was noted when the pressure was applied as a negative value (i.e. suction), compared to when the pressure was applied as a positive value.

Significant variation in the deflection was noted in the EPCs tested. For example, under an applied pneumatic load of 200 kPa, deflections were noted ranging from 0.01 mm to 0.18 mm. This is a large range and needs to be carefully considered when interpreting the results from the field.

Drying Box Tests

Three Drying Box tests were conducted to investigate the performance of the remote monitoring system over a range of conditions.

The first test, Drying Box 1, was conducted over 11 months. The intent of this test was to verify the performance of the entire remote monitoring system. With modifications made to the logging code and battery used to power the system, a configuration was found and tested that allowed the remote monitoring system to perform effectively for six months without external intervention. During this test, it was again confirmed that the TEROS 21 WPS are not appropriate for use in the monitoring of gold tailings as they perform poorly at low suctions (<10 kPa) and are slow to

© University of Pretoria

equilibrate to changes in suction due to drying (in the order of 27 days in some cases). It was also found that the steel-cased Tuks tensiometers are more resilient and should be used in favour of the epoxy-cased Tuks tensiometers for long-term monitoring of gold tailings.

During the five-month period after the last deposition event, some evidence of the thermal influence on the performance of the Geosense VWTPC-4000 EPCs under constant load was noted. These thermal influences were not captured by the thermal correction factors provided by the manufacturer and when expressed in terms of kPa/°C, ranged from 0.1 to 0.6 kPa/°C.

The second test, Drying Box 2, was much shorter and was only conducted over 16 days. This test focused on the response of the EPCs immediately after deposition. This was due to the small negative pressures interpreted from the site installations. One of the reasons for these negatives stresses was believed to be small tensile forces in the soil as a result of desiccation. The purpose of this test was to investigate this postulation. The EPCs were logged at five-minute intervals during filling and the tailings was then allowed to dry. At the end of the test, the measured suctions were approaching 30 kPa and no evidence of negative interpreted pressures were noted. Rather, it was postulated that the observed negative pressures are a result of inaccurate zero readings and small thermal influences on site.

The third and final test, Drying Box 3 was conducted over a nine-month period. This test comprised two main phases and focused on the temperature effects on the EPCs under constant load. The first phase focussed on the daily temperature variations on the response from the EPCs under zero load, and low hydraulic stresses. The second phase was more long-term in nature and focused on the seasonal ambient temperature variations on the response from the EPCs under zero load over a period of eight months. For both phases it was found that there are thermal influences on the response of the EPCs, and that these influences are evident despite the use of the thermal correction factors recommended by the manufacturer. When expressed in terms of kPa/°C, the magnitude of these influences varied between 0.1 kPa/°C and 0.5 kPa/°C for the tests conducted.

© University of Pretoria

6 FIELD MONITORING

6.1 INTRODUCTION

The initial plan for this research was to deploy the remote monitoring system onto three different tailings tams: a gold tailings dam, an iron ore tailings dam, and a platinum tailings dam. Unfortunately, for reasons that will be described later in this section, only reliable, long-term data were generated for one site: the gold tailings site.

Despite the fact that no long-term data were available for the iron ore and platinum sites, the same level of care was taken for these installations. Therefore, although the data are short-term in nature, the information is still useful and can assist in showing the value of remote monitoring of the stress regime in tailings dams. This chapter therefore presents details regarding the installation, monitoring and interpretation of the remote monitoring systems at the three tailings sites.

In the text, the remote monitoring systems are sometimes referred to as “stations” or “installations”. These terms are used interchangeably in this section and refer to the remote monitoring system installed at the various locations on the three tailings dams being monitored.

6.2 GOLD TAILINGS SITE

6.2.1 Site description

The gold tailings site used for this study is located in the East Rand of Gauteng. Details of the gold tailings are provided in Section 3.3. As part of the research agreement between the University and the Mine, the name and exact location of the Mine cannot be specified. However, details relevant to the research can be provided. The University had been monitoring this site for several years prior to this research and this has led to a number of research outputs (e.g. Basson, 2023) with several more in the process of being published.

Based on publicly available satellite images, it was determined that construction of the tailings dam had already commenced by March 2010. The site slopes gently from West-to-East and a starter wall was constructed along the Eastern perimeter. Although the construction records were not available, based on discussions with site personnel, it was determined that a basal drainage system was constructed as part of the starter wall. The stress stations were installed along Piezometer Line A, along the Eastern Embankment of the dam which has the highest wall height.

© University of Pretoria

At the time of installation of the stress stations, in March 2022, the dam was approximately 22 m in height and had an active surface area of 50 ha. As mentioned earlier, the starter wall was only constructed along the Eastern Embankment. However, at the time of installation, a bench (hereafter referred to as the first bench) had been established along the entire perimeter at an elevation of approximately 1615 mamsl.

During the monitoring period, a new bench (the second bench) was established at an elevation of approximately 1624 mamsl. The dam is constructed with 9 m wide benches with 9 m lifts between benches. This results in intermediate slopes of 1(v):1.5(h), and an overall slope of approximately 1(v):3(h). This is a common construction configuration used on upstream constructed gold tailings dams in South Africa.

A single, 600 mm diameter concrete-ring penstock system is in place for decanting surface water. The tailings dam has a dedicated return water dam so surface water is kept to a minimum. An independent operating contractor with many decades of experience operating large tailings dams in South Africa is appointed for the daily operation of the tailings dam. The operating contractor has a comprehensive monitoring system in place which includes monthly readings of 22 standpipe piezometers installed at five key cross-sections along the perimeter.

According to the monitoring system currently in place at the site, the site has experienced a mean annual rainfall of 916 mm. This value is slightly higher than those values reported by nearby rainfall stations (Adamson, 1981). Table 6.1 provides hydrological details obtained from the nearby rainfall stations. To maintain the anonymity of the site, the rainfall station names have been removed. Over the review period, from January 2020 to June 2024, the highest single day rainfall event occurred on 14 February 2023 when 59 mm of rainfall were recorded. Over these four years, the mean annual rainfall was 800 mm.

Table 6.1: Key rainfall characteristics of the gold site (after Adamson, 1981)

Rainfall Station	**Distance from site (km)**	**Years of record**	**Mean annual rainfall (mm)**	**1:50yr, 1 day event (mm)**	**1:00yr, 1-day event (mm)**
Rain Gauge #1	42.3	57	650	126	145
Rain Gauge #2	46.3	61	660	151	177
Rain Gauge #3	40.9	66	716	143	167
Rain Gauge #4	41.1	62	768	146	169
Site data (all)		13	916	133	N/A

© University of Pretoria

Where available, monitoring data are presented over a period from January 2020 to June 2024. Figure 6.1 shows the monthly recorded rainfall at the gold site, for reference the monitoring period has also been highlighted. It can be seen that for the two years preceding the monitoring period, less-than-average rainfall was recorded while in the first year of monitoring, slightly above-average rainfall was recorded. However for the second year of monitoring, less than half the annual rainfall was recorded.

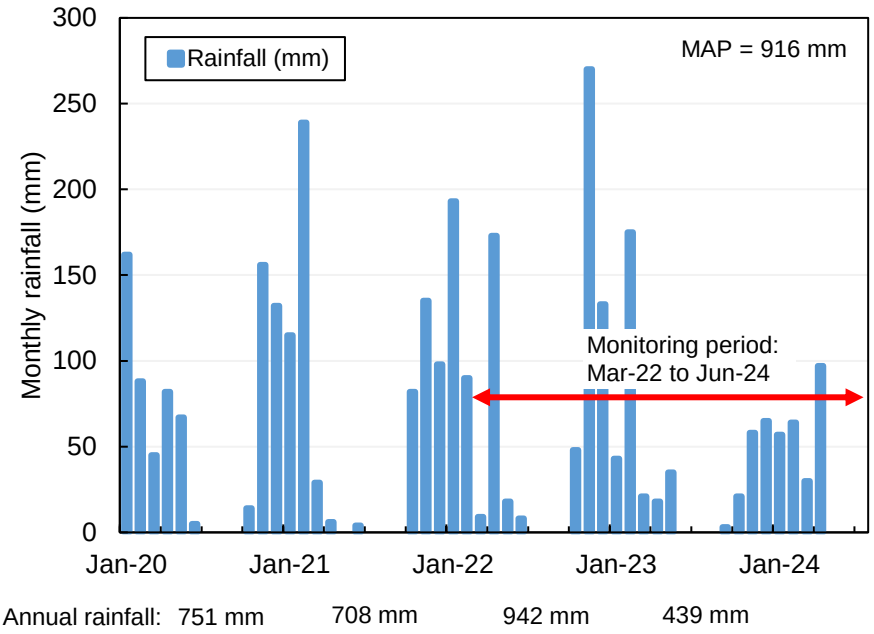


Figure 6.1: Monthly rainfall records at the gold tailings dam over the monitoring period

Figure 6.2 shows key monitoring data over the review period, as provided by the operating contractor. Figure 6.2(a) shows the monthly dry deposition tons, against a target of 120 000 t per month. It can be seen that there is some variation in the monthly deposition with some months receiving more than the target and some months receiving less. This is normal as the deposition is closely linked to the plant's processing output which varies with the mining plan but also due to external factors such as breakdowns, etc. In November and December 2023, significantly lower deposition tonnages were noted due to industrial action which led to extended plant stoppages. Over a longer term, it can be seen that the cumulative monthly deposition is slightly below the target.

The influence of the variation in monthly deposition tonnages can be seen in the monthly elevation of the dam, shown in Figure 6.2(b). Two elevations are presented: the elevation of the tailings at the penstock, and the average crest elevation. It can be seen that there is a difference between

© University of Pretoria

the two elevations with the penstock elevation being lower than the crest elevation. The reason for the height difference is due to the natural inwards slope of the dam created as a result of the deposition methodology, combined with the daywall-paddock method which ensures the daywalls are maintained at a higher elevation than the basin to provide sufficient vertical freeboard. Although there are some monthly variations, over the longer term these trajectories appear stable, this is an indication of a well-managed dam.

Although it is useful to monitor the monthly elevation changes, it is more useful to monitor the Rate of Rise (RoR) of the dam. Two trends for the RoR are presented in Figure 6.2(c), the first trend is determined based on the monthly tailings elevation reported at the penstock and is shown in blue. The second trend is determined based on the average monthly crest elevation of the entire dam and is shown in yellow. Both values are calculated using the cumulative height changes with time so naturally more variation can be expected early in the reporting period. Both methods indicate a long-term RoR of approximately 2.0 m/year which is in line with the design requirements.

© University of Pretoria

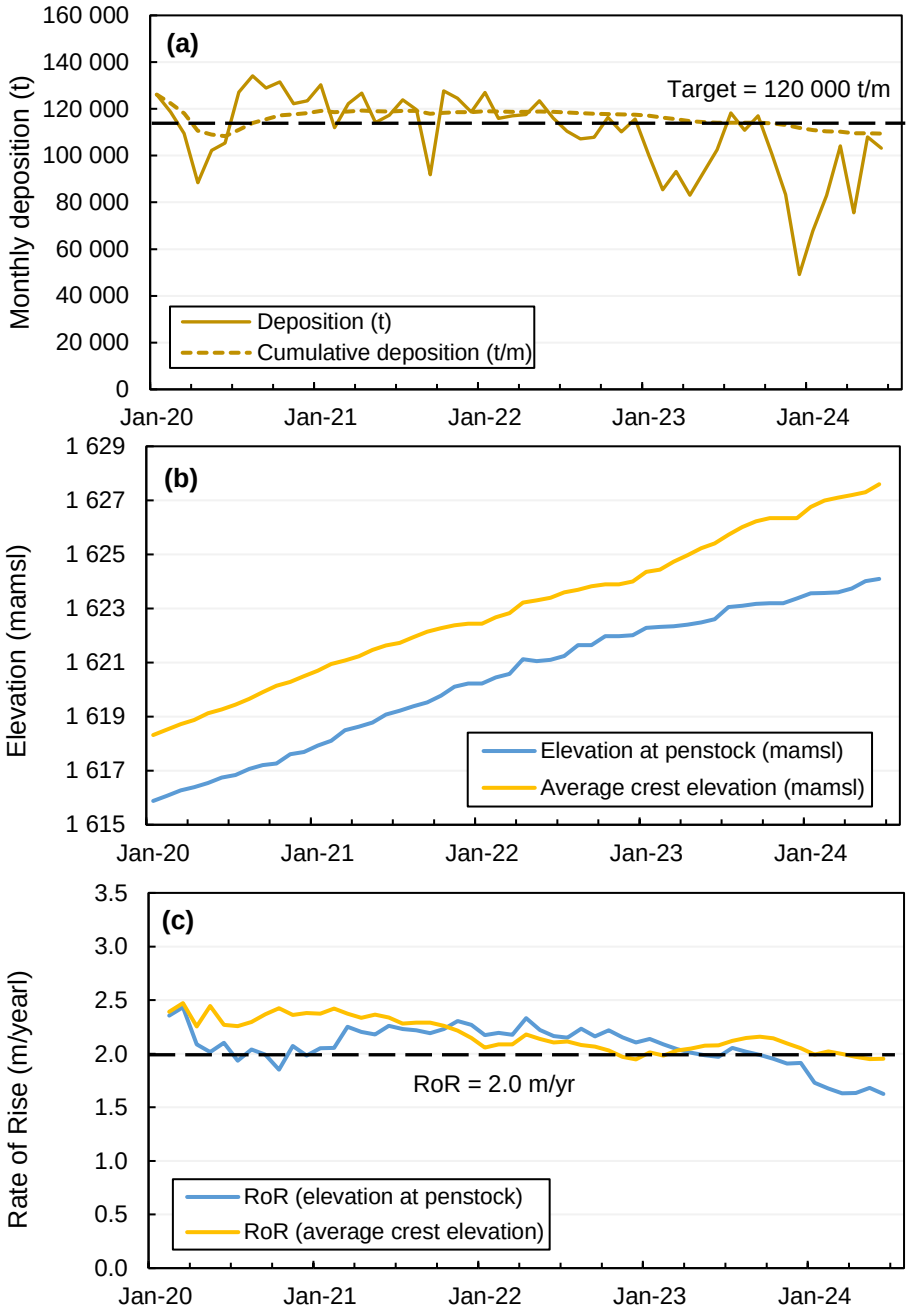


Figure 6.2: Key monitoring data at the gold tailings dam over the review period showing: (a) monthly deposition, (b) elevation, and (c) RoR

Figure 6.3 shows the results from the monthly standpipe piezometer monitoring at the cross section where the remote monitoring systems were installed. The location of these piezometers along the slope is shown in Figure 6.7. The water column height is defined as the height of the water column within the standpipe piezometer, relative to the base of the standpipe. This height was determined monthly by the operating contractor. Piezometers 1A and 1C were reported as blocked so no meaningful data were obtained from these piezometers. Significantly more scatter was noted for piezometer 1D, compared to piezometer 1B. However, both piezometers show a steady increase

© University of Pretoria

in saturation of the slope with time which is expected.

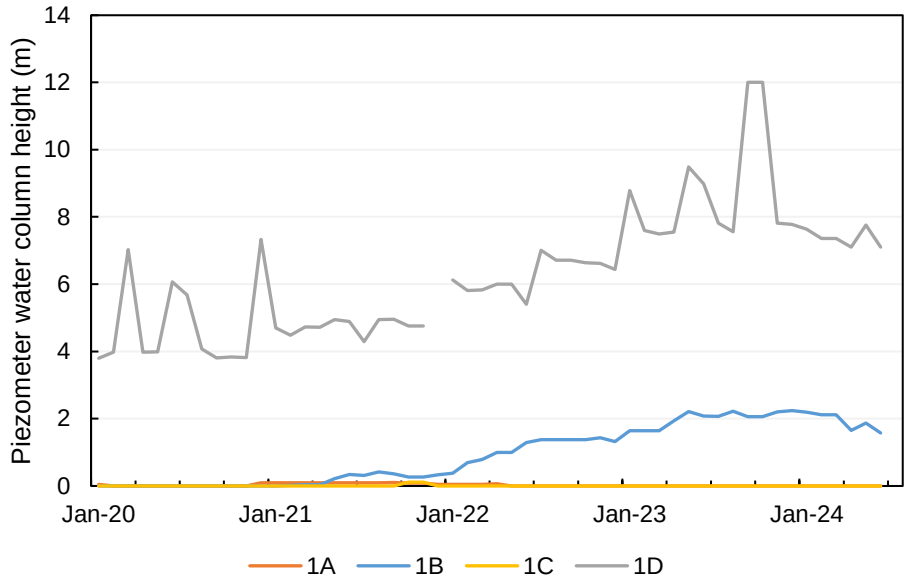


Figure 6.3: Monthly piezometer water column heights at the gold tailings dam over the monitoring period

6.2.2 Installation details

Three remote monitoring stations were installed on the gold tailings dam as shown in Figure 6.7. The location of these stations was based on previous monitoring on the dam by the University, as well as proximity to existing monitoring equipment, specifically standpipe piezometer Line A. Standpipe piezometer Line A comprises four standpipe piezometers. Piezometer 1A is located on the stater wall, while piezometer 1B is located on the first bench. Piezometer 1C was located in the daywall at the time of the installation. As at the end of June 2024, this piezometer was located on the recently-established second bench.

Piezometer 1D is furthest into the tailings dam (initially in the basin but as of June 2024, was located in the daywall). The first station was installed in the daywall close to the outer wall, adjacent to standpipe piezometer 1C. The second station was also installed on the daywall but closer to the pond. The third station was installed in the basin, adjacent to standpipe piezometer 1D.

Figure 6.4(a) shows a photograph of the location of the three installations during the planning stage. Figure 6.4(b) shows a photograph taken during the installation process. In this photograph, the shallow excavation for Station 1 can be seen in the foreground, while the cabling to is being laid to Station 3 (indicated in the background by the green arrow). Figure 6.4(c) shows a photograph taken at the end of the installation, once the logger boxes were erected on the slope.

© University of Pretoria

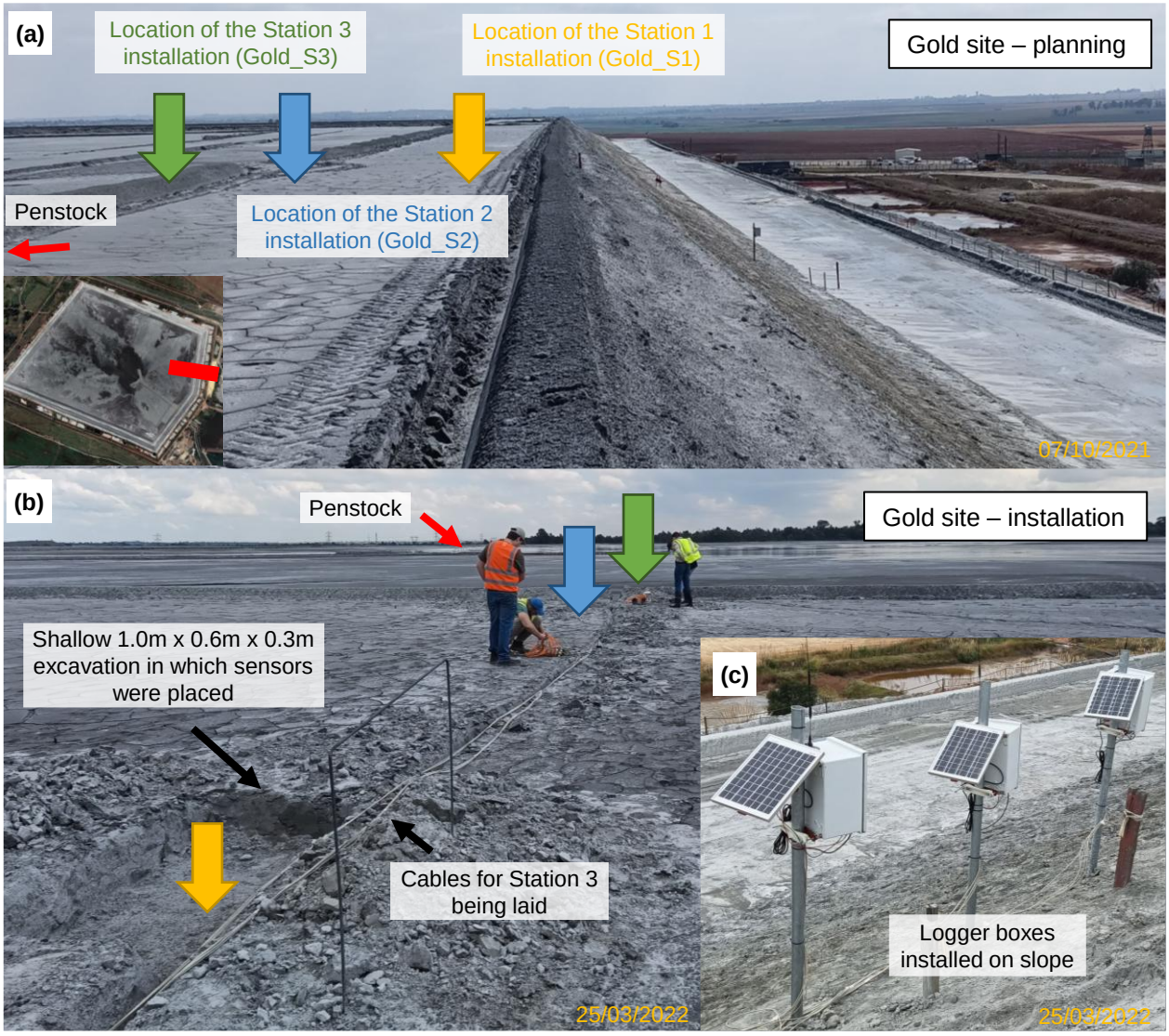


Figure 6.4: Photographs showing the gold site: (a) planning, (b) installation, and (c) the logger boxes installed on the slope

An initial excavation approximately 1.0 m long, 0.6 m wide, and 0.3m deep was made for each installation. The sensors were then placed within this excavation. Figure 6.5 shows a photograph taken during the installation of Station 3. In the figure, tensiometer 1 can be seen being carried from the water bottle to the installation. The EPC used to measure vertical stress is referred to as the vertical EPC and this EPC was installed in a slurry and levelled. The EPC used to measure horizontal stress is referred to as the horizontal EPC and this EPC was suspended from a segment of reinforcing steel using wire and levelled horizontally.

After this photograph was taken, the second tensiometer was installed and the excavation was carefully and loosely backfilled with the same tailings initially excavated. Within a few days, the operating contractor commenced with routine tailings deposition in the area and the installations

© University of Pretoria

were successfully submerged in slurried tailings. Figure 6.6(a) shows Station 3 at the end of the installation day (after backfilling) but before deposition while Figure 6.6(b) shows Station 3 on day 13 of the monitoring period, after deposition had occurred in the area.



Figure 6.5: Sensor installation at the gold tailings site, Station 3

© University of Pretoria

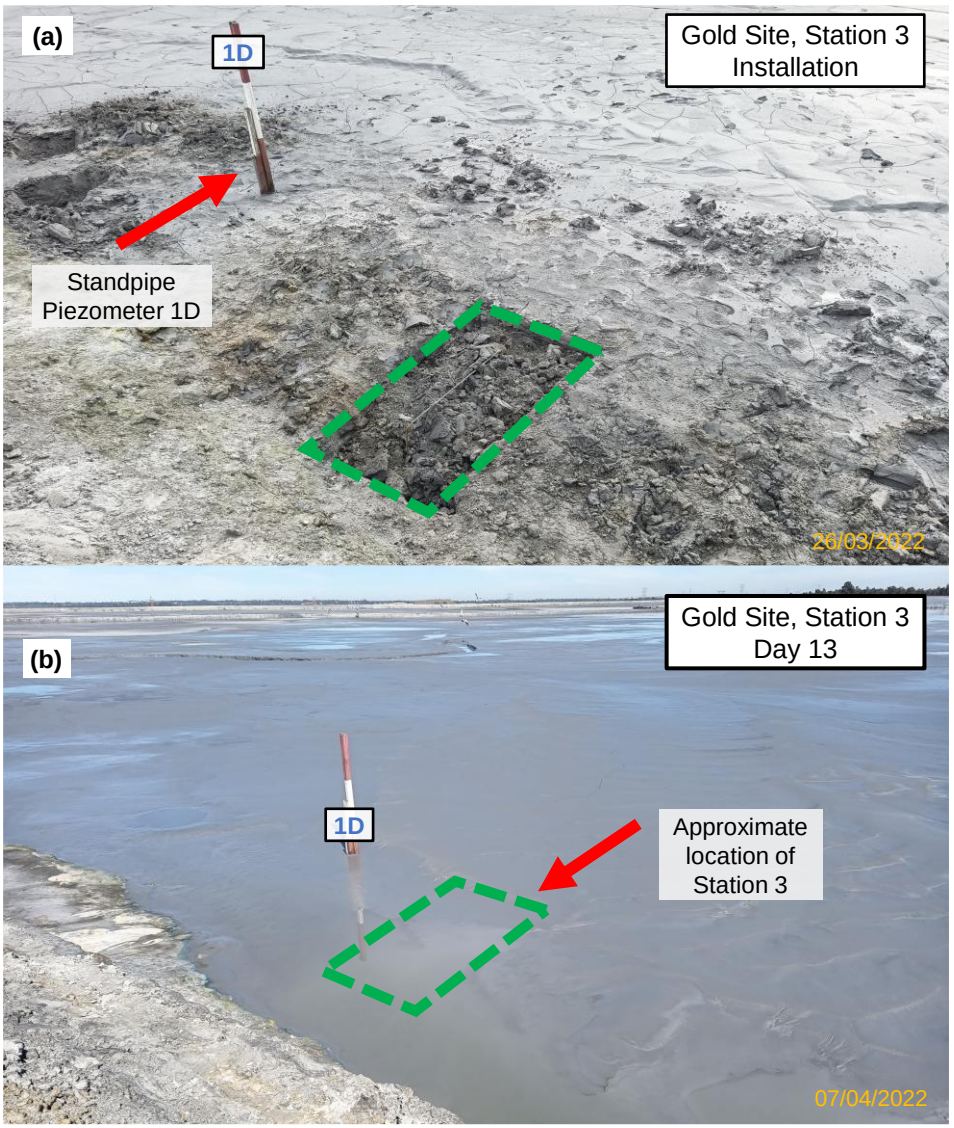


Figure 6.6: Station 3 at the gold tailings site: (a) on the day of installation, and (b) on day 13 of monitoring

Table 6.2 provides an overview of the key events at the gold monitoring site. In particular, the dates for the station installation, first deposition in the area, and the start of the step-in construction are provided. The importance of these dates is discussed in the subsequent sections.

Table 6.2: Key events at the gold site

Date	**Event**
25 March 2022	Installation of Stations 1, 2 and 3. Start of logging.
28 March 2022	First deposition in the area.
1 March 2023	Start of Step-in construction (establishment of the second bench).

© University of Pretoria

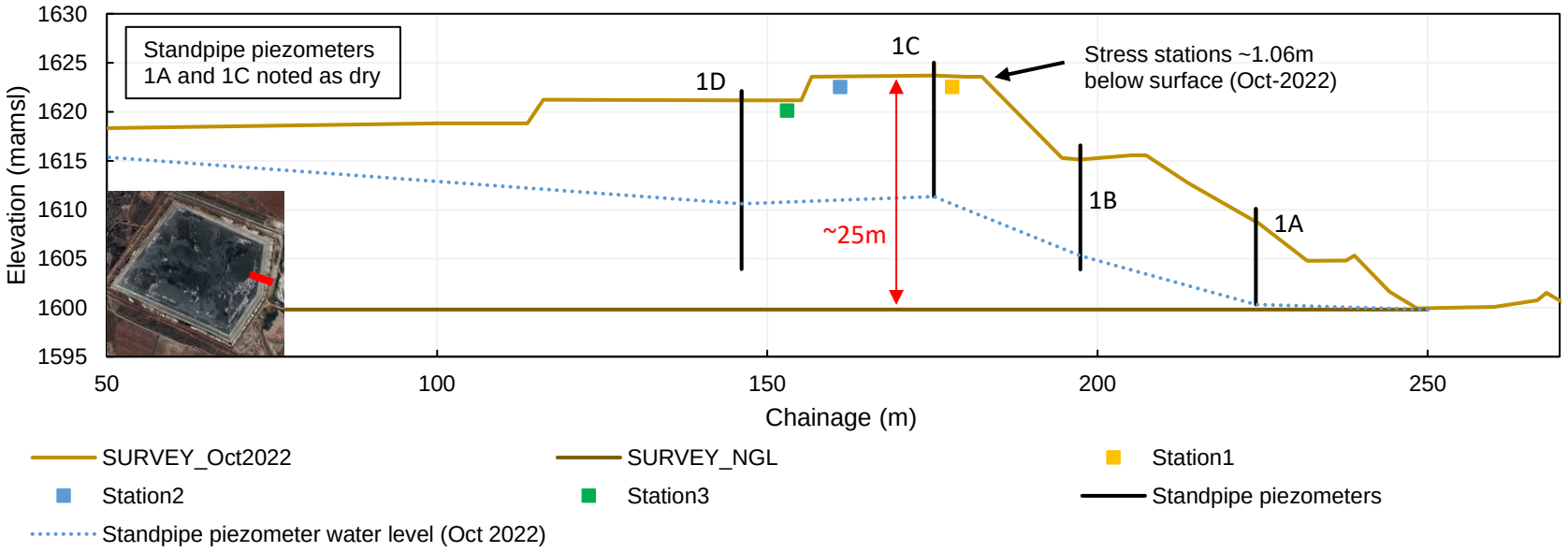


Figure 6.7: Cross section showing the installation details at the gold tailings dam

© University of Pretoria

6.2.3 Results

Key results from the remote monitoring system installed at the gold tailings dam are shown in this section. Due to the nature of the monitoring, a significant volume of data was collected over the monitoring period. Therefore, the results are split into distinct phases. The first phase comprises the initial monitoring data, where the response from the individual sensors is shown. The second phase shows the results for the first twelve months of monitoring (i.e. up until the start of the step-in). The third phased shows the results for the entire monitoring period. The fourth phase focuses specifically on the response from the moisture probe and the VWC estimation, while the fifth phase focuses on the temperature influences on the EPCs after the step-in.

6.2.3.1 Initial data (first month)

Results from the first month of monitoring are provided for each station at the gold site in Appendix C. Details of the first deposition event are provided, as well as installation details for the tensiometers. The zero readings for the EPCs and tensiometers are also shown for reference. What is also of interest is the interpretation of the raw data reported from the sensors, and the conversion to engineering units. This is done by showing a side-by-side comparison of the raw and interpreted data for each sensor.

6.2.3.2 Initial data (selected months)

Figure 6.8(a) shows the VWC and suctions measurements for the three stations at the gold tailings site during the drying phase after the first rewetting. In the initial drying stages there is a marginal change in the VWC for a moderate change in suctions which start from close to zero. This indicates that the soil is near saturation after first rewetting. The saturated VWCs for the three stations are shown for reference.

Figure 6.8(b) shows the VWC and suction responses recorded for the three stations during the drying and wetting cycles experienced during month six of the monitoring. During this period it can be seen that there are moderate changes in VWC with suction during both the wetting and drying phases. It is likely that these wetting and drying paths lie on scanning curves between the primary wetting and drying curve as described in Section 2.3.3.

Additional details noted for the various sensors for selected months can be found in Appendix C. In particular, it is shown how climatic factors such as rainfall have a decreasingly smaller influence on the response of the sensors as the depth of overlying tailings increases.

© University of Pretoria

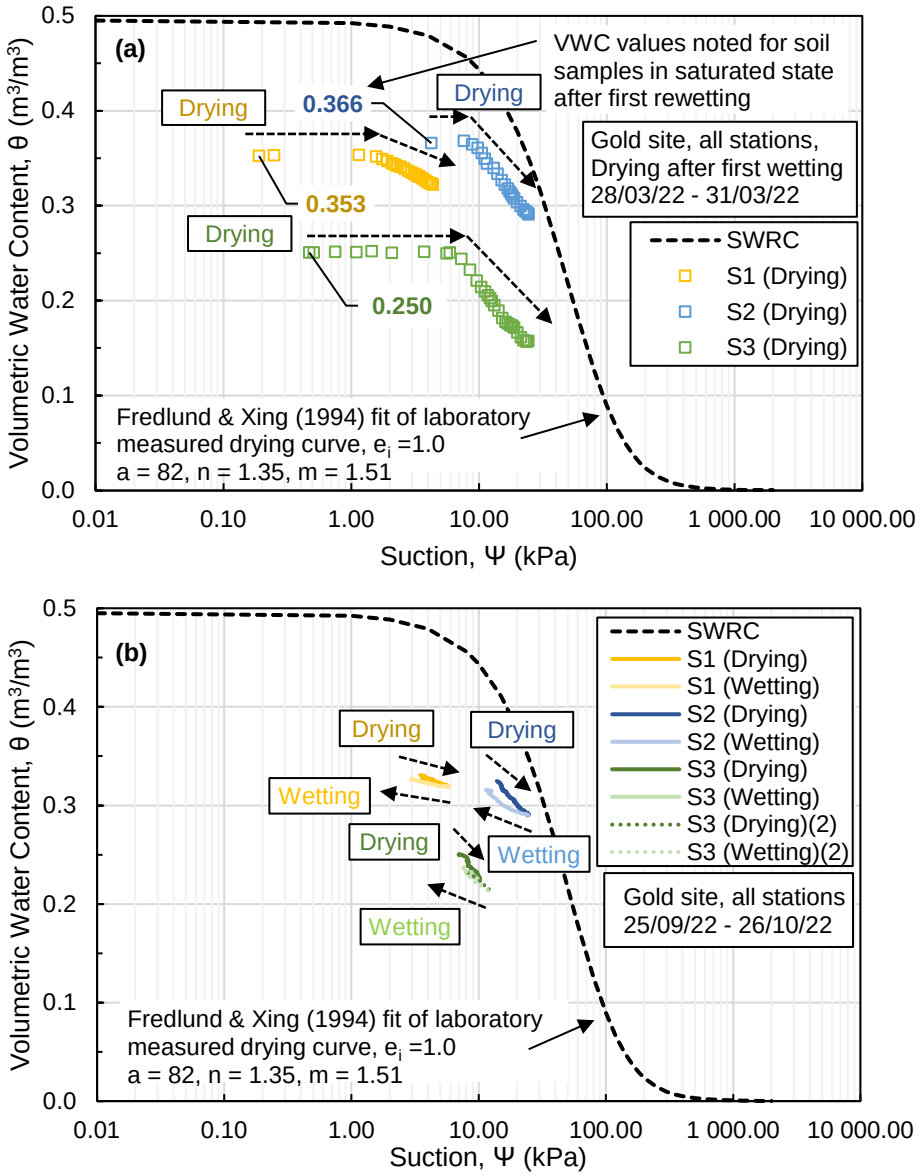


Figure 6.8: VWC and suction responses at the gold site after: (a) first rewetting, and (b) wetting and drying in month six

6.2.3.3 Combined data (first year)

Figure 6.9 shows the results from the three remote monitoring stations installed at the gold tailings site, from installation in March 2022, up to the step-in in March 2023. As was done with the Drying Box experiments, the results are presented with time, and the key results are shown directly below each other. This allows for site influences to be seen across all the sensors. Figure 6.9(a) shows the results from the EPCs. The same colour scheme as was shown in the installation section has been retained. Station 1 (closest to the outer wall) is shown in yellow, Station 2 (between Station 1 and Station 3) is shown in blue, while Station 3 (closest to the penstock) is shown in green. In this

© University of Pretoria

particular figure, the vertical total stresses are shown in a darker shade, while the horizontal stresses are shown in a lighter shade. It is clear that there is a distinct difference between the magnitude of the interpreted horizontal stresses and the interpreted vertical stresses, with the vertical stresses being consistently greater.

Also shown for reference are black squares which indicate the approximate vertical total stress at the stations. These values were determined by multiplying the height of tailings above the sensors and the assumed bulk density of the overlying tailings. The height of the tailings was determined by subtracting the known installation elevation of the sensors from the average monthly crest elevation determined by the mine surveyors. This information was included in the monthly monitoring reports provided by the operating contractor on site. Similarly, the density was based on the average bulk density determined from the numerous samples collected from site over the monitoring period.

As shown in Figure 6.7, Stations 2 and 3 are further from the outer wall compared to Station 1. This means that as the dam was raised, the rate of increase in the vertical depth of tailings above the stations was initially the same for all three stations. However, at some point the slope extended over Station 1 such that as the dam continued to be raised, the rate of increase in depth of tailings above Station 1 deviated from the rate of increase in depth of tailings above Stations 2 and 3. Based on the results shown in Figure 6.9(a), it can be seen that this occurred at some point in November 2022. After this point, the estimated vertical stresses for Stations 2 and 3 continued to track the vertical stress estimated from the site elevations as the slope remained far from these stations. Based on the above, it can be seen that there is good agreement with the measured vertical stresses. These indirect checks help provide confidence in the measured stress data.

Upon closer inspection of the horizontal stresses, it can be seen that initially negative values were interpreted. This is more pronounced for the horizontal stress at Station 3. Although these values are small (less than 10 kPa), it is important to determine whether these are true negative pressures caused by tensile forces in the soil, or whether these are artifacts of the interpretation methods due to temperature effects, and not true tensile forces in the soil. This was one the main reasons for the Drying Box 2 experiment.

As was discussed in Section 5.6.2, and as will be shown in Section 7.4, it is believed that these interpreted negative stresses are not a result of tensile forces in the soil but rather a result of small temperature influences. These influences are difficult to correct but become less of a concern once the magnitudes of the variation in temperature reduces, which naturally occurs as the height of the overlying tailings increases with time. Therefore, it was decided that no changes to the

© University of Pretoria

interpretations were necessary.

Figure 6.9(b) shows the response from the tensiometers. Excellent correlation can be seen between the tensiometer pairs at each station. As expected, there are rapid changes in the pore pressure due to deposition and subsequent drying. Therefore, the use of the TEROS 21 WPS would not be particularly useful at this stage of the monitoring. During this period, the pore pressures recorded from the tensiometers fell within a fairly narrow band of -35 kPa and 5 kPa. Interestingly, the tensiometers at Station 1 (closest to the outer wall), reported pore pressures in a much narrower band of between -10 kPa and 0 kPa.

Figure 6.9(c) shows the interpreted VWC of the tailings, as well as the rainfall recorded on site. Although it is difficult to see on this graph, the influence of rainfall on the response from the was meaningful initially, when the sensors were close to surface. However, this influence gradually reduced over time as the height of the overlying tailings increased.

Figure 6.9(d) shows the interpreted stress ratios. After some initial variability, the stress ratios appear to stabilise to a fairly narrow band of between 0.4 and 0.5. Unlike the Drying Box experiments, this stabilisation was not simply due to the large magnitude of suction developed in the soil compared to the total stress values. In this case, moderate total stress values were measured and the suctions were not as large in comparison to the total stresses. This is discussed further in Section 7.2. The interpreted stress ratios also show a good correlation with the stress ratio estimated using the Jaky (1944) equation.

© University of Pretoria

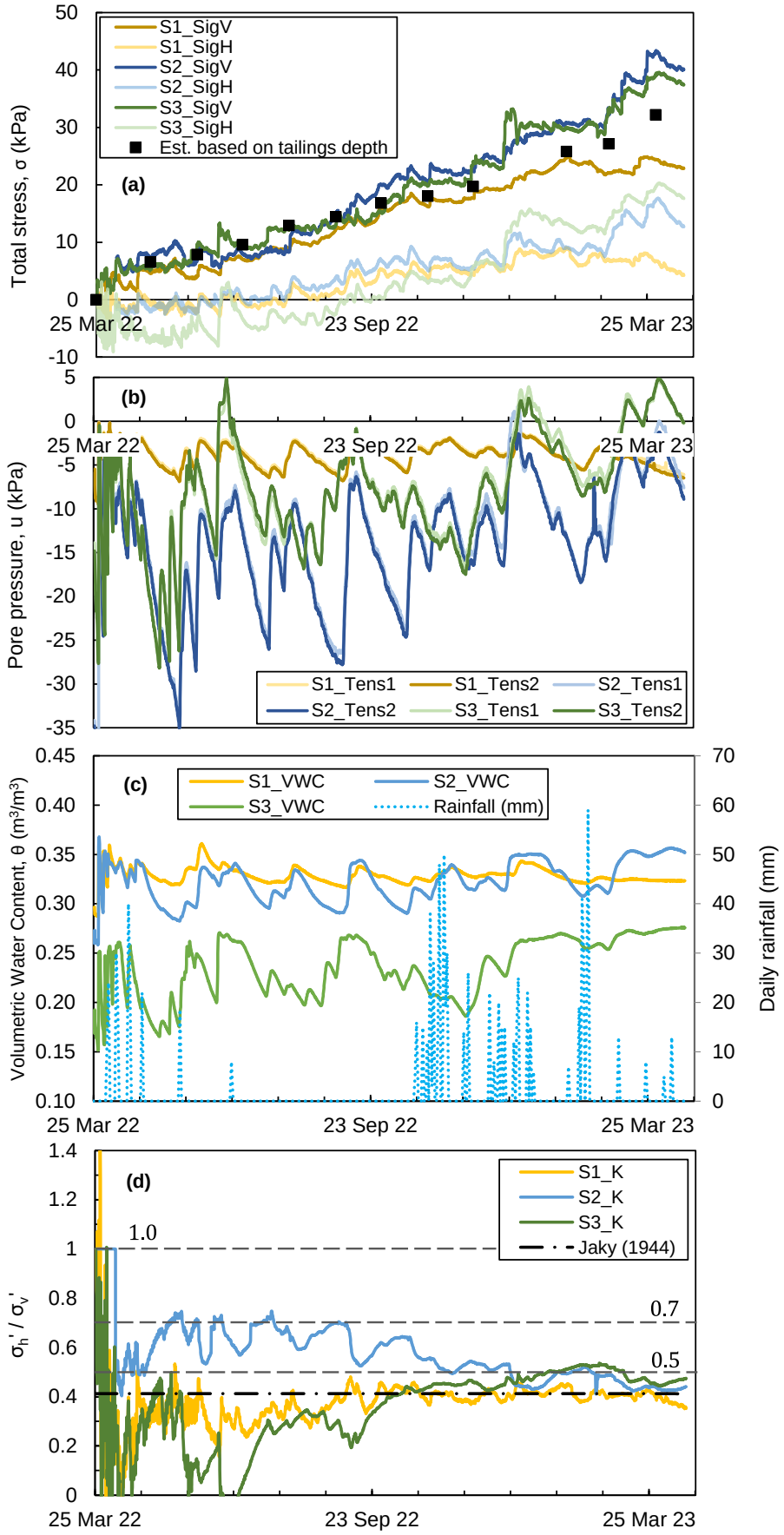


Figure 6.9: Results from the gold site, prior to the step-in showing: (a) total stresses, (b) pore pressures, (c) VWC, and (d) stress ratios

© University of Pretoria

6.2.3.4 Combined data (entire period)

Figure 6.10 shows the results from the remote monitoring system for the gold site over the entire monitoring period., from March 2022 to June 2024. Figure 6.10(a) shows the results from the EPCs. The black squares, representing the estimated vertical stress based on the height of tailings above the sensors, show a good correlation to the vertical stresses determined calculated for the EPCs at Stations 2 and 3. Due to several incidents of industrial action towards the end of 2023, there were many days of interrupted production at the plant. The tonnages sent to the tailings dam were therefore lower in these months which resulted in virtually no increase in the height of the tailings dam during this time.

Figure 6.10(b) shows the results from the tensiometers. Remarkably, over the two-year period, all four tensiometers at Stations 2 and 3 are still providing reliable results. Unfortunately both tensiometers at Station 1 cavitated shortly after the step-in. Over the monitoring period, the pore pressures at the gold site varied between -35 kPa and 5 kPa. The effect of the reduced tonnages in increasing the suctions can also be seen in this figure. A key aspect that this figure shows is the reliability of the suctions within the tailings dam over this period. This is particularly important if suction is to be considered in the strength component of the soil in design and safety evaluations. At these depths of approximately 3.5 m, there appears to be very little influence of rainfall on the pore pressures.

Figure 6.10(c) shows the interpreted VWC at the three stations. During the recent rainy season, it can be seen that there is hardly any response in the VWC to the daily rainfall events. Over the monitoring period, the VWC was noted to vary between 0.26 and 0.37 m^3/m^3 for Stations 1 and 2, and between 0.15 and 0.28 m^3/m^3 for Station 3. As shown in Figure 6.15, these VWC result in a degree of saturation of between 60 and 100%.

Figure 6.10(d) shows the interpreted stress ratio over the monitoring period. After some variability in the first nine months, these ratios appear to have stabilised. Based in this figure, the in-situ stress state at the gold tailings dam, defined by the geostatic stress ratio, appears to vary between a fairly narrow band of 0.4 and 0.6. For the period from October 2022 to June 2024, this stress ratio was found to average 0.48, with a standard deviation of 0.04.

Figure 6.11 shows the VWC and suction values measured over the entire monitoring period at the gold tailings site. Also plotted on this figure is the Fredlund & Xing (1994) fit of a laboratory measured drying SWRC. It can be seen that although the response is similar for all three stations, the magnitude of the VWC for Station 3 is distinctly different to the VWC values measures at Stations 1 and 2.

© University of Pretoria

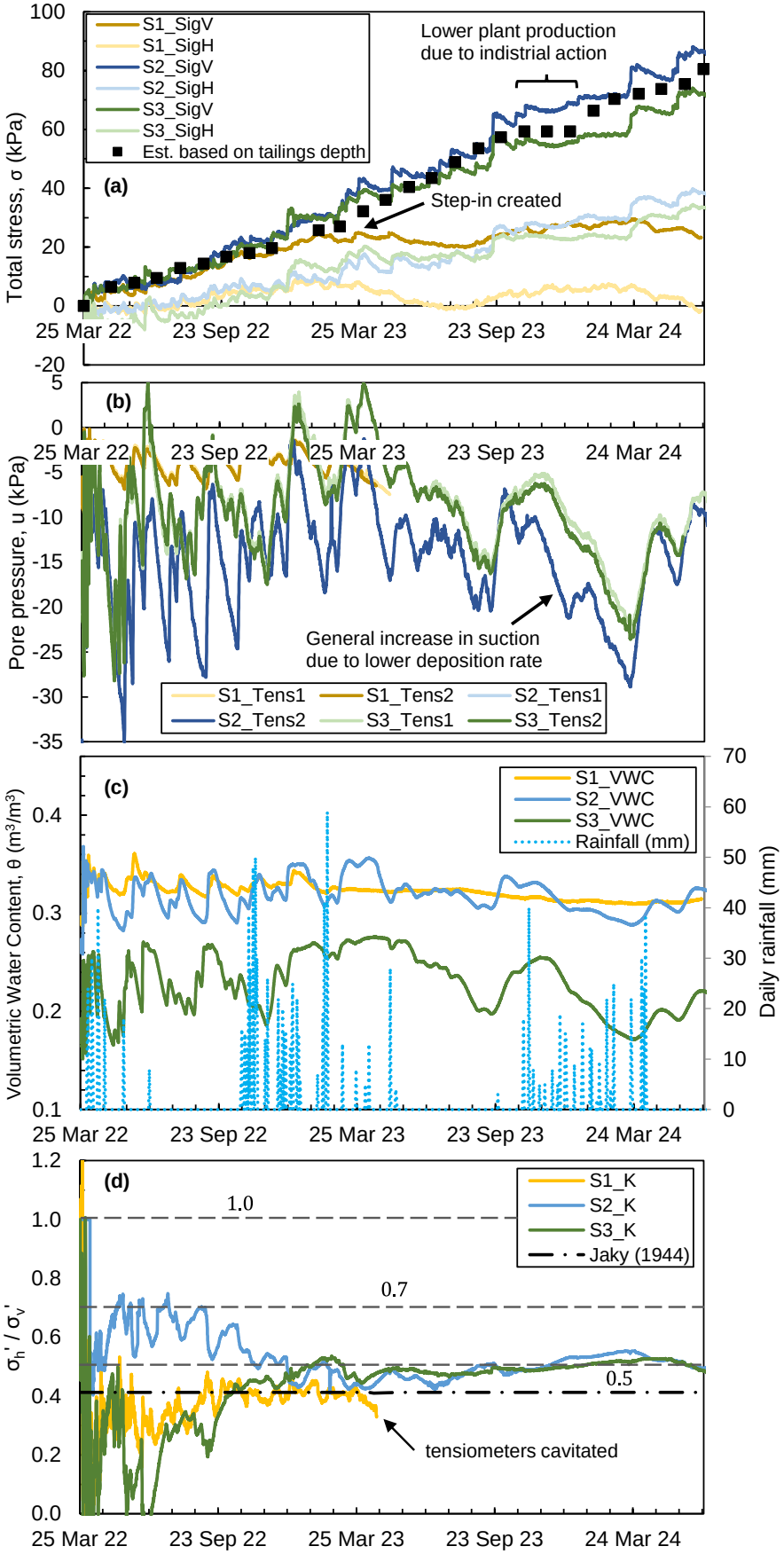


Figure 6.10: Results for the gold tailings site over the entire monitoring period showing: (a) total stresses, (b) pore pressures, (c) VWC, and (d) stress ratios

© University of Pretoria

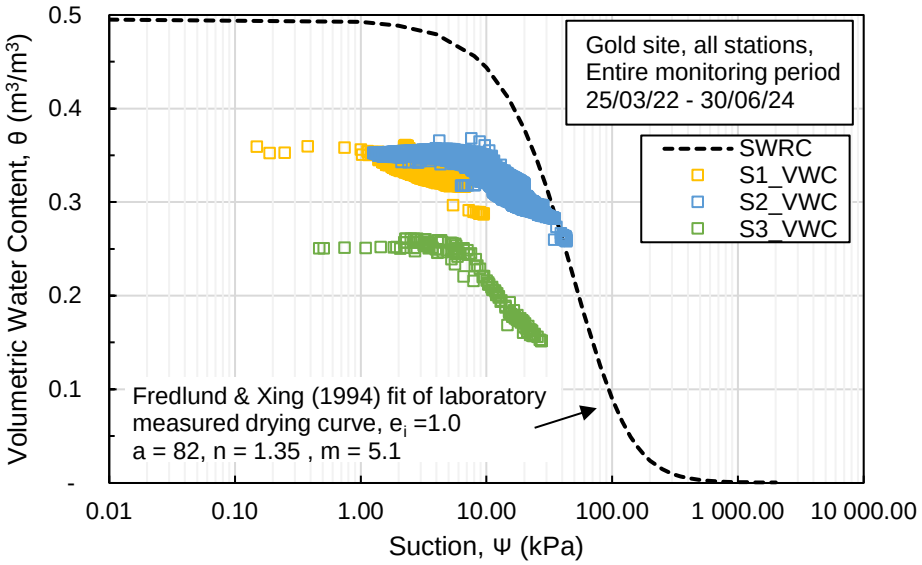


Figure 6.11: VWC and suction values measured at the gold tailings site

6.2.3.5 Stress paths

Although it is interesting to observe the changes in stress, pore pressure and moisture content varying with time, it would be more useful to view these changes from a CSSM perspective. One way to achieve this is to use stress invariants and plot stress paths. The stress invariants s' and t were calculated according to Equation (12) and Equation (13), respectively.

$$s' = \frac{1}{2}(\sigma'_v + \sigma'_h) \tag{12}$$

$$t = \frac{1}{2}(\sigma'_v - \sigma'_h) \tag{13}$$

Figure 6.12 shows the interpreted stress paths for Station 2 at the gold site for the period from 1 November 2022 to 9 December 2022. Two cycles comprising a wetting and drying phase are shown. The first phase shows the drying period where there is a progressive increase in effective stress. The second stage show the large reduction in effective stress as a result of the wetting process caused by routine deposition. Any increase in total stress is initially masked by the increase in pore pressure due to the wetting. As the material dries again, the effective stress as well as the shear stress increases as part of phase three. This continues until the next wetting cycle starts as shown in phase four. These continuous cycles result in a ratcheting movement can be seen with the stress state gradually moving upwards and to the right when plotted in $t - s'$ space.

© University of Pretoria

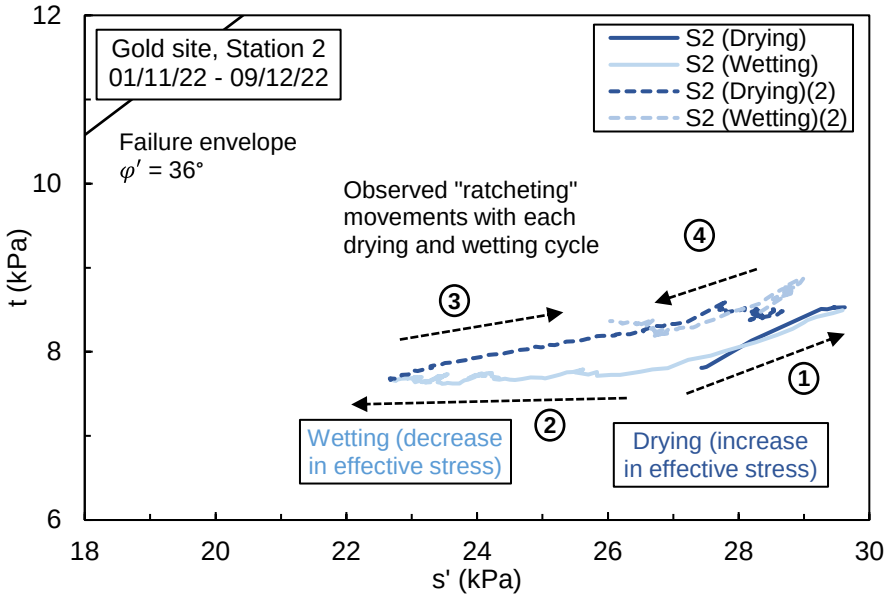


Figure 6.12: Selected stress paths for Station 2

Similarly, key wetting and drying cycles were identified for all three stations in November 2022. This is shown in Figure 6.13. From the figure, it is clear that only small changes occur between subsequent cycles. However, over a longer period of time, these changes can be quite large.

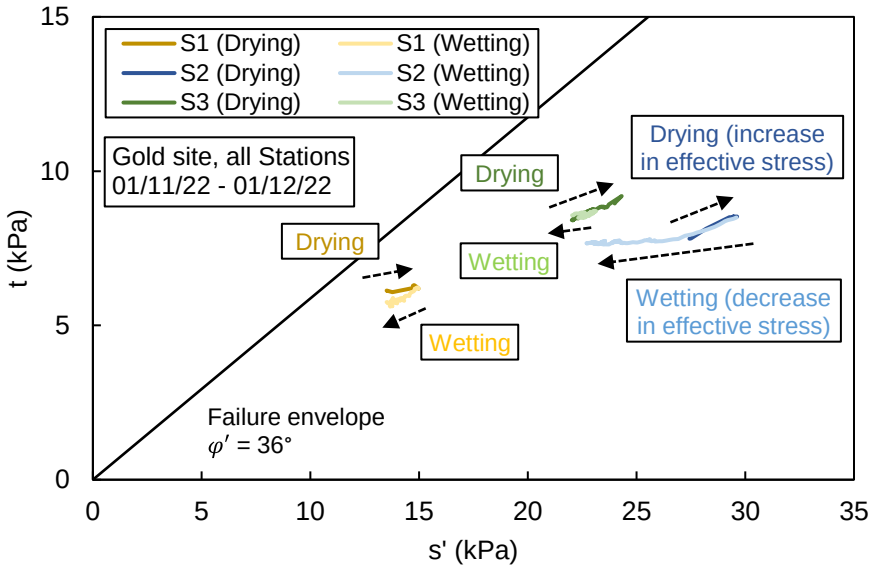


Figure 6.13: Interpreted stress paths for all three stations at the gold site during November 2022

Figure 6.14 shows the results from all three stations over the entire monitoring period. It can be seen that there quite a large difference between the location of the stress paths at the start of the monitoring period, compared to their location at the end. The fact that the stress paths for Station 2 and Station 3 coincide at moderate stresses is supported by the plots of the stress ratio as was

© University of Pretoria

shown earlier. As was seen earlier, there is a general increase from left to right in the stress paths when viewed in $t - s'$ space.

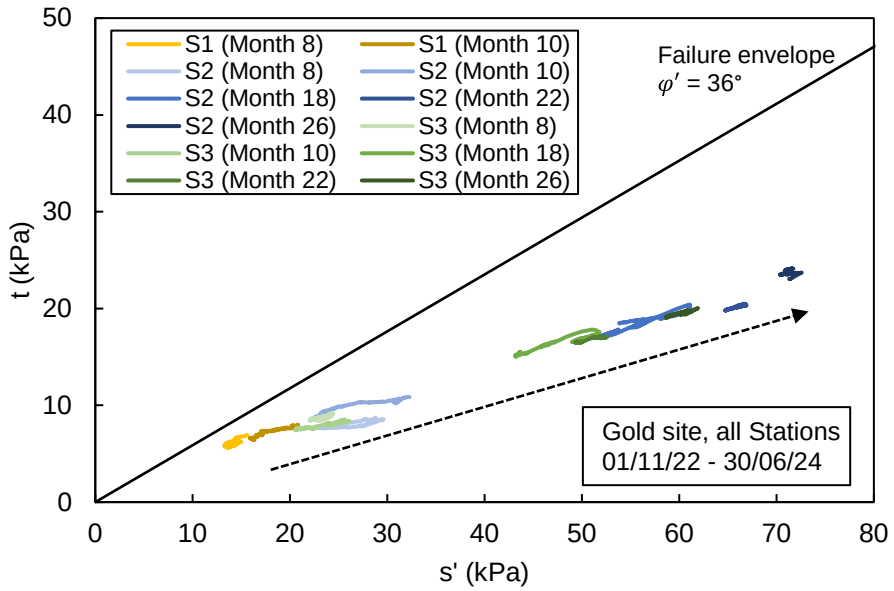


Figure 6.14: Combined stress path results for the gold site

6.2.3.6 Stress ratios

Figure 6.15 shows the S_r (estimated using the VWC as described in Section 5.5) and suction values measured at the gold tailings site. To simplify the plots, it was decided to only present the values at month-end. It can be seen that the values correlate well with the laboratory measured SWRC and that S_r varied between 0.6 and 1.0 over the monitoring period.

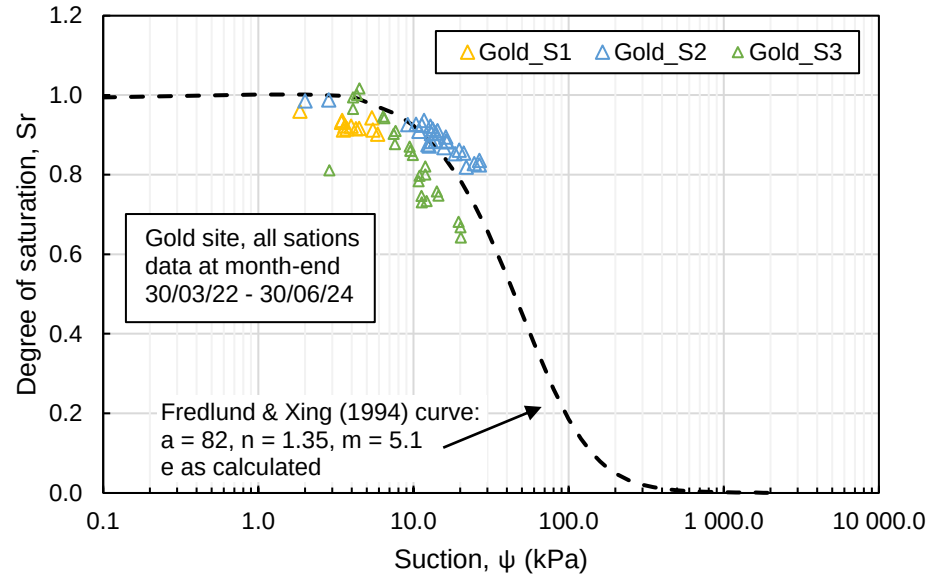


Figure 6.15: Month-end Sr and suction values at the gold tailings site

© University of Pretoria

Figure 6.16 shows the month-end stress ratios measured at the gold site. Although there is some initial scatter, the stress ratio appears to stabilise after six months to a K_0 value of approximately 0.5. This is lower than the value of 0.7 which is commonly assumed for loose, sandy soils (e.g. Bentley Systems, 2023b). At these moderate stress levels, the equation proposed by Jaky (1944) appears to be a lower-bound value for the measured stress ratios. This is in line with the findings of Graham & Jefferies (1986) for loosely deposited Erksak sand.

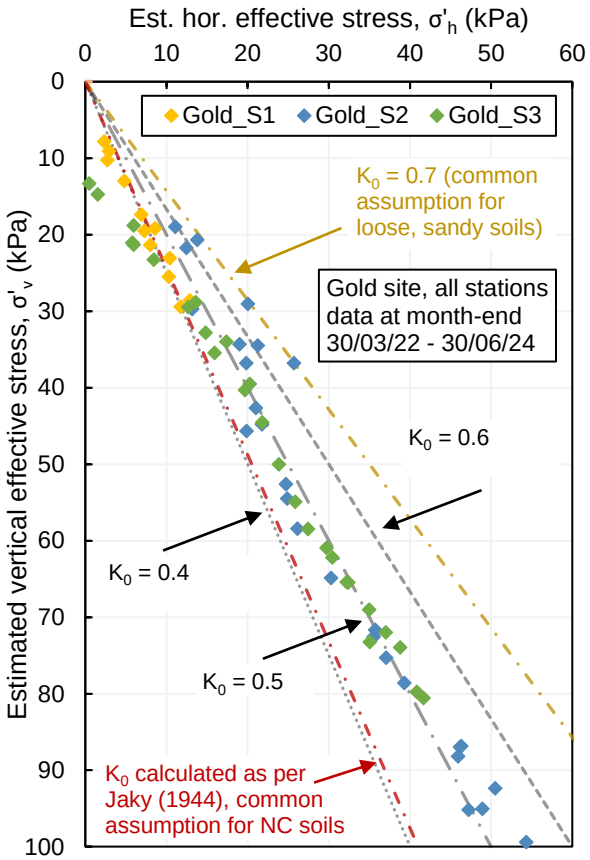


Figure 6.16: Month-end vertical and horizontal effective stresses at the gold site

6.2.3.7 Changes after the step-in

Figure 6.17 shows the ground temperature variations as recorded by the EPCs for the monitoring period at the gold tailings site. Initially, as the EPCs were close to the surface, there were large variations in daily temperature. However, as the depth of the EPCs increased, this daily change in temperature reduced significantly. Over a longer period, the seasonal ground temperature variations can be observed. After start of the step-in construction in March 2023, it can be seen that there is a larger variation in temperature observed for Station 1, when compared to the temperature variations observed for Stations 2 and 3. In the next section, it will be shown how this seasonal variation in temperature had a meaningful influence on the EPCs installed at Station 1,

© University of Pretoria

which were essentially under constant load for the period after the step-in.

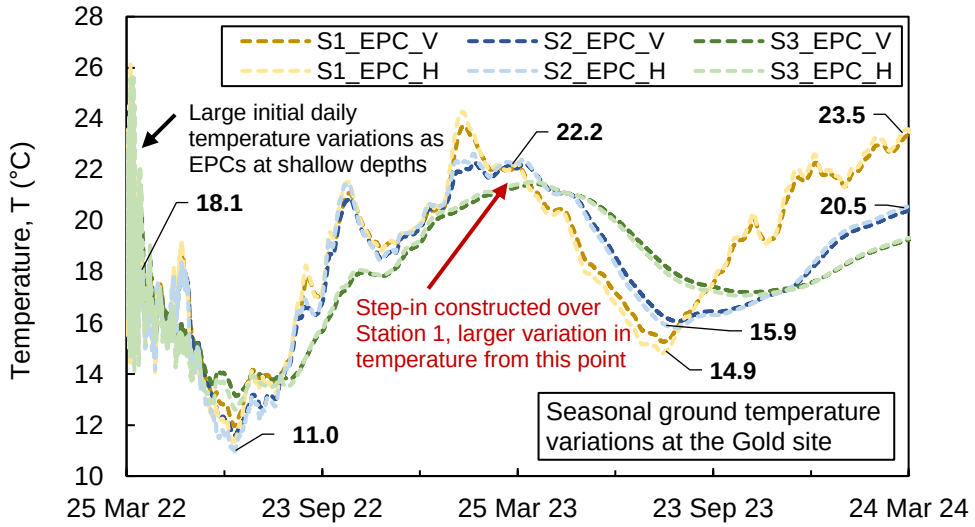


Figure 6.17: Seasonal ground temperature variations at the gold site

Figure 6.18 shows the results from the remote monitoring system at the gold site for the EPCs at Station 1 after the step-in. Figure 6.18(a) shows the temperatures recorded by both EPCs. It can be seen that over the 10-month monitoring period, a change in temperature of between 7°C and 8°C was noted for the vertical and horizontal EPCs. This change in temperature is due to seasonal changes and is dampened due to the presence of approximately 1.5 m of tailings above the sensors. Temperature readings recorded using the logger at surface indicated ambient temperature changes of approximately 18°C over the same period.

Figure 6.18(b) shows the frequency response from both the horizontal and vertical EPCs. It can be seen that there is a very similar change in frequency for the two EPCs, with both values being approximately 12 Hz. The unit change in frequency as a result of temperature changes for the two EPCs can be calculated as 1.5 Hz/°C, 1.6 Hz/°C for the horizontal and vertical EPCs installed at Station 1, respectively. Although it is known that the interpreted stress is influenced by the square of the frequency and not the frequency itself, it is believed that it is still useful to quantify the observed thermal influence in terms of the frequency. This allows direct comparison of the magnitude of observed changes in measured frequency due to true applied pressure changes and those changes only due to temperature effects.

Figure 6.18(c) shows the interpreted stress for the EPCs. It can be seen that there is a change in stress for both EPCs, even though no change in stress was applied to the EPCs on site. These changes in interpreted stress are fairly similar for the horizontal and vertical EPCs and are

© University of Pretoria

approximately 9 kPa in magnitude. The unit change in interpreted stress as a result of temperature changes can be calculated as 1.1 kPa/C and 1.2 kPa/C for the horizontal and vertical EPCs for Station 1, respectively.

Additional details regarding this monitoring period are provided in Appendix B.

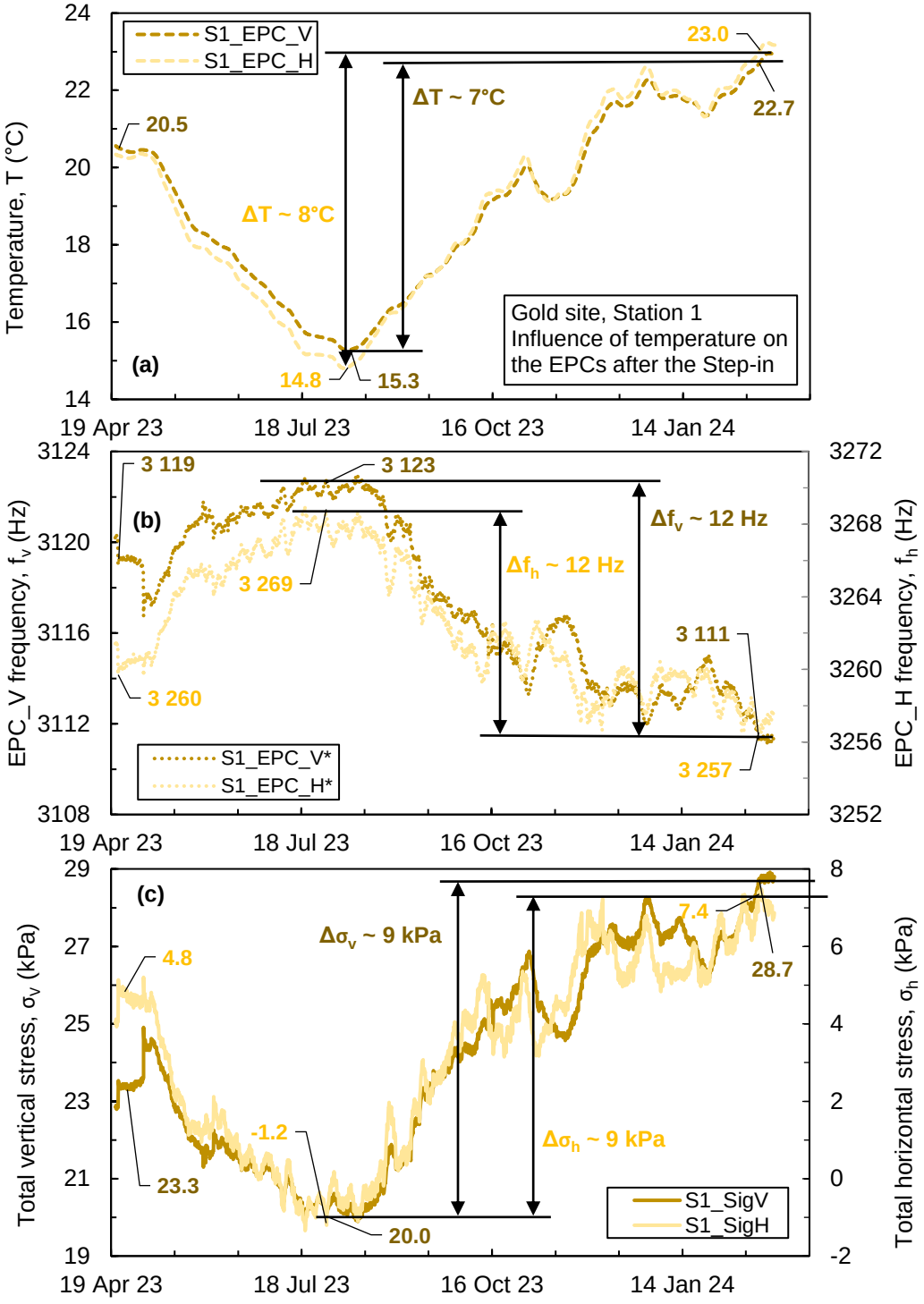


Figure 6.18: Influence of temperature on the EPCs installed at Station 1, after the step-in showing: (a) temperatures, (b) EPC frequencies, and (c) interpreted total stress

© University of Pretoria

6.3 IRON ORE TAILINGS SITE

6.3.1 Site description

The iron ore tailings site used for this study is located in the Northern Cape Province of South Africa. The mine has a single, upstream constructed tailings dam which was historically split into eight compartments: four outer compartments designed to store the coarser tailings and four inner compartments designed to store the finer tailings.

A ring-main delivery system is installed around the perimeter of the dam and the tailings is hydraulically deposited using a spigot system with target slurry density of 1.35 t/m^3. A gravity penstock at the centre of each compartment is used to remove excess water off the dam. This water is stored in a dedicated return water dam. The deposition plan is designed such that each compartment has periods of activity, followed by periods of rest where the tailings is allowed to consolidate, as recommended by Donaldson (1960).

This site presented a unique opportunity as there would be two installations: a surface installation, similar to the gold and platinum installations, as well as a deep installation. This was possible due to the excavation of a trench for an outfall pipe for a new decanting system that was to be installed. Unfortunately, there was a last-minute change in deposition plans for both the compartments where the shallow and deep installations were installed. Therefore only short-term data are presented for the shallow installation during the period when the dam was active. However, this presented an opportunity to observe the long-term response of the EPCs under a constant load.

Based on testing conducted by the EoR, the iron ore tailings can be characterised using a φ' of 28°. With a surface area of 42 ha and a monthly deposition of 200 000 t, the compartments are raised at an average RoR of 0.9 m/year. Figure 6.19 shows a grading curve of the fine and coarse samples of the iron ore tailings. It can be seen that the grading of the coarse tailings is similar to the grading of the gold tailings, while the fine tailings is significantly finer.

© University of Pretoria

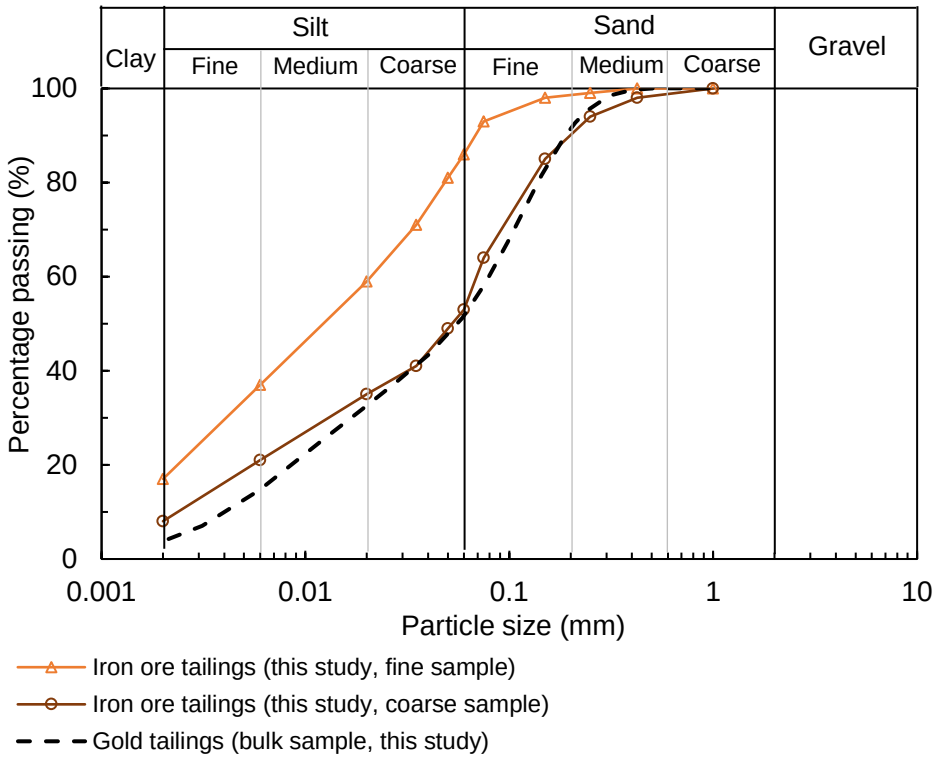


Figure 6.19: Grading curves for the iron ore tailings, compared to the gold tailings

XRD testing was conducted on samples of the iron ore tailings obtained in the basin, near the monitoring sites. A summary of this testing, showing the approximate mineralogical composition of the iron ore tailings is shown in Table 6.3. As with the other tailings samples, Carbon was used to coat the material before testing. It can be seen that the majority of the sample comprises Hematite with smaller quantities of Quartz, Muscovite and Kaolinite. The XRD spectrograph of the iron ore tailings basin sample is provided in Appendix B.

Table 6.3: Composition of the iron ore tailings (basin sample)

Mineral	**Composition (%)**
Hematite	87.4
Quartz	10.5
Muscovite	1.4
Kaolinite	0.7

6.3.2 Installation details

The shallow installation comprised two installations at surface while the deep installation comprised a single installation at a depth of 8 m below the tailings surface. As shown in Figure 6.20, the

© University of Pretoria

shallow installation included two stations approximately 20 m apart from each other. The intent was to monitor the response from the remote monitoring system due to the influence of routine deposition and subsequent drying. Unfortunately, due to changes to the planned deposition schedule, there were extended periods where no deposition occurred. The test therefore comprised three distinct phases. The first phase occurred prior to deposition on the dam, the second phase occurred while the dam was active, and the third phase occurred after deposition ceased on the dam. Details of these three phases, as well as key events at the iron ore site are shown in Table 6.4.

Table 6.4: Key events at the iron ore site

Date	**Event**
31 March 2022	Installation of Station 1 and Station 2 (shallow installation)
23 May 2022	Tensiometer replacements at Station 1 and Station 2
01 June 2022	Start of deposition on Compartment 1 (shallow installation)
31 August 2022	Installation of Station 3 (deep installation)
30 November 2022	End of deposition on Compartment 1
28 August 2023	Start of excavation backfilling at Station 3
29 September 2023	End of excavation backfilling at Station 3

The first phase covered a two-month period starting in March 2022, where no deposition occurred on the compartment. During this period, the EPCs were exposed to low stresses (approximately 3 kPa) and were subjected to large daily changes in temperature. All four tensiometers cavitated during this phase.

The second phase started in June 2022 when the compartment was recommissioned. Replacement tensiometers were installed prior to recommissioning. This phase continued for six months. During this period, approximately 1.3 Mt of material was hydraulically deposited onto the compartment which resulted in 1.30 m of tailings being placed above the sensors.

The third phase covered a 10-month period starting in November 2022, when deposition ceased. During this period, the EPCs were exposed to moderate stresses (approximately 27 kPa). Due to the depth of tailings above the sensors, the EPCs were influenced more by the seasonal temperature changes than the daily temperature changes over this period.

Figure 6.20(a) shows the proposed locations of the installations during the planning stage, while Figure 6.20(b) shows a photograph of Station 1 and 2 after installation. Figure 6.20(c) shows the

© University of Pretoria

erected logger boxes. With the exception of the piece of reinforcing steel used to suspend the horizontal EPC, the same process as described for the gold site installation was followed. Instead of suspending the horizontal EPC, the excavation was backfilled with slurried tailings and the EPC was carefully placed within the tailings.

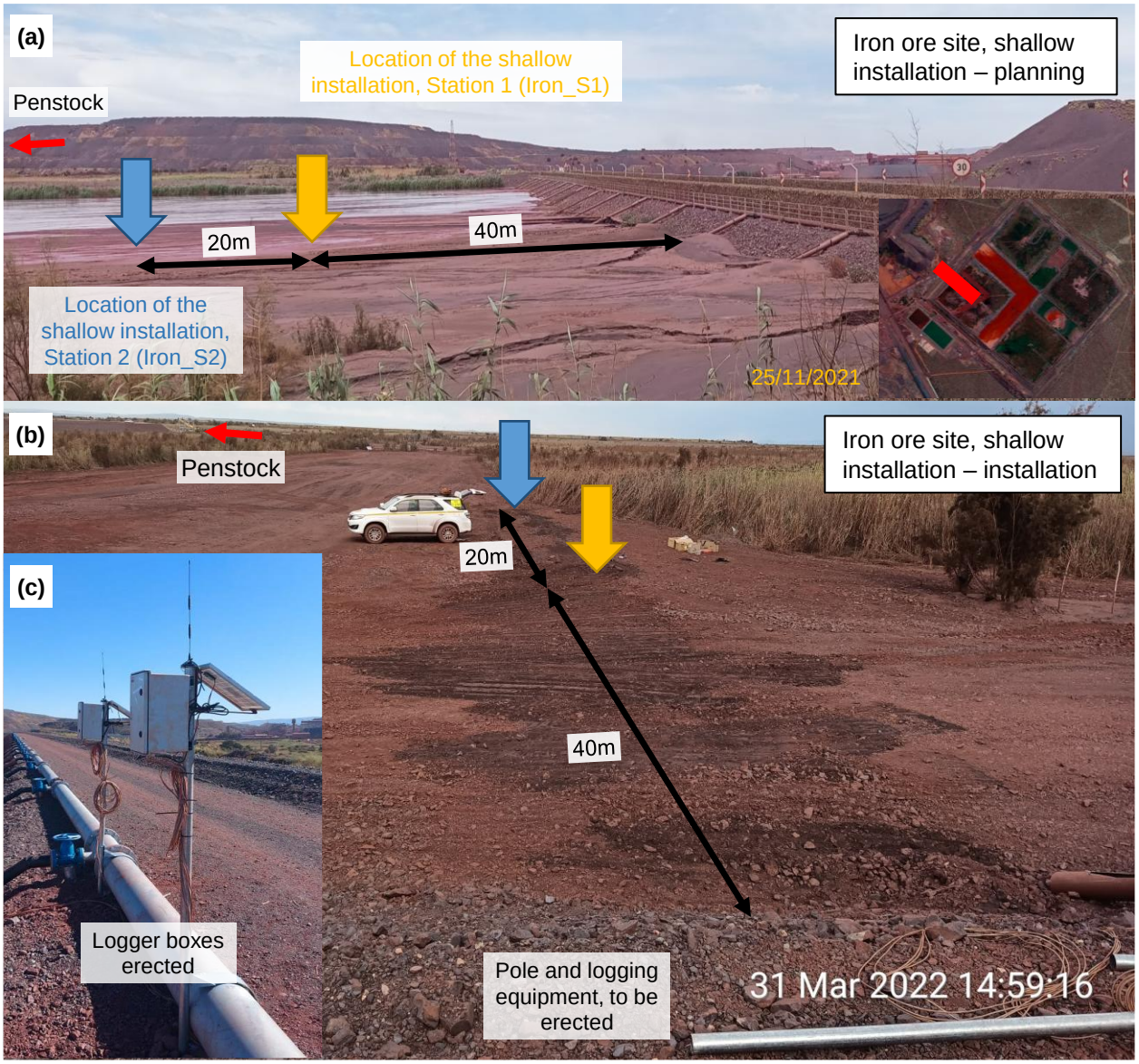


Figure 6.20: Photographs taken for the iron ore shallow installation showing: (a) planning, (b) installation, and (c) the erected logger boxes

Similar issues regarding a change in deposition plan were faced at the deep installation. In particular, the excavation remained open for approximately one year after the installation of the sensors. This extended period resulted in the tensiometers cavitating and significant temperature influences. The deep installation was completed on 31 August 2022.

© University of Pretoria

Like the shallow installation, the deep installation was split into two distinct phases. The first phase covered a 12-month period from August 2022 during which the excavation remained open. The EPCs were therefore exposed to seasonal temperature variations under low stresses. The second phase covered a six-month period from August 2023 to March 2024. During this period the excavation was backfilled but the compartment was not active.

Figure 6.21 shows selected photographs taken during the planning and installation stages of the deep installation. Figure 6.21(a) shows the location of deep installation within the excavation. Figure 6.21(b) shows the completed installation and Figure 6.21(c) shows the erected logger box on an access bench on the outer wall.

© University of Pretoria

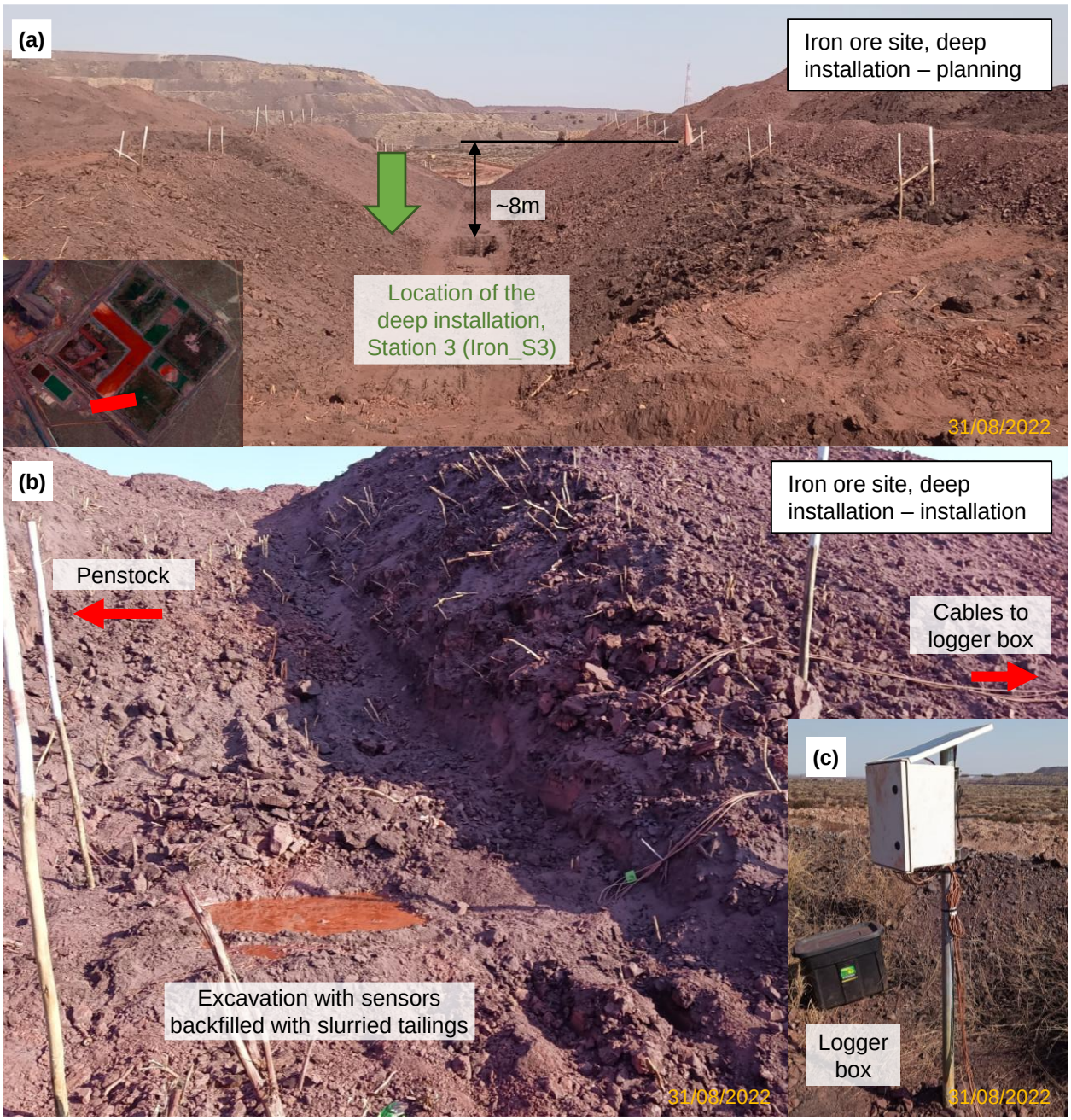


Figure 6.21: Photograph for the deep installation showing: (a) planning, (b) installation, and (c) the erected logger box

6.3.3 Results – shallow installation

The results are split into several sections. The first section shows the data recorded during the first month of monitoring. The second section shows the period prior to deposition, where meaningful daily temperature influences were noted on the response from the EPCs. The third section focusses on the six-month period when the compartment was active. This section is followed by a period of over 12 months where the EPCs seemed to be influenced by seasonal temperature

© University of Pretoria

variations. Finally, the interpreted stress paths are shown for the period when the compartment was active.

6.3.3.1 Initial data (first month)

Results from the first month of monitoring are provided for Station 1 and 2 at the iron ore site in Appendix C. Details of the first deposition event are provided, as well as installation details for the tensiometers. The zero readings for the EPCs and tensiometers are also shown for reference. What is also of interest is the interpretation of the raw data reported from the sensors, and the conversion to engineering units. This is done by showing a side-by-side comparison of the raw and interpreted data for each sensor.

6.3.3.2 Initial data (selected months)

Figure 6.22 shows the VWC and suctions measurements for the two stations at the shallow iron ore installation during the first wetting and drying phases. In the initial drying stages there is a marginal change in the VWC for a moderate change in suctions which start from close to zero. This indicates that the soil is near saturation after first rewetting. The saturated VWC for the two stations is shown for reference. Additional details noted for the various sensors for selected months can be found in Appendix C.

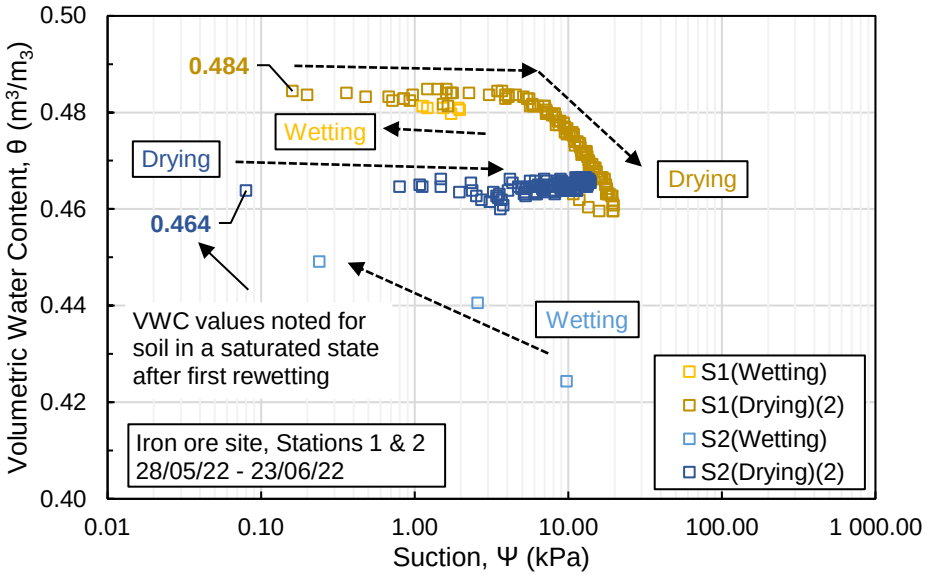


Figure 6.22: VWC and suction measurements during the first wetting and drying cycles at the shallow iron ore installation

© University of Pretoria

6.3.3.3 Temperature influences (prior to recommissioning)

Figure 6.23 shows the influence of temperature on the readings from the EPCs at the iron ore site, prior to recommissioning of the compartment. Figure 6.23(a) shows the temperature recorded by each EPC. In general, there is a good correlation between the four EPCs. It can be seen that over the two-month monitoring period, a change in temperature of approximately 10°C was noted. This change in temperature is due to daily temperature changes and is dampened somewhat due to the presence of approximately 0.15 m of tailings above the sensors. Temperature readings recorded from the logger installed on surface indicated changes in ambient temperature of 21°C over the same period.

Figure 6.23(b) shows the frequency response from the EPCs installed at both Station 1 and Station 2. There is a difference in the change in frequency for the four EPCs, with the vertical EPCs showing a larger frequency change, compared to the horizontal EPCs. Only the vertical EPC will be assessed in further detail in this section. Frequency changes of 30 Hz and 43 Hz were recorded for the vertical EPCs. The unit change in frequency as a result of temperature changes for the two EPCs can be calculated as 3.1 Hz/°C and 4.4 Hz/°C for the vertical EPCs installed at Station 1 and Station 2, respectively.

Figure 6.23(c) shows the interpreted stress for the EPCs. It can be seen that there is a change in interpreted stress for all four EPCs, even though no stress was applied to the EPCs during the monitoring period. As was noted for the frequency changes, a larger difference in interpreted stress was noted for the vertical EPCs, when compared to the horizontal EPCs. These changes in interpreted stresses vary between 24 kPa and 29 kPa. The unit change in interpreted stress as a result of temperature changes can be calculated as 2.9 kPa/°C and 2.5 kPa/°C for the vertical EPCs installed at Station 1 and Station 2, respectively.

© University of Pretoria

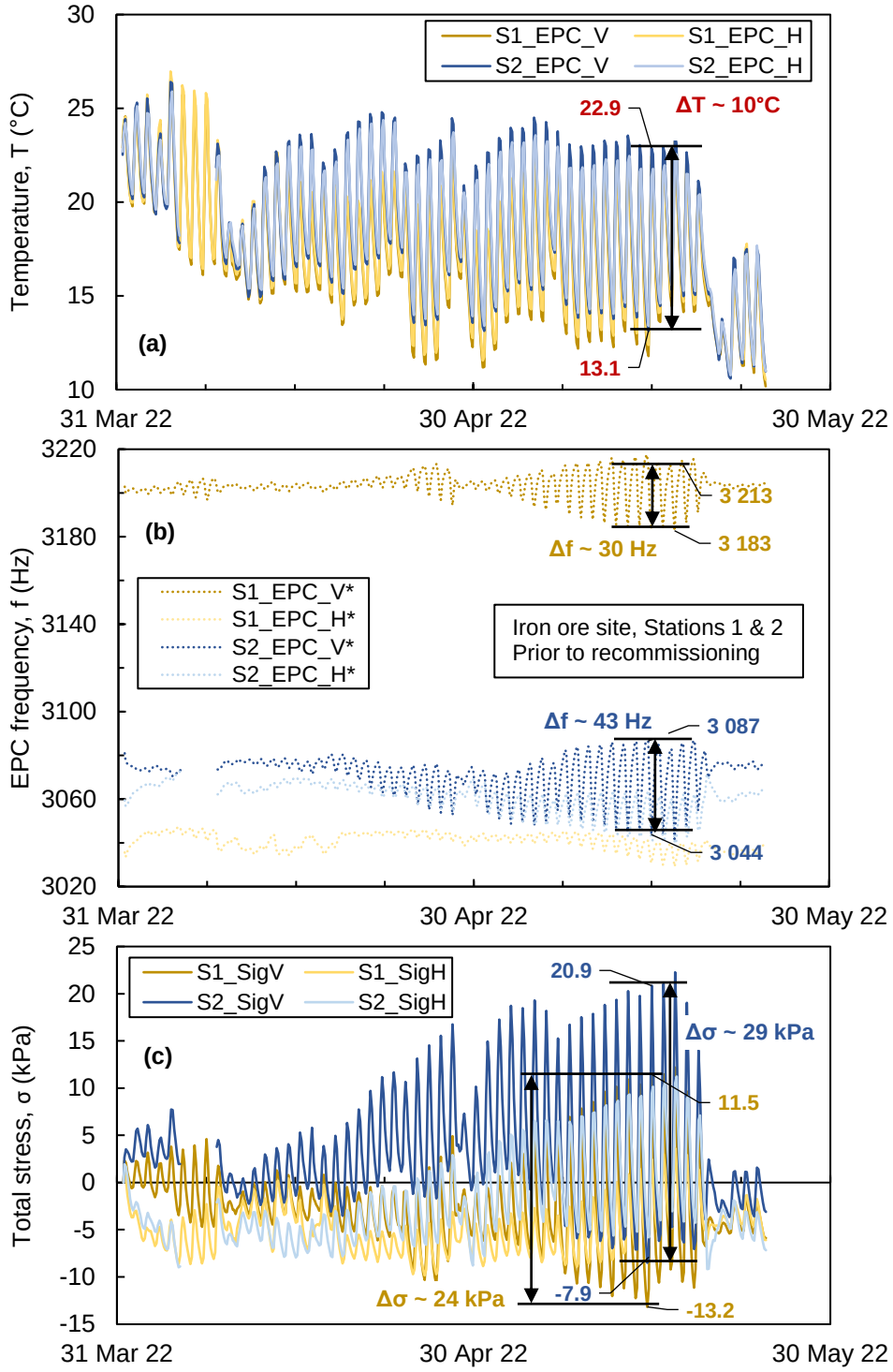


Figure 6.23: Temperature influences prior to recommissioning showing: (a) temperatures, (b) EPC frequencies, and (c) interpreted total stresses

6.3.3.4 Active period

Figure 6.24 shows the results from the remote monitoring system at the iron ore site for the period when the compartment was active. Figure 6.24(a) shows the interpreted total stresses, as well as the same black squares that were shown for the gold site representing the estimated vertical

© University of Pretoria

stresses. It can be seen that there is not a good correlation between this indirect check and the response noted from the vertical EPCs at either station. The stresses noted at Station 1 are smaller, while the stresses noted at Station 2 are larger. Interestingly, there is also an initial period where the interpreted stresses are negative.

Figure 6.24(b) shows the pore pressures recorded by the tensiometers. Although there is a fair correlation between the tensiometer pairs at each station, the correlation is not as good as was noted on the gold site. It can also be seen how the tensiometers immediately started showing large negative pressures once deposition had ceased. All four tensiometers cavitated within 15 days of deposition ceasing on the compartment. In this case, it would have perhaps been useful to have the TEROS 21 WPS installed so that the monitoring of the suctions could have continued.

Figure 6.24(c) shows the interpreted VWC from the TEROS 12 moisture probes. As was seen in the EPC data, there appears to be a difference in the behaviour of the tailings at the two stations, despite the stations being only 20 m apart on site.

Figure 6.24(d) shows the interpreted stress ratios. Before the drying out period, these ratios appeared to be stable. For Station 1, this ratio stabilised at 0.7, while for Station 2, this ratio stabilised at 0.5. The reason for this difference in stress ratio for the two adjacent stress stations in unclear. The interpreted stress ratio for Station 2 showed good correlation with the estimated stress ratio determined using the Jaky (1944) equation. For the period from 01/09/2022 to 30/11/2022, this stress ratio was found to average 0.70, with a standard deviation of 0.09.

© University of Pretoria

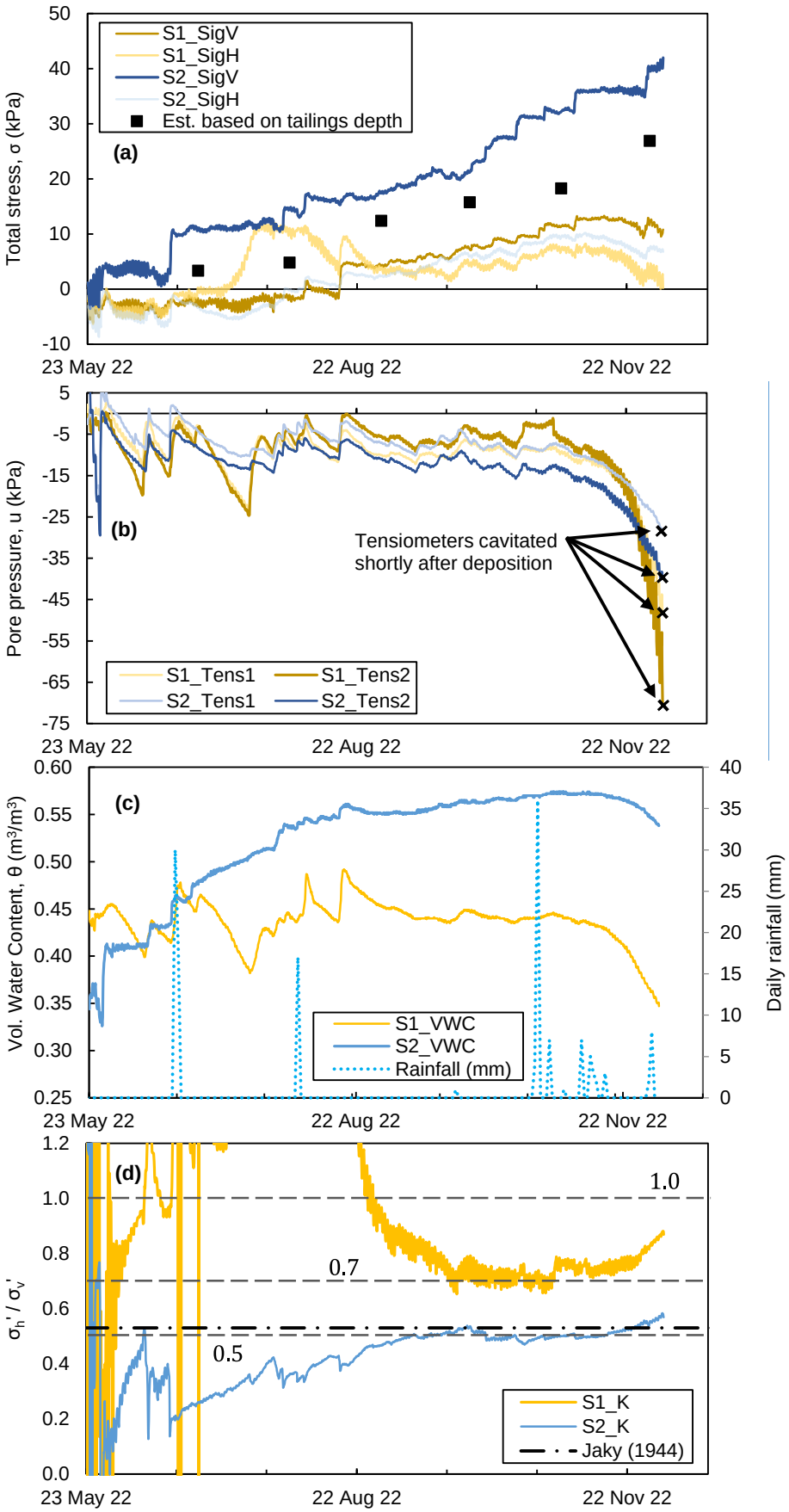


Figure 6.24: Results from the shallow installation at the iron ore site showing: (a) total stress, (b) pore pressure, (c) VWC, and (d) stress ratios

© University of Pretoria

Figure 6.25(a) shows the VWC and suction response from both stations at the shallow iron ore installation. It can be seen that in general there was not a very large change in moisture content while the compartment was active. However, a peculiar trend is noted for Station 2. This is shown in greater detail in Figure 6.25(b). The reason for this behaviour is perhaps explained by the long-term response of the moisture probe as shown in Figure 6.26. Based on this figure, it appears that the soil at Station 2 took approximately six months to re-saturate which explains the gradually increasing VWC.

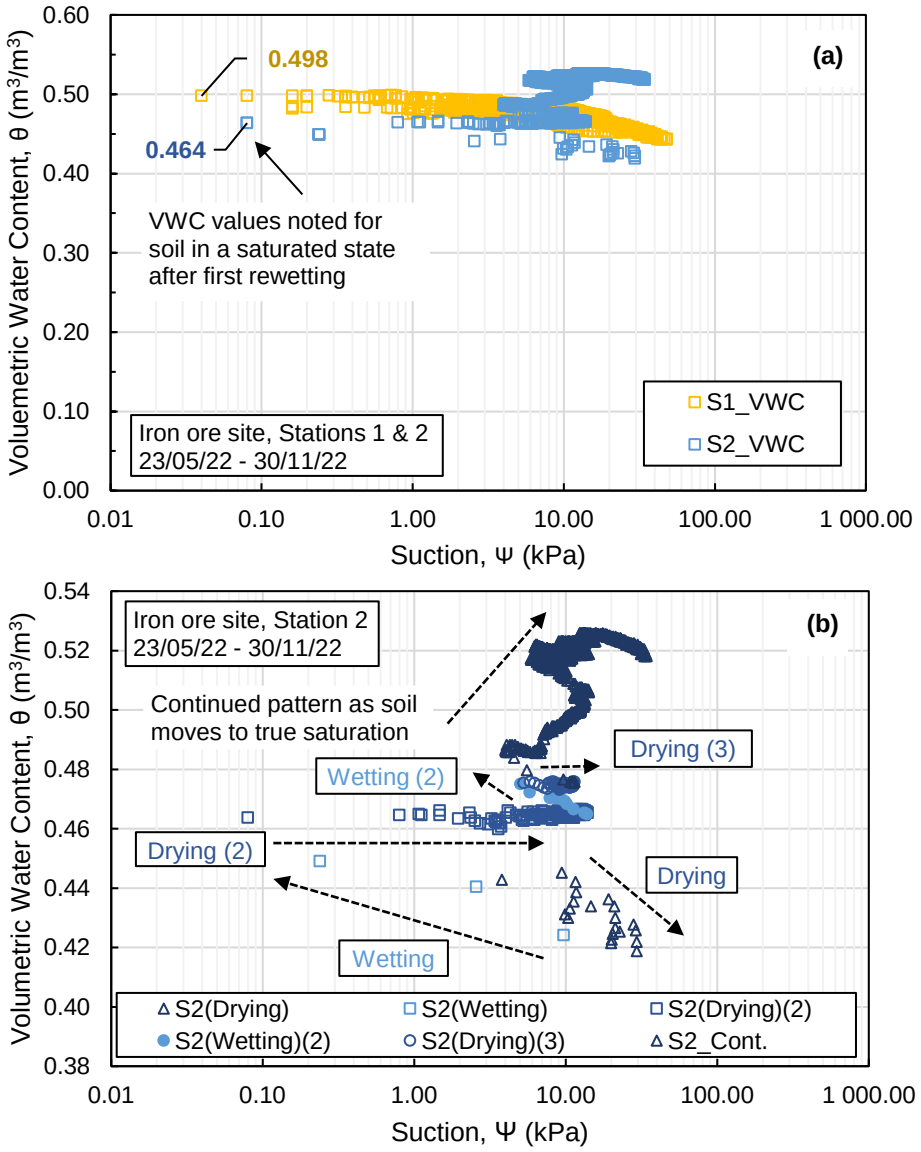


Figure 6.25: VWC and suction responses at the shallow iron ore site for: (a) both stations, and (b) Station 2 only

© University of Pretoria

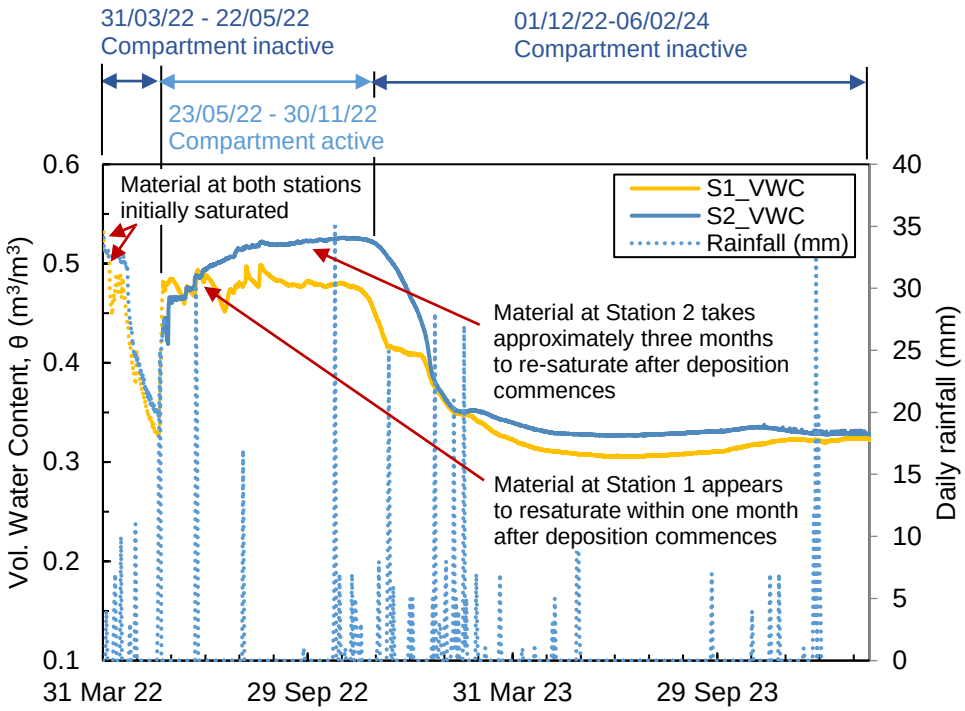


Figure 6.26: VWC responses at the iron ore site (shallow installation)

6.3.3.5 Temperature influences (after deposition ceased)

Figure 6.27 shows the response from the EPCs at the iron ore tailings site after deposition had ceased on the compartment. The purpose of this section is to explore the influence of seasonal temperature variations on the response from the EPCs installed at Station 1 and Station 2, which were essentially under constant load during this period.

Figure 6.27(a) shows the temperature recorded by each EPC. It can be seen that there although the trends are similar, there is a distinct difference in temperature measured at Station 1 and Station 2. Over the eight-month monitoring period, a change in temperature of approximately 13°C was noted for Station 1. A slightly lower change of 11°C was noted for Station 2. Unlike the period before deposition, which was dominated by daily temperature variations, this period was dominated by seasonal temperature changes. This change is also dampened to a larger extent due to the presence of approximately 1.30 m of tailings above the sensors. Temperature readings recorded from the loggers installed at surface indicated ambient temperature changes of 39°C over the same period.

Figure 6.27(b) shows the frequency response from the EPCs installed at both Station `1 and Station 2. It can be seen that there is a difference in the change in frequency for all four EPCs, with the vertical EPCs showing a greater change, compared to the horizontal EPCs. The values ranged

© University of Pretoria

from 61 Hz to 120 Hz. The unit change in frequency as a result of temperature changes for the four EPCs can be calculated as 4.6 Hz/°C and 11.0 Hz/°C for the vertical EPC installed at Station 1 and Station 2, respectively.

Figure 6.27(c) shows the interpreted stress for the EPCs. It can be seen that there is a change in interpreted stress for both EPCs, even though no change in stress was applied to the EPCs over the monitoring period. Larger changes in interpreted stresses were noted for the vertical EPCs, compared to the horizontal EPCs. The change in interpreted stress for the vertical EPCs varied between 50 kPa and 70 kPa. The unit change in interpreted stress as a result of temperature changes can be calculated as 3.7 kPa/°C and 6.5 kPa/°C for the vertical EPCs installed at Station 1 and Station 2, respectively.

© University of Pretoria

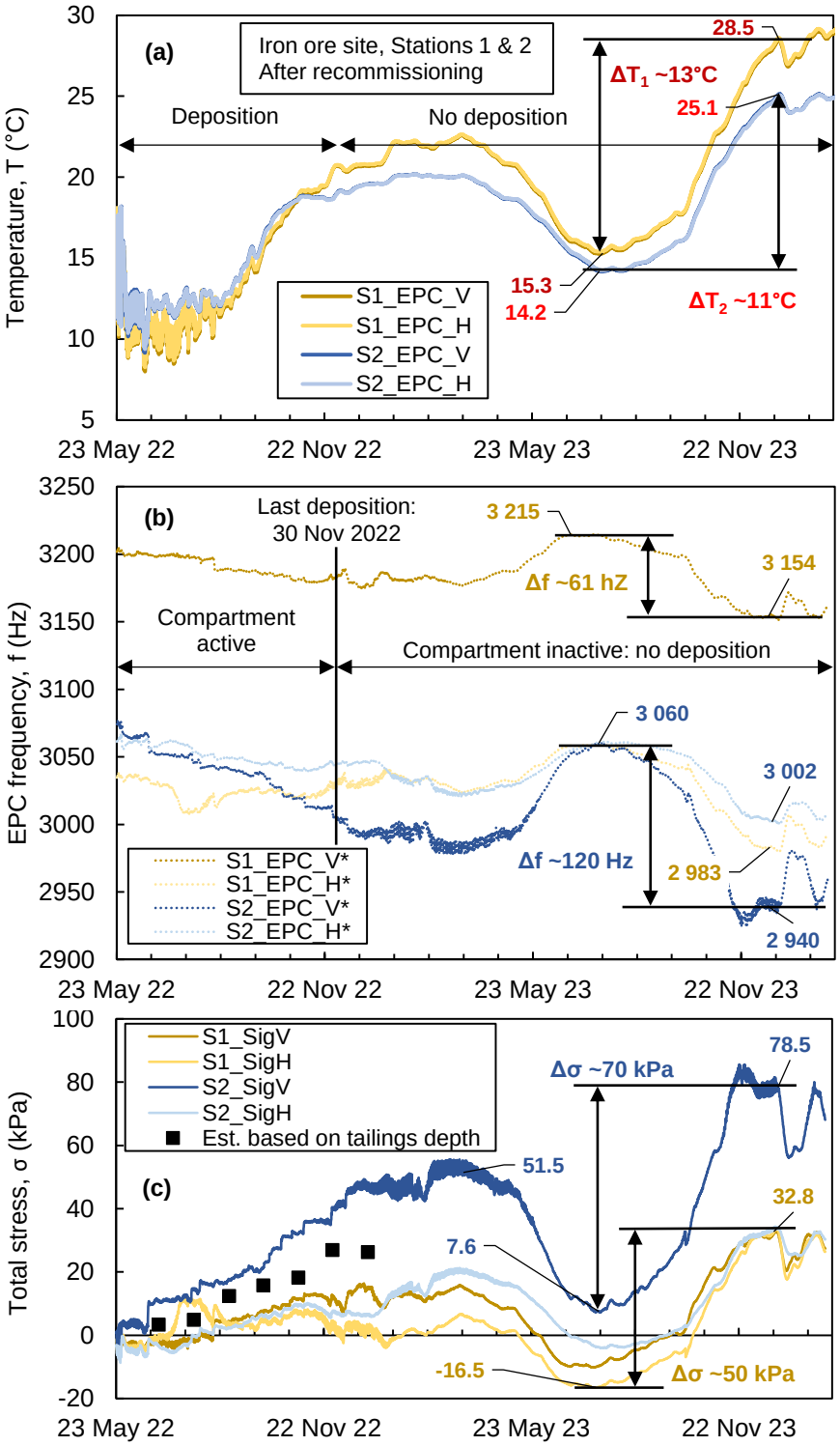


Figure 6.27: EPC response post deposition ceasing showing: (a) temperatures, (b) EPC frequencies, and (c) interpreted total stresses

6.3.3.6 Stress paths

Figure 6.28 shows the stress paths for the shallow installation stations at the iron ore site. As was noted in the stress ratios, the slopes of the stress paths for the two stations are distinctly different.

© University of Pretoria

However, both stress paths clearly show a gradual movement upwards and to the right when plotted in $t - s'$ space.

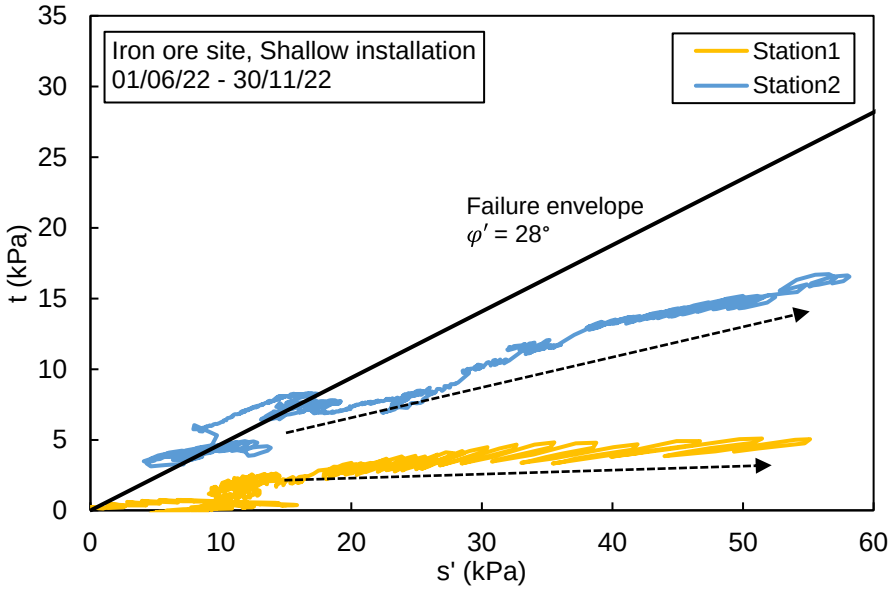


Figure 6.28: Stress paths for the shallow installation at the iron ore site

6.3.3.7 Stress ratios

Figure 6.29 shows the month-end stress ratios for both stress stations at the shallow installation at the iron ore tailings site. This site was the site with perhaps the most uncertainty of the three tailings sites. This uncertainty was largely due to the plasticity of the tailings (see Figure 6.32), the prolific reed growth in the basin (see Figure 6.20(b)), and the relatively short period of activity. As was found for the gold tailings, the equation proposed by Jaky (1944) appears to be a lower-bound for the measured stress ratios. Interestingly, in contrast to the results from the gold site, the results from Station 1 appear to fit quite well with the common assumption of 0.7 for loose, sandy soils (e.g. Bentley Systems, 2023b).

© University of Pretoria

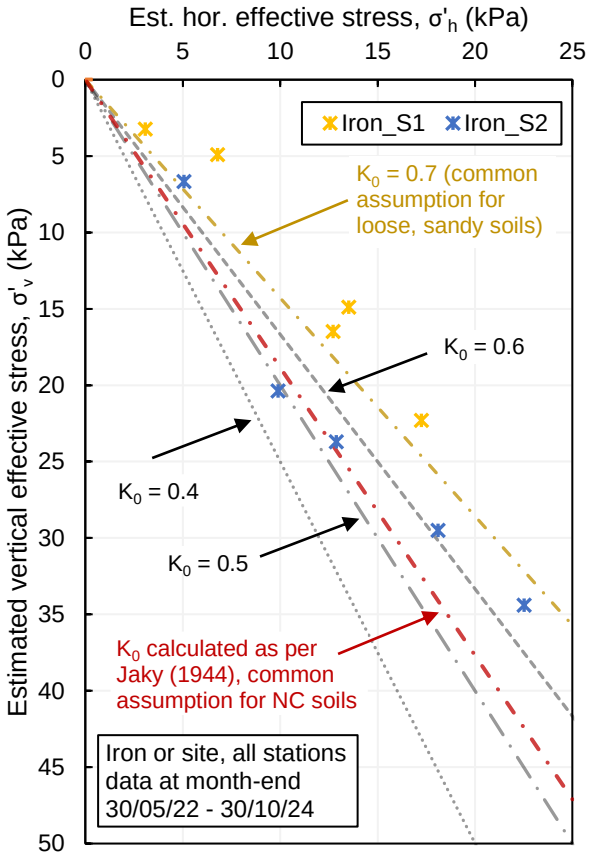


Figure 6.29: Month-end stress ratios for the iron ore tailings site

6.3.4 Results – deep installation

As has been done previously, the monitoring results are split into key stages. The first stage shows the initial data recorded during the first month of monitoring. The second stage shows the seasonal temperature influences on the EPCs prior to the excavation backfilling, while the third stage shows the monitoring data during and after the backfilling. Since there was no deposition on this compartment, no stress path data are provided.

6.3.4.1 Initial data (first month)

Results from the first month of monitoring are provided for Station 3 at the iron ore site in Appendix C. Details of the first deposition event are provided, as well as installation details for the tensiometers. The zero readings for the EPCs and tensiometers are also shown, as well as the interpretation of the raw data reported from the sensors, and the subsequent conversion to engineering units. This is done by showing a side-by-side comparison of the raw and interpreted data for each sensor.

© University of Pretoria

6.3.4.2 Prior to backfilling

Figure 6.30 shows the results of the influence of temperature on the responses recorded from the EPCs for the deep installation at the iron ore site, prior to backfilling of the excavation. Figure 6.30(a) shows the temperature recorded by both EPCs. In general, there is excellent correlation between the two EPCs. It can be seen that over the 12-month monitoring period, a change in temperature of approximately 19°C was noted. This change in temperature is due to seasonal changes and is dampened somewhat due to the presence of approximately 0.15 m of tailings above the sensors. Temperature readings recorded from the logger installed on surface indicated ambient temperature changes of 33°C over the same period.

Figure 6.30(b) shows the frequency response from both the horizontal and vertical EPCs installed at Station 3. It can be seen that there is a change in frequency for both EPCs, with the values being very similar at approximately 16 Hz. The unit change in frequency as a result of temperature changes can be calculated as 0.8 Hz/°C for both the horizontal and vertical EPCs installed at Station 3.

Figure 6.30(c) shows the interpreted stress for the EPCs. It can be seen that there is a change in interpreted stress for both EPCs, even though no change in stress was imposed on the EPCs over this period. These changes in interpreted stresses are similar for the horizontal and vertical EPCs and are approximately 16 kPa in magnitude. The unit change in interpreted stress as a result of temperature changes can be calculated as 0.9 kPa/°C and 0.8 kPa/°C for the horizontal and vertical EPCs for Station 3, respectively. Additional details regarding these temperature changes and their influence on the response recorded from the EPCs are provided in Appendix B.

Figure 6.30(d) shows the response from the TEROS 12 probe and the interpreted VWC. It can be seen that there is a gradual reduction in moisture content of the tailings as the material dried out. Initial attempts were made to keep the tensiometers saturated, but these were soon abandoned when it was realised that the backfilling would be delayed for serval months.

© University of Pretoria

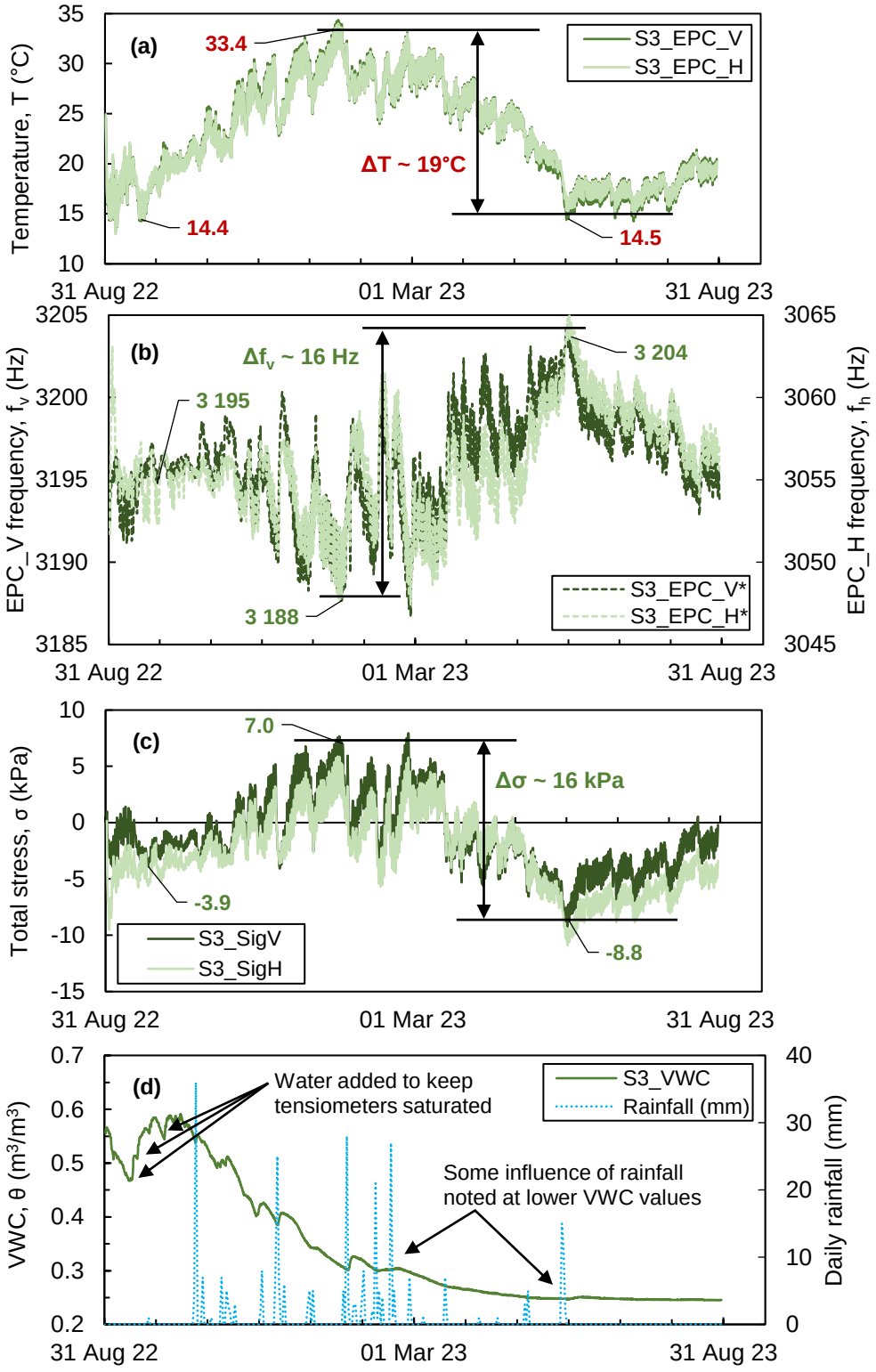


Figure 6.30: Results from the deep installation at the iron ore site showing: (a) temperatures, (b) EPC frequencies, (c) interpreted total stresses, and (d) water content estimates

6.3.4.3 After backfilling

Figure 6.31 shows the results from the deep installation for the entire monitoring period. The

© University of Pretoria

backfilling of the excavation can clearly be seen in Figure 6.31(a), with activities commencing on the 30th of August 2023 and ending around the 31st of September 2023. At the time of the most recent readings, the total vertical stress had stabilised to approximately 92 kPa. However, the horizontal total stress at this time was only 5.7 kPa. It is unclear at this stage why there is such a large difference between the vertical and horizontal total stresses. It is known known that that the iron ore tailings does contain some plastic fines which results in large desiccation cracks, as shown in Figure 6.32. This photograph was taken near the existing penstock, several months after deposition has ceased on the compartment.

It is plausible that a crack similar to the one noticed on site developed near the horizontal EPC. Such a crack would have a significant influence on the interpreted horizontal stress. However, it is believed that once the compartment is recommissioned and the tailings is resaturated, a more meaningful response will be obtained from the stress station. Alternatively, the geometry of the installation location could have resulted in some arching occurring between the battered trench sides.

Interestingly, the TEROS 12 moisture probe showed an increase in moisture content in the soil once the backfilling had started as shown in Figure 6.31(c). This is in line with the strategy to backfill the excavation with slurried tailings to maintain a zone of low permeability around the penstock outfall pipe. Although this has definitely increased the saturation of the tailings, it is perhaps not sufficient to completely resaturate the tailings around the EPCs.

© University of Pretoria

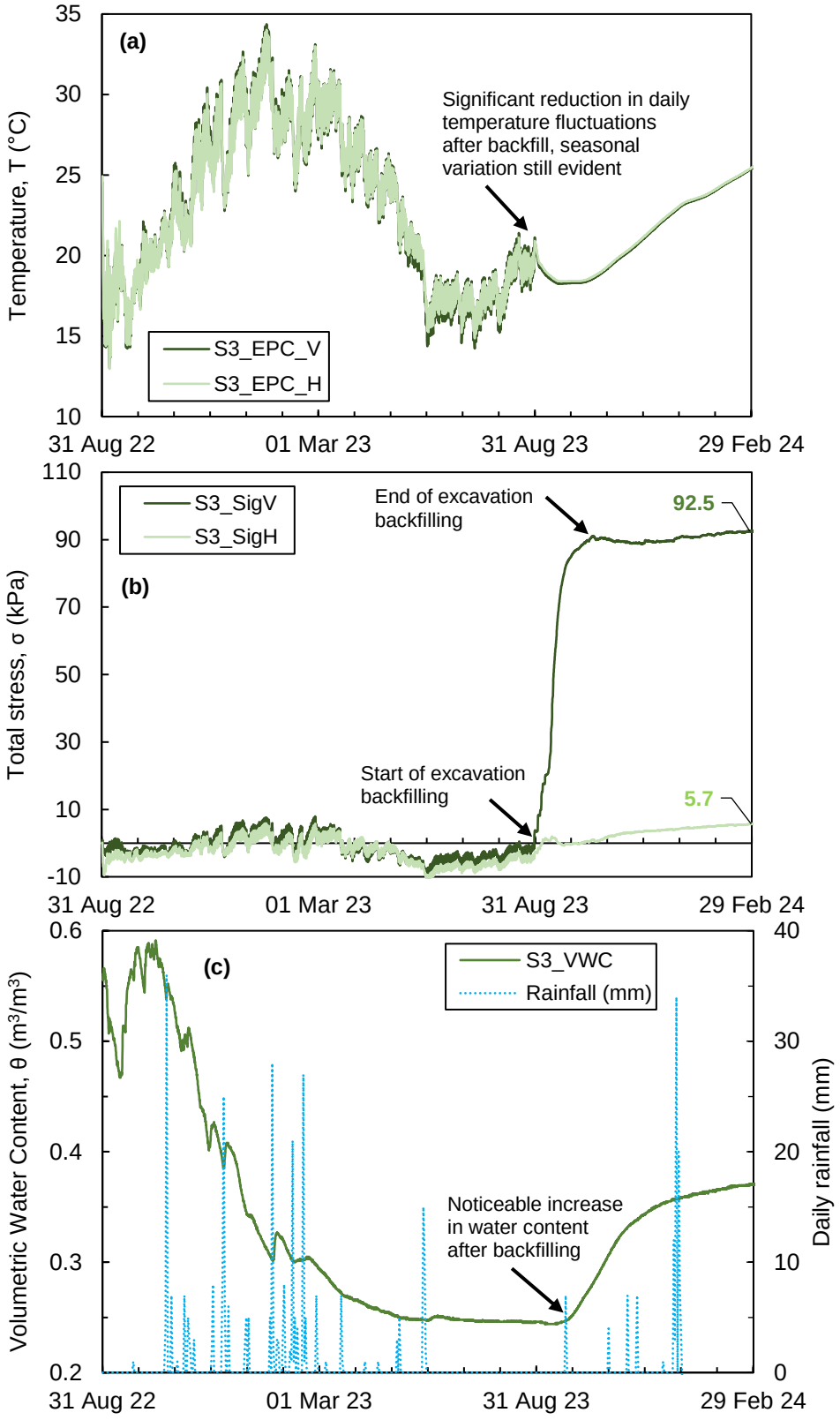


Figure 6.31: Results from the remote monitoring system at the deep installation at the iron ore site showing: (a) temperatures, (b) total stresses, and (c) VWC

© University of Pretoria



Figure 6.32: Photograph showing the large desiccation cracks noted near the penstock at the iron ore site

Another interesting observation that can be made at Station 3 is in terms of temperature influences. Figure 6.33 shows the daily temperature variations recorded by the vertical EPCs for a five-day period, from 1 January to 6 January, but for two different years. The 2023 period is indicated by the solid line, while the 2024 period is indicated by the dotted line. It can be seen that although there is a general upward trajectory for both these lines (as a result of seasonal temperature variations), the magnitude of the daily temperature variations is quite different. For 2023, these daily temperature variations are in the order of 3.6°C. However, for 2024 these daily variations are negligible as they are dampened due to the backfilling of the excavation.

© University of Pretoria

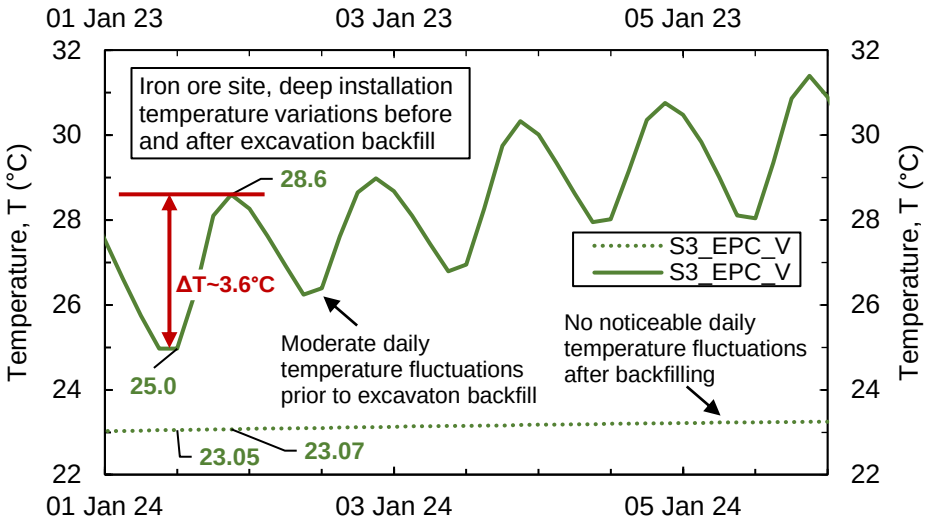


Figure 6.33: Daily temperature variations before and after backfilling of the excavation

© University of Pretoria

6.4 PLATINUM TAILINGS SITE

6.4.1 Site Description

The platinum tailings site used for this study is located in the Limpopo Province of South Africa. Unlike the other two tailings dams instrumented, which are upstream constructed dams, this dam was converted from an upstream constructed dam to a downstream constructed dam. In a similar process to what was followed at Mount Polley, waste rock from the open pit operations was used to initially buttress the outer walls. At this site, this was then continued such that the outer walls were raised in a downstream manner. The hydraulically deposited tailings was then impounded within this outer wall. An engineered filter layer was constructed between the rock wall and the tailings to prevent piping.

With the change in operational philosophy from upstream to downstream, this dam was expected to experience a higher rate of rise compared to similarly sized platinum tailings dams in the country. Therefore, although this would no longer be an upstream tailings dam, the opportunity to experience higher stress levels in the time available for the study seemed quite attractive. This was especially true considering some of the uncertainties encountered during the analysis of the data from the Drying Box 1 experiment and the data from the gold site, where initial negative interpreted horizontal stresses were noted.

The tailings dam that was instrumented at the platinum site has been active since October 2013 and currently receives approximately 1 Mt of dry tailings per month. With an active surface are of 155 ha, this deposition rate results in a RoR of approximately 5.5 m/year. Unfortunately, as was the case with the iron ore tailings dams, long-term monitoring was not successful on this site. In this case, this was due to theft and cable damage as is discussed in the next section.

Based on internal testing conducted by the Mine and the EoR, the platinum tailings can be characterised using an effective friction angle of 33°. Figure 6.34 shows the average grading curve of the platinum tailings. It can be seen that the material is finer than the gold tailings, with more than 80% of the material by mass passing the 0.075 mm sieve.

© University of Pretoria

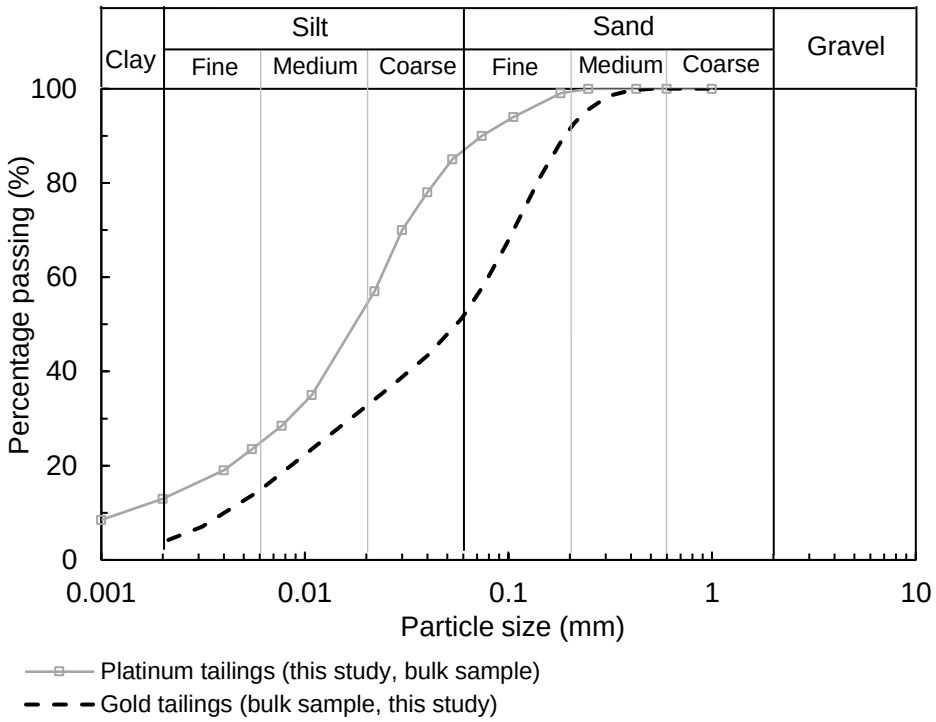


Figure 6.34: Grading curve of the platinum tailings, compared to the gold tailings

XRD testing was conducted on samples of the platinum tailings obtained in the basin, near the monitoring sites. A summary of this testing, showing the approximate mineralogical composition of the platinum tailings is shown in Table 6.5. It can be seen that most common mineral is Enstatite, followed by Plagioclase and Chromite. Trace amounts of Augite and Talc were also present. The XRD spectrograph of the platinum tailings wall sample is provided in Appendix B.

Table 6.5: Composition of the platinum tailings (basin sample)

Mineral	**Composition (%)**
Enstatite	60.5
Plagioclase	22.6
Chromite	14.2
Augite	2.1
Talc	0.6

6.4.2 Installation details

The installation of the two stations at the platinum site was conducted on 24 August 2022. Figure 6.35 shows selected photographs taken during this time. Figure 6.35(a) shows the cross section with the location of the two installations, which are approximately 20 m apart. Station 1 is

© University of Pretoria

closer to the outer wall and approximately 30 m upstream of the rock wall, while Station 2 is closer to the penstock. The engineered filter layer can be seen between the outer rock wall and the tailings.

To remain out of the way of the future filter and tailings, the logger boxes were placed on the crest of the outer rock wall. The location of the cross section is shown on a layout of the dam in an insert. The same installation process as described for the iron ore site was followed. Figure 6.35(b) shows the laying of the cables during installation. The photograph was taken from the location of the logger boxes, looking towards the stress stations. A protective sleeve, which was used for the cables along the waste rock slope, can also be seen in the photograph. Figure 6.35(c) shows the erected logger boxes on the crest of the rock wall.

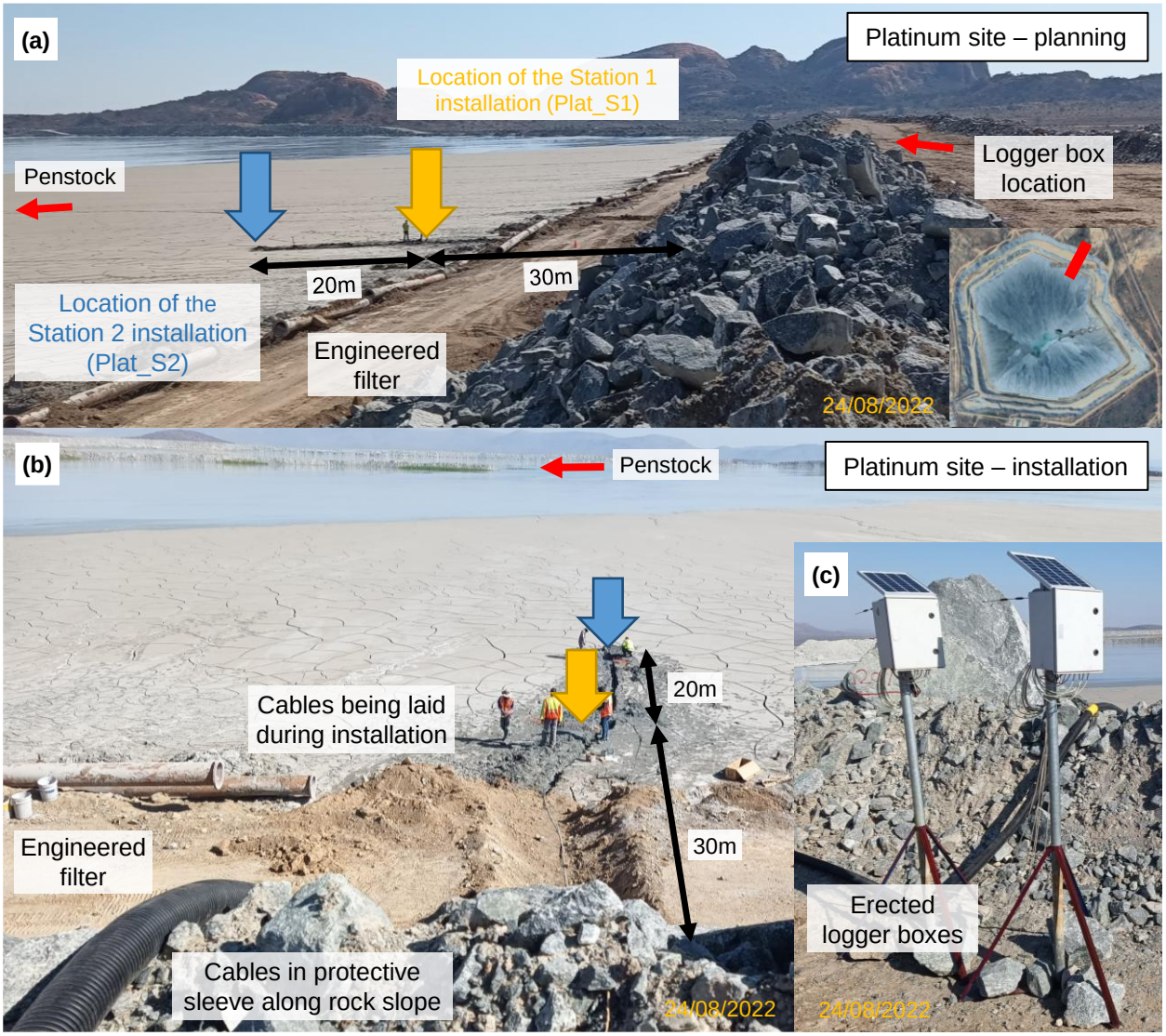


Figure 6.35: Photograph for the platinum installation showing: (a) planning, (b) installation, and (c) the erected logger boxes

© University of Pretoria

As discussed earlier, long-term monitoring data were note obtained from the platinum site. This was due to a number of factors which are summarised in Table 6.6. In addition to details regarding the theft and damage, the dates when the systems were installed, and when deposition in the area was started is also provided in the table. It can be seen that although the installation was conducted on 24 August 2022, deposition in the area only occurred on 22 September 2022. On 22 October 2022, the logger boxers were vandalised. It took some time to complete the investigation into the theft, and to decide on measures to put in place to prevent the incident from recurring. In addition, some new equipment was required, and the procurement lead times were several weeks.

The logging system was successfully reinstated on 23 March 2023. However, between 27 June 2023 and 04 July 2023, extensive cable damage was reported on site and no further logging was possible. Attempts were made to repair the cables but these were ultimately unsuccessful. On 11 August 2023 it was decided that no further attempts would be made to reinstate the logging system. This was due to the extensive damage that had occurred, as well as the next waste rock wall raise which was imminent and would mean the logging equipment would need to be relocated again within a few months. It is however hoped that this monitoring will continue in the future.

Table 6.6: Key events at the platinum site

Date	Event
24 August 2022	Installation of Station 1 and Station 2, start of logging
22 September 2022	First deposition in the area
22 October 2022	Logger boxes vandalised, no further logging possible
02 February 2023	First attempt to reinstate cables, work disrupted by heavy rainfall.
23 March 2023	Cables successfully spliced and extended, data logging resumed
22 June 2023	Trip to the Mine to manually download the data and replace the batteries.
27 June 2023	Cables damage reported on site, logging stopped
04 July 2023	Additional cable damage reported on site
27 July 2023	Cables spliced and extended, unfortunately several of the sensors did not provide reliable readings. It was suspected that there was additional cable damage further inside the dam. No further logging was possible.
11 August 2023	Acknowledging the existing cable damage, a decision was made to return the logging equipment to the University until a long-term solution to reinstate the monitoring system could be found.

© University of Pretoria

6.4.3 Results

As was done with the previous installations, the results from the remote monitoring stations are split into key periods. The first period presents the initial data from the first month of monitoring. In this section, results from the individual sensors are discussed. The second period represents the combined data from all the sensors for the monitoring period. Finally, the results are plotted as stress paths.

6.4.3.1 Initial data (first month)

Results from the first month of monitoring are provided for both stations at the platinum site in Appendix C. Details of the first deposition event are provided, as well as installation details for the tensiometers. The zero readings for the EPCs and tensiometers are also shown for reference. Also of interest is the interpretation of the raw data reported from the sensors, and the conversion to engineering units. This is done by showing a side-by-side comparison of the raw and interpreted data for each sensor.

As was discussed earlier, deposition in the area was delayed so the material around the sensors started drying out with time. To ensure the tensiometers did not cavitate, the site personnel assisted in pouring water over the installations. The addition of this water resulted in an increase in saturation of the tailings around the sensors, which can be seen in the relevant figures. However, the limited volume of water that could practically be added resulted in only a small increase in pore pressure (reduction in suction) being recorded. These attempts were masked by the gradual drying of the tailings. This temporary increase in saturation is confirmed by the response noted from the moisture probes.

6.4.3.2 Initial data (selected months)

Figure 6.36 shows the VWC and suctions measurements for the two stations at the platinum site during the first rewetting phase. It can be seen that there is a marginal change in the VWC for a moderate change in suctions which approach zero. This indicates that the soil is near saturation at the start of the drying phase. The saturated VWC for the two stations is shown for reference. Additional details noted for the various sensors for selected months can be found in Appendix C.

© University of Pretoria

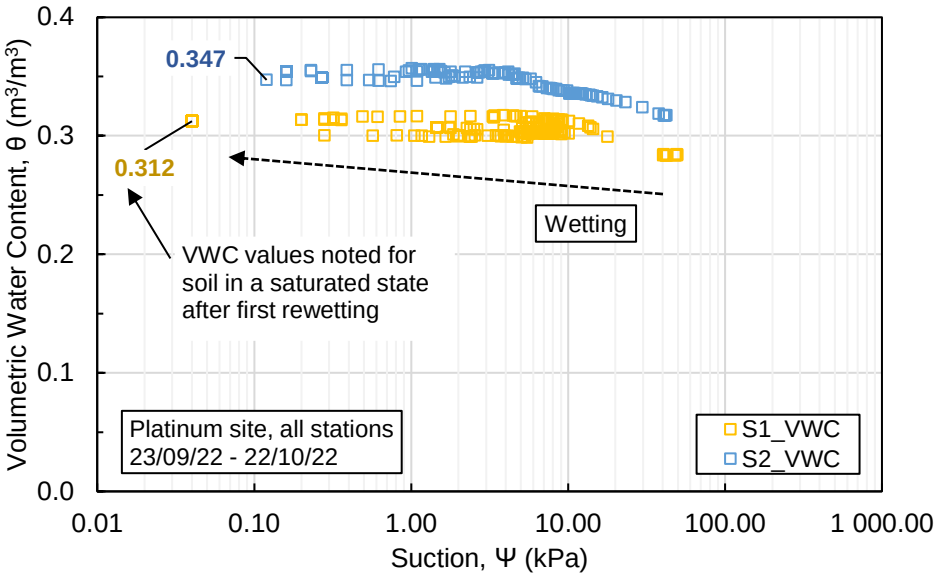


Figure 6.36: VWC and suction data for the first rewetting phase at the platinum site

6.4.3.3 Combined data

Figure 6.37 shows the results from the two stress stations at the platinum site over the monitoring period. During the first monitoring period, from August 2022 to October 2022, excellent correlation was noted between the two stations. No data were recorded from October 2022 to March 2023 due to the theft of the logging equipment. The next monitoring period, from March 2023 to June 2023 also proved successful. However, no further monitoring was possible after this period.

Figure 6.37(a) shows the interpreted total stresses from the EPCs. Once again, the black squares shown represent the estimated vertical total stress at the stations based on the reported crest elevations and the bulk density of the tailings. Unlike the gold and iron ore site, the high RoR meant that the initial negative interpreted stresses were quickly overcome. At the end of the monitoring period, the sensors were estimated to be below 3.8 m of tailings.

Figure 6.37(b) shows the pore pressures interpreted from the tensiometers. Two tensiometers (one at each station) stopped responding during installation. Therefore only one tensiometer is available per station. Initially, good correlation was noted between the tensiometers at the two stations. Some deviation was noted for the second monitoring period. Interestingly, for the second period relatively high positive pore pressures of between 5 and 15 kPa were noted. This is unusual for such a shallow installation, however, with such a rapid RoR this may be plausible.

Figure 6.37(c) shows the VWC interpreted by the moisture probes. The gradual reduction in moisture content prior to deposition is clear for both stations. However, once deposition had

© University of Pretoria

commenced in the area, the tailings essentially remained saturated for the entire monitoring period. This is entirely consistent with the high RoR on the dam.

Figure 6.37(d) shows the interpreted stress ratios for the two stations. It can be seen that once deposition commenced, both stations reported a stress ratio of between 0.3 and 0.5. Some data are missing but as the total stresses increased due to routine deposition, it can be seen that this band moved such that the interpreted stress ratios varied between 0.4 and 0.6. There is also a good correlation between the interpreted stress ratios, and the stress ratio estimated using the Jaky (1944) equation. For the period from October 2022 to June 2023, this stress ratio was found to average 0.46, with a standard deviation of 0.05.

© University of Pretoria

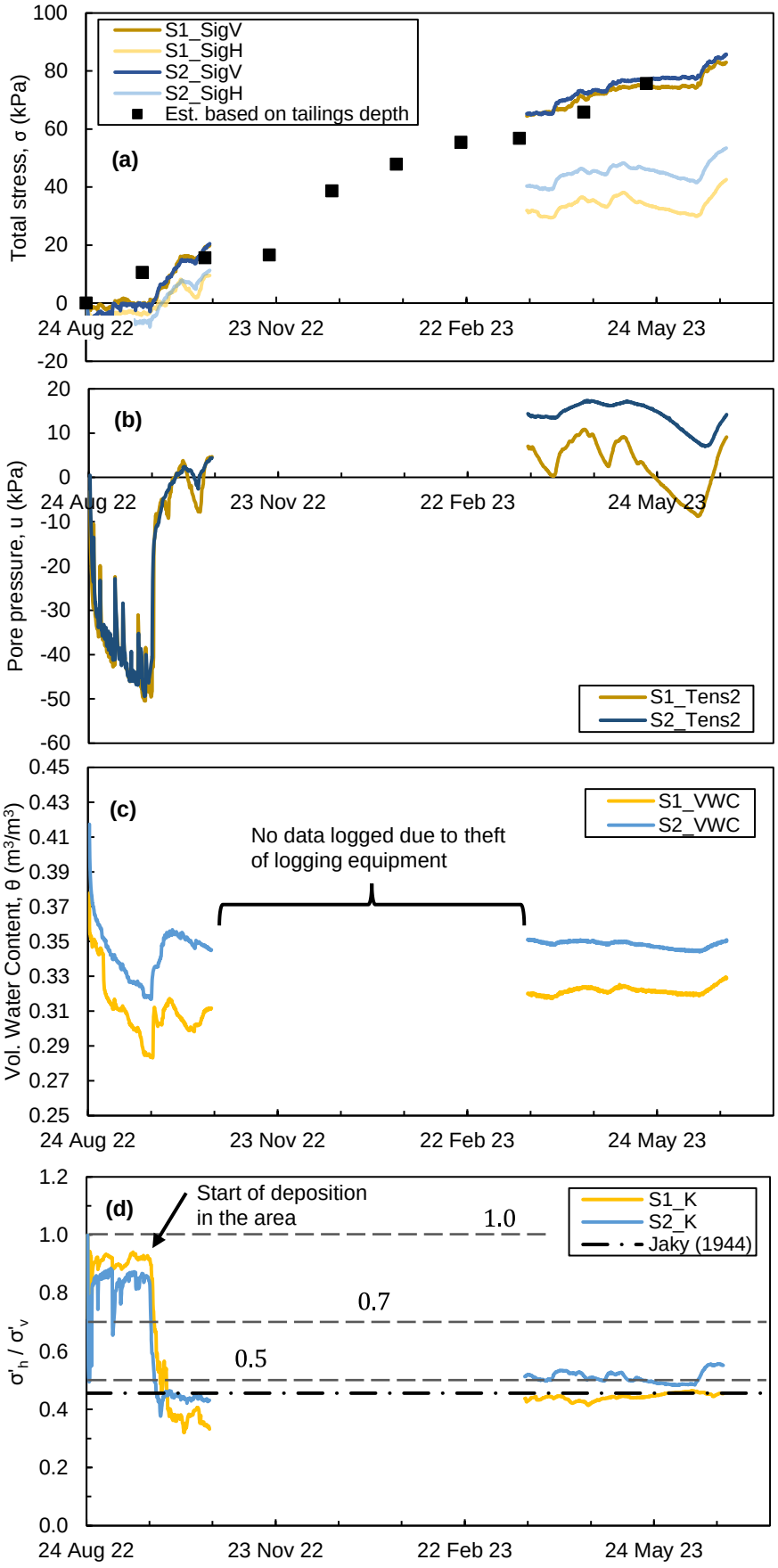


Figure 6.37: Results from the remote monitoring stations at the platinum site showing: (a) total stress, (b) pore pressures, (c) VWC, and (d) stress ratios

© University of Pretoria

Figure 6.38 shows the VWC and suctions responses for both stations at the platinum site, over the entire monitoring period. It can be seen that there is a distinct difference in the drying behaviour during the initial drying period and the first drying period after first wetting. During the second wetting periods, the HCTs reported positive pore pressures for both stations. These results therefore do not plot on this figure. The VWC for the tailings in a saturated state after the first wetting are also indicated for reference. Additional details regarding these features are provided in Appendix C.

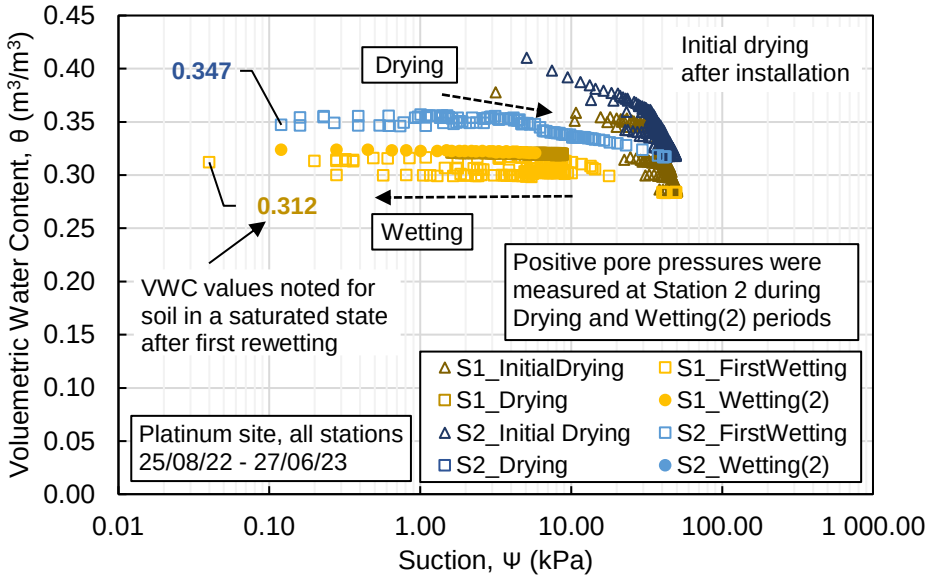


Figure 6.38: VWC and suctions responses at the platinum site

6.4.3.4 Stress paths

Figure 6.39 shows the interpreted stress paths for the two stations at the platinum site. It can be seen that there is a break in the data, corresponding to the period when the logging equipment was not in place. For the available data, there is good correlation noted between the two stress paths. In general, there is a gradual increase in the stress paths from left to right when plotted in $t - s'$ space.

© University of Pretoria

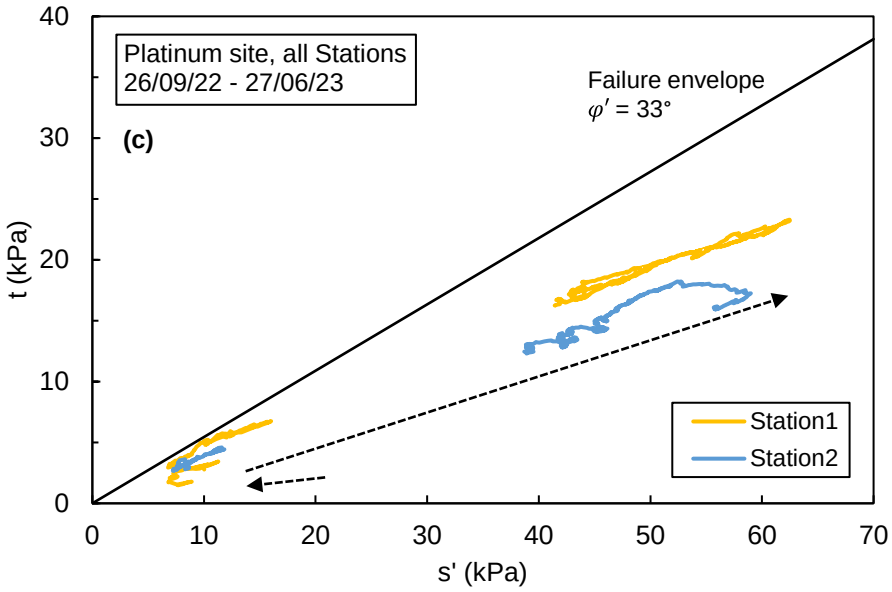


Figure 6.39: Stress paths for the platinum site

6.4.3.5 Stress ratios

Figure 6.40 shows the interpreted month-end stress ratios at the platinum tailings site. Although the data are limited, it can be seen that the stress ratios consistently plot around a value of 0.5. This is lower than the value of 0.7 which is commonly assumed for loose, sandy soils (e.g. Bentley Systems, 2023b). The interpreted stress ratios show a good correlation with the equation proposed by Jaky (1944).

© University of Pretoria

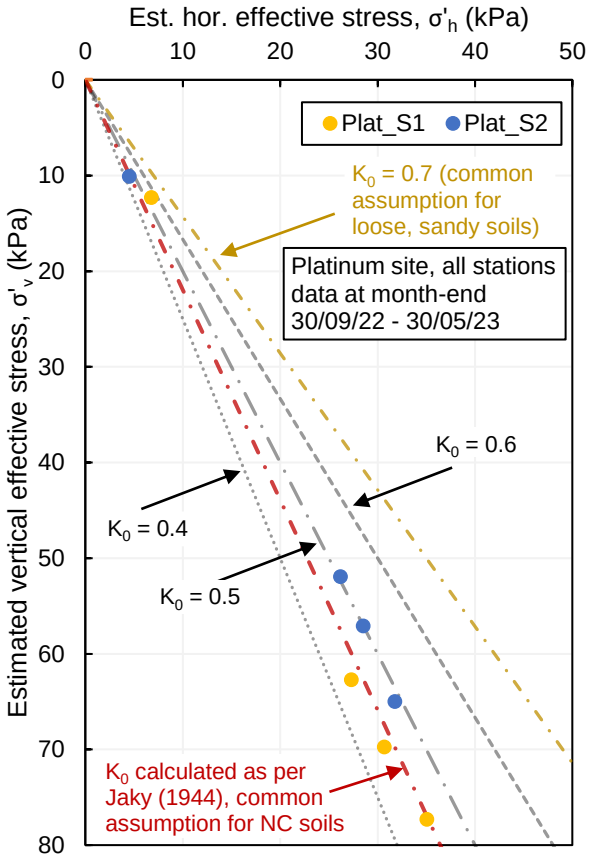


Figure 6.40: Month-end stress ratios at the platinum tailings site

6.5 TEMPERATURE EFFECTS OF THE EPCS

During the course of monitoring the responses from the EPCs, it was noticed that there appeared to be a correlation between the temperature measured on site and the response recorded from the EPCs. This was particularly evident for the EPCs installed at the iron ore site and the gold site.

Table 6.7 shows a summary of the results of the influence of temperature on the EPCs installed in the field as part of this study. A total of eight EPCs were tested over a range of time periods (between two to 14 months). Imposed stress levels varied between 1 and 27 kPa and the temperatures investigated ranged from 13 to 33°C. These values are discussed further in Section 7.4, where they are compared to other values reported in the literature, as well as to values determined from similar tests conducted in the laboratory. Additional details regarding these tests can be found in Appendix B.

© University of Pretoria

Table 6.7: Summary of temperature influence on EPCs under constant load

	Starting stresses (kPa)	**Temperatures (°C)**	**Changes in interpreted stress (kPa/°C)**	**Manufacturer's thermal factors (kPa/°C)**
This study, field tests	1.6 – 26.9	13 - 33	0.8 – 6.5	0.1 – 0.5

6.6 COMBINED RESULTS

At the outset, three tailings dams were identified for monitoring: a gold tailings dam, an iron ore tailings dam and a platinum tailings dam. For a number of reasons, long-term monitoring was not possible on two of the three sites. Therefore, only long-term data for the gold tailings dam were presented. Where possible, short-term data were presented for the iron ore and platinum tailings sites.

6.6.1 In-situ stress states

The in-situ stress state was evaluated using the responses from several sensors incorporated in the remote monitoring system. In particular, this stress state was represents using the geostatic stress ratio, K_0, which is simply the ratio between the horizontal and vertical effective stress. For consistency, the symbol K is used to represent this stress ratio as no attempt was made to ensure zero lateral strain, which is a requirement for true K_0-conditions.

Based on the results from this study, it was found that the measured stress state across the three tailings dams is not isotropic. Rather K values ranging between 0.4 and 0.8 were found for the three tailings materials as shown in Figure 6.41. Interestingly, for the gold and platinum tailings, this ratio only varied between 0.4 and 0.6 as shown in Figure 6.41(a) and Figure 6.41(c) respectively. For the iron ore site, this stress ratio varied between 0.5 and 0.8, as shown in Figure 6.41(b). For each site, the stress ratio estimated using the Jaky (1944) equation is also shown for reference. It can be seen stress ratio estimated using the remote monitoring system shows a fair correlation to the stress ratio estimate using Jaky's equations. With the exception of Station 1 at the iron ore site, the difference between these two stress ratios for all three materials was found to be less than 0.2 once the ratios had stabilised.

© University of Pretoria

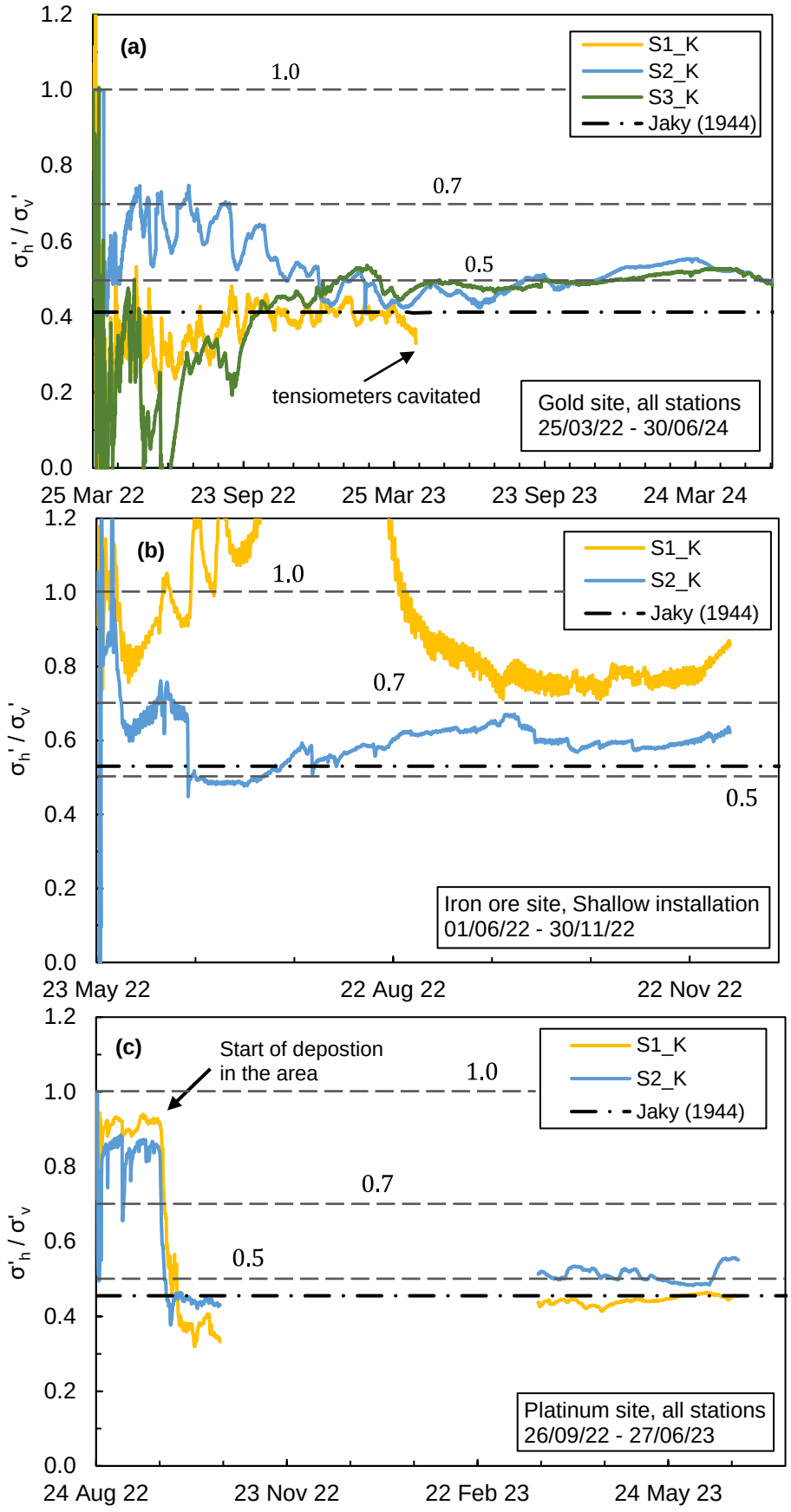


Figure 6.41: Stress ratios for the: (a) gold, (b) iron ore, and (c) platinum sites

© University of Pretoria

6.6.2 Stress ratios

Figure 6.42 shows the interpreted stress ratios for the three sites at the end of each month. Figure 6.42(a) shows the results for the gold site, Figure 6.42(b) shows the results for the iron ore sire, Figure 6.42(c) shows the results for the platinum site. Also shown on the figures are the K_0 values determined using the equation proposed by Jaky (1944), as well as some commonly-assumed values. It can be seen that the stress ratios appear to stabilise for all three sites as the magnitude of the stresses increase.

© University of Pretoria

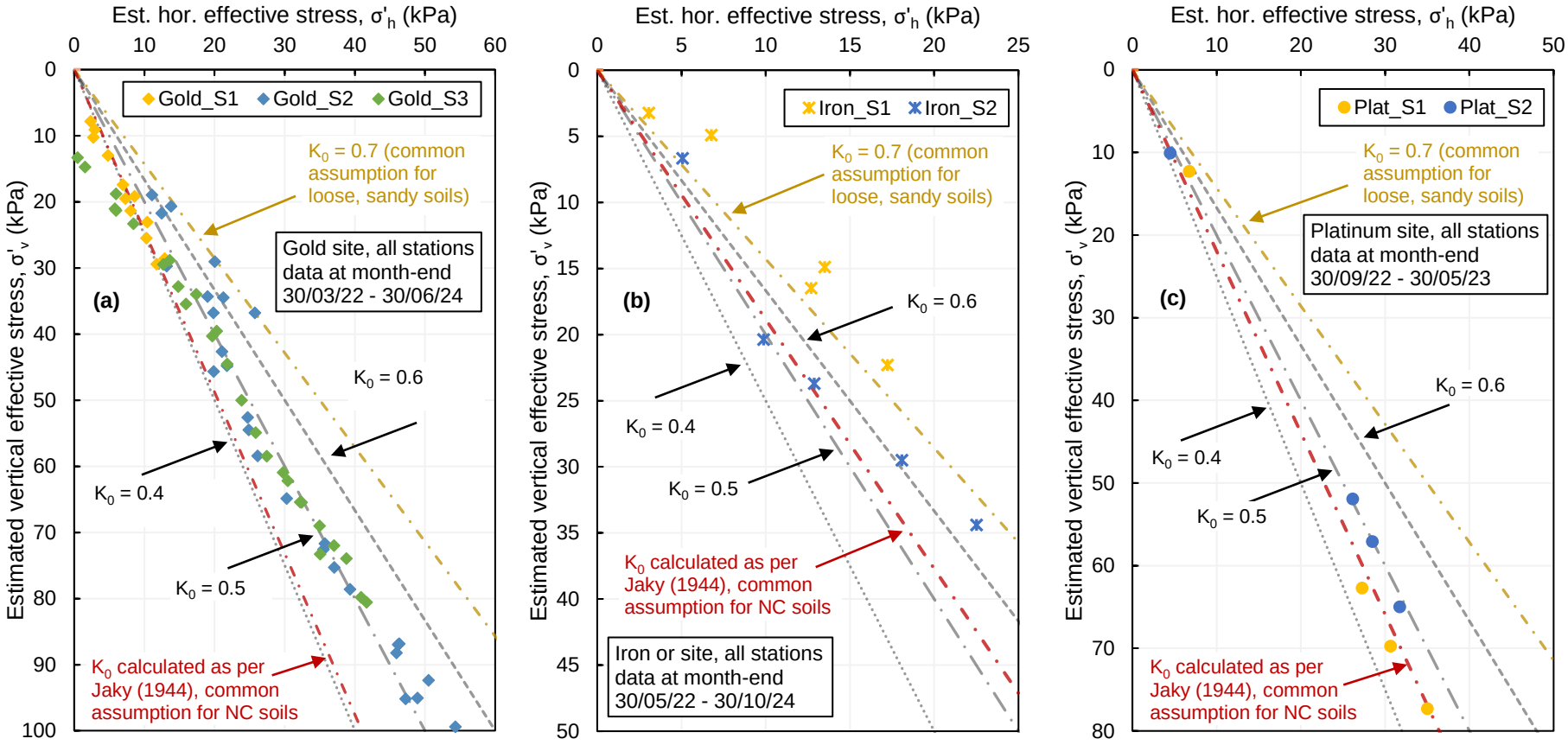


Figure 6.42: Summary of the interpreted stress ratios for the: (a) gold, (b) iron ore, and (c) platinum sites

© University of Pretoria

6.6.3 Stress paths

Although it is of interest to know the in-situ stress state, it is more useful to plot the stress paths of the material. This is important as it is known that the stress history plays an important role in the behaviour of sandy soils. For this study, the stress invariants s' and t were used. To calculate these parameters, it was assumed that the vertical and horizontal stresses were the major and minor principal stresses, respectively.

The interpreted stress paths for all three tailings materials are shown in Figure 6.43. Figure 6.43(a) shows the stress paths for the gold tailings. Figure 6.43(b) shows the stress paths for the iron ore tailings. Figure 6.43(c) shows the stress paths for the platinum tailings. In general, it can be seen that the stress paths are anisotropic in nature and in some cases approach and even cross the drained failure envelope, probably due to measurement inaccuracies.

© University of Pretoria

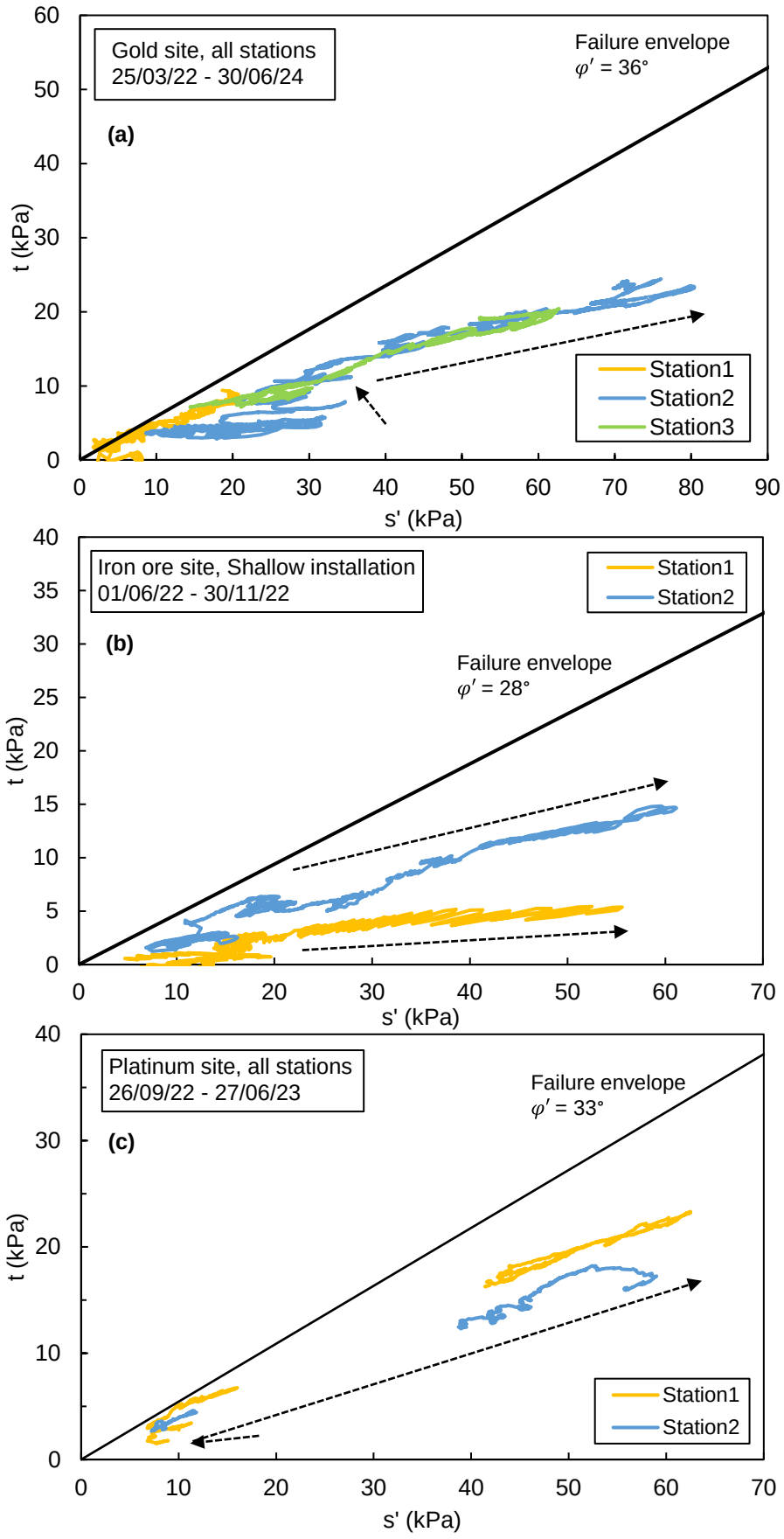


Figure 6.43: Interpreted stress paths for the: (a) gold, (b) iron ore, and (c) platinum sites

© University of Pretoria

7 INTERPRETATION OF LABORATORY AND FIELD DATA

7.1 INTRODUCTION

So far, results from field and laboratory tests have been presented. However, they have for the most part been presented in isolation. The intent of this chapter is to interpret the results of the laboratory and field tests in a soil mechanics context. In addition, some key assumptions made during the interpretation of the field and laboratory data are discussed in detail.

7.2 INTERPRETED STRESS RATIOS

This section discussed the stress ratios interpreted for the three tailings sites over the various monitoring periods. To simplify the plots, only the measurements at the end of each month are presented. More detailed results can be found in Chapter 6 and Appendix C.

As described in Section 5.5, the calculation of the effective stress according to the Bolzon et al. (1996) interpretation of Bishop effective stress requires the estimation of the degree of saturation. Figure 7.1 shows the month-end S_r values recorded at the three sites using the assumptions discussed in Section 5.5. Aside from the outliers noted at Station 2 at the iron ore site, S_r values of between 0.6 and 1.0 were noted. Reasonable correlation was noted for the gold site measurements and the drying SWRC determined in the laboratory.

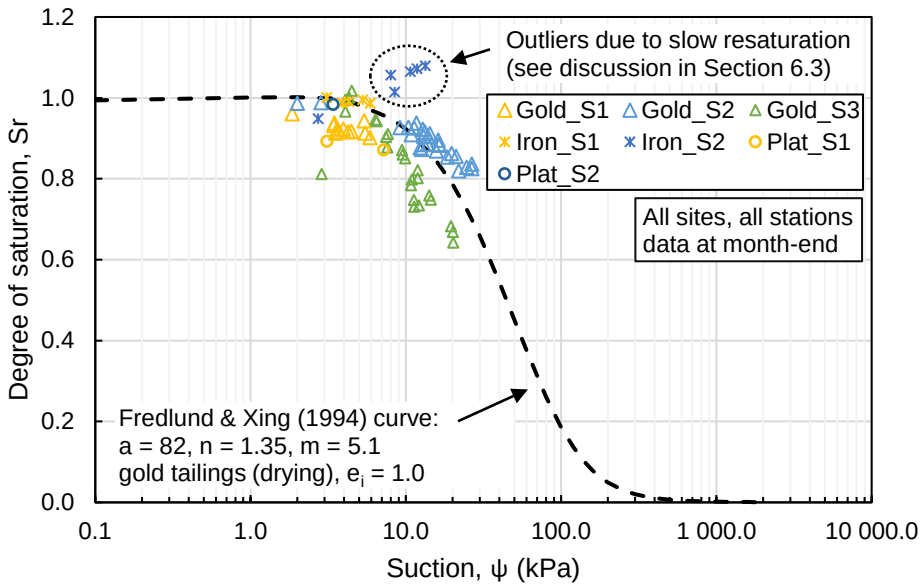


Figure 7.1: Estimated month-end S_r values during the field monitoring

© University of Pretoria

Figure 7.2 shows the estimated month-end horizontal and vertical stresses for all three tailings sites. There is some scatter noted in the data at the lower stress ranges. However, at higher stresses, the stress ratios appear quite consistent. In general, the measured field stress ratios appear to be bounded by stress ratio values of 0.4 and 0.7, with an average value of 0.5 at higher stresses.

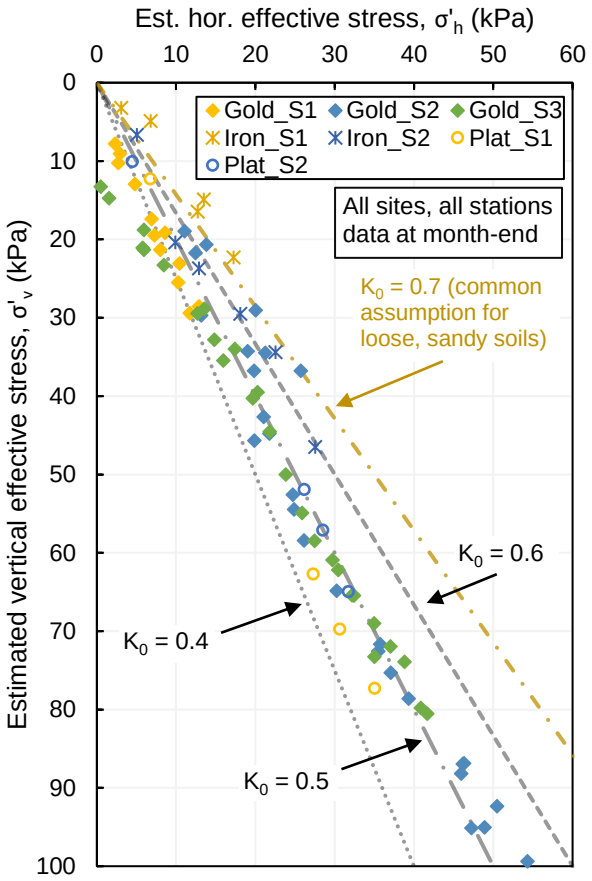


Figure 7.2: Estimated month-end stresses over the course of the field monitoring

A summary of the field measured K values after the initial period of variability is provided in Table 7.1. The average values and the associated standard deviations were calculate considering all the datapoints and not just the month-end datapoints. It can be seen that the stress ratios determined for the gold and platinum tailings sites are similar, with fairly low standard deviation values, indicating that the variability in the data is not too large. These values are considerably lower than the value of 0.7 that is commonly-assume for loose, sandy soils (e.g. Bentley Systems, 2023b). The stress ratio determined for the iron ore site is higher and has a larger standard deviation, indicating more variability in the data. As discussed in Section 6.3.3, there is more uncertainty regarding this site so the values should be considered with that in mind.

© University of Pretoria

In general, the K_0 values estimated using the Jaky (1944) equation appear to be a lower-bound for the measured stress ratios. This is in line with the findings of Graham & Jefferies (1986) for loose, hydraulically-deposited Erksak sand.

Table 7.1: Summary of field measured K_0 values

Site	Monitoring period	Average K (±standard deviation)	K_0 after Jaky (1944)
Gold tailings	01/09/2022-30/06/2024	0.48 (±0.04)	0.41
Iron ore tailings	01/09/2022-30/11/2022	0.70 (±0.09)	0.53
Platinum tailings	01/10/2022-27/06/2023	0.46 (±0.05)	0.46

7.3 BEHAVIOURAL FRAMEWORK

A series of laboratory tests were conducted to investigate the influence of various aspects of soil state on the compression and shear behaviour of the gold tailings. It was found that the undrained shear response of the gold tailings is highly dependent on the void ratio, as well as the stress ratio (i.e. the magnitude of stress anisotropy).

Based on the results from the remote monitoring system presented in Section 6.2.3, the stress ratios observed at the gold site varied between 0.4 and 0.6. As discussed in Section 2.5.1, there is some uncertainty in the literature regarding whether the stress ratios measured under specific stress conditions need to be scaled when applied to other stress conditions. Assuming the stress ratio determined in field (K) can be directly compared to the stress ratio imposed during the triaxial test (K_c), it would appear that the gold tailings on site can expect to exhibit a yield undrained strength ratio of between 0.36 and 0.50, and a Brittleness Index of between 0.48 and 0.65. Considering the average K value of 0.48 measured between October 2022 and June 2024, a yield undrained strength ratio of 0.46, and a Brittleness Index value of 0.65 could be expected. These values are based on the results obtained from the triaxial tests described in Section 3.5. It should be noted that using this approach ignores principal stress angle effects which can have an influence on the stress ratio as the depth of the monitoring points below the slope increases.

Regardless, it is clear that these are not strength ratios and Brittleness Index values that would be considered for isotropically consolidated samples, which would likely be in the order of 0.20 and 0.77, respectively. Therefore, laboratory testing plans need to be carefully designed to enable useful comparisons such as this to be drawn. Another aspect that needs to be carefully considered

© University of Pretoria

is the fabric of the soil used for the triaxial tests. If the appropriate densities can be repeatedly achieved, it is perhaps prudent to consider additional tests on SD samples to verify the observed response on the MT samples.

As discussed by (Zheng, 2022) and (France et al., 2022), the selected K_0 value can have play a significant role in the outcome of stability assessments of tailings dams and water-retaining embankments. Therefore, these results also have implications in the assumptions made during designs and safety evaluations of tailings dams and water-retaining embankments.

7.4 TEMPERATURE INFLUENCES ON THE EPCS UNDER CONSTANT LOAD

A series of long-term laboratory and field tests were conducted to investigate the thermal effects on the Geosense VWTPC-4000 EPCs under constant load. As shown in Table 7.3, a total of two laboratory tests, and three field tests were conducted. The tests covered a range of stress levels (0 kPa to 26 kPa), materials (gold and iron ore tailings), and durations (two to 12 months).

Table 7.2 show a summary of the thermal influence on the response recorded from various EPCs under constant load. The data are based on results of this study, as well as data obtained from literature, specifically the work conducted by Yang et al. (2001) and Daigle & Zhao (2004). A few points can be made.

Firstly, it can be seen that for both the tests performed as part of this study, as well as the tests performed by others, the change in interpreted stress was lower for the laboratory tests, compared to the field tests. Since the tests were performed over a similar range of temperature changes, this difference in attributed to the lower stress levels imposed in the laboratory tests, compared to the field tests.

Secondly, it can be seen that the magnitude of changes in interpreted stress due to temperature determined for this study (0.3 and 6.5 kPa/°C) fall within the range of those reported in the literature (between 0.2 and 7.0 kPa/°C). Finally, with the exception of the laboratory tests performed as part of this study, all the tests showed temperature influences significantly greater than those suggested by the manufacturer's thermal factors which varied between 0.03 and 0.5 kPa/°C. As the manufacturer's thermal factors are only intended to compensate for thermal effects of the pressure transducer itself and not for the entire cell assembly (see Section 2.6.1), these results suggests there can be meaningful thermal influences on the entire cell assembly which are not addressed using the thermal factors provided by the manufacturer. This needs to be carefully considered for

© University of Pretoria

situations where EPCs are subjected to large temperature variations.

Table 7.2: Summary of temperature influence noted for the EPCs under constant load

	Starting stresses (kPa)	**Temperatures (°C)**	**Changes in interpreted stress (kPa/°C)**	**Manufacturer's thermal factors (kPa/°C)**
This study, laboratory tests	0 - 7.1	13 - 28	0.3 – 0.5	0.1 – 0.5
Data from literature, laboratory tests	0 – 77	-10 - +30	0.2 – 2.3	0.03 – 0.2
This study, field tests	1.6 – 26.9	13 - 33	0.8 – 6.5	0.1 – 0.5
Data from literature, field test	18 - 367	0 - 22	0.6 – 7.0	0.05 – 0.1

As suggested by Dunnicliff (1997), there is likely an influence on the type and magnitude of confining stress applied to the EPC on these thermal influences. This concept is explored in Figure 7.3, which shows a plot of the unit change in interpreted stress versus the initial stress for all the field and laboratory data generated as part of this study as well as the data collected from the literature. Although there is scatter in the data, it is clear that there is a general trend of an increase in thermal influence with increasing initial stress level. Note that for display purposes, the EPCs tested under zero load were assigned an initial stress of 0.1 kPa in Figure 7.3.

© University of Pretoria

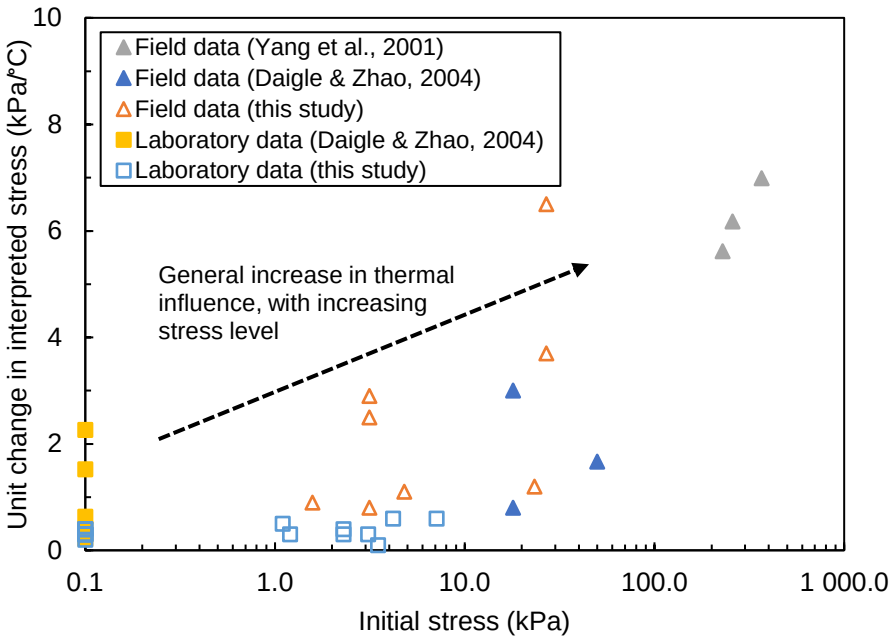


Figure 7.3: Summary of the thermal effects on the interpreted stress response from the EPCs under constant load

© University of Pretoria

Table 7.3: Summary of EPCs tests conducted to investigate thermal effects under constant load

Test	Internal Ref	Description	Key Features
Laboratory Test 1	Drying Box 1	Laboratory test to simulate the expected field conditions at the gold site. After the last deposition event, the EPCs were monitored for an additional five months to investigate the influence of seasonal temperature variations.	Laboratory test, gold tailings, low stress levels, five-month monitoring period.
Laboratory Test 2	Drying Box 3	Laboratory test to investigate the influence of natural ambient temperature variations on the recorded response from the EPCs. The EPCs were monitored in a zero-load state for a period of eight months.	Laboratory test, zero stress, eight-month monitoring period.
Field Test 1	Gold site	Field test at the gold tailings site. A step-in was constructed at the location of monitoring Station 1, so the vertical stress remained constant at approximately 23 kPa. The response of the EPCs to seasonal temperature variations over a 10-month period was monitored.	Field test, gold tailings, moderate stresses, 10-month monitoring period.
Field Test 2a	Iron ore site (shallow installation)	Field test at the iron ore tailings site. The EPCs were installed in a shallow excavation but deposition was delayed. The response of the EPCs to seasonal temperature variations over a two-month period prior to deposition was monitored.	Field test, iron ore tailings, low stress levels, two-month monitoring period.
Field Test 2b	Iron ore site (shallow installation)	Field test at the iron ore tailings site. The compartment was active for six months, after which deposition was ceased. The response of the EPCs to seasonal temperature variations over a 14-month period after deposition ceased was monitored.	Field test, iron ore tailings, moderate stress levels, 14-month monitoring period.
Field Test 3	Iron ore site (deep installation)	Field test at the iron ore tailings site. The EPCs were installed in a deep excavation which was not backfilled. The response of the EPCs to seasonal temperature variations over a 12-month period prior to backfilling was monitored.	Field test, iron ore tailings, low stress levels, 12-month monitoring period

© University of Pretoria

7.5 SUMMARY

This chapter provided a discussion of some of the key aspects of this study. A brief summary of these aspects, as well as the outcome of the discussion, is provided here.

The interpreted stress ratios for the three tailings sites were reviewed based on the month-end values over the monitoring period. Some initial scatter was noted for all three sites, however this was found to reduce as the effective stress increased. The interpreted stress ratios appeared to be bounded by values of 0.4 and 0.7, with an average value of 0.5 at higher stresses. For each site, average stress ratios were calculated, with an associated standard deviation. The gold and platinum site exhibited similar average stress ratios of 0.48 and 0.46, respectively, with the iron ore site exhibiting a higher average stress ratio of 0.70. The stress ratio estimates were also compared to those obtained using the Jaky (1944) equation. In general, a surprisingly good correlation was noted between these values across all three tailings sites, with the value estimated by Jaky's equation appearing to be a lower-bound value.

The behavioural framework established in Chapter 3 was discussed. Assuming the stress ratio determined from site (K), could be directly compared to the stress ratio imposed in the triaxial apparatus (K_c), it was possible to determine a range of yield undrained shear strengths and Brittleness Index values to expect from the gold tailings on site. These ranges were determined to be between 0.36 and 0.50, and between 0.48 and 0.65 for the yield undrained shear strength and Brittleness Index, respectively. These values are distinctly different to the values of 0.20 and 0.77 that would be considered for isotropically consolidated samples and this needs to be carefully considered.

Finally, the temperature influences on the EPCs under constant load was discussed. Based on the results from this study, it was found that in some cases the Geosense VWTPC-4000 EPCs are susceptible to temperature effects that cannot be addressed using the thermal correction factors provided by the manufacturer. This influence was found to be in the order of 0.3 kPa/C and 6.5 kPa/°C. In addition, some evidence was noted to support the view that this thermal influence appears to vary depending on the imposed stress on the EPC. However, additional testing is required to verify this finding.

© University of Pretoria

8 CONCLUSIONS AND RECOMMENDATIONS

8.1 INTRODUCTION

Although this study attempted to address several uncertainties related to the in-situ stress state in upstream constructed tailings dams, there are still some unanswered questions. This chapter is therefore split into two broad sections. In the first section, conclusions are provided for those objectives stated in Chapter 1. In the second section, recommendations are then provided for the remaining uncertainties that are related to this study topic.

8.2 CONCLUSIONS

The conclusions of this study are linked directly to objectives as presented in Chapter 1. The conclusions are based on the interpretation of the results from the experimental work conducted as part of this study and placed within a framework based on the literature review conducted regarding the current knowledge of soil behaviour.

8.2.1 The influence of K_c on the undrained shear response of the gold tailings

As described earlier, some care needs to be taken when describing stress ratios to avoid confusion regarding boundary conditions imposed on the soil. This is particularly important when comparing field and laboratory data where boundary conditions are likely to be different. For this study, the term K_c has been used to describe the ratio of the horizontal to vertical effective stress in the triaxial test (e.g. Fotovvat & Sadrekarimi, 2022), while for the field data, the term K_0 has been used to describe the same ratio (e.g. Shuttle et al., 2021). Direct comparisons of K_c and K_0 were then made, as has been done by other researchers (e.g. Morgenstern et al., 2015; Jefferies et al., 2019; France et al., 2022).

A series of triaxial compression tests were conducted on the gold tailings obtained from the monitoring site to investigate the influence of the magnitude of stress anisotropy imposed during consolidation on the mechanical response during undrained shearing. The magnitude of stress anisotropy was determined using the stress ratio K_c. The samples were prepared to a loose initial void ratio of 1.0 using the MT method and then saturated using conventional procedures. After saturation was confirmed, the samples were consolidated in three stages to a mean effective stress value of 100 kPa and then sheared undrained. A total of six tests were conducted with K_c values ranging from 0.41 to 0.95. An additional test was conducted at a K_c value of 0.31, but this sample

© University of Pretoria

failed during consolidation. The purpose of these tests was to define a framework in which the measured stress ratios from the field monitoring could be viewed.

It was found that both brittleness, represented by the Brittleness Index (I_B), and the yield undrained shear strength, represented by the yield undrained shear strength ratio ($S_{u(yield)}/p'_0$) are influenced by the stress anisotropy. This is important as both parameters are used directly in design and safety evaluations in some guidelines (e.g. ICOLD, 2022).

For a change in K_c from 0.95 to 0.41, the gold tailings exhibited a progressive change in undrained shear response, with ($S_{u(yield)}/p'_0$) changed from 0.20 to 0.50. In particular, it was found that for a change in K_c of 0.41 (from K_c = 0.95 to K_c = 0.54) I_B changed from 0.77 to 0.49, while ($S_{u(yield)}/p'_0$) changed from 0.20 to 0.36.

In addition to the increase in yield undrained shear strength, and reduction in brittleness, it was found that for the samples prepared at the same initial void ratio but consolidated under decreasing K_c values, there is a general decrease in axial strain required to reach the yield point. An alternative view, as described by Rosenzweig et al. (2020), is that as K_c decreases, the soil has progressively less capacity to handle an increase in shear stress before collapse is initiated. Therefore, knowledge of the in-situ stress state (which can be described using K_0) is of importance for both design engineers and regulators.

Importantly, the density of the sample was shown to have a much larger influence on the undrained shearing behaviour, when compared to the stress anisotropy. For a change in void ratio from 0.69 to 0.84, the gold tailings exhibited a progressive change in behaviour from strain-hardening to strain-softening. For the loose samples, it was specifically found that only a small change in void ratio of 0.04 changed the behaviour significantly. In terms of brittleness, I_B changed from 0.24 to 0.62, as the void ratio increased from 0.74 to 0.78. Similarly, in terms of yield undrained shear strength, $S_{u(yield)}/p'_0$ changed from 0.44 to 0.22. These are significant changes in material response for a relatively small change in void ratio.

8.2.2 The uniqueness of the NCL for the gold tailings

It is known that the compression behaviour of fine-grained soils such as plastic clays is vastly different to the compression behaviour of coarse-grained soils such as clean sands. The former appear to exhibit a unique NCL while the latter appear to have an infinite number of NCLs. Knowledge of the compression behaviour of a soil is important for the planning and implementation

© University of Pretoria

of laboratory testing plans, as well as for design and safety evaluations of new and existing tailings dams where an increase in stress level is anticipated. This is particularly important for aspects related to classifying whether a soil is contractive or dilative at large strains.

Gold tailings, which typically classify as a silty soil, are neither a clean sand nor a clay of high plasticity and there is some uncertainty regarding their compression behaviour. To investigate this, a series of oedometer and triaxial tests were conducted on remoulded gold tailings samples obtained from the gold site. All samples were prepared using the MT method, so the findings are limited to this fabric.

Seven oedometer tests were conducted on samples prepared to different initial densities and with different stress histories, such that samples with various degrees of overconsolidation were created. At large stresses of approximately 3 200 kPa, all the samples approached the same compression curve. Therefore, there appears to be a unique 1D-NCL for the gold tailings. An additional four triaxial compression tests were conducted on samples with similar states as the oedometer tests. At large stresses of approximately 1 600 kPa, all the samples approached the same compression curve.

It should be noted that there was a slight offset noted between the curves of approximately e = 0.04. Interestingly, this is the same value that was determined by Reid et al. (2021) to be the accuracy to which the CSL can be reasonably expected to be determined using modern triaxial testing techniques. Since the same approach that is used to determine the CSL is also used to determine the NCL in terms of the void ratio estimate, it seems reasonable to assume that this accuracy applies to the NCL as well. Therefore, for practical purposes, it was concluded that there exists a unique NCL for the gold tailings tested.

By assuming a K_0 value proposed by other researchers for gold tailings from the same ore body, the known vertical stress could be converted to a mean effective stress so that the 1D-NCL and NCL could be directly compared. For the gold tailings, it was found that the 1D-NCL is parallel to the NCL when plotted in $e - p'$ space.

In terms of particle crushing, samples were taken for grading analysis before and after the tests. Based on the results of these tests, no meaningful evidence of particle crushing was noted, even for the samples loaded to 3 200 kPa.

In terms of identifying whether the gold tailings is a transitional soil, the fact that a unique NCL and CSL could be identified suggests that the gold tailings tested is not a transitional soil, and that the

© University of Pretoria

behaviour of this soil can be captured by traditional CSSM concepts.

In summary, based on the oedometer and triaxial test results conducted, it was found that from a practical perspective, the gold tailings used as part of this study exhibits a unique NCL. Although the NCL and CSL were found to not be parallel, for low to moderate mean effective stress levels of between 50 kPa and 400 kPa, the lines are sufficiently offset in the $e - \ln p'$ space. For example, for a NC sample the state parameter changes from 0.126 to 0.100 as the mean effective stress increases from 50 kPa to 400 kPa. Therefore, for the purposes of defining whether the soil is contractive or dilative at large strains, the NCL and CSL can be considered parallel.

8.2.3 The performance of several geotechnical sensors for long-term monitoring of gold tailings

This study comprised several long-term tests in gold tailings, including both laboratory tests and field tests. Several sensor types were used in the various tests, and it was found that certain sensors performed better than others.

In particular, based on the results from the long-term Drying Box 1 experiment, it was found that the steel-cased Tuks tensiometers performed better than the epoxy-cased Tuks tensiometers. Although the steel-cased tensiometer are more expensive to construct, they proved more resistant to cracking of the ceramic, which was observed for the epoxy-cased Tuks tensiometers. This is a concern as once the ceramic cracks, the Tuks tensiometers are no longer able to provide reliable pressure measurements.

In the same test, it was found that the TEROS 21 WPS is not appropriate for suction measurements in gold tailings. Despite the reported higher capacity in terms of suction measurement of the WPS, and its resistance to cavitation (which is a concern for any high capacity tensiometers), this sensor was not able to capture the rapid changes in pore pressures in the gold tailings due to routine deposition and subsequent drying. Rather, a time-lag was noted between the tensiometers, which showed a rapid response, and the WPS. This lag varied from 4 days for the smaller, moisture probe calibration tests to between 13 and 27 days for the larger Drying Box 1 experiment. In addition, the WPS was found to perform poorly at suction values smaller than 10 kPa.

Regarding the EPCs, it was found that these sensors appear to be susceptible to temperature effects that are not captured by the thermal correction factors provided by the manufacturer in the datasheets. This is due to the fact that the thermal correction factors provided by the manufacturer

© University of Pretoria

are for the pressure transducer itself, and not the entire sell assembly (e.g. Dunnicliff, 1997). Therefore, there may be thermal influences on the entire cell assembly that are not captured by the calibration equations which will result in incorrect stress interpretations if not addressed appropriately.

To investigate this, a number of laboratory and field tests were conducted using the Geosense VWTPC-4000 EPCs under constant load. The error in the interpreted stress was normalised by the change in temperature up to that point during the test. This normalised error was described as a unit change in interpreted stress due to temperature and presented in terms of kPa/°C. The maximum unit change was presented for each test.

It was found that this change in interpreted stress due to temperature changes for the EPCs under constant load varied between 0.3 and 0.5 kPa/°C for the laboratory tests, and between 0.8 and 6.5 kPa/°C for the field tests. This is comparable to the range of 0.2 to 7.0 kPa/°C as found by other researchers on similar EPCs (e.g. Yang et al., 2001; Daigle & Zhao, 2004) and is very different to the thermal factors provided by the manufacturer which ranged from 0.1 to 0.5 kPa/°C.

There is also some evidence that this error increases as the magnitude of confining stress increases however this needs to be investigated further before any meaningful conclusions can be drawn.

8.2.4 Development and implementation a remote monitoring system capable of measuring the in-situ stress state in an upstream constructed tailings dam

A remote monitoring system was successfully developed for the measurement of the in-situ stresses in an upstream constructed tailings dam. A systematic process was followed with the first step being the design of the system. The design followed a two-stage approach. In the first stage, the key requirements of the system were listed. These includes aspects such as accessibility, reliability, durability, longevity, etc. In the second stage, individual components were selected to meet the above-mentioned requirements. These components included various sensors, dataloggers, batteries, solar panels, etc.

Once the individual components were selected, each component was rigorously tested to ensure that it would meet the performance requirements. Once these verification tests were passed, the individual components were assembled into the remote monitoring system. The entire system was then successfully tested in the geotechnical engineering laboratory at the University of Pretoria. A

© University of Pretoria

Drying Box experiment was conducted to simulate the expected field conditions and the remote monitoring system performed independently for a period of 11 months.

Based on the verification tests, a few modifications were made to the system. For example, it was decided that the epoxy-cased Tuks tensiometers would be replaced by the steel-cased Tuks tensiometers to improve their long-term performance. In addition, the logging code was optimised. This was specifically done to power down the cellular module during periods of inactivity which greatly reduced the power consumption of the remote monitoring system.

The updated system was then successfully installed and operated on an active gold tailings dam for a period of over 27 months. In addition, the system was installed on an iron ore tailings dam, and a platinum tailings dam. However, due to various factors including last-minute changes to the deposition plan and theft, it was not possible to obtain long-term monitoring data from the iron ore and platinum sites. Regardless, the remote monitoring systems are still installed on both the gold and iron ore site and provide the opportunity to continue this monitoring for many years to come.

8.2.5 Evaluation of the in-situ stress state in an upstream constructed tailings dam

Although measurements were made on the iron ore and platinum tailings dams, the focus of this study is the gold tailings dam. The remote monitoring system described above was used to estimate the in-situ stresses. A specific focus of this study was to investigate the change in this stress state due to routine deposition and subsequent drying. These values were then displayed in terms of a stress ratio, K.

A key finding from the long-term monitoring at the gold tailings site is the reliability of the suctions within the tailings dam. Initially, the pore pressures were observed to be greatly influenced by deposition and rainfall events and suctions were reduced to close to zero in many instances. However, as the depths of tailings cover increased, this influence gradually reduced. At depths of approximately 3.5 m, there appeared to be very little influence of deposition or rainfall on the measured pore pressures and the soil suctions remained within a fairly narrow range of between 5 and 30 kPa. This is a particularly important aspect to be considered if soil suctions are to be used as part of the soil strength in design and safety evaluations.

As perhaps expected, there was some initial variability in the measured data. However, over the medium-term the responses started to stabilise. Based on the results from the remote monitoring system installed on the gold tailings dam, over a period of 27 months it was found that the in-situ

© University of Pretoria

stress state in not isotropic. Rather, this value was found to vary between 0.4 and 0.6. Based on the measurements recorded from October 2022 to June 2024, the stress ratios at the gold tailings site were found to average 0.48 with a standard deviation of 0.04. These values are quite different to the commonly-assumed value of 0.7 for loose, sandy soils (e.g. Bentley Systems, 2023b). As discussed in Section 7.3, this difference can have meaningful effects on design and safety evaluations. In addition, as was noted by Graham & Jefferies (1986) for loose, hydraulically-deposited Erksak sand, the equation proposed by Jaky (1944) appeared to be a lower-bound for the measured data.

Similar stress ratios were determined for the systems installed on the iron ore and platinum tailings dams. These values are in line with estimates made by other researchers on other upstream constructed tailings dams as discussed in Section 2.5.5.

8.3 RECOMMENDATIONS

There are several recommendations for future work based on the results from this study. These have been split into several categories as shown below.

8.3.1 Additional field testing to estimate the in-situ stress ratio, K

Perhaps the most obvious next step following this study is to verify the proposed in-situ stress state values with alternate methods. As presented in Section 2.5.5, there are several field methods available to estimate the in-situ K value, each with its own set of advantages and limitations. Of all the current methods, the self-boring pressuremeter appears to be considered the method that results in the least soil disturbance. Unfortunately, this equipment is rarely used in South Africa, and it was not possible to arrange testing on the site within the timeframes of this study.

However, the remote monitoring system is still operational at the gold and iron ore sites, so there is still an opportunity to perform these tests and compare the results to those interpreted from the remote monitoring system. This activity will prove invaluable in challenging some of the assumptions made as part of this study, specifically those relating to the orientation of the principal planes and the associated effects on the interpretation of the stress values from the EPCs.

8.3.2 Additional sites for field monitoring

Although the initial intent of this study was to present long-term monitoring data for three different

© University of Pretoria

tailings materials, this ultimately proved unsuccessful due to a number of reasons. These reasons included last-minute operational changes in the long-term deposition plans in the case of the iron ore site, as well as theft and accidental cable damage in the case of the platinum site. Therefore, only long-term monitoring data were collected for the gold tailings site.

To expand on this knowledge, it is recommended that additional tailings dams are instrumented using the remote monitoring system. This system has been shown to work effectively and is relatively cost-effective. Naturally, to be able to comment on the observed stresses to the same extent as was done for the gold tailings site, any monitoring of soils other than gold tailings will require a similar effort to establish the soil behavioural framework as was presented in Chapter 3. If it is not possible to instrument additional sites, then additional locations on the existing dam should be instrumented.

8.3.3 Additional calibrations for the Earth Pressure Cells

As discussed earlier, there is some uncertainty regarding the performance of EPCs in soil, specifically regarding embedment cells. In this study, a limited attempt was made to verify the calibration coefficients provided by the manufacturer. This was done by performing pneumatic loading tests.

This can be improved upon. Ideally, verification tests should be conducted using physical calibration chambers that are designed to be capable of measuring the key test parameters with high accuracy. In this way the manufacturer's calibration coefficients can be verified in conditions that more closely represent the conditions expected in the field.

8.3.4 Additional sensors for field installations

With regard to the composition of the remote monitoring system, it was identified that the inclusion of additional sensors would likely improve the usefulness of the system, as well as help reduce the number of assumptions that needed to be made. Details regarding these additional sensors are provided in this section.

8.3.4.1 Installation of additional EPCs on inclined planes

A limitation of standard EPCs is that they can only measure normal stress (i.e. stress applied perpendicular to the face of the cell). However, it is known that the true soil stress state comprises both normal stresses (those acting in a direction perpendicular to the soil element) and shear

© University of Pretoria

stresses (those acting in a direction parallel to the soil element). The inability of a standard EPC to measure shear stresses results in assumptions having to be made regarding the orientation of the major and minor principal stresses. However, this assumption may not need to be made if additional EPCs, inclined at various orientations, are used. At the very least, the additional information provided by the cells could be used to quantify the likely error based on various assumptions.

For future studies, it is recommended that additional EPCs be placed at varying orientations in close proximity to each other. In this way, if the stress state is defined using a Mohr circle, then more points on the Mohr circle can be defined. All these points will still be lacking the shear stress component, this information is still valuable and can help reduce any uncertainty regarding the orientation of the principal stress planes.

8.3.4.2 Installation of additional EPCs to capture temperature influences on EPCs under constant load

In this study, it was found that in some cases the Geosense VWTPC-4000 EPCs under constant load are susceptible to seasonal temperature changes that cannot be corrected using the thermal correction factors provided by the manufacturer. It is believed that these changes are due to thermal effects on the entire cell assembly, and not just the influence on the pressure transducer, which is the basis for the thermal correction factors provided by the manufacturer.

It is therefore recommended that if the EPC are to be used in situations like this, a “redundant” EPC be installed on the site that is only subject to thermal influence and no changes in stress. This will help determine whether any additional thermal corrections are required for the “active” EPCs at the site. If corrections are required, these “redundant” cells could prove quite valuable in determining how these corrections should be implemented.

8.3.4.3 Additional sensors to measure soil suction

One of the key areas where the remote monitoring system proposed as part of this research can add value is in terms of long-term monitoring. At the time of installation, it was decided to omit the additional suction probes for several reasons, including budget and delivery time constraints.

Although it has been shown that these sensors do not perform optimally at low suctions, or in situations where there are fairly rapid changes in suction, these sensors have proved to be remarkably durable. Specifically, these sensors are not susceptible to cavitation which means that this could be particularly useful for long-term monitoring of dormant or decommissioned tailings

© University of Pretoria

dams where large suctions are expected to develop. Conversely, the Tuks tensiometers are susceptible to cavitation and are more suitable for short to medium term monitoring, especially in such environments where low degrees of saturation are expected.

Therefore, a combination of two steel-cased Tuks tensiometers, and a TEROS 21 WPS could be an ideal installation. The tensiometers will perform well at low suctions and will be able to track the rapid changes during deposition and the subsequent drying. The dual tensiometers will also provide some assurance on the accuracy of the measured suction. Although the WPS will not function effectively at low suctions, in cases where deposition ceases for an extended period of time, the sensor will continue to function once the tensiometers cavitate and will be able to provide reliable suction readings up to 100 MPa.

8.3.5 Additional Laboratory Element Testing

Although a fairly extensive laboratory testing campaign was conducted on the gold tailings, there is still some scope for further testing. Four particular areas are recommended for future work:

8.3.5.1 Triaxial testing of intact samples recovered from site to determine the undrained shear response

As discussed extensively earlier in this document, soil fabric plays an important role in the undrained shear behaviour of sandy soils such as mine tailings. In particular, there is evidence that remoulded samples created in the laboratory simply cannot reproduce the same undrained shear response as samples with the in-situ stress history and fabric (e.g. Chang et al., 2011).

In this study, extensive comments were made based on the observed undrained stress-strain response of the remoulded samples. However, this behaviour may be different for samples with the in-situ stress history and fabric. It therefore may be useful to repeat some of the tests conducted on intact samples recovered from site to verify whether these observations are still for samples with the in-situ stress history and fabric.

8.3.5.2 Triaxial testing of intact samples recovered from site to determine K_0

For this study, K_0 values were determined based on results from the remote monitoring system. To link these K_0 values to the associated undrained shear response of the gold tailings, a series of triaxial tests were conducted at various K_c values. However, there was no attempt made to compare the K_0 value determined on site to a K_0 value determined by performing K_0-consolidation

© University of Pretoria

in the laboratory. K_0-consolidation requires the use of a radial calliper to monitor changes in the diameter of the sample. Although there is equipment with this capability at the University, this equipment was not available at the time of the testing, so these tests were not conducted.

For future testing, it is recommended that K_0-consolidation of intact samples recovered from site be done to compare the K_0 value obtained from these tests, to the K_0 value determined from the remote monitoring system.

8.3.5.3 Triaxial testing of remoulded samples to determine K_0

In addition to performing K_0-consolidation for intact samples recovered from site, it may be useful to perform K_0-consolidation using remoulded samples. Samples can be prepared using the MT and SD techniques.

Although this may not be particularly useful in the greater context, especially considering how varied the stress state of the site samples may be, it may help expand our current understanding of the behavioural differences between remoulded and intact tailings samples.

8.3.5.4 Triaxial testing of remoulded samples prepared using slurry deposition

The triaxial testing conducted as part of this study focused predominantly on MT samples. A total of 21 tests were conducted and in general every test showed good compliance with the unique CSL that was proposed.

Limited testing was performed on SD samples, which were created using the air-drying technique as described by Reid et al. (2022b). These sample did not conform to the CSL established using the MT samples. Although this behaviour has been noted by others for gold tailings (Reid et al., 2022b) and iron ore tailings (Mmbando et al., 2023), both those studies were limited in nature.

Since the gold tailings was determined to not be a transitional soil, this is a concern, and it is recommended that this be investigated further. More tests should be conducted at various stress levels and under both drained and undrained shearing conditions. A specific attempt should be made to create SD samples in a loose state. With careful planning, this should be possible using the air-drying technique. Alternatively, methods such as those proposed by Vaid & Negussey (1988) could be used.

© University of Pretoria

9 REFERENCES

Adamson, P. T. 1981. *Southern African storm rainfall*. Department of Environmental Affairs. Technical Report TR 102.

Alabi, A. A., Akinyemi, O. D., and Adewale, A. 2013. Seismicity pattern in southern Africa from 1986 to 2009. *Earth Science Research*, 2(2), pp 1-10.

Askegaard, V. 1963. Measurement of pressure in solids by means of pressure cells. *In Bulletin Number 17*. Copenhagen: Structural Research Laboratory, Technical University of Denmark.

American Society for Testing and Materials **(ASTM)**. 2011. *ASTM D2435-04 Standard test methods for one-dimensional consolidation properties of soils using incremental loading*.

American Society for Testing and Materials **(ASTM)**. 2014. ASTM D5550-14: Standard Test Method for Specific Gravity of Soil Solids by Gas Pycnometer.

American Society for Testing and Materials **(ASTM)**. 2016a. ASTM D4253-16:Standard Test Methods for Maximum Index Density and Unit Weight of Soils Using a Vibratory Table.

American Society for Testing and Materials **(ASTM)**. 2016b. ASTM D4254-16: Standard Test Methods for Minimum Index Density and Unit Weight of Soils and Calculation of Relative Density. American Society for Testing and Materials.

American Society for Testing and Materials **(ASTM)**. 2017. ASTM D2487-17: Standard practice for classification of soils for engineering purposes (unified soil classification system).

American Society for Testing and Materials **(ASTM)**. 2020. ASTM D4767-11: Standard Test Method for Consolidated Undrained Triaxial Compression Test for Cohesive Soils. American Society for Testing and Materials.

Atkinson, J. H., and Bransby, P. L. 1978. *The mechanics of soils: an introduction to critical state soil mechanics*.

Audibert, J. M. E., and Tavenas, F. A. 1975. Discussion of “Evaluation of Stress Cell Performance.” *Journal of the Geotechnical Engineering Division*, 101(7), pp 705–707.

Basson, J. A. 2023. *Contribution of matric suction to the slope stability of tailings dams*. MEng Thesis, University of Pretoria, Pretoria.

Bates, R. C. 1969. SMRL Soil Stress Cell. *Proceedings of the Engineering Geology and Soils Engineering Symposium*, pp 9–32. Moscow.

Bedin, J., Schnaid, F., Da Fonseca, A. V, and Costa Filho, L. D. M. 2012. Gold tailings liquefaction under critical state soil mechanics. *Géotechnique*, 62(3), pp 263–267.

Been, K. 2016. Characterizing mine tailings for geotechnical design. *Australian Geomechanics Journal*, 50(4), pp 59–78.

Been, K., and Jefferies, M. G. 1985. A state parameter for sands. *Géotechnique*, 35(2), pp 99–112.

© University of Pretoria

Benkelman, A. C., and Lancaster, R. J. 1940. Important considerations in the design and use of soil pressure cells. *Proceedings of the Highway Research Board*, 20, pp 299–313.

Bentley Systems. 2023a. PLAXIS 2D Reference Manual.

Bentley Systems. 2023b. PLAXIS User Defined Soil Models - NorSand: An elasto-plastic model for soil behaviour with static liquefaction.

Biscontin, G. 2001. *Modeling the dynamic behaviour of lightly overconsolidated soil deposits on submerged slopes*. PhD Dissertation, University of California, California.

Bishop, A. W. 1959. The principal of effective stress. *Teknisk Ukeblad*, 106(39), pp 859–863.

Bishop, Alan W. 1971. Shear strength parameters for undisturbed and remolded soil specimens. *Roscoe Memorial Symposium*, pp 3–58.

Bishop, A. W, and Blight, G. E. 1963. Some aspects of effective stress in saturated and partly saturated soils. *Géotechnique*, 13(3), pp 177–197.

Bishop, A. W., and Henkel, D. J. 1962. *The measurement of soil properties in the triaxial test,* 2nd Edition. London: Edward Arnold Publishers.

Bjerrum, L., and Anderson, K. H. 1972. In-situ measurement of lateral pressures in clay. *Norwegian Geotechnical Institute Publication*, (91).

Blight, G. 2009. *Geotechnical engineering for mine waste storage facilities*. CRC Press.

Blight, G E, and Ofer, Z. 1984. Laboratory determination of K0 and comparison with prototype silo observations. *Proceedings of the Fourth Australia-New Zealand Conference on Geomechanics*, pp 83–87. Perth.

Blight, Geoffrey E. 1988. Some less familiar aspects of hydraulic fill structures. *Hydraulic Fill Structures*, pp 1000–1027.

Bolzon, G., Schrefler, B. A., and Zienkiewicz, O. C. 1996. Elastoplastic soil constitutive laws generalized to partially saturated states. *Géotechnique*, 46(2), pp 279–289.

Bordes, J. L., and Debreuille, P. J. 1984. Some facts about long-term reliability of vibrating wire instruments. *Reliability of Geotechnical Instrumentation*, pp 20–27.

Bozozuk, M. 1970. Field instrumentation of soil. *Proceedings of the Conference on the Design and Installation of Pile Foundations and Cellular Structures*, pp 145–157. Bethlehem: Lehigh University.

Brackley, I. J. A., and Sanders, P. J. 1992. In situ measurement of total natural horizontal stresses in an expansive clay. *Géotechnique*, 42(3), pp 443–451.

Brandt, M. 2011. *Seismic Hazard in South Africa*, Council for Geoscience Report Number: 2011-0061. Belville.

British Standards Institution **(BSI)**. *1990. BS 1377-7: Methods of test for soils for civil engineering purposes - shear strength tests*. London.

British Standards Institution **(BSI)**. 1999. *BS 5930: Code of practice for site investigations*. London.

Brown, S F. 1977. *State of the art report on field instrumentation for pavement experiments.*

© University of Pretoria

Transportation Research Record, (640), pp 13–28.

Brown, Stephen F, and Pell, P. S. 1967. Subgrade stress and deformation under dynamic load. *Journal of the Soil Mechanics and Foundations Division*, 93(1), pp 17–46.

Bruggemann, D. A., and Gosden, J. D. 2004. The Performance of Thika Dam, Kenya. *Long-Term Benefits and Performance of Dams: Proceedings of the 13th Conference of the British Dam Society and the ICOLD European Club Meeting*, University of Kent, Canterbury, UK from 22 to 26 June 2004., pp 421–432.

Campbell Scientific Inc. 2019. *TEROS 12 advanced soil moisture and temperature sensor with electrical conductivity brochure*.

Carder, D. R. 1976. Finite element analysis of the performance of rigid plate soil pressure cells. *Ground Engineering*, 9(8), pp 40–46.

Carraro, J. A. H., and Prezzi, M. 2008. A new slurry-based method of preparation of specimens of sand containing fines. *Geotechnical Testing Journal*, 31(1), pp 1–11.

Carrera, A., Coop, M. R., and Lancellotta, R. 2011. Influence of grading on the mechanical behaviour of Stava tailings. *Géotechnique*, 61(11), pp 935–946.

Cartwright, A., Coop, M. R., and Fourie, A. B. 2022. The implications of transitional behaviour for tailings. *Proceedings of the 20th International Conference on Soil Mechanics and Geotechnical Engineering*, pp 4351–4356. Sydney.

Castonguay, V., and Konrad, M. J. 2016. Prediction of the Fraser River sand response to oedometric loading using the NorSand soil model. *Proceedings of the 69th Canadian Geotechnical Conference*. Vancouver.

Castro, G. 1969. *Liquefaction of sands*. PhD Dissertation, Harvard Soil Mechanics.

Chadwick, P. 2019. *Brazil: shocking video captures moment of deadly dam collapse*. Retrieved February 23, 2020, from The Guardian website: https://www.theguardian.com/world/2019/feb/01/brazil-mining-dam-video-captures-moment-collapse

Chang, N. 2009. *The effect of fabric on the behaviour of gold tailings*. PhD Dissertation, University of Pretoria, Pretoria.

Chang, N., Heymann, G., and Clayton, C. 2011. The effect of fabric on the behaviour of gold tailings. *Géotechnique*, 61(3), pp 187–197.

Choquet, P., Juneau, F., Debreuille, P. J., and Bessette, J. 1999. Reliability, long-term stability and gage performance of vibrating wire sensors with reference to case histories. *Proceedings of the 5th International Symposium on Field Measurements in Geomechanics*, 1(3).

Choudhury, S. P. 1977. *A study of reinforced earth retaining walls with sand backfill by centrifugal modelling*. PhD Dissertation. The University of Manchester, United Kingdom.

Chu, J., and Gan, C. L. 2004. Effect of void ratio on K0 of loose sand. *Géotechnique*, 54(4), pp 285–288.

© University of Pretoria

International Centre for Numerical Methods in Engineering **(CIMNE)**. 2021. *Computational analyses of dam 1 failure at the Corrego de Feijão mine in Brumadinho. Barcelona*.

Collins, L. E. 1954. Some foundation experiences in the Durban area. *Civil Engineering*, 1954(8), pp 219–238.

Collins, R., Lee, K. J., Lilly, G. P., and Westmann, R. A. 1972. Mechanics of pressure cells: A theoretical and experimental analysis of miniature semiconductor strain gages is presented. *Experimental Mechanics*, 12(11), pp 514–519.

Coop, M. R. 2015. Limitations of a critical state framework applied to the behaviour of natural and "transitional" soils. *Proceedings of 6th International Symposium on Deformation Characteristics of Geomaterials (IS-Buenos Aires)*, pp 115–155.

Coop, M. R. 1990. The mechanics of uncemented carbonate sands. *Géotechnique*, 40(4), pp 607–626.

Corrêa, M. M., and Oliveira Filho, W. L. 2019. Impact of methods used to reconstitute tailings specimens on the liquefaction potential assessment of tailings dams. *REM-International Engineering Journal*, 72(3), pp 507–513.

Cullity, B. D. 1956. *Elements of X-ray Diffraction*. Addison-Wesley Publishing.

da Fonseca, A. V., Cordeiro, D., and Molina-Gómez, F. 2021. Recommended procedures to assess critical state locus from triaxial tests in cohesionless remoulded samples. *Geotechnics*, 1(1), pp 95–127.

Daigle, L., and Zhao, J. Q. 2004. The influence of temperature on earth pressure cell readings. *Canadian Geotechnical Journal*, 41(3), pp 551–559.

Daliri, F. 2013. *The influence of desiccation and stress history on monotonic and cyclic shear response of thickened gold tailings*. PhD Dissertation, Carleton University, Ontario.

Davis, J. L., and Chudobiak, W. J. 1975. In-situ meter for measuring relative permittivity of soils. *Geological Survey of Canada Paper 75-1A*, pp 75-79, Ottawa.

de Mello Martins, P., Alves, H. O., Moghaddam, R., and Gagnon, A. 2022. Assessing dilative conditions of cyclone underflow tailings. *Proceedings of Tailings and Mine Waste 2022*. Colorado.

Deák, F., Ván, P., and Vásárhelyi, B. 2012. Hundred years after the first triaxial test. *Periodica Polytechnica Civil Engineering*, 56(1), pp 115–122.

Desrues, J., Chambon, R., Mokni, M., and Mazerolle, F. 1996. Void ratio evolution inside shear bands in triaxial sand specimens studied by computed tomography. *Géotechnique,* 46(3), pp 529–546.

Department: Minerals and Energy **(DME)**. 2000. *Guideline for the compilation of a mandatory code of practice on mine residue deposits*. DME reference number: 16/3/2/2-A1.

Engineers and Geologists British Columbia **(EGBC)**. 2022. *Disciplinary Hearings and Notices*. Retrieved December 3, 2023, from https://www.egbc.ca/Complaints-Discipline/Complaints-

© University of Pretoria

Discipline/Discipline-Hearings-Notices#disciplineary_orders

Dladla, S. D., and Ramsamy, S. 2022. Practical steps to Global Industry Standard on Tailings Management (GISTM) compliance for operational tailings storage facilities in South Africa. *Journal of the Southern African Institute of Mining and Metallurgy*, 122(6), pp 283–290.

Dludla, N. 2022. *South Africa mine dam wall collapses killing 1 and injuring 40*. Retrieved September 12, 2022, from Reuters website: https://www.reuters.com/world/africa/south-africa-mine-dam-wall-collapses-killing-three-injuring-40-2022-09-11/

Doanh, T., Ibraim, E., and Matiotti, R. 1997. Undrained instability of very loose Hostun sand in triaxial compression and extension. Part 1: experimental observations. *Mechanics of Cohesive-Frictional Materials: An International Journal on Experiments, Modelling and Computation of Materials and Structures*, 2(1), pp 47–70.

Donaldson, G W. 1960. The stability of slimes dams in the gold mining industry. *Journal of the Southern African Institute of Mining and Metallurgy*, 61(3), pp 183–199.

Donaldson, G. W. 1965. The effects of capillary action on the consolidation and shear strength of silt in a hydraulic fill dam. *Proceedings of the 6th International Conference on Soil Mechanics and Foundation Engineering*, pp 459–463. Montreal.

Dunn, C. S., and Billam, J. 1966. A study of the response characteristics of a new miniature earth pressure cell. *Civil Engineering and Public Works Review*, 61(715), pp 181–186.

Dunnicliff, J. 1997. Temperature sensitivity of earth pressure cells. *Geotechnical Instrumentation News*, 15(2), pp 42.

Dunnicliff, J, and Green, G. E. 1988. *Geotechnical instrumentation for monitoring field performance*. New York: John Wiley and Sons.

Department: Water Affairs and Forestry **(DWAF)**. 1996. *South African Water Quality Guidelines: Volume 1 - Domestic Use.*

Department: Water and Sanitation **(DWS)**. 2023. *Water and Sanitation outlines progress regarding its response to Jagersfontein tailings dam collapse*. Retrieved September 14, 2023, from https://www.gov.za/speeches/water-and-sanitation-outlines-progress-regarding-its-response-Jagersfontein-tailings-dam

Dyvik, R., Berre, T., Lacasse, S., and Raadim, B. 1987. Comparison of truly undrained and constant volume direct simple shear tests. *Géotechnique*, 37(1), pp 3–10.

Eckersley, D. 1990. Instrumented laboratory flowslides. *Géotechnique*, 40(3), pp 489–502.

Elbanna, M., Quinn, J., and Martens, S. 2011. SPT - CPT correlations for oilsands tailings sand. *Proceedings of Tailings and Mine Waste 2011*.

ESI Technology **(ESI)**. 2021. Genspec GS4200: General purpose pressure transmitter datasheet. ESI Technology.

Fanni, R., Reid, D., and Smith, K. 2019. On some considerations related to pore fluid chemistry in tailings critical state testing. *Proceedings of Tailings and Mine Waste 2019*, pp 965–977.

© University of Pretoria

Vancouver.

Fanni, R., Reid, D., and Fourie, A. 2022. On reliability of inferring liquefied shear strengths from simple shear testing. *Soils and Foundations*, 62(3), pp 101151.

Felio, G. Y., and Bauer, G. E. 1986. Factors affecting the performance of a pneumatic earth pressure cell. *Geotechnical Testing Journal*, 9(2), pp 102–106.

Fellner-Feldegg, H. 1969. Measurement of dielectrics in the time domain. *The Journal of Physical Chemistry*, 73(3), pp 616–623.

The Federal Emergency Management Agency **(FEMA)**. 2005. *Technical Manual: Conduits through Embankment Dams.*

Fotovvat, A., and Sadrekarimi, A. 2022. Instability of a gold mine tailings subjected to different stress paths. *Journal of Geotechnical and Geoenvironmental Engineering*, 148(5), 4022020.

Fotovvat, A., Sadrekarimi, A., and Etezad, M. 2022. Instability of gold mine tailings subjected to undrained and drained unloading stress paths. *Géotechnique*, pp 1–19.

Fourie, A. B., Blight, G. E., and Papageorgiou, G. 2001. Static liquefaction as a possible explanation for the Merriespruit tailings dam failure. *Canadian Geotechnical Journal*, 38(4), pp 707–719.

Fourie, A. B., and Papageorgiou, G. 2001. Defining an appropriate steady state line for Merriespruit gold tailings. *Canadian Geotechnical Journal*, 38(4), pp 695–706.

Fourie, A. B., and Tshabalala, L. 2005. Initiation of static liquefaction and the role of K0 consolidation. *Canadian Geotechnical Journal*, 42(3), pp 892–906.

Fourie, A. B., Verdugo, R., Bjelkevik, A., Torres-Cruz, L. A., and Znidarcic, D. 2022. Geotechnics of mine tailings: a 2022 state of the art. *Proceedings of the 20th International Conference on Soil Mechanics and Geotechnical Engineering*, pp 121–182. Sydney.

Fourie, A. B., and Reid, D. 2021. *Static liquefaction workshop*. Western Australia: Australian Centre for Geomechanics.

Fukagawa, R., and Ohta, H. 1988. Effect of some factors on K0-value of a sand. *Soils and Foundations*, 28(4), pp 93–106.

France, J. W., Alvi, I. A., Dickson, P. A., Falvey, H. T., Rigbey, S. J., and Trojanoswki, J. T. 2018. *Independent forensic team report: Orville dam spillway incident*. California.

France, J. W., Alvi, I. A., Miller, A. C., Williams, J. L., and Higinbotham, S. 2022. *Investigation into failures of Edenville and Sanford dams - final report.*

Franke, E., Kiekbusch, M., and Schuppener, B. 1979. A new direct simple shear device. *Geotechnical Testing Journal*, 2(4), pp 190–199.

Fredlund, D. G. 1973. *Volume change behaviour of unsaturated soils*. PhD Dissertation, University of Alberta.

Fredlund, D. G. 2017. Role of the soil-water characteristic curve in unsaturated soil mechanics. *Proceedings of the 19th International Conference on Soil Mechanics and Geotechnical*

© University of Pretoria

Engineering, pp 17–22.

Fredlund, D. G. 2019. Determination of unsaturated soil property functions for engineering practice. *Proceedings of the 17th African Regional Conference on Soil Mechanics and Geotechnical Engineering*, pp 3–19. Cape Town.

Fredlund, D. G., and Xing, A. 1994. Equations for the soil-water characteristic curve. *Canadian Geotechnical Journal*, 31(4), pp 521-532.

Gallage, C. P. K., and Uchimura, T. 2010. Effects of dry density and grain size distribution on soil-water characteristic curves of sandy soils. *Soils and Foundations*, 50(1), pp 161–172.

Global Digital Systems **(GDS)** Instruments. 2017. *GDSLAB v2.5.4 - The GDS Laboratory Users Handbook*, United Kingdom.

Geldenhuys, L., Narainsamy, Y., and Hörtkorn, F. 2019. The limitations of standpipe piezometers in stability analysis. *Proceedings of the 17th African Regional Conference on Soil Mechanics and Geotechnical Engineering*, pp 435–440. Cape Town.

Geldenhuys, N. P. 2014. *Ownership of historic mine and tailings dumps and expropriation*. LLM Thesis, North-West University.

George, A. 2022. *Aberfan disaster*. Retrieved September 21, 2022, from http://www.alangeorge.co.uk/AberfanDisaster.htm

Geosense Ltd. 2016. *Total pressure cells VWTPC-4000 instruction manual*. Retrieved from https://www.geosense.co.uk/wp-content/uploads/2021/04/Total-Pressure-Cell-VWTPC-4000-Manual-V1.5.pdf

Geosynthetic Institute 2017. GRI GT13(a) - *ASTM Version Standard Specification for Test method and properties for geotextiles used as separation between subgrade soil and aggregate*. Folsom.

Graham, J., and Jefferies, M.G. 1986. Some examples of in situ lateral stress determinations in hydraulic fills using the self-boring pressuremeter. *Proceedings of the 39th Canadian Geotechnical Conference*. Ottawa, Canada.

Grebby, S., Sowter, A., Gluyas, J., Toll, D., Gee, D., Athab, A., and Girindran, R. 2021. Advanced analysis of satellite data reveals ground deformation precursors to the Brumadinho tailings dam collapse. *Communications Earth and Environment*, 2(1), pp 1-9.

Grognet, M. 2011. *The boundary conditions in direct simple shear tests - developments for peat testing at low normal stress*. MSc Thesis, Delft University of Technology, Delft.

Growcol International Technology Company **(Growcol)**. 2021. *Monocystalline 10W Solar Panel Datasheet*. Growcol.

Hadala, P. F. 1967. The effect of placement method on the response of soil stress gauges. *Proceedings of the International Symposium on Wave Propagation and Dynamic Properties of Earth Materials*, pp 255–263. Albuquerque: University of New Mexico.

Hamouche, K. K., Leroueil, S., Roy, M., and Lutenegger, A. J. 1995. In situ evaluation of K0 in

© University of Pretoria

eastern Canada clays. *Canadian Geotechnical Journal*, 32(4), pp 677–688.

Handy, R. L. 1983. Discussion of "K0-OCR Relationships in Soils" by Paul W. Mayne and Fred H. Kulhawy (1982). *Journal of Geotechnical Engineering*, 109(6), pp 862–864.

Hatton, C. N., Spencer, D. L., Bareither, C. A., and Ward, K. J. 2020. All hands on deck! - a semi-quantitative attempt to characterise the impending qualified tailings professional resource shortage*. Proceedings of Tailings and Mine Waste 2020*, pp 551–565. Virtual Event: Colorado State University.

Hayat, T. M. 1992. *The coefficient of earth pressure at rest*. PhD Dissertation, University of Illinois, Illinois.

Harmony Gold Mining Company Limited **(HGM)** (2023). *Mineral Resources and Reserves: 30 June 2023*.

High Court of South Africa. 2007. *De Beers vs. Ataqua Mining*, Case No. 3215/06, High Court of South Africa – Orange Free State Provincial Division.

High Court of South Africa. 2017. *De Beers vs. Lucky Seekoei*, Case No. 1488/17, High Court of South Africa - Northern Cape Provincial Division.

Howell, G., and Kirsten, A. 2016. Interface shear: towards understanding the significance in geotechnical structures. *Proceedings of the First Southern African Geotechnical Conference,* pp 269-274. Rustenburg.

Hughes, C. 1966. *Report of the tribunal appointed to inquire into the disaster at Aberfan on October 21st, 1966*. London.

Hvorslev, M. J. 1951. *Time lag and soil permeability in ground-water observations*. Waterways Experiment Station, Corps of Engineers, US Army.

Hvorslev, M. J. 1976. *The changeable interaction between soils and pressure cells: tests and reviews at the waterways experiment station*.

International Council for Mining and Metals **(ICMM)**. 2021a. *Conformance protocols: global industry standard on tailings management.*

International Council for Mining and Metals **(ICMM)**. 2021b. *Tailings management: good practice guide*.

International Commission on Large Dams **(ICOLD)**. 2022. *Bulletin No. 194: Tailings dam safety*, Paris.

International Electrotechnical Commission **(IEC)**. 2001. *IEC 60529: Degrees of protection provided by enclosures (IP Code)*. Geneva.

Ingram, J. K. 1965. The development of a free-field soil stress gage for static and dynamic measurements. *Instruments and Apparatus for Soil and Rock Mechanics (STP 392)*, pp 20–36.

Ishihara, K. 1993. Liquefaction and flow failure during earthquakes. *Géotechnique*, 43(3), pp 351–451.

International Organisation of Standardisation **(ISO)**. 2020. *ISO 13320:2020 Particle size analysis -*

© University of Pretoria

Laser diffraction methods.

Itasca Consulting Group Incorporated **(Itasca)**. 2015. *FLAC 3D - Fast Lagrangian Analysis of Continua in Three-Dimensions*. Minneapolis.

Jacobsz, S. W. 2018. Low cost tensiometers for geotechnical applications. *Physical Modelling in Geotechnics*, pp 305–310. CRC Press.

Jacobsz, S. W. 2019. TUKS tensiometer measures to--1.7 Mega Pascal. *SAICE Civil Engineering*, 27(1), pp 24–26.

Jaky, J. 1944. The coefficient of earth pressure at rest. *Journal of the Society of Hungarian Architects and Engineers*, 78(22), pp 355–358.

Jaky, J. 1948. Pressure in silos. *Proceedings of the 2nd International Conference on Soil Mechanics*, 1, pp 103–107. Rotterdam.

Jamiolkowski, M. 1995. Opening address. *Proceedings of the International Symposium on Cone Penetration Testing*, pp 7–15. Linkoping.

Jamiolkowski, M., Leroueil, S., and Lo Presti, D. C. F. 1991. Design parameters from theory to practice. *Proceedings of the International Conference on Geotechnical Engineering for Coastal Development*, 2, pp 877–917.

Jefferies, M. G., and Been, K. 2000. Implications for critical state theory from isotropic compression of sand. *Géotechnique*, 50(4), pp 419–429.

Jefferies, M. G., and Been, K. 2015. *Soil liquefaction: a critical state approach*. 2nd edition, CRC press.

Jefferies, M. G. 1993. Nor-Sand: a simple critical state model for sand. *Géotechnique*, 43(1), pp 91–103.

Jefferies, M. G., Morgenstern, N. R., Van Zyl, D., and Wates, J. 2019. *Report on NTSF embankment failure*. Sydney, Australia: Cadia Valley Operations, for Ashurst Australia.

Jefferies, M. G. 2022. Improving governance will not be sufficient to avoid dam failures. *Proceedings of the Institution of Civil Engineers-Geotechnical Engineering*, 175(2), pp 166–180.

Jefferies, M. G., and Shuttle, D. A. 2005. NorSand: Features, calibration and use. *Soil Constitutive models: evaluation, selection, and calibration*, pp 204–236.

Jin, Y.-F., Yin, Z.-Y., Shen, S.-L., and Hicher, P.-Y. 2016. Investigation into MOGA for identifying parameters of a critical-state-based sand model and parameters correlation by factor analysis. *Acta Geotechnica*, 11(5), pp 1131–1145.

erse Kablo (2021). *LIYCY cable datasheet.*

Kallstenius, T., and Bergau, W. 1956. Investigations of soil pressure measuring by means of cells. *Royal Swedish Geotechnical Institute Proceedings No 12*. Statens geotekniska institut.

Kato, S., Ishihara, K., and Towhata, I. 2001. Undrained shear characteristics of saturated sand under anisotropic consolidation. *Soils and Foundations*, 41(1), pp 1–11.

Kennard, M. F., Penman, A. D. M., and Vaughan, P. R. 1967. Stress and strain measurements in

© University of Pretoria

the clay core at Balderhead Dam. *Transactions of the 9th International Congress on Large Dams*, Volume 3, pp 129–151. Istanbul.

Klotz, E. U., and Coop, M. R. 2002. On the identification of critical state lines for sands. *Geotechnical Testing Journal*, 25(3), pp 289–302.

König, U., Norberg, N., and Gobbo, L. 2017. From iron ore to iron sinter - process control using X-Ray Diffraction (XRD*). Anais Dos Seminários de Redução, Minério de Ferro e Aglomeração*, pp 146–153. Rio de Janeiro.

Konrad, J. M. 1993. Undrained response of loosely compacted sands during monotonic and cyclic compression tests. *Géotechnique*, 43(1), pp 69–89.

Kudla, W., Rosenzweig, T., Szczyrba, S., and Weissbach, J. 2022. Research results on soil liquefaction of mine dumps in Eastern Germany. *Proceedings of the 20th International Conference on Soil Mechanics and Geotechnical Engineering*, pp 4363–4368. Sydney.

Kulhawy, F. H., and Mayne, P. W. 1982. K0-OCR relationship in soil*. ASCE Journal of the Geotechnical Engineering Division*, 108, pp 851–872.

Ladd, R. S. 1978. Preparing test specimens using undercompaction. *Geotechnical Testing Journal*, 1(1), pp 16–23.

Lade, P. V. 2016. *Triaxial testing of soils*. John Wiley and Sons.

le Roux, G. 2002. The effectiveness of single and multiple open standpipe piezometers in monitoring of the pore pressure regime in tailings dams. *Proceedings of Tailings and Mine Waste 2002*. Colorado.

le Roux, P. 2019. *The measurement of soil-water retention curves using the tensiometer method*. MEng Thesis, University of Pretoria, Pretoria.

Lefebvre, G., Bozozuk, M., Philibert, A., and Hornych, P. 1991. Evaluating K0 in Champlain clays with hydraulic fracture tests. *Canadian Geotechnical Journal*, 28(3), pp 365–377.

Leyden, P., and Mametse, A. 2020. *The unregulated terrain of historic mine dumps in South Africa*. Retrieved February 13, 2023, from Herbert Smith Freehills website: https://hsfnotes.com/africa/2020/07/08/the-unregulated-terrain-of-historic-mine-dumps-in-south-africa/

Li, W. 2017. *The mechanical behaviour of tailings*. PhD Dissertation, City University of Hong Kong, Hong Kong.

Lindgård, A., and Ofstad, C. S. 2016. *An evaluation of methods to determined K0 in clays*, MSc Thesis, Norwegian University of Science and Technology, Trondheim.

Lu, N., and Likos, W. J. 2004. *Unsaturated soil mechanics*, 1st Edition. New Jersey: John Wiley and Sons.

Lu, N., Godt, J. W., and Wu, D. T. 2010. A closed-form equation for effective stress in unsaturated soil. *Water Resources Research*, 46(5), W05515.

Madabhushi, G. 2017. *Centrifuge modelling for civil engineers*, 1st Edition. Boca Raton: CRC

© University of Pretoria

Press.

Marchetti, S. 1980. In situ tests by flat dilatometer. *Journal of the Geotechnical Engineering Division*, 106(3), pp 299–321.

Martin, T. E., and McRoberts, E. C. 1999. Some considerations in the stability analysis of upstream tailings dams. *Proceedings of the Sixth International Conference on Tailings and Mine Waste*, 99, pp 287–302.

Mathiba, G. 2022. *The Jagersfontein tragedy of 11 September 2022: Who must be held accountable for mine tailings dump management failure - the DMRE or De Beers or Superkolong?* Retrieved February 13, 2023, from AfricLaw website: https://africlaw.com/2022/09/16/the-jagersfontein-tragedy-of-11-september-2022-who-must-be-held-accountable-for-mine-tailings-dump-management-failure-the-dmre-or-de-beer-or-superkolong/

Minerals Council of South Africa **(MCSA)**. 2020. *We care and we remember: Merriespruit, 22 February 1994*. Retrieved November 18, 2023, from https://www.mineralscouncil.org.za/industry-news/we-care-we-remember/324-we-remember-merriespruit%0A

Mele, L., Tian, J. T., Lirer, S., Flora, A., and Koseki, J. 2019. Liquefaction resistance of unsaturated sands: experimental evidence and theoretical interpretation. *Géotechnique*, 69(6), pp 541–553.

Mesri, G., and Hayat, T. M. 1993. The coefficient of earth pressure at rest. *Canadian Geotechnical Journal*, 30(4), pp 647–666.

METER Group. 2018. *TEROS 12 user manual.*

METER Group. 2020. *TEROS 21 (Gen 2) user manual.*

Michalowski, R. L. 2005. Coefficient of earth pressure at rest. *Journal of Geotechnical and Geoenvironmental Engineering*, 131(11), pp 1429–1433.

Michigan Live **(MLive)**. 2020. *Michigan dam failure caught on video*. Retrieved November 20, 2023, from https://www.youtube.com/watch?v=Hc3u_CHVHJ8

Mmbando, E., Fourie, A. B., and Reid, D. 2023. Mechanics of an Iron Ore Tailings Exhibiting Transitional Behaviour. *Geotechnical and Geological Engineering*, pp 1–10.

Monfore, G. E. 1950. *An analysis of the stress distributions in and near stress gages embedded in elastic solids*. US Bureau of Reclamation.

Morgenstern, N. R. 2020. *Fundão Tailings Dam Failure*. Retrieved October 10, 2022, from MB Geotech website: https://www.youtube.com/watch?v=ZCaPPmdDgXY

Morgenstern, N. R., Vick, S. G., and Van Zyl, D. 2015. *Report on Mount Polley tailings storage facility breach*. Report of Independent Expert Engineering Investigation and Review Panel. Prepared on Behalf of the Government of British Columbia and the Williams Lake and Soda Creek Indian Bands.

Morgenstern, N. R., Vick, S. G., Viotti, C. B., and Watts, B. D. 2016. *Fundão tailings dam review*

© University of Pretoria

panel report on the immediate causes of the failure of the Fundão dam. SAMARCO, SA, Vale, SA, Eds, 76.

Narainsamy, Y., Geldenhuys, L., and Hörtkorn, F. 2019. Use of mode of shear for undrained slope stability analysis. Proceedings of the *17th African Regional Conference on Soil Mechanics and Geotechnical Engineering*, pp 727–732. Cape Town.

Narainsamy, Y., and Jacobsz, S. W. 2022. Influence of K0 consolidation on yield undrained shear strength in triaxial compression. *Proceedings of the 8th International Conference on Tailings Management*, pp 123–130. Online Conference.

Narainsamy, Y., and Jacobsz, S. W. 2023a. A review of geostatic stress measurements in mine tailings. *Proceedings of the Southern African Institute of Mining and Metallurgy Conference on Next Generation Tailings - Opportunity or Risk?,* pp 29–40. Johannesburg.

Narainsamy, Y., and Jacobsz, S. W. 2023b. Evaluating the performance of three sensor types for long-term measurement of suction in gold tailings. *Proceedings of the 8th International Conference on Unsaturated Soils.* Milos.

Newman, P., Bruton, M., Burgos, J., and Purrington, J. 2022. Innovations in tailings management - hydraulic dry stacking. *Proceedings of Tailings and Mine Waste 2022*, pp 1129-1140. Colorado.

Newman, P., Bruton, M., Lopez, A., Burgos, J., and Purrington, J. 2023. Successes with hydraulic dewatered stacking at the El Soldado demonstration facility. *Proceedings of Tailings and Mine Waste 2023*, pp 1587–1600. Vancouver.

O'Connor, B. H., and Raven, M. D. 1988. Application of the Rietveld refinement procedure in assaying powdered mixtures. *Powder Diffraction*, 3(1), pp 2–6.

Oberle, B. 2020. *Global industry standard on tailings management (GISTM)*.

Obrician, V. 1969. Determination of lateral pressure associated with consolidation of granular soils. *Highway Research Record*, (284).

Ofer, Z. 1981. Laboratory instrument for measuring lateral soil pressure and swelling pressure. *Geotechnical Testing Journal*, 4(4), pp 177–182.

Olalla, C., and Cuellar, V. 2001. Failure mechanism of the Aznalcóllar dam, Seville, Spain. *Géotechnique*, 51(5), pp 399–406.

Olson, S. M. (2001). *Liquefaction analysis of level and sloping ground using field case histories and penetration resistance*, PhD Dissertation, University of Illinois, Illinois.

Olson, S. M., and Stark, T. D. 2003. Use of laboratory data to confirm yield and liquefied strength ratio concepts. *Canadian Geotechnical Journal*, 40(6), pp 1164–1184.

Omar, T., and Sadrekarimi, A. 2014. Effects of multiple corrections on triaxial compression testing of sands. *Journal of GeoEngineering*, 9(2), pp 75–83.

Pang, P. L. R. 1986. A new boundary stress transducer for small soil models in the centrifuge. *Geotechnical Testing Journal*, 9(2), pp 72–79.

© University of Pretoria

Papageorgiou, G. 2004. *Liquefaction assessment and flume modelling of the Merriespruit gold and Bafokeng platinum tailings*. PhD Dissertation, University of the Witwatersrand, Johannesburg.

Parry, R. H. G. 2004. *Mohr circles, stress paths and geotechnics*. CRC Press.

Peattie, K. R., and Sparrow, R. W. 1954. The fundamental action of earth pressure cells. *Journal of the Mechanics and Physics of Solids*, 2(3), pp 141–155.

Philip, L. 2016. Jagersfontein – the forgotten gem of the Free State. *New Contree*, 76(0), 22.

Plewes, H. D., Davies, M. P., and Jefferies, M. G. 1992. CPT based screening procedure for evaluating liquefaction susceptibility. *Proceedings of the 45th Canadian Geotechnical Conference*, 4, pp 1–9. Toronto.

Ponzoni, E., Nocilla, A., Coop, M. R., and Colleselli, F. 2014. Identification and quantification of transitional modes of behaviour in sediments of Venice lagoon. *Géotechnique*, 64(9), pp 694–708.

Prisco, C. di, Matiotti, R., and Nova, R. 1995. Theoretical investigation of the undrained stability of shallow submerged slopes. *Géotechnique*, 45(3), pp 479–496.

Rankine, W. J. M. 1856. On the Stability of Loose Earth. *Proceedings of the Royal Society of London*, pp 185–187.

Rankka, K. 1990. Measuring and predicting lateral earth pressured in slopes in soft clays in Sweden. *Transportation Research Board*, pp 172–182.

Reid, D. 2021. Some considerations on the engineering performance of subaqueasly-deposited silts. *Proceedings of Mine Waste and Tailings 2021*. Brisbane.

Reid, D., Dickinson, S., Mital, U., Fanni, R., and Fourie, A. 2022a. On some uncertainties related to static liquefaction triggering assessments. *Proceedings of the Institution of Civil Engineers-Geotechnical Engineering,* 175(2), pp 181–199.

Reid, D., Fourie, A. B., Ayala, J. L., Dickinson, S., Ochoa-Cornejo, F., Fanni, R., Garfias, J., de Fonseca, A. V., Ghafghazi, M., Ovalles, C., Riemer, M., Rismanchian, A., Olivera, R. and Suazo, G. 2021. Results of a critical state line testing round robin programme. *Géotechnique*, 71(7), pp 616–630.

Reid, D., Fourie, A. B., Castro, J., and Lupo, J. 2018. Undrained shear strength evolution with loading on an undisturbed block sample of desiccated gold tailings. *Proceedings of Tailings and Mine Waste 2018*, pp 365-376. Colorado.

Reid, D., Fourie, A. B., and Fanni, R. 2022b. Layering--the missing factor in fabric studies? *Proceedings of the 20th International Conference on Soil Mechanics and Geotechnical Engineering*, pp 209-214, Sydney.

Reid, D., Simms, P., Sivathayalan, S., Fanni, R., and Fourie, A. B. 2022c. The “air dried” specimen reconstitution technique--review, refinements, and applications. *Proceedings of Tailings and Mine Waste 2022, pp 451-451. Colorado.*

Reiff, C. M., and Linger, D. A. 1967. Investigation of Buried Domes-Phase I-Evaluation of

© University of Pretoria

Instrumentation and Preliminary Tests. *Technical Report AFWL-TR-67--110*, Airforce Weapons Laboratory. NM Kirtland Airforce Base.

Rendulic, L. 1936. Relation between void ratio and effective principal stresses for a remoulded, silty clay. *Proceedings of the International Conference on Soil Mechanics and Foundation Engineering*, pp 48–51. Cambridge: Harvard University.

Rendulic, L. 1937. Ein grundgesetz der tonmechanik und sein experimenteller beweis (A fundamental law of clay mechanics and its experimental proof). *Bauingenieur*, 18(31), pp 459–467.

Rico, M., Benito, G., and Diez-Herrero, A. 2008. Floods from tailings dam failures. *Journal of Hazardous Materials*, 154(1–3), pp 79–87.

Riemer, M. F., and Seed, R. B. 1997. Factors affecting apparent position of steady-state line. *Journal of Geotechnical and Geoenvironmental Engineering*, 123(3), pp 281–288.

Rietveld, H. M. 1969. A profile refinement method for nuclear and magnetic structures. *Journal of Applied Crystallography*, 2(2), pp 65–71.

Riveros, G. A., and Sadrekarimi, A. 2021. Static liquefaction behaviour of gold mine tailings. *Canadian Geotechnical Journal*, 58(6), pp 889–901.

Rivet, S. 2023. *Preliminary Survey Report for Jagersfontein*. Vancouver.

Robertson, P K. 2017. Evaluation of flow liquefaction: Influence of high stresses. *Proceedings of the 3rd International Conference on Performance Based Design (PBD-III)*. Vancouver.

Robertson, P K, de Melo, L., Williams, D. J., and Wilson, G. W. 2019. *Report on the expert panel on the technical causes of the failure of the Feijão dam 1.*

Robertson, Peter K, Brouwer, K., Sully, T. E., and Gagnon, A. 2023. Influence of Increased Confining Stress on Undrained Behavior of Tailings: A Case History at the Candelaria Mine. *ISSMGE International Journal of Geoengineering Case Histories*, 7(3), pp 34–55.

Romero, E., Gens, A., and Lloret, A. 1999. Water permeability, water retention and microstructure of unsaturated compacted Boom clay. *Engineering Geology*, 54(1–2), pp 117–127.

Rosenzweig, T., Szczyrba, S., and Kudla, W. 2020. Spannungszustaende in Abraumfoerderbrueckenkippenitle (Stress state in conveyor bridge dumps). *Geotechnik*, 43(4), pp 237–247.

Rowe, P. W., and Barden, L. 1964. Importance of free ends in triaxial testing. *Journal of the Soil Mechanics and Foundations Division*, 90(1), pp 1–27.

Rozina, E., Mizani, S., Malek, M., and Simms, P. 2015. Model bearing capacity tests in a large laboratory simulation of polymer amended MFT. *68th Canadian Geotechnical Conference*. Québec.

Republic of South Africa **(RSA)**. 1993. *Occupational Health and Safety Act*. Government Gazette 14918, Vol 337, Published 2 July 1993.

Republic of South Africa **(RSA)**. 1996. *Mine Health and Safety Act*. Government Gazette 17242,

© University of Pretoria

Vol 584, No 967, Published 14 June 1996.

Republic of South Africa **(RSA)**. 2013a. National Environmental Management: Waste Act. Act no. 59 of 2008, *government notice R634 (GN634)*. Government Gazette 36784.

Republic of South Africa **(RSA)**. 2013b. National Environmental Management: Waste Act. Act no. 59 of 2008, *government notice R635 (GN635)*. Government Gazette 36784.

Republic of South Africa **(RSA)**. 2013c. National Environmental Management: Waste Act. Act no. 59 of 2008, *government notice R636 (GN636).* Government Gazette 36784.

South Africa Bureau of Standards **(SABS)**. 1998. *SABS 10286: Code of practice for mine residue*.

South Africa Bureau of Standards **(SABS)**. 2015. *SANS 241-2:2015 Drinking Water Part 2: Application of SANS 241-1*.

Sadrekarimi, A. 2014. Effect of the mode of shear on static liquefaction analysis. *Journal of Geotechnical and Geoenvironmental Engineering*, 140(12), 4014069.

Sachan, A. 2011. Shear testing data of soil: a function of boundary friction in triaxial setup. *Indian Geotechnical Journal*, 41(4), pp 168–176.

Sasitharan, S., Robertson, P. K., Sego, D. C., and Morgenstern, N. R. 1993. Collapse behavior of sand. *Canadian Geotechnical Journal*, 30(4), pp 569–577.

Scarlett, N. V. Y., Madsen, I. C., Pownceby, M. I., and Christensen, A. N. 2004. In situ X-ray diffraction analysis of iron ore sinter phases. *Journal of Applied Crystallography*, 37(3), pp 362–368.

Schofield, A. N., and Wroth, P. 1968. *Critical state soil mechanics*. McGraw-hill London.

United States Securities and Exchange Commission **(SEC)**. 2022. *Press release: SEC charges Brazilian mining company with misleading investors about safety prior to deadly dam collapse*. Retrieved May 2, 2022, from https://www.sec.gov/news/press-release/2022-72

United States Securities and Exchange Commission **(SEC)**. 2023. *Press release: Brazilian mining company to pay $55.9 million to settle charges related to misleading disclosures prior to deadly dam collapse*. Retrieved April 3, 2023, from https://www.sec.gov/news/press-release/2023-63

Selig, E. T. 1964. A review of stress and strain measurement in soil. *Proceedings of the Symposium on Soil-Structure Interaction*, pp 172–186. Tuscon.

Selig, E. T., and Tobin, H. G. 1967. Investigation of piezoresistive soil stress gauges. *Proceedings of the International Symposium on Wave Propagation and Dynamic Properties of Earth Materials*, pp 239–254. Albuquerque: University of New Mexico.

Sellers, B. 2000. Temperature effects on earth pressure and concrete stress cells - some theoretical consideration. *Geotechnical Instrumentation News*, 18(1), pp 23–24.

Shannon & Wilson Incorporated (**Shannon & Wilson Inc)**. 1972. *Soil behaviour under earthquake loading conditions*. Tennessee.

Shuttle, D. A., Martens, S., and Jefferies, M. G. 2021. Geostatic stress in oil-sand tailings. *Proceedings of the Institution of Civil Engineers-Geotechnical Engineering*, pp 1–10.

© University of Pretoria

Skempton, A. W. 1944. Notes on the compressibility of clays. *Quarterly Journal of the Geological Society*, 100(1–4), pp 119–135.

Sladen, J. A., D'hollander, R. D., and Krahn, J. 1985. The liquefaction of sands, a collapse surface approach. *Canadian Geotechnical Journal*, 22(4), pp 564–578.

Sladen, J. A., and Handford, G. 1987. A potential systematic error in laboratory testing of very loose sands. *Canadian Geotechnical Journal*, 24(3), pp 462–466.

Smith, E. S., and Connell, D. H. 1979. The role of water in the failure of tailings dams. *Mine Drainage: San Francisco*, Miller Freeman Publications, pp 627–650.

Smart Solar. 2018. *HP Series Smart Solar Charge Controller Datasheet*.

Sottile, M., Labanda, N. A., Cier, R. J., Reid, D., and Fourie, A. B. 2023. Numerical study of moist tamping and end platens lubrication effect on undrained triaxial test of a sand. *Proceedings of the 10th European Conference on Numerical Methods in Geotechnical Engineering*. London.

Sparrow, R. W., and Tory, A. C. 1966. Behavior of a soil mass under dynamic loading. *Journal of the Soil Mechanics and Foundations Division*, 92(3), pp 59–93.

Spencer, L. 2021. Characterizing tailings professional labor demand. MSc Thesis, Colorado State University, Colorado.

Spies, L. H. 2020. Design of a lined platinum tailings storage facility in South Africa. *Journal of the Southern African Institute of Mining and Metallurgy*, 120(7), pp 399–404.

Station, W. E. 1944. Soil pressure cell investigation, *Technical Memorandum No. 210-1*. Vicksburg, Mississippi.

Susha Lekshmi, S. U., Singh, D. N., Tarantino, A., and Baghini, M. S. 2018. Evaluation of the Performance of TDR and Capacitance Techniques for Soil Moisture Measurement. *Geotechnical Testing Journal*, 41(2), 20160240.

Swanepoel, N. 2016. *A single health and safety act for mining and industry in South Africa*. LLM Thesis, North-West University, Potchefstroom.

Symons, I. F., and Murray, R. T. 1988. Conventional retaining walls: pilot and full-scale studies. *Proceedings of the Institution of Civil Engineers*, 84(3), pp 519–538.

Take, W. A. 1997. *Lateral earth pressure behind rigid fascia retaining walls*. MSc Thesis, University of New Brunswick, Fredericton.

Take, W. A., and Bolton, M. D. 2003. Tensiometer saturation and the reliable measurement of soil suction. *Géotechnique*, 53(2), pp 159–172.

Taylor, D. W. 1945. Review of pressure distribution theories, earth pressure cell investigations and pressure distribution data, *Soil mechanics fact finding survey, Progress Report*. Waterways Experiment Station, Vicksburg, Mississippi.

Taylor, D. W. 1947. *Pressure distribution theories, earth pressure cell investigations and pressure distribution data*. US Waterways Experiment Station.

Taylor, D. W. 1948. *Fundamentals of Soil Mechanics*. New York: John Wiley and Sons.

© University of Pretoria

TE Connectivity. (2018). *MS54XX miniature SMD pressure sensor datasheet*.

Topp, G. C., Davis, J. L., and Annan, A. P. 1980. Electromagnetic determination of soil water content: Measurements in coaxial transmission lines. *Water Resources Research*, 16(3), pp 574–582.

Torres-Cruz, L. A. 2016. *Use of the cone penetration test to assess the liquefaction potential of tailings storage facilities*, PhD Dissertation, University of the Witwatersrand, Johannesburg.

Torres-Cruz, L. A. 2021. The Plewes method: a word of caution. *Mining, Metallurgy and Exploration*, pp 1–10.

Torres-Cruz, L. A., and O'Donovan, C. 2023. Public remotely sensed data raise concerns about history of failed Jagersfontein dam. *Scientific Reports*, 13(1), 4953.

Tory, A. C., and Sparrow, R. W. 1967. The influence of diaphragm flexibility on the performance of an earth pressure cell. *Journal of Scientific Instruments*, 44(9), pp 781-785.

Triandafilidis, G. E. 1974. Soil-stress gauge design and evaluation. *Journal of Testing and Evaluation*, 2(3), pp 146–158.

Tripathy, S., Al-Khyat, S., Cleall, P. J., Baille, W., and Schanz, T. 2016. Soil suction measurement of unsaturated soils with a sensor using fixed-matrix porous ceramic discs. *Indian Geotechnical Journal*, 46, pp 252–260.

Trollope, D. H., and Lee, I. K. 1957. The performance of laboratory earth pressure cells. *Australian Journal of Applied Sciences*, 8(2), pp 84–97.

Tshabalala, L. 2003. *The effect of consolidation and loading stress paths on the static liquefaction of mine tailings*. MSc Thesis, University of the Witwatersrand, Johannesburg.

TÜV-SÜD. 2018. *Auditoria Técnica de Segurança 2° Ciclo 2018*.

Vaid, Y. P., and Negussey, D. 1988. Preparation of reconstituted sand specimens. *Advanced Triaxial Testing of Soil and Rock*, pp 405–417.

Vaid, Y. P., and Sivathayalan, S. 2000. Fundamental factors affecting liquefaction susceptibility of sands. *Canadian Geotechnical Journal*, 37(3), pp 592–606.

Vandoorne, R., Gräbe, P. J., and Heymann, G. 2021. Soil suction and temperature measurements in a heavy haul railway formation. *Transportation Geotechnics*, 31, 100675.

Verdugo, R., and Ishihara, K. 1996. The steady state of sandy soils. *Soils and Foundations*, 36(2), pp 81–91.

Vermeulen, N. J. 2001. The composition and state of gold tailings. PhD Dissertation, University of Pretoria, Pretoria.

Vick, S. G. 1983. *Planning, design, and analysis of tailings dams*. Wiley New York.

Wagener, F, Van der Berg, J., and Jacobsz, S. W. 1998. Monitoring of the seepage regime in tailings dams. *South African Institution of Civil Engineering Magazine*, pp 23–26.

Wagener, F. 1997. The Merriespruit slimes dam failure: overview and lessons learnt. *Journal of the South African Institution of Civil Engineering*, 39(3), pp 11–15.

© University of Pretoria

Wanatowski, D., and Chu, J. 2012. Factors affecting pre-failure instability of sand under plane-strain conditions. *Géotechnique*, 62(2), pp 121–135.

Wang, S., Luna, R., and Stephenson, R. W. 2011. A slurry consolidation approach to reconstitute low-plasticity silt specimens for laboratory triaxial testing. *Geotechnical Testing Journal,* 34(4), pp 288–296.

Wates, J. A. 2018. Keynote presentation: SANS10286 being world class. *Proceedings of the 6th International Mining and Industrial Waste Management Conference.* Polokwane.

Wates, J. A., and Lyell, K. 2018. A review of the evolution of tailings management and the impact on improved safety in South Africa*. Proceedings of the 6th International Mining and Industrial Waste Management Conference*, pp 109–116. Polokwane.

Weiler, W. A., and Kulhawy, F. H. 1982. Factors affecting stress cell measurements. *Journal of the Geotechnical Engineering Division*, pp 442–449.

Weiler, W. A., and Kulhawy, F. H. 1978. Behavior of stress cells in soil, *Contract Report B-49(4) to Niagara Mohawk Power Corporation*. Ithica.

Wen, B., Aydin, A., and Duzgoren-Aydin, N. 2002. A comparative study of particle size analyses by sieve-hydrometer and laser diffraction methods. *Geotechnical Testing Journal*, 25(4), pp 434–442.

Westraad, D. 2004. *Suction induced shear strength of gold mine tailings*. MEng Thesis, University of Pretoria, Pretoria.

Williams, A. A. B., and Brown, S. F. 1971. The use of earth pressure cells in some road experiments. *Proceedings of the 5th Regional Conference on Soil Mechanics and Foundation Engineering*, (124), pp 15–21. Luanda.

Wortmann, H. 2007. *Sedimentation and desiccation of gold mine tailings*. MEng Thesis, University of Pretoria, Pretoria.

Wroth, C. P. 1984. The interpretation of in situ soil tests. *Géotechnique*, 34(4), pp 449–489.

Yang, M. Z. 2000. *Evaluation of factors affecting earth pressures on buried box culverts*. PhD Dissertation, University of Tennessee, Tennessee.

Yang, M. Z., Drumm, E. C., Bennett, R. E., and Mauldon, M. 2001. Temperature effects on contact earth pressure cells: inferences from long term field instrumentation. *Geotechnical Instrumentation News*, 19(2), pp 25–28.

Yoshimi, Y., Tanaka, K., and Tokimatsu, K. 1989. Liquefaction resistance of a partially saturated sand. *Soils and Foundations*, 29(3), pp 157–162.

Yoshimine, M., Ishihara, K., and Vargas, W. 1998. Effects of principal stress direction and intermediate principal stress on undrained shear behavior of sand. *Soils and Foundations*, 38(3), pp 179–188.

Youd, T. L., and Craven, T. N. 1975. Lateral stress in sands during cyclic loading. *Journal of the Geotechnical Engineering Division*, 101(2), pp 217-221.

© University of Pretoria

Yu, H. S. 1998. CASM: A unified state parameter model for clay and sand. *International Journal for Numerical and Analytical Methods in Geomechanics*, 22(8), pp 621–653.

Zadeh, S. G. (2019). *Shear behaviour of geosynthetic clay liners and textured geomembranes in mining applications*. PhD Dissertation, Colorado State University, Colorado.

Zhang, H., and Garga, V. K. 1997. Quasi-steady state: a real behaviour? *Canadian Geotechnical Journal*, 34(5), pp 749–761.

Zhang, C., Chen, Q., Pan, Z., and Ma, C. 2020. Mechanical behavior and particle breakage of tailings under high confining pressure. *Engineering Geology*, 265, 105419.

Zhang, X., and Houston, S. 2024. Indefinability of effective stress for unsaturated soils. *Journal of Geotechnical and Geoenvironmental Engineering*, 150(8), 04024064.

Zheng, J. (2022). Discussion on “Procedure for assessing the liquefaction vulnerability of tailings dams.” *Computers and Geotechnics*, 149, 104870.

Zhu, F., and Clark, J. I. 1994. The effect of dynamic loading on lateral stress in sand. *Canadian Geotechnical Journal*, 31(2), pp 308-311.

Zlatovic, S., and Ishihara, K. 1997. Normalized behavior of very loose non-plastic soils: effects of fabric. *Soils and Foundations*, 37(4), pp 47–56.

© University of Pretoria